International Journal of
*Molecular Sciences*

# Aptamers

Edited by
Julian Alexander Tanner, Andrew Brian Kinghorn and
Yee-Wai Cheung

Printed Edition of the Special Issue Published in *IJMS*

www.mdpi.com/journal/ijms

MDPI

# Aptamers

# Aptamers

Special Issue Editors

**Julian Alexander Tanner**
**Andrew Brian Kinghorn**
**Yee-Wai Cheung**

MDPI • Basel • Beijing • Wuhan • Barcelona • Belgrade

*Special Issue Editors*
Julian Alexander Tanner, Andrew Brian Kinghorn and Yee-Wai Cheung
The University of Hong Kong
China

*Editorial Office*
MDPI
St. Alban-Anlage 66
Basel, Switzerland

This edition is a reprint of the Special Issue published online in the open access journal *International Journal of Molecular Sciences* (ISSN 1422-0067) from 2017–20181 (available at: http://www.mdpi.com/journal/ijms/special_issues/aptamers).

For citation purposes, cite each article independently as indicated on the article page online and as indicated below:

LastName, A.A..; LastName, B.B.; LastName, C.C. Article title. *Journal Name* **Year**, Article number, Page Range.

**ISBN 978-3-03897-059-0 (Pbk)**
**ISBN 978-3-03897-060-6 (PDF)**

Cover image courtesy of Masayo Kotaka, it is a depiction of a DNA aptamer binding to *Plasmodium falciparum* lactate dehydrogenase.

# Contents

# About the Special Issue Editors

**Julian Alexander Tanner** is Associate Professor in the School of Biomedical Sciences at the University of Hong Kong. Julian's research interests are highly interdisciplinary, intersecting nucleic acid nanotechnology, chemical biology, diagnostics technologies, and polyphosphate biochemistry. He has published over 60 papers in these areas, and chaired the conference "Aptamers 2018" at the University of Oxford. Julian has been awarded the Outstanding Young Researcher, Outstanding Research Student Supervisor, and Outstanding Teacher awards by the University of Hong Kong.

**Andrew Brian Kinghorn** is a Postdoctoral Fellow in the School of Biomedical Sciences at the University of Hong Kong. Andrew received his B.Biotech with first class honours from the University of Queensland in 2008 and received his PhD from the University of Hong Kong in 2016. Kinghorn's wet lab research interests include directed molecular evolution, aptamer selection, microarray-based aptamer optimization, and applying aptamers as point-of-care diagnostics. Kinghorn's computational research interests include modelling of complex systems, simulation of directed molecular evolution, and coding of bioinformatics tools.

**Yee-Wai Cheung** is a Postdoctoral Fellow in the School of Biomedical Sciences at the University of Hong Kong. She performed her PhD research on the selection and structural elucidation of DNA aptamers for malaria diagnosis. She has over ten years' experience in aptamer science and specialises in aptamer selection and diagnostics development. Her research focuses on elucidation of aptamer-target interactions and the development of biosensors using emerging nucleic acid technologies.

# Preface to "Aptamers"

Aptamers are in vitro selected oligonucleotides capable of specific, high-affinity binding to a wide variety of target molecules. These features enable their application in diagnostics, therapeutics, targeted delivery, fluorescence imaging, and biosensing. Aptamers are isolated via systematic evolution of ligands by exponential enrichment (SELEX), an iterative cycle of selection and amplification steps that enriches a randomly synthesised oligonucleotide library to a pool of specific, high-affinity aptamers. Since the inception of aptamers in 1990, the methods by which aptamers are selected has been improved, yielding a robust system capable of producing aptamers rapidly and at low cost. Recently, there has been an explosion in the field of aptamers including innovations in enhanced selection strategies, bioinformatics approaches, riboswitches, unnatural base pairs, nucleic acid nanostructures, and DNAzymes.

We are pleased to introduce this book "Aptamers" based on a Special Issue of International Journal of Molecular Sciences (MDPI). This book is the result of contributions from aptamer scientists and consolidates the best ideas in the Aptamers Special Issue. From initial SELEX library design to the modification and optimisation of identified aptamers and the final endpoint application, the fifteen articles presented herein cover a wide range of areas in aptamer science. Eleven review papers are included in this book in three areas:

Aptamer Identification

- SELEX-based aptamer selection starts with the design of the initial nucleic acid library. Vorobyeva et al. [1] compiled literature examples specifying both the general considerations and the many important, selection-specific features of library design. Consideration of aspects such as structural complexity, chemical repertoire, the randomisation approach, and sequence formatting are discussed. The library design checklist is a useful way to categorise and illustrate aptamer libraries.
- Aptamer serum stability and bloodstream retention time are challenges for the use of aptamers as therapeutics. Ni et al. [2] reviewed different post-SELEX chemical modifications for the optimisation of aptamers for clinical use. The suitability of different chemical modifications for resisting nuclease degradation and renal clearance and improving affinity and specificity are discussed.
- Aptamers are genetic in nature, so bioinformatics approaches can improve both aptamers and their selection methodologies. Kinghorn et al. [3] reviewed several categories of aptamer bioinformatics, including the simulation of aptamer selection, fragment-based aptamer design, the patterning of libraries, the identification of lead aptamers from high-throughput sequencing (HTS) data, and in silico aptamer optimization.
- Riboswitches are a major topic in aptamer science. Based on structural changes induced by target-RNA aptamer binding, gene expression can be controlled. Gong et al. [4] reviewed different computational approaches used to model structures of RNA aptamers and designing riboswitches.
- Amyloid β-protein is associated with Alzheimer's disease, cancer, and Down syndrome. Of particular interest is amyloid β-protein's misfolding to form Amyloid plaques. Using a case study of aptamers targeting amyloid β-protein, Rahimi [5] deliberated the controversies and methodological limitations of identifying aptamers against intrinsically disordered proteins.
- DNA damage and repair are critical determinants in cancer, aging, and many other diseases. McKeague [6] provides an excellent summary of the current literature on aptamers relating to DNA damage and repair.

Fluorogenic Aptamers

- The recent development of aptamer-based fluorogenic modules facilitates the application of imaging RNA in the cell, RNA tracking, and the biosensing of metabolites in cells.

Bouhedda et al. [7] provide an excellent overview of the development and application of several different RNA-based fluorogenic modules.

Aptamer Applications

- One property of aptamers that sets them apart from antibodies is the potential for expansion of their chemical repertoire. Röthlisberger et al. [8] discuss the function and application of various aptamer conjugates and recent advances in chemical modifications for aptamers. The applications of aptamers in neurosciences are specifically highlighted.
- Prion protein (PrP) is intrinsic to the nervous system; however, its misfolding leads to transmissible spongiform encephalopathies. Macedo and Cordeiro [9] review the implications and potential advances of aptamers selected against PrP and other amyloidogenic proteins for application as therapeutics and diagnostics for neurogenic disorders.
- Glioblastoma is a highly aggressive primary brain tumour with poor clinical prognosis due to its varied genetic profiles and infiltrative growth. Hays et al. [10] summarise the current aptamers targeting glioblastoma cells or biomarkers for brain tumour.
- Interleukin-6 (IL-6) plays an important role in the immune response. The signal transduction of IL-6 is initiated by recognition of IL-6 by IL-6 receptors on cell surface. Hahn [11] introduced the concept of "Charomers", which are IL-6 receptor-specific aptamers that internalise after binding to the IL-6 receptor. Charomers have been used for the targeted delivery of chemopathic agents and in photodynamic therapy.

To demonstrate the different selection approaches currently used and the downstream applications of identified aptamers, four research articles are included in this book:

- Osteoblast differentiation is a target of regenerative medicine, as it is associated with bone formation. Nuclear WW domain containing E3 ubiquitin ligase 1 (WWP1) is involved in osteoblast differentiation by regulating the ubiquitination of Runt-related transcription factor 2.. Tucker et al. [12] selected DNA aptamers that target the homologous E6-AP carboxyl terminus (HECT) domain of WWP1. One characterised aptamer showed an affinity to WWP1 in the low micromolar range and was shown to promote extracellular mineralisation in cell culture experiments. These results demonstrate that aptamer-mediated inhibition of protein ubiquitination has potential as a novel therapeutic strategy.
- *Bifidobacterium bifidum* is a probiotic bacteria commonly found in humans. Hu et al. [13] performed a whole cell SELEX against B. bifidum to isolate DNA aptamers. One identified aptamer was able to differentiate *B. bifidum* from other *Bifidobacterium* spp. This aptamer was incorporated into a colorimetric micotitre plate bioassay for the detection of B. bifidum.
- Fipronil is a commonly used insecticide linked to human health and environmental risk. Hong and Sooter [14] isolated aptamers against fipronil, with one characterised aptamer exhibiting specific binding to fipronil with a low nanomolar dissociation constant. This aptamer was developed into a microtiter plate detection assay to determine fibronil-spiked river water samples.
- *Staphylococcus aureus* is a common cause of infection in humans. Reich et al. [15] demonstrated the development of an aptasensor for *S. aureus* using a ferri-/ferricyanide probe. The developed biosensor could discriminate *S. aureus* from *Escherichia coli* and *Staphylococcus epidermidis* with an excellent detection limit.

We thank the article authors again for their excellent contributions. We hope this book will not only be beneficial and interesting to aptamer scientists, but also to extended audiences across biomedical, chemical, and environmental sciences.

**References**

1. Vorobyeva, M.; Davydova, A.; Vorobjev, P.; Pyshnyi, D. Venyaminova A: Key Aspects of Nucleic

Acid Library Design for in Vitro Selection. *Int. J. Mol. Sci.* **2018**, *19*, 470.
2. Ni, S.; Yao, H.; Wang, L.; Lu, J.; Jiang, F.; Lu, A.; Zhang, G. Chemical Modifications of Nucleic Acid Aptamers for Therapeutic Purposes. *Int. J. Mol. Sci.* **2017**, *18*, 1683.
3. Kinghorn, A.; Fraser, L.; Liang, S.; Shiu, S.; Tanner, J. Aptamer Bioinformatics. *Int. J. Mol. Sci.* **2017**, *18*, 2516.
4. Gong, S.; Wang, Y.; Wang, Z.; Zhang, W. Computational Methods for Modeling Aptamers and Designing Riboswitches. *Int. J. Mol. Sci.* **2017**, *18*, 2442.
5. Rahimi, F. Aptamers Selected for Recognizing Amyloid β-Protein—A Case for Cautious Optimism. *Int. J. Mol. Sci.* **2018**, *19*, 668.
6. McKeague, M. Aptamers for DNA Damage and Repair. *Int. J. Mol. Sci.* **2017**, *18*, 2212.
7. Bouhedda, F.; Autour, A.; Ryckelynck, M. Light-Up RNA Aptamers and Their Cognate Fluorogens: From Their Development to Their Applications. *Int. J. Mol. Sci.* **2018**, *19*, 44.
8. Röthlisberger, P.; Gasse, C.; Hollenstein, M. Nucleic Acid Aptamers: Emerging Applications in Medical Imaging, Nanotechnology, Neurosciences, and Drug Delivery. *Int. J. Mol. Sci.* **2017**, *18*, 2430.
9. Macedo, B.; Cordeiro, Y. Unraveling Prion Protein Interactions with Aptamers and Other PrP-Binding Nucleic Acids. *Int. J. Mol. Sci.* **2017**, *18*, 1023.
10. Hays, E.; Duan, W.; Shigdar, S. Aptamers and Glioblastoma: Their Potential Use for Imaging and Therapeutic Applications. *Int. J. Mol. Sci.* **2017**, *18*, 2576.
11. Hahn, U. Charomers—Interleukin-6 Receptor Specific Aptamers for Cellular Internalization and Targeted Drug Delivery. *Int. J. Mol. Sci.* **2017**, *18*, 2641.
12. Tucker, W.; Kinghorn, A.; Fraser, L.; Cheung, Y.-W.; Tanner, J. Selection and Characterization of a DNA Aptamer Specifically Targeting Human HECT Ubiquitin Ligase WWP1. *Int. J. Mol. Sci.* **2018**, *19*, 763.
13. Hu, L.; Wang, L.; Lu, W.; Zhao, J.; Zhang, H.; Chen, W. Selection, Characterization and Interaction Studies of a DNA Aptamer for the Detection of *Bifidobacterium bifidum*. *Int. J. Mol. Sci.* **2017**, *18*, 883.
14. Hong, K.; Sooter, L. In Vitro Selection of a Single-Stranded DNA Molecular Recognition Element against the Pesticide Fipronil and Sensitive Detection in River Water. *Int. J. Mol. Sci.* **2018**, *19*, 85.
15. Reich, P.; Stoltenburg, R.; Strehlitz, B.; Frense, D.; Beckmann, D. Development of An Impedimetric Aptasensor for the Detection of *Staphylococcus aureus*. *Int. J. Mol. Sci.* **2017**, *18*, 2484.

**Julian Alexander Tanner, Andrew Brian Kinghorn and Yee-Wai Cheung**
*Special Issue Editors*

International Journal of
*Molecular Sciences*

MDPI

*Review*

# Unraveling Prion Protein Interactions with Aptamers and Other PrP-Binding Nucleic Acids

**Bruno Macedo * and Yraima Cordeiro ***

Faculty of Pharmacy, Federal University of Rio de Janeiro (UFRJ), Av. Carlos Chagas Filho 373, Bloco B, Subsolo, Sala 17, Rio de Janeiro, RJ 21941-902, Brazil

* Correspondence: brunomacedo@ufrj.br (B.M.); yraima@pharma.ufrj.br (Y.C.); Tel.: +55-21-2260-9192 (B.M. & Y.C.)

Academic Editors: Julian Alexander Tanner, Andrew Brian Kinghorn and Yee-Wai Cheung
Received: 8 March 2017; Accepted: 4 May 2017; Published: 17 May 2017

**Abstract:** Transmissible spongiform encephalopathies (TSEs) are a group of neurodegenerative disorders that affect humans and other mammals. The etiologic agents common to these diseases are misfolded conformations of the prion protein (PrP). The molecular mechanisms that trigger the structural conversion of the normal cellular PrP ($PrP^{C}$) into the pathogenic conformer ($PrP^{Sc}$) are still poorly understood. It is proposed that a molecular cofactor would act as a catalyst, lowering the activation energy of the conversion process, therefore favoring the transition of $PrP^{C}$ to $PrP^{Sc}$. Several in vitro studies have described physical interactions between PrP and different classes of molecules, which might play a role in either PrP physiology or pathology. Among these molecules, nucleic acids (NAs) are highlighted as potential PrP molecular partners. In this context, the SELEX (Systematic Evolution of Ligands by Exponential Enrichment) methodology has proven extremely valuable to investigate PrP–NA interactions, due to its ability to select small nucleic acids, also termed aptamers, that bind PrP with high affinity and specificity. Aptamers are single-stranded DNA or RNA oligonucleotides that can be folded into a wide range of structures (from harpins to G-quadruplexes). They are selected from a nucleic acid pool containing a large number ($10^{14}$–$10^{16}$) of random sequences of the same size (~20–100 bases). Aptamers stand out because of their potential ability to bind with different affinities to distinct conformations of the same protein target. Therefore, the identification of high-affinity and selective PrP ligands may aid the development of new therapies and diagnostic tools for TSEs. This review will focus on the selection of aptamers targeted against either full-length or truncated forms of PrP, discussing the implications that result from interactions of PrP with NAs, and their potential advances in the studies of prions. We will also provide a critical evaluation, assuming the advantages and drawbacks of the SELEX (Systematic Evolution of Ligands by Exponential Enrichment) technique in the general field of amyloidogenic proteins.

**Keywords:** prion protein; nucleic acids; SELEX (Systematic Evolution of Ligands by Exponential Enrichment); aptamers

## 1. Introduction

Aberrant prion proteins (PrPs) responsible for the transmissible spongiform encephalopathies (TSEs) are misfolded conformations of the natively expressed prion protein, the innocuous cellular PrP ($PrP^{C}$) [1]. The misfolded conformers, termed scrapie PrP ($PrP^{Sc}$), have the ability to self-perpetuate and to become infectious entities [1]. Therefore, they are the primary culprit of TSEs, which form a group of fatal neurodegenerative disorders that affect humans and other mammals [1]. Currently, the "prion" term has emerged as a new phenomenon in molecular biology, describing proteins with the ability to undergo autoconversion, autopropagation, and dissemination between cells [2]. Remarkably, pathogenic PrPs can be transmitted not only between cells but also among organisms of the same

species and this can ultimately lead to epidemic outbreaks [3]. To date, only the prion protein fulfills the infectious characteristics of true prions. There is, apparently, a lack of conformational properties in other prion-like proteins to define them as bona fide prions.

$PrP^{C}$ is a constitutive cell-surface glycoprotein, highly conserved among species, expressed in several cell types, mainly in the central nervous system (CNS) [1]. High-resolution studies have revealed two structurally distinct domains: the flexible N-terminal region (residues 23–~120) and the globular C-terminal domain (residues ~120–231), the latter composed of three α-helices and a small antiparallel β-sheet [4,5]. Is it still not known how the drastic conformational changes occur in the $PrP^{C}$ structure—even without any mutations in the *PRNP* gene—to give rise to the abnormal $PrP^{Sc}$. However, once formed, $PrP^{Sc}$ can propagate in an autocatalytic manner, recruiting more $PrP^{C}$ to fold into new $PrP^{Sc}$, leading to its accumulation in tissues with severe cellular damage and further neurodegeneration [6]. In contrast to $PrP^{C}$, $PrP^{Sc}$ is a β-structure-rich protein, insoluble, and resistant to proteolysis. It can form toxic oligomers and aggregates either with an amyloid-like architecture or with an amorphous disposition [6]. Besides prion diseases, protein aggregation is the central event of many other neurodegenerative disorders, including Alzheimer's (AD) and Parkinson's (PD) diseases [7]. In each scenario, the misfolding of a specific protein, that is, the amyloid β-protein (Aβ) for AD, α-synuclein (α-syn) for PD, and the prion protein itself (PrP) for TSEs, can lead to its aggregation and cell-to-cell transfer, forming insoluble deposits or plaques in different regions of the brain (depending on the particular protein under discussion) [8]. To date, there is no available treatment to halt or to delay the neurodegeneration process triggered by one or more of these misfolded and aggregated proteins in the CNS; therefore, these diseases are still invariably fatal. Understanding the molecular basis of protein misfolding and conformational conversion are major priorities in the search for therapeutic strategies that could block or modulate the aggregation process from its very beginning.

The mechanisms that lead a soluble and natively folded protein to adopt an aberrant conformation with a higher tendency to form aggregates depend on the different intermediate structures formed during the folding process, the free energy of these intermediates, the energy barrier between them, and the exposition of hydrophobic surfaces that should be normally buried and solvent-excluded in a functional conformation [9]. Misfolded forms are normally degraded by cell protein quality control mechanisms, but during aging these mechanisms begin to fail, losing or reducing their ability to prevent protein accumulation [10]. Mutations, posttranslational modifications, environmental variations, or interactions with external agents are also factors that can drive protein misfolding and aggregation [11]. PrP is also known as a "promiscuous" protein that can bind to different classes of molecules, including metallic ions, glycosaminoglycans, lipids, and nucleic acids. The biological relevance of most of these interactions is still not clear, but these ligands may participate in the PrP structural conversion and, consequently, in disease progression [12–17].

Nowadays, the cofactor hypothesis has gained more visibility. It postulates that the presence of an adjuvant factor that interacts with PrP favors its interconversion, aggregation, and infectivity [13,16,18–20]. Such a cofactor may act as a catalyst in PrP conversion, lowering the high-energy barrier that prevents the spontaneous conversion of $PrP^{C}$ into $PrP^{Sc}$ (Figure 1). In this context, nucleic acid (NAs) molecules have been ascribed an important role. PrP has been shown to interact with DNAs and RNAs both in vitro and in vivo [21–26], indicating their suitable involvement in PrP pathophysiology. Many studies have evaluated the effects of NAs as molecular cofactors for PrP conversion into $PrP^{Sc}$-like species. The in vitro-methodology called SELEX (Systematic Evolution of Ligands by Exponential Enrichment) [27,28] is an interesting tool that has been used to identify and select small oligonucleotides, known as "aptamers" that bind with high affinity and high specificity to the wild-type (full-length) PrP and/or its different domains.

In this review, we will focus on published studies about PrP–NA interactions, the SELEX methodology, the knowledge these bring to the prion field, and the new avenues they offer for the therapy and diagnosis of such devastating diseases. Besides PrP, several other amyloid-forming proteins related to conformational diseases can also bind nucleic acids [25]; therefore, we will also

present an overall critical assessment of the aptamer literature in the general field of amyloids, reviewing some relevant SELEX studies against other amyloidogenic proteins, focusing also on the possible drawbacks of this approach regarding aptamer specificity and selectivity against the monomeric or fibrillar forms of these proteins.

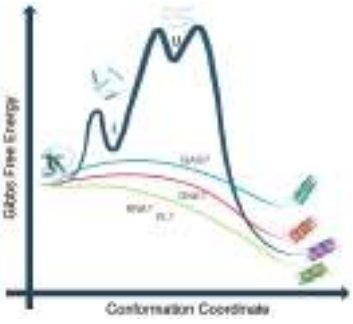


**Figure 1.** Free energy diagram representing the role of cofactors in prion protein (PrP) conformational conversion. DNA, RNA, phospholipid (PL), and glycosaminoglycan (GAG) candidates may interact with $PrP^{C}$, lowering the energy barrier that prevents its spontaneous conversion to the $PrP^{Sc}$. Different cofactor molecules may stimulate the conversion to the different PrP pathogenic forms and may result in the generation of $PrP^{Sc}$ with varying conformations, providing a possible explanation for the existence of various prion strains. I: intermediate state; U: unfolded state. Reproduced from [9].

## 2. PrP and Nucleic Acids Interactions

The crosstalk between PrP and NAs has captured the attention of the prion research community for the last twenty years. The first study was conducted by Pradip Nandi in 1997 with the human-derived neurotoxic prion peptide ($PrP^{106–126}$) and showed, through fluorescence measurements, the ability of this peptide to bind to a small single-stranded DNA (ssDNA) sequence with micromolar affinity and that this interaction induced a structural change in the DNA molecule [29]. In subsequent publications, Nandi showed that $PrP^{106–126}$ polymerizes into amyloid aggregates in the presence of DNA, either in its circular or in its linearized forms, under experimental conditions where the peptide alone did not polymerize [30]. Wild-type murine recombinant PrP (rPrP) also underwent polymerization in a nucleic acid aqueous solution [31]. In 2001, our group was the first to show the dual role of NAs in changing PrP conformation and aggregation [21]. While PrP interaction with double-stranded DNA (dsDNA) induced the conversion of the full-length recombinant PrP (rPrP) to β-sheet-rich structures and led to rPrP aggregation as revealed by spectroscopic techniques, the same dsDNA oligonucleotides inhibited the aggregation of a PrP hydrophobic domain, the $PrP^{109–149}$ [21]. $PrP^{109–149}$ undergoes prompt aggregation when diluted from a denaturing condition into an aqueous solution; however, the aggregation is completely inhibited in the presence of DNA in a concentration-dependent manner, as verified by light scattering (LS) measurements and through transmission electron microscopy [21,24]. It was also reported that an anti-DNA antibody (OCD4), as well as the gene 5 protein, a DNA-binding protein, is able to catch PrP only from the brain material of prion-infected humans or animals, but they do not capture PrP from non-infected brains [26]. OCD4 seems to present immunoreaction with DNA-associated molecules and this antibody can form a complex with PrP in prion diseases [26]. Moreover, OCD4 detects $PrP^{Sc}$ over ten times more efficiently than an antibody against PrP [26] supporting the proposal that nucleic acids are associated with $PrP^{Sc}$ in vivo. Collectively, these results reinforce the proposal by our group that DNA can participate in PrP misfolding, shifting the equilibrium between $PrP^{C}$ and $PrP^{Sc}$ by reducing protein mobility and favoring protein–protein interactions [21,32].

Following these initial observations, many groups started evaluating the interaction of NAs with both $PrP^{C}$ and $PrP^{Sc}$, unraveling many aspects of this crosstalk. One important area of exploration was

to characterize the DNA-binding site on PrP. Studies with different rPrP constructs, mainly using nuclear magnetic resonance (NMR) and small angle X-ray spectroscopy (SAXS) measurements, identified at least two DNA-binding sites in rPrP; one of them in the C-terminal globular domain and the other in the flexible N-terminal region [33–35]. In 2012, our group showed that different small dsDNA sequences can individually bind to rPrP, inducing protein aggregation in a supramolecular structure resembling less-ordered amyloid fibrils [24]. We have observed different effects on the structure, stability, and aggregation of rPrP upon interaction with different DNA sequences [24]. The resultant PrP–DNA complex was toxic to murine neuroblastoma (N2a) cell lines, depending on the DNA sequence, but caused no toxicity to human kidney (HK-2) cell lines [24]. Our results suggested that the DNA GC-content is important to dictate the aggregation pattern and the formation of toxic species; in addition, the PrP expression level or some specific factors from the cellular lineage also appeared to be important to mediate PrP toxicity [24]. In 2013, Cavaliere et al. showed that G-quadruplex forming DNA can bind to different forms of PrP with nanomolar affinity and, in accordance with our previous studies, the PrP–DNA interaction led to loss of the secondary structure of both the PrP and the DNA molecule, indicating that there are reciprocal structural changes after DNA binds to PrP [24,36].

PrP–RNA interactions have also been described. The work of the Darlix group showed that PrP has nucleic acid chaperoning activities, similar to nucleocapsid retroviral proteins, indicating that PrP might participate in nucleic acid metabolism (both RNA and DNA) [37,38]. Indeed, rPrP binds different RNAs with high affinity in vitro and in vivo. This interaction promotes the formation of PrP aggregates where PrP becomes resistant to proteinase K (PK) digestion and the RNAs bound to the complex are resistant to ribonuclease (RNase) attack [22,23,39,40]. This interaction is normally abolished when the PrP construct has its N-terminal region truncated (residues 23–~121), as shown by different groups, suggesting that the flexible PrP N-terminal region is important to establish the interaction with RNA [33,40]. In 2003, Deleault et al. described the role of RNA molecules in stimulating prion protein conversion in vitro [23]. The amplification of a protease-resistant $PrP^{Sc}$-like molecule, termed $PrP^{Res}$ (from the PK-resistance property), was evaluated by the in vitro conversion assay based on the protein-misfolding cyclic amplification (PMCA) method [41,42]. PMCA uses diluted prion-infected brain homogenate as a seed to trigger the conversion of $PrP^{C}$ in healthy brain homogenates; the final amplified $PrP^{Res}$ shares many specific characteristics with the scrapie prion propagated in vivo; therefore, it is widely used in prion conversion studies [41]. It was found that RNase inhibits $PrP^{Res}$ amplification in a dose-dependent manner, evidencing that RNA is required for the efficient formation and accumulation of scrapie-like PrP in vitro. Moreover, only the addition of specific RNAs (isolated from mammalian brains) was able to stimulate this conversion reaction [23]. Subsequent work, using only purified and synthetic molecules, revealed that $PrP^{C}$, $PrP^{Sc}$, co-purified lipids, and poly-A RNA can form the minimal set of components necessary to amplify the $PrP^{Res}$ conformation in vitro with the ability to infect normal wild-type hamsters in vivo [18]. The requirement of a negatively charged accessory molecule for the efficient production of infectious prions in vitro (synthetic prions) is in good agreement with the proposed cofactor hypothesis, where endogenous or extracellular factors may participate in prion propagation in vivo. Nevertheless, more studies are required to determine what the exact molecular characteristics of PrP conversion catalysts are and to establish whether one or more cofactors could be considered 'ideal' for forming true prions in vitro or to participate in prion pathogenesis in vivo. Our group showed, through several biophysical approaches, that depending on the RNA source—whether from mammalian, yeast, or bacterial cells—the interaction with murine rPrP led to aggregation with different extents. rPrP–RNA interaction led to secondary structural changes in both rPrP, which loses α-helical content, and in the RNA molecule [40]. Finally, only the aggregated species formed upon incubation with RNA extracted from N2a cells were highly toxic to N2a cells in culture [40]. RNA-binding to ovine PrP was also investigated, and the results revealed a likewise PrP conformational shift to a higher β-sheet content, as well as the neurotoxicity of this complex [39]. In accordance with previous work, the PrP N-terminal region seems to be essential to mediate these effects [40,43].

Although $PrP^C$ is typically localized anchored at the plasmatic membrane, it has been reported that it can be found in the nucleus of neuronal and endocrine cells and can interact with chromatin [44]. The translocation and deposition of misfolded PrPs in the nucleus of infected cells, where the misfolded PrP was able to interact with chromatin components, has also been shown [45]. Although converging experimental evidence indicates that the endocytic pathway is the principal site of prion conversion [46,47], one might speculate that an abnormal nuclear compartmentalization of PrP may contribute to its encounter with non-native partners that could be involved in prion pathogenesis. Nevertheless, PrP and nucleic acids could crosstalk even along the endocytic pathway, as would be the case of endocytosis of exogenous (or from the membrane) PrP bound to nucleic acid. It would also be possible that cytosolic forms of PrP [46] encounter small NAs in the cytoplasm, triggering conversion. In fact, cytosolic PrP has been shown to induce the formation of large ribonucleoprotein organelles in the N2a cell line [48]. Moreover, $PrP^C$ to $PrP^{Sc}$ conversion can also occur on the plasma membrane, being the primary site of conversion when the host is infected with scrapie from external sources [49,50]. In this latter case, a nucleic acid released from a cell or from an exogenous source could encounter $PrP^C$/$PrP^{Sc}$ at the membrane.

Altogether, the evidence compiled here concerning PrP–NA interactions strongly suggest that these molecules can be partners in vivo. Both of them can trigger PrP misfolding, leading to its aggregation in vitro, and they can also stimulate $PrP^{Sc}$ conversion and propagation in vivo. Although they are not identical, the misfolded PrPs formed can be toxic to cultured cells depending on the nucleic acid sequence evaluated. We strongly believe that the sequence and structure adopted by the NAs are essential to dictate those effects. More studies about this partnership may be fundamental not only to understand prion function or dysfunction but also for the development of effective therapeutic approaches.

## 3. SELEX Technique and the Aptamer Discovery

The SELEX technique consists of finding NA ligands with high affinity and specificity against a given target [27,28]. In this review, our target is the PrP. Generally, the core of the selection process consists of the following essential steps: (i) incubation of a randomly synthesized DNA or RNA library (containing $10^{14}$–$10^{16}$ different oligonucleotides sequences) with the selected target to allow binding; (ii) separation of bound from non-bound species (unbound oligonucleotides are removed by several stringent washing steps of the binding complexes); (iii) elution of the target-bound oligonucleotides with higher salt concentrations; and (iv) amplification of the oligonucleotide bound species by a polymerase chain reaction (PCR). A new enriched pool of selected oligonucleotides is generated by purification of ssDNAs from the PCR products (DNA SELEX) or by in vitro transcription (RNA SELEX). Then, this selected NA pool is used for the next selection round. This process can be repeated several times to enhance the affinity and specificity of the isolated NA sequences. The final selected NA sequences are called aptamers; they have to be cloned and individual aptamers have to be sequenced and validated against its target (Figure 2). The stoichiometry of the target and the NAs can be altered as well as the number of washes, and competitive inhibitors can also be added to the binding buffer to enhance the stringency of the SELEX conditions [51]. A counter-SELEX procedure can also be performed to exclude sequences recognizing other non-interested targets by using similar structural targets, therefore increasing the selectivity of the aptamers [52]. Over the years, many modifications and improvements have been introduced to the classical SELEX methodology in order to decrease the selection time and enhance the binding affinity, which include capillary electrophoresis (CE)-SELEX, automated SELEX, and whole cell SELEX [52]. The cell–SELEX technique is fast, straightforward, and very promising because it can be performed with normal living cells, thus guaranteeing that target proteins on the cell maintain their native conformation and function along the selection procedures [52]. Some aptamers have already been discovered to work against different cancer cells by this method; for example, one of them could specifically recognize leukemia cells [53]. To date, there is only one federally approved aptamer, the Pegaptanib drug, selected against vascular endothelial growth factor

(VEGF) to treat the age-related macular degeneration, although there are more than 10 aptamers under different stages of clinical trials for treatment of coagulation, inflammation, cancer, etc. [54]. However, various crucial aspects have delayed the clinical translation of therapeutic aptamers, including their intrinsic physicochemical properties and the lack of safety data.

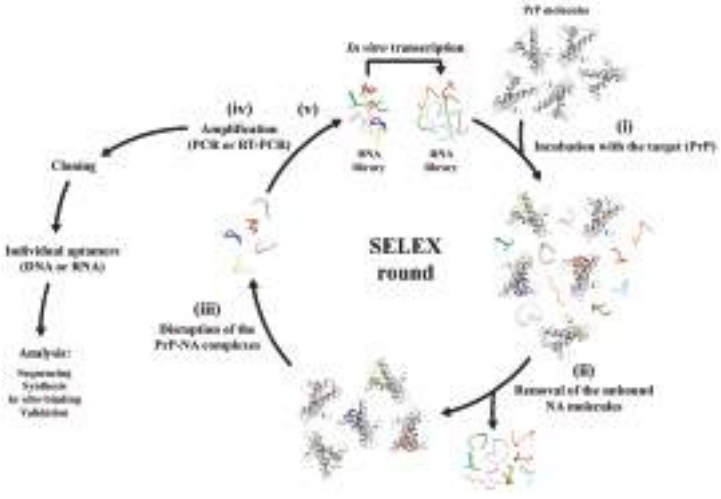


**Figure 2.** General scheme of the SELEX method using recombinant PrP as the target. A SELEX round consists of the following essential steps: (i) binding after the incubation of a randomly synthesized DNA or RNA library (containing $10^{14}$–$10^{16}$ different sequences) with the molecular target (full-length recombinant PrP or other PrP constructions); (ii) removal of the non-bound NA species; (iii) elution of NA sequences from the immobilized PrP (either in-column, in ELISA dishes, or other); (iv) amplification of the eluted NA sequences; (v) back to Step (i). This process can be repeated several times to enhance the affinity and specificity of the isolated NA sequences. The final selected NA pool contains the aptamers that have to be further cloned, and individual aptamers have to be sequenced and validated for binding against its target, PrP.

Aptamers are small single-stranded DNA or RNA nucleotides with a length varying from 20 to 100 bases, flanked by two constant sequences that contain the primer-binding sites [48]. This name comes from the Latin "aptus," which means "fit". Single-stranded NAs can fold into a variety of loops, stems, hairpins, quadruplexes, and bugles, among other shapes, to generate a vast range of secondary and tertiary NAs structures [52]. A well-defined three-dimensional structure of these oligonucleotides can specifically recognize and interact with several target molecules, including amino acids [55,56], proteins [57], antibodies [58], or even whole cells [59]. The interaction affinity occurs in the nanomolar to femtomolar range and is established by various intermolecular forces such as hydrogen bonding, van der Waals forces, and base stacking. To date, thousands of aptamers have already been selected against a wide range of target ligands [52]. They are compared to antibodies but have more advantages over them. They are smaller in size, which allows them to reach the cellular target more easily than classical antibodies; they might have more affinity to the specific target; they are easier to synthesize; and they are non-toxic and non-immunogenic [52]. Aptamers are also more thermally stable and can restore their original structure easily and quickly if denatured, while antibodies cannot. These characteristics support the evaluation of aptamers as great therapeutic candidates. Their clinical limitations—such as low stability, because of nucleases' action in blood, and fast clearance, due to their smaller size—can be easily overcome by further chemical modifications [60]. Site-specific modifications are difficult to make in antibodies, in contrast to aptamers, where chemical modifications can be

easily introduced at any desired position in the nucleotide sequence. Because of their ability to bind to proteins and to block their functions, they are also being investigated in the interruption or prevention of misfolded protein accumulation, which is related to many diseases, as discussed here. Moreover, aptamers might differentiate even between isoforms of a given protein, which would aid the understanding of prion function and/or dysfunction, in addition to the diagnostic potential.

## 4. Nucleic Acids Aptamers against PrP

Considering PrP interaction with a large variety of NAs, this protein was proposed as a NA chaperone, although many doubts still persist concerning either its functional or pathological role. Pursuing the main objectives of dissecting PrP–NA interaction, elucidating PrP conformational conversion, identifying specific NAs with which PrPs from different species may interact, and looking for therapeutic and/or diagnostic methods, several studies have applied the SELEX method [61]. With regard to therapeutic perspectives, aptamer(s) binding to PrPs could prevent their conversion and accumulation by stabilizing $PrP^{C}$ or $PrP^{Sc}$, inhibiting $PrP^{C}$-$PrP^{Sc}$ interaction, or blocking $PrP^{C}$ binding to some pathological stimulating cofactor. Specific aptamers for PrPs could also set up new diagnostic tools, since early diagnosis is crucial and will definitely improve the efficacy of any attempt at therapy.

The first aptamer for PrP was selected by Weiss et al. in 1997 using the SELEX method directed against recombinant Syrian hamster full-length prion protein ($rPrP^{23–231}$). The isolated unmodified RNA aptamer did not recognize the C-terminal domain construct ($rPrP^{90–231}$) that lacks almost all the N-terminal residues [33]. They mapped the RNA aptamer-binding site between amino acid residues 23–52 at the PrP N-terminal region. They also suggested that these RNA aptamers may fold into guanine(G)-quartet-containing structural elements that seem to be essential for PrP recognition since the G replacement for uridines (U) in the aptamer sequence abolished its binding to PrP [33]. These individual RNA aptamers interact specially with $PrP^{C}$ from brain homogenates of healthy mice, hamsters, and cattle but did not recognize $PrP^{Res}$ in brain homogenates from prion-infected mice; moreover, the interaction was not observed in PrP knockout mice [33]. The conservation of the specially $PrP^{C}$–RNA interaction in different species provided the first landmark to the development of new diagnostic assays for prion diseases using aptamers.

The same group in 2001 was also the first to show the therapeutic potential of aptamers against prion diseases by selecting the 2′-amino-2′-deoxypyrimidine-modified RNA aptamer (DP7) that was able to reduce $PrP^{Sc}$ accumulation in prion-infected neuroblastoma cells [62]. The RNA chemical modification was made—after using SELEX—as a strategy to enhance the RNA resistance to nucleases. DP7 was highly specific to human $PrP^{90–129}$, a region involved in PrP pathological conversion, and its binding was sustained even for full-length PrP from different species, including humans, mice, and hamsters [62]. One might speculate that blocking this region could supply promise for controlling the conversion. In 2003, Rhie et al. were the first to characterize RNA aptamers that bind preferentially to the infection-related conformations of PrP [63]. The 2′fluoro-RNA aptamer against scrapie-associated fibrils (SAF-93) had a tenfold higher affinity for $PrP^{Sc}$ than for $PrP^{C}$ and inhibited prion propagation in an in vitro conversion assay, highlighting its therapeutic and diagnostic potential [63].

Following these studies, many authors have used the SELEX methodology either against $PrP^{23–231}$ from different species, the PrP C-terminal domains, PrP peptides, or pathogenic-related conformations (Table 1). It has been revealed that aptamer interaction with PrP is sustained even after immobilization and aptamer chemical modification [64]. Briefly, the first DNA aptamers were selected against recombinant human cellular $PrP^{23–231}$ and interacted specially with mammalian PrPs from normal brain homogenates of sheep, calf, piglets, and deer as well as with $PrP^{C}$ expressed in N2a cells [65]. None of them bound to PK-digested prion-infected ScN2a cells, suggesting that these aptamers hold specificity for $PrP^{C}$ [65]. Their binding affinity appeared to be both aptamer sequence- and structure-dependent, with dissociation constants in the micromolar to nanomolar range, in accordance with our work with nucleic-acid ligands selected individually [65]. The work from King et al. selected aptamers against the globular domain (residues 90–231) of hamster PrP, folded into an α-helical-rich native

conformation, identifying a thioaptamer (with phosphorothioate modification to enhance their stability against nucleases) with an affinity of 0.58 (+/−0.1) nM for hamster PrP [66]. Lower affinities for bovine (Bo) and human (Hu) PrP were found, suggesting some specificity where the interaction is dependent on the primary structure of PrP [66]. A control oligonucleotide with the same length and a scrambled consensus sequence could not differentiate among the three PrP sequences, and control oligonucleotides encompassing non-selected sequences bound to PrP at a sequence-independent DNA-binding site with much lower affinities [66]. The results confirm that the high-affinity binding of thioaptamers to PrP depends on backbone modifications, oligonucleotide sequence, and PrP sequence [66].

As well as RNA aptamers, the ssDNA thioaptamers designed by Kocisko et al., were able to bind $PrP^{C}$ on live cells, to be cell-internalized and potently inhibit $PrP^{Res}$ accumulation in infected-cultured cells [67]. Interestingly enough, prophylactic treatments with these modified oligonucleotides tripled scrapie survival periods in mice [67]. A prolonged survival time was also observed when these phosphorothioate aptamers were previously mixed with the infectious brain inoculum [67]. The potent anti-scrapie activity of these modified nucleic acids represents a new class of drugs that hold promises for the treatment of prion diseases [67,68]. Mashima et al. in 2009 provided the first report, showing the high-resolution structure of an RNA aptamer (R12) against isolated domains of the bovine PrP by NMR. The GGAGGAGGAGGA sequence from R12 aptamer forms an intramolecular parallel G-quadruplex structure [69]. G-quadruplexes are formed by G-rich sequences and are built around tetrads of hydrogen-bonded guanine bases (Hoogsteen base pair). Two or more G-tetrads can stack on top of each other to form the structure, and the quadruplex is stabilized by a cation, especially potassium [70]. Two R12 quadruplexes form a dimer through intermolecular hexad–hexad stacking [69]. Most of the RNA aptamers obtained by this group contain GGA tandem repeats and bind both $rPrP^{C}$ and the beta-form of PrP with high affinities [71]. The DNA counterpart aptamer (D12) can also bind to PrP, but the affinity is weaker for both cellular PrP and its β-form [36,69]. The GGA tandem repeats form peculiar quadruplex structures that appear to be critical for the higher affinities and recognition of PrP. This tight binding is expected to stabilize $PrP^{C}$ or block its interconversion and to thereby prevent the onset of prion diseases.

NMR measurements also provide the first high-resolution 3D-structure of the complex formed with N-terminal PrP peptides (P1 and P16) and the R12 aptamer [72]. The G-quadruplex structured RNA is preserved even after interaction with PrP. The RNA forms a dimer where each monomer simultaneously binds to two portions of the $PrP^{C}$ N-terminal region, which can explain the strong binding, where electrostatic and stacking interactions drive the affinity of each portion [72]. Additionally, the authors demonstrate that the driving force for the binding between R12 and P16 (a PrP peptide) is a robust gain of water entropy, and the energy decrease driven by attractive interactions between R12 and P16 is compensated by the energetic dehydration effect after binding or vice-versa. The interaction of the complex occurs via stacking of flat moieties, via electrostatic interactions, including specific hydrogen bonding, and through molecular geometry complementarity [73].

One should not forget that an appropriate geometrical correspondence of hydrogen bond donors and acceptors may allow more stable complexes to be formed, but it is mainly due to stacking interactions that significant stabilization occurs [74]. Moreover, R12 was shown to reduce the accumulation of $PrP^{Sc}$ levels in scrapie-infected neuronal cells, demonstrating its great therapeutic potential [65]. Remarkably, G-quadruplex forming NAs were shown to change the $PrP^{C}$ structure after binding, so that they may actually lower the free energy barrier between the two conformers and therefore prompt the conversion process [36]. As one of the strongest PrP binders, more attention should be given to these peculiar NA structures. In fact, many NA ligands directed against PrP discussed here might form G-quadruplex structures, as they contain at least four GG repeats in their sequence that could form quadruplexes after dimerization. The PrP messenger RNA (mRNA) itself has sequences with the propensity to form G-quadruplex depending on environmental conditions such as fluctuations in potassium levels [75]. One cannot rule out the possibility that PrP interaction with its own mRNA might be involved in their physiological or pathological pathways.

**Table 1.** Binding characteristics of mammalian PrPs and nucleic acids.

| Author, Year (Ref.) | Nucleic Acid Type | $K_D$ [1] (nM) | Binding Assay | PrP SELEX Target | PrPs Recognized | PrP Binding Region(s) |
|---|---|---|---|---|---|---|
| Weiss, 1997 [33] | RNA-aptamer | ND | Gel-shift of labeled aptamer | Hamster $rPrP^{23-231}$ | Mouse, hamster, cow (PrP in brain homogenates) | (23–36) |
| Nandi, 1997 [29–31] | Plasmid DNA | 250 | Fluorescent dye displacement | NS | Human $rPrP^{106-126}$ and $rPrP^{23-231}$ | ND |
| Cordeiro, 2001 [21] | Short dsDNAs | 25 | Fluorescence polarization | NS | Murine $rPrP^{23-231}$ | N-terminal and C-terminal domains |
| Gabus, 2001 [76] | HIV-1 LTR DNA (1000 bp) | ND | Gel-shift assay | NS | Human $rPrP^{23-231 \text{ or } 23-144}$ | N-terminal |
| Gabus, 2001 [37] | HIV-1 5′-leader RNA (415 nt) | ND | Gel shift assay | NS | Human $rPrP^{23-231}$; Ovine $rPrP^{25-234}$ | N-terminal |
| Proske, 2002 [62] | RNA-aptamer | 100 | Filter-binding assay | Human $PrP^{90-129}$ | Hamster, mouse or human rPrP | (90–129) |
| Adler, 2003 [22] | Small, highly structured RNAs | 3.8 | Gel shift, filter-binding assay | NS | Human rPrP, PrP from brain homogenates of mouse, rat and hamster | N-terminal domain |
| Rhie, 2003 [63] | RNA-aptamer | 16 | Homologous competition binding assay | SAF material from infected brain homogenates | Bovine rPrP in b-oligomeric or a-helical form, PK-untreated SAF, PK-treated SAF | N-terminal and SAF conformation-specific site in (110–230) |
| Sayer, 2004 [77] | RNA-aptamer | 6.8 | Equilibrium binding | Bovine $rPrP^{23-230}$ | Bovine rPrP | ND |
| Sekiya, 2005 [78] | RNA-aptamer | ND | ND | Murine $rPrP^{23-231}$ and murine SAF infected material | Murine $rPrP^{23-231}$ and mouse SAF | (23–108) of Murine rPrP and mouse SAF |
| Sekiya, 2006 [79] | RNA-aptamer | 5.6 | Filter-binding assay | Murine $rPrP^{23-231}$ with competitive selection | Murine $rPrP^{23-231}$, Bovine rPrP, Mouse PrP in brain homogenate | (23–108) and (23–88) |
| Mercey, 2006 [35] | RNA-aptamer | 15 | Surface plasmon resonance, filter-binding assay | Ovine $PrP^{23-231}$ with mutations associated with disease | Ovine rPrP(ARR, VRQ, AHQ, ARQ), Murine rPrP, Bovine rPrP | (25–34) and (101–110) |
| Lima, 2006 [34] | Short dsDNAs | 90 | Fluorescence polarization and SAXS | NS | Murine $rPrP^{23-231}$ | N-terminal and C-terminal |
| Takemura, 2006 [65] | DNA-aptamer | 16 | End-point titration method in microplate, gel-shift, and dot-blot assays | Human $rPrP^{23-231}$ | Murine $rPrP^{23-231}$, PrP from brain homogenates of sheep, calves, pigs, deer, PK-untreated PrP from ScN2a cells | (23–89) |

**Table 1.** *Cont.*

| Author, Year (Ref.) | Nucleic Acid Type | $K_D$ [1] (nM) | Binding Assay | PrP SELEX Target | PrPs Recognized | PrP Binding Region(s) |
|---|---|---|---|---|---|---|
| Ogasawara, 2007 [80] | DNA-aptamer | 100 | Surface plasmon resonance, dot-blot, competitive selection and fluorescence measurements | Murine $rPrP^{23-231}$ | Murine $rPrP^{23-231}$ | ND |
| Murakami, 2008 [71] | RNA-aptamer | 31 | Surface plasmon resonance | Bovine $PrP^{23-231}$ | Bovine $rPrP^{23-231}$ | (125–231) |
| Bibby, 2008 [81] | DNA-aptamer | 18 | Saturation binding using PrP-coated Ni-NTA beads | Ni-NTA beads coated Murine $PrP^{90-231}$ | Murine $rPrP^{90-231}$, Ovine rPrP and Human $rPrP^{90-231}$ | (90–230) |
| Mashima, 2009 [69] | G4 RNA-aptamer | 8.5 | Northwestern blotting assay | Bovine $PrP^{23-231}$ | Bovine $PrP^{C}$ | (25–34) and (110–118) |
| | G4 RNA-aptamer | 280 | | | Amyloidogenic bovine PrP-β | ND |
| | G4 DNA-aptamer | 85 | | | Bovine $PrP^{C}$ | (25–34) and (110–118) |
| | G4 DNA-aptamer | >280 | | | Amyloidogenic Bovine PrP-β | ND |
| Wang, 2011 [82] | DNA-aptamer biosensor immobilized | 22 | Surface plasmon resonance | $PrP^{Sc}$ from brain tissues of scrapie-infected animals with counter-selection with $PrP^{C}$ | Pathological isoforms of PrP from distinct species | ND |
| Macedo, 2012 [24] | Small dsDNAs | ND | Fluorescence measurements | NS | murine $rPrP^{23-231}$ and $rPrP^{109-149}$ | N-terminal and C-terminal domains |
| Cavaliere, 2013 [36] | G4 DNA-aptamer | 62 | Surface plasmon resonance and Isothermal Titration Calorimetry (ITC) | Ovine rPrP-23–231 | Ovine $rPrP^{23-24}$ | 23-134 |
| | G4 RNA-aptamer | 75 | | | Ovine $rPrP^{23-24}$ | |
| | G4 DNA-aptamer | 300 | | | Amyloidogenic Ovine PrP-β | ND |
| | G4 RNA-aptamer | 400 | | | Amyloidogenic Ovine PrP-β | |

We chose the KD (dissociation constant) value of the best interaction when several aptamers were described by the same study. When many types of PrP were investigated in binding assays, the PrP species or fragment with the lowest KD value is the first shown. NS: non-SELEX (NA sequences found individually); ND: non-determined.

## 5. Aptamers against Other Amyloidogenic Proteins

The prion protein has been understood as the etiological agent of TSEs amyloidosis, but nowadays the term "prion" has evolved to describe a phenomenon in molecular biology that is more ubiquitous than previously thought and that is shared by other prion-like proteins, especially the ones that can aggregate into amyloid fibrils through a highly ordered mechanism. Unrelated proteins in their sequence or structure can form amyloid aggregates that possess a common cross-architecture with a β-sheet enriched core; it appears that the amyloid fibril formation is the result of an intrinsic, conservative, and generic process of proteins, and amyloids formed by the same protein sequence can still be found with different structural and phenotypic properties [7]. Evidence indicates that amyloid fibrils share specific structural characteristics and aggregate morphologies; however, some structural polymorphisms between amyloids can be found either in vivo or in vitro [83]. Although our review focuses on PrP interactions with nucleic acids, we find it useful to also provide an overall critical consideration regarding aptamer interactions with other prion-like amyloid proteins.

In this context, RNA aptamers were selected by SELEX against the wild-type bovine PrP (bPrP); the recognition was shown to occur mainly through the PrP N-terminal (25–131) region, as expected and confirmed by other researchers [40,71]. However, and interestingly, those same aptamers also bound to bPrP in the β-conformation (bPrP-β), which resembles the amyloid core, but with a tenfold lower interaction affinity [71]. Thus, it led the group to conclude that the selected aptamers bind with high affinity to both native PrP and the amyloid-like PrP conformation. The transition from the native α-form to a β-form was achieved, and it occurs briefly in the presence of phospholipid micelle solutions at pH 5.0 [71]. One question raised is this: How did an aptamer selected against a non-amyloid prion form recognize the β-conformation? The same bPrP-β formation protocol was applicable to human, cow, elk, pig, dog, and mouse PrP, even in wild-type or truncated PrP forms, and it showed that part of the flexible domain encompassing the 105–120 region must be present for the generation of bPrP-β [71]. Although that region is normally unfolded in the native PrP, it can also undergo dynamic structural shifts. This region is normally positively charged but also contains hydrophobic amino acids, both important for NA-binding. One might speculate that the epitope recognition motif found in the 105–120 PrP region can be found both in the native or in the amyloid PrP conformation; the aptamer interaction is established with high affinity for the two forms (bPrP and bPrP-β), but with a significant difference between them, probably because, for the latter, the new structure potentially adopted by the 105–120 region might change the dissociation constant value. Besides, the results showed that the high affinity for bPrP-β by the selected aptamer is abolished at a high salt concentration (1M NaCl); this behavior is not observed for the native bPrP, which maintains approximately the same interaction affinity for the same selected aptamer in equal experimental conditions [71]. This suggests that this aptamer interaction with the amyloid PrP form occurs mainly through electrostatic interactions, but for the native PrP, electrostatic interactions may bring the two partners in proximity, allowing them to establish more specific intermolecular forces (hydrophobic and base stacking), resulting in a higher affinity for the native PrP. In addition, when minimizing the aptamers' length, they lose their affinity for the bPrP-β (30-fold less) in comparison to bPrP, demonstrating that a differential aptamer specificity indeed exists for the two PrP conformations [71]. We thus suggest the use of non-aggregated PrP forms as competitors to improve selection and binding-ability to β-forms of PrP.

Besides PrP, we will also discuss briefly some studies about other amyloidogenic proteins related to diseases, such as Aβ protein and β-2-microgobulin (β2m), regarding their interaction with aptamers. RNA aptamers were selected against Alzheimer's amyloid Aβ peptide (1–40), and, apparently, the selection targeting a non-amyloid Aβ conformation led to the selection of aptamers that recognized the β-sheet-rich fibrils of Aβ [84]. Aβ (1–40) presents a hydrophobic domain that aggregates easily, especially in amyloid fibrils, but the experimental condition of Aβ (1–40) immobilization for the SELEX process in this particular study did not guarantee that the monomeric conformation of Aβ (1–40), that is, the SELEX target, was maintained in-column [84]. Aβ (1–40) could possibly aggregate in-column and/or will also be found in the trimeric or tetrameric form. It cannot be ruled

out that those oligomeric forms present a β-sheet core enriched enough to be considered a pre-amyloid aggregate, which could explain the positive selection of these aptamers to the mature amyloid fibrils as well. Preformed aggregates induce fast aggregation of amyloidogenic proteins, resulting in poor experimental reproducibility [85], and are not desirable in aptamer selection for non-aggregated, non-fibrillar forms of the respective proteins. The interaction of Aβ (1–40) fibrils with these particular RNA aptamers can be easily detected through electron microscopy; the aptamer was labeled with colloidal gold that stained as black dots along the amyloid-fibrils, showing that the interaction occurs in specific regions of the fibril with an apparently specific distribution pattern [84]. Again, the addition of experimental controls like other amyloid fibrils or completely non-aggregated proteins is of interest to refine the executed assay.

Subsequently, the study performed by Rahimi et al. provided a step forward, exploiting aptamers' interaction with amyloid fibrils formed by distinct proteins [86]. The results showed that an aptamer selection targeting a non-fibrillar Aβ preparation led to a selection of aptamers that recognized fibrils of Aβ and fibrils of other amyloidogenic proteins [86]. Although we consider this work strongly relevant, some considerations can be explored for relevant discussion and speculation of other possibilities regarding the experimental evidences and conditions; some of them were also raised by the authors [87]. One of the aptamer selection targets was the cross-linked trimeric form of the Aβ protein using the filter-binding SELEX assay. The authors selected the Aβ trimeric conformation by direct purification from the SDS-PAGE and stored it for approximately twenty-four hours in a solution containing traces of SDS before the final procedure, which consisted of long-term dialysis to remove impurities until the sample was ready for the SELEX's first round [88]. These procedures suggest that traces of SDS may have been present in the sample and/or the extensive dialysis duration might have accelerated Aβ self-aggregation, enhancing the β-sheet content and/or favoring protein–protein interaction and aggregation, as verified for other proteins [89,90]. In addition, a nitrocellulose filter-binding assay is not the most suitable way to retain low-molecular-weight proteins such as Aβ (1–40), due to the poor retention of the peptide on the filter. This approach might result in the apparent unexpected lack of interaction between the aptamers selected against this specific Aβ assembly (in the trimeric expected conformation), with the same expected assembly verified through a filter-binding assay [86]. The aptamers were probably not selected against a homogeneous non-aggregated Aβ-form; we therefore believe the SELEX target was a common cross-beta structure present both in the trimeric form, oligomers and in the amyloid fibrils. Moreover, the evidence that two aptamers have different binding affinities between fibrils formed with the Aβ (1–40) and Aβ (1–42) reveals that there must be some specificity governing the aptamer interaction [84]. The reactivity of aptamers against Aβ (1–42) fibrils was somewhat lower than their reactivity with Aβ (1–40) fibrils, again suggesting moderate specificity for Aβ (1–40) [84]. Given that observation, there are minor differences between Aβ (1–40) and Aβ (1–42) that come from a dissimilar enzymatic cleavage site of the amyloid precursor protein (APP), and there are still significant differences upon binding to the selected RNA aptamers, strongly suggesting some specificity, which we are still looking for. Remarkably, these same aptamers recognize fibrils of other amyloidogenic proteins, including insulin, islet amyloid polypeptide, calcitonin, lysozyme, and $PrP^{106–126}$, but with significant differences between some fibrils that might correlate with residual specificity [86].

Similar results were obtained in other work, where aptamers were selected against fibrils of β2-microglobulin (β2-m) or against monomeric β2-m at low pH [91]. The aptamers bind with high affinity to β2-m fibrils with different morphologies formed under different conditions in vitro, as well as to amyloid fibrils isolated from tissues of β2-m-related amyloidosis patients, demonstrating that they can detect conserved epitopes between different fibrillar assemblies of β2-m, including those formed in vivo. At this time, the group's data demonstrate that the selections generated aptamers able to bind with high affinity to all three forms of β2-m, including two distinct fibrils and the low pH monomeric form [91]. The validation of the interaction was performed through surface plasmon resonance (SPR), a more suitable and refined method for this approach than dot-blot only [91]. These results suggest that

the β2-m fibrils share at least one epitope in common with the monomeric β2-m, and the higher affinity for the fibrillar form might be due to more epitopes being available and the greater ease of interacting with these aptamers in the macromolecular structure of the fibril. The aptamers also reacted with some (but not all) other amyloid fibrils, either generated in vitro or isolated from ex vivo sources; but for these other proteins, none of the aptamers were able to bind to native monomers, confirming that the epitopes being recognized are fibril specific [91]. Thus, the native folded species seem not to share epitopes in common with the fibrillar and pre-fibrillar states. SPR measurements also showed that there are large signal differences between the naive SELEX RNA pool and the final selected individual aptamers against the target, confirming that the SPR responses seen are due to specific binding and not to inherent affinity of the oligonucleotides for fibrillar amyloid structures [91]. The same behavior was reported for certain antibodies, which could recognize conformational epitopes in Aβ assemblies and interact with similar assemblies of other amyloid-forming proteins [92–95]; some antibodies were raised against oligomers but reacted with both oligomeric and fibrillar assemblies [96–98].

One must conclude, based on these observations, that, although amyloid fibrils have many common structural properties, they also have features that are unique to individual fibril types. Some amyloids may hinder more structural differences than others, and because of these structural polymorphisms, aptamers selected against a specific amyloidogenic protein can interact with other unrelated amyloid-forming proteins with similar or significantly different affinities, depending on the amyloid protein aggregated structure. There were also cases where these aptamers have not at all recognized amyloid fibrils from other amyloidogenic proteins, such as apomyoglobin, Aβ (1–40), or transthyretin, but significant binding was observed to fibrils formed from lysozyme [91]. The aptamer binding to lysozyme fibrils cannot be the cause of nonspecific interactions, as evidenced by the inability of the aptamer to bind to native monomeric lysozymes together with the observation that the naive RNA SELEX pool binds relatively weakly to the lysozyme fibrils under these conditions [91]. Although these aptamers recognize an epitope present in different amyloid fibrils, the epitope for each aptamer must be either distinct or differentially accessible between different amyloids. Understanding the structural molecular basis of why some aptamers and antibodies raised against monomeric proteins can recognize either the oligomeric forms or the amyloid polymeric architecture requires an ongoing investigation, but will definitely improve the discussion about their potential in the pharmaceutical and biotechnology fields.

## 6. Conclusions and Perspectives

Over the last twenty years, NAs have been proposed as potential cofactors that can bind to different disease-related proteins and can trigger their misfolding and aggregation processes [9,99]. Protein interactions with NAs are governed by several molecular forces, including hydrogen bonding mediated by aqueous solvent, electrostatic, hydrophobic, and stacking interactions [52]. Because of the many structural motifs existing both in proteins and NAs, as well as the variations in the nucleotide sequences, it is very difficult to characterize a single model for protein–NA interactions. Hydrophobic interactions seem to be more efficient than charge effects for driving protein aggregation [100]. However, both factors (hydrophobic and charge effects) can be critical and determinant for protein aggregation and need to be considered for understanding the process in vivo and the role of amino acid composition, sequence, and substitutions in protein misfolding diseases and protein design [100,101].

The knowledge acquired from the PrP studies discussed here permitted us to map the NA-binding sites on PrP. This interaction involves at least three different binding sites: two of them localized at the N-terminal flexible region and the other in the structured globular C-terminal domain. Apparently, the two lysine clusters in the N-terminal domain, encompassing residues 23–52 and 101–110, are involved in all non-specific NA interactions, since this is a positively charged region with enough flexibility to bind DNAs, RNAs, and even heparin molecules, mainly through electrostatic interactions with the sugar-phosphate backbone [35,63]. Through NMR studies, residues encompassing the lysine cluster were shown to mediate the interaction with DNA [34] or RNA [72]. Although

contributions from hydrophobic interactions appear to be more important than those involving charge interactions, the influence of charge factors on protein aggregation must not be underestimated [100]. Structural data show that the PrP globular domain in the normal conformation can interact with DNA but not with RNA [35,40]. However, conformational changes in the C-terminal domain, especially in its transition to beta forms, can expose structural or sequence motifs that are able to bind even RNA aptamers through more specific interactions than those established with the N-terminal region [63].

Although many efforts have been made to find the sequence specificity governing PrP-NA interactions, no consensus has yet been found. Partial consensus sequences are clearly present, confirming that selection had occurred, but there has been no obviously dominant epitope-binding consensus. Comparison of the aptamers sequences reported elsewhere for either anti-PrP or anti-Aβ (1–40) or anti-β2-m aptamers did not show significant sequence motif matches, suggesting that the aptamers raised are specific to their selection targets. Some structural features can be highlighted, such as the G-forming quadruplex in many DNA and RNA ligands that provides tight bonding; however, other structural motifs, such as hairpins and the double helix, have also been described and proven to have a high affinity for PrPs [24,36]. Through NMR studies, it appears that the geometric characteristics (overall shapes, sizes, and detailed polyatomic structures) of the molecules are the most important factors governing PrP recognition [73]. The strong diversity between PrP nucleic acid ligands should not rule out the existence of some specificity, once many modifications in the NA molecule can alter its PrP-binding affinity and can trigger different changes on PrP properties [24,33].

NA molecules might play a dual role in prion biology, either by triggering PrP conversion and aggregation or by preventing them. Understanding this intriguing partnership could be critical to explaining how prion diseases arise, and to developing effective diagnostic and therapeutic methodologies. In terms of the pathological aspect, NA-binding to PrP could lead to reciprocal conformational changes, altering both the PrP and NA structure and promoting distinct modes of polymerization depending on the NA source. Possibly the charge neutralization of the positively charged PrP N-terminal domain after NA binding favors the association of PrP molecules, which might explain the immediate NA-induced PrP aggregation [102].

What remains to be elucidated is whether these interactions are relevant in vivo, regarding either the pathology or biology of prions. Although RNA molecules were found to be associated with plaques in the brains of AD-diseased patients [103–105], no direct evidence of in vivo association of specific nucleic acid sequences with PrP scrapie in affected humans has been found yet. Nevertheless, the work of Manuelidis' group showed that circular DNAs could be co-purified along with infectivity in 22L-infected cell lines, in hamster 263K scrapie-infected brain samples, and in FU-CJD infected mouse brain [106]. Additionally, the same group showed that prion infectivity was retained when PrP was digested; in contrast, when different prion strains were treated with nucleases, infectivity (prion titer) was substantially reduced [107]. In addition, PrP-NA interaction was shown to be fundamental in generating synthetic scrapie prions; free small RNAs, extracted from highly infectious scrapie-associated fibrils (SAFs) and incubated with $PrP^{C}$, were shown to promote $PrP^{C}$–$PrP^{Sc}$ conversion with the acquisition of infectivity, inducing prion disease in wild-type healthy Syrian hamsters [108]. These results indicate that nucleic acids are essential for prion infectivity and might be involved in prion pathogenesis.

Altogether, these studies show that NAs are potential PrP cofactors able to catalyze the formation of $PrP^{Sc}$ in vivo. The "NA cofactor hypothesis" initially proposed by our group and reinforced by other contemporaneous studies does not necessarily refute the commonly accepted "protein-only hypothesis", where PrP is the solely proteinaceous infectious agent. In fact, we otherwise add to this vision the suitable participation of molecules that could facilitate protein aggregation and the formation of infectious conformations that could, even alone, template the conversion of normal PrPs into abnormal conformations, thus leading to prion disease progression.

Protein folding and protein aggregation are dynamic and competitive events constantly fighting inside the cell and driven by the same molecular forces, which explains why these processes are

well controlled and balanced by the protein quality control of the cell machinery [109]. The process is so complex that an increasing number of proteins with the same amino acid sequence were shown to adopt, under native conditions, various folded conformations that coexist in dynamic equilibrium [109]. Especially for the amyloid aggregation pathway, there are many precursor species along the way to fibril maturation: amyloid seeds, oligomeric forms, prefibrillar, and fibrillar states [7]. Therefore, amyloid aggregation is also a dynamic and potentially reversible process where different species may be present even after fibril formation. Regarding aptamer selection against amyloid prions, the characterization of aptamers is particularly important, because the natural affinity of oligonucleotides for fibrillar amyloid structures potentially hinders the development of aptamers that are specific for non-fibrillar amyloid proteins under physiological conditions [86]. Particular studies discussed in this review describe the selection of nucleic acids that inherently bind fibrillar or β-sheet-rich structures of amyloid proteins. This tendency must be more deeply explored. In addition, it is important to determine the size distribution profile of the amyloid aggregates as well as the morphology of each species that can coexist in the aggregation protocols used in those studies, making it more difficult to guarantee which exact species are exposing the exact epitope that led to the aptamer selection. In general, aptamers selected against amyloidogenic proteins recognize a structural motif, probably the backbone of the proteins in a cross-β structure that is common to the fibrillar state of these proteins. Nucleic acid reactivity clearly depends on the protein assembly state and to some extent on the protein sequence. Based on the idea that the amyloid fold is ancient and may have co-evolved with RNAs [110,111], it is plausible to propose that such proteins present a general nucleic acid binding property resulting from this evolution process. NA-binding can thus result in ribonucleoprotein complexes that possess important cellular functions, for instance, being related to functional amyloids [112] or to amyloidogenic diseases [99]. Accordingly, it is expected that amyloids and amyloid-forming proteins will present promiscuous RNA- (or even DNA)-binding characteristics.

Developing effective therapies against prion diseases and other amyloidosis remains a hard challenge. Together with the therapeutic potential of aptamers against PrP, ligands able to bind and stabilize the native state of an amyloidogenic protein provide one such potential strategy for controlling protein accumulation and the disease progression of many neurodegenerative disorders including Alzheimer's and Parkinson's diseases [51]. Efforts to generate aptamers that would specifically recognize oligomeric pre-amyloid species have also been a challenge, likely due to the dynamic nature of the oligomers preventing long-lasting NA–oligomer interactions. This inherent, apparently sequence-independent, affinity of oligonucleotides may have led to the generation of fibril-cross-reactive aptamers in studies aiming to generate aptamers for non-fibrillar amyloidogenic proteins. Recently, Takahashi et al. have selected aptamers against an oligomeric model of Aβ (1–40) and demonstrated an interaction with monomeric Aβ with micromolar affinity [112]. However, the cross-reactivity of these aptamers with fibrillar Aβ (1–40) or with other fibrillar amyloidogenic proteins was not determined [113]. In addition, data in the literature indicate that aptamers can also be used to detect early β-sheet formation more sensitively than the common thioflavin-T (ThT) amyloid dye [86]. Thus, these aptamers could be highly efficient detection tools of β-sheet formation in histopathological and in biophysical studies in vitro.

Overall, if aptamers are to be obtained for diagnostic and therapeutic approaches in amyloid diseases, the use of such a selective powerful tool is yet to be achieved in this field. Additional experiments to generate devoted and specific aptamers for prefibrillar assemblies (including monomers and oligomers) will have to deal with the apparent inherent affinity of oligonucleotides for fibrillar structures. Nevertheless, small differences in specificity and affinity of aptamers for amyloid and monomeric proteins may indeed allow their application in diagnosis or therapy.

In the context of the biology and pathology of prion proteins as well as in other protein-misfolding diseases, it would be valuable for those who would like to continue researching aptamers and their applications to find the ideal aptamer against therapeutic targets of the future, specific enough to warrant their use as recognition tools or therapeutics. Maybe the literature is being too optimistic in

this regard, but we cannot forget those are still invariably fatal diseases where researchers are avidly waiting for a new drug discovery to treat or cure illnesses for both humans and animals. Several nucleic acids, especially the aptamers for PrP, have been shown to bind to $PrP^{C}$ or $PrP^{Sc}$ and to interfere with $PrP^{Sc}$ biogenesis, providing a new class of promising molecules that could be used for the treatment of prion diseases. Even if they bind monomeric $PrP^{C}$ to some extent, the benefit of preventing conversion into $PrP^{Sc}$ would surpass the drawback of lack of specificity. Some of the investigated nucleic acids have shown therapeutic efficacy in infected mice models by tripling their survival time [67], but to our knowledge none of them have proceeded to clinical studies so far. Alternative attempts based on antibody therapy also have potential [114]; however, the stimulation of the autoimmune system presents challenges to further developments in this area [114].

Unfortunately, there is no therapy to treat or prevent prion diseases. Most of the lead compounds found in the drug screening for anti-scrapie activity lack efficacy (possibly due to prion strain specificity), and have poor pharmacokinetic profiles, such as high toxicity and/or an inability to efficiently cross the blood–brain barrier (BBB) [115]. In fact, the aptamer pharmacokinetic profile is especially relevant for neurodegenerative disorders, pushing the development of strategies towards crossing the BBB, as it is unlikely that they can easily enter the brain. Nevertheless, aptamers may surpass this barrier via pinocytosis, transcytosis, channel, and/or receptors to their uptake [116]. Additionally, quadruplex-structured aptamers may cross the BBB through binding to nucleolin via micropinocytosis [117]. Using a nicely executed in vivo selection protocol, Cheng and collaborators selected aptamers that permeated the brain after peripheral injection of the library in wild-type mice [118]. Fortunately, aptamers are molecules that can be easily modified to overcome their clinical limitations: for example, nanoparticle-encapsulated aptamers were reported to cross the BBB, and delivery of liposome-based aptamers was well tolerated in clinical trials [119]. We still do not have the safety profile of these molecules, although they are expected to be non-toxic and non-immunogenic [52].

In conclusion, NA aptamers can distinguish normal and abnormal conformations of PrP, representing the first reagents able to identify PrP pathological conformations from multiple host species. They can even differentiate prion strains and can be used to detect infectious prions in blood samples, which cannot be accomplished using conventional diagnostic tools that rely on antibody-based detection methods. The hard challenge of prion disease diagnosis before the symptomatic stage is how to discriminate and detect the minute quantity of disease-associated prion protein isoform ($PrP^{Res}$) sensitively and selectivity in complex biological samples, from plasma to brain homogenate. The development of a dual-aptamer strategy for diagnostic tools began with an investigation of the advantages of aptamers, the great separation ability of magnetic microparticles (MMPs), and the high fluorescence emission features of quantum dots (QDs) [120]. Two aptamers were coupled to the surfaces of MMPs and QDs, respectively, which then could be co-associated through the specific interaction of the two aptamers with their two corresponding different PrP epitopes, forming an aptasensor platform [120]. Moreover, aptamers can enrich a target, for example, the PrP molecule, from biological fluids; in this context, RNA aptamers have been successfully utilized for the concentration of $PrP^{C}$ and $PrP^{res}$ taken from serum, urine, and brain homogenate [121]. There is also an interesting proposal for $PrP^{Sc}$-enrichment, using $PrP^{C}$-specific aptamers to capture normal prions from biological samples, which could be used as a diagnostic tool in double ligand assay systems and other aptasensors [65]. There is an urgent necessity to develop more sensitive and more efficient assays to detect the pathological forms of PrP in pre-symptomatic screening of tissue, blood, or other body fluids. Based on these promising studies, NA aptamers appear to be good candidates to reach this goal. Although many aptamers have been identified against PrP, with great potential for use in diagnostic tools, the community is still relying on antibody-based detection methods. Among the limiting factors that make aptamers especially promising is the sensitivity of detection. Thus, many efforts are now being made to build aptasensing platforms based on electrochemical or dual-signal systems to develop highly sensitive prion assays [122,123]. This new class of molecules thus has great potential.

**Acknowledgments:** We thank the Fundação de Amparo a Pesquisa do Estado do Rio de Janeiro (FAPERJ) and INCT-INBEB from CNPq (process #465395/2014-7) for financial support. We are thankful to Lucas M. Ascari for the art design of Figure 2 and to Professors Julia R. Clarke, Luís M. T. R. Lima, Monica S. Freitas from UFRJ and Sotiris Missailidis from FIOCRUZ for critical revision of the manuscript.

**Author Contributions:** Bruno Macedo wrote the manuscript, and Yraima Cordeiro revised it critically for important intellectual content.

**Conflicts of Interest:** The authors declare no conflict of interest.

## References

1. Prusiner, S.B. Nobel Prize Lecture: Prions. *Proc. Natl. Acad. Sci. USA* **1998**, *95*, 13363–13383. [CrossRef] [PubMed]
2. Aguzzi, A.; Lakkaraju, A.K.K. Cell Biology of Prions and Prionoids: A Status Report. *Trends Cell Biol.* **2016**, *26*, 40–51. [CrossRef] [PubMed]
3. Collinge, J. Prion diseases of humans and animals: Their causes and molecular basis. *Annu. Rev. Neurosci.* **2001**, *24*, 519–550. [CrossRef] [PubMed]
4. Riek, R.; Hornemann, S.; Wider, G.; Billeter, M.; Glockshuber, R.; Wüthrich, K. NMR structure of the mouse prion protein domain $PrP^{121–231}$. *Nature* **1996**, *382*, 180–182. [CrossRef] [PubMed]
5. Knaus, K.J.; Morillas, M.; Swietnicki, W.; Malone, M.; Surewicz, W.K.; Yee, V.C. Crystal structure of the human prion protein reveals a mechanism for oligomerization. *Nat. Struct. Biol.* **2001**, *8*, 770–774. [CrossRef] [PubMed]
6. Caughey, B.; Baron, G.S.; Chesebro, B.; Jeffrey, M. Getting a grip on prions: Oligomers, amyloids, and pathological membrane interactions. *Annu. Rev. Biochem.* **2009**, *78*, 177–204. [CrossRef] [PubMed]
7. Knowles, T.P.J.; Vendruscolo, M.; Dobson, C.M. The amyloid state and its association with protein misfolding diseases. *Nat. Rev. Mol. Cell Biol.* **2014**, *15*, 384–396. [CrossRef] [PubMed]
8. Guo, J.L.; Lee, V.M.Y. Cell-to-cell transmission of pathogenic proteins in neurodegenerative diseases. *Nat. Med.* **2014**, *20*, 130–138. [CrossRef] [PubMed]
9. Silva, J.L.; Cordeiro, Y. The "Jekyll and Hyde" Actions of Nucleic Acids on the Prion-like Aggregation of Proteins. *J. Biol. Chem.* **2016**, *291*, 15482–15490. [CrossRef] [PubMed]
10. Chiti, F.; Dobson, C.M. Protein Misfolding, Functional Amyloid, and Human Disease. *Annu. Rev. Biochem.* **2006**, *75*, 333–366. [CrossRef] [PubMed]
11. Uversky, V.N.; Dunker, A.K. Understanding protein non-folding. *Biochim. Biophys. Acta Proteins Proteom.* **2010**, *1804*, 1231–1264. [CrossRef] [PubMed]
12. Yen, C.-F.; Harischandra, D.S.; Kanthasamy, A.; Sivasankar, S. Copper-induced structural conversion templates prion protein oligomerization and neurotoxicity. *Sci. Adv.* **2016**, *2*, e1600014. [CrossRef] [PubMed]
13. Silva, J.L.; Gomes, M.P.; Vieira, T.C.; Cordeiro, Y. PrP interactions with nucleic acids and glycosaminoglycans in function and disease. *Front. Biosci.* **2010**, *15*, 132–150. [CrossRef]
14. Vieira, T.C.R.G.; Reynaldo, D.P.; Gomes, M.P.B.; Almeida, M.S.; Cordeiro, Y.; Silva, J.L. Heparin binding by murine recombinant prion protein leads to transient aggregation and formation of rna-resistant species. *J. Am. Chem. Soc.* **2011**, *133*, 334–344. [CrossRef] [PubMed]
15. Liu, C.; Zhang, Y. Nucleic acid-mediated protein aggregation and assembly. *Adv. Protein Chem. Struct. Biol.* **2011**, *84*, 1–40. [PubMed]
16. Supattapone, S. Elucidating the role of cofactors in mammalian prion propagation. *Prion* **2014**, *8*, 100–105. [CrossRef] [PubMed]
17. Critchley, P.; Kazlauskaite, J.; Eason, R.; Pinheiro, T.J.T. Binding of prion proteins to lipid membranes. *Biochem. Biophys. Res. Commun.* **2004**, *313*, 559–567. [CrossRef] [PubMed]
18. Deleault, N.R.; Harris, B.T.; Rees, J.R.; Supattapone, S. Formation of native prions from minimal components in vitro. *Proc. Natl. Acad. Sci. USA* **2007**, *104*, 9741–9746. [CrossRef] [PubMed]
19. Miller, M.B.; Wang, D.W.; Wang, F.; Noble, G.P.; Ma, J.; Woods, V.L.; Li, S.; Supattapone, S. Cofactor molecules induce structural transformation during infectious prion formation. *Structure* **2013**, *21*, 2061–2068. [CrossRef] [PubMed]
20. Soto, C. Prion hypothesis: The end of the controversy? *Trends Biochem. Sci.* **2011**, *36*, 151–158. [CrossRef] [PubMed]

21. Cordeiro, Y.; Machado, F.; Juliano, L.; Juliano, M.A.; Brentani, R.R.; Foguel, D.; Silva, J.L. DNA Converts Cellular Prion Protein into the β-Sheet Conformation and Inhibits Prion Peptide Aggregation. *J. Biol. Chem.* **2001**, *276*, 49400–49409. [CrossRef] [PubMed]
22. Adler, V.; Zeiler, B.; Kryukov, V.; Kascsak, R.; Rubenstein, R.; Grossman, A. Small, highly structured RNAs participate in the conversion of human recombinant PrPSen to PrPRes in vitro. *J. Mol. Biol.* **2003**, *332*, 47–57. [CrossRef]
23. Deleault, N.R.; Lucassen, R.W.; Supattapone, S. RNA molecules stimulate prion protein conversion. *Nature* **2003**, *425*, 717–720. [CrossRef] [PubMed]
24. Macedo, B.; Millen, T.A.; Braga, C.A.C.A.; Gomes, M.P.B.; Ferreira, P.S.; Kraineva, J.; Winter, R.; Silva, J.L.; Cordeiro, Y. Nonspecific prion protein-nucleic acid interactions lead to different aggregates and cytotoxic species. *Biochemistry* **2012**, *51*, 5402–5413. [CrossRef] [PubMed]
25. Chaves, J.A.P.; Sanchez-López, C.; Gomes, M.P.B.; Sisnande, T.; Macedo, B.; de Oliveira, V.E.; Braga, C.A.C.; Rangel, L.P.; Silva, J.L.; Quintanar, L.; et al. Biophysical and morphological studies on the dual interaction of non-octarepeat prion protein peptides with copper and nucleic acids. *J. Biol. Inorg. Chem.* **2014**, *19*, 839–851. [CrossRef] [PubMed]
26. Zou, W.-Q.; Zheng, J.; Gray, D.M.; Gambetti, P.; Chen, S.G. Antibody to DNA detects scrapie but not normal prion protein. *Proc. Natl. Acad. Sci. USA* **2004**, *101*, 1380–1385. [CrossRef] [PubMed]
27. Tuerk, C.; Gold, L. Systematic evolution of ligands by exponential enrichment: RNA ligands to bacteriophage T4 DNA polymerase. *Science* **1990**, *249*, 505–510. [CrossRef] [PubMed]
28. Ellington, A.D.; Szostak, J.W. In vitro selection of RNA molecules that bind specific ligands. *Nature* **1990**, *346*, 818–822. [CrossRef] [PubMed]
29. Nandi, P.K. Interaction of prion peptide HuPrP106–126 with nucleic acid: Brief report. *Arch. Virol.* **1997**, *142*, 2537–2545. [CrossRef] [PubMed]
30. Nandi, P.K. Polymerization of human prion peptide HuPrP 106–126 to amyloid in nucleic acid solution. *Arch. Virol.* **1998**, *143*, 1251–1263. [CrossRef] [PubMed]
31. Nandi, P.K.; Leclerc, E. Polymerization of murine recombinant prion protein in nucleic acid solution. *Arch. Virol.* **1999**, *144*, 1751–1763. [CrossRef] [PubMed]
32. Cordeiro, Y.; Silva, J.L. The hypothesis of the catalytic action of nucleic acid on the conversion of prion protein. *Protein Pept. Lett.* **2005**, *12*, 251–255. [CrossRef] [PubMed]
33. Weiss, S.; Proske, D.; Neumann, M.; Groschup, M.H.; Kretzschmar, H.A.; Famulok, M.; Winnacker, E.L. RNA aptamers specifically interact with the prion protein PrP. *J. Virol.* **1997**, *71*, 8790–8797. [PubMed]
34. Lima, L.M.T.R.; Cordeiro, Y.; Tinoco, L.W.; Marques, A.F.; Oliveira, C.L.P.; Sampath, S.; Kodali, R.; Choi, G.; Foguel, D.; Torriani, I.; et al. Structural insights into the interaction between prion protein and nucleic acid. *Biochemistry* **2006**, *45*, 9180–9187. [CrossRef] [PubMed]
35. Mercey, R.; Lantier, I.; Maurel, M.C.; Grosclaude, J.; Lantier, F.; Marc, D. Fast, reversible interaction of prion protein with RNA aptamers containing specific sequence patterns. *Arch. Virol.* **2006**, *151*, 2197–2214. [CrossRef] [PubMed]
36. Cavaliere, P.; Pagano, B.; Granata, V.; Prigent, S.; Rezaei, H.; Giancola, C.; Zagari, A. Cross-talk between prion protein and quadruplex-forming nucleic acids: A dynamic complex formation. *Nucleic Acids Res.* **2013**, *41*, 327–339. [CrossRef] [PubMed]
37. Gabus, C.; Derrington, E.; Leblanc, P.; Chnaiderman, J.; Dormont, D.; Swietnicki, W.; Morillas, M.; Surewicz, W.K.; Marc, D.; Nandi, P.; et al. The Prion Protein Has RNA Binding and Chaperoning Properties Characteristic of Nucleocapsid Protein NCp7 of HIV-1. *J. Biol. Chem.* **2001**, *276*, 19301–19309. [CrossRef] [PubMed]
38. Guichard, C.; Ivanyi-Nagy, R.; Sharma, K.K.; Gabus, C.; Marc, D.; Mély, Y.; Darlix, J.L. Analysis of nucleic acid chaperoning by the prion protein and its inhibition by oligonucleotides. *Nucleic Acids Res.* **2011**, *39*, 8544–8558. [CrossRef] [PubMed]
39. Liu, M.; Yu, S.; Yang, J.; Yin, X.; Zhao, D. RNA and CuCl2 induced conformational changes of the recombinant ovine prion protein. *Mol. Cell. Biochem.* **2007**, *294*, 197–203. [CrossRef] [PubMed]
40. Gomes, M.P.B.; Millen, T.A.; Ferreira, P.S.; Cunha E Silva, N.L.; Vieira, T.C.R.G.; Almeida, M.S.; Silva, J.L.; Cordeiro, Y. Prion protein complexed to N2a cellular RNAs through its N-terminal domain forms aggregates and is toxic to murine neuroblastoma cells. *J. Biol. Chem.* **2008**, *283*, 19616–19625. [CrossRef] [PubMed]

41. Saborio, G.P.; Permanne, B.; Soto, C. Sensitive detection of pathological prion protein by cyclic amplification of protein misfolding. *Nature* **2001**, *411*, 810–813. [CrossRef] [PubMed]
42. Lucassen, R.; Nishina, K.; Supattapone, S. In vitro amplification of protease-resistant prion protein requires free sulfhydryl groups. *Biochemistry* **2003**, *42*, 4127–4135. [CrossRef] [PubMed]
43. Cordeiro, Y.; Kraineva, J.; Gomes, M.P.B.; Lopes, M.H.; Martins, V.R.; Lima, L.M.T.R.; Foguel, D.; Winter, R.; Silva, J.L. The amino-terminal PrP domain is crucial to modulate prion misfolding and aggregation. *Biophys. J.* **2005**, *89*, 2667–2676. [CrossRef] [PubMed]
44. Strom, A.; Wang, G.S.; Picketts, D.J.; Reimer, R.; Stuke, A.W.; Scott, F.W. Cellular prion protein localizes to the nucleus of endocrine and neuronal cells and interacts with structural chromatin components. *Eur. J. Cell. Biol.* **2011**, *90*, 414–419. [CrossRef] [PubMed]
45. Mangé, A.; Crozet, C.; Lehmann, S.; Béranger, F. Scrapie-like prion protein is translocated to the nuclei of infected cells independently of proteasome inhibition and interacts with chromatin. *J. Cell. Sci.* **2004**, *117*, 2411–2416. [CrossRef] [PubMed]
46. Marijanovic, Z.; Caputo, A.; Campana, V.; Zurzolo, C. Identification of an intracellular site of prion conversion. *PLoS Pathog.* **2009**, *5*, e1000426. [CrossRef] [PubMed]
47. Yim, Y.-I.; Park, B.-C.; Yadavalli, R.; Zhao, X.; Eisenberg, E.; Greene, L.E. The multivesicular body is the major internal site of prion conversion. *J. Cell. Sci.* **2015**, 1434–1443. [CrossRef] [PubMed]
48. Beaudoin, S.; Vanderperre, B.; Grenier, C.; Tremblay, I.; Leduc, F.; Roucou, X. A large ribonucleoprotein particle induced by cytoplasmic PrP shares striking similarities with the chromatoid body, an RNA granule predicted to function in posttranscriptional gene regulation. *Biochim. Biophys. Acta Mol. Cell. Res.* **2009**, *1793*, 335–345. [CrossRef] [PubMed]
49. Baron, G.S.; Magalhães, A.C.; Prado, M.A.M.; Caughey, B. Mouse-adapted scrapie infection of SN56 cells: Greater efficiency with microsome-associated versus purified PrP-res. *J. Virol.* **2006**, *80*, 2106–2117. [CrossRef] [PubMed]
50. Rouvinski, A.; Karniely, S.; Kounin, M.; Moussa, S.; Goldberg, M.D.; Warburg, G.; Lyakhovetsky, R.; Papy-Garcia, D.; Kutzsche, J.; Korth, C.; et al. Live imaging of prions reveals nascent $PrP^{Sc}$ in cellsurface, raft-associated amyloid strings and webs. *J. Cell. Biol.* **2014**, *204*, 423–441. [CrossRef] [PubMed]
51. Qu, J.; Yu, S.; Zheng, Y.; Zheng, Y.; Yang, H.; Zhang, J. Aptamer and its applications in neurodegenerative diseases. *Cell. Mol. Life Sci.* **2017**, *74*, 683–695. [CrossRef] [PubMed]
52. Zhou, J.; Rossi, J. Aptamers as targeted therapeutics: Current potential and challenges. *Nat. Rev. Drug Discov.* **2017**, *16*, 181–202. [CrossRef] [PubMed]
53. Shangguan, D.; Li, Y.; Tang, Z.; Cao, Z.C.; Chen, H.W.; Mallikaratchy, P.; Sefah, K.; Yang, C.J.; Tan, W. Aptamers evolved from live cells as effective molecular probes for cancer study. *Proc. Natl. Acad. Sci. USA* **2006**, *103*, 11838–11843. [CrossRef] [PubMed]
54. Gogtay, N.J.; Sridharan, K. Therapeutic Nucleic Acids: Current clinical status. *Br. J. Clin. Pharmacol.* **2016**, *82*, 659–672.
55. Famulok, M. Molecular Recognition of Amino Acids by RNA-Aptamers: An L-Citrulline Binding RNA Motif and Its Evolution into an L-Arginine Binder. *J. Am. Chem. Soc.* **1994**, *116*, 1698–1706. [CrossRef]
56. Lupold, S.E.; Hicke, B.J.; Lin, Y.; Coffey, D.S. Identification and characterization of nuclease-stabilized RNA molecules that bind human prostate cancer cells via the prostate-specific membrane antigen. *Cancer Res.* **2002**, *62*, 4029–4033. [PubMed]
57. Tabarzad, M.; Jafari, M. Trends in the Design and Development of Specific Aptamers Against Peptides and Proteins. *Protein J.* **2016**, *35*, 81–99. [CrossRef] [PubMed]
58. Williams, K.P.; Liu, X.H.; Schumacher, T.N.; Lin, H.Y.; Ausiello, D.A.; Kim, P.S.; Bartel, D.P. Bioactive and nuclease-resistant L-DNA ligand of vasopressin. *Proc. Natl. Acad. Sci. USA* **1997**, *94*, 11285–11290. [CrossRef] [PubMed]
59. Tang, Z.; Shangguan, D.; Wang, K.; Shi, H.; Sefah, K.; Mallikratchy, P.; Chen, H.W.; Li, Y.; Tan, W. Selection of aptamers for molecular recognition and characterization of cancer cells. *Anal. Chem.* **2007**, *79*, 4900–4907. [CrossRef] [PubMed]
60. Yu, Y.; Liang, C.; Lv, Q.; Li, D.; Xu, X.; Lui, B.; Lu, A.; Zhang, G. Molecular Selection, Modification and Development of Therapeutic Oligonucleotide Aptamers. *Int. J. Mol. Sci.* **2016**, *17*, 358. [CrossRef] [PubMed]
61. Marc, D. Aptamers to explore prion protein interactions with nucleic acids. *Front. Biosci.* **2010**, *15*, 550–563. [CrossRef]

62. Proske, D.; Gilch, S.; Wopfner, F.; Schatzl, H.M.; Winnacker, E.L.; Famulok, M. Prion-protein-specific aptamer reduces PrPSc formation. *ChemBioChem* **2002**, *3*, 717–725. [CrossRef]
63. Rhie, A.; Kirby, L.; Sayer, N.; Wellesley, R.; Disterer, P.; Sylvester, I.; Gill, A.; Hope, J.; James, W.; Tahiri-Alaoui, A. Characterization of 2'-fluoro-RNA aptamers that bind preferentially to disease-associated conformations of prion protein and inhibit conversion. *J. Biol. Chem.* **2003**, *278*, 39697–39705. [CrossRef] [PubMed]
64. Kouassi, G.K.; Wang, P.; Sreevatan, S.; Irudayaraj, J. Aptamer-mediated magnetic and gold-coated magnetic nanoparticles as detection assay for prion protein assessment. *Biotechnol. Prog.* **2007**, *23*, 1239–1244. [CrossRef] [PubMed]
65. Takemura, K.; Wang, P.; Vorberg, I.; Surewicz, W.; Priola, S.A.; Kanthasamy, A.; Pottathil, R.; Chen, S.G.; Sreevatsan, S. DNA aptamers that bind to $PrP^{C}$ and not $PrP^{Sc}$ show sequence and structure specificity. *Exp. Biol. Med.* **2006**, *231*, 204–214.
66. King, D.J.; Safar, J.G.; Legname, G.; Prusiner, S.B. Thioaptamer Interactions with Prion Proteins: Sequence-specific and Non-specific Binding Sites. *J. Mol. Biol.* **2007**, *369*, 1001–1014. [CrossRef] [PubMed]
67. Kocisko, D.A.; Vaillant, A.; Lee, K.S.; Arnold, K.M.; Bertholet, N.; Race, R.E.; Olsen, E.A.; Juteau, J.M.; Caughey, B. Potent antiscrapie activities of degenerate phosphorothioate oligonucleotides. *Antimicrob. Agents Chemother.* **2006**, *50*, 1034–1044. [CrossRef] [PubMed]
68. Karpuj, M.V.; Giles, K.; Gelibter-Niv, S.; Scott, M.R.; Lingappa, V.R.; Szoka, F.C.; Peretz, D.; Denetclaw, W.; Prusiner, S.B. Phosphorothioate oligonucleotides reduce PrP levels and prion infectivity in cultured cells. *Mol. Med.* **2007**, *13*, 190–198. [CrossRef] [PubMed]
69. Mashima, T.; Matsugami, A.; Nishikawa, F.; Nishikawa, S.; Katahira, M. Unique quadruplex structure and interaction of an RNA aptamer against bovine prion protein. *Nucleic Acids Res.* **2009**, *37*, 6249–6258. [CrossRef] [PubMed]
70. Burge, S.; Parkinson, G.N.; Hazel, P.; Todd, A.K.; Neidle, S. Quadruplex DNA: Sequence, topology and structure. *Nucleic Acids Res.* **2006**, *34*, 5402–5415. [CrossRef] [PubMed]
71. Murakami, K.; Nishikawa, F.; Noda, K.; Yokoyama, T.; Nishikawa, S. Anti-bovine prion protein RNA aptamer containing tandem GGA repeat interacts both with recombinant bovine prion protein and its beta isoform with high affinity. *Prion* **2008**, *2*, 73–80. [CrossRef] [PubMed]
72. Mashima, T.; Nishikawa, F.; Kamatari, Y.O.; Fujiwara, H.; Saimura, M.; Nagata, T.; Kodaki, T.; Nishikawa, S.; Kuwata, K.; Katahira, M. Anti-prion activity of an RNA aptamer and its structural basis. *Nucleic Acids Res.* **2013**, *41*, 1355–1362. [CrossRef] [PubMed]
73. Hayashi, T.; Oshima, H.; Mashima, T.; Nagata, T.; Katahira, M.; Kinoshita, M. Binding of an RNA aptamer and a partial peptide of a prion protein: Crucial importance of water entropy in molecular recognition. *Nucleic Acids Res.* **2014**, *42*, 6861–6875. [CrossRef] [PubMed]
74. Yakovchuk, P.; Protozanova, E.; Frank-Kamenetskii, M.D. Base-stacking and base-pairing contributions into thermal stability of the DNA double helix. *Nucleic Acids Res.* **2006**, *34*, 564–574. [CrossRef] [PubMed]
75. Olsthoorn, R.C.L. G-quadruplexes within prion mRNA: The missing link in prion disease? *Nucleic Acids Res.* **2014**, *42*, 9327–9333. [CrossRef] [PubMed]
76. Gabus, C.; Auxilien, S.; Péchoux, C.; Dormont, D.; Swietnicki, W.; Morillas, M.; Surewicz, W.; Nandi, P.; Darlix, J.L. The prion protein has DNA strand transfer properties similar to retroviral nucleocapsid protein. *J. Mol. Biol.* **2001**, *307*, 1011–1021. [CrossRef] [PubMed]
77. Sayer, N.M.; Cubin, M.; Rhie, A.; Bullock, M.; Tahiri-Alaoui, A.; James, W. Structural Determinants of Conformationally Selective, Prion-binding Aptamers. *J. Biol. Chem.* **2004**, *279*, 13102–13109. [CrossRef] [PubMed]
78. Sekiya, S.; Nishikawa, F.; Noda, K.; Kumar, P.K.R.; Yokoyama, T.; Nishikawa, S. In vitro selection of RNA aptamers against cellular and abnormal isoform of mouse prion protein. *Nucleic Acids Symp. Ser.* **2005**, 361–362. [CrossRef] [PubMed]
79. Sekiya, S.; Noda, K.; Nishikawa, F.; Yokoyama, T.; Kumar, P.K.R.; Nishikawa, S. Characterization and application of a novel RNA aptamer against the mouse prion protein. *J. Biochem.* **2006**, *139*, 383–390. [CrossRef] [PubMed]
80. Ogasawara, D.; Hasegawa, H.; Kaneko, K.; Sode, K.; Ikebukuro, K. Screening of DNA aptamer against mouse prion protein by competitive selection. *Prion* **2007**, *1*, 248–254. [CrossRef] [PubMed]

81. Bibby, D.F.; Gill, A.C.; Kirby, L.; Farquhar, C.F.; Bruce, M.E.; Garson, J.A. Application of a novel in vitro selection technique to isolate and characterise high affinity DNA aptamers binding mammalian prion proteins. *J. Virol. Methods* **2008**, *151*, 107–115. [CrossRef] [PubMed]
82. Wang, P.; Hatcher, K.L.; Bartz, J.C.; Chen, S.G.; Skinner, P.; Richt, J.; Liu, H.; Sreevatsan, S. Selection and characterization of DNA aptamers against $PrP^{Sc}$. *Exp. Biol. Med.* **2011**, *236*, 466–476. [CrossRef] [PubMed]
83. Eisenberg, D.; Jucker, M. The amyloid state of proteins in human diseases. *Cell* **2012**, *148*, 1188–1203. [CrossRef] [PubMed]
84. Ylera, F.; Lurz, R.; Erdmann, V.A.; Fürste, J.P. Selection of RNA aptamers to the Alzheimer's disease amyloid peptide. *Biochem. Biophys. Res. Commun.* **2002**, *290*, 1583–1588. [CrossRef] [PubMed]
85. Jucker, M.; Walker, L.C. Self-propagation of pathogenic protein aggregates in neurodegenerative diseases. *Nature* **2013**, *501*, 45–51. [CrossRef] [PubMed]
86. Rahimi, F.; Murakami, K.; Summers, J.L.; Chen, C.H.B.; Bitan, G. RNA aptamers generated against oligomeric Aβ40 recognize common amyloid aptatopes with low specificity but high sensitivity. *PLoS ONE* **2009**, *4*, e7694. [CrossRef] [PubMed]
87. Rahimi, F.; Bitan, G. Selection of aptamers for amyloid β-protein, the causative agent of Alzheimer's disease. *J. Vis. Exp.* **2010**, *13*, 1–7. [CrossRef] [PubMed]
88. Bitan, G.; Teplow, B. Preparation of Aggregate-Free, Low Molecular Weight Amyloid beta for Assembly and Toxicity Assays. *Methods Mol. Biol. Protein* **2005**, *299*, 3–9.
89. Pesarrodona, M.; Unzueta, U.; Vázquez, E. Dialysis: A characterization method of aggregation tendency. In *Insoluble Proteins: Methods and Protocols*; Springer: Berlin, Germany, 2014; pp. 321–330.
90. Hamada, H.; Arakawa, T.; Shiraki, K. Effect of additives on protein aggregation. *Curr. Pharm. Biotechnol.* **2009**, *10*, 400–407. [CrossRef] [PubMed]
91. Bunka, D.H.J.; Mantle, B.J.; Morten, I.J.; Tennent, G.A.; Radford, S.E.; Stockley, P.G. Production and characterization of RNA aptamers specific for amyloid fibril epitopes. *J. Biol. Chem.* **2007**, *282*, 34500–34509. [CrossRef] [PubMed]
92. Kayed, R.; Head, E.; Sarsoza, F.; Saing, T.; Cotman, C.W.; Necula, M.; Margol, L.; Wu, J.; Breydo, L.; Thompson, J.L.; et al. Fibril specific, conformation dependent antibodies recognize a generic epitope common to amyloid fibrils and fibrillar oligomers that is absent in prefibrillar oligomers. *Mol. Neurodegener.* **2007**, *2*, 18. [CrossRef] [PubMed]
93. Kayed, R.; Glabe, C.G. Conformation-Dependent Anti-Amyloid Oligomer Antibodies. *Methods Enzymol.* **2006**, *413*, 326–344. [PubMed]
94. O'Nuallain, B.; Wetzel, R. Conformational Abs recognizing a generic amyloid fibril epitope. *Proc. Natl. Acad. Sci. USA* **2002**, *99*, 1485–1490. [CrossRef] [PubMed]
95. Kayed, R.; Head, E.; Thompson, J.L.; McIntire, T.M.; Milton, S.C.; Cotman, C.W.; Glabe, C.G. Common structure of soluble amyloid oligomers implies common mechanism of pathogenesis. *Science* **2003**, *300*, 486–489. [CrossRef] [PubMed]
96. Lambert, M.P.; Velasco, P.T.; Chang, L.; Viola, K.L.; Fernandez, S.; Lacor, P.N.; Khuon, D.; Gong, Y.; Bigio, E.H.; Shaw, P.; et al. Monoclonal antibodies that target pathological assemblies of Aβ. *J. Neurochem.* **2007**, *100*, 23–35. [CrossRef] [PubMed]
97. Lacor, P.N.; Buniel, M.C.; Chang, L.; Fernandez, S.J.; Gong, Y.; Viola, K.L.; Lambert, M.P.; Velasco, P.T.; Bigio, E.H.; Finch, C.E.; et al. Synaptic targeting by Alzheimer's-related amyloid β oligomers. *J. Neurosci.* **2004**, *24*, 10191–10200. [CrossRef] [PubMed]
98. Lee, E.B.; Leng, L.Z.; Zhang, B.; Kwong, L.; Trojanowski, J.Q.; Abel, T.; Lee, V.M.Y. Targeting amyloid-β peptide (Aβ) oligomers by passive immunization with a conformation-selective monoclonal antibody improves learning and memory in Aβ precursor protein (APP) transgenic mice. *J. Biol. Chem.* **2006**, *281*, 4292–4299. [CrossRef] [PubMed]
99. Cordeiro, Y.; Macedo, B.; Silva, J.L.; Gomes, M.P.B. Pathological implications of nucleic acid interactions with proteins associated with neurodegenerative diseases. *Biophys. Rev.* **2014**, *6*, 97–110. [CrossRef]
100. Calamai, M.; Taddei, N.; Stefani, M.; Ramponi, G.; Chiti, F. Relative Influence of Hydrophobicity and Net Charge in the Aggregation of Two Homologous Proteins. *Biochemistry* **2003**, *42*, 15078–15083. [CrossRef] [PubMed]
101. Chiti, F. Relative Importance of Hydrophobicity, Net Charge, and Secondary Structure Propensities in Protein Aggregation. *Analysis* **2004**, *4*, 43–59.

102. Groveman, B.R.; Kraus, A.; Raymond, L.D.; Dolan, M.A.; Anson, K.J.; Dorward, D.W.; Caughey, B. Charge neutralization of the central lysine cluster in prion protein (PrP) promotes $PrP^{Sc}$-Like folding of recombinant PrP amyloids. *J. Biol. Chem.* **2015**, *290*, 1119–1128. [CrossRef] [PubMed]
103. Ginsberg, S.D.; Galvin, J.E.; Chiu, T.S.; Lee, V.M.Y.; Masliah, E.; Trojanowski, J.Q. RNA sequestration to pathological lesions of neurodegenerative diseases. *Acta Neuropathol.* **1998**, *96*, 487–494. [CrossRef] [PubMed]
104. Ginsberg, S.D.; Crino, P.B.; Hemby, S.E.; Weingarten, J.A.; Lee, V.M.Y.; Eberwine, J.H.; Trojanowski, J.Q. Predominance of neuronal mRNAs in individual Alzheimer's disease senile plaques. *Ann. Neurol.* **1999**, *45*, 174–181. [CrossRef]
105. Marcinkiewicz, M. BetaAPP and furin mRNA concentrates in immature senile plaques in the brain of Alzheimer patients. *J. Neuropathol. Exp. Neurol.* **2002**, *61*, 815–829. [CrossRef] [PubMed]
106. Manuelidis, L. Nuclease resistant circular DNAs copurify with infectivity in scrapie and CJD. *J. Neurovirol.* **2011**, *17*, 131–145. [CrossRef] [PubMed]
107. Botsios, S.; Manuelidis, L. CJD and Scrapie Require Agent-Associated Nucleic Acids for Infection. *J. Cell. Biochem.* **2016**, *117*, 1947–1958. [CrossRef] [PubMed]
108. Simoneau, S.; Thomzig, A.; Ruchoux, M.-M.; Vignier, N.; Daus, M.L.; Poleggi, A.; Lebon, P.; Freire, S.; Durand, V.; Graziano, S.; et al. Synthetic Scrapie Infectivity: Interaction between Recombinant PrP and Scrapie Brain-Derived RNA. *Virulence* **2015**, *6*, 132–144. [CrossRef] [PubMed]
109. Hartl, F.U.; Bracher, A.; Hayer-Hartl, M. Molecular chaperones in protein folding and proteostasis. *Nature* **2011**, *475*, 324–332. [CrossRef] [PubMed]
110. Maury, C.P.J. Self-Propagating beta-sheet polypeptide structures as prebiotic informational molecular entities: The amyloid world. *Orig. Life Evol. Biosph.* **2009**, *39*, 141–150. [CrossRef] [PubMed]
111. Si, K. Prions: What Are They Good For? *Annu. Rev. Cell. Dev. Biol* **2015**, *31*, 149–169. [CrossRef] [PubMed]
112. Maury, C.P.J. The emerging concept of functional amyloid. *J. Intern. Med.* **2009**, *265*, 329–334. [PubMed]
113. Takahashi, T.; Tada, K.; Mihara, H. RNA aptamers selected against amyloid β-peptide (Aβ) inhibit the aggregation of Abeta. *Mol. Biosyst.* **2009**, *5*, 986–991. [PubMed]
114. Burchell, J.T.; Panegyres, P.K. Prion diseases: Immunotargets and therapy. *ImmunoTargets Ther.* **2016**, *5*, 57–68. [PubMed]
115. Cordeiro, Y.; Ferreira, N.C. New approaches for the selection and evaluation of anti-prion organic compounds. *Mini Rev. Med. Chem.* **2015**, *15*, 84–92. [PubMed]
116. Hanss, B.; Leal-Pinto, E.; Bruggeman, L.; Copeland, T.; Klotman, P. Identification and characterization of a cell membrane nucleic acid channel. *Proc. Natl. Acad. Sci. USA* **1998**, *95*, 1921–1926. [PubMed]
117. Reyes-Reyes, E.M.; Teng, Y.; Bates, P.J. A new paradigm for aptamer therapeutic AS1411 action: Uptake by macropinocytosis and its stimulation by a nucleolin-dependent mechanism. *Cancer Res.* **2010**, *70*, 8617–8629. [PubMed]
118. Cheng, C.; Chen, Y.H.; Lennox, K.A.; Behlke, M.A.; Davidson, B.L. In vivo SELEX for Identification of Brain-penetrating Aptamers. *Mol. Ther. Nucleic Acids* **2013**, *2*, E67. [PubMed]
119. Kim, Y.; Wu, Q.; Hamerlik, P.; Hitomi, M.; Sloan, A.E.; Barnett, G.H.; Weil, R.J.; Leahy, P.; Hjelmeland, A.B.; Rich, J.N. Aptamer identification of brain tumor-initiating cells. *Cancer Res.* **2013**, *73*, 4923–4936. [PubMed]
120. Xiao, S.J.; Hu, P.P.; Wu, X.D.; Zou, Y.L.; Chen, L.Q.; Peng, L.; Ling, J.; Zhen, S.J.; Zhan, L.; Li, Y.F.; et al. Sensitive discrimination and detection of prion disease-associated isoform with a dual-aptamer strategy by developing a sandwich structure of magnetic microparticles and quantum dots. *Anal. Chem.* **2010**, *82*, 9736–9742. [PubMed]
121. Zeiler, B.; Adler, V.; Kryukov, V.; Grossman, A. Concentration and removal of prion proteins from biological solutions. *Biotechnol. Appl. Biochem.* **2003**, *37*, 173–182. [PubMed]
122. Yu, P.; Zhang, X.; Xiong, E.; Zhou, J.; Li, X.; Chen, J. A label-free and cascaded dual-signaling amplified electrochemical aptasensing platform for sensitive prion assay. *Biosens. Bioelectron.* **2016**, *85*, 471–478. [CrossRef] [PubMed]
123. Zhou, J.; Battig, M.R.; Wang, Y. Aptamer-based molecular recognition for biosensor development. *Anal. Bioanal. Chem.* **2010**, *398*, 2471–2480. [CrossRef] [PubMed]


International Journal of
*Molecular Sciences*

MDPI

*Review*

# Chemical Modifications of Nucleic Acid Aptamers for Therapeutic Purposes

**Shuaijian Ni [1,2,†], Houzong Yao [1,2,†], Lili Wang [1,2,†], Jun Lu [1,2], Feng Jiang [1,2,3,*], Aiping Lu [1,2,*] and Ge Zhang [1,2,*]**

1 Institute of Precision Medicine and Innovative Drug Discovery, School of Chinese Medicine, Hong Kong Baptist University (HKBU), Hong Kong 999077, China; jack6shuai@163.com (S.N.); yaohouzong@163.com (H.Y.); wanglili9413@163.com (L.W.); ljaaa111@163.com (J.L.)

2 Institute for Advancing Translational Medicine in Bone & Joint Diseases, School of Chinese Medicine, Hong Kong Baptist University (HKBU), Hong Kong 999077, China

3 Faculty of Materials Science and Chemical Engineering, the State Key Laboratory Base of Novel Functional Materials and Preparation Science, Ningbo University, Ningbo 315211, Zhejiang, China

* Correspondence: jiangfeng@nbu.edu.cn (F.J.); aipinglu@hkbu.edu.hk (A.L.); zhangge@hkbu.edu.hk (G.Z.); Tel.: +852-3411-2456 (A.L.); +852-3411-2958 (G.Z.)

† These authors contributed equally to this work.

Received: 10 July 2017; Accepted: 1 August 2017; Published: 2 August 2017

**Abstract:** Nucleic acid aptamers have minimal immunogenicity, high chemical synthesis production, low cost and high chemical stability when compared with antibodies. However, the susceptibility to nuclease degradation, rapid excretion through renal filtration and insufficient binding affinity hindered their development as drug candidates for therapeutic applications. In this review, we will discuss methods to conquer these challenges and highlight recent developments of chemical modifications and technological advances that may enable early aptamers to be translated into clinical therapeutics.

**Keywords:** nucleic acid aptamer; nuclease degradation; rapid excretion; binding affinity; chemical modification

## 1. Introduction

In 1990, several groups isolated the first nucleic acid aptamers by "SELEX" (Systematic Evolution of Ligands by Exponential Enrichment) or "in vitro selection" (a demarcation resulting from whether the technique was learned from Tuerk and Gold [1] or Ellington and Szostak [2], respectively). Through 3D conformational complementarities, aptamers bind to a wide range of targets, including small metal ions and organic molecules, peptides, proteins, viruses, bacteria, whole cells and even targets within live animals [3]. Being similar to the binding of antibodies and antigens, the binding between aptamer and its target has comparable binding affinity and specificity, which makes aptamers a promising class of therapeutic alternatives to antibodies [4].

In addition, nucleic acid aptamers have minimal immunogenicity, high chemical synthesis production, low cost and high chemical stability, drawing extensive attention of researchers to the development of aptamer therapeutics [5].

However, the susceptibility to nuclease degradation and rapid excretion through renal filtration severely limit the practical usage of aptamers [6,7]. Many aptamers with potent activities have unacceptable short half-lives in vivo [8,9]. Besides, the binding affinity and specificity of unmodified nucleic acid aptamers are sometimes insufficient for successful implementation as therapeutic agent [10]. The generation of high quality aptamers from conventional SELEX is generally below 30% [11]. Therefore, many attempts of post-SELEX chemical modifications should be done in order to solve these challenges (Figure 1).

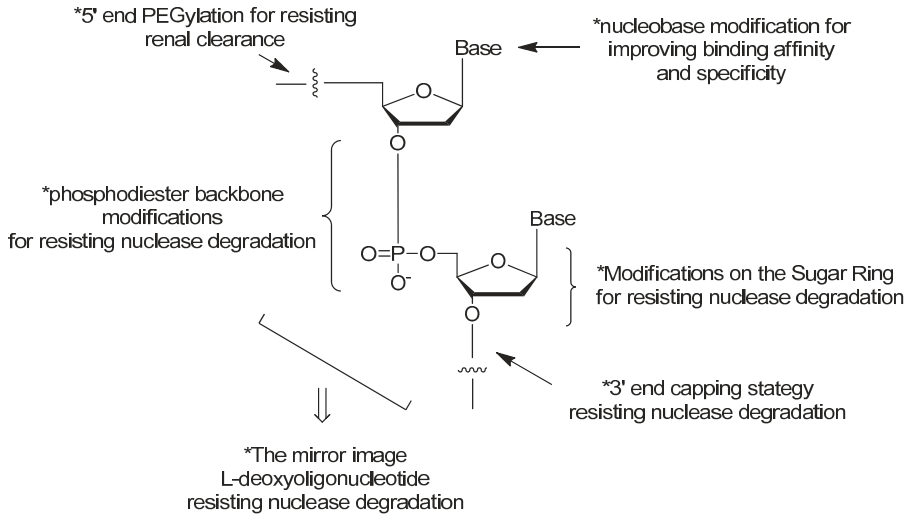


**Figure 1.** The common strategies in the chemical modifications of nucleic acid aptamers and their purposes. Among the modifications, such as modifications on the terminals of nucleic acids, modifications on the phosphodiester linkage, modifications on the sugar ring and modifications on the bases, the 3′ end capping with inverted thymidine [6,12] and PEGylation [13] have been the common strategies in the chemical modifications of nucleic acid aptamers for development clinical therapeutics [14–17].

In this review, the standard synthetic method of solid phase phosphoramidite chemistry for nucleic acid aptamers preparation will be introduced firstly [18,19]. Then, the chemical modification strategies of aptamers for resisting nuclease degradation [12,20–26], improving target binding affinities [10,27–31] and resisting renal clearance [32–36] will be summarized, sequentially. Among the modifications, such as modifications on the terminals of nucleic acids, modifications on the phosphodiester linkage, modifications on the sugar ring and modifications on the bases, the 3′ end capping with inverted thymidine [6,12] and PEGylation [13] have been the common strategies in the chemical modifications of nucleic acid aptamers for development clinical therapeutics (e.g., pegaptanib [14–17], etc.). More excitingly, aptamers with improved binding affinities are being generated with modifications on the bases [29] or substitutions of two non-bridging phosphate oxygen atoms in nucleic acids by sulfur replacement [10] (see "SOMAmers" and "PS2 walk" below).

## 2. Chemical Synthesis of Nucleic Acid Aptamers

### *2.1. Synthesis of DNA Aptamers*

DNA aptamers can be synthesized through the classic solid phase phosphoramidite four-step process on the automated DNA synthesizer [18].

The four-step method is shown in Figure 2. First, the 4,4′-Dimethoxytriphenylmethyl (DMT) group is removed from the deoxynucleoside (5′-end) which is linked to the control pore glass (CPG) columns. Large excess of acid solution (trichloroacetic acid (TCA)) could be used for the deprotection of DMT. In the second step of the cycle, an internucleotide bond called phosphite trimester is synthesized. Then, in the third step, the reaction product from Step 2 should be treated with capping agent to cap the unreacted free 5′-OH group. In the last step (Step 4), the new phosphite is oxidized to the corresponding phosphotriester by iodine. The cycle is repeated, once for each base, to produce the required oligonucleotide. Finally, the nucleic acid aptamers could be cleaved from the CPG by

concentrated ammonium hydroxide. The protecting groups for phosphates and heterocyclic bases could be removed at the same time [18,37,38].

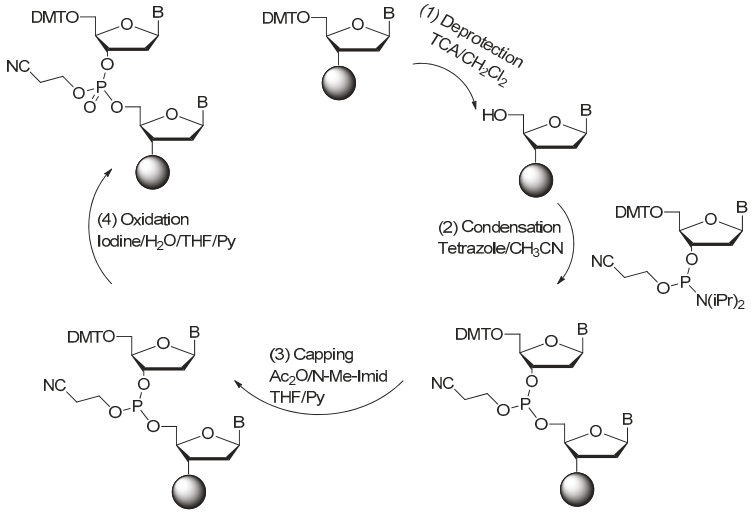


**Figure 2.** Four-step phosphoramidite oligodeoxynucleotide synthesis cycle (adapted from [18]). The phosphoramidite method, pioneered by Marvin Caruthers in the early 1980s, and enhanced by the application of solid-phase technology and automation, is now firmly established as the method of choice. Phosphoramidite oligonucleotide synthesis proceeds in the 3′ to 5′ direction (opposite to the 5′ to 3′ direction of DNA biosynthesis in DNA replication). One nucleotide is added per synthesis cycle. The phosphoramidite DNA synthesis cycle consists of a series of steps outlined in the figure.

At present, the application of four-step method is very common. For the most part, progress in the solid phase nucleic acid synthesis field has not changed this fundamental approach. For R&D purposes, shortened aptamers with 20 to 50 nucleotides in length can be generated in individual labs using "lab scale" DNA or RNA synthesizers [39] (e.g., Expedite 8909, ABI394).

### 2.2. Synthesis of RNA Aptamers

Several of synthetic strategies for the solid-phase synthesis of RNA had been reported [19,40–42]. Among the combinations of different coupling/activation chemistries and protecting groups for the 2′-hydroxyl and exocyclic amine groups, the tert-butyldimethylsilyl protection of the ribose 2′-hydroxyl group combined with the standard protecting groups for the exocyclic amine groups (benzoyl for adenosine, acetyl for cytidine, and isobutyryl for guanosine) were most widely used [40,43]. Phosphoramidite monomers were usually activated with 4,5-dicyanoimidazole, 5-ethylthio-1*H*-tetrazole (ETT) or 5-benzylthio-1*H*-tetrazole (BTT) (Figure 3). The solid supports for RNA synthesis were polymeric supports or CPGs with different linkers and pore sizes. The final product could be cleaved from the CPG by concentrated ammonium hydroxide. The protection groups can also be removed at the same time [19,40,44–46].

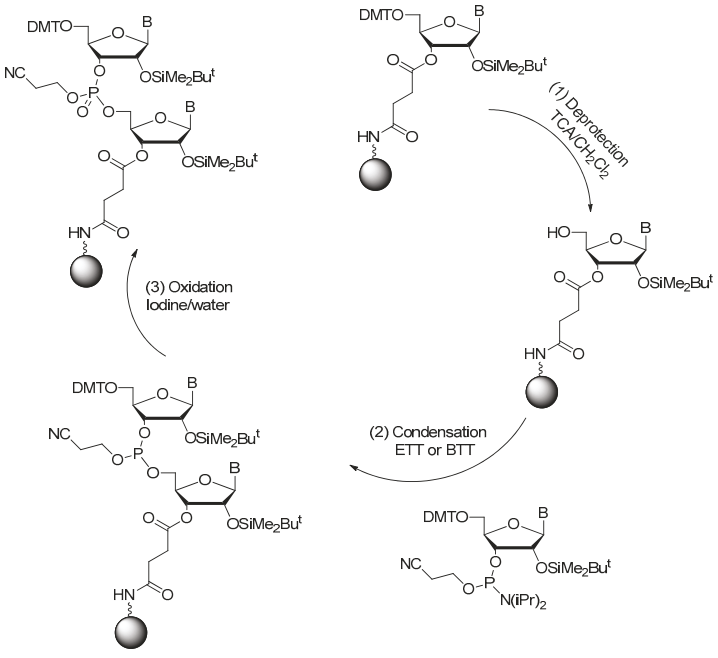


**Figure 3.** Solid-phase RNA synthesis via the phosphoramidite method (adapted from [19]). In RNA synthesis, the 2′-hydroxy group is protected with TBDMS (*t*-butyldimethylsilyl) group, which can be removed by treatment with fluoride ion.

## 3. Modifications of Nucleic Acid Aptamers

### *3.1. Aptamer Derivatives for Resisting Nuclease Degradation*

#### 3.1.1. Terminal 3′–3′ and 5′–5′ Internucleotide Linkage

The 3′–3′ and 5′–5′ inversions were tested in 1991 by Seliger et al. [12]. The 3′-end capping with inverted thymidine has also been a common strategy among aptamers for diseases therapy in ongoing or completed clinical trials [15,47]. Research suggested that 3′-inverted dT modification could increase the stability and resistance of aptamers to 3′-exonuclease in human serum. Synthesis of 3′-inverted dT modified aptamers (Figure 4) needed modified CPG with the 5′-hydroxyl of the first nucleoside attached, followed by chain elongation in standard 3′→5′ fashion [12,20,21].

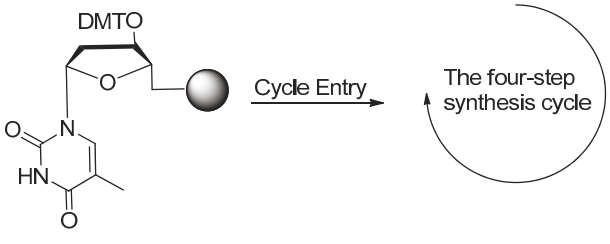


**Figure 4.** Solid-phase synthesis of 3′-inverted dT modified aptamers. Synthesis of 3′-inverted dT modified aptamers needs modified CPG with the 5′-hydroxyl of the first nucleoside attached, followed by chain elongation in standard 3′→5′ fashion.

### 3.1.2. 3′-Biotin Conjugates

In some ways, 3′-biotin (Figure 5) could resist the activity of 3′-exonuclease, which was similar to 3′-inverted dT modification. Dougan et al. [36] investigated the 3′-biotin-streptavidin conjugates of the thrombin aptamer to find that the 3′-biotin rendered resistance to the 3′-exonuclease in the blood of mouse or rabbits. In addition, the 3′-biotin-streptavidin conjugates slowed down the clearance rate of aptamers in blood circulation system in vivo [36]. A similar 3′-biotin approach was also used to protect the DNA aptamer targeting the SARS coronavirus helicase for up to 31 and 16 h in 5% and 10% fetal bovine serum, whereas the original aptamer can only sustain half of that time [20].

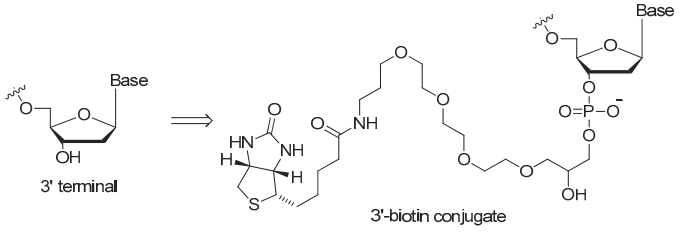


**Figure 5.** Structure of the 3′-biotin conjugate. 3′-Biotin could inhibit the activity of 3′-exonuclease, which was similar to 3′-inverted dT modification. In addition, the 3′-biotin conjugates slowed down the clearance rate in blood circulation system in vivo.

### 3.1.3. Modifications on the Sugar Ring

#### 2′-Substitutions

Modifications to the sugars such as 2′-fluoro (2′-F) or 2′-amino (2′-$NH_2$) ribose groups (Figure 6) on the pyrimidine residues have been available for incorporation into enzymatically derived nucleic acids for some years. Although both are effective at improving serum half-life, 2′-F modifications quickly garnered favor over 2′-$NH_2$ due to the increased coupling efficiency during solid-phase synthesis, and elimination of extra deprotection steps during 2′-$NH_2$ purification. The more bulky 2′-O-methyl (2′-OMe) modifications have been previously used as a post-selection modification due to their increased nuclease resistance and high duplex melting temperature which could be seen in the clinical examples [48,49].

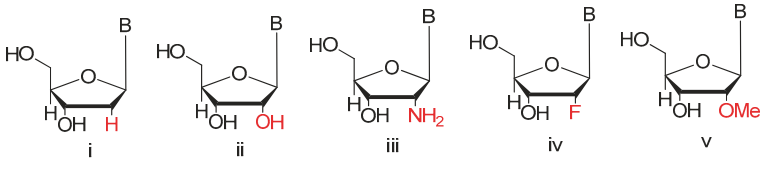


**Figure 6.** 2′-substitutions utilized to enhance the stability of aptamers in vivo (adapted from [39]). 2′-Substitutions can easily be incorporated into aptamers during chemical synthesis and include: (**i**) 2′-H; (**ii**) 2′-OH; (**iii**) 2′-$NH_2$; (**iv**) 2′-F; and (**v**) 2′-OMe.

#### LNA, UNA, 2′-F ANA

Locked nucleic acid (LNA) (Figure 7) is an analog of ribonucleotide with a methylene linkage between 2′-O and 4′-C of the sugar ring. This modification showed great resistance to nucleases and increased thermostability thus could be used to generate the most stable pairs [50,51]. Darfeuille et al. also found that the LNA/DNA chimera LNA5, a stable complex that against HIV-1 trans-activating response (TAR) RNA, was able to maintain the intact structure within 20 h in bovine serum [52].

Shi et al. developed a new LNA/DNA chimeric aptamer probe through proper LNA incorporation and 3′-3′-thymidine (3′-3′-T) capping. The serum stability of original aptamer was gradually enhanced while its specificity and affinity were perfectly maintained. Especially TD05.6 aptamer which had a 7-base pair-LNA substitution exhibited a ten-fold elevated stability in serum and a much slower clearance rate in mice [53].

Unlike LNA, a structurally rigid modification that increases the thermostability of a modified-oligonucleotide thus protects it from nucleases degradation in cells, unlocked nucleic acid (UNA) (Figure 7) in which a bond between C2′ and C3′ of the sugar ring was absent makes aptamers more flexible [54]. Due to its nature of flexibility, UNA could alleviate strain in tight loop structures. Pasternak et al. found that UNA modifications on the loop regions of a 15-mer thrombin targeted DNA aptamer increased its thermodynamic stability. However, modifications within the G-quartet structures were unfavorable for quadruplex formation [55]. They also demonstrated that UNA could be placed in many positions without affecting the thrombin-binding affinity and anticoagulant efficiency of the aptamer [55].

It has been found that modifications at the 2′-position of the sugar ring would bring about different effects on thermostability based on the molecularity of G-quadruplex. Peng et al. discovered that, in both anti-HIV phosphorothioate aptamer and thrombin-binding aptamer, substitution of guanines (G) that adopted anti-conformation with 2′-F-G could maintain the quadruplex conformation, while substituting guanines with syn-conformation was not favored [25]. More importantly, two 2′-F-modified thrombin-binding aptamers (PG13 and PG14) showed approximately four-fold increased binding affinity to thrombin and up to seven-fold higher nuclease resistance. As a result, the 2′-deoxy-2′-fluoro-D-arabinonucleic acid (2′-F ANA) (Figure 7) modification was very suitable for improving the biological and physicochemical properties of DNA G-quartets [25].

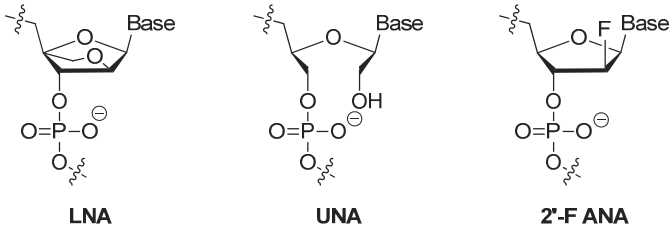


**Figure 7.** Structures of Locked nucleic acid (LNA), unlocked nucleic acid (UNA) and 2′-deoxy-2′-fluoro-D-arabinonucleic acid (2′-F ANA). LNA is an analog of ribonucleotide with a methylene linkage between 2′-O and 4′-C of the sugar ring. UNA misses a bond between C2′ and C3′ of the sugar ring. 2′-F ANA adopts anti-conformation with 2′-F-G.

### 3.1.4. Modifications on the Phosphodiester Linkage

#### Methylphosphonate or Phosphorothioate

Replaced phosphodiester linkage of DNA with methylphosphonate or phosphorothioate analog is commonly used for aptamer modification. Thermodynamic studies revealed that loss of the negative charge of the phosphate backbone, as the methylphosphonate analog (Figure 8), destabilized the G-quadruplex structure [56]. The ionic radii of the oligonucleotide backbone atoms also have an impact in the stabilization of G-quadruplex structures. Sacca et al. found that substitution of the phosphate backbone atom O with S (phosphorothioate analog, Figure 8) might influence the thermal stability of the G-quadruplex structure in a molecularity-dependent manner [56].

The thermodynamic stability of the phosphodiester linkage of the thrombin-binding aptamer d(GGTTGGTGTGGTTGG) with thiophosphoryl substitutions at different internucleotide sites were studied [23,24]. Complete substitution by thiophosphorylated oligonucleotides was limited as their

high toxicities, so partial substitutions with the maximum thermal stability were selected for evaluating their stabilities under conditions of nuclease RQ1 DNAse hydrolysis and their antithrombin activities in blood plasma [24]. Aptamer d(GGSTSTSGGTGTGGSTSTSGG) with thio-substitutions in both TT loops exhibited similar antithrombin efficiency to the unmodified aptamer but better resistance to the degradation of DNA nuclease in blood serum [23].

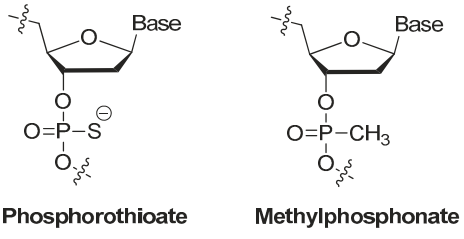


**Figure 8.** Structures of methylphosphonate and phosphorothioate.

More recently, phosphorodiothioate linkages (PS2) were employed to stabilize phosphate backbone. The substitution of both non-bridging oxygen atoms with sulfur could give rise to a phosphorodithioate linkage, which, similar to natural DNA, is achiral at phosphorus. In addition, it was reported that PS2 substitutions dramatically improved target binding affinity by ~1000-fold (see PS2 walk below) [10].

Replaced by Triazole

Replacement of the oligonucleotide phosphodiester linkage with triazole linkages has shown great promise [57–60]. These triazole analogs can be obtained through automated phosphoramidite synthesis with modified dinucleoside blocks [61] or the click reaction between azide- and alkyne-bearing nucleosides [62,63]. Figure 9 shows three types of promising triazole internucleotide modifications [64].

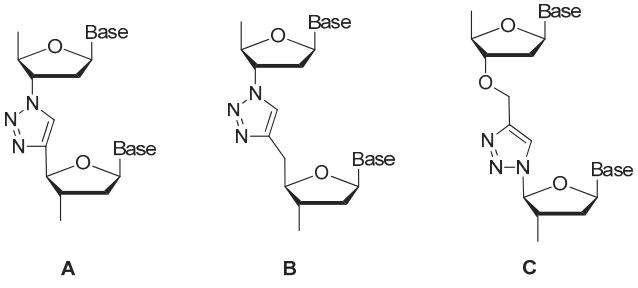


**Figure 9.** Fragments of oligonucleotide analogs with different types of triazole internucleotide modifications (adapted from [64]). A, B, C represent three different types of triazole internucleotide modifications.

Varizhuk et al. synthesized several new oligonucleotide analogs with triazole internucleotide linkages through the click reaction as shown in Figure 10. These analogs bore DNA hybridization affinities similar to those of original oligonucleotides and increased resistance to nuclease cleavage [64].

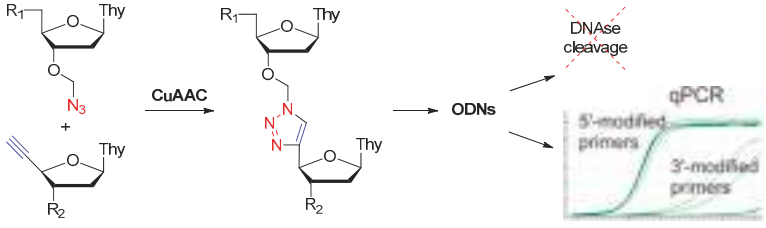


**Figure 10.** Synthesis of the triazole internucleoside linked oligonucleotide analogs with increased resistance to DNAses and polymerases (adapted from [64]).

Later in 2013, Varizhuk et al. synthesized a series of triazole-modified DNA aptamers with structure similar to thrombin-inhibiting G-quadruplexes TBA15 (Thrombin-Binding Aptamer) and TBA31, then tested their secondary structure stabilities, binding affinities for thrombin and anticoagulant effects [65]. A modification in the central loop of the aptamer quadruplex resulted in an anticoagulant activity similar to that of TBA15. Although the modification failed to enhance thrombin binding affinity, it protected aptamers from nuclease hydrolysis thus increased their stabilities. The novel aptamers were potent thrombin inhibitors and could be an alternative to the known anticoagulant drugs [59].

### 3.1.5. The Mirror Image L-DNA

Natural DNAs are all in D-form. A chiral transition could result in the mirror image L-DNA (Figure 11) that may display high resistance to the degradation of nucleases and retain the affinity to targets. Based on the sequences of D-form aptamers, the L-enantiomeric oligonucleotide aptamers (also called as Spiegelmers) were then chemically synthesized [66]. Based on the domain approach, Purschke et al. found a 65-mer Spiegelmer that bound to a stable 25-amino acids length domain of bacterial staphylococcal enterotoxin B [64]. The L-DNA Spiegelmer showed comparable binding affinity to the L-peptide domain and slightly reduced affinity to the whole bacterial staphylococcal enterotoxin B protein.

Through an in vitro-selection process, which was started from a random pool of oligonucleotides, a 67-mer Spiegelmer with a dissociation constant (Kd) of 20 nM for gonadotropin-releasing hormone (GnRH) was reported by Wlotzka et al. [67]. This Spiegelmer was an effective antagonist to GnRH in Chinese hamster and castrated rat models. Besides, the PEGylated Spiegelmer showed more pronounced inhibition activity and longer plasma half-life [67]. Towards the same target, other Spiegelmers with high specificity and affinity were identified through the usage of Spiegelmer technology by Leva et al. [68]. Firstly, aptamers that bind to D-GnRH with Kd of 50–100 nM were isolated, and then their enantiomers were synthesized. The resulting Spiegelmers had similar affinities to that of D-aptamers [68]. Many clinical evaluated aptamers such as NOX-A12, NOX-H94 and NOX-E36 are all L-aptamers [69,70].

A number of different strategies and chemical modifications are now available to enhance the stability of aptamers to nuclease (Table 1). Among these modifications, 2′-fluoro or 2′-*O*-methyl-substitutions and 3′ end capping with inverted thymidine have been the common strategies in the chemical modifications of nucleic acid aptamers for resisting nuclease degradation.

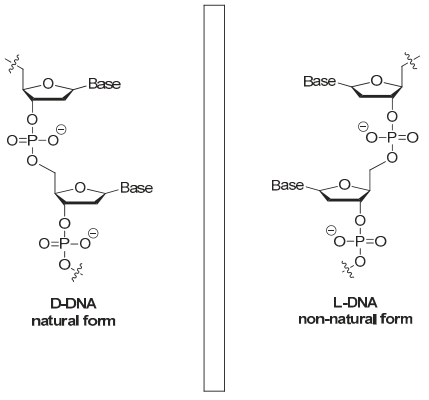


**Figure 11.** Structures of L-deoxyoligonucleotide (L-DNA). Mirror image aptamers are composed of non-natural L-ribose nucleotides. The molecules are initially selected from natural D-ribose aptamer libraries against a non-natural target, for example a D-peptide. Once optimized as a D-aptamer, the mirror image L-aptamer (Spiegelmer) is synthesized chemically and intrinsically bound to the natural L-target, such as a naturally occurring protein.

**Table 1.** Chemical modifications of nucleic acid aptamers for resisting nuclease degradation.

| Modification Sites | Strategy | Applications |
| --- | --- | --- |
| ends of nucleic acid chain | terminal 3′–3′or 5′–5′internucleotide linkage[1], 3′-biotin conjugates; | [12,15,36,47] |
| sugar ring of nucleoside | 2′-fluoro, 2′-*O*-methyl and 2′-amino-substitutions [1], locked nucleic acid (LNA), unlocked nucleic acid (UNA) and 2′-deoxy-2′-fluoro-D-arabinonucleic acid (2′-F ANA); | [25,48,49,52–55] |
| phosphodiester linkage | methylphosphonate or phosphorothioate, replaced by triazole; | [23,24,56–59] |
| mirror image | L-enantiomeric oligonucleotide aptamers (Spiegelmers) | [66–70] |

[1] 2′-fluoro or 2′-*O*-methyl-substitutions and 3′ end capping with inverted thymidine have been the common strategies in the chemical modifications of nucleic acid aptamers for resisting nuclease degradation.

### *3.2. Aptamer Derivatives for Resisting Renal Clearance*

#### 3.2.1. 5′-End with Cholesterol

Even with stabilizing backbone modification, small aptamers are subjected to rapid excretion through renal clearance mainly through glomerular filtration. Formulation with bulky moiety enlarges the size of aptamers, overcoming the renal filtration and extending circulation time, evidently [32,33].

Cholesterol can be derivatized to the 5′-end of an aptamer to form a cholesterol-oligonucleotide (cholODN) conjugate. Smidt et al. added cholesterol at the 5′-end of a 16-mer oligonucleotide (ODN) through a phosphate spacer (Figure 12), the half-time of the resulting cholODN (9–11 min) in plasma was considerably longer than the unmodified ODN (<1 min) [71]. The resulting cholODN can be further linked with low-density lipoprotein (LDL) to form cholODN-LDL complex that turned out to be stable against degradation by rat serum nucleases. The cholODN had a roughly 10-fold longer plasma half-life than the unmodified ODN [71].

Lee and coworkers modified a 29 nucleotide-long 2′-F pyrimidine modified RNA aptamer with cholesterol to form a cholesterol-conjugated aptamer (chol-aptamer) (Figure 12) which can be efficiently absorbed into the cell and inhibits Hepatitis C virus RNA replication [71]. The chol-aptamer had no toxicity in vitro or in vivo. It did not induce any notable alteration in the gene expression profile, including innate immune-related genes. Moreover, administration of the chol-aptamer was well

tolerated in mice without any abnormalities observed. Noticeably, cholesterol conjugation showed longer half-life with approximately nine times lower of clearance rate in plasma. In other words, it extended the duration time that the aptamer stayed in plasma, thus enhanced the stability when the aptamer was exposed to body [32].

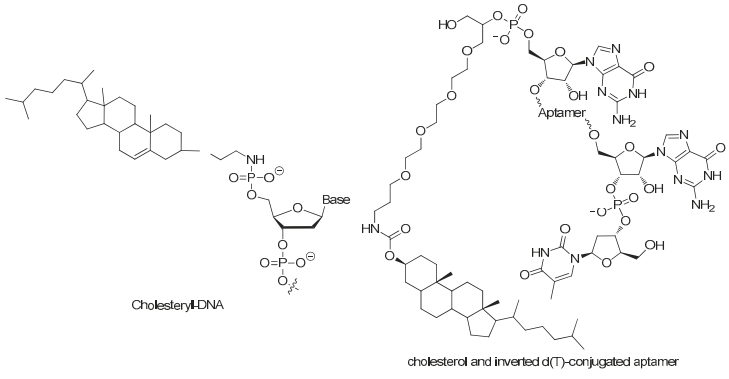


**Figure 12.** Structures of cholesterol-oligonucleotide conjugates (adapted from [71]). Cholesterol can be derivatized to the 5′-end of an aptamer to form a cholesterol-oligonucleotide (cholODN) conjugate. The half-time of the resulting cholODN in plasma was considerably longer than the control ODN.

### 3.2.2. 5′-End with Dialkyl Lipids

Willis et al. reported the preparation and functional properties of a nuclease-resistant vascular endothelial growth factor (VEGF) aptamer which was attached to liposome bilayers through a lipid group. The resulting liposome-anchored aptamer maintained the high binding affinity to VEGF. Moreover, the residence time in plasma was considerably improved when compared with that of the original aptamer [72]. They used the solid phase phosphoramidite method to prepare a dialkylglycerol (DAG) modified VEGF aptamer in which two 18-carbon saturated unbranched hydrocarbon chains were attached via a tetraethylene glycol linker. The DAG phosphoramidite was synthesized in seven steps and then introduced to the 5′-end of the VEGF aptamer (Figure 13) [73]. Afterwards, the DAG-modified VEGF aptamer was incorporated into the bilayers of liposomes, which resulted in aptamers with improved inhibitory activity toward VEGF-induced endothelial cell proliferation in vitro and increased vascular permeability in vivo [73].

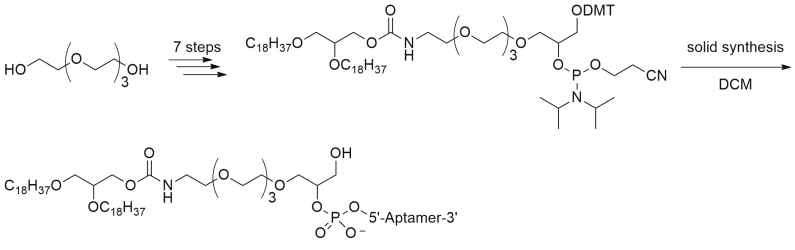


**Figure 13.** Synthesis of the dialkylglycerol (DAG) modified VEGF aptamer (adapted from [72]). Liposome-anchored aptamer maintained the high binding affinity to VEGF. Moreover, the plasma residence time was considerably improved when compared with that of the original aptamer.

### 3.2.3. 5′-End PEGylation

In 2011, Hoffmann et al. described the PEGylation of amino-modified NOX-E36 oligonucleotide by using *N*-hydroxysuccinimide (NHS)-ester-activated polyethylene glycol (PEG), which was most widely used, especially for manufacturing large quantities of PEGylated oligonucleotides. Following synthesis and two-step deprotection, the resulting intermediate amino-modified oligonucleotide reacted with NHS-ester-activated PEG to form oligonucleotide-PEG conjugate (Figure 14). Other coupling methods such as activation by *p*-nitrophenyl carbonate or thiol-maleimide coupling could also be used [74]. The choice of coupling strategies should be made under consideration of the following factors: (1) compatibility with the oligonucleotide; (2) accessibility of the modified oligonucleotide; and (3) reactivity of the activated PEG, which should only react at the functionalization site of the oligonucleotide.

MP7 is one of the DNA aptamers that bind specifically to the murine extracellular domain of PD-1 (Programmed death protein 1) and block the PD-1:PD-L1 (Programmed death-ligand 1) interaction. However, the unmodified DNA aptamer exhibited very short in vivo half-time (<1 h) owing to the rapid renal filtration of such small molecule [75]. It has been reported that conjugation of aptamers with high molecular weight PEG could limit the rate of filtration and extended half-life up to 24–48 h [32,75]. Thus, MP7 was modified at its 5′-termini with a 40 kDa PEG (Figure 15). The PEGylated form of MP7 retained the ability to block PD-1 binding to PD-L1, and significantly suppressed the growth of PD-L1 positive colon carcinoma in vivo [76,77] (Table 2).

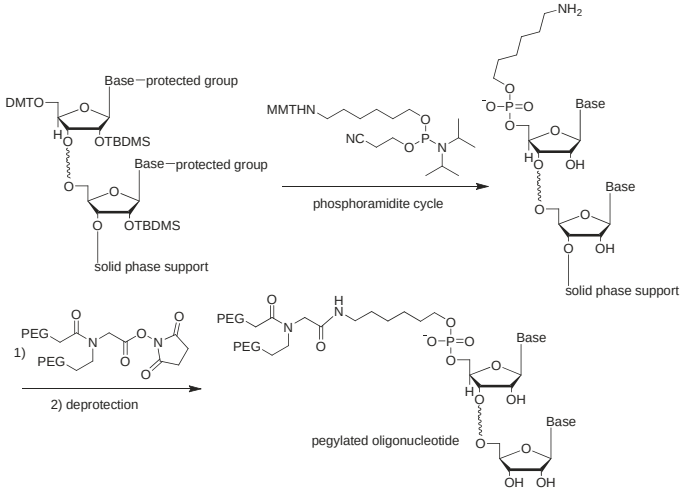


**Figure 14.** Addition of the aminolinker to 5′-end of the oligonucleotide and PEGylation of amino-modified oligonucleotide with 40 kDa Y-shaped PEG ($n$ = ~450) (adapted from [74]). Amino-modified oligonucleotide could be reacted with NHS-ester-activated PEG to form oligonucleotide-PEG conjugate. Conjugation of aptamers with high molecular weight PEG could limit the rate of filtration and extended half-life up to 24–48 h.

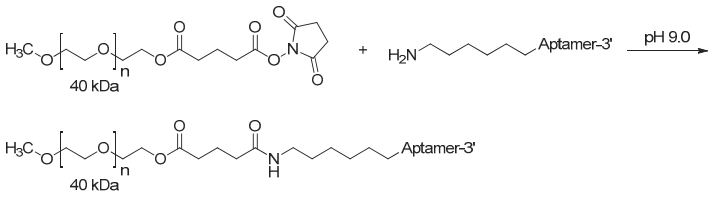


**Figure 15.** Reaction scheme of aptamer conjugating to a 40 kDa polyethylene glycol (PEG) at the 5′-termini (adapted from [76]).

**Table 2.** Aptamer derivatives for resisting renal clearance.

| Modification Sites | Strategy | Applications |
|---|---|---|
| ends of nucleic acid chain | 5′-end with cholesterol;<br>5′-end with dialkyl lipids;<br>5′-end PEGylation [1] | [32,33,71–77] |

[1] Terminal PEGylation has been the common strategy in the chemical modifications of nucleic acid aptamers for resisting renal clearance.

### *3.3. Aptamer Derivatives for Improving Binding Affinity and Target Selectivity*

#### 3.3.1. Modifications on the Bases; SOMAmers

Aptamers with improved binding affinities are being generated with modifications on the base. AS1411 aptamer is a 26-mer single strand DNA 5-d(GGTGGTGGTGGTTGTGGTGGTGGTGG)-3′ which binds to the nucleolin protein expressed on the surfaces of cancer cells [78–80]. Recent research has shown that 5-BzdU (5-(*N*-benzylcarboxyamide)-2-deoxyuridine) modification (Figure 16) of the AS1411 aptamer might selectively increase its targeting affinity to cancer cells while the normal healthy cells have no significant influence [26].

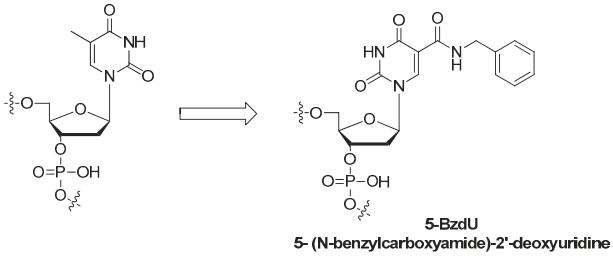


**Figure 16.** Structure of 5-BzdU (5-(*N*-benzylcarboxyamide)-2′-deoxyuridine).

The benzyl could be replaced by the other functional groups such as naphtyl, triptamino, isobutyl and so on (Figure 17). These additional groups might increase the affinities of aptamers to their targets [81–84] (Table 3).

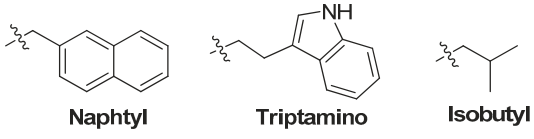


**Figure 17.** Structures of naphtyl, triptamino and isobutyl.

**Table 3.** Aptamer derivatives for improving binding affinity and specificity.

| Modification Sites | Strategy | Applications |
| --- | --- | --- |
| base of nucleoside | 5-(*N*-benzylcarboxyamide)-2′-deoxyuridine modification [1], Slow Off-rate Modified Aptamers (SOMAmers) | [78–84] |
| phosphodiester linkage | phosphorodithioate (PS2) substitution | [10,85,86] |

[1] The benzyl could be replaced by the other functional groups such as naphtyl, triptamino, isobutyl and so on.

The base modifications have also made significant advancements to give aptamers protein-like functionality [11,87]. The SOMAmers (Slow Off-rate Modified Aptamers) not only display improved binding affinities and binding kinetics (in particular, slow off-rates) when compared to traditional aptamers, but also the inclusion of these modifications in their libraries significantly increased the selection "hit rate" [88]. The power of this kind of base modifications has been further demonstrated through the discovery of a 32 nucleotide SOMAmer, SL1025, which binds IL-6 with 200 pmol/L binding affinity and exhibits very little nuclease degradation over a 48-hour incubation in human serum [47,89].

#### 3.3.2. Crystal Structure Based Modifications

Nucleic acid aptamers are much smaller than antibodies. In recent years, there are many studies on the crystallization and X-ray diffraction analysis of aptamers or the complex of aptamers and enzyme [90–93]. It is an effective method to develop modified aptamers with higher affinity and selectivity according to the crystal structures. Autotaxin (ATX) is a plasma lysophospholipase D which can hydrolyze lysophosphatidylcholine (LPC) and generate lysophosphatidic acid (LPA) [94,95]. DNA aptamer RB011 is an inhibitor against ATX. Nureki and coworkers had investigated the crystal structure of ATX in complex with RB011 [96]. The results showed that RB011 inhibited the activity of ATX by preventing its binding to LPC substrates. The hydrophobic pocket of ATX could be occupied by some inhibitors such as HA155 or 3BoA [97,98], but RB011 did not occlude the hydrophobic pocket. Thus, the researchers introduced some hydrophobic groups such as *p*-methyl and *p*-isopropyl into the backbone phosphate of RB011, resulting in RB012 and RB013, respectively. The activities of both RB012 and RB013 ($IC_{50}$ values for LPC were 1.8 and 0.85 nM, respectively) were more potent than that of RB011 (4.4 nM) [96]. These results suggested that modifications aimed to occlude the hydrophobic pocket could significantly increase inhibitory activity. This is a successful modification based on the crystal structural information.

#### 3.3.3. NMR Spectroscopy Guided Aptamer Optimization

Nucleic acid aptamers are widely used for biotechnological or biomedical purpose. High resolution structure information of aptamer–ligand complexes could help reveal the fundamental aspects of nucleic acid folding and nucleic acid-small molecule interactions. Structure information of aptamers and aptamer–ligand complexes constitute the starting point for rational function directed chemical modifications. Duchardt-Ferner E et al. reported the NMR resonance assignment of an RNA aptamer binding to the fluorescent ligand tetramethylrhodamine (TMR) in complex with the ligand 5-carboxy-tetramethylrhodamine (5-TAMRA) as a starting point for a high-resolution structure determination using NMR spectroscopy in solution [99]. This and other reports indicated that NMR guided aptamer optimization could be an optional strategy for aptamer improving binding affinity [100–102].

#### 3.3.4. PS2 Walk

The binding affinity and specificity of unmodified nucleic acid aptamers are sometimes insufficient for successful implementation as therapeutic agents, compared with monoclonal antibody. Post-SELEX

optimization of one Bn-dU and one Nap-dU SOMAmer led to improvements in IL-6 binding (10-fold) and inhibition activity (greater than 20-fold), resulting in lead SOMAmers with sub-nanomolar affinity ($K_d$ = 0.2 nM) and potency ($IC_{50}$ = 0.2 nM) [92]. The PS2 (phosphorodithioate) walk strategy is another option [85,86] (Figure 18). It was reported that the application of the PS2 substitution on a single nucleotide of nucleic acid aptamers could significantly improve target binding affinity by ~1000-fold (from nanomolar to picomolar). An X-ray co-crystal structure of the α-thrombin-PS2-aptamer complex revealed a localized induced-fit folding of the PS2-containing aptamer which leads to increased target interaction [10].

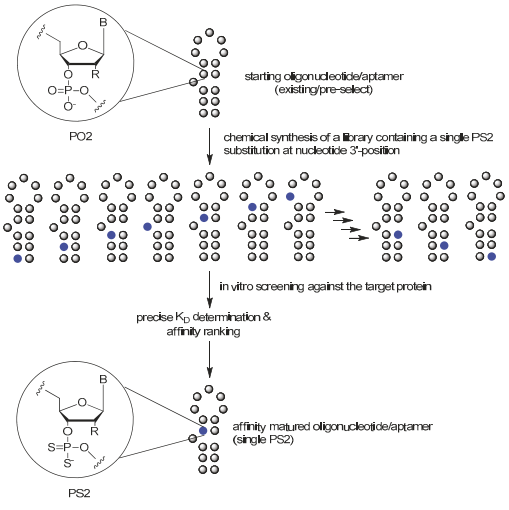


**Figure 18.** Schematic of the PS2-walk library of sequence variants each containing a single PS2 modification. Modification hot spots along the phosphate backbone of the aptamer could be identified by phosphorodithioate (PS2) substitution on a single nucleotide of nucleic acid sequences.

It is worth noting that the effect of PSO substitution (see Section 3.1.4. above) cannot be predicted since the PSO backbone modification is chiral and the chemical synthesis of PSO using phosphoramidite methodology typically results in a mixture of diastereoisomers with a fairly limited influence on the affinity improvement. The promising PS2 derivatives are achiral, representing a class of closely related mimics of natural nucleic acids.

## 4. Conclusions

In this review, we introduced the general solid phase synthesis method of nucleic acid aptamers. In addition, a number of chemical modifications of both DNA and RNA aptamers are summarized here. Among all the modifications shown in the Figure 19, 5′-end PEGylation (for resisting renal clearance) and 3′-end capping strategy (for resisting nuclease degradation) with inverted thymidine are the most commonly used strategy in recent studies. These two methods have been used in the aptamers for disease therapy in ongoing or completed clinical trials [15,47].

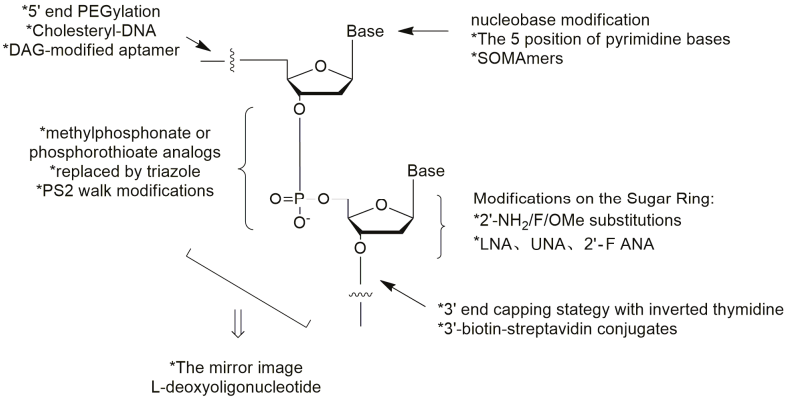


**Figure 19.** Summary of the chemical modifications of nucleic acid aptamers.

The nucleobase and phosphodiester linkage modifications (for improving target binding affinity) can also optimize the properties of aptamers. Excitingly, the established technologies provide an opportunity to generate nucleic acid aptamers of substantially improved affinity with a SOMAmer strategy or a single PS2-moiety substitution and without negatively affecting specificity. These technologies also provide crucial insights that could significantly accelerate the development of nucleic acid aptamer-based therapeutics for clinical applications. With the development of post-SELEX modifications of nucleic acid aptamers, the inherent physicochemical characteristics (metabolic instability, insufficient binding affinity and rapid renal filtration) of nucleic acid aptamers have been improved constantly, which provide a strong impetus of developing nucleic acid aptamers for therapeutic purposes (Table 4).

**Table 4.** Chemical modifications of nucleic acid aptamers for different purposes.

| Strategy | Nuclease Resistance | Improving Binding Affinity and Target Selectivity | Resistance to Renal Clearance |
|---|---|---|---|
| 3′-3′inversion/ 3′-T capping | [12,20,21] | | |
| 5′-5′inversion | [12] | | |
| 3′-biotin conjugates | [20,36] | | |
| 2′-fluoro, 2′-*O*-methyl and 2′-amino-substitutions1 | [39,48,49] | | |
| locked nucleic acid (LNA) | [52,53] | | |
| unlocked nucleic acid (UNA) | [54,55] | | |
| 2′-deoxy-2′-fluoro-D-arabinonucleic acid (2′-F ANA) | [25] | | |
| methylphosphonate | [56] | | |
| phosphorothioate | [23,24] | | |
| replaced by triazole | [57–60] | | |
| L-enantiomeric oligonucleotide aptamers (Spiegelmers) | [66–70] | | |
| 5′-end with cholesterol | | [32,33,71] | |
| 5′-end with dialkyl lipids | | [72,73] | |
| 5′-end PEGylation | | [32,74–77] | |
| 5-(*N*-benzylcarboxyamide)-2-deoxyuridine modification1, Slow Off-rate Modified Aptamers (SOMAmers) | | | [78–84] |
| phosphorodithioate (PS2) substitution | | | [10,85,86] |

**Acknowledgments:** We thank the other academic staff members in Aiping Lu and Ge Zhang's group at Hong Kong Baptist University (Hong Kong, China). We also thank Hong Kong Baptist University (Hong Kong, China) and the State Key Laboratory of Bioorganic and Natural Products Chemistry (Shanghai, China) for providing critical comments and technical support. This study was supported by the Hong Kong General Research Fund (HKBU12102914 to Ge Zhang), the Faculty Research Grant of Hong Kong Baptist University (FRG2/12-13/027 to Ge Zhang) and Open Project of Shanghai Institute of Organic Chemistry (SKLBNPC17344 to Feng Jiang).

**Author Contributions:** Shuaijian Ni, Houzong Yao, Lili Wang and Jun Lu wrote the manuscript. Feng Jiang, Aiping Lu and Ge Zhang revised and approved the manuscript.

**Conflicts of Interest:** The authors declare no conflict of interest.

## References


1. Tuerk, C.; Gold, L. Systematic evolution of ligands by exponential enrichment: RNA ligands to bacteriophage T4 DNA polymerase. *Science* **1990**, *249*, 505–510. [CrossRef] [PubMed]
2. Ellington, A.D.; Szostak, J.W. In vitro selection of RNA molecules that bind specific ligands. *Nature* **1990**, *346*, 818. [CrossRef] [PubMed]
3. Zhou, J.; Rossi, J. Aptamers as targeted therapeutics: Current potential and challenges. *Nat. Rev. Drug Discov.* **2017**, *16*, 181–202. [CrossRef] [PubMed]
4. Gelinas, A.D.; Davies, D.R.; Janjic, N. Embracing proteins: Structural themes in aptamer-protein complexes. *Curr. Opin. Struct. Biol.* **2016**, *36*, 122–132. [CrossRef] [PubMed]
5. Ashrafuzzaman, M. Aptamers as both drugs and drug-carriers. *BioMed Res. Int.* **2014**, *2014*. [CrossRef] [PubMed]
6. Dass, C.R.; Saravolac, E.G.; Li, Y.; Sun, L.Q. Cellular uptake, distribution, and stability of 10–23 deoxyribozymes. *Antisense Nucleic Acid Drug Dev.* **2002**, *12*, 289–299. [CrossRef] [PubMed]
7. Morrissey, D.V.; Blanchard, K.; Shaw, L.; Jensen, K.; Lockridge, J.A.; Dickinson, B.; McSwiggen, J.A.; Vargeese, C.; Bowman, K.; Shaffer, C.S.; et al. Activity of stabilized short interfering RNA in a mouse model of hepatitis B virus replication. *Hepatology* **2005**, *41*, 1349–1356. [CrossRef] [PubMed]
8. Griffin, L.C.; Tidmarsh, G.F.; Bock, L.C.; Toole, J.J.; Leung, L.L. In vivo anticoagulant properties of a novel nucleotide-based thrombin inhibitor and demonstration of regional anticoagulation in extracorporeal circuits. *Blood* **1993**, *81*, 3271–3276. [PubMed]
9. Pagratis, N.C.; Bell, C.; Chang, Y.F.; Jennings, S.; Fitzwater, T.; Jellinek, D.; Dang, C. Potent 2′-amino-, and 2′-fluoro-2′-deoxyribonucleotide RNA inhibitors of keratinocyte growth factor. *Nat. Biotechnol.* **1997**, *15*, 68–73. [CrossRef] [PubMed]
10. Abeydeera, N.D.; Egli, M.; Cox, N.; Mercier, K.; Conde, J.N.; Pallan, P.S.; Mizurini, D.M.; Sierant, M.; Hibti, F.E.; Hassell, T.; et al. Evoking picomolar binding in RNA by a single phosphorodithioate linkage. *Nucleic Acids Res.* **2016**, *44*, 8052–8064. [CrossRef] [PubMed]
11. Gold, L.; Ayers, D.; Bertino, J.; Bock, C.; Bock, A.; Brody, E.N.; Carter, J.; Dalby, A.B.; Eaton, B.E.; Fitzwater, T.; et al. Aptamer-based multiplexed proteomic technology for biomarker discovery. *PLoS ONE* **2010**, *5*, e15004. [CrossRef] [PubMed]
12. Ortigao, J.R.; Rosch, H.; Montenarh, M.; Frohlich, A.; Seliger, H. Oligonucleotide analogs with terminal 3′, 3′-and 5′, 5′-internucleotidic linkages as antisense inhibitors of viral replication. *Antisense Res. Dev.* **1991**, *1*, 380. [CrossRef]
13. Ng, E.W.; Shima, D.T.; Calias, P.; Cunningham, E.T., Jr.; Guyer, D.R.; Adamis, A.P. Pegaptanib, a targeted anti-VEGF aptamer for ocular vascular disease. *Nat. Rev. Drug Discov.* **2006**, *5*, 123–132. [CrossRef] [PubMed]
14. Doggrell, S.A. Pegaptanib: The first antiangiogenic agent approved for neovascular macular degeneration. *Expert Opin. Pharmacother.* **2005**, *6*, 1421–1423. [CrossRef] [PubMed]
15. Fine, S.L.; Martin, D.F.; Kirkpatrick, P. Pegaptanib sodium. *Nat. Rev. Drug Discov.* **2005**, *4*, 187–188. [CrossRef] [PubMed]
16. Kiire, C.A.; Morjaria, R.; Rudenko, A.; Fantato, A.; Smith, L.; Smith, A.; Chong, V. Intravitreal pegaptanib for the treatment of ischemic diabetic macular edema. *Clin. Ophthalmol.* **2015**, *9*, 2305–2311. [CrossRef] [PubMed]
17. Vinores, S.A. Technology evaluation: Pegaptanib, Eyetech/Pfizer. *Curr. Opin. Mol. Ther.* **2003**, *5*, 673–679. [PubMed]
18. Caruthers, M.H.; Barone, A.D.; Beaucage, S.L.; Dodds, D.R.; Fisher, E.F.; McBride, L.J.; Matteucci, M.; Stabinsky, Z.; Tang, J.Y. Chemical synthesis of deoxyoligonucleotides by the phosphoramidite method. *Methods Enzymol.* **1987**, *154*, 287–313. [PubMed]
19. Sproat, B.S. RNA synthesis using 2′-*O*-(tert-butyldimethylsilyl) protection. *Oligonucleotide Synth.* **2005**, 17–31.
20. Shum, K.T.; Tanner, J.A. Differential inhibitory activities and stabilisation of DNA aptamers against the SARS coronavirus helicase. *Chembiochem* **2008**, *9*, 3037–3045. [CrossRef] [PubMed]

21. Shaw, J.P.; Kent, K.; Bird, J.; Fishback, J.; Froehler, B. Modified deoxyoligonucleotides stable to exonuclease degradation in serum. *Nucleic Acids Res.* **1991**, *19*, 747–750. [CrossRef] [PubMed]
22. De Smidt, P.C.; le Doan, T.; de Falco, S.; van Berkel, T.J. Association of antisense oligonucleotides with lipoproteins prolongs the plasma half-life and modifies the tissue distribution. *Nucleic Acids Res.* **1991**, *19*, 4695–4700. [CrossRef] [PubMed]
23. Zaitseva, M.; Kaluzhny, D.; Shchyolkina, A.; Borisova, O.; Smirnov, I.; Pozmogova, G. Conformation and thermostability of oligonucleotide d(GGTTGGTGTGGTTGG) containing thiophosphoryl internucleotide bonds at different positions. *Biophys. Chem.* **2010**, *146*, 1–6. [CrossRef] [PubMed]
24. Pozmogova, G.; Zaitseva, M.; Smirnov, I.; Shvachko, A.; Murina, M.; Sergeenko, V. Anticoagulant effects of thioanalogs of thrombin-binding DNA-aptamer and their stability in the plasma. *Bull. Exp. Biol. Med.* **2010**, *150*, 180–184. [CrossRef] [PubMed]
25. Peng, C.G.; Damha, M.J. G-quadruplex induced stabilization by 2′-deoxy-2′-fluoro-D-arabinonucleic acids (2′F-ANA). *Nucleic Acids Res.* **2007**, *35*, 4977–4988. [CrossRef] [PubMed]
26. Lee, K.Y.; Kang, H.; Ryu, S.H.; Lee, D.S.; Lee, J.H.; Kim, S. Bioimaging of nucleolin aptamer-containing 5-(*N*-benzylcarboxyamide)-2′-deoxyuridine more capable of specific binding to targets in cancer cells. *J. Biomed. Biotechnol.* **2010**, *2010*, 168306. [CrossRef] [PubMed]
27. Pallan, P.S.; Yang, X.; Sierant, M.; Abeydeera, N.D.; Hassell, T.; Martinez, C.; Janicka, M.; Nawrot, B.; Egli, M. Crystal structure, stability and Ago2 affinity of phosphorodithioate-modified RNAs. *Rsc. Adv.* **2014**, *4*, 64901–64904. [CrossRef]
28. Ashley, S.L.; Xia, M.; Murray, S.; O'Dwyer, D.N.; Grant, E.; White, E.S.; Flaherty, K.R.; Martinez, F.J.; Moore, B.B. Six-SOMAmer Index relating to immune, protease and angiogenic functions predicts progression in IPF. *PLoS ONE* **2016**, *11*, e0159878. [CrossRef] [PubMed]
29. Eid, C.; Palko, J.W.; Katilius, E.; Santiago, J.G. Rapid slow off-rate modified aptamer (SOMAmer)-based detection of C-reactive protein using isotachophoresis and an ionic spacer. *Anal. Chem.* **2015**, *87*, 6736–6743. [CrossRef] [PubMed]
30. Kraemer, S.; Vaught, J.D.; Bock, C.; Gold, L.; Katilius, E.; Keeney, T.R.; Kim, N.; Saccomano, N.A.; Wilcox, S.K.; Zichi, D.; et al. From SOMAmer-based biomarker discovery to diagnostic and clinical applications: A SOMAmer-based, streamlined multiplex proteomic assay. *PLoS ONE* **2011**, *6*, e26332. [CrossRef] [PubMed]
31. Park, N.J.; Wang, X.; Diaz, A.; Goos-Root, D.M.; Bock, C.; Vaught, J.D.; Sun, W.; Strom, C.M. Measurement of cetuximab and panitumumab-unbound serum EGFR extracellular domain using an assay based on slow off-rate modified aptamer (SOMAmer) reagents. *PLoS ONE* **2013**, *8*, e71703. [CrossRef] [PubMed]
32. Healy, J.M.; Lewis, S.D.; Kurz, M.; Boomer, R.M.; Thompson, K.M.; Wilson, C.; McCauley, T.G. Pharmacokinetics and biodistribution of novel aptamer compositions. *Pharm. Res.* **2004**, *21*, 2234–2246. [CrossRef] [PubMed]
33. Watson, S.R.; Chang, Y.F.; O'Connell, D.; Weigand, L.; Ringquist, S.; Parma, D.H. Anti-L-selectin aptamers: Binding characteristics, pharmacokinetic parameters, and activity against an intravascular target in vivo. *Antisense Nucleic Acid Drug Dev.* **2000**, *10*, 63–75. [CrossRef] [PubMed]
34. Gilbert, J.C.; DeFeo-Fraulini, T.; Hutabarat, R.M.; Horvath, C.J.; Merlino, P.G.; Marsh, H.N.; Healy, J.M.; Boufakhreddine, S.; Holohan, T.V.; Schaub, R.G. First-in-human evaluation of anti von Willebrand factor therapeutic aptamer ARC1779 in healthy volunteers. *Circulation* **2007**, *116*, 2678–2686. [CrossRef] [PubMed]
35. Van Eijk, L.; Swinkels, D.; John, A.; Schwoebel, F.; Fliegert, F.; Summo, L.; Vauleon, S.; Laarakkers, J.; Riecke, K.; Pickkers, P. Randomized double-blind placebo-controlled PK/PD study on the effects of a single intravenous dose of the anti-hepcidin Spiegelmer NOX-H94 on serum iron during experimental human endotoxemia. *Crit. Care* **2013**, *17*, P352.
36. Dougan, H.; Lyster, D.M.; Vo, C.V.; Stafford, A.; Weitz, J.I.; Hobbs, J.B. Extending the lifetime of anticoagulant oligodeoxynucleotide aptamers in blood. *Nucl. Med. Biol.* **2000**, *27*, 289–297. [CrossRef]
37. Dellinger, D.J.; Betley, J.R.; Wyrzykiewicz, T.K.; Caruthers, M.H. Synthesis of DNA using a new two-step cycle. *Oligonucleotide Synth.* **2005**, *288*, 1–16.
38. Beaucage, S.L.; Caruthers, M.H. Synthetic strategies and parameters involved in the synthesis of oligodeoxyribonucleotides according to the phosphoramidite method. *Curr. Protoc. Nucleic Acid Chem.* **2001**. [CrossRef]
39. Maier, K.E.; Levy, M. From selection hits to clinical leads: Progress in aptamer discovery. *Mol. Ther. Methods Clin. Dev.* **2016**, *5*, 16014. [CrossRef] [PubMed]

40. Usman, N.; Ogilvie, K.; Jiang, M.; Cedergren, R. The automated chemical synthesis of long oligoribuncleotides using 2′-*O*-silylated ribonucleoside 3′-*O*-phosphoramidites on a controlled-pore glass support: Synthesis of a 43-nucleotide sequence similar to the 3′-half molecule of an *Escherichia coli* formylmethionine tRNA. *J. Am. Chem. Soc.* **1987**, *109*, 7845–7854.
41. Shiba, Y.; Masuda, H.; Watanabe, N.; Ego, T.; Takagaki, K.; Ishiyama, K.; Ohgi, T.; Yano, J. Chemical synthesis of a very long oligoribonucleotide with 2-cyanoethoxymethyl (CEM) as the 2′-*O*-protecting group: Structural identification and biological activity of a synthetic 110mer precursor-microRNA candidate. *Nucleic Acids Res.* **2007**, *35*, 3287–3296. [CrossRef] [PubMed]
42. Ohgi, T.; Masutomi, Y.; Ishiyama, K.; Kitagawa, H.; Shiba, Y.; Yano, J. A new RNA synthetic method with a 2′-*O*-(2-cyanoethoxymethyl) protecting group. *Org. Lett.* **2005**, *7*, 3477–3480. [CrossRef] [PubMed]
43. Usman, N.; Pon, R.T.; Ogilvie, K.K. Preparation of ribonucleoside 3′-*O*-phosphoramidites and their application to the automated solid phase synthesis of oligonucleotides. *Tetrahedron Lett.* **1985**, *26*, 4567–4570. [CrossRef]
44. Sinha, N.; Davis, P.; Usman, N.; Perez, J.; Hodge, R.; Kremsky, J.; Casale, R. Labile exocyclic amine protection of nucleosides in DNA, RNA and oligonucleotide analog synthesis facililating N-deacylation, minimizing depurination and chain degradation. *Biochimie* **1993**, *75*, 13–23. [CrossRef]
45. Welz, R.; Müller, S. 5-(Benzylmercapto)-1*H*-tetrazole as activator for 2′-O-TBDMS phosphoramidite building blocks in RNA synthesis. *Tetrahedron Lett.* **2002**, *43*, 795–797. [CrossRef]
46. Westman, E.; Stromberg, R. Removal of t-butyldimethylsilyl protection in RNA-synthesis. Triethylamine trihydrofluoride (TEA, 3HF) is a more reliable alternative to tetrabutylammonium fluoride (TBAF). *Nucleic Acids Res.* **1994**, *22*, 2430–2431. [CrossRef] [PubMed]
47. Gupta, S.; Hirota, M.; Waugh, S.M.; Murakami, I.; Suzuki, T.; Muraguchi, M.; Shibamori, M.; Ishikawa, Y.; Jarvis, T.C.; Carter, J.D.; et al. Chemically modified DNA aptamers bind interleukin-6 with high affinity and inhibit signaling by blocking its interaction with interleukin-6 receptor. *J. Biol. Chem.* **2014**, *289*, 8706–8719. [CrossRef] [PubMed]
48. Padilla, R.; Sousa, R. Efficient synthesis of nucleic acids heavily modified with non-canonical ribose 2′-groups using a mutantT7 RNA polymerase (RNAP). *Nucleic Acids Res.* **1999**, *27*, 1561–1563. [CrossRef] [PubMed]
49. Ruckman, J.; Green, L.S.; Beeson, J.; Waugh, S.; Gillette, W.L.; Henninger, D.D.; Claesson-Welsh, L.; Janjic, N. 2′-Fluoropyrimidine RNA-based aptamers to the 165-amino acid form of vascular endothelial growth factor (VEGF165). Inhibition of receptor binding and VEGF-induced vascular permeability through interactions requiring the exon 7-encoded domain. *J. Biol. Chem.* **1998**, *273*, 20556–20567. [CrossRef] [PubMed]
50. Obika, S.; Nanbu, D.; Hari, Y.; Morio, K.-I.; In, Y.; Ishida, T.; Imanishi, T. Synthesis of 2′-O,4′-C-methyleneuridine and -cytidine. Novel bicyclic nucleosides having a fixed C3, -endo sugar puckering. *Tetrahedron Lett.* **1997**, *38*, 8735–8738. [CrossRef]
51. Koshkin, A.A.; Singh, S.K.; Nielsen, P.; Rajwanshi, V.K.; Kumar, R.; Meldgaard, M.; Olsen, C.E.; Wengel, J. LNA (Locked Nucleic Acids): Synthesis of the adenine, cytosine, guanine, 5-methylcytosine, thymine and uracil bicyclonucleoside monomers, oligomerisation, and unprecedented nucleic acid recognition. *Tetrahedron* **1998**, *54*, 3607–3630. [CrossRef]
52. Darfeuille, F.; Hansen, J.B.; Orum, H.; Di Primo, C.; Toulme, J.J. LNA/DNA chimeric oligomers mimic RNA aptamers targeted to the TAR RNA element of HIV-1. *Nucleic Acids Res.* **2004**, *32*, 3101–3107. [CrossRef] [PubMed]
53. Shi, H.; He, X.; Cui, W.; Wang, K.; Deng, K.; Li, D.; Xu, F. Locked nucleic acid/DNA chimeric aptamer probe for tumor diagnosis with improved serum stability and extended imaging window in vivo. *Anal. Chim. Acta* **2014**, *812*, 138–144. [CrossRef] [PubMed]
54. Campbell, M.A.; Wengel, J. Locked vs. unlocked nucleic acids (LNA vs. UNA): Contrasting structures work towards common therapeutic goals. *Chem. Soc. Rev.* **2011**, *40*, 5680–5689. [CrossRef] [PubMed]
55. Pasternak, A.; Hernandez, F.J.; Rasmussen, L.M.; Vester, B.; Wengel, J. Improved thrombin binding aptamer by incorporation of a single unlocked nucleic acid monomer. *Nucleic Acids Res.* **2011**, *39*, 1155–1164. [CrossRef] [PubMed]
56. Sacca, B.; Lacroix, L.; Mergny, J.L. The effect of chemical modifications on the thermal stability of different G-quadruplex-forming oligonucleotides. *Nucleic Acids Res.* **2005**, *33*, 1182–1192. [CrossRef] [PubMed]
57. El-Sagheer, A.H.; Brown, T. Click chemistry with DNA. *Chem. Soc. Rev.* **2010**, *39*, 1388–1405. [CrossRef] [PubMed]

58. Mutisya, D.; Selvam, C.; Kennedy, S.D.; Rozners, E. Synthesis and properties of triazole-linked RNA. *Bioorg. Med. Chem. Lett.* **2011**, *21*, 3420–3422. [CrossRef] [PubMed]
59. Sau, S.P.; Hrdlicka, P.J. C2′-pyrene-functionalized triazole-linked DNA: Universal DNA/RNA hybridization probes. *J. Org. Chem.* **2012**, *77*, 5–16. [CrossRef] [PubMed]
60. El-Sagheer, A.H.; Brown, T. Click nucleic acid ligation: Applications in biology and nanotechnology. *Acc. Chem. Res.* **2012**, *45*, 1258–1267. [CrossRef] [PubMed]
61. Chandrasekhar, S.; Srihari, P.; Nagesh, C.; Kiranmai, N.; Nagesh, N.; Idris, M.M. Synthesis of readily accessible triazole-linked dimer deoxynucleoside phosphoramidite for solid-phase oligonucleotide synthesis. *Synthesis* **2010**, *2010*, 3710–3714. [CrossRef]
62. Nuzzi, A.; Massi, A.; Dondoni, A. Model studies toward the synthesis of thymidine oligonucleotides with triazole internucleosidic linkages via iterative Cu(I)-promoted azide–alkyne ligation chemistry. *Mol. Inform.* **2007**, *26*, 1191–1199.
63. Lucas, R.; Zerrouki, R.; Granet, R.; Krausz, P.; Champavier, Y. A rapid efficient microwave-assisted synthesis of a 3′,5′-pentathymidine by copper (I)-catalyzed [3 + 2] cycloaddition. *Tetrahedron* **2008**, *64*, 5467–5471. [CrossRef]
64. Varizhuk, A.M.; Kaluzhny, D.N.; Novikov, R.A.; Chizhov, A.O.; Smirnov, I.P.; Chuvilin, A.N.; Tatarinova, O.N.; Fisunov, G.Y.; Pozmogova, G.E.; Florentiev, V.L. Synthesis of triazole-linked oligonucleotides with high affinity to DNA complements and an analysis of their compatibility with biosystems. *J. Org. Chem.* **2013**, *78*, 5964–5969. [CrossRef] [PubMed]
65. Varizhuk, A.M.; Tsvetkov, V.B.; Tatarinova, O.N.; Kaluzhny, D.N.; Florentiev, V.L.; Timofeev, E.N.; Shchyolkina, A.K.; Borisova, O.F.; Smirnov, I.P.; Grokhovsky, S.L.; et al. Synthesis, characterization and in vitro activity of thrombin-binding DNA aptamers with triazole internucleotide linkages. *Eur. J. Med. Chem.* **2013**, *67*, 90–97. [CrossRef] [PubMed]
66. Hoellenriegel, J.; Zboralski, D.; Maasch, C.; Rosin, N.Y.; Wierda, W.G.; Keating, M.J.; Kruschinski, A.; Burger, J.A. The Spiegelmer NOX-A12, a novel CXCL12 inhibitor, interferes with chronic lymphocytic leukemia cell motility and causes chemosensitization. *Blood* **2014**, *123*, 1032–1039. [CrossRef] [PubMed]
67. Wlotzka, B.; Leva, S.; Eschgfaller, B.; Burmeister, J.; Kleinjung, F.; Kaduk, C.; Muhn, P.; Hess-Stumpp, H.; Klussmann, S. In vivo properties of an anti-GnRH Spiegelmer: An example of an oligonucleotide-based therapeutic substance class. *Proc. Natl. Acad. Sci. USA* **2002**, *99*, 8898–8902. [CrossRef] [PubMed]
68. Leva, S.; Lichte, A.; Burmeister, J.; Muhn, P.; Jahnke, B.; Fesser, D.; Erfurth, J.; Burgstaller, P.; Klussmann, S. GnRH binding RNA and DNA Spiegelmers: A novel approach toward GnRH antagonism. *Chem. Biol.* **2002**, *9*, 351–359. [CrossRef]
69. Yu, Y.; Liang, C.; Lv, Q.; Li, D.; Xu, X.; Liu, B.; Lu, A.; Zhang, G. Molecular selection, modification and development of therapeutic oligonucleotide aptamers. *Int. J. Mol. Sci.* **2016**, *17*, 358. [CrossRef] [PubMed]
70. Purschke, W.G.; Radtke, F.; Kleinjung, F.; Klussmann, S. A DNA Spiegelmer to staphylococcal enterotoxin B. *Nucleic Acids Res.* **2003**, *31*, 3027–3032. [CrossRef] [PubMed]
71. Lee, C.H.; Lee, S.H.; Kim, J.H.; Noh, Y.H.; Noh, G.J.; Lee, S.W. Pharmacokinetics of a cholesterol-conjugated aptamer against the Hepatitis C Virus (HCV) NS5B Protein. *Mol. Ther. Nucleic Acids* **2015**, *4*, e254. [CrossRef] [PubMed]
72. Willis, M.C.; Collins, B.D.; Zhang, T.; Green, L.S.; Sebesta, D.P.; Bell, C.; Kellogg, E.; Gill, S.C.; Magallanez, A.; Knauer, S.; et al. Liposome-anchored vascular endothelial growth factor aptamers. *Bioconjug. Chem.* **1998**, *9*, 573–582. [CrossRef] [PubMed]
73. Green, L.S.; Jellinek, D.; Bell, C.; Beebe, L.A.; Feistner, B.D.; Gill, S.C.; Jucker, F.M.; Janjic, N. Nuclease-resistant nucleic acid ligands to vascular permeability factor/vascular endothelial growth factor. *Chem. Biol.* **1995**, *2*, 683–695. [CrossRef]
74. Hoffmann, S.; Hoos, J.; Klussmann, S.; Vonhoff, S. RNA aptamers and spiegelmers: Synthesis, purification, and post-synthetic PEG conjugation. *Curr. Protoc. Nucleic Acid Chem.* **2011**, *46*, 1–30.
75. Da Pieve, C.; Blackshaw, E.; Missailidis, S.; Perkins, A.C. PEGylation and biodistribution of an anti-MUC1 aptamer in MCF-7 tumor-bearing mice. *Bioconjug. Chem.* **2012**, *23*, 1377–1381. [CrossRef] [PubMed]
76. Prodeus, A.; Abdul-Wahid, A.; Fischer, N.W.; Huang, E.H.; Cydzik, M.; Gariépy, J. Targeting the PD-1/PD-L1 immune evasion axis with DNA aptamers as a novel therapeutic strategy for the treatment of disseminated cancers. *Mol. Ther. Nucleic Acids* **2015**, *4*, e237. [CrossRef] [PubMed]

77. Tan, L.; Neoh, K.G.; Kang, E.T.; Choe, W.S.; Su, X. PEGylated anti-MUC1 aptamer-doxorubicin complex for targeted drug delivery to MCF7 breast cancer cells. *Macromol. Biosci.* **2011**, *11*, 1331–1335. [CrossRef] [PubMed]
78. Bates, P.J.; Laber, D.A.; Miller, D.M.; Thomas, S.D.; Trent, J.O. Discovery and development of the G-rich oligonucleotide AS1411 as a novel treatment for cancer. *Exp. Mol. Pathol.* **2009**, *86*, 151–164. [CrossRef] [PubMed]
79. Reyes-Reyes, E.M.; Teng, Y.; Bates, P.J. A new paradigm for aptamer therapeutic AS1411 action: Uptake by macropinocytosis and its stimulation by a nucleolin-dependent mechanism. *Cancer Res.* **2010**, *70*, 8617–8629. [CrossRef] [PubMed]
80. Trinh, T.L.; Zhu, G.; Xiao, X.; Puszyk, W.; Sefah, K.; Wu, Q.; Tan, W.; Liu, C. A synthetic aptamer-drug adduct for targeted liver cancer therapy. *PLoS ONE* **2015**, *10*, e0136673. [CrossRef] [PubMed]
81. Kimoto, M.; Yamashige, R.; Matsunaga, K.I.; Yokoyama, S.; Hirao, I. Generation of high-affinity DNA aptamers using an expanded genetic alphabet. *Nat. Biotechnol.* **2013**, *31*, 453–457. [CrossRef] [PubMed]
82. Sefah, K.; Yang, Z.; Bradley, K.M.; Hoshika, S.; Jimenez, E.; Zhang, L.; Zhu, G.; Shanker, S.; Yu, F.; Turek, D.; et al. In vitro selection with artificial expanded genetic information systems. *Proc. Natl. Acad. Sci. USA* **2014**, *111*, 1449–1454. [CrossRef] [PubMed]
83. Yang, Z.; Durante, M.; Glushakova, L.G.; Sharma, N.; Leal, N.A.; Bradley, K.M.; Chen, F.; Benner, S.A. Conversion strategy using an expanded genetic alphabet to assay nucleic acids. *Anal. Chem.* **2013**, *85*, 4705–4712. [CrossRef] [PubMed]
84. Chumakov, A.; Yuhina, E.; Frolova, E.; Kravchenko, J.; Chumakov, S. Expanding the application potential of DNA aptamers by their functionalization. *Russ. J. Bioorg. Chem.* **2016**, *42*, 1–13. [CrossRef]
85. Tonkinson, J.L.; Guvakova, M.; Khaled, Z.; Lee, J.; Yakubov, L.; Marshall, W.S.; Caruthers, M.H.; Stein, C. Cellular pharmacology and protein binding of phosphoromonothioate and phosphorodithioate oligodeoxynucleotides: A comparative study. *Antisense Res. Dev.* **1994**, *4*, 269–278. [CrossRef] [PubMed]
86. Zandarashvili, L.; Nguyen, D.; Anderson, K.M.; White, M.A.; Gorenstein, D.G.; Iwahara, J. Entropic enhancement of protein-DNA affinity by oxygen-to-sulfur substitution in DNA phosphate. *Biophys. J.* **2015**, *109*, 1026–1037. [CrossRef] [PubMed]
87. Vaught, J.D.; Bock, C.; Carter, J.; Fitzwater, T.; Otis, M.; Schneider, D.; Rolando, J.; Waugh, S.; Wilcox, S.K.; Eaton, B.E. Expanding the chemistry of DNA for in vitro selection. *J. Am. Chem. Soc.* **2010**, *132*, 4141–4151. [CrossRef] [PubMed]
88. Davies, D.R.; Gelinas, A.D.; Zhang, C.; Rohloff, J.C.; Carter, J.D.; O'Connell, D.; Waugh, S.M.; Wolk, S.K.; Mayfield, W.S.; Burgin, A.B.; et al. Unique motifs and hydrophobic interactions shape the binding of modified DNA ligands to protein targets. *Proc. Natl. Acad. Sci. USA* **2012**, *109*, 19971–19976. [CrossRef] [PubMed]
89. Rohloff, J.C.; Gelinas, A.D.; Jarvis, T.C.; Ochsner, U.A.; Schneider, D.J.; Gold, L.; Janjic, N. Nucleic acid ligands with protein-like side chains: Modified aptamers and their use as diagnostic and therapeutic agents. *Mol. Ther. Nucleic Acids* **2014**, *3*, e201. [CrossRef] [PubMed]
90. Forster, C.; Brauer, A.B.; Brode, S.; Schmidt, K.S.; Perbandt, M.; Meyer, A.; Rypniewski, W.; Betzel, C.; Kurreck, J.; Furste, J.P.; et al. Comparative crystallization and preliminary X-ray diffraction studies of locked nucleic acid and RNA stems of a tenascin C-binding aptamer. *Acta Crystallogr. Sect. F Struct. Biol. Cryst. Commun.* **2006**, *62 Pt 7*, 665–668. [CrossRef] [PubMed]
91. Forster, C.; Oberthuer, D.; Gao, J.; Eichert, A.; Quast, F.G.; Betzel, C.; Nitsche, A.; Erdmann, V.A.; Furste, J.P. Crystallization and preliminary X-ray diffraction data of an LNA 7-mer duplex derived from a ricin aptamer. *Acta Crystallogr. Sect. F Struct. Biol. Cryst. Commun.* **2009**, *65 Pt 9*, 881–885. [CrossRef] [PubMed]
92. Gelinas, A.D.; Davies, D.R.; Edwards, T.E.; Rohloff, J.C.; Carter, J.D.; Zhang, C.; Gupta, S.; Ishikawa, Y.; Hirota, M.; Nakaishi, Y.; et al. Crystal structure of interleukin-6 in complex with a modified nucleic acid ligand. *J. Biol. Chem.* **2014**, *289*, 8720–8734. [CrossRef] [PubMed]
93. Hottin, A.; Marx, A. Structural insights into the processing of nucleobase-modified nucleotides by DNA polymerases. *Acc. Chem. Res.* **2016**, *49*, 418–427. [CrossRef] [PubMed]
94. Umezu-Goto, M.; Kishi, Y.; Taira, A.; Hama, K.; Dohmae, N.; Takio, K.; Yamori, T.; Mills, G.B.; Inoue, K.; Aoki, J. Autotaxin has lysophospholipase D activity leading to tumor cell growth and motility by lysophosphatidic acid production. *J. Cell Biol.* **2002**, *158*, 227–233. [CrossRef] [PubMed]

95. Tokumura, A.; Majima, E.; Kariya, Y.; Tominaga, K.; Kogure, K.; Yasuda, K.; Fukuzawa, K. Identification of human plasma lysophospholipase D, a lysophosphatidic acid-producing enzyme, as autotaxin, a multifunctional phosphodiesterase. *J. Biol. Chem.* **2002**, *277*, 39436–39442. [CrossRef] [PubMed]
96. Kato, K.; Ikeda, H.; Miyakawa, S.; Futakawa, S.; Nonaka, Y.; Fujiwara, M.; Okudaira, S.; Kano, K.; Aoki, J.; Morita, J.; et al. Structural basis for specific inhibition of autotaxin by a DNA aptamer. *Nat. Struct. Mol. Biol.* **2016**, *23*, 395–401. [CrossRef] [PubMed]
97. Hausmann, J.; Kamtekar, S.; Christodoulou, E.; Day, J.E.; Wu, T.; Fulkerson, Z.; Albers, H.M.; van Meeteren, L.A.; Houben, A.J.; van Zeijl, L.; et al. Structural basis of substrate discrimination and integrin binding by autotaxin. *Nat. Struct. Mol. Biol.* **2011**, *18*, 198–204. [CrossRef] [PubMed]
98. Kawaguchi, M.; Okabe, T.; Okudaira, S.; Nishimasu, H.; Ishitani, R.; Kojima, H.; Nureki, O.; Aoki, J.; Nagano, T. Screening and X-ray crystal structure-based optimization of autotaxin (ENPP2) inhibitors, using a newly developed fluorescence probe. *ACS Chem. Biol.* **2013**, *8*, 1713–1721. [CrossRef] [PubMed]
99. Duchardt-Ferner, E.; Juen, M.; Kreutz, C.; Wöhnert, J. NMR resonance assignments for the tetramethylrhodamine binding RNA aptamer 3 in complex with the ligand 5-carboxy-tetramethylrhodamine. *Biomol. NMR Assign.* **2017**, *11*, 29–34. [CrossRef] [PubMed]
100. Amano, R.; Aoki, K.; Miyakawa, S.; Nakamura, Y.; Kozu, T.; Kawai, G.; Sakamoto, T. NMR monitoring of the SELEX process to confirm enrichment of structured RNA. *Sci. Rep.* **2017**, *7*, 283. [CrossRef] [PubMed]
101. Minagawa, H.; Onodera, K.; Fujita, H.; Sakamoto, T.; Akitomi, J.; Kaneko, N.; Shiratori, I.; Kuwahara, M.; Horii, K.; Waga, I. Selection characterization and application of artificial DNA aptamer containing appended bases with sub-nanomolar affinity for a salivary biomarker. *Sci. Rep.* **2017**, *7*, 42716. [CrossRef] [PubMed]
102. Thirunavukarasu, D.; Chen, T.; Liu, Z.; Hongdilokkul, N.; Romesberg, F.E. Selection of 2′-fluoro-modified aptamers with optimized properties. *J. Am. Chem. Soc.* **2017**, *139*, 2892–2895. [CrossRef] [PubMed]


International Journal of
*Molecular Sciences*

MDPI

*Review*

# Aptamers for DNA Damage and Repair

**Maureen McKeague**

Department of Health Sciences and Technology, ETH Zürich, Schmelzbergstrasse 9, 8092 Zurich, Switzerland; maureen.mckeague@hest.ethz.ch; Tel.: +41-44-632-3282

Received: 4 October 2017; Accepted: 20 October 2017; Published: 22 October 2017

**Abstract:** DNA is damaged on a daily basis, which can lead to heritable mutations and the activation of proto-oncogenes. Therefore, DNA damage and repair are critical risk factors in cancer, aging and disease, and are the underlying bases of most frontline cancer therapies. Much of our current understanding of the mechanisms that maintain DNA integrity has been obtained using antibody-based assays. The oligonucleotide equivalents of antibodies, known as aptamers, have emerged as potential molecular recognition rivals. Aptamers possess several ideal properties including chemical stability, in vitro selection and lack of batch-to-batch variability. These properties have motivated the incorporation of aptamers into a wide variety of analytical, diagnostic, research and therapeutic applications. However, their use in DNA repair studies and DNA damage therapies is surprisingly un-tapped. This review presents an overview of the progress in selecting and applying aptamers for DNA damage and repair research.

**Keywords:** aptamer; DNA damage; DNA repair; in vitro selection; SELEX; mutation; therapeutics

## 1. Introduction

While DNA was originally considered an extremely stable molecule, Tomas Lindahl determined that the nucleobases of DNA react slowly with water. This insight led him to discover the molecular machinery by which cells repair damaged DNA and won him, along with Aziz Sancar and Paul Modrich, the Nobel Prize in Chemistry in 2015 [1–3]. Indeed, our DNA is damaged on a daily basis by radiation, ultraviolet light and contaminants in our food and in our environment. DNA damage can lead to heritable mutations and the activation of proto-oncogenes. DNA damage is therefore a critical risk factor in cancer, aging and heritable diseases [4], and is the underlying basis for most frontline cancer therapies [5,6] (Figure 1).

**Figure 1.** Our DNA is damaged by normal cell processes, contaminants in our food and environment, radiation and ultraviolet light. Damage may include strand-breaks, crosslinks (yellow line in DNA), or adducts (black and red stars). If not repaired, DNA damage can lead to cell death or heritable mutations and cancer.

Cells have a number of strategies to detect (e.g., damage checkpoints) and deal with (i.e., repair pathways) damage to DNA. If such detection and repair mechanisms are impaired, cells may experience genomic instability, apoptosis or senescence, and furthermore, predispose organisms to immunodeficiency, neurological disorders and cancer. Antibodies have been widely used as the molecular recognition platform of choice for the detection of DNA adducts and repair signaling and activation [7,8]. Over the past several decades, their use in DNA damage and repair research has facilitated the discovery of and insight into the mechanisms by which cells respond to DNA damage and initiate repair.

More recently, the nucleic acid analogues to antibodies, known as aptamers, have emerged. Since their discovery, aptamers have been compared to antibodies due to their similar ability to bind to specific targets. However, aptamers offer several broad advantages over antibodies as molecular recognition molecules (reviewed elsewhere [9,10]). Antibodies must be developed in vivo, whereas aptamers are composed of oligonucleotides which can be selected in vitro (using a process termed the systematic evolution of ligands by exponential enrichment, SELEX). As a result, aptamers can be selected against DNA-damaging toxins or the resulting lethal DNA adducts that are challenging for antibody generation. Furthermore, the nucleic acid composition affords aptamers with the ability to reversibly change conformation, making it possible to develop aptamers in conditions with varying pH, temperatures and ionic strengths that would cause antibodies to be irreversibly denatured. Finally, aptamers can be chemically modified during their synthesis to increase shelf life and nuclease resistance, as well as impart different chemical functionality (e.g., fluorescence and electrochemical properties) [11].

The unique combination of aptamer qualities listed above has led to a surge in the application of aptamers for analytical and diagnostic detection, therapeutics and drug delivery, intracellular imaging, and for gene regulation and control. With this increased interest in aptamers, coupled to a growing concern of the quality of commercial research antibodies [12], it is surprising that the application of aptamers to the study and detection of DNA damage and repair processes is limited. This review covers the aptamers that have been selected for DNA damage and repair proteins to-date and discusses the challenges in their selection and potential applications.

## 2. Aptamers for Damaged DNA

Damage to DNA includes oxidation, depurination or depyrimidation, single-strand or double-strand DNA breaks, deamination or alkylation. In this section, aptamers that can be potentially used to detect these types of DNA damage are highlighted.

### *2.1. Guanine Oxidation*

The most abundant oxidatively-damaged base is 8-oxoguanine (8-oxoG.) When occurring in the genome, mismatched pairing of 8-oxoG with adenine results in G to T transversion mutations [13]. G to T mutations are often observed in oxidative stress-associated diseases, such as cancer, atherosclerosis, diabetes and pathologies of the central nervous system, as well as during aging. Therefore, it is not surprising that this damaged-nucleobase has been the focus of recent detection strategies [14], and the target of many aptamer-related selections. 8-oxoG can be further oxidized, leading to the formation of a variety of products, including the spiroiminodihydantoin (Sp) lesion. Unlike the 8-oxoG lesion, the Sp lesion is not planar. Instead, it is shaped like a propeller. Given this unusual shape, both Sp lesions strongly destabilize the DNA duplex [15] (Figure 2).

The first example of an aptamer that recognized DNA damage was reported in 1998 by Rink et al. Following ten rounds of conventional SELEX using an 8-oxodG affinity matrix, a specific RNA aptamer (Clone R10-B35) that exhibited highly specific binding to 8-oxodG compared to dG and other nucleosides was selected [16]. Using the electrophoretic mobility-shift assay (EMSA), the authors demonstrated that the aptamer bound to a single-strand DNA sequence containing a 3′ terminal

8-oxodG with an apparent dissociation constant ($K_d$) of 270 nM. Surprisingly, the RNA aptamer also recognized 8-oxodG present in the center of a 19 nt ssDNA with an apparent $K_d$ of 2.8 μM.

Almost ten years later, in 2009, the first DNA aptamer that recognized the oxidative lesion 8-oxodG was reported. To select these aptamers, Miyachi and co-workers used guanosine-monophosphate as an analog of 8-oxodG (due to the difficulty in immobilizing sufficiently high concentrations of 8-oxodG). The highest affinity aptamer that emerged from their selection was capable of binding to the free nucleoside with a $K_d$ of 0.1 μM [17].

In 2012, an aptamer for 8-oxoG (the free base) was rationally designed. To achieve this, the thermal stability of nine 8-oxodG-containing hairpin DNA triplexes were compared. Next, the 8-oxoG moiety was removed from the two most stable triplexes. As a result, the abasic site allowed for the free oxidized base to bind in a specific manner [18]; thus creating a "rationally designed aptamer". The same group also tested several aliphatic side chain modifications at the abasic site to improve binding specificity. Introduction of a β-alanine side chain allowed selective binding of the 8-oxoG nucleobase with a dissociation constant of 5.5 μM [19].

Finally, in 2015, the Burrows group employed the recently described "structure-switching" SELEX [20] to isolate DNA aptamers for several products of guanine oxidation, including 8-oxodG and its nucleobase (8-oxo-G), the dSp nucleoside diastereomers: (−),-(*R*)-dSp and (+),-(*S*)-dSp and one of the Sp nucleobase enantiomers: (−),-(*R*)-Sp. The DNA aptamers resulting from this work bound to their respective targets with $K_d$ values in the low nanomolar range, with the exception of the aptamer for 8-oxo-dG, which bound in the micromolar range (Table 1) [21].

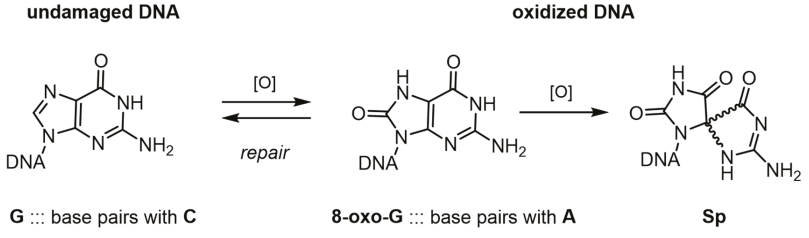


**Figure 2.** When guanine is oxidized, forming 8-oxoguanine (8-oxo-G), the resulting preferential basepairing to A ultimately leads to a G to T tranversion mutation. Further oxidation results in the spiroiminodihydantoin (Sp) adduct diastereomers, for example, which are highly destabilizing to the DNA duplex.

**Table 1.** Aptamers for DNA damage and repair targets.

| Target Class | Target | Nucleic Acid | $K_d$ [1] | Reference |
|---|---|---|---|---|
| DNA Adducts | 8-oxodG | RNA | 270 nM | [16] |
| | 8-oxodG | DNA | 100 nM | [17] |
| | 8-oxoG | DNA [2] | 5.5 μM | [19] |
| | 8-oxoG | DNA | 3 nM | [21] |
| | 8-oxodG | DNA | 25 μM | [21] |
| | (−),-(*R*)-dSp | DNA | 28 nM | [21] |
| | (+),-(*S*)-dS | DNA | 76 nM | [21] |
| | (−),-(*R*)-Sp | DNA | 12 nM | [21] |
| | $m^7$-GTP | RNA | 500 nM | [22] |
| | benzylguanine | RNA | 200 nM | [23] |
| Strand Breaks | homopurine/pyrimidine duplex | RNA | 1 μM | [24] |
| | 20 bp duplex | DNA [3] | 43.9 nM | [25] |
| | 3′LTR | RNA | 300 nM | [26] |
| | Ku protein | RNA | 2 nM | [27] |

**Table 1.** *Cont.*

| Target Class | Target | Nucleic Acid | $K_d$ [1] | Reference |
|---|---|---|---|---|
| Repair Proteins | Fpg (DNA glycosylase) | RNA | 2.5 nM | [28] |
| | Polβ/polκ | RNA | 290 nM | [29] |
| | MutS | DNA | 3.6 nM | [30] |
| | AlkB | DNA | 20 nM | [31] |
| | AlkB homologue 2 | DNA | 85 nM | [32] |
| Mutated Gene | $KRAS^{V12}$ | RNA | 4.04 nM | [33] |

[1] Only aptamers with $K_d$ values are reported; for each, the best $K_d$ is included. [2] With a β-alanine side chain. [3] Presence of benzoindoloquinolin required.

### 2.2. Guanine Alkylation

Adduct formation is the result of covalent binding between reactive electrophilic substances and nucleophilic sites (ring nitrogens and exocyclic oxygen atoms) of DNA bases. The N7 atom of guanine is the most vulnerable site for attack by alkylating agents [34]. Other common sites of DNA alkylation include the $N^3$ and $N^1$ positions of adenine, as well as the $N^3$ position of cytosine. Furthermore, even though *O*-alkyl lesions are generated to a much lesser extent than *N*-alkyl adducts, the induction of $O^6$-alkyl-G lesions is of significant interest because $O^6$-alkyl-G can readily mispair with thymine during DNA replication to cause mutagenic and cytotoxic biological effects.

While there are no reports of aptamers that directly bind to the adduct $N^7$-methylguanine ($m^7dG$), there are a few potential examples that might be explored in the future. As one example, Haller et al. reported the selection of RNA aptamers that bind to the methylated ribose, 7-methyl-guanosine ($m^7G$) which is typically part of the 5′ cap at the ends of mRNA transcripts in eukaryotes. The authors performed conventional SELEX with the goal of isolating aptamers capable of inhibiting translation of capped mRNA transcripts. The resulting aptamers bound to $m^7G$ with modest affinity (0.5 μM) and high specificity, discriminating between non-methylated nucleotides by over 2000 fold. Interestingly, the presence of phosphate groups, or the identity of the purine group (e.g., adenine vs. guanine) had little effect on binding [22]. Therefore, it is possible that these aptamers may recognize the $m^7dG$ adduct.

As another example, Larguinho and co-workers used an RNA aptamer that binds to xanthine [35] to develop nanoprobes that preferentially detected glycidamide (GA) adducts. GA is an epoxide metabolite of the genotoxic carcinogen acrylamide, and alkylates the $N^7$ position of guanine. Surprisingly, the authors were able to preferentially detect GA adducts compared to similar compounds (e.g., dGTP and glycidamide metabolites). While the sensor was capable of detecting the GA adducts, it was unfortunately ineffective in the presence of high concentrations of nucleotides [36].

Finally, Xu et al. developed an RNA aptamer that binds benzylguanine [23]. While benzylguanine is not a biologically-relevant DNA adduct, it is frequently used in place of $O^6$-methylguanine for studies [37]. The best selected aptamer displayed high affinity for the target (~200 nM), but most importantly, it exhibited a 20,000 fold selectivity compared to other guanine metabolites.

Together, these examples suggest that aptamers could be selected to recognize and bind to biologically-relevant alkylated guanine adducts in the future.

### 2.3. Double-Strand Breaks

The most dangerous forms of DNA damage are double-strand breaks (DSB). DNA DSBs occur when the two complementary stands of the double helix are simultaneously broken at locations that are close enough to one another, so that base pairing and chromatin structure cannot keep the two DNA ends together. As a consequence, repair is difficult and detrimental recombination with other sites in the genome may occur [38].

Despite their importance, there have been no reports of selecting aptamers to specifically recognize the termini of DSBs. This is expected to be difficult due to the electrostatic repulsion

of the sugar–phosphate backbone of DNA that would prevent single strand aptamer binding to the DNA duplex. However, there have been several efforts in the past two decades to overcome the challenges presented by binding oligonucleotides to duplex DNA.

The Maher group reported the first example in 1996. The authors applied conventional SELEX against a 21 nt homopurine/homopyrimidine duplex DNA target. Following 26 rounds of selection under conditions that increased from pH 5.0–7.4, several aptamers emerged that bound to the duplex target with modest affinity (less than 1 μM) at pH 6, and approximately 10 μM at physiological pH [24]. Importantly, these selected aptamers approach the binding affinity of a 21 nt RNA oligonucleotide that forms a canonical triple helix with the duplex. Building on the success of this SELEX approach, selection of oligonucleotides to a duplex was performed again 13 years later, this time at neutral pH and in the presence of the triplex stabilizing agent, benzoindoloquinoline (BIQ). Following only seven rounds of selection, aptamers were capable of binding a 20 bp duplex with a $K_d$ of 43.9 nM. However, in the absence of BIQ, no binding was observed [25]. Together, these examples indicate that there are strategies to reduce the electrostatic repulsion between DNA and potential aptamers; thus, potentially enabling future approaches for aptamer-based detection of DSBs.

As a final exciting example, Srisawat et al. performed SELEX using the 3′ long terminal repeat (LTR) of human immunodeficiency virus type 1. This 325 bp DNA duplex lacks a long polypurine/polypyrimiding tract and is therefore unlikely to favor triplex formation. The goal of this work was to identify aptamers that bind to the internal region of the LTR and thereby regulate its transcription. As such, several efforts were made to promote binding of the aptamer library to the internal region. The authors found that the selected RNA aptamers had a tendency to bind to the "ends" of the dsDNA; some aptamers were specific for the 3′ end while others recognized the 5′ end of the LTR [26]. This result suggests that aptamers might be selected to recognize the damaged ends of double-strand breaks.

## 3. Aptamers for Repair Proteins

Cells have unique molecular pathways to correct common types of DNA damage. The major pathways include non-homologous end joining, homologous recombination, mismatch repair, nucleotide excision repair, base excision repair and direct repair [39]. Below, the aptamers that bind to the repair proteins that mediate these repair pathways are described. The repair mechanisms and proteins involved in each pathway have been extensively reviewed by others (see for example [40,41]); however, a short overview is also provided. To our knowledge, there are no aptamers available for the components of homologous recombination repair pathways. Furthermore, there are no aptamers that specifically interact with proteins from transcription-coupled repair (TC-NER) involving the transcription factor TFIIH. However, a recent review describes many aptamers that bind to the transcription factor, TFIIA [42]. This suggests that the TC-NER pathway may be a suitable target for future aptamer development.

### *3.1. Non-Homologous End Joining*

Double-strand breaks (DSBs) are repaired by the non-homologous end joining (NHEJ) and homologous recombination repair (HR) pathways. While the HR pathways require a homologous template, the NHEJ pathway repairs DSBs by directly ligating the ends. There are at least two genetically distinct sub-pathways of NHEJ: the classical-NHEJ (C-NHEJ) and alternative-NHEJ (A-NHEJ). The C-NHEJ pathway requires at least seven different proteins [43]. Two of these proteins, Ku70 and Ku86, form a heterodimer that functions as a molecular scaffold for the other NHEJ proteins to bind and initiate repair [44,45].

The first example of aptamer selection for a repair protein was performed in 1998 to the important scaffolding protein Ku. Here, Yoo et al. performed electrophoretic mobility shift assay (EMSA)–SELEX using an RNA library against the dimeric Ku protein purified from HeLa cell extracts. Their selection yielded 18 individual aptamers, each binding to the Ku protein with dissociation constants below

2 nM [27]. Excitingly, four of the aptamers were sufficiently selective that they were able to bind to the Ku protein in crude Hela cell extracts. Furthermore, these aptamers inhibited the binding and catalytic activity of the DNA dependent protein kinase catalytic subunit (DNA-PK), which is normally recruited to broken ends of DNA by the Ku protein [27].

### 3.2. Base Excision Repair

The base excision repair (BER) pathway is responsible for repairing small, non-helix-distorting damaged bases. BER is initiated by DNA glycosylases that recognize and remove the damaged base, creating an abasic site (AP site). Next, an AP endonuclease cleaves the AP site, and DNA polymerase β (polβ) removes the resulting 5′-deoxyribose phosphate via its 5′ to 3′ nuclease activity. Finally, the gap is filled by either short-patch (polβ replaces a single nucleotide) or long-patch BER (2–10 nucleotides are newly synthesized) [46,47].

There are currently two known examples of aptamers selected to BER-related proteins. First, as a proof-of-concept study, the Beal lab selected RNA aptamers to formamidopyrimidine DNA glycosylase (Fpg). Fpg (also known as 8-oxoguanine DNA glycosylase) is found in bacteria and repairs a wide range of oxidized purines. In this work, Vuyisich et al. used conventional SELEX with Fpg isolated from *E. coli* as the target. However, the authors were interested in isolating ligand-induced binding aptamers (i.e., those that only bind to the target in certain conditions). Therefore, the selections included a range of neomycin concentrations. As a result, the emerging aptamers could only bind to the target, Fpg, in the presence of the antibiotic, neomycin. Regardless, the best aptamer displayed high affinity to this repair protein, with a reported $K_d$ of 7.5 nM [28]. Next, in 2006, Gening and co-workers performed seven rounds of selection to uncover RNA aptamers that bind to polβ isolated from *E. coli*. Upon further characterization, these aptamers bound to polβ with $K_d$ values as low as 290 nM. Unfortunately, the aptamers did not display high specificity, binding also to polκ with similar affinity ($K_d$ = 410 nM). More impressively, the aptamers were able to inhibit the activity of both polymerases in primer extension assays [29], highlighting potential applications for these aptamers.

### 3.3. Mismatch Repair

Mismatches in the genome can occur due to mis-incorporation during the replication process, or as a result of chemical damage to a complementary nucleobase. If the mismatches are not removed by the proofreading activities of the replisome, then the post-replicative "Mismatch Repair System" (MMRS) is activated. For simplicity, the process in *E. coli* is described; however, homologues of all these proteins are found in eukaryotes. This process is initiated by MutS, a protein that recognizes and binds to mispaired nucleotides. MutS then works together with MutL to direct the excision of the newly synthesized DNA strand by MutH [48]. This is followed by removal of the mismatch and subsequent re-synthesis by DNA polymerases [49].

The Krylov group has been using non-equilibrium capillary electrophoresis of equilibrium mixtures (NECEEM) SELEX [50] to identify many aptamers to various repair proteins. In 2006, NECEEM was first used to select aptamers to MutS from *Thermus aquaticus*. The isolated aptamers displayed dissociation constants as low as 3.6 nM to the isolated protein [30]. Other selections by the Krylov group have focused on DNA dealkylating proteins (see below).

### 3.4. Direct Repair

The simplest form of repairing DNA damage is direct repair, because cleavage of the phosphodiester backbone is not required. As a result, highly specialized proteins are involved for each type of damage [51]. Direct reversal is primarily used for correcting damage caused by DNA alkylating agents. For example, $O^6$-alkylguanine DNA alkyltransferase (AGT) is known to specifically reverse $O^6$-methylguanine back to guanine. As another example, the repair protein AlkB directly repairs $N^1$-methyladenine and $N^3$-methylcytosine base lesions [52,53].

In 2011, the Krylov group selected DNA aptamers using the NECEEM SELEX platform to the AlkB protein isolated from *E. coli*. The resulting aptamers displayed $K_d$ values in the nanomolar range (as low as 20 nM) [31]. Later, these aptamers were shown to also inhibit AlkB activity by binding through an allosteric mechanism [54]. Next, the Krylov group was interested in obtaining aptamers to the human repair protein homologue, AlkB homologue 2 (ABH2). Original attempts failed due to challenges with the target (including instability and high positive charge). However, in 2014, NECEEM was coupled to emulsion PCR to efficiently amplify potential sequences. As a result, aptamers were isolated within three rounds that bound specifically to ABH2 with $K_d$ values as low as 85 nM [32].

## 4. Aptamers That Recognize Mutated Gene Products

If DNA adducts are not repaired, mutations accumulate in the genome. When these mutations occur in oncogenes or tumor suppressor genes, it is possible that the mutations confer a growth advantage (driver mutations), thus resulting in the promotion of cancer [55]. Hot spot mutations may arise from either potentially damage-prone or repair-inaccessible locations in the genome. Ongoing research aims to determine the exact mechanism behind this selection preference [56]. Such mutations occur in tumor samples more frequently than the background [57], and have been identified in several genes. As a result, these mutated gene products provide some of the best-studied targets for chemotherapy [57], which explains why there have been some efforts towards isolating aptamers for these cancer driver gene products.

Codon 12 of the *KRAS* gene is the most frequently mutated codon in human cancers. As a result, many aptamers have been generated to mutant KRAS proteins and peptides [58,59]. In the most recent example, an RNA aptamer was generated that specifically bound to a mutant KRAS protein with a point mutation in codon 12 ($KRAS^{V12}$). Excitingly, binding to the wild-type KRAS was more than 50 fold lower than the mutant [33]. A second example is the *p53* gene which is considered the "guardian of the genome". *p53* is lost or mutated in about half of human cancer cases [60,61]. The single amino acid substitution p53R175H is one mutation which abolishes p53 function. In 2015, Chen et al. were able to isolate an RNA aptamer that binds to the p53 mutant p53R175H. Remarkably, this RNA aptamer (p53R175H-APT) also displayed a significantly stronger affinity to p53R175H than to the wild-type p53 in both in vitro and in vivo assays [62].

## 5. Selection Challenges and Considerations

The SELEX process involves iterative rounds of in vitro binding, partitioning and amplification (Figure 3) [63–65]. Despite the simplicity, a major advantage of the process is the flexibility in the enrichment strategy, binding conditions and nucleic acids design and type [66,67]. Due to this flexibility, aptamers have been selected to a wide range of targets, including whole cells, viruses, proteins and small molecules [68]. For reviews on the many modifications and improvements to the SELEX procedure over the past 25 years, see [69–71]. Here, conditions specific to DNA damage and repair targets are highlighted.

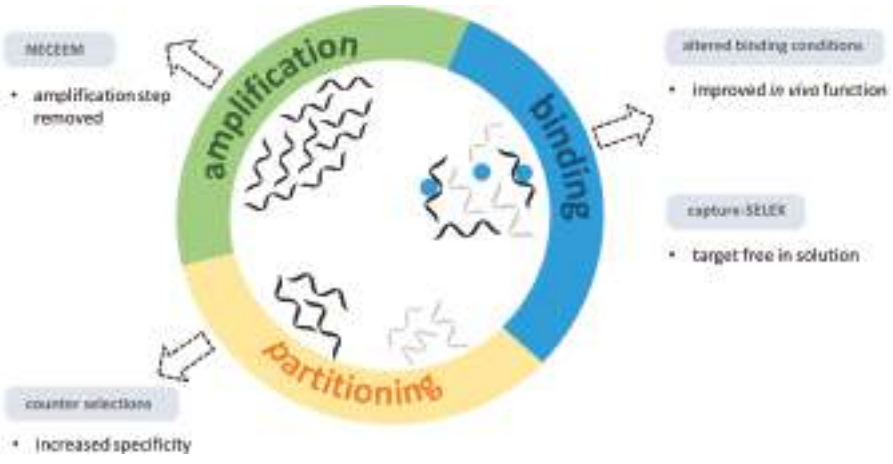


**Figure 3.** Conceptual representation of classic Systematic Evolution of Ligands by EXponential enrichment (SELEX) and important modifications. Classic SELEX consists of iterative rounds of binding, partitioning and PCR amplification. Single-stranded DNA or RNA libraries are incubated with the target-of-interest (blue circles). A partitioning step removes non-specific sequences (light grey strands). PCR amplification is then used to make multiple copies of the selected sequences (dark grey). Modifications to the classic SELEX process to isolate aptamers for DNA damage and repair targets include: the use of "capture-SELEX" for small molecules allowing them to be selected without immobilization; altered binding conditions to improve binding to strand breaks and improving activity in vivo; rigorous counter selection to ensure binding specificity; and the use of NECEEM for difficult protein targets.

### *5.1. DNA Adducts*

The nucleobases of DNA have molecular weights ranging from approximately 110–150 g/mol. Nucleosides range from 240–285 g/mol, and nucleotides are around 500 g/mol. As a result, the selection targets for DNA damage aptamer libraries are very small, and therefore pose some of the same challenges as small molecule SELEX. Several reviews and methods highlight the conceptual and technical challenges in isolating aptamers to targets of less than 1000 g/mol [11,72]. This explains, in part, the relatively small number of different DNA adduct aptamers as compared to repair proteins, and is consistent with the general trend of fewer small molecule aptamers as compared to aptamers to large targets such as proteins and even cells [68].

The biggest potential break-through in addressing the challenges associated with small molecule aptamer selection was the development of Capture-SELEX, which yields structure-switching aptamers [73]. This method circumvents the needs to immobilize small molecules on a solid-support and further introduces a selection pressure for the selected aptamers to undergo a large structural rearrangement upon binding to the target. This feature is often desired in development detection applications with aptamers [74]. As a result, future aptamer selection efforts to damaged nucleobases and nucleosides should make further use of the Capture-SELEX strategy.

### *5.2. Strand Breaks*

Overcoming electrostatic repulsion of the sugar–phosphate backbone of DNA typically requires the alteration of binding conditions in the selection of aptamers. This may include high concentrations of cations (to shield the charge), lowering the selection pH or adding triplex-stabilizing agents. However, a relatively unexplored strategy is the incorporation of non-natural nucleotides. One potential option would be the use of peptide nucleic acids (PNA), where the negatively charged

phosphate backbone is replaced by a neutral amide backbone [75]. As a result, PNA can selectively bind and invade the DNA duplex [76]. There are several examples of DNA aptamers being synthesized as PNA or developing aptamer-PNA conjugates [77]. Furthermore, the Liu lab has described an in vitro selection and amplification system for peptide nucleic acids [78]. Therefore, future efforts should evaluate the use of PNA to improve the binding affinity and specificity of detecting strand breaks.

### 5.3. Proteins

There are several methods available for selecting aptamers to protein targets; each possessing their own unique advantages and difficulties. Regardless of the method employed, the most important consideration for aptamers in applications involving DNA damage and repair is ensuring specificity. This is particularly critical for targeting both repair proteins and mutated gene products. In the selections described for mutated genes (Section 4), counter selection rounds were imperative to ensure that the resulting aptamers did not bind to the non-mutated, wild-type proteins. Without including these counter measures, it is possible that the aptamers would also recognize and bind to the wild-type proteins. For example, in the polβ selection (Section 3.2), counter selections were not performed. As a result, the aptamers were able to additionally bind and inhibit polκ, a polymerase from a different family. Therefore, highly stringent counter selection steps should be performed to ensure the specificity of the isolated aptamers.

## 6. Promising Applications

There is a disproportionately large number of publications and patents describing aptamer applications compared to the number of publications describing new aptamers [79]. This trend is consistent across most areas of aptamer research including food safety [80], neuroscience [81], medicine [82] and gene control [83]. In contrast, the opposite appears to be true in the field of DNA damage and repair; there are fewer examples of aptamer applications compared to the number of selections (Table 1). Here, some of the promising future applications are described (Figure 4). The challenges that must be addressed to make these potential applications a reality are summarized.

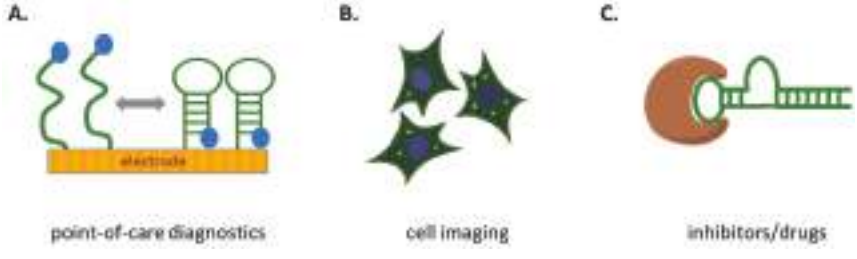


**Figure 4.** Conceptual figure highlighting potential applications of aptamers for DNA damage and repair. (**A**) Aptamers (green strands) could be incorporated into several platforms to create rapid analysis or point-of-care diagnostic kits to measured DNA lesion levels; (**B**) Aptamers combined with RNA tools such as "Spinach" could replace antibodies in cell imaging (allowing fluorescent imaging (bright dots) of damage/ repair proteins inside cells); (**C**) Highly specific aptamers (green strand) that inhibit repair proteins and polymerases (brown shape) could be used in cancer treatment and gene therapy.

### 6.1. Diagnostics

The detection of DNA adducts poses a major analytical challenge due to their very low abundance in genomic samples. As a result, methods must be both very sensitive and highly specific [84]. DNA lesion investigations from the 1980s were typically accomplished using the $^{32}$P-postlabeling methodology. This method was capable of detecting lesions at frequencies as

low as one lesion in $10^{10}$ nucleotides [85]. More recently, mass spectrometry (MS) coupled with liquid chromatography–electrospray ionization spectrometry (ESI-LC-MS) has been employed [86], and can currently be used to detect one lesion per $10^8$–$10^9$ nucleotides. Regardless, these methods require significant quantities of purified DNA for quantifications. As a result, there have been several recent efforts toward specifically amplifying DNA adducts or mapping adducts within a genome. As an example, the Sturla group has developed a strategy to PCR-amplify DNA adducts of interest using mutated polymerases capable of specifically incorporating non-natural nucleosides [87]. As another example, the Burrows group has applied nanopore sequencing, and developed a biotin-labelling strategy to enrich and sequence oxidative damage [88,89]. These strategies are powerful, yet time-consuming and costly. Therefore, there is still an unmet need for simple, inexpensive methods that could be used as point-of-care diagnostic tools for decision-making about further DNA damage testing. Aptamers have been readily incorporated into nanoparticle- [90] and electrochemical-based [91] platforms to create point-of-care diagnostics. Therefore, the aptamers described in Table 1, could be easily used to rapidly screen or test for target DNA adducts.

### 6.2. Cellular Imaging

Immunofluorescent staining of DNA damage and the damage response has led to several important insights into DNA repair processes [92]. However, antibody staining must be performed after fixing of tissue or cell samples [93], and therefore cannot capture real-time or dynamic repair information. To image real-time processes inside cells, Jaffrey and co-workers developed "Spinach", another breakthrough aptamer technology [94]. Spinach, and several newer variants, is an RNA aptamer capable of specifically binding to a small molecule dye. Only upon interaction with the RNA aptamer does the dye fluoresce, creating a "light-up aptamer". These RNA aptamers have been encoded in the genomes of bacteria, yeast and mammalian cells to quantify, image and track specific RNA molecules in real-time [95,96]. More importantly, the Spinach aptamer can be directly coupled to a second aptamer, creating a system where fluorescence is observed only in the presence of the aptamer's target [97]. As a result, metabolites have been imaged and quantified in live cells (see review [98]). Therefore, it is feasible that the same strategy could be applied to imaging and quantification of DNA adducts and repair proteins in live cells and whole animals.

### 6.3. Therapeutic Targets

With several candidates in the clinical pipeline, aptamers have gained therapeutic visibility [99]. Aptamers have been used to impair cancer development, inflammatory disease, viral infection and cardiovascular illness [99]. However, the most successful example continues to be Pegaptanib, a vascular endothelial growth factor antagonist aptamer which was approved in 2004 for treatment of age-related macular degeneration [100]. Recently, aptamer applications in therapeutics have focused on cancer drugs and targeted drug delivery [101]. The aptamers described in this review could be leveraged for these applications.

In particular, alkylating agents are commonly used in chemotherapy due to their ability to cause DNA damage-induced apoptosis [102]. However, the efficiency of chemotherapeutic agents is strongly reduced by DNA repair systems. Aptamers that bind to the active site of repair proteins or polymerases involved in repair could be used to specifically inhibit their activities in cells [54]. This is a particularly exciting application for aptamers, compared to antibodies, given that aptamers are sufficiently small to fit inside tight binding pockets [27]. As one example, the aptamer selected by the Krylov group, not only bound to the NER repair protein AlkB, but also was capable of efficiently inhibiting catalysis at nanomolar concentrations [31].

As another possible direction, aptamers could be used to target specific cells or "turn on" drug activity in the presence of altered repair processes. It is known that repair processes are altered in cancer cells and that DNA damage and defects in DNA repair can both cause cancer [103]. Certainly, aptamers that recognize cancer cell surface proteins may be useful in delivering DNA damaging

chemotherapeutics or DNA repair inhibitors. Alternatively, typical mutated proteins arising from DNA damage (or lack of repair) may be useful for ensuring chemotherapeutics are successfully distributed and/or activated once inside their target cells (in this case, cells that indicate increased DNA damage or altered repair). For example, the aptamer that binds to the mutated p53 protein was only able to interact with the mutated protein in cancer cells in vitro as well as in tumor xenografts [62], and had no impact on the wild-type p53 protein. Therefore, it is feasible that aptamers that bind to mutated gene products could be loaded with drugs that target repair processes, providing a means to target cells that are either cancerous or that may lead to further damage and mutation.

### 6.4. Application Roadblocks

Despite the exciting potential, it is clear that there have been very limited demonstrations of using aptamers in DNA damage and repair applications. This lack of utility is likely due to several technical and conceptual challenges. For diagnostic applications, perhaps the biggest roadblock is that there is still much to learn concerning the quantitative importance of DNA damage. For example, the linear dose response for genotoxicant-induced gene mutations and chromosomal damage has been challenged [104]. Furthermore, there is a gap in our understanding of the link between sequence-specific DNA adducts and mutational patterns [56,105,106]. Until these questions are addressed, it is not clear if there is a need for rapid point-of-care diagnostics or testing DNA adducts as a biomarkers in disease.

In contrast, cellular imaging with aptamers is a much-needed application, particularly in the field of DNA damage and repair. However, this application has only been very recently demonstrated. It is likely "only a matter of time" before in vivo or cellular imaging of DNA damage and repair processes with aptamers are demonstrated. One challenge is the internalization of the cellular imaging probes. However, researchers have developed many clever transport and delivery strategies to overcome this hurdle (see review [98]), and thus it is no longer a critical issue. However, a bottleneck that has not been tested with this set of aptamers is the in vivo activity. Unfortunately, many of the available aptamers were selected in conditions that are not physiologically relevant. In particular, many aptamers were selected using high concentrations of magnesium. This can be a limitation when genetically-encoding or delivering aptamers into the cellular environment, where free magnesium is much less abundant [107]. Therefore, it is possible that additional aptamer selections, under physiologically relevant conditions, may be needed to enable the successful use of aptamers in cellular imaging of DNA damage and repair.

The majority of the aptamers selected for DNA damage and repair proteins used proof-of-concept targets, including prokaryotic versions of repair proteins. These aptamers would not be useful for therapeutic applications (as they likely do not bind to the human orthologues), but demonstrate the potential for future aptamer selections targeting human repair proteins. In general, the main challenge in applying aptamers that recognize DNA damage and repair targets to therapeutic applications are the same obstacles for all aptamer therapeutic targets. These challenges include efficient internalization of the aptamers into the cell (and nucleus), off-target binding, half-life and stability in vivo and renal clearance. These difficulties, in combination with a general reluctance to divert from conventional antibody-based approaches, account for the long delay in the clinical translation and distribution of therapeutic aptamers [99]. As the number of aptamer modifications increases, these challenges will no longer hinder the therapeutic use of aptamers in general. Subsequently, it is expected that the therapeutic applications for aptamers targeting DNA damage and repair processes will also improve.

## 7. Conclusions

There are few examples of aptamers that bind to DNA adducts or modified nucleic acids, damage repair proteins and mutated gene products involved in carcinogenesis. However, there are many targets for which future aptamer selection would be beneficial. For example, there are no aptamers that bind to damage resulting from deamination or crosslinking. Furthermore,

aptamers could be selected for a long list of repair proteins, including those involved in the NER and HR pathways. Despite the potential, direct evidence of the utility of aptamers in the field of DNA damage and repair is currently limited. Therefore, demonstration of these exciting potential applications should be performed. It is expected that several ongoing advances in the field of aptamers, particularly in the context of targeted therapeutics, will help address current challenges limiting the applications of aptamers in DNA damage and repair. Ultimately, this may motivate the researchers to undertake additional selections to increase the list of aptamers that bind to DNA adducts and repair proteins.

**Acknowledgments:** The author thanks Shana Sturla for support and insight. This work was supported by the Swiss National Science Foundation.

**Conflicts of Interest:** The author declares no conflict of interest. The founding sponsors had no role in the design of the study; in the collection, analyses, or interpretation of data; in the writing of the manuscript, and in the decision to publish the results.

## Abbreviations

| | |
|---|---|
| ABH2 | AlkB homologue 2 |
| AGT | $O^6$-alkylguanine DNA alkyltransferase |
| BER | Base excision repair |
| BIQ | Benzoindoloquinoline |
| bp | Base pair |
| DSB | Double-strand break |
| dsDNA | Double-strand DNA |
| EMSA | Electrophoretic mobility shift assay |
| Fpg | Formamidopyrimidine DNA glycosylase |
| GA | Glycidamide |
| HR | Homologous recombination |
| $K_d$ | Dissociation constant |
| LTR | Long terminal repeat |
| $m^7$-GTP | 7-methylguanosine 5′-triphosphate |
| NECEEM | Non-equilibrium capillary electrophoresis of equilibrium mixtures |
| NER | Nucleotide excision repair |
| NHEJ | Non non-homologous end joining |
| N7-meG | $N^7$-methylguanine |
| 8-oxoG | 8-oxoguanine |
| PNA | Peptide nucleic acid |
| SELEX | Systematic evolution of ligands by EXPonential enrichment |
| Sp | Spiroiminodihydantoin |

## References

1. Lindahl, T.; Andersson, A. Rate of chain breakage at apurinic sites in double-stranded deoxyribonucleic acid. *Biochemistry* **1972**, *11*, 3618–3623. [CrossRef] [PubMed]
2. Lindahl, T.; Nyberg, B. Rate of depurination of native deoxyribonucleic acid. *Biochemistry* **1972**, *11*, 3610–3618. [CrossRef] [PubMed]
3. Lindahl, T.; Nyberg, B. Heat-induced deamination of cytosine residues in deoxyribonucleic acid. *Biochemistry* **1974**, *13*, 3405–3410. [CrossRef] [PubMed]
4. Knoch, J.; Kamenisch, Y.; Kubisch, C.; Berneburg, M. Rare hereditary diseases with defects in DNA-repair. *Eur. J. Dermatol.* **2012**, *22*, 443–455. [PubMed]
5. Leone, G.; Pagano, L.; Ben-Yehuda, D.; Voso, M.T. Therapy-related leukemia and myelodysplasia: Susceptibility and incidence. *Haematologica* **2007**, *92*, 1389–1398. [CrossRef] [PubMed]
6. Wood, M.E.; Vogel, V.; Ng, A.; Foxhall, L.; Goodwin, P.; Travis, L.B. Second malignant neoplasms: Assessment and strategies for risk reduction. *J. Clin. Oncol.* **2012**, *30*, 3734–3745. [CrossRef] [PubMed]

7. Santella, R.M.; Yang, X.Y.; Hsieh, L.L.; Young, T.L. Immunologic methods for the detection of carcinogen adducts in humans. *Prog. Clin. Biol. Res.* **1990**, *340C*, 247–257. [PubMed]
8. Shia, J.; Ellis, N.A.; Klimstra, D.S. The utility of immunohistochemical detection of DNA mismatch repair gene proteins. *Virchows Arch.* **2004**, *445*, 431–441. [CrossRef] [PubMed]
9. Chen, A.; Yang, S. Replacing antibodies with aptamers in lateral flow immunoassay. *Biosens. Bioelectron.* **2015**, *71*, 230–242. [CrossRef] [PubMed]
10. Toh, S.Y.; Citartan, M.; Gopinath, S.C.; Tang, T.H. Aptamers as a replacement for antibodies in enzyme-linked immunosorbent assay. *Biosens. Bioelectron.* **2015**, *64*, 392–403. [CrossRef] [PubMed]
11. McKeague, M.; Derosa, M.C. Challenges and opportunities for small molecule aptamer development. *J. Nucleic Acids* **2012**, *2012*, 748913. [CrossRef] [PubMed]
12. Voskuil, J.L. The challenges with the validation of research antibodies. *F1000Research* **2017**, *6*, 161. [CrossRef] [PubMed]
13. Suzuki, T.; Kamiya, H. Mutations induced by 8-hydroxyguanine (8-oxo-7,8-dihydroguanine), a representative oxidized base, in mammalian cells. *Genes Environ.* **2017**, *39*, 2. [CrossRef] [PubMed]
14. Fleming, A.M.; Ding, Y.; Burrows, C.J. Sequencing DNA for the oxidatively modified base 8-oxo-7,8-dihydroguanine. *Methods Enzymol.* **2017**, *591*, 187–210. [PubMed]
15. Alenko, A.; Fleming, A.M.; Burrows, C.J. Reverse transcription past products of guanine oxidation in rna leads to insertion of a and c opposite 8-oxo-7,8-dihydroguanine and a and g opposite 5-guanidinohydantoin and spiroiminodihydantoin diastereomers. *Biochemistry* **2017**, *56*, 5053–5064. [CrossRef] [PubMed]
16. Rink, S.M.; Shen, J.C.; Loeb, L.A. Creation of rna molecules that recognize the oxidative lesion 7,8-dihydro-8-hydroxy-2′-deoxyguanosine (8-oxodg) in DNA. *Proc. Natl. Acad. Sci. USA* **1998**, *95*, 11619–11624. [CrossRef] [PubMed]
17. Miyachi, Y.; Shimizu, N.; Ogino, C.; Fukuda, H.; Kondo, A. Selection of a DNA aptamer that binds 8-ohdg using gmp-agarose. *Bioorg. Med. Chem. Lett.* **2009**, *19*, 3619–3622. [CrossRef] [PubMed]
18. Zhang, Q.; Wang, Y.; Meng, X.; Dhar, R.; Huang, H. Triple-stranded DNA containing 8-oxo-7,8-dihydro-2′-deoxyguanosine: Implication in the design of selective aptamer sensors for 8-oxo-7,8-dihydroguanine. *Anal. Chem.* **2013**, *85*, 201–207. [CrossRef] [PubMed]
19. Roy, J.; Chirania, P.; Ganguly, S.; Huang, H. A DNA aptamer sensor for 8-oxo-7,8-dihydroguanine. *Bioorg. Med. Chem. Lett.* **2012**, *22*, 863–867. [CrossRef] [PubMed]
20. Stoltenburg, R.; Nikolaus, N.; Strehlitz, B. Capture-selex: Selection of DNA aptamers for aminoglycoside antibiotics. *J. Anal. Methods Chem.* **2012**, *2012*, 415697. [CrossRef] [PubMed]
21. Ghude, P.; Burrows, C.J. Structure-Switching Selex for Selection of Aptamers of Damaged Nucleosides and Nucleobases 8-Oxoguanine and Spiroiminodihydantoin. Ph.D. Thesis, The University of Utah, Salt Lake City, UT, USA, 2015.
22. Haller, A.A.; Sarnow, P. In vitro selection of a 7-methyl-guanosine binding rna that inhibits translation of capped mrna molecules. *Proc. Natl. Acad. Sci. USA* **1997**, *94*, 8521–8526. [CrossRef] [PubMed]
23. Xu, J.; Carrocci, T.J.; Hoskins, A.A. Evolution and characterization of a benzylguanine-binding rna aptamer. *Chem. Commun.* **2016**, *52*, 549–552. [CrossRef] [PubMed]
24. Soukup, G.A.; Ellington, A.D.; Maher, L.J., III. Selection of rnas that bind to duplex DNA at neutral ph. *J. Mol. Biol.* **1996**, *259*, 216–228. [CrossRef] [PubMed]
25. Ayel, E.; Escude, C. In vitro selection of oligonucleotides that bind double-stranded DNA in the presence of triplex-stabilizing agents. *Nucleic Acids Res.* **2010**, *38*, e31. [CrossRef] [PubMed]
26. Srisawat, C.; Engelke, D.R. Selection of RNA aptamers that bind hiv-1 ltr DNA duplexes: Strand invaders. *Nucleic Acids Res.* **2010**, *38*, 8306–8315. [CrossRef] [PubMed]
27. Yoo, S.; Dynan, W.S. Characterization of the RNA binding properties of ku protein. *Biochemistry* **1998**, *37*, 1336–1343. [CrossRef] [PubMed]
28. Vuyisich, M.; Beal, P.A. Controlling protein activity with ligand-regulated RNA aptamers. *Chem. Biol.* **2002**, *9*, 907–913. [CrossRef]
29. Gening, L.V.; Klincheva, S.A.; Reshetnjak, A.; Grollman, A.P.; Miller, H. Rna aptamers selected against DNA polymerase beta inhibit the polymerase activities of DNA polymerases beta and kappa. *Nucleic Acids Res.* **2006**, *34*, 2579–2586. [CrossRef] [PubMed]
30. Drabovich, A.P.; Berezovski, M.; Okhonin, V.; Krylov, S.N. Selection of smart aptamers by methods of kinetic capillary electrophoresis. *Anal. Chem.* **2006**, *78*, 3171–3178. [CrossRef] [PubMed]

31. Krylova, S.M.; Karkhanina, A.A.; Musheev, M.U.; Bagg, E.A.; Schofield, C.J.; Krylov, S.N. DNA aptamers for as analytical tools for the quantitative analysis of DNA-dealkylating enzymes. *Anal. Biochem.* **2011**, *414*, 261–265. [CrossRef] [PubMed]
32. Yufa, R.; Krylova, S.M.; Bruce, C.; Bagg, E.A.; Schofield, C.J.; Krylov, S.N. Emulsion pcr significantly improves nonequilibrium capillary electrophoresis of equilibrium mixtures-based aptamer selection: Allowing for efficient and rapid selection of aptamer to unmodified ABH2 protein. *Anal. Chem.* **2015**, *87*, 1411–1419. [CrossRef] [PubMed]
33. Jeong, S.; Han, S.R.; Lee, Y.J.; Kim, J.H.; Lee, S.W. Identification of rna aptamer specific to mutant kras protein. *Oligonucleotides* **2010**, *20*, 155–161. [CrossRef] [PubMed]
34. Fu, D.; Calvo, J.A.; Samson, L.D. Balancing repair and tolerance of DNA damage caused by alkylating agents. *Nat. Rev. Cancer* **2012**, *12*, 104–120. [CrossRef] [PubMed]
35. Kiga, D.; Futamura, Y.; Sakamoto, K.; Yokoyama, S. An RNA aptamer to the xanthine/guanine base with a distinctive mode of purine recognition. *Nucleic Acids Res.* **1998**, *26*, 1755–1760. [CrossRef] [PubMed]
36. Larguinho, M.; Santos, S.; Almeida, J.; Baptista, P.V. DNA adduct identification using gold-aptamer nanoprobes. *IET Nanobiotechnol.* **2015**, *9*, 95–101. [CrossRef] [PubMed]
37. Wyss, L.A.; Nilforoushan, A.; Eichenseher, F.; Suter, U.; Blatter, N.; Marx, A.; Sturla, S.J. Specific incorporation of an artificial nucleotide opposite a mutagenic DNA adduct by a DNA polymerase. *J. Am. Chem. Soc.* **2015**, *137*, 30–33. [CrossRef] [PubMed]
38. Scharer, O.D. Chemistry and biology of DNA repair. *Angew. Chem. Int. Ed. Engl.* **2003**, *42*, 2946–2974. [CrossRef] [PubMed]
39. Dexheimer, T.S. DNA repair pathways and mechanisms. In *DNA Repair of Cancer Stem Cells*; Mathews, L.A., Cabarcas, S.M., Hurt, E.M., Eds.; Springer: Dordrecht, The Netherlands, 2013; pp. 19–32.
40. Chatterjee, N.; Walker, G.C. Mechanisms of DNA damage, repair, and mutagenesis. *Environ. Mol. Mutagen.* **2017**, *58*, 235–263. [CrossRef] [PubMed]
41. Pei, D.S.; Strauss, P.R. Zebrafish as a model system to study DNA damage and repair. *Mutat. Res.* **2013**, *743–744*, 151–159. [CrossRef] [PubMed]
42. Mondragon, E.; Maher, L.J., III. Anti-transcription factor RNA aptamers as potential therapeutics. *Nucleic Acid Ther.* **2016**, *26*, 29–43. [CrossRef] [PubMed]
43. Fattah, F.; Lee, E.H.; Weisensel, N.; Wang, Y.; Lichter, N.; Hendrickson, E.A. Ku regulates the non-homologous end joining pathway choice of DNA double-strand break repair in human somatic cells. *PLoS Genet.* **2010**, *6*, e1000855. [CrossRef] [PubMed]
44. Wang, H.; Xu, X. Microhomology-mediated end joining: New players join the team. *Cell Biosci.* **2017**, *7*, 6. [CrossRef] [PubMed]
45. Durdikova, K.; Chovanec, M. Regulation of non-homologous end joining via post-translational modifications of components of the ligation step. *Curr. Genet.* **2016**, *63*, 591–605. [CrossRef] [PubMed]
46. Beard, W.A.; Prasad, R.; Wilson, S.H. Activities and mechanism of DNA polymerase beta. *Methods Enzymol.* **2006**, *408*, 91–107. [PubMed]
47. Idriss, H.T.; Al-Assar, O.; Wilson, S.H. DNA polymerase beta. *Int. J. Biochem. Cell Biol.* **2002**, *34*, 321–324. [CrossRef]
48. Fishel, R. Mismatch repair. *J. Biol. Chem.* **2015**, *290*, 26395–26403. [CrossRef] [PubMed]
49. Li, G.M. Mechanisms and functions of DNA mismatch repair. *Cell Res.* **2008**, *18*, 85–98. [CrossRef] [PubMed]
50. Musheev, M.U.; Krylov, S.N. Selection of aptamers by systematic evolution of ligands by exponential enrichment: Addressing the polymerase chain reaction issue. *Anal. Chim. Acta* **2006**, *564*, 91–96. [CrossRef] [PubMed]
51. Yi, C.; He, C. DNA repair by reversal of DNA damage. *Cold Spring Harb. Perspect. Biol.* **2013**, *5*, a012575. [CrossRef] [PubMed]
52. Johannessen, T.C.; Prestegarden, L.; Grudic, A.; Hegi, M.E.; Tysnes, B.B.; Bjerkvig, R. The DNA repair protein alkbh2 mediates temozolomide resistance in human glioblastoma cells. *Neuro Oncol.* **2013**, *15*, 269–278. [CrossRef] [PubMed]
53. Yi, C.; Chen, B.; Qi, B.; Zhang, W.; Jia, G.; Zhang, L.; Li, C.J.; Dinner, A.R.; Yang, C.G.; He, C. Duplex interrogation by a direct DNA repair protein in search of base damage. *Nat. Struct. Mol. Biol.* **2012**, *19*, 671–676. [CrossRef] [PubMed]

54. Krylova, S.M.; Koshkin, V.; Bagg, E.; Schofield, C.J.; Krylov, S.N. Mechanistic studies on the application of DNA aptamers as inhibitors of 2-oxoglutarate-dependent oxygenases. *J. Med. Chem.* **2012**, *55*, 3546–3552. [CrossRef] [PubMed]
55. Tokheim, C.J.; Papadopoulos, N.; Kinzler, K.W.; Vogelstein, B.; Karchin, R. Evaluating the evaluation of cancer driver genes. *Proc. Natl. Acad. Sci. USA* **2016**, *113*, 14330–14335. [CrossRef] [PubMed]
56. Adar, S.; Hu, J.; Lieb, J.D.; Sancar, A. Genome-wide kinetics of DNA excision repair in relation to chromatin state and mutagenesis. *Proc. Natl. Acad. Sci. USA* **2016**, *113*, E2124–E2133. [CrossRef] [PubMed]
57. Chang, M.T.; Asthana, S.; Gao, S.P.; Lee, B.H.; Chapman, J.S.; Kandoth, C.; Gao, J.; Socci, N.D.; Solit, D.B.; Olshen, A.B.; et al. Identifying recurrent mutations in cancer reveals widespread lineage diversity and mutational specificity. *Nat. Biotechnol.* **2016**, *34*, 155–163. [CrossRef] [PubMed]
58. Gilbert, B.A.; Sha, M.; Wathen, S.T.; Rando, R.R. RNA aptamers that specifically bind to a k ras-derived farnesylated peptide. *Bioorg. Med. Chem.* **1997**, *5*, 1115–1122. [CrossRef]
59. Tanaka, Y.; Akagi, K.; Nakamura, Y.; Kozu, T. RNA aptamers targeting the carboxyl terminus of kras oncoprotein generated by an improved selex with isothermal rna amplification. *Oligonucleotides* **2007**, *17*, 12–21. [CrossRef] [PubMed]
60. Pfeifer, G.P.; Denissenko, M.F.; Olivier, M.; Tretyakova, N.; Hecht, S.S.; Hainaut, P. Tobacco smoke carcinogens, DNA damage and p53 mutations in smoking-associated cancers. *Oncogene* **2002**, *21*, 7435–7451. [CrossRef] [PubMed]
61. Hang, B. Formation and repair of tobacco carcinogen-derived bulky DNA adducts. *J. Nucleic Acids* **2010**, *2010*, 709521. [CrossRef] [PubMed]
62. Chen, L.; Rashid, F.; Shah, A.; Awan, H.M.; Wu, M.; Liu, A.; Wang, J.; Zhu, T.; Luo, Z.; Shan, G. The isolation of an rna aptamer targeting to p53 protein with single amino acid mutation. *Proc. Natl. Acad. Sci. USA* **2015**, *112*, 10002–10007. [CrossRef] [PubMed]
63. Tuerk, C.; Gold, L. Systematic evolution of ligands by exponential enrichment: RNA ligands to bacteriophage t4 DNA polymerase. *Science* **1990**, *249*, 505–510. [CrossRef] [PubMed]
64. Ellington, A.D.; Szostak, J.W. In vitro selection of rna molecules that bind specific ligands. *Nature* **1990**, *346*, 818–822. [CrossRef] [PubMed]
65. Robertson, D.L.; Joyce, G.F. Selection in vitro of an RNA enzyme that specifically cleaves single-stranded DNA. *Nature* **1990**, *344*, 467–468. [CrossRef] [PubMed]
66. Jijakli, K.; Khraiwesh, B.; Fu, W.; Luo, L.; Alzahmi, A.; Koussa, J.; Chaiboonchoe, A.; Kirmizialtin, S.; Yen, L.; Salehi-Ashtiani, K. The in vitro selection world. *Methods* **2016**, *106*, 3–13. [CrossRef] [PubMed]
67. Sun, H.; Zu, Y. A highlight of recent advances in aptamer technology and its application. *Molecules* **2015**, *20*, 11959–11980. [CrossRef] [PubMed]
68. McKeague, M.; McConnell, E.M.; Cruz-Toledo, J.; Bernard, E.D.; Pach, A.; Mastronardi, E.; Zhang, X.; Beking, M.; Francis, T.; Giamberardino, A.; et al. Analysis of in vitro aptamer selection parameters. *J. Mol. Evol.* **2015**, *81*, 150–161. [CrossRef] [PubMed]
69. Djordjevic, M. Selex experiments: New prospects, applications and data analysis in inferring regulatory pathways. *Biomol. Eng.* **2007**, *24*, 179–189. [CrossRef] [PubMed]
70. Xi, Z.; Huang, R.; Deng, Y.; He, N. Progress in selection and biomedical applications of aptamers. *J. Biomed. Nanotechnol.* **2014**, *10*, 3043–3062. [CrossRef] [PubMed]
71. Catuogno, S.; Esposito, C.L. Aptamer cell-based selection: Overview and advances. *Biomedicines* **2017**, *5*, 49. [CrossRef] [PubMed]
72. Ruscito, A.; McConnell, E.M.; Koudrian, A.; Velu, R.; Mattic, C.; Hung, V.; McKeague, M.; DeRosa, M.C. In vitro selection and characterization of DNA aptamers to a small molecule target. *Curr. Protoc. Chem. Biol.* **2017**, *9*, 1–36.
73. Yang, K.A.; Pei, R.; Stojanovic, M.N. In vitro selection and amplification protocols for isolation of aptameric sensors for small molecules. *Methods* **2016**, *106*, 58–65. [CrossRef] [PubMed]
74. Nutiu, R.; Li, Y. Structure-switching signaling aptamers. *J. Am. Chem. Soc.* **2003**, *125*, 4771–4778. [CrossRef] [PubMed]
75. Nielsen, P.E.; Egholm, M.; Berg, R.H.; Buchardt, O. Sequence-selective recognition of DNA by strand displacement with a thymine-substituted polyamide. *Science* **1991**, *254*, 1497–1500. [CrossRef] [PubMed]

76. Peffer, N.J.; Hanvey, J.C.; Bisi, J.E.; Thomson, S.A.; Hassman, C.F.; Noble, S.A.; Babiss, L.E. Strand-invasion of duplex DNA by peptide nucleic acid oligomers. *Proc. Natl. Acad. Sci. USA* **1993**, *90*, 10648–10652. [CrossRef] [PubMed]
77. Scheibe, C.; Wedepohl, S.; Riese, S.B.; Dernedde, J.; Seitz, O. Carbohydrate-pna and aptamer-pna conjugates for the spatial screening of lectins and lectin assemblies. *Chembiochem* **2013**, *14*, 236–250. [CrossRef] [PubMed]
78. Brudno, Y.; Birnbaum, M.E.; Kleiner, R.E.; Liu, D.R. An in vitro translation, selection and amplification system for peptide nucleic acids. *Nat. Chem. Biol.* **2010**, *6*, 148–155. [CrossRef] [PubMed]
79. McKeague, M.; Derosa, M.C. Aptamers and selex: Tools for the development of transformative molecular recognition technology. *Aptamers Synth. Antib.* **2014**, *1*, 12–16.
80. McKeague, M.; Velu, R.; De Girolamo, A.; Valenzano, S.; Pascale, M.; Smith, M.; DeRosa, M.C. Comparison of in-solution biorecognition properties of aptamers against ochratoxin A. *Toxins* **2016**, *8*, 336. [CrossRef] [PubMed]
81. McConnell, E.M.; Holahan, M.R.; DeRosa, M.C. Aptamers as promising molecular recognition elements for diagnostics and therapeutics in the central nervous system. *Nucleic Acid Ther.* **2014**, *24*, 388–404. [CrossRef] [PubMed]
82. Kruspe, S.; Giangrande, P.H. Aptamer-sirna chimeras: Discovery, progress, and future prospects. *Biomedicines* **2017**, *5*, 45. [CrossRef] [PubMed]
83. Schneider, C.; Suess, B. Identification of rna aptamers with riboswitching properties. *Methods* **2016**, *97*, 44–50. [CrossRef] [PubMed]
84. Klaene, J.J.; Sharma, V.K.; Glick, J.; Vouros, P. The analysis of DNA adducts: The transition from (32)p-postlabeling to mass spectrometry. *Cancer Lett.* **2013**, *334*, 10–19. [CrossRef] [PubMed]
85. Phillips, D.H.; Arlt, V.M. Genotoxicity: Damage to DNA and its consequences. *EXS* **2009**, *99*, 87–110. [PubMed]
86. Guo, J.; Yun, B.H.; Upadhyaya, P.; Yao, L.; Krishnamachari, S.; Rosenquist, T.A.; Grollman, A.P.; Turesky, R.J. Multiclass carcinogenic DNA adduct quantification in formalin-fixed paraffin-embedded tissues by ultraperformance liquid chromatography-tandem mass spectrometry. *Anal. Chem.* **2016**, *88*, 4780–4787. [CrossRef] [PubMed]
87. Wyss, L.A.; Nilforoushan, A.; Williams, D.M.; Marx, A.; Sturla, S.J. The use of an artificial nucleotide for polymerase-based recognition of carcinogenic $o^6$-alkylguanine DNA adducts. *Nucleic Acids Res.* **2016**, *44*, 6564–6573. [CrossRef] [PubMed]
88. Riedl, J.; Ding, Y.; Fleming, A.M.; Burrows, C.J. Identification of DNA lesions using a third base pair for amplification and nanopore sequencing. *Nat. Commun.* **2015**, *6*, 8807. [CrossRef] [PubMed]
89. Ding, Y.; Fleming, A.M.; Burrows, C.J. Sequencing the mouse genome for the oxidatively modified base 8-oxo-7,8-dihydroguanine by og-seq. *J. Am. Chem. Soc.* **2017**, *139*, 2569–2572. [CrossRef] [PubMed]
90. McKeague, M.; Foster, A.; Miguel, Y.; Giamberardino, A.; Verdin, C.; Chan, J.Y.S.; DeRosa, M.C. Development of a DNA aptamer for direct and selective homocysteine detection in human serum. *RSC Adv.* **2013**, *3*, 24415–24422. [CrossRef]
91. Schoukroun-Barnes, L.R.; Glaser, E.P.; White, R.J. Heterogeneous electrochemical aptamer-based sensor surfaces for controlled sensor response. *Langmuir* **2015**, *31*, 6563–6569. [CrossRef] [PubMed]
92. Bennett, B.T.; Bewersdorf, J.; Knight, K.L. Immunofluorescence imaging of DNA damage response proteins: Optimizing protocols for super-resolution microscopy. *Methods* **2009**, *48*, 63–71. [CrossRef] [PubMed]
93. Luise, C.; Nuciforo, P. Immunohistochemistry protocol for γH2AX detection (formalin-fixed paraffin-embedded sections). *Protoc. Exch.* **2006**. [CrossRef]
94. Paige, J.S.; Wu, K.Y.; Jaffrey, S.R. RNA mimics of green fluorescent protein. *Science* **2011**, *333*, 642–646. [CrossRef] [PubMed]
95. Nilaratanakul, V.; Hauer, D.A.; Griffin, D.E. Development and characterization of sindbis virus with encoded fluorescent rna aptamer spinach2 for imaging of replication and immune-mediated changes in intracellular viral rna. *J. Gen. Virol.* **2017**, *98*, 992–1003. [CrossRef] [PubMed]
96. Huang, K.; Doyle, F.; Wurz, Z.E.; Tenenbaum, S.A.; Hammond, R.K.; Caplan, J.L.; Meyers, B.C. Fastmir: An RNA-based sensor for in vitro quantification and live-cell localization of small rnas. *Nucleic Acids Res.* **2017**, *45*, e130. [CrossRef] [PubMed]
97. McKeague, M.; Wong, R.S.; Smolke, C.D. Opportunities in the design and application of rna for gene expression control. *Nucleic Acids Res.* **2016**, *44*, 2987–2999. [CrossRef] [PubMed]

98. Alsaafin, A.; McKeague, M. Functional nucleic acids as in vivo metabolite and ion biosensors. *Biosens. Bioelectron.* **2017**, *94*, 94–106. [CrossRef] [PubMed]
99. Zhou, J.; Rossi, J. Aptamers as targeted therapeutics: Current potential and challenges. *Nat. Rev. Drug Discov.* **2017**, *16*, 440. [CrossRef] [PubMed]
100. Ng, E.W.; Shima, D.T.; Calias, P.; Cunningham, E.T., Jr.; Guyer, D.R.; Adamis, A.P. Pegaptanib, a targeted anti-vegf aptamer for ocular vascular disease. *Nat. Rev. Drug Discov.* **2006**, *5*, 123–132. [CrossRef] [PubMed]
101. Poolsup, S.; Kim, C.Y. Therapeutic applications of synthetic nucleic acid aptamers. *Curr. Opin. Biotechnol.* **2017**, *48*, 180–186. [CrossRef] [PubMed]
102. Soll, J.M.; Sobol, R.W.; Mosammaparast, N. Regulation of DNA alkylation damage repair: Lessons and therapeutic opportunities. *Trends Biochem. Sci.* **2017**, *42*, 206–218. [CrossRef] [PubMed]
103. Kelley, M.R.; Logsdon, D.; Fishel, M.L. Targeting DNA repair pathways for cancer treatment: What's new? *Futur. Oncol.* **2014**, *10*, 1215–1237. [CrossRef] [PubMed]
104. Thomas, A.D.; Fahrer, J.; Johnson, G.E.; Kaina, B. Theoretical considerations for thresholds in chemical carcinogenesis. *Mutat. Res. Rev. Mutat. Res.* **2015**, *765*, 56–67. [CrossRef] [PubMed]
105. Li, W.; Hu, J.; Adebali, O.; Adar, S.; Yang, Y.; Chiou, Y.Y.; Sancar, A. Human genome-wide repair map of DNA damage caused by the cigarette smoke carcinogen benzo[a]pyrene. *Proc. Natl. Acad. Sci. USA* **2017**, *114*, 6752–6757. [CrossRef] [PubMed]
106. Hu, J.; Selby, C.P.; Adar, S.; Adebali, O.; Sancar, A. Molecular mechanisms and genomic maps of DNA excision repair in escherichia coli and humans. *J. Biol. Chem.* **2017**, *292*, 15588–15597. [CrossRef] [PubMed]
107. McKeague, M.; Wang, Y.H.; Smolke, C.D. In vitro screening and in silico modeling of rna-based gene expression control. *ACS Chem. Biol.* **2015**, *10*, 2463–2467. [CrossRef] [PubMed]

International Journal of
*Molecular Sciences*

MDPI

*Review*

# Nucleic Acid Aptamers: Emerging Applications in Medical Imaging, Nanotechnology, Neurosciences, and Drug Delivery

**Pascal Röthlisberger [1], Cécile Gasse [2,*] and Marcel Hollenstein [1,*]**

[1] Institut Pasteur, Department of Structural Biology and Chemistry, Laboratory for Bioorganic Chemistry of Nucleic Acids, CNRS UMR3523, 28, rue du Docteur Roux, 75724 Paris CEDEX 15, France; pascal.rothlisberger@pasteur.fr

[2] Institute of Systems & Synthetic Biology, Xenome Team, 5 rue Henri Desbruères Genopole Campus 1, University of Evry, F-91030 Evry, France

* Correspondence: cecile.gasse@univ-evry.fr (C.G.); marcel.hollenstein@pasteur.fr (M.H.); Tel.: +33-1-44-38-9466 (M.H.)

Received: 26 October 2017; Accepted: 9 November 2017; Published: 16 November 2017

**Abstract:** Recent progresses in organic chemistry and molecular biology have allowed the emergence of numerous new applications of nucleic acids that markedly deviate from their natural functions. Particularly, DNA and RNA molecules—coined aptamers—can be brought to bind to specific targets with high affinity and selectivity. While aptamers are mainly applied as biosensors, diagnostic agents, tools in proteomics and biotechnology, and as targeted therapeutics, these chemical antibodies slowly begin to be used in other fields. Herein, we review recent progress on the use of aptamers in the construction of smart DNA origami objects and MRI and PET imaging agents. We also describe advances in the use of aptamers in the field of neurosciences (with a particular emphasis on the treatment of neurodegenerative diseases) and as drug delivery systems. Lastly, the use of chemical modifications, modified nucleoside triphosphate particularly, to enhance the binding and stability of aptamers is highlighted.

**Keywords:** aptamers; systematic evolution of ligands by exponential enrichment (SELEX); modified triphosphates; medical imaging; drug delivery; gene regulation; DNA origami; neurodegenerative diseases

## 1. Introduction

Over the last decades, the repository of genetic information in living organisms—DNA—and the vector for gene expression—RNA—have seen an impressive expansion in applications that substantially deviate from their natural functions. Indeed, nucleic acids play a key role in the development of gene silencing therapeutic agents [1,2], the construction of novel nanomaterials [3], and the crafting of biocatalysts [4–6]. In this context, aptamers are rapidly developing nucleic acid tools that consist of single stranded DNA or RNA molecules comprising 20–100 nucleotides [7], and that are capable of selective binding to a broad array of targets with remarkable affinity [8,9]. Hence, these functional nucleic acids are often considered as the nucleic acid equivalent of protein antibodies. However, unlike their proteinaceous counterparts, aptamers are not plagued by physical or chemical instability or by potential immunogenicity and can be produced on a relatively large scale by standard chemical synthesis with little batch-to-batch variation [10]. Even though natural aptamers interacting with RNA polymerases have recently been identified [11], these functional nucleic acids are generally isolated in vitro by a combinatorial method coined SELEX (Systematic Evolution of Ligands by Exponential Enrichment) [9,12,13]. During SELEX, large libraries of oligonucleotides

(typically $10^{14}$–$10^{15}$ individual molecules) are challenged to bind to the intended target and iterative rounds of selection-amplification cycles are utilized to enrich the populations with high binding species. Since the invention of the SELEX protocol in the early 1990s, thousands of aptamers have been selected for targets ranging from small molecules [14] to larger entities such as proteins [15,16] or cells [17–19], and databases have been created to canalize this exponential growth of aptameric sequences and wealth of information [20–22]. The binding capacity of an aptamer is best described by its dissociation constant $K_d$, which in turn is given by the ratio of the dissociation and association rate constants ($k_{off}/k_{on}$) [23]. Typically, values in the low nM or even pM range are observed for potent aptamers. These impressive properties are reflected by the numerous clinical trials involving aptamers and the first FDA-approved oligonucleotide-based drug (Macugen®) [24,25]. Moreover, the versatility of the selection protocol and the high binding affinities have propelled aptamers in the forefront of numerous applications including for instance biosensing [26,27], proteomics [28], purification and biotechnology [29–31], therapeutics [25,32], and diagnostics [33,34]. Herein, we have chosen to give an overview and a brief description of the emerging but rapidly growing applications of aptamers. Particularly, we will discuss recent implications of aptamers as radiopharmaceutical tools for medical imaging purposes (MRI and PET imaging) and in neurosciences for the treatment and detection of Alzheimer's and Parkinson's diseases. We also discuss the combined use of aptamers with DNA origamis to develop novel nanomaterials and biosensing platforms. Since the development of all these new therapeutic, imaging, and sensing agents require means of targeted delivery, we also cover the use of aptamers as drug delivery systems and as gene silencing agents. The last facet of this review will involve a discussion on the possibility of using chemical modifications to enhance the general properties of aptamers and we will focus particularly on the direct use of modified nucleoside triphosphates (dN*TPs) in SELEX experiments.

## 2. Medical Imaging (MRI and PET)

The ease of chemical modification at both 3′- and 5′-ends [35] combined with the high target affinity and selectivity dramatically increases the potential of aptamers to serve as molecular imaging agents, particularly for magnetic resonance imaging (MRI) and positron emission tomography (PET) [36].

### *2.1. Aptamers and MRI*

MRI is a highly efficient technique that provides non-invasive three-dimensional images of living systems and of biological events with sub-millimeter spatial resolution [37]. In MRI, exogenous contrast agents—mainly small molecules based on $Gd^{3+}$-complexes—are used to enhance the image contrast by increasing the longitudinal ($T_1$) or transverse ($T_2$) relaxation times [38,39]. An important research avenue in the field of MRI consists in the development of smart or responsive contrast agents which consist either of systems that induce a change in magnetic relaxation in the presence of a biochemical stimuli (Figure 1A) or conjugates that vector MRI probes to their intended targets and sites (Figure 1B) [40]. Smart contrast agents based on aptamers have been devised by the application of both strategies. Indeed, in a proof-of-principle article, Yigit et al. developed a method for the detection and bisosensing of adenosine in vitro [41]. The contrast agent chosen in this system relied on biocompatible superparamagnetic iron oxide nanoparticles (SPIONs) due to their excellent capacity at changing the nuclear spin relaxation of neighbouring water protons [42]. The SPIONs were coated with cross-linked dextran which in turn could be functionalized with 3′- or 5′-thiol-modified DNA sequences that were designed so as to partially hybridize to a potent anti-adenosine aptamer [43]. In the presence of the adenosine analyte, the aptameric section refolded into its three-dimensional binding pocket concomitantly disrupting the hybridization to the SPION carrying oligonucleotides. The disruption of the SPION clusters led to the dispersion of single nanoparticles which display larger $T_2$ values compared to the initial bioconjugate [41]. The observed brightening of the MR images was ascribed to the resulting increase in $T_2$ values. In a related system, anti-thrombin aptamers [15,44]

were immobilized on cross-linked dextran coated SPIONs and upon binding to the thrombin target, the nanoparticles assembled into larger aggregates which led to a decrease in $T_2$ values (and thus a reduction of the brightness of MR images); a strategy that is often preferred in $T_2$-weighted MR imaging [45]. More recently, a similar strategy was applied however by replacing the SPIONs with a $Gd^{3+}$-based $T_1$-weighted contrast agent [46]. Indeed, a Gd-DOTA complex was connected (by standard amide bond formation chemistry) to the 3′-amino modified end of a DNA oligonucleotide designed to be partially complementary to the adenosine aptamer. The aptameric part was connected to streptavidin and released the Gd-DOTA-modified oligonucleotide from the large streptavidin complex upon binding to the target adenosine. The release of the contrast agent bearing oligonucleotide in turn led to an increase in $T_1$ value (and thus of the brightness of the MRI signal). In a conceptually related strategy, a catalytic DNA molecule (DNAzyme) [4,5] was used to release Gd-DOTA from a bulky complex [47]. Indeed, the RNA substrate was equipped with the Gd-DOTA complex while the $UO_2^{2+}$-dependent DNAzyme was connected to the protein streptavidin via a biotin moiety anchored at its 3′-end. In the presence of the analyte ($UO_2^{2+}$), the DNAzyme adopted its catalytically active structure and hydrolyzed the single embedded rA unit, releasing the contrast agent.

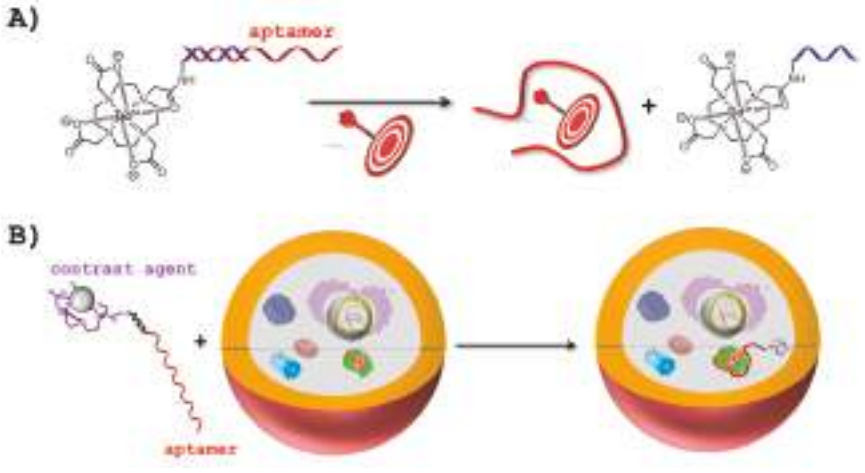


**Figure 1.** Strategies for the construction of aptamers acting as smart contrast agents: (**A**) Response to a biochemical stimuli: An oligonucleotide is equipped with a $Gd^{3+}$-DOTA complex. This oligonucleotide is complementary to part of the aptamer and upon binding to the target, the structural reorganization causes the $Gd^{3+}$-DOTA-labeled strand to dissociate from the duplex, which in turn increases the relaxation time and thus the brightness of the MRI signal [46]; (**B**) Vectoring to intended target: An aptamer is equipped with a contrast agent and will vector the probe directly to the intended target.

Monoclonal antibodies have been employed as tumor-specific ligands for the delivery of contrast agents [48,49]. By analogy to their proteinaceous counterparts, aptamers can play the role of vectors to transport contrast agents to specific regions of interest for MR imaging in vivo (Figure 1B) [50]. For instance, in a proof-of-principle study, the anti-thrombin aptamer was coupled to a Gd-DPTA (DPTA = diethylenetriaminepentaacetic acid) complex [51]. When the aptamer-Gd-DPTA bioconjugate was incubated with thrombin, significant relaxivity enhancements could be observed due to target interaction which increases the size of the contrast agent and concomitantly the rotational tumbling time [52]. In an ingenious system, Wang et al. bioconjugated a 2′-fluoropyrimidine-modified RNA aptamer specific for prostate cancer cells [53] on thermally cross-linked SPION [54]. The resulting construct not only allowed the transport of a contrast agent to the intended target and the concomitant MRI detection of prostate cancer cells in vitro but also served as a convenient scaffold for the selective

delivery of the anticancer agent doxorubicin (DOX) [55]. The same RNA aptamer-SPION construct was then later used for the in vivo MRI detection of prostate tumors in a mouse model [56]. Related to this approach, a G-rich 26-nucleotide long aptamer coined AS1411 [57] was first conjugated to silver nanoclusters (Ag NCs) and then coupled to ultra-small gadolinium oxide ($Gd_2O_3$) nanoparticles [58]. The resulting $Gd_2O_3$-aptamer-Ag NCs system was successfully employed for the detection of MCF-7 tumor cells by MR and fluorescence imaging in vitro. Similarly, a variant of cell-SELEX was recently used to isolate aptamers that specifically bound inflamed human aortic endothelial (HAE) cells [59]. The resulting aptamer tightly bound the desired target ($K_d$ = 82 and 460 nM for fixed and free HAE cells, respectively) and was conjugated to magnetic iron oxide particles for the efficient and selective in vitro detection of activated HAE cells.

### 2.2. Aptamers and PET Imaging

Positron emission tomography (PET) is another highly accurate biomedical imaging modality that is used worldwide in clinical diagnostic applications due to its capacity at providing tomographic resolution at any tissue depth [60,61]. Several radioisotopes (e.g., $^{18}F$, $^{64}Cu$, $^{11}C$, $^{13}N$, $^{124}I$, and $^{68}Ga$) display suitable properties for PET, namely a decay by emission of a positively charged particle (the positron ($\beta^+$)). Of these potential positron emitting radionuclides, $^{18}F$ is often preferred due to its rather convenient half-life ($t_{1/2}$ = 110 min), facile production, and favorable physical properties (clean decay and low emission energy) [62]. Besides the development of $^{18}F$-based synthons and radiolabeling strategies, an important challenge in the field of PET imaging is the crafting of target-specific imaging agents [61]. The potential of aptamers at delivering radionuclide probes was realized early on by Lange et al. who photoconjugated an $^{18}F$-labeled precursor on the 5′-amino-modified DNA thrombin aptamer [63]. More recently, an aptamer (sgc8) selective for the protein tyrosine kinase 7 (PTK7) [19] was $^{18}F$-radiolabeled and the resulting bioconjugate was used for the detection and the quantification by PET imaging of the expression of PTK7 both in vitro and in different tumor mouse models [64]. Similarly, the very same sgc8 aptamer was radiolabeled by application of the copper (I)-catalyzed alkyne-azide cycloaddition (CuAAC or click reaction) using a metabolically stable $^{18}F$-areene-arene derivative (Figure 2A) [65]. The affinity of the resulting $^{18}F$-sgc8 aptamer for the PTK7 target could be determined ($K_d$ = 1.1 nM) by PET imaging in vivo and further used for the mapping of tumoral PTK7 expression (Figure 2B). $^{18}F$-arene tags were also connected by standard amide bond formation to an aptamer selective for the extracellular matrix glycoprotein tenascin-C which has been identified as a potential biomarker for various diseases, including myocarditis as well as different forms of cancer [66,67]. The anti-tenascin-C aptamer was also radiolabeled with a $^{64}Cu$-NOTA complex and both the $^{64}Cu$ and $^{18}F$-labeled aptamers were used for the in vitro and in vivo PET imaging analysis of the stability of the aptameric construct and for tumor localization in a mouse model [67]. These first examples of in vivo PET imaging guided by aptamer ligands were followed by a recent article by Zhu et al. where DNA aptamers were screened both in vitro and in vivo against the cell membrane HER2 which is overexpressed in various types of cancer [68]. In a first step, a traditional in vitro selection experiment was carried out using a His-tagged extracellular domain of HER2 to isolate aptamers against this biomarker. Following eight rounds of the protein-based selection, seven rounds of cell-SELEX were applied with live SKOV3 ovarian cancer cells as targets to ensure proper binding of the aptamer candidates under in vivo-like conditions. This dual selection strategy allowed for the isolation of different high affinity ($K_D$ values in the low nM range) aptamers against SKOV3 cells, which were subsequently $^{18}F$-radiolabeled by application of a click reaction protocol. The $^{18}F$-labeled aptamers were injected intravenously into an SKOV3 xenograft tumor and their tumor uptake efficiency was evaluated by PET imaging analysis. The most efficient radiolabeled aptamer was then successfully used for the PET imaging detection of HER2 in an ovarian cancer mouse model [68].

In an alternative methodology, a hybridization reaction between a radiolabeled sequence that is partially complementary to an aptamer can be used to circumvent the tedious and material consuming purification step involved in the direct labeling of an aptamer. In this context, using click chemistry,

Park et al. $^{18}$F-radiolabeled an oligonucleotide that recognizes the anti-nucleolin aptamer AS1411 [57] and used the resulting duplex for the in vitro and in vivo PET imaging detection and targeting of C6 tumors in a mouse model [69]. As clearly shown in this section, the potential of aptamers to serve as PET imaging agents only begins to be explored and additional and alternative $^{18}$F-radiolabeling strategies [70–73] will certainly facilitate the application of aptamers in this imaging modality.

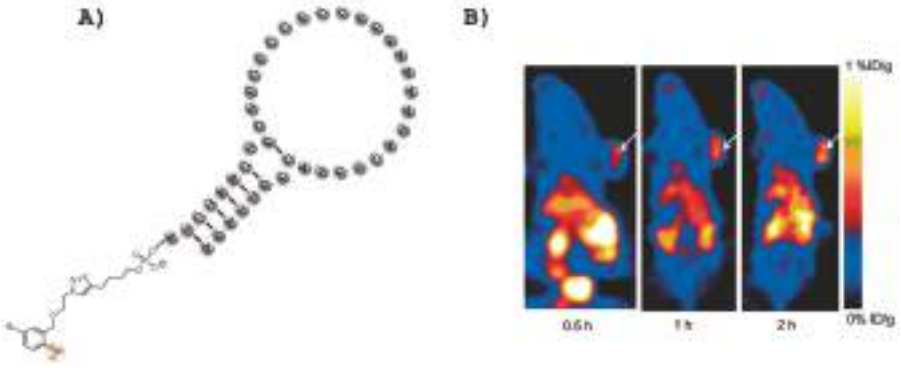


**Figure 2.** (**A**) Hypothetical secondary structure of the sgc8 aptamer and the $^{18}$F-label; and (**B**) positron emission tomography (PET) images of a mouse model with HCT116 tumors, white arrows represent the HCT116 xenograft [65].

Aptamers have also been used in the related imaging technique SPECT (single photon emission computed tomography) where radionuclides (e.g., $^{99m}$Tc or $^{111}$In) decay by emitting a single γ-ray [74]. In a recent example, a 2′-fluoro-modified RNA aptamer (F3B) was raised against the human Matrix MetalloProtease-9 (hMMP-9) which is implicated in angiogenesis and believed to favor tumor cell formation [75]. The unmodified purine ribonucleotides were converted to 2′-*O*-methyl-modified units after SELEX and the resulting aptamer (F3Bomf) displayed a very high specificity and binding affinity for its intended hMMP-9 target ($K_d$ = 20 nM). The fully modified aptamer F3Bomf could be connected to a $^{99m}$Tc complex and successfully used for the detection of the tumor biomarker hMMP-9 in human glioblastoma sections [75]. The same aptamer F3Bomf was subsequently radiolabelled with $^{99m}$Tc and $^{111}$In complexes which revealed to be excellent candidates for the in vivo detection of hMMP-9 in mice bearing human melanoma tumors [76].

## 3. Aptamers for the Treatment and Diagnostics of Neurological Diseases

Aptamers can prevent protein-protein interactions, protein aggregation, and inhibit enzymes and thus represent alluring biomolecules for the modulation and mechanistic investigation of biological events related to neurodegenerative diseases. Surprisingly, the use of aptamers in the field of neurosciences is rather modest but is steadily increasing since new perspectives of traversing the blood brain barrier are rising for those molecules [77–79].

### *3.1. Aptamers and Neurotransmitters*

The transmission of signals between two neurons is relayed by the exocytotic release of a battery of distinct chemical entities called neurotransmitters (see Figure 3A). Neurotransmitters consist mainly of single amino acids and their metabolites (e.g., glutamate and GABA, respectively) [80], biogenic monoamines (e.g., dopamine (DA), norepinephrine (NE), acetylcholine (Ach), and serotonin (5-HT)) [81], soluble gases (mainly NO, CO, and $H_2S$), and neuropeptides (e.g., neurokinin A and B, substance P or neuropeptide Y) [82]. In addition to their critical roles in numerous physiological functions, abnormal levels of neurotransmitters are indicators of various diseases including tumors [83],

tauopathies [84], and psychological and mood disorders such as schizophrenia [82,85], However, due to the presence of only low amounts, complex and delicate matrix composition, and the inherent chemical nature of neurotransmitters, detection of variation of their local concentrations is a rather difficult undertaking, even on samples obtained by ex vivo preparation [81], Aptamers have already demonstrated their capacity at recognizing and sensing various neurotransmitters [86]. Indeed, in an early report, Mannironi et al. have isolated an RNA aptamer that specifically recognized dopamine ($K_d$ = 1.6 μM for the free molecule in solution) [87]. This RNA aptamer was fundamental in the development of a potent dopamine biosensing system. This approach exploited the three-dimensional folding produced by the binding event which in turn favored gold nanoparticle aggregation leading to a colorimetric change [88]. Similarly, the RNA aptamer was used for the selective (despite the presence of competitive catecholamines) and sensitive (100 nM to 5 μM concentration range) electrochemical detection of DA [89]. Surprisingly, when the sequence of this anti-DA RNA aptamer was converted into its DNA counterpart, the affinity of the aptamer was increased and the specificity retained [90]. This DNA version of the DA aptamer was recently used in an in vivo study assessing its capacity at reversing cognitive deficits caused by the non-competitive NMDA-receptor antagonist, MK-801 in a rat model [91]. However, the specificity and binding capacity of the DNA homolog was seriously questioned recently, and the authors even suggested that it was not acting as a true aptamer [92].

Additionally, aptamers were also raised against the biogenic monoamines norepinephrine [93], acetylcholine [94], and serotonin (developed by Base Pair Biotechnologies, Inc., Pearland, TX, USA) [95].

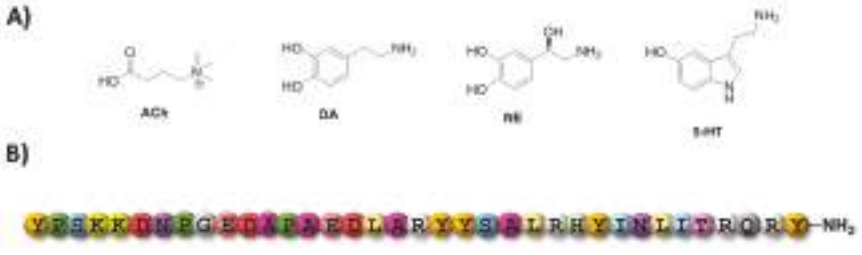


**Figure 3.** (**A**) Chemical structure of the main biogenic monoamine neurotransmitters; and (**B**) amino acid sequence of neuropeptide Y [96].

Neuropeptides represent the largest family of neuromessengers and can modulate both gene expression and synaptic communication [82,97]. Due to their larger size and broader chemical diversity, neuropeptides bind to their targets with higher affinities than biogenic monoamines and are consequently present in even lower quantities. Neuropeptides thus represent attractive targets for aptamer selection to devise potent sensing and quantification systems. In this context, first selection campaigns aimed at raising aptamers against neuropeptide Y (Figure 3B), which is negatively charged (pI = 5.52) at pH 7.0, and thus represents a challenging target [98,99]. First, an RNA aptamer was isolated and shown to bind tightly to the C terminus of neuropeptide Y ($K_d$ = 370 nM) and displayed no cross-reactivity with the closely related (~50% sequence homology) human pancreatic polypeptide (hPP) [99]. More recently, DNA aptamers were also raised against neuropeptide Y and displayed similar affinities ($K_d$ values in the 0.3–1 μM range) and selectivities to the RNA counterpart [98]. One DNA aptamer was integrated in a graphene-gold nanocomposite-based sensing platform for the fast, selective, and precise in vitro detection of neuropeptide Y [100]. This sensing platform displays a detection limit of 10 pM as well as high selectivity and fast response. Similarly, Banerjee et al. developed an aptasensor based on carbon fiber amperometry to detect neuropeptide Y in pheochromocytoma 12 cells [101].

The undecapeptide substance P is a member of the tachykinin family and is an essential excitatory transmitter involved in numerous important biological activities and functions. In light of its high

biological and neurological significance, an RNA aptamer was isolated against substance P [102]. Indeed, an automated SELEX procedure with the D-peptide of substance P as target was applied to isolate an L-RNA aptamer which could be converted to its corresponding Spiegelmer (D-RNA) [103] which bound to the naturally occurring L-substance P with high affinity ($K_d$ = 40 nM). This Spiegelmer was also efficiently used to inhibit the substance P-mediated calcium release in human AR42J cells ($IC_{50}$ = 45 nM). A similar strategy was applied in the isolation of a Spieglemer (D-RNA) aptamer against the neuropeptide nociceptin/orphanin FQ (N/OFQ), involved in numerous capital biological and neurological responses such as anxiety, pain, and stress [104]. The most potent Spiegelmer, NOX 2149, recognized N/OFQ with high affinity ($K_d$ = 0.2 μM) and concomitantly prevented N/OFQ from binding to its receptor ($IC_{50}$ = 110 nM). Aptamers have also been raised against the neuropeptides somatostatin [105], ghrelin [106], Glucagon [107], angiotensin II [108], and calcitonin gene-related peptide 1 (α-CGRP) [109], as well as against certain receptors such as neurotensin receptors [110,111], and the cholecystokinin B receptor [112].

### 3.2. Aptamers and Tauopathies

Tauopathies are progressive neurodegenerative disorders including Alzheimer's disease (AD), Parkinson's disease (PD), Huntington's and prion diseases, and are characterized by the presence of aggregates of the microtubule-associated protein tau in the brain [113]. Even though the exact origins and the molecular mechanisms are vastly unknown, it is believed that misfolded and abnormal forms (often hyperphosphorylated) of the wild-type proteins are involved in the physiopathology of these diseases by acting as seeds for the aggregation of these proteins. Aptamers could thus contribute to this field as tools for the investigation of the origin of tauopathies and for the detection, the prevention, and the treatment of these disorders [77,78], as highlighted in this section for AD and PD.

#### 3.2.1. Alzheimer's Disease

In AD, the combined accumulation and deposition of abnormal forms of tau protein and amyloid β (Aβ) peptides in the human brain is followed by a progressive functional disruption of neuronal networks [114]. Consequently, both tau and Aβ proteins represent valid targets for aptamer selection experiments.

Tau proteins play an important role in the stabilization and assembly of microtubules and display little propensity at aggregating and oligomerizing when found in their native folds and states. In AD, aggregates of hyperphosphorylated tau are thought to be transmitted in a prion-like manner that proceeds along connected neurons throughout the brain (the so-called tau-hypothesis) [115]. The understanding of how and why tau protein aggregates are capable of propagating in the brain is an important issue in neurosciences. In order to develop new tools to investigate and prevent this aggregation, Kim et al. have recently reported the isolation of an RNA aptamer against the longest isoform of human tau (tau40, 2N4R) [116]. The resulting aptamer efficiently prevented the oligomerization of tau monomers in vitro without affecting its degradation but on the other hand was not capable of disentangling pre-existing tau oligomers. Interestingly, the RNA aptamer could also delay tau oligomerization in DOX-inducible tau HEK293 cells and significantly reduced interneuronal tau propagation in primary rat neuronal cells, underscoring the inhibitory potential of aptamers for the regulation of tau oligomerization. A ssDNA sequence capable of binding to the human tau isoforms 381 and 410 ($K_d$ = 0.19 and 0.35 μM, respectively) was identified not by SELEX but by kinetic capillary electrophoresis [117]. This DNA oligonucleotide was subsequently used in an aptamer-antibody sandwich assay for the detection of tau 381 in human plasma (limit of detection of 10 fM) [118].

In addition to abnormal tau protein accumulation, the deposition of rather short (~4 kDa) Aβ peptides is believed to be a key step in the progression of AD—known as the Aβ-hypothesis [119]. Aβ peptides stem from the sequential cleavage of the larger transmembrane glycoprotein amyloid precursor protein (APP) mainly mediated by the combined action of a β-secretase (also known as β-site APP cleaving enzyme-1; BACE1) and a γ-secretase complex (Figure 4). Both aspartyl proteases

hydrolyze APP into several Aβ isoforms (mainly Aβ38, Aβ40, and Aβ42) which first assemble into synaptotoxic oligomers and then into amyloid fibrils, often considered as one of the major toxic agents in AD [119]. Lastly, Aβ oligomers also seem capable of binding to normal prion protein ($PrP^C$) with high affinity which might be at the origin of the toxicity of these oligomers [120]; this hypothesis, however, remains somewhat controversial [121–123]. Consequently, $PrP^C$, Aβ monomers and oligomers, BACE1, and the γ-secretase complex all represent relevant targets for aptamer selections to modulate, inhibit, or understand their functions [78,79].

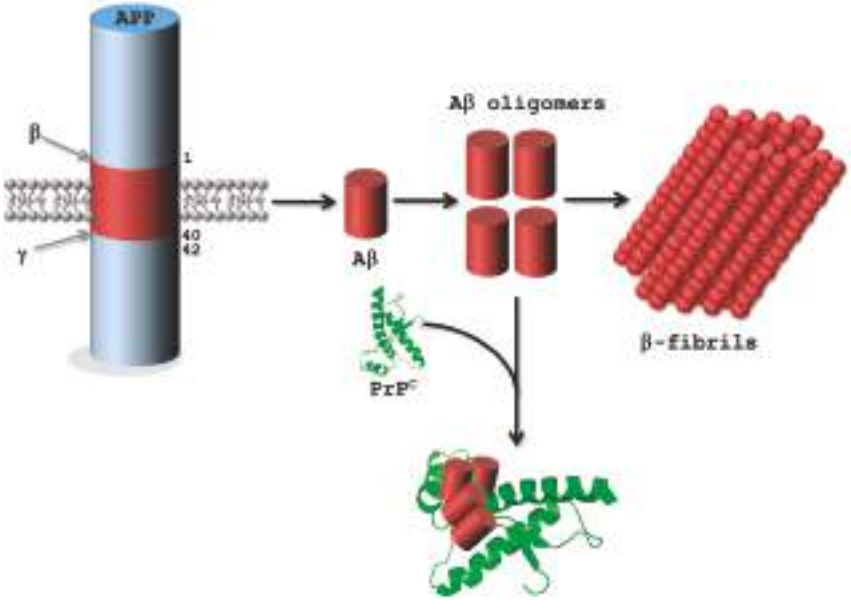


**Figure 4.** Schematic depiction of the formation of Aβ fibrils: BACE1 cleaves APP (Aβ sequence numbers are shown only) in the extracellular domain and the resulting fragment remains membrane-bound where it is cleaved by the γ-secretase complex into Aβ peptides (only the main Aβ40 and Aβ42 isoforms are shown). Monomeric Aβ peptides then aggregate to form oligomers and eventually β-fibrils. The cellular prion protein $PrP^C$ can also bind to Aβ oligomers [78,119].

Inhibition of the catalytic activity of BACE1 or the γ-secretase complex could directly hinder the formation of the toxic Aβ oligomers and β-fibrils. Consequently, both a natural and a modified DNA aptamer have been raised against the transmembrane protease BACE1 [124]. The natural DNA aptamer binds BACE1 with high affinity ($K_d$ = 69 nM) and was shown by a FRET assay to inhibit its activity both in vitro ($IC_{50}$ = 242 nM) and in an AD cell model [124]. The modified aptamers, selected with the triphosphate 5-chloro-dUTP and 7-deaza-dATP [125], displayed similar properties to the unmodified sequence, albeit with a slightly higher binding affinity and an interesting agonist/antagonist behavior [126]. Similarly, an RNA aptamer (called S10) was selected against the cytoplasmic tail B1-CT of BACE1 and showed a remarkable affinity for both phosphorylated and nonphosphorylated BACE1 ($K_d$ = 330 and 360 nM, respectively) [127]. Aptamer S10 was also capable of binding to cellular BACE1 and did not prevent binding of the protein factor GGA1 to the cytoplasmic tail or the casein kinase-mediated phosphorylation of the single serine S498 located in the B1-CT tail. Thus far, no aptamers have been raised against the membrane bound γ-secretase nor any of its constitutive proteins (i.e., presenilins, nicastrin, APH-1, and PEN-2) [119].

The Aβ40 and Aβ42 isoforms readily associate to form soluble but toxic Aβ oligomers. In this context, an RNA aptamer coined β55 was identified by SELEX and shown to recognize its intended target Aβ40 with high affinity ($K_d$ = 29 nM), albeit not in its monomeric or oligomeric forms but as fibrillar assemblies [128]. Furthermore, Farrar et al. also demonstrated that β55 was capable of binding to amyloid plaques in ex vivo human AD brain tissue slices. Remarkably, this binding event was also confirmed in vivo using a fluorescently labeled β55 in a transgenic mouse model [129]. Having realized that β55 only bound to Aβ40 polymers despite using a monomeric species in SELEX, Rahimi et al. set up an in vitro selection experiment that involved covalently-stabilized oligomers of Aβ40 [130]. Surprisingly, the resulting RNA aptamers did not bind to Aβ40 oligomers but only to Aβ40 fibrils, showing the high and natural propensity of nucleic acids to recognize fibrillar motifs in protein assemblies. This propensity was further confirmed by the substantial cross-reactivity of the isolated aptamers with Aβ42 and other amyloid fibrils. Another set of RNA aptamers was obtained through a selection experiment that used monomeric Aβ40 conjugated to gold nanoparticles; this target was hypothesized to act as a model of Aβ oligomerization and to allow both binding to the Aβ40 peptide and facile separation from unbound material [131]. Two aptamers, obtained by different elution protocols from the Aβ40-gold nanoparticles, indeed recognized monomeric Aβ40 ($K_d$ values of 22 and 11 μM) and were capable of inhibiting Aβ fibrilization.

Lastly, the prion protein (native $PrP^C$ or infectious isoform $PrP^{Sc}$) is an interesting target for aptamer selection due to its implication in AD (Figure 4) and prion diseases such as spongiform encephalopathies. Consequently, various DNA and RNA aptamers have been isolated against bovine [132], mouse [133], and human [134] $PrP^C$ as well as $PrP^{Sc}$ [135]. However, we refer the interested reader to a recent and concise review article thoroughly covering this topic [77].

#### 3.2.2. Parkinson's Disease

As for AD, the origin of the PD pathology is believed to be connected to the formation of misfolded protein aggregates. However, in PD, the presynaptic neuronal, 140 amino acid-long protein α-synuclein and not Aβ has been identified as a possibly responsible agent for the pathogenesis [136]. The aggregation of α-synuclein proteins into oligomers eventually leads to the formation of fibrils which then accumulate in cytosolic filamentous inclusions called Lewy bodies, which are the hallmark of PD [137]. Consequently, the first example of a DNA aptamer against α-synuclein—coined M5-15—was obtained by SELEX using the monomeric protein as target in the selection protocol [138]. However, M5-15 preferentially bound to α-synuclein oligomers and did not recognize the monomeric form. This inherent conformation specificity prompted the authors to isolate other DNA aptamers using a competitive screening method based on aptamer blotting and α-synuclein oligomers as target [139,140]. The resulting aptamers presented $K_d$ values in the low nM range that selectively recognized the oligomeric form of α-synuclein over monomers and fibrils [140]. Interestingly, the isolated aptamers also bound to Aβ40 oligomers (with slightly lower $K_d$ values), hinting at the possibility of a selective recognition of aggregates with β-sheet-rich proteins. One of the isolated aptamers (T-SO517) was recently integrated in a potent label-free aptasensor system for the selective detection of α-synuclein oligomers (the limit of detection was in the low nM or pM depending on the analysis method) [141]. Aptamer T-SO517 was also integrated in a fluorescent sensing platform that enabled the detection of Aβ40 oligomers down to 12.5 nM [142]. Similarly, a nanocomposite of aptamer T-SO508, gold nanoparticles, and thionine was used as probe for the selective and sensitive detection of Aβ40 oligomers (100 pM limit of detection) [143]. Lastly, variants of T-SO508 were either grafted on magnetic nanoparticles to detect Aβ oligomers (detection limit of 36 pM) [144] or combined with abasic site-containing molecular beacons to monitor Aβ aggregation [145].

Lastly, low levels of dopamine are also frequently found in patients suffering from PD and thus, all the anti-DA aptamers described in Section 3.1 could be of use for the detection, monitoring, and treatment of PD. Other potential targets are the other two members of the synuclein family, namely β-synuclein and γ-synuclein which might be involved in neurodegenerative diseases.

## 4. Aptamers as Key Components in the Fabrication of Smart DNA Origami Objects

The predictable nature and the high degree of fidelity of DNA base pairing are the origin of the development of a plethora of DNA-based nanomaterials [3,146]. Of particular interest are DNA origamis which are created by combining large single-stranded DNA frameworks (e.g., M13 bacteriophage genomic DNA (7249 nucleotides) [147]) with hundreds of shorter (20–60 nucleotides) oligonucleotides (called staple strands) partially complementary to particular sequences on the genomic DNA scaffold so as to form pre-designed two- and/or three-dimensional folds [3,148]. Since both aptamers and DNA origami are made out of the very same biopolymer and because of the inherent binding capacity of aptamers, a combination of both nucleic acid-based materials has been used for different applications including: (1) defined spatial positioning of proteins (and other ligands of interest) on DNA arrays for medical diagnostic, biosensing, or tissue and material engineering purposes [149,150]; (2) development of nanorobots for the delivery of drugs and other payloads [151,152]; and (3) the creation of multimodal sensing platforms [153].

Chhabra et al. were the first to report on the immobilization of proteins at specific locations of two-dimensional DNA nanoarrays [149]: two tile double-crossed (DX) DNA molecules [154] were equipped either with the thrombin aptamer [44] or an aptamer raised against the Platelet-derived growth factor (PDGF) [155] and combined with another set of DX tiles to form a two-dimensional DNA network with interspaced alternating lines of both aptamers. An atomic force microscopy (AFM) analysis showed that the corresponding target proteins successfully bound to their respective aptamers following their sequential addition on the network. This approach was then extended to a DNA origami constructed with 200 staple strands which resulted in the formation of rectangular two-dimensional DNA nanoarrays. The inclusion of the two aforementioned aptamers controlled the spatial positioning of the respective targets (i.e., thrombin and PDGF proteins) and therefore the generation of programmable high-density protein-DNA nanoarrays [149]. In a conceptually related construct, two aptamers binding to different epitopes of thrombin [15,44] were appended at different locations of rigid four- or five-helix bundle DNA tiles to evaluate the optimal inter-aptamer distance that ensures the highest binding to thrombin after formation of the hetero-aptamer system [150]. The optimal inter-aptamer distance appears to be at around 5.3 nM (i.e., slightly over the size of thrombin) for high affinity bivalent binding ($K_d$ ~10 nM). The same strategy was then applied for the construction of a rectangular-shaped two-dimensional DNA origami object [156] two lines of each aptamer separated by 5.3 nM were included in the scaffold of the origami tile resulting in efficient bivalent binding to thrombin by dual-aptamer lines. These initial proof-of-principle studies paved the way for the development of smart DNA origami objects. For instance, in a landmark work, Douglas and co-workers designed a DNA nanorobot in the form of a hexagonal barrel (Figure 5A) consisting of 196 staple oligonucleotides and the 7308 nucleotide-long genomic DNA of an M13-like phage [151]. The two domains that constitute the barrel are connected by single-stranded oligonucleotidic hinges at the rear and closed in the front by an aptamer sequence hybridized to a partially complementary sequence. In the presence of protein tyrosine kinase 7 (PTK7), the sgc8c aptamers (specific for PTK7) [19] dissociate from the lock-duplexes and the DNA nanorobot opens as a direct consequence of the formation of the aptamer-ligand complex. The different payloads (i.e., either 5-nm gold nanoparticles or antibody fragments against the human leukocyte antigen–A/B/C) are affixed on the inner walls of the barrel (either through 5′-thiol or 5′-amino modified linkers, respectively) and can be released upon opening of the DNA nanorobot. This ingenious system was incubated with different cell lines expressing the HLA–A/B/C antigen with a combination of molecular inputs. An increase in fluorescence caused by the binding of the antibody fragments on the cell surface could only be detected in the presence of the correct "key", namely PTK7. Lastly, the DNA origami system could be extended to yield a more discriminatory system by incorporating combinations of aptamers recognizing different targets.

Godonoga et al. recently reported a DNA origami-aptamer construct for the specific recognition of a malaria biomarker [152]. In this system, a rectangular DNA origami [156] was fabricated by including

the aptamer 2008s that specifically recognizes the malaria biomarker *Plasmodium falciparum* lactate dehydrogenase (*Pf*LDH) with high affinity ($K_d$ = 42 nM) through the formation of a 2:1 aptamer:ligand complex [157]. An AFM analysis clearly revealed that only *Pf*LDH and not the related human homolog (hLDH) bound to the surface of the DNA origami decorated with the aptamer 2008s (Figure 5B), thus clearly demonstrating that large supramolecular DNA constructs could be used as diagnostic tools for diseases.

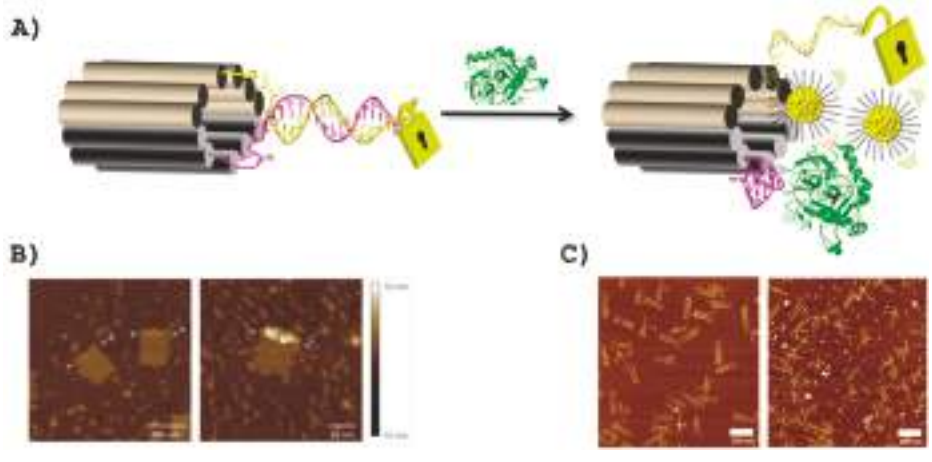


**Figure 5.** (**A**) Schematic representation of the aptamer-gated DNA nanorobot [151]: the aptamer (magenta) is locked in a double-stranded form by a partially complementary sequence (yellow) and both are grafted on the nanorobot. The payloads (either gold nanoparticles (shown) or antibody fragments) are constrained to remain within the DNA construct and only the recognition of intended target by the aptamer (green) will unlock the DNA nanorobot and enable the delivery of the payload; (**B**) AFM images of a DNA origami-aptamer construct in the presence of a non-target protein (hLDH; left-hand side) and presence of the target protein (*Pf*LDH; right-hand side) [152]; (**C**) AFM analysis of a DNA origami equipped with a split aptamer system in the closed (left-hand side) and open (right-hand side) forms [153].

Lastly, DNA origami-aptamers systems can also be used as smart biosensing platforms. In a recent contribution, Walter et al. blended the pinching capacity of a nanomechanical DNA origami forceps [158] with the biosensing capacity of split aptamer systems [159]. Indeed, the constituting sequences of the ATP-specific split aptamer were equipped with green- and red-emitting photostable cyanine dyes that act as energy donor and acceptor, respectively [160] and were subsequently appended on one arm of the DNA origami forceps. In the absence of the analyte (i.e., ATP) the constructs remained in an open form (Figure 5C) and emitted green light (absence of energy transfer). On the other hand, in the presence of ATP, the split aptamer sequences bound together which resulted in the closure of the DNA origami forceps which concomitantly led to red light emission due to an efficient energy transfer (Figure 5C). The sensing event can be observed by both AFM (Figure 5C) or by the change in fluorescence from green to red, hence following the concept of DNA traffic lights [161].

## 5. Aptamers as Drug Carriers and Gene Regulating Agents

Repair of the biological damage or chemical imbalance caused by a disease often requires an intervention in the form of a drug at the precise location of the inflicted disorder. Depending on the disease, the nature and the location of the damaged biomaterial can vary substantially ranging from simpler constructs such as proteins or nucleic acids to larger systems such as cells or entire tissues. In order to improve the therapeutic index of drugs and reduce offside effects and some

inherent toxicity, numerous systems have been devised to carry drugs in a stable form to the intended sites [162,163]. In this context, aptamers represent ideal candidates as delivery systems for conventional or encapsulated drugs, but also for therapeutic oligonucleotides and peptides due to their properties (vide supra) [25].

### 5.1. Nanomaterials Conjugated Aptamers

Due to the ease of functionalization of oligonucleotides, aptamers can be conjugated to virtually any type of nanomaterial [164]. Amongst these, graphene oxide (GO) holds high promises for the development of advanced materials due to its interesting optical and electronic properties but also because of the possibility of constructing barrier films and new classes of membranes. In addition, graphene oxide consists of interspaced sheets that form 2D structures which are known to exhibit low toxicity, high mechanical flexibility, a large accessible surface, and an excellent quenching capacity of fluorophores [165]. Consequently, numerous reports exist on the crafting of GO-aptamers conjugates, especially for the development of biosensors [166]. In a highly interesting approach, Nellore et al. explored the potential of immobilizing aptamers selective for biomarkers on GO to capture and identify circulating tumor cells (CTCs) in blood—an approach that is reminiscent of that described earlier in this review for the immobilization of aptamers on DNA origamis (see Section 4) [167]. Thus, aptamers selective for the prostate-specific membrane antigen (PSMA), HER2, and the carcinoembryonic antigen (CEA) biomarkers were covalently affixed on two-dimensional GO sheets by standard amide bond formation with the carboxylic acid residues present on GO and then converted to a three-dimensional architecture using polyethyleneglycol (PEG) as a cross-linking agent. The high capacity of the resulting aptamer-coated 3D GO foam-based membrane at capturing tumor cells was proven by separating the different cells from infected rabbit blood. In a related study, Bahreyni et al. connected aptamers selective against the membrane protein mucin MUC1 which is overexpressed in various epithelial carcinomas, through $\pi$-$\pi$ stacking interactions with the GO surface [168]. GO was charged either with the anti-MUC1 aptamer or a fluorescently-labeled aptamer selective for MUC1 cytochrome C. Upon successful internalization of the labeled aptamer nano complex into target MDA-MB-231 and MCF-7 cells, a strong fluorescent signal was observed indicating binding and release of the fluorescein labeled aptamers to cytochrome C, while no effects were observed with non-targeted cell lines (HepG2). This theranostic system appeared to be non-invasive and selective for the targeted cells inducing apoptosis.

An elegant "on and off" strategy reported by Tang et al. required a non-covalent assembly of the Cy5.5-labeled AS1411 aptamer, targeting nucleolin, on the surface of a GO-wrapped, DOX-loaded mesoporous silica nanoparticle [169]. This system allowed a light induced administration of DOX that could be monitored by fluorometric measurements: a first fluorescent signal of the Cy5.5-labeled aptamer indicated real time endocytosis of the aptamers into the target cell, while a second fluorescent signal was induced by laser irradiation because absorption and transduction of the near infrared light by the GO structures lead to local heat and expansion of the GO sheets and thus the release of the DOX molecules in a light dependent manner.

Besides GO, gold-based nanomaterials and derivatives have attracted considerable attention for the crafting of aptamer-based materials and devices due to their stability and their advantageous optical and electronic properties [170–172]. In particular, gold nanoparticles have served as drug delivery systems for aptamers since they generally increase the stability of ssDNA towards nuclease degradation, the cellular uptake capacity of oligonucleotides, as well as their biocompatibility and usually induce a limited immune response [173,174]. For instance, Huang and coworkers used gold nanoparticles to attach thrombin-binding aptamers on their surface [175]. The complexed thrombin on the gold nanoparticles (d = 13 nM) efficiently inhibited the thrombin activity against fibrinogen upon activation with green laser light. The anticoagulant activity of these complexes was found to be 30 times more potent than recent commercially available drugs (heparin, argatroban, hirudin,

or warfarin) exhibiting a good biocompatibility, low toxicity and showed excellent half-life stability in serum ($t_{1/2}$ >14 d) [175].

Besides the use of gold nanoparticles as drug delivery systems and diagnostic tools, Niu et al. demonstrated that conjugation of the sgc8c aptamer [19] with a gold *N*-heterocyclic gold (I) complex (NHC-$Au^{I}$-aptamer), known to induce cell apoptosis, resulted in internalization of the bioconjugate specifically into CCRF-CEM leukemia cells and exhibited excellent cytotoxicity [171]. The sgc8c-7aptamer employed in this strategy targeted the receptor protein tyrosine kinase 7 (PTK-7) that is overexpressed in CCRF-CEM leukemia cells and allowed for a 30-fold increase in cytotoxicity compared to the unmodified NHC-$Au^{I}$ complex. No toxicity to off-target cells (in this case, K526 cells) was observed with the bioconjugate, on the other hand, a dose-dependent toxicity was observed with CCRF-CEM cells, underscoring the usefulness of this approach.

Quantum dots (QDs) represent another very attractive class of inorganic nanoparticles for the formation of aptamer bioconjugates [176–178]. QDs have unique photophysical properties, including color tunability and bright and extremely photostable fluorescence, that is keeping them in the forefront of numerous sensing applications [178]. In addition, QDs have also been used in dual imaging-drug delivery systems based on aptamers [179]. For instance, Su and co-workers covalently attached a capture sequence on a near infrared $CuInS_2$-QD via amide coupling to connect a MUC1-aptamer to this nanoparticle through the formation of Watson–Crick base pairs [180]. Multiple CG-motifs present in the resulting duplex served as intercalation sites for daunorubicin (DNR), which is a drug for the treatment of acute myeloid leukemia. This system allowed a specific delivery of the DNR to prostate cancer cells in vitro and a concomitant sensing of the presence of DNR in the construct due to a marked drop in fluorescence intensity upon binding of the drug. A high cytotoxicity was found for MUC1 positive PC-3M cells but not for MUC1 negative HepG2 cells when treated with the DNR-loaded bioconjugate [180].

In addition to inorganic frameworks, aptamers can be coupled to various organic nanomaterials including DNA constructs [164], DNA micelles [181,182], aptamer-based hydrogels [183], lipids [184], or even vitamins [185,186]. Recently, Dai et al. developed a DNA tetrahedron (Td) labeled with an aptamer targeting MUC1. In this drug delivery system, the aptamer serves for the targeted delivery to MUC1-positive breast cancer cells while the DNA tetrahedron is instrumental for the intercalation of DOX [187]. A fluorescence-based drug loading experiment showed that each aptamer-Td construct with an average size of 12.4 nM could carry up to 25 DOX molecules. A high red fluorescent signal of free DOX molecules could be observed upon binding of the negatively charged complex to the MUC1 positive breast cancer cells but not with MUC1 negative cells. Accordingly, a very high cytotoxicity was observed when MUC1 positive cancer cells were treated with the aptamer-Td conjugate [187].

A last category of nanoparticles that will be considered consist of linear block copolymers and dendritic polymers which have been extensively used as encapsulating devices in drug delivery systems [188,189]. Aptamers have also been used to decorate the surface of these polymeric entities and to facilitate targeted delivery. This concept was developed by the Langer laboratory who reported a strategy for a drug encapsulation by a triblock copolymer comprising a controlled release polymer (poly (lactic-co-glycolic-acid); PLGA), a hydrophilic polymer (PEG), and the 2′-fluoro-modified RNA A10 aptamer (see Sections 5.5 and 6) that selectively recognizes the prostate cancer specific membrane antigene (PSMA) [55,190]. By systematically changing the composition of the complex, a narrow ratio between PEG and aptamer could be determined that enabled maximal specific binding to the target and cellular uptake, efficient drug (in this case the anticancer drug Docetaxel) release, high antibiofouling properties, and minimized self-aggregation and thus undesired accumulation in the spleen [190]. A similar approach was also used to selectively deliver a Pt(IV)-prodrug [191], a cisplatin prodrug [192], and other anticancer drugs [193–195], while dendritic polymers-aptamer systems have also successfully been used for in vivo [196] and in vitro [197] tumor imaging and drug delivery [198].

### 5.2. Micelles and Liposomes Conjugated Aptamers

Liposomes are small spherical and artificial vesicles with one or multiple lipid bilayers and have already been suggested as potentially highly efficient drug deliver systems at an early stage [199]. Indeed, Huwyler and co-workers already described in the early 1990s the use of liposomes decorated with monoclonal antibodies to delivery encapsulated tritium-radiolabeled daunomycin in a directed manner to target cells [200]. This strategy has many benefits including the modulation of the affinity of the bionconjugate complex by simply changing the ratio of antibodies present on the lipid bilayer surface along with the impressive quantity of drug molecules (>10,000) that can be delivered in a selective manner [200,201]. In a more recent study, Ara et al. used liposomes composed of lipid bilayers that are labeled with an aptamer instead of a monoclonal antibody [202] to ensure selective cellular uptake [203]. The aptamers were covalently linked on PEG 2000 disteraoyl phosphotheanolamine and targeted the primary cultured mouse tumor endothelial cells (mTEC). By application of a standard lipid hydration method, the corresponding aptamer-labeled PEG2000 liposomes and PEG200 liposomes (negative control) were formed. Fluorescent measurements and confocal laser scanning microscopy showed an increased uptake in mTEX cells of the aptamer-PEG liposomes compared to the unlabeled liposomes. In vitro experiments revealed that approximately 39% of the aptamer-PEG-liposomes could escape the endosomes in a receptor mediated way followed by clathrin-mediated endocytosis. Lastly, in vivo experiments with the aptamer-conjugated liposomes were performed with human renal cell carcinoma (OS-RC-2 cells) inoculating mice using confocal laser scanning microscopy. These experiments clearly indicated that the aptamer modified liposomes strongly accumulated (co-localization ratio of 25%) on tumor vasculature compared to non-labeled liposomes, where a co-localization ratio of only 3% accumulation was observed [203]. In a similar approach, a 2′-fluoro-modified RNA aptamer against the cancer stem cells (CSC) surface markers CD44 was affixed on the surface of a PEG-functionalized liposome by application of the thiol-maleimide click reaction [204]. The resulting construct was shown to act as a very efficient potential drug delivery system due to its high selectivity and specificity for CD44 positive cells.

In a recent study by Plourde et al., the high binding capacity of aptamers served as a driving force for the incorporation of DOX into cationic liposomes (Figure 6A) [205]. Indeed, different versions of an anti-DOX DNA aptamer [206] were designed by either adding an additional base-pair on the binding motif or by including two binding motifs into one construct. Upon intercalation of DOX into the aptamer its intrinsic fluorescence was quenched and was used to determine both the loading efficiency and the binding affinity. The drug aptamer complexes were incorporated into cationic liposomes (d < 200 nM) via electrostatic interactions, where encapsulation of DOX into liposomes was greatly enhanced (ten times higher) when using an aptamer compared to negative controls without any specific DOX binding sites. This aptameric-encapsulation was compared to the Doxil-like formulation, which is a commercialized version of liposomes of DOX that allows the loading of up to 10,000 molecules through strong entrapment but concomitantly reduces the therapeutic efficiency due to a slow release [207]. The aptamer-based loading strategy offered a number of advantages over the Doxil-like formulation including similar loading capacity, faster release, and a higher therapeutic efficiency. Cytotoxicity assays revealed that liposomes with aptamers having an intermediate affinity ($K_d$ = 334 nM) for DOX exhibited the higher therapeutic effects. The same approach was then extended to the amphiphilic drug tobramycin used for the treatment of lung infections. It is known that encapsulation of tobramycin in liposomes increases the in vivo efficacy compared to the free drug. The low encapsulation efficiency of tobramycin in liposomes is a limiting factor in this approach. The active loading with an aptamer allowed the encapsulation of up to six times more drug compared to passive encapsulation. Therefore, the authors reasoned that this strategy could find a broad application to load a large variety of drugs into liposomes.

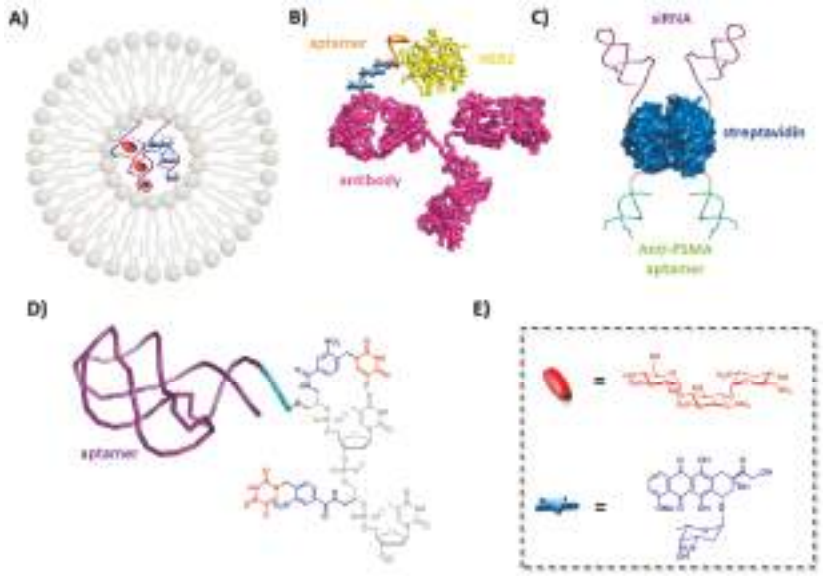


**Figure 6.** Illustrative examples of aptameric-based systems used as drug delivery systems: (**A**) encapsulation of aptamer-drug complexes in liposome [205]; (**B**) antibody-aptamer pincers (AAPs) for selective targeting of HER2 and delivery of DOX [208]; (**C**) streptavidin serves as the core for the connection of two anti-PSMA aptamers and two siRNA molecules [209]; (**D**) delivery of the 5-fluorouracil (5-FU; shown in red) drug connected to an aptamer-oligonucleotide scaffold via a photo-cleavable linker (shown in blue) [210]; and (**E**) chemical structures of tobramycin (red) and DOX (blue).

### *5.3. Aptamer-Drug Conjugates*

Aptamers have also been considered to guide drugs directly and selectively to their intended targets by direct conjugation to the therapeutic agent or through a small linker arm [211]. An early example of a covalent attachment of a drug on an aptamer is the appendage of DOX on the sgc8c-aptamer via a short linker. Indeed, the linker was connected to the aptamer by means of the thiol-ene click reaction and to DOX via a hydrazone moiety. The hydrazone unit was chosen because of the compatibility with the ketone group found on DOX and a possible hydrolysis in the acidic environment (pH 4.5–5.5) of endosomes [212]. In vitro tests showed that the administration of unconjugated DOX exhibited a higher toxicity towards non-targeted cells compared to the aptamer-DOX conjugate.

In an attempt to overcome low aptamers-drug ratios, Wang et al. synthesized an aptamer containing multiple copies of 5-fluorouracil (5-FU), a drug against colorectal and pancreatic cancer, via a photo-cleavable linker in order to spatially and temporarily control the drug release (Figure 6D) [210]. Besides covalent attachment of drugs on aptamers, a few examples of non-covalently attached drug-aptamer conjugates have also been reported, mainly by intercalation. The benefit of this strategy stems from the steady increase in loading capacity of the intercalating drug on aptamers with aptamer vs. drug ratios that improved from 1/1.2 in 2006 [55] to nearly 1/50 in 2013 by the use of self-assembling dsDNA drug intercalation sites directly appended to the desired aptamers [213].

Most drug delivery systems rely on the presence of a single type of aptamer which results in an efficient escorting of drugs to the intended target. However, since aptamers are usually obtained by in vitro selection experiments, small conformational changes of their targets caused by their in vivo environments might interfere or even impede their binding activities [68,214,215]. A multimeric aptamer-drug delivery strategy was developed in order to face this potential drop in binding affinity.

The system consists of two distinct aptamers specific for different cancer subtypes and DOX intercalated in the double-stranded portions created by the self-assembly of the two aptameric species [216].

### 5.4. Aptamer-Antibody Conjugate

The conjugation of aptamers with their proteinaceous counterpart antibodies is used to increase the affinity of the resulting construct for a single target [7]. The rationale behind this strategy is based on the observation that antibody dimerization causes a decrease in $K_d$ value (caused by lower $k_{off}$ and higher $k_{on}$ rates) compared to the two individual antibodies [208,217]. This working hypothesis was validated by an inhibition study of the VEGF-A and PDGF-B signaling pathways [218] as well as for the fluorescence detection of human CD4 [217]. More recently, Kang and Hah reported a drug delivery strategy based on the formation of an antibody-aptamer hybrid complex in order to improve the specificity of the construct for thrombin or the anti-human epidermal growth factor 2 (HER2) as model systems (Figure 6B). The resulting so-called antibody-aptamer pincers (AAPs) were found to increase the affinity for thrombin of the conjugate compared to the individual aptamers or antibody by 35-fold or 100-fold, respectively ($K_d$ value of 567 pM). The DOX loaded AAP constructed with the anti-HER2 aptamer and antibody was also found to exhibit a 3–6 fold higher cytotoxicity than the individual antibody DOX conjugate or unconjugated DOX [208].

The conjugation of an aptamer with an antibody (a so-called oligobody) can also be helpful to overcome both the poor pharmacokinetics for systemic administration of the small aptamers and the limited tissue penetration of the rather large antibodies (~150 kDa) [219]. The combination of an anti-cotinine antibody (cot-body) with a cotinine labeled vascular endothelial growth factor (VEGF) targeting aptamer (cot-pega) led to the formation of an oligobody that exhibited no loss in affinity to cancer cells compared to the aptamer only, penetrated deep into tumor tissue of an A549-xenograft mouse model, displayed extended half-life times in serum ($t_{1/2}$ = 8.3 h) and reduced tumor growth. All these studies clearly demonstrate the potential of aptamer-antibody conjugates in anticancer therapeutics.

### 5.5. Aptamers and Gene Regulating Agents

Aptamers, being of nucleic acid nature, can easily be conjugated to relevant RNA or DNA sequences (for instance to sgRNA in the gene editing system CRISPR/Cas9 [220,221]) and particularly to therapeutic oligonucleotides (siRNA, miRNA, or antisense agents) [222–224].

The first siRNA-aptamer conjugate was reported by McNamara et al. who tried to improve the therapeutic efficacy of siRNAs by constructing a chimera with aptamers as vectors to achieve targeted delivery [225]. The aptamer-siRNA chimera was constructed to target the cell surface receptor prostate specific membrane antigen (PSMA) overexpressed in prostate cancer cells via the A10 RNA aptamer [53], while the delivered siRNA targeted the polo-like kinase 1 (PLK1) and B-cell lymphoma 2 (BCL2) genes, which are overexpressed in numerous human tumors [225]. Upon internalization and processing of the RNAs by Dicer, the siRNA is directed to the RNAi pathway and silence their cognate mRNAs which in turn leads to the depletion of the PLK1 and BCL2 survival genes and ultimately cell death. The benefit of that system compared to chimeras of siRNA with antibodies is the low immunogenicity of the RNA aptamers and also an increased in vivo tissue penetration due to the small size. Additionally, it was demonstrated that the genes were only regulated in cells expressing PSMAs on their surface. Dassie et al. further improved this system by optimizing both parts of the chimeric species in order to allow systemic administration, which should simplify clinical applications [226]. The fabrication of the second generation of optimized PSMA-Plk1 chimeras involved a reduction of the length of the aptamers (from 71 down to 39 nucleotides) to facilitate chemical synthesis while introduction of 2′ fluoropyrimidines residues in the longer RNA strand increased serum stability. In addition, the gene silencing activity was enhanced by fine-tuning the siRNA sequence for Dicer recognition, RISC complex formation, and mimicking endogenous miRNA precursors. This optimization included the inclusion of a UU 3′-overhang, engineering of a wobble

base pair, swapping of the passenger and guide strands, and introduction of a short stem loop chimera. The second-generation chimeras were found to be active at concentration 50-fold lower than the first generation chimeras and produced a target-specific apoptotic activity [226].

A similar approach was followed in a recent study by Liu et al. where an RNA based aptamer siRNA chimera was engineered to target PSMAs of prostate cancer (PCa) [227]. The bivalent aptamer-dual siRNA chimeric system that was used consisted of an anti-PSMA aptamer [228] connected to an siRNA targeted against the survivin oncogene while the second moiety was composed of the same aptamer but linked to an siRNA for the EGFR gene. Upon binding to prostate cancer cells and internalization, the bivalent chimera was divided into the aptamer and the siRNA parts by digestion of the stem-loops by the Dicer activating RNAi machinery. The siRNAs then inhibited both EGFR and survivin simultaneously by selective mRNA cleavage and ultimately induced apoptosis. Both in vitro and in vivo studies revealed that the combination therapy where two oncogenic pathways are targeted simultaneously is a highly efficient strategy for the eradication of tumor growth and angiogenesis. In another similar approach followed by Jeong et al., DOX was intercalated into a multivalent aptamer-siRNA chimera in order to target multidrug resistant mucin1-overexpressing breast cancer cells (MCF7) [229]. A multimeric antisense siRNA construct was first built by covalent attachment of about 18 single 3′- and 5′-end dithiolated BCL2-specific siRNA sequences through a dithio-bis-maleimidoethane linker and by application of the thiol-ene click reaction. The resulting multivalent template was designed to bind to a chimera comprising a complementary siRNA sequence (the sense strand) and an anti-MUC1 aptamer for the selective delivery of the siRNA to the intended target. DOX was loaded on the construct in the double-stranded regions and the subsequent in vitro tests showed that the DOX-aptamer-siRNA efficiently reduced the viability of the cancer cells after one day by activating the apoptotic caspase-3/7 and releasing DOX as a therapeutic agent. Compared to monovalent DOX-aptamer-siRNA or free DOX, administration of the multivalent complex was the only one that led to a low recovery rate of the cancer cells. The construct thus fulfilled its intended purposes: selective delivery of DOX and efficient antisense activity.

Wilner et al. targeted the transferrin receptor CD71 (TfR) which is overexpressed in malignant cells with a liposome labeled with aptamers and loaded with an anti-enhanced green fluorescent protein siRNA [230]. To achieve specific delivery, they developed a nuclease-resistant aptamer that was obtained through application of a modified SELEX protocol. Indeed, in the first step of the hybrid in vitro selection protocol, a traditional SELEX was carried out using 2′-fluoro-pyrmidine NTPs (in lieu of the natural UTP and CTP) and recombinant hTfR immobilized on a solid support. After the 5th round of selection, a second, "internalization selection", step was included which consisted of incubation of the enriched RNA libraries stemming from the different generations with HeLa cells and extraction and amplification of the RNA molecules internalized by the cells. This ingenious selection protocol allowed for the isolation of a highly potent RNA aptamer ($K_d$ = 17 nM) that could efficiently penetrate Jurkat cells and retain its high binding affinity. The selected anti-TfR aptamer could be engineered into a truncated version ($K_d$ = 102 nM) and was then used to functionalize stable nucleic acid lipid particles (SNALP) containing the siRNA by connection with a thiol maleimide linker. Upon internalization of the functionalized SNALPs, an efficient gene knockdown activity was observed in HeLa cells in vitro, thus providing evidence for the successful activation of the RNAi pathway of the siRNA.

Paralleling these efforts, an elegant approach for aptamer-mediated siRNA delivery was developed by Chu et al. in 2006 in which streptavidin served as a tetravalent core to connect two identical biotinylated anti-PSMA aptamers and two identical biotinylated siRNAs directed against lamin A/C (Figure 6C). In vitro studies with LNCaP cells overexpressing PSMA showed that the chimeric construct was internalized within 30 min and that the gene expression was significantly reduced only when both the siRNA and the anti PSMA aptamers were present on the construct [209]. Control experiments with PSMA-negative PC3 cells demonstrated no cytotoxic effects and no reduction of gene expression, highlighting the potential of such a set up as a gene therapeutic agent despite

a potential immunogenicity of the streptavidin adducts which could limit the delivery of such constructs [231]. The same anti-PSMA aptamer was recently involved in the construction of a pRNA-3WJ core based system for the specific delivery of a miRNA LNA to LNCaP prostate cancer cells and to knock down the oncogenes miR17 and miR21 [232]. In addition to the miRNA and the aptamer, a Cy5 dye was introduced in the framework to follow the in vitro internalization into cells. The ultra-stable and serum resistant constructs bound to PSMA in an excellent manner at RNA concentrations as low as 100 nM and were shown to deliver the miRNA specifically to the LNCap cells but not to PC-3 cells. Systemic in vivo administration to xenograft tumors in nude mice showed that the aptamer-pRNA-siRNA construct specifically bound to tumor cells with little or no accumulation in healthy cells. A reduced tumor growth could be found even days post administration without any indication of toxicity as a result of the specific delivery.

Lastly, aptamers have also been linked to catalytic DNA (DNAzymes [4]) and RNA (ribozymes [233]) molecules. For instance, a two-step selection protocol was developed to generate RNA molecules capable of both recognizing and binding to the inteRNAl ribosome entry site (IRES) of hepatitis C virus (HCV) and cleavage of the genomic viral RNA at a specific location [234]. This selection experiment led to the identification of seven distinct groups of aptamer-ribozyme chimeras that selectively bound to the intended target ($K_d$ values of ~5–200 nM) and cleaved the viral RNA with appreciable rate constants ($k_{obs} \cong 0.01–0.04\ min^{-1}$) [234,235]. Recently, a partial randomization of the sequence of an isolated aptamer-ribozyme followed by reselection allowed improving the inhibitory properties of such RNA molecules [236].

In the context of catalytic DNA molecules, a hemin/G-quadruplex (hGQ) horseradish peroxidase-mimicking DNAzyme [237] was linked to various aptamers specific for certain small molecules—yielding constructs coined nucleoapzymes—to expand the catalytic repertoire of these biocatalysts [238]. Particularly, when the DNAzyme was conjugated with DA- and arginine-binding aptamers, increased yields of oxidation (with multiple turnover kinetics) could be observed with the respective substrates (i.e., DA and N-hydroxy-L-arginine) compared to the individual functional nucleic acids.

## 6. Recent Chemical Modifications of Aptamers

Aptamers are often referred to as nucleic acids antibodies, however the chemical arsenal of DNA and RNA is rather limited when compared to that of proteins. In addition, unmodified, natural nucleic acids are highly prone to hydrolytic degradation by nucleases. The possibility of using chemical modifications in SELEX might help to alleviate these shortcomings [239]. Over the last quarter century, it was shown by several groups that incorporation of nucleoside triphosphates modified at the level of the α-phosphate, the sugar scaffold (mainly at the 2′ position), or at the level of the nucleobase (5 position of pyridines or 7 position of purines) can enhance the target affinity as well as the serum stability compared to aptamers that are restricted to natural nucleotides. Since the principle of using modified nucleotides in SELEX is a known strategy that has been reviewed extensively [240–244], this section will only highlight recent advances in this field.

### *6.1. Base Modified Aptamers*

Gawande et al. recently investigated the influence on the outcome of a selection process when using a library comprising two amino acid-like 5′-modified pyrimidine bases ($dC^X$ 1, $dU^X$; Figure 7) or a similar population of oligonucleotides but prepared with only one base modification [245]. A systematic study with all the possible pairwise combinations (i.e., 18 different libraries) of dCTPs equipped with two different side-chains (Nap and Pp) and five different modifications on dUTP (Nap, Tyr, Moe, Thr, and Pp) to find high affinity ligands for proprotein convertase substilisin/kexin type 9 (PCSK9) showed that after six rounds of selection, the libraries made with a single dN*TP were enriched with the modification while libraries prepared with two modifications displayed an increased content of the modified $dC^X$ only. Ligands that showed a high affinity for PCSK9 with

two modifications were in general more frequent than ligands with only one modification, with the selection experiments exploiting the combination of Tyr-dU and Pp-dC or Nap-dC performing best. A synergistic behavior of the two modifications with respect to affinity could be observed in some cases when compared to aptamers containing only one of the modifications separately. Interestingly, a useful property of double modified aptamers is the high abundance of the modified nucleotides within the sequence. It could be demonstrated that this allows truncating the aptamers with a lower loss of functionality compared to aptamers bearing only one modification. In addition, the serum stability was higher for SOMAmers with two distinct modification compared to natural or ligands with only a single modification. Lastly, another favorable property of using multiple modifications is a higher epitope coverage compared to natural aptamers or ligands containing only a single modification.

With the rationale of using nucleobases equipped with an amino acid-like modification to mimic the hypervariable domains of certain antibodies where tyrosine is overrepresented, Perrin et al. used a phenol modified 5′-deoxyuridine triphosphate ($d^yUTP$) [246] to raise aptamers against *E. coli* DH5α cells [247]. Despite the lower incorporation efficiency by the Vent ($exo^-$) DNA polymerase of $d^yUTP$ compared to natural dTTP, a relative high abundance of the modified nucleotide (much larger than if introduced randomly) was found in the ligands obtained and sequenced after 12 rounds of a whole cell-SELEX. Unexpectedly, sequencing of the enriched library revealed a vast diversity of sequences that could not be classified into families, thus showing a low abundance of sequence identity. It was hypothesized that this lack of sequence identity was caused by the vast diversity of targets expressed on the cell surface of such a bacteria. Analysis of the binding specificity of the four most abundant aptamers compared with an unmodified aptamer as control for the gram positive cells showed that: (1) the modification is required for high affinity binding; and (2) that cross-reactivity with other cell strains was minimal. The apparent dissociation constant of the most promising aptamer was determined by saturation experiments to be 27.4 nM, which is about 10-fold lower than unmodified RNA aptamers recently reported for DH5α cells [248].

Minagawa et al. used a base-appended base (BAB) in a 75 nucleotide long modified library with a 30 mer randomized region to select aptamers against salivary α-amylase (sAA) [249]. Indeed, replacement of the thymidine nucleotide with a triphosphate displaying an adenine attached to the C5 position of the nucleobase ($dU^{ad}TP$ [250], Figure 7) in the selection protocol led to the isolation of seven aptamers against sAA with an abundance of over 5% of the enriched pool after eight rounds of selection. SPR measurements revealed that the most potent aptamer bound to the target with an affinity of 559 pM, which is sufficient for potential applications as a biosensor of the stress biomarker sAA [251]. When the selection experiment was carried out in the absence of $dU^{ad}TP$ (only natural dNTPs), no enrichment of the library was observed, further highlighting the usefulness and the potential of modified nucleoside triphosphates in SELEX. An optimization study of the initial 75 mer aptamer showed that the full-length sequence could be truncated down to a 36 mer species without inducing a substantial loss of binding affinity. Additionally, imino-proton NMR spectra were recorded at different temperatures to elucidate the structural properties of the sAA binding aptamer. This NMR analysis suggested that the imino-protons of the adenine part of $dU^{ad}$ were engaged in additional hydrogen-bonding interactions, thus leading to the assumption that the BAB modification induced a well-defined and compact secondary structure. Finally, the potential of the selected aptamer was highlighted with the detection of human sAA in human saliva using capillary electrophoresis, pull down, and lateral flow assays.

Examples of base-modified RNA aptamers are not as common as for DNA, which reflects both the lower tolerance of natural RNA polymerases for base-modified NTPs and the restricted choice of engineered RNA polymerases. Despite these limitations, allyl-amino-UTP ($U^{aa}TP$) was used in an in vitro selection experiment aimed at raising an anti-ATP aptamer [252]. More recently, Kabza and Sczepanski used the same $U^{aa}TP$ to isolate an aptamer against the oncogenic precursor microRNA 19a (pre-miR-19a) which was converted to its Spiegelmer via solid-phase synthesis using the L-$U^{aa}$-phosphoramidite [253]. The resulting L-RNA aptamer bound its target with a slightly lower

affinity than its D-counterpart ($K_d$ values of 2.2 and 0.72 nM, respectively) but efficiently inhibited the Dicer-mediated processing of the miR target ($IC_{50} \cong 4$ nM) in vitro.

Lastly, the Hili laboratory is currently exploring an interesting approach—coined LOOPER (Ligase-catalyzed OligOnucleotide PolymERization)—for the increase of chemical diversity without the involvement of dN*TPs and relying on the ligation of base-modified pentanucleotides [254,255]. This strategy was recently expanded to the Darwinian evolution of aptamers against human α-thrombin [256]. Indeed, a library containing 16 different pentanucleotidic codons (and as many functional groups ranging from hydrophobic to Brønsted acids and bases) was subjected to six rounds of SELEX. The most highly represented sequence displayed a remarkable affinity ($K_d$ = 1.6 nM) and selectivity for its target (no cross-reactivity with BSA) and strictly required the presence of the modifications for binding. In addition to ablating the need for dN*TPs (and to an extent engineered polymerases), this strategy allows for the introduction of a broad variety of functional groups and will certainly be used for the evolution of other aptamers and potentially DNAzymes.

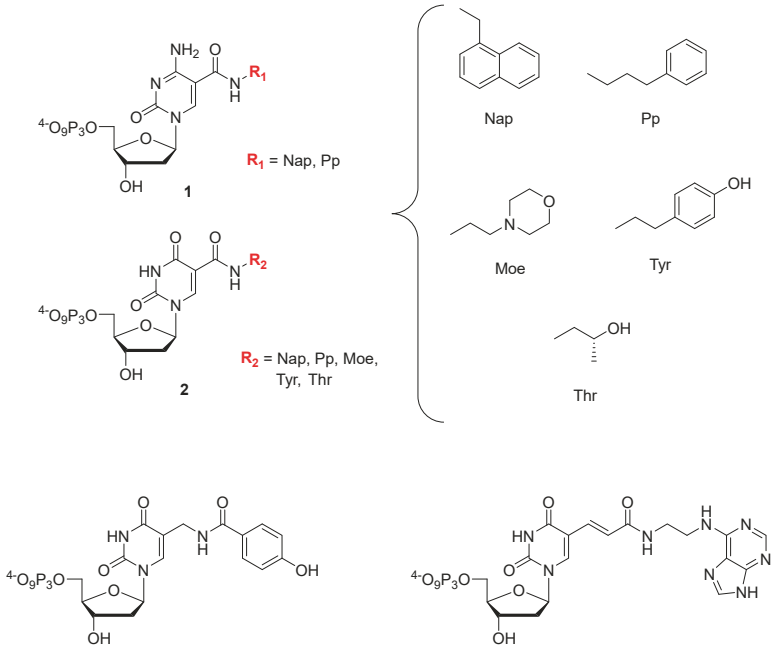


**Figure 7.** Chemical structures of base-modified nucleoside triphosphates used in selection experiments of aptamers with an expanded chemical repertoire.

### *6.2. Aptamers with an Extended Genetic Alphabet*

Expanding the genetic code from a two- to a three- or even a four-base-pair system is a long standing goal in synthetic biology since this would enable the creation of functional nucleic acids with improved properties and ultimately to semi-synthetic organisms with proteins that potentially display novel structures and/or functions [257]. In this context, Hirao and colleagues have developed the ex-SELEX (genetic alphabet expansion for systematic evolution of ligands by exponential enrichment) method where an additional artificial Ds-Px base pair (Figure 8) complements the two natural Watson–Crick base pairs to isolate aptamers against the vascular endothelial growth factor ($VEGF_{165}$) [258,259]. In the ex-SELEX strategy, the hydrophobic base Ds is introduced into DNA by solid-phase synthesis at predetermined locations and specifically binds to its unnatural

partner Px in PCR for the amplification of the generations during SELEX. The localization of the Ds modifications in each sublibrary—a key step in the ex-SELEX protocol—is possible through the combination of a unique barcode system and replacement PCR. In a new approach aimed at exploring a larger chemical space, a fully randomized library containing the unnatural base was used to isolate aptamers targeting the Willebrand factor A1 domain (vWF) [260]. Although the selection with the randomized additional base in the sequences led to higher affinity ligands compared to the selection with natural base pairs or the ex-SELEX selection procedure with limited sublibraries, it also increased the complexity of the system and led to scaling problems. The new complexity and the possibility of misincorporation of the Ds base during PCR experiments required the introduction of a novel sequencing method to elucidate the exact location of the Ds modification. The authors took advantage of the fact that only dATP misincorporated opposite Px by the Taq polymerase but none of the dye-carrying 2′,3′-dideoxynucleoside-5′-triphosphates were incorporated at these positions, which led to the formation of a gap in the sequencing peak pattern at the position of the unnatural base. By comparing the sequencing pattern with that of a clone after a replacement PCR, the exact positions of the modifications could be inferred. Lastly, both the serum stability and the thermostability of the anti-vWF aptamers could be enhanced by introducing additional mini-hairpin motifs containing GNA loops (N = A, G, C or T) [261] without a loss of affinity in both the natural ($K_d$ = 182 pM) and the modified aptamer ($K_d$ = 61 pM), which thus represents a convenient strategy for the improvement and construction of functional aptamers [259,262,263].

In the context of an expansion of the genetic alphabet, Benner and co-workers developed a third base pair dZ-dP (Figure 5) that can be used in SELEX and the related strategy was coined "laboratory in vitro evolution based on an artificial expanded genetic information system" (LIVE-AEGIS) [264,265]. Initial selection experiments using a 20 nucleotide long randomized library with a nucleotide composition of T/G/A/C/Z/P ≅ 1.5/1.2/1.0/1.0/1.0/0.5 by solid-phase synthesis and amplified in the selection rounds Hot Start Taq polymerase in the presence of natural and modified dNTPs led to the isolation of a high affinity aptamer ($K_d$ = 30 nM) against MDA-MB 231 breast cancer cells [266]. In order to perform deep sequencing of the enriched populations at the end of the LIVE-AEGIS protocol, a conversion technique was used where the dZ nucleotides were converted into dC and dT and dP into dA and dG, allowing to assign the positions of the two modifications. Analysis of the sequence composition showed that only one dZ was present in the most potent aptamer which additionally lost its binding affinity when the modification was replaced with a natural nucleotide. The depletion of dZ and dP nucleotides in the isolated aptamer (an average of three dZ and 1.5 dP would be expected for a 20 nucleotide long sequence) was ascribed to a slight disadvantage of the modified triphosphates during PCR compared to the natural nucleotides. A similar observation was made in another study by Zhang et al. using the AEGIS system for cells engineered to place glypican 3 (hGPC3) on their surface where a ligand with only one dZ was found that bound with an affinity of 6 nM [267]. Analogues without the dZ showed a significant loss in activity again demonstrating the importance of the modification. The most recent AEGIS-LIVE study by Biondi et al. targeting the protective antigen (PA63), a cleaved version of the precursor protein PA83 from *Bacillus anthracis*, brought forth an aptamer that binds to PA63 and thus blocks the toxin channel by displacing the lethal factor and finally inhibiting translocation of toxins into infected cell [268]. Analysis of the sequences stemming from the AEGIS-LIVE selections revealed that no survivor contained a dZ modification but different dP-containing sequences were isolated [268]. The most abundant sequence of the enriched pool comprised two dP nucleotides and this aptameric species displayed a very high affinity for PA63 ($K_d$ ~35 nM). This underrepresentation of modifications in the surviving sequences was ascribed to the conformational constraint imposed by the modified nucleotides. An intensive analysis of the secondary structure of the aptamer revealed interesting features resembling the formation of a higher folded structure [269] upon addition of cations that was not described in the literature before and which was also found to increase the stability against nuclease degradation.

Other prominent base-modified nucleoside and nucleotide analogs that have not (yet) been used to generate aptamers with enhanced properties include the DNAM-5dSICS unnatural base pair (UBP) developed by the Romesberg laboratory and used in the development of a semi-synthetic organism [270,271], artificial metallo-base pairs [272,273], and nucleotides modified with other functional groups [125,274–278].

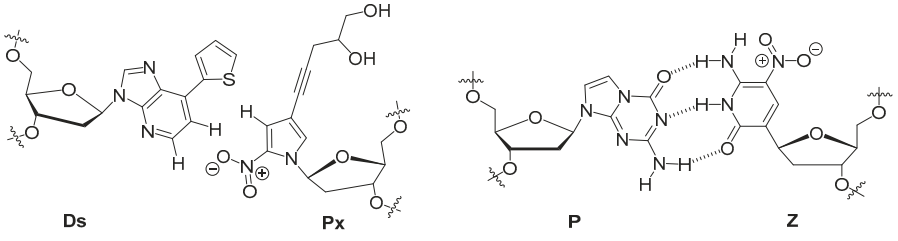


**Figure 8.** Chemical structures of the unnatural base pairs Ds Px and dP dZ used in the expansion of the genetic code.

### *6.3. Sugar Modified Aptamers*

2′-fluoro-nucleotides (**3** in Figure 9) are popular modifications that are often introduced into aptameric scaffolds to increase their nuclease resistance, a strategy that culminated in the development of pegaptanib sodium (Macugen®) [25,240]. However, 2′-fluoro-modified nucleoside triphosphates are rather poor substrates for DNA polymerases which restricts their use in selection experiments and often require a time consuming reverse transcription in order to convert the 2′-modified sequences into natural oligonucleotides that can be amplified and then transcribed back into modified sequences [279]. In order to circumvent these shortcomings, the Romesberg laboratory evolved a thermostable polymerase that could PCR-amplify oligonucleotides containing 2′-fluoro- and 2′-OMe-nucleotides [280]. This polymerase, SFM4-3, was then recently used in a selection experiment with 2′-fluorine-modified purine nucleotides to raise aptamers that could bind human neutrophil elastase (NHE) [281]. With the engineered thermostable DNA polymerase SFM4-3, the need for a reverse transcription step was ablated which significantly shortened and simplified the selection process. After six rounds of selection, two aptamers were identified that displayed very high affinity ($K_d$ = 20–170 nM) for the NHE target, albeit with slightly lower affinity than that of the sequences that did not contain the 2′-fluoro-modifications ($K_d$ = 11–17 nM). In order to exclude nonspecific electrostatic interactions of the aptamers with the positively charged HNE, an experiment suppressing the charges with high salt concentrations (i.e., 1 M NaCl) was performed, where the natural variant of the aptamers lost its affinity to HNE but the ligand with the 2′-fluoro modification remained bound. Lastly, $^{19}$F NMR experiments revealed that the secondary structure of the aptamer was influenced by the presence of the 2′-modifications which disfavours duplex formation and therefore allows the formation of a more soluble species that specifically recognized the target. A similar selection experiment was carried out to isolate fully-modified 2′-OMe-aptamers by combining an engineered polymerase and a reverse transcriptase. One particular aptamer, 2mHNE-4, bound its intended target, human neutrophil elastase, with good affinity ($K_d$ = 45 nM) [282].

Other sugar modifications such as HNA (hexitol nucleic acid **8**) [283], LNA (locked nucleic acid **5**) [283], FANA (2′-fluoro-arabinose **4**) [284], and TNA (threose nucleic acid **6**) [285] have all been used for the generation of highly potent modified aptamers, while other nucleotides such as 7′,5′-bicyclo-DNA **9** [286], xylonucleic acids **7** [287], 2′-selenomethyl nucleotides [288], and 4′thio-DNA [289,290] have recently been suggested as potential candidates to explore new chemistries in selection experiments (Figure 9) [279,291].

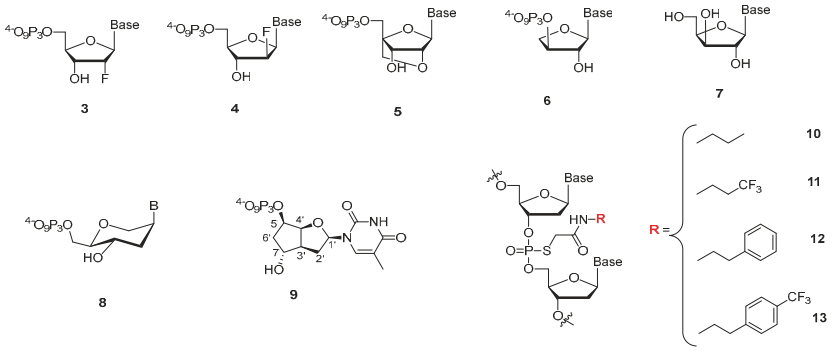


**Figure 9.** Chemical structures of sugar and phosphate modified nucleotides.

### *6.4. Phosphate Modified Aptamers*

The possibilities for the modification at the level of the phosphate unit are more limited than in the case of the sugar and nucleobases moieties and most efforts have focused on the α-phosphate, particularly α-phosphorothioates [242,279,292–294]. In this context, Yang et al. have explored the alkylation of phosphorothioated thrombine-binding aptamers (TBA) with aim of improving the antitumor properties of the ligands by reducing the thrombin binding affinity [295]. Alkylation of the phosphorothiate moieties was achieved by a simple substitution reaction with four different brominated substrates (**10** to **13** in Figure 9). Previous X-ray [296] and NMR studies [297] of the TBA showed that the TT or TGT loop of the G-quadruplex structure was responsible for effective binding. Therefore, the modifications were systematically introduced at these positions. The presence of the phenyl moiety (**12** in Figure 9) was shown to reduce the flexibility of the loop regions through interaction with nucleobases which resulted in an inhibition of G-quadruplex formation which in turn is believed to cause a lowering of the binding affinity ($K_d$ = 0.5 μM) for thrombin compared to the unmodified aptamer ($K_d$ = 0.19 μM). The higher dissociation constants for the aptamers modified with the phenyl moiety also resulted in a reduction of the anticoagulation properties. The antiproliferation experiments with the natural aptamers as control revealed that the TBAs with the phenyl modification exhibited excellent inhibition of the proliferation of about 80% with the lung carcinoma cell line A549 but no activity against the human breast cancer cell line MCF-7.

Substitution of an oxygen atom on the α-phosphate with a $BH_3$ moiety instead of a sulfur atom was used for the selection of a potent anti-ATP aptamer but no further examples have been reported since [298].

## 7. Conclusions and Prospects

In view of their impressive functional properties, nucleic acid aptamers certainly deserve their description as chemical antibodies [25]. The high degree of structural flexibility associated with an impressive target specificity and selectivity has propelled aptamers into the forefront of numerous therapeutic and diagnostic applications. Moreover, aptamers are continuously employed in proof-of-concept studies to further expand the boundaries of the realm of aptamer-based technologies. Particularly, aptamers have recently started to infiltrate the fields of medical imaging and there is no doubt that aptamers will mature into valuable and smart imaging agents. In addition, aptamers commence to be used as tools in neuroscience for the detection of the variation of small concentrations of various neurotransmitters and abnormal protein folds. Hopes for the in vivo use of aptamers in neurosciences are spurred by a recent selection experiment of an aptamer for its capacity at penetrating the blood–brain barrier (BBB) [299] as well as a novel bioconjugation method to polymeric nanoparticles which has allowed the in vivo BBB passage [300]. Furthermore, due to their chemical malleability, aptamers can easily be conjugated to small molecules, other nucleic acid oligonucleotides, or larger

constructs such as antibodies, liposomes, and DNA origamis that undoubtedly will improve their cellular uptake and help in the development of aptamer-mediated drug delivery systems as well as biosensing platforms. However, aptamers still suffer from temperature- and nuclease-mediated degradation and the restricted chemical arsenal available to natural nucleic acids precludes binding to difficult targets such as single enantiomers of small organic molecules or glycosylated proteins [240,301]. The use of modified nucleoside triphosphates, along with engineered polymerases [291,302] and new selection strategies [256,285,303–305], will certainly help in alleviating these predicaments.

All the emerging applications described in this Review along with technological and synthetic progress will certainly improve the limited commercial success of aptamers in the near future.

**Acknowledgments:** The authors gratefully acknowledge financial support from the Institut Pasteur start-up funds.

**Author Contributions:** Pascal Röthlisberger, Cécile Gasse, and Marcel Hollenstein contributed to the conception of the article, literature collection, and preparation of the manuscript. Marcel Hollenstein contributed to reviewing and revising the manuscript. All authors read and approved the final version of the manuscript.

**Conflicts of Interest:** The authors declare no conflict of interest.

## Abbreviations

| | |
|---|---|
| CTC | Circulating Cancer Cells |
| GO | Graphene oxide |
| AFM | Atomic Force Microscopy |
| SELEX | Systematic Evolution of Ligands by Exponential Enrichment |
| PET | Positron Emission Tomography |
| MRI | Magnetic Resonance Imaging |
| DOTA | 1,4,7,10-tetraazacyclododecane-1,4,7,10-tetraacetic acid |
| $K_D$ | Dissociation constant |
| XNA | Xeno nucleic acid |
| SPIONs | Superparamagnetic iron oxide nanoparticles |
| NOTA | 1,4,7-triazacyclononane-triacetic acid |
| DNAzyme | DNA enzyme or catalytic DNA |
| SPECT | Single Photon Emission Computed Tomography |
| HER2 | Human Epidermal Growth Factor Receptor 2 |
| DOX | Doxorubicin |
| QD | Quantum Dot |
| PEG | Polyethyleneglycol |
| siRNA | Small interfering RNA |
| miRNA | Micro RNA |
| sgRNA | Single guide RNA |
| pRNA | Packaging RNA |
| 3WJ | Three-way junction |
| GABA | γ-Aminobutyric acid |
| BSA | Bovine Serum Albumin |
| Aβ | Amyloid β |

## References

1. Goyenvalle, A.; Griffith, G.; Babbs, A.; El Andaloussi, S.; Ezzat, K.; Avril, A.; Dugovic, B.; Chaussenot, R.; Ferry, A.; Voit, T.; et al. Functional correction in mouse models of muscular dystrophy using exon-skipping tricyclo-DNA oligomers. *Nat. Med.* **2015**, *21*, 270–275. [CrossRef] [PubMed]
2. Khvorova, A.; Watts, J.K. The chemical evolution of oligonucleotide therapies of clinical utility. *Nat. Biotechnol.* **2017**, *35*, 238–248. [CrossRef] [PubMed]
3. Wang, P.; Meyer, T.A.; Pan, V.; Dutta, P.K.; Ke, Y. The beauty and utility of DNA origami. *Chem* **2017**, *2*, 359–382. [CrossRef]

4. Hollenstein, M. DNA catalysis: The chemical repertoire of DNAzymes. *Molecules* **2015**, *20*, 20777–20804. [CrossRef] [PubMed]
5. Silverman, S.K. Catalyic DNA: Scope, applications, and biochemistry of deoxyribozymes. *Trends Biochem. Sci.* **2016**, *41*, 595–609. [CrossRef] [PubMed]
6. Rioz-Martinez, A.; Roelfes, G. DNA-based hybrid catalysis. *Curr. Opin. Chem. Biol.* **2015**, *25*, 80–87. [CrossRef] [PubMed]
7. Yu, Y.Y.; Liang, C.; Lv, Q.X.; Li, D.F.; Xu, X.G.; Liu, B.Q.; Lu, A.P.; Zhang, G. Molecular selection, modification and development of therapeutic oligonucleotide aptamers. *Int. J. Mol. Sci.* **2016**, *17*, 358. [CrossRef] [PubMed]
8. Ellington, A.D.; Szostak, J.W. In vitro selection of RNA molecules that bind specific ligands. *Nature* **1990**, *346*, 818–822. [CrossRef] [PubMed]
9. Tuerk, C.; Gold, L. Systematic evolution of ligands by exponential enrichment: RNA ligands to bacteriophage T4 DNA polymerase. *Science* **1990**, *249*, 505–510. [CrossRef] [PubMed]
10. Zhang, L.Q.; Wan, S.; Jiang, Y.; Wang, Y.Y.; Fu, T.; Liu, Q.L.; Cao, Z.J.; Qiu, L.P.; Tan, W.H. Molecular elucidation of disease biomarkers at the interface of chemistry and biology. *J. Am. Chem. Soc.* **2017**, *139*, 2532–2540. [CrossRef] [PubMed]
11. Sedlyarova, N.; Rescheneder, P.; Magan, A.; Popitsch, N.; Rziha, N.; Bilusic, I.; Epshtein, V.; Zimmermann, B.; Lybecker, M.; Sedlyarov, V.; et al. Natural RNA polymerase aptamers regulate transcription in *E. coli*. *Mol. Cell* **2017**, *67*, 30–43. [CrossRef] [PubMed]
12. Joyce, G.F. Forty years of in vitro evolution. *Angew. Chem. Int. Ed.* **2007**, *46*, 6420–6436. [CrossRef] [PubMed]
13. Robertson, D.L.; Joyce, G.F. Selection in vitro of an RNA enzyme that specifically cleaves single-stranded DNA. *Nature* **1990**, *344*, 467–468. [CrossRef] [PubMed]
14. Pfeiffer, F.; Mayer, G. Selection and biosensor application of aptamers for small molecules. *Front. Chem.* **2016**, *4*. [CrossRef] [PubMed]
15. Bock, L.C.; Griffin, L.C.; Latham, J.A.; Vermaas, E.H.; Toole, J.J. Selection of single-stranded-DNA molecules that bind and inhibit human thrombin. *Nature* **1992**, *355*, 564–566. [CrossRef] [PubMed]
16. Nimjee, S.M.; White, R.R.; Becker, R.C.; Sullenger, B.A. Aptamers as therapeutics. *Annu. Rev. Pharmacol. Toxicol.* **2017**, *57*, 61–79. [CrossRef] [PubMed]
17. Chen, M.; Yu, Y.Y.; Jiang, F.; Zhou, J.W.; Li, Y.S.; Liang, C.; Dang, L.; Lu, A.P.; Zhang, G. Development of cell-SELEX technology and its application in cancer diagnosis and therapy. *Int. J. Mol. Sci.* **2016**, *17*, 2079. [CrossRef] [PubMed]
18. Sefah, K.; Shangguan, D.; Xiong, X.L.; O'Donoghue, M.B.; Tan, W.H. Development of DNA aptamers using cell-SELEX. *Nat. Protoc.* **2010**, *5*, 1169–1185. [CrossRef] [PubMed]
19. Shangguan, D.; Li, Y.; Tang, Z.W.; Cao, Z.H.C.; Chen, H.W.; Mallikaratchy, P.; Sefah, K.; Yang, C.Y.J.; Tan, W.H. Aptamers evolved from live cells as effective molecular probes for cancer study. *Proc. Natl. Acad. Sci. USA* **2006**, *103*, 11838–11843. [CrossRef] [PubMed]
20. Lee, J.F.; Hesselberth, J.R.; Meyers, L.A.; Ellington, A.D. Aptamer database. *Nucleic Acids Res.* **2004**, *32*, D95–D100. [CrossRef] [PubMed]
21. Cruz-Toledo, J.; McKeague, M.; Zhang, X.R.; Giamberardino, A.; McConnell, E.; Francis, T.; DeRosa, M.C.; Dumontier, M. Aptamer base: A collaborative knowledge base to describe aptamers and SELEX experiments. *Database* **2012**, *8*. [CrossRef] [PubMed]
22. Wu, Y.X.; Kwon, Y.J. Aptamers: The "evolution" of SELEX. *Methods* **2016**, *106*, 21–28. [CrossRef] [PubMed]
23. Gupta, S.; Hirota, M.; Waugh, S.M.; Murakami, I.; Suzuki, T.; Muraguchi, M.; Shibamori, M.; Ishikawa, Y.; Jarvis, T.C.; Carter, J.D.; et al. Chemically modified DNA aptamers bind interleukin-6 with high affinity and inhibit signaling by blocking its interaction with interleukin-6 receptor. *J. Biol. Chem.* **2014**, *289*, 8706–8719. [CrossRef] [PubMed]
24. Sundaram, P.; Kurniawan, H.; Byrne, M.E.; Wower, J. Therapeutic RNA aptamers in clinical trials. *Eur. J. Pharm. Sci.* **2013**, *48*, 259–271. [CrossRef] [PubMed]
25. Zhou, J.H.; Rossi, J. Aptamers as targeted therapeutics: Current potential and challenges. *Nat. Rev. Drug Discov.* **2017**, *16*, 181–202. [CrossRef] [PubMed]
26. Meng, H.M.; Liu, H.; Kuai, H.L.; Peng, R.Z.; Mo, L.T.; Zhang, X.B. Aptamer-integrated DNA nanostructures for biosensing, bioimaging and cancer therapy. *Chem. Soc. Rev.* **2016**, *45*, 2583–2602. [CrossRef] [PubMed]

27. Ku, T.H.; Zhang, T.T.; Luo, H.; Yen, T.M.; Chen, P.W.; Han, Y.Y.; Lo, Y.H. Nucleic acid aptamers: An emerging tool for biotechnology and biomedical sensing. *Sensors* **2015**, *15*, 16281–16313. [CrossRef] [PubMed]
28. Gold, L.; Ayers, D.; Bertino, J.; Bock, C.; Bock, A.; Brody, E.N.; Carter, J.; Dalby, A.B.; Eaton, B.E.; Fitzwater, T.; et al. Aptamer-based multiplexed proteomic technology for biomarker discovery. *PLoS ONE* **2010**, *5*, e15004. [CrossRef] [PubMed]
29. Bunka, D.H.J.; Stockley, P.G. Aptamers come of age—At last. *Nat. Rev. Microbiol.* **2006**, *4*, 588–596. [CrossRef] [PubMed]
30. Famulok, M.; Hartig, J.S.; Mayer, G. Functional aptamers and aptazymes in biotechnology, diagnostics, and therapy. *Chem. Rev.* **2007**, *107*, 3715–3743. [CrossRef] [PubMed]
31. Forier, C.; Boschetti, E.; Ouhammouch, M.; Cibiel, A.; Duconge, F.; Nogre, M.; Tellier, M.; Bataille, D.; Bihoreau, N.; Santambien, P.; et al. DNA aptamer affinity ligands for highly selective purification of human plasma-related proteins from multiple sources. *J. Chromatogr. A* **2017**, *1489*, 39–50. [CrossRef] [PubMed]
32. Keefe, A.D.; Pai, S.; Ellington, A. Aptamers as therapeutics. *Nat. Rev. Drug Discov.* **2010**, *9*, 537–550. [CrossRef] [PubMed]
33. Zhou, W.Z.; Huang, P.J.J.; Ding, J.S.; Liu, J. Aptamer-based biosensors for biomedical diagnostics. *Analyst* **2014**, *139*, 2627–2640. [CrossRef] [PubMed]
34. Jo, H.; Ban, C. Aptamer–nanoparticle complexes as powerful diagnostic and therapeutic tools. *Exp. Mol. Med.* **2016**, *48*, e230. [CrossRef] [PubMed]
35. Uzawa, T.; Tada, S.; Wang, W. Expansion of the aptamer library from a "natural soup" to an "unnatural soup". *Chem. Commun.* **2013**, *49*, 1786–1795. [CrossRef] [PubMed]
36. Wang, A.Z.; Farokhzad, O.C. Current progress of aptamer-based molecular imaging. *J. Nucl. Med.* **2014**, *55*, 353–356. [CrossRef] [PubMed]
37. Boros, E.; Gale, E.M.; Caravan, P. MR imaging probes: Design and applications. *Dalton Trans.* **2015**, *44*, 4804–4818. [CrossRef] [PubMed]
38. Hingorani, D.V.; Bernstein, A.S.; Pagel, M.D. A review of responsive MRI contrast agents: 2005–2014. *Contrast Media Mol. Imaging* **2015**, *10*, 245–265. [CrossRef] [PubMed]
39. Que, E.L.; Chang, C.J. Responsive magnetic resonance imaging contrast agents as chemical sensors for metals in biology and medicine. *Chem. Soc. Rev.* **2010**, *39*, 51–60. [CrossRef] [PubMed]
40. Gale, E.M.; Jones, C.M.; Ramsay, I.; Farrar, C.T.; Caravan, P. A janus chelator enables biochemically responsive MRI contrast with exceptional dynamic range. *J. Am. Chem. Soc.* **2016**, *138*, 15861–15864. [CrossRef] [PubMed]
41. Yigit, M.V.; Mazumdar, D.; Kim, H.K.; Lee, J.H.; Dintsov, B.; Lu, Y. Smart "turn-on" magnetic resonance contrast agents based on aptamer-functionalized superparamagnetic iron oxide nanoparticles. *ChemBioChem* **2007**, *8*, 1675–1678. [CrossRef] [PubMed]
42. Thomas, R.; Park, I.K.; Jeong, Y.Y. Magnetic iron oxide nanoparticles for multimodal imaging and therapy of cancer. *Int. J. Mol. Sci.* **2013**, *14*, 15910–15930. [CrossRef] [PubMed]
43. Huizenga, D.E.; Szostak, J.W. A DNA aptamer that binds adenosine and ATP. *Biochemistry* **1995**, *34*, 656–665. [CrossRef] [PubMed]
44. Tasset, D.M.; Kubik, M.F.; Steiner, W. Oligonucleotide inhibitors of human thrombin that bind distinct epitopes. *J. Mol. Biol.* **1997**, *272*, 688–698. [CrossRef] [PubMed]
45. Yigit, M.V.; Mazumdar, D.; Lu, Y. MRI detection of thrombin with aptamer functionalized superparamagnetic iron oxide nanoparticles. *Bioconjug. Chem.* **2008**, *19*, 412–417. [CrossRef] [PubMed]
46. Xu, W.C.; Lu, Y. A smart magnetic resonance imaging contrast agent responsive to adenosine based on a DNA aptamer-conjugated gadolinium complex. *Chem. Commun.* **2011**, *47*, 4998–5000. [CrossRef] [PubMed]
47. Xu, W.C.; Xing, H.; Lu, Y. A smart T-1-weighted MRI contrast agent for uranyl cations based on a DNAzyme-gadolinium conjugate. *Analyst* **2013**, *138*, 6266–6269. [CrossRef] [PubMed]
48. Artemov, D.; Mori, N.; Ravi, R.; Bhujwalla, Z.M. Magnetic resonance molecular imaging of the Her-2/neu receptor. *Cancer Res.* **2003**, *63*, 2723–2727. [PubMed]
49. Zhou, Z.X.; Lu, Z.R. Gadolinium-based contrast agents for magnetic resonance cancer imaging. *Wiley Interdiscip. Rev. Nanomed. Nanobiotechnol.* **2013**, *5*, 1–18. [CrossRef] [PubMed]
50. Hicke, B.J.; Stephens, A.W.; Gould, T.; Chang, Y.F.; Lynott, C.K.; Heil, J.; Borkowski, S.; Hilger, C.S.; Cook, G.; Warren, S.; et al. Tumor targeting by an aptamer. *J. Nucl. Med.* **2006**, *47*, 668–678. [PubMed]

51. Bernard, E.D.; Beking, M.A.; Rajamanickam, K.; Tsai, E.C.; DeRosa, M.C. Target binding improves relaxivity in aptamer-gadolinium conjugates. *J. Biol. Inorg. Chem.* **2012**, *17*, 1159–1175. [CrossRef] [PubMed]
52. Caravan, P. Protein-targeted gadolinium-based magnetic resonance imaging (MRI) contrast agents: Design and mechanism of action. *Acc. Chem. Res.* **2009**, *42*, 851–862. [CrossRef] [PubMed]
53. Lupold, S.E.; Hicke, B.J.; Lin, Y.; Coffey, D.S. Identification and characterization of nuclease-stabilized RNA molecules that bind human prostate cancer cells via the prostate-specific membrane antigen. *Cancer Res.* **2002**, *62*, 4029–4033. [PubMed]
54. Wang, A.Z.; Bagalkot, V.; Vasilliou, C.C.; Gu, F.; Alexis, F.; Zhang, L.; Shaikh, M.; Yuet, K.; Cima, M.J.; Langer, R.; et al. Superparamagnetic iron oxide nanoparticle-aptamer bioconjugates for combined prostate cancer imaging and therapy. *Chem. Med. Chem.* **2008**, *3*, 1311–1315. [CrossRef] [PubMed]
55. Farokhzad, O.C.; Cheng, J.J.; Teply, B.A.; Sherifi, I.; Jon, S.; Kantoff, P.W.; Richie, J.P.; Langer, R. Targeted nanoparticle-aptamer bioconjugates for cancer chemotherapy in vivo. *Proc. Natl. Acad. Sci. USA* **2006**, *103*, 6315–6320. [CrossRef] [PubMed]
56. Yu, M.K.; Kim, D.; Lee, I.H.; So, J.S.; Jeong, Y.Y.; Jon, S. Image-guided prostate cancer therapy using aptamer-functionalized thermally cross-linked superparamagnetic iron oxide nanoparticles. *Small* **2011**, *7*, 2241–2249. [CrossRef] [PubMed]
57. Bates, P.J.; Laber, D.A.; Miller, D.M.; Thomas, S.D.; Trent, J.O. Discovery and development of the G-rich oligonucleotide AS1411 as a novel treatment for cancer. *Exp. Mol. Pathol.* **2009**, *86*, 151–164. [CrossRef] [PubMed]
58. Li, J.J.; You, J.; Dai, Y.; Shi, M.L.; Han, C.P.; Xu, K. Gadolinium oxide nanoparticles and aptamer-functionalized silver nanoclusters-based multimodal molecular imaging nanoprobe for optical/magnetic resonance cancer cell imaging. *Anal. Chem.* **2014**, *86*, 11306–11311. [CrossRef] [PubMed]
59. Ji, K.L.; Lim, W.S.; Li, S.F.Y.; Bhakoo, K. A two-step stimulus-response cell-SELEX method to generate a DNA aptamer to recognize inflamed human aortic endothelial cells as a potential in vivo molecular probe for atherosclerosis plaque detection. *Anal. Bioanal. Chem.* **2013**, *405*, 6853–6861. [CrossRef] [PubMed]
60. Ametamey, S.M.; Honer, M.; Schubiger, P.A. Molecular imaging with PET. *Chem. Rev.* **2008**, *108*, 1501–1516. [CrossRef] [PubMed]
61. Perrin, D.M. [$^{18}$F]-Organotrifluoroborates as radioprosthetic groups for PET imaging: From design principles to preclinical applications. *Acc. Chem. Res.* **2016**, *49*, 1333–1343. [CrossRef] [PubMed]
62. Bernard-Gauthier, V.; Bailey, J.J.; Liu, Z.B.; Wangler, B.; Wangler, C.; Jurkschat, K.; Perrin, D.M.; Schirrmacher, R. From unorthodox to established: The current status of F-18-trifluoroborate- and F-18-SiFA-based radiopharmaceuticals in PET nuclear imaging. *Bioconjug. Chem.* **2016**, *27*, 267–279. [CrossRef] [PubMed]
63. Lange, C.W.; VanBrocklin, H.F.; Taylor, S.E. Photoconjugation of 3-azido-5-nitrobenzyl-[$^{18}$F] fluoride to an oligonucleotide aptamer. *J. Label. Compd. Radiopharm.* **2002**, *45*, 257–268. [CrossRef]
64. Jacobson, O.; Weiss, I.D.; Wang, L.; Wang, Z.; Yang, X.Y.; Dewhurst, A.; Ma, Y.; Zhu, G.Z.; Niu, G.; Kiesewetter, D.O.; et al. $^{18}$F-Labeled single-stranded DNA aptamer for PET imaging of protein tyrosine kinase-7 expression. *J. Nucl. Med.* **2015**, *56*, 1780–1785. [CrossRef] [PubMed]
65. Wang, L.; Jacobson, O.; Avdic, D.; Rotstein, B.H.; Weiss, I.D.; Collier, L.; Chen, X.Y.; Vasdev, N.; Liang, S.H. Ortho-stabilized $^{18}$F-Azido click agents and their application in PET imaging with single-stranded DNA aptamers. *Angew. Chem. Int. Ed.* **2015**, *54*, 12777–12781. [CrossRef] [PubMed]
66. Daniels, D.A.; Chen, H.; Hicke, B.J.; Swiderek, K.M.; Gold, L. A tenascin-c aptamer identified by tumor cell-SELEX: Systematic evolution of ligands by exponential enrichment. *Proc. Natl. Acad. Sci. USA* **2003**, *100*, 15416–15421. [CrossRef] [PubMed]
67. Jacobson, O.; Yan, X.F.; Niu, G.; Weiss, I.D.; Ma, Y.; Szajek, L.P.; Shen, B.Z.; Kiesewetter, D.O.; Chen, X.Y. PET imaging of tenascin-c with a radio labeled single-stranded DNA aptamer. *J. Nucl. Med.* **2015**, *56*, 616–621. [CrossRef] [PubMed]
68. Zhu, G.Z.; Zhang, H.M.; Jacobson, O.; Wang, Z.T.; Chen, H.J.; Yang, X.Y.; Niu, G.; Chen, X.Y. Combinatorial screening of DNA aptamers for molecular imaging of her2 in cancer. *Bioconjug. Chem.* **2017**, *28*, 1068–1075. [CrossRef] [PubMed]
69. Park, J.Y.; Lee, T.S.; Song, I.H.; Cho, Y.L.; Chae, J.R.; Yun, M.; Kang, H.; Lee, J.H.; Lim, J.H.; Cho, W.G.; et al. Hybridization-based aptamer labeling using complementary oligonucleotide platform for PET and optical imaging. *Biomaterials* **2016**, *100*, 143–151. [CrossRef] [PubMed]

70. Schulz, J.; Vimont, D.; Bordenave, T.; James, D.; Escudier, J.M.; Allard, M.; Szlosek-Pinaud, M.; Fouquet, E. Silicon-based chemistry: An original and efficient one-step approach to F-18 -nucleosides and F-18 -oligonucleotides for PET imaging. *Chem. Eur. J.* **2011**, *17*, 3096–3100. [CrossRef] [PubMed]
71. James, D.; Escudier, J.M.; Amigues, E.; Schulz, J.; Vitry, C.; Bordenave, T.; Szlosek-Pinaud, M.; Fouquet, E. A 'click chemistry' approach to the efficient synthesis of modified nucleosides and oligonucleotides for PET imaging. *Tetrahedron Lett.* **2010**, *51*, 1230–1232. [CrossRef]
72. Li, Y.; Schaffer, P.; Perrin, D.M. Dual isotope labeling: Conjugation of P-32-oligonucleotides with F-18-aryltrifluoroborate via copper(I) catalyzed cycloaddition. *Bioorg. Med. Chem. Lett.* **2013**, *23*, 6313–6316. [CrossRef] [PubMed]
73. Kuhnast, B.; de Bruin, A.; Hinnen, F.; Tavitian, B.; Dolle, F. Design and synthesis of a new F-18 fluoropyridine-based haloacetamide reagent for the labeling of oligonucleotides: 2-bromo-*N*-3-(2-F-18-fluoropyridin-3-yloxy)propyl acetamide. *Bioconjug. Chem.* **2004**, *15*, 617–627. [CrossRef] [PubMed]
74. James, M.L.; Gambhir, S.S. A molecular imaging primer: Modalities, imaging agents, and applications. *Physiol. Rev.* **2012**, *92*, 897–965. [CrossRef] [PubMed]
75. Gomes, S.D.; Miguel, J.; Azema, L.; Eimer, S.; Ries, C.; Dausse, E.; Loiseau, H.; Allard, M.; Toulme, J.J. Tc-99m-MAG3-aptamer for imaging human tumors associated with high level of matrix metalloprotease-9. *Bioconjug. Chem.* **2012**, *23*, 2192–2200. [CrossRef] [PubMed]
76. Kryza, D.; Debordeaux, F.; Azema, L.; Hassan, A.; Paurelle, O.; Schulz, J.; Savona-Baron, C.; Charignon, E.; Bonazza, P.; Taleb, J.; et al. Ex vivo and in vivo imaging and biodistribution of aptamers targeting the human matrix metalloprotease-9 in melanomas. *PLoS ONE* **2016**, *11*, e0149387. [CrossRef] [PubMed]
77. Macedo, B.; Cordeiro, Y. Unraveling prion protein interactions with aptamers and other PrP-binding nucleic acids. *Int. J. Mol. Sci.* **2017**, *18*, 1023. [CrossRef] [PubMed]
78. Qu, J.; Yu, S.Q.; Zheng, Y.; Zheng, Y.; Yang, H.; Zhang, J.L. Aptamer and its applications in neurodegenerative diseases. *Cell. Mol. Life Sci.* **2017**, *74*, 683–695. [CrossRef] [PubMed]
79. Wolter, O.; Mayer, G. Aptamers as valuable molecular tools in neurosciences. *J. Neurosci.* **2017**, *37*, 2517–2523. [CrossRef] [PubMed]
80. Nedergaard, M.; Takano, T.; Hansen, A.J. Beyond the role of glutamate as a neurotransmitter. *Nat. Rev. Neurosci.* **2002**, *3*, 748–755. [CrossRef] [PubMed]
81. Perry, M.; Li, Q.; Kennedy, R.T. Review of recent advances in analytical techniques for the determination of neurotransmitters. *Anal. Chim. Acta* **2009**, *653*, 1–22. [CrossRef] [PubMed]
82. Hokfelt, T.; Bartfai, T.; Bloom, F. Neuropeptides: Opportunities for drug discovery. *Lancet Neurol.* **2003**, *2*, 463–472. [CrossRef]
83. Li, B.R.; Hsieh, Y.J.; Chen, Y.X.; Chung, Y.T.; Pan, C.Y.; Chen, Y.T. An ultrasensitive nanowire-transistor biosensor for detecting dopamine release from living pc12 cells under hypoxic stimulation. *J. Am. Chem. Soc.* **2013**, *135*, 16034–16037. [CrossRef] [PubMed]
84. Kumar, A.; Singh, A.; Ekavali. A review on Alzheimer's disease pathophysiology and its management: An update. *Pharmacol. Rep.* **2015**, *67*, 195–203. [CrossRef] [PubMed]
85. Castren, E. Is mood chemistry? *Nat. Rev. Neurosci.* **2005**, *6*, 241–246. [CrossRef] [PubMed]
86. McConnell, E.M.; Holahan, M.R.; DeRosa, M.C. Aptamers as promising molecular recognition elements for diagnostics and therapeutics in the central nervous system. *Nucleic Acid Ther.* **2014**, *24*, 388–404. [CrossRef] [PubMed]
87. Mannironi, C.; DiNardo, A.; Fruscoloni, P.; TocchiniValentini, G.P. In vitro selection of dopamine RNA ligands. *Biochemistry* **1997**, *36*, 9726–9734. [CrossRef] [PubMed]
88. Zheng, Y.; Wang, Y.; Yang, X.R. Aptamer-based colorimetric biosensing of dopamine using unmodified gold nanoparticles. *Sens. Actuator B Chem.* **2011**, *156*, 95–99. [CrossRef]
89. Farjami, E.; Campos, R.; Nielsen, J.S.; Gothelf, K.V.; Kjems, J.; Ferapontova, E.E. RNA aptamer-based electrochemical biosensor for selective and label-free analysis of dopamine. *Anal. Chem.* **2013**, *85*, 121–128. [CrossRef] [PubMed]
90. Walsh, R.; DeRosa, M.C. Retention of function in the DNA homolog of the RNA dopamine aptamer. *Biochem. Biophys. Res. Commun.* **2009**, *388*, 732–735. [CrossRef] [PubMed]

91. Holahan, M.R.; Madularu, D.; McConnell, E.M.; Walsh, R.; DeRosa, M.C. Intra-accumbens injection of a dopamine aptamer abates MK-801-induced cognitive dysfunction in a model of schizophrenia. *PLoS ONE* **2011**, *6*, e22239. [CrossRef] [PubMed]
92. Alvarez-Martos, I.; Ferapontova, E.E. A DNA sequence obtained by replacement of the dopamine RNA aptamer bases is not an aptamer. *Biochem. Biophys. Res. Commun.* **2017**, *489*, 381–385. [CrossRef] [PubMed]
93. Kammer, M.N.; Olmsted, I.R.; Kussrow, A.K.; Morris, M.J.; Jackson, G.W.; Bornhop, D.J. Characterizing aptamer small molecule interactions with backscattering interferometry. *Analyst* **2014**, *139*, 5879–5884. [CrossRef] [PubMed]
94. Bruno, J.G.; Carrillo, M.P.; Phillips, T.; King, B. Development of DNA aptamers for cytochemical detection of acetylcholine. *In Vitro Cell. Dev. Biol. Anim.* **2008**, *44*, 63–72. [CrossRef] [PubMed]
95. Chavez, J.L.; Hagen, J.A.; Kelley-Loughnane, N. Fast and selective plasmonic serotonin detection with aptamer-gold nanoparticle conjugates. *Sensors* **2017**, *17*, 8. [CrossRef] [PubMed]
96. Tatemoto, K. Neuropeptide Y: Complete amino-acid-sequence of the brain peptide. *Proc. Natl. Acad. Sci. USA* **1982**, *79*, 5485–5489. [CrossRef] [PubMed]
97. Van den Pol, A.N. Neuropeptide transmission in brain circuits. *Neuron* **2012**, *76*, 98–115. [CrossRef] [PubMed]
98. Mendonsa, S.D.; Bowser, M.T. In vitro selection of aptamers with affinity for neuropeptide Y using capillary electrophoresis. *J. Am. Chem. Soc.* **2005**, *127*, 9382–9383. [CrossRef] [PubMed]
99. Proske, D.; Hofliger, M.; Soll, R.M.; Beck-Sickinger, A.G.; Famulok, M. A Y2 receptor mimetic aptamer directed against neuropeptide Y. *J. Biol. Chem.* **2002**, *277*, 11416–11422. [CrossRef] [PubMed]
100. Fernandez, R.E.; Sanghavi, B.J.; Farmehini, V.; Chavez, J.L.; Hagen, J.; Kelley-Loughnane, N.; Chou, C.F.; Swami, N.S. Aptamer-functionalized graphene-gold nanocomposites for label-free detection of dielectrophoretic-enriched neuropeptide Y. *Electrochem. Commun.* **2016**, *72*, 144–147. [CrossRef]
101. Banerjee, S.; Hsieh, Y.J.; Liu, C.R.; Yeh, N.H.; Hung, H.H.; Lai, Y.S.; Chou, A.C.; Chen, Y.T.; Pan, C.Y. Differential releases of dopamine and neuropeptide Y from histamine-stimulated pc12 cells detected by an aptamer-modified nanowire transistor. *Small* **2016**, *12*, 5524–5529. [CrossRef] [PubMed]
102. Eulberg, D.; Buchner, K.; Maasch, C.; Klussmann, S. Development of an automated in vitro selection protocol to obtain RNA-based aptamers: Identification of a biostable substance P antagonist. *Nucleic Acids Res.* **2005**, *33*, e45. [CrossRef] [PubMed]
103. Vater, A.; Klussmann, S. Turning mirror-image oligonucleotides into drugs: The evolution of spiegelmer therapeutics. *Drug Discov. Today* **2015**, *20*, 147–155. [CrossRef] [PubMed]
104. Faulhammer, D.; Eschgfaller, B.; Stark, S.; Burgstaller, P.; Englberger, W.; Erfurth, J.; Kleinjung, F.; Rupp, J.; Vulcu, S.D.; Schroder, W.; et al. Biostable aptamers with antagonistic properties to the neuropeptide nociceptin/orphanin FQ. *RNA* **2004**, *10*, 516–527. [CrossRef] [PubMed]
105. Takenaka, M.; Amino, T.; Miyachi, Y.; Ogino, C.; Kondo, A. Screening and evaluation of aptamers against somatostatin, and sandwich-like monitoring of somatostatin based on atomic force microscopy. *Sens. Actuator B Chem.* **2017**, *252*, 813–821. [CrossRef]
106. Kobelt, P.; Helmling, S.; Stengel, A.; Wlotzka, B.; Andresen, V.; Klapp, B.F.; Wiedenmann, B.; Klussmann, S.; Monnikes, H. Anti-ghrelin spiegelmer NOX-B11 inhibits neurostimulatory and orexigenic effects of peripheral ghrelin in rats. *Gut* **2006**, *55*, 788–792. [CrossRef] [PubMed]
107. Vater, A.; Sell, S.; Kaczmarek, P.; Maasch, C.; Buchner, K.; Pruszynska-Oszmalek, E.; Kolodziejski, P.; Purschke, W.G.; Nowak, K.W.; Strowski, M.Z.; et al. A mixed mirror-image DNA/RNA aptamer inhibits glucagon and acutely improves glucose tolerance in models of type 1 and type 2 diabetes. *J. Biol. Chem.* **2013**, *288*, 21136–21147. [CrossRef] [PubMed]
108. Heiat, M.; Ranjbar, R.; Latifi, A.M.; Rasaee, M.J. Selection of a high-affinity and in vivo bioactive ssDNA aptamer against angiotensin II peptide. *Peptides* **2016**, *82*, 101–108. [CrossRef] [PubMed]
109. Vater, A.; Jarosch, F.; Buchner, K.; Klussmann, S. Short bioactive spiegelmers to migraine-associated calcitonin gene-related peptide rapidly identified by a novel approach: Tailored-SELEX. *Nucleic Acids Res.* **2003**, *31*, e130. [CrossRef] [PubMed]
110. Kahsai, A.W.; Wisler, J.W.; Lee, J.; Ahn, S.; Cahill, T.J.; Dennison, S.M.; Staus, D.P.; Thomsen, A.R.B.; Anasti, K.M.; Pani, B.; et al. Conformationally selective RNA aptamers allosterically modulate the β(2)-adrenoceptor. *Nat. Chem. Biol.* **2016**, *12*, 709–716. [CrossRef] [PubMed]
111. Daniels, D.A.; Sohal, A.K.; Rees, S.; Grisshammer, R. Generation of RNA aptamers to the G-protein-coupled receptor for neurotensin, NTS-1. *Anal. Biochem.* **2002**, *305*, 214–226. [CrossRef] [PubMed]

112. Clawson, G.A.; Abraham, T.; Pan, W.H.; Tang, X.M.; Linton, S.S.; McGovern, C.O.; Loc, W.S.; Smith, J.P.; Butler, P.J.; Kester, M.; et al. A cholecystokinin B receptor-specific DNA aptamer for targeting pancreatic ductal adenocarcinoma. *Nucleic Acid Ther.* **2017**, *27*, 23–35. [CrossRef] [PubMed]
113. Costanzo, M.; Zurzolo, C. The cell biology of prion-like spread of protein aggregates: Mechanisms and implication in neurodegeneration. *Biochem. J.* **2013**, *452*, 1–17. [CrossRef] [PubMed]
114. Verwilst, P.; Kim, H.-R.; Seo, J.; Sohn, N.-W.; Cha, S.-Y.; Kim, Y.; Maeng, S.; Shin, J.-W.; Kwak, J.H.; Kang, C.; et al. Rational design of in vivo tau tangle-selective near-infrared fluorophores: Expanding the BODIPY universe. *J. Am. Chem. Soc.* **2017**, *139*, 13393–13403. [CrossRef] [PubMed]
115. Guo, J.L.; Lee, V.M.Y. Seeding of normal tau by pathological tau conformers drives pathogenesis of Alzheimer-like tangles. *J. Biol. Chem.* **2011**, *286*, 15317–15331. [CrossRef] [PubMed]
116. Kim, J.H.; Kim, E.; Choi, W.H.; Lee, J.; Lee, J.H.; Lee, H.; Kim, D.E.; Suh, Y.H.; Lee, M.J. Inhibitory RNA aptamers of tau oligomerization and their neuroprotective roles against proteotoxic stress. *Mol. Pharm.* **2016**, *13*, 2039–2048. [CrossRef] [PubMed]
117. Krylova, S.M.; Musheev, M.; Nutiu, R.; Li, Y.F.; Lee, G.; Krylov, S.N. Tau protein binds single-stranded DNA sequence specifically—The proof obtained in vitro with non-equilibrium capillary electrophoresis of equilibrium mixtures. *FEBS Lett.* **2005**, *579*, 1371–1375. [CrossRef] [PubMed]
118. Kim, S.; Wark, A.W.; Lee, H.J. Femtomolar detection of tau proteins in undiluted plasma using surface plasmon resonance. *Anal. Chem.* **2016**, *88*, 7793–7799. [CrossRef] [PubMed]
119. Hamley, I.W. The amyloid β peptide: A chemist's perspective. Role in Alzheimer's and fibrillization. *Chem. Rev.* **2012**, *112*, 5147–5192. [CrossRef] [PubMed]
120. Lauren, J.; Gimbel, D.A.; Nygaard, H.B.; Gilbert, J.W.; Strittmatter, S.M. Cellular prion protein mediates impairment of synaptic plasticity by amyloid-β oligomers. *Nature* **2009**, *457*, 1128–1132. [CrossRef] [PubMed]
121. Balducci, C.; Beeg, M.; Stravalaci, M.; Bastone, A.; Sclip, A.; Biasini, E.; Tapella, L.; Colombo, L.; Manzoni, C.; Borsello, T.; et al. Synthetic amyloid-β oligomers impair long-term memory independently of cellular prion protein. *Proc. Natl. Acad. Sci. USA* **2010**, *107*, 2295–2300. [CrossRef] [PubMed]
122. Kessels, H.W.; Nguyen, L.N.; Nabavi, S.; Malinow, R. The prion protein as a receptor for amyloid-β. *Nature* **2010**, *466*, E3–E4. [CrossRef] [PubMed]
123. Benilova, I.; De Strooper, B. Prion protein in alzheimer's pathogenesis: A hot and controversial issue. *EMBO Mol. Med.* **2010**, *2*, 289–290. [CrossRef] [PubMed]
124. Liang, H.Y.; Shi, Y.S.; Kou, Z.W.; Peng, Y.H.; Chen, W.J.; Li, X.W.; Li, S.J.; Wang, Y.; Wang, F.; Zhang, X.M. Inhibition of bace1 activity by a DNA aptamer in an Alzheimer's disease cell model. *PLoS ONE* **2015**, *10*, e0140733. [CrossRef] [PubMed]
125. Eremeeva, E.; Abramov, M.; Margamuljana, L.; Rozenski, J.; Pezo, V.; Marliere, P.; Herdewijn, P. Chemical morphing of DNA containing four noncanonical bases. *Angew. Chem. Int. Ed.* **2016**, *55*, 7515–7519. [CrossRef] [PubMed]
126. Gasse, C.; Zaarour, M.; Noppen, S.; Abramov, M.; Marliere, P.; Liekens, S.; De Strooper, B.; Herdewijn, P. Modulation of BACE1 activity by chemically modified aptamers. *Chembiochem* **2017**. submitted.
127. Rentmeister, A.; Bill, A.; Wahle, T.; Walter, J.; Famulok, M. RNA aptamers selectively modulate protein recruitment to the cytoplasmic domain of β-secretase BACE1 in vitro. *RNA* **2006**, *12*, 1650–1660. [CrossRef] [PubMed]
128. Ylera, F.; Lurz, R.; Erdmann, V.A.; Furste, J.P. Selection of RNA aptamers to the Alzheimer's disease amyloid peptide. *Biochem. Biophys. Res. Commun.* **2002**, *290*, 1583–1588. [CrossRef] [PubMed]
129. Farrar, C.T.; William, C.M.; Hudry, E.; Hashimoto, T.; Hyman, B.T. RNA aptamer probes as optical imaging agents for the detection of amyloid plaques. *PLoS ONE* **2014**, *9*, e89901. [CrossRef] [PubMed]
130. Rahimi, F.; Murakami, K.; Summers, J.L.; Chen, C.-H.B.; Bitan, G. RNA aptamers generated against oligomeric aβ40 recognize common amyloid aptatopes with low specificity but high sensitivity. *PLoS ONE* **2009**, *4*, e7694. [CrossRef] [PubMed]
131. Takahashi, T.; Tada, K.; Mihara, H. RNA aptamers selected against amyloid β-peptide (Aβ) inhibit the aggregation of ab. *Mol. Biosyst.* **2009**, *5*, 986–991. [CrossRef] [PubMed]
132. Murakami, K.; Nishikawa, F.; Noda, K.; Yokoyama, T.; Nishikawa, S. Anti-bovine prion protein RNA aptamer containing tandem gga repeat interacts both with recombinant bovine prion protein and its β isoform with high affinity. *Prion* **2008**, *2*, 73–80. [CrossRef] [PubMed]

133. Ogasawara, D.; Hasegawa, H.; Kaneko, K.; Sode, K.; Ikebukuro, K. Screening of DNA aptamer against mouse prion protein by competitive selection. *Prion* **2007**, *1*, 248–254. [CrossRef] [PubMed]
134. Proske, D.; Gilch, S.; Wopfner, F.; Schatzl, H.M.; Winnacker, E.L.; Famulok, M. Prion-protein-specific aptamer reduces PrPSc formation. *ChemBioChem* **2002**, *3*, 717–725. [CrossRef]
135. Wang, P.; Hatcher, K.L.; Bartz, J.C.; Chen, S.G.; Skinner, P.; Richt, J.; Liu, H.; Sreevatsan, S. Selection and characterization of DNA aptamers against PrPSc. *Exp. Biol. Med.* **2011**, *236*, 466–476. [CrossRef] [PubMed]
136. Goedert, M. Alpha-synuclein and neurodegenerative diseases. *Nat. Rev. Neurosci.* **2001**, *2*, 492–501. [CrossRef] [PubMed]
137. Spillantini, M.G.; Schmidt, M.L.; Lee, V.M.Y.; Trojanowski, J.Q.; Jakes, R.; Goedert, M. Alpha-synuclein in Lewy bodies. *Nature* **1997**, *388*, 839–840. [CrossRef] [PubMed]
138. Tsukakoshi, K.; Harada, R.; Sode, K.; Ikebukuro, K. Screening of DNA aptamer which binds to alpha-synuclein. *Biotechnol. Lett.* **2010**, *32*, 643–648. [CrossRef] [PubMed]
139. Hasegawa, H.; Sode, K.; Ikebukuro, K. Selection of DNA aptamers against VEGF(165) using a protein competitor and the aptamer blotting method. *Biotechnol. Lett.* **2008**, *30*, 829–834. [CrossRef] [PubMed]
140. Tsukakoshi, K.; Abe, K.; Sode, K.; Ikebukuro, K. Selection of DNA aptamers that recognize alpha-synuclein oligomers using a competitive screening method. *Anal. Chem.* **2012**, *84*, 5542–5547. [CrossRef] [PubMed]
141. Sun, K.; Xia, N.; Zhao, L.J.; Liu, K.; Hou, W.J.; Liu, L. Aptasensors for the selective detection of alpha-synuclein oligomer by colorimetry, surface plasmon resonance and electrochemical impedance spectroscopy. *Sens. Actuator B Chem.* **2017**, *245*, 87–94. [CrossRef]
142. Liu, L.; Chang, Y.; Yu, J.; Jiang, M.S.; Xia, N. Two-in-one polydopamine nanospheres for fluorescent determination of β-amyloid oligomers and inhibition of β-amyloid aggregation. *Sens. Actuator B Chem.* **2017**, *251*, 359–365. [CrossRef]
143. Zhou, Y.L.; Zhang, H.Q.; Liu, L.T.; Li, C.M.; Chang, Z.; Zhu, X.; Ye, B.X.; Xu, M.T. Fabrication of an antibody-aptamer sandwich assay for electrochemical evaluation of levels of β-amyloid oligomers. *Sci. Rep.* **2016**, *6*, 35186. [CrossRef] [PubMed]
144. Jiang, L.F.; Chen, B.C.; Chen, B.; Li, X.J.; Liao, H.L.; Huang, H.M.; Guo, Z.J.; Zhang, W.Y.; Wu, L. Detection of ab oligomers based on magnetic-field-assisted separation of aptamer-functionalized $Fe_3O_4$ magnetic nanoparticles and $bayf_5$:Yb,er nanoparticles as upconversion fluorescence labels. *Talanta* **2017**, *170*, 350–357. [CrossRef] [PubMed]
145. Zhu, L.L.; Zhang, J.Y.; Wang, F.Y.; Wang, Y.; Lu, L.L.; Feng, C.C.; Xu, Z.A.; Zhang, W. Selective amyloid β oligomer assay based on abasic site-containing molecular beacon and enzyme-free amplification. *Biosens. Bioelectron.* **2016**, *78*, 206–212. [CrossRef] [PubMed]
146. McLaughlin, C.K.; Hamblin, G.D.; Sleiman, H.F. Supramolecular DNA assembly. *Chem. Soc. Rev.* **2011**, *40*, 5647–5656. [CrossRef] [PubMed]
147. Rothemund, P.W.K. Folding DNA to create nanoscale shapes and patterns. *Nature* **2006**, *440*, 297–302. [CrossRef] [PubMed]
148. Endo, M.; Yang, Y.; Sugiyama, H. DNA origami technology for biomaterials applications. *Biomater. Sci.* **2013**, *1*, 347–360. [CrossRef]
149. Chhabra, R.; Sharma, J.; Ke, Y.G.; Liu, Y.; Rinker, S.; Lindsay, S.; Yan, H. Spatially addressable multiprotein nanoarrays templated by aptamer-tagged DNA nanoarchitectures. *J. Am. Chem. Soc.* **2007**, *129*, 10304–10305. [CrossRef] [PubMed]
150. Rinker, S.; Ke, Y.G.; Liu, Y.; Chhabra, R.; Yan, H. Self-assembled DNA nanostructures for distance-dependent multivalent ligand-protein binding. *Nat. Nanotechnol.* **2008**, *3*, 418–422. [CrossRef] [PubMed]
151. Douglas, S.M.; Bachelet, I.; Church, G.M. A logic-gated nanorobot for targeted transport of molecular payloads. *Science* **2012**, *335*, 831–834. [CrossRef] [PubMed]
152. Godonoga, M.; Lin, T.Y.; Oshima, A.; Sumitomo, K.; Tang, M.S.L.; Cheung, Y.W.; Kinghorn, A.B.; Dirkzwager, R.M.; Zhou, C.S.; Kuzuya, A.; et al. A DNA aptamer recognising a malaria protein biomarker can function as part of a DNA origami assembly. *Sci. Rep.* **2016**, *6*, 21266. [CrossRef] [PubMed]
153. Walter, H.K.; Bauer, J.; Steinmeyer, J.; Kuzuya, A.; Niemeyer, C.M.; Wagenknecht, H.A. "DNA origami traffic lights" with a split aptamer sensor for a bicolor fluorescence readout. *Nano Lett.* **2017**, *17*, 2467–2472. [CrossRef] [PubMed]
154. Liu, F.R.; Sha, R.J.; Seeman, N.C. Modifying the surface features of two-dimensional DNA crystals. *J. Am. Chem. Soc.* **1999**, *121*, 917–922. [CrossRef]

155. Green, L.S.; Jellinek, D.; Jenison, R.; Ostman, A.; Heldin, C.H.; Janjic, N. Inhibitory DNA ligands to platelet-derived growth factor B-Chain. *Biochemistry* **1996**, *35*, 14413–14424. [CrossRef] [PubMed]
156. Ke, Y.G.; Lindsay, S.; Chang, Y.; Liu, Y.; Yan, H. Self-assembled water-soluble nucleic acid probe tiles for label-free RNA hybridization assays. *Science* **2008**, *319*, 180–183. [CrossRef] [PubMed]
157. Cheung, Y.W.; Kwok, J.; Law, A.W.L.; Watt, R.M.; Kotaka, M.; Tanner, J.A. Structural basis for discriminatory recognition of plasmodium lactate dehydrogenase by a DNA aptamer. *Proc. Natl. Acad. Sci. USA* **2013**, *110*, 15967–15972. [CrossRef] [PubMed]
158. Kuzuya, A.; Sakai, Y.; Yamazaki, T.; Xu, Y.; Komiyama, M. Nanomechanical DNA origami 'single-molecule beacons' directly imaged by atomic force microscopy. *Nat. Commun.* **2011**, *2*, 449. [CrossRef] [PubMed]
159. Chen, A.L.; Yan, M.M.; Yang, S.M. Split aptamers and their applications in sandwich aptasensors. *Trac-Trends Anal. Chem.* **2016**, *80*, 581–593. [CrossRef]
160. Walter, H.K.; Bohlander, P.R.; Wagenknecht, H.A. Development of a wavelength-shifting fluorescent module for the adenosine aptamer using photostable cyanine dyes. *Chemistry* **2015**, *4*, 92–96. [CrossRef] [PubMed]
161. Holzhauser, C.; Wagenknecht, H.A. DNA and RNA "traffic lights": Synthetic wavelength-shifting fluorescent probes based on nucleic acid base substitutes for molecular imaging. *J. Org. Chem.* **2013**, *78*, 7373–7379. [CrossRef] [PubMed]
162. Bertrand, N.; Wu, J.; Xu, X.Y.; Kamaly, N.; Farokhzad, O.C. Cancer nanotechnology: The impact of passive and active targeting in the era of modern cancer biology. *Adv. Drug Deliv. Rev.* **2014**, *66*, 2–25. [CrossRef] [PubMed]
163. Strebhardt, K.; Ullrich, A. Paul Ehrlich's magic bullet concept: 100 years of progress. *Nat. Rev. Cancer* **2008**, *8*, 473–480. [CrossRef] [PubMed]
164. Liu, Q.L.; Jin, C.; Wang, Y.Y.; Fang, X.H.; Zhang, X.B.; Chen, Z.; Tan, W.H. Aptamer-conjugated nanomaterials for specific cancer cell recognition and targeted cancer therapy. *NPG Asia Mater.* **2014**, *6*, e95. [CrossRef]
165. Nair, R.R.; Wu, H.A.; Jayaram, P.N.; Grigorieva, I.V.; Geim, A.K. Unimpeded permeation of water through helium-leak-tight graphene-based membranes. *Science* **2012**, *335*, 442–444. [CrossRef] [PubMed]
166. Kim, J.; Park, S.J.; Min, D.H. Emerging approaches for graphene oxide biosensor. *Anal. Chem.* **2017**, *89*, 232–248. [CrossRef] [PubMed]
167. Nellore, B.P.V.; Kanchanapally, R.; Pramanik, A.; Sinha, S.S.; Chavva, S.R.; Hamme, A.; Ray, P.C. Aptamer-conjugated graphene oxide membranes for highly efficient capture and accurate identification of multiple types of circulating tumor cells. *Bioconjug. Chem.* **2015**, *26*, 235–242. [CrossRef] [PubMed]
168. Bahreyni, A.; Yazdian-Robati, R.; Hashemitabar, S.; Ramezani, M.; Ramezani, P.; Abnous, K.; Taghdisi, S.M. A new chemotherapy agent-free theranostic system composed of graphene oxide nano-complex and aptamers for treatment of cancer cells. *Int. J. Pharm.* **2017**, *526*, 391–399. [CrossRef] [PubMed]
169. Tang, Y.; Hu, H.; Zhang, M.G.; Song, J.; Nie, L.; Wang, S.; Niu, G.; Huang, P.; Lu, G.; Chen, X. An aptamer-targeting photoresponsive drug delivery system using "off-on" graphene oxide wrapped mesoporous silica nanoparticles. *Nanoscale* **2015**, *7*, 6304–6310. [CrossRef] [PubMed]
170. Yang, L.; Zhang, X.B.; Ye, M.; Jiang, J.H.; Yang, R.H.; Fu, T.; Chen, Y.; Wang, K.M.; Liu, C.; Tan, W.H. Aptamer-conjugated nanomaterials and their applications. *Adv. Drug Deliv. Rev.* **2011**, *63*, 1361–1370. [CrossRef] [PubMed]
171. Niu, W.; Chen, X.; Tan, W.; Veige, A.S. N-Heterocyclic Carbene–Gold(I) complexes conjugated to a Leukemia-Specific DNA aptamer for targeted drug delivery. *Angew. Chem. Int. Ed.* **2016**, *55*, 8889–8893. [CrossRef] [PubMed]
172. Siafaka, P.I.; Okur, N.U.; Karavas, E.; Bikiaris, D.N. Surface modified multifunctional and stimuli responsive nanoparticles for drug targeting: Current status and uses. *Int. J. Mol. Sci.* **2016**, *17*, 1440. [CrossRef] [PubMed]
173. Latorre, A.; Posch, C.; Garcimartin, Y.; Celli, A.; Sanlorenzo, M.; Vujic, I.; Ma, J.; Zekhtser, M.; Rappersberger, K.; Ortiz-Urda, S.; et al. DNA and aptamer stabilized gold nanoparticles for targeted delivery of anticancer therapeutics. *Nanoscale* **2014**, *6*, 7436–7442. [CrossRef] [PubMed]
174. Massich, M.D.; Giljohann, D.A.; Schmucker, A.L.; Patel, P.C.; Mirkin, C.A. Cellular response of polyvalent oligonucleotide-gold nanoparticle conjugates. *ACS Nano* **2010**, *4*, 5641–5646. [CrossRef] [PubMed]
175. Huang, S.-S.; Wei, S.-C.; Chang, H.-T.; Lin, H.-J.; Huang, C.-C. Gold nanoparticles modified with self-assembled hybrid monolayer of triblock aptamers as a photoreversible anticoagulant. *J. Control. Release* **2016**, *221*, 9–17. [CrossRef] [PubMed]

176. Swift, B.J.F.; Shadish, J.A.; DeForest, C.A.; Baneyx, F. Streamlined synthesis and assembly of a hybrid sensing architecture with solid binding proteins and click chemistry. *J. Am. Chem. Soc.* **2017**, *139*, 3958–3961. [CrossRef] [PubMed]
177. Geissler, D.; Linden, S.; Liermann, K.; Wegner, K.D.; Charbonniere, L.J.; Hildebrandt, N. Lanthanides and quantum dots as forster resonance energy transfer agents for diagnostics and cellular imaging. *Inorg. Chem.* **2014**, *53*, 1824–1838. [CrossRef] [PubMed]
178. Zhou, D.J. Quantum dot-nucleic acid/aptamer bioconjugate-based fluorimetric biosensors. *Biochem. Soc. Trans.* **2012**, *40*, 635–639. [CrossRef] [PubMed]
179. Elgqvist, J. Nanoparticles as theranostic vehicles in experimental and clinical applications-focus on prostate and breast cancer. *Int. J. Mol. Sci.* **2017**, *18*, 1102. [CrossRef] [PubMed]
180. Lin, Z.; Ma, Q.; Fei, X.; Zhang, H.; Su, X. A novel aptamer functionalized cuins2 quantum dots probe for daunorubicin sensing and near infrared imaging of prostate cancer cells. *Anal. Chim. Acta* **2014**, *818*, 54–60. [CrossRef] [PubMed]
181. Wu, Y.R.; Sefah, K.; Liu, H.P.; Wang, R.W.; Tan, W.H. DNA aptamer-micelle as an efficient detection/delivery vehicle toward cancer cells. *Proc. Natl. Acad. Sci. USA* **2010**, *107*, 5–10. [CrossRef] [PubMed]
182. Liu, H.P.; Zhu, Z.; Kang, H.Z.; Wu, Y.R.; Sefan, K.; Tan, W.H. DNA-based micelles: Synthesis, micellar properties and size-dependent cell permeability. *Chem. Eur. J.* **2010**, *16*, 3791–3797. [CrossRef] [PubMed]
183. Kim, J.; Kim, D.; Lee, J.B. DNA aptamer-based carrier for loading proteins and enhancing the enzymatic activity. *RSC Adv.* **2017**, *7*, 1643–1645. [CrossRef]
184. Xiong, X.L.; Liu, H.P.; Zhao, Z.L.; Altman, M.B.; Lopez-Colon, D.; Yang, C.J.; Chang, L.J.; Liu, C.; Tan, W.H. DNA aptamer-mediated cell targeting. *Angew. Chem. Int. Ed.* **2013**, *52*, 1472–1476. [CrossRef] [PubMed]
185. Lale, S.V.; Aswathy, R.G.; Aravind, A.; Kumar, D.S.; Koul, V. AS1411 aptamer and folic acid functionalized pH-responsive atrp fabricated pPEGMA-PCL-pPEGMA polymeric nanoparticles for targeted drug delivery in cancer therapy. *Biomacromolecules* **2014**, *15*, 1737–1752. [CrossRef] [PubMed]
186. Sun, P.C.; Zhang, N.; Tang, Y.F.; Yang, Y.N.; Chu, X.; Zhao, Y.X. Sl2b aptamer and folic acid dual-targeting DNA nanostructures for synergic biological effect with chemotherapy to combat colorectal cancer. *Int. J. Nanomed.* **2017**, *12*, 2657–2672. [CrossRef] [PubMed]
187. Dai, B.; Hu, Y.; Duan, J.; Yang, X.-D. Aptamer-guided DNA tetrahedron as a novel targeted drug delivery system for muc1-expressing breast cancer cells in vitro. *Oncotarget* **2016**, *7*, 38257–38269. [CrossRef] [PubMed]
188. Stiriba, S.E.; Frey, H.; Haag, R. Dendritic polymers in biomedical applications: From potential to clinical use in diagnostics and therapy. *Angew. Chem. Int. Ed.* **2002**, *41*, 1329–1334. [CrossRef]
189. MacEwan, S.R.; Chilkoti, A. From composition to cure: A systems engineering approach to anticancer drug carriers. *Angew. Chem. Int. Ed.* **2017**, *56*, 6712–6733. [CrossRef] [PubMed]
190. Gu, F.; Zhang, L.; Teply, B.A.; Mann, N.; Wang, A.; Radovic-Moreno, A.F.; Langer, R.; Farokhzad, O.C. Precise engineering of targeted nanoparticles by using self-assembled biointegrated block copolymers. *Proc. Natl. Acad. Sci. USA* **2008**, *105*, 2586–2591. [CrossRef] [PubMed]
191. Dhar, S.; Gu, F.X.; Langer, R.; Farokhzad, O.C.; Lippard, S.J. Targeted delivery of cisplatin to prostate cancer cells by aptamer functionalized Pt(IV) prodrug-PLGA-PEG nanoparticles. *Proc. Natl. Acad. Sci. USA* **2008**, *105*, 17356–17361. [CrossRef] [PubMed]
192. Dhar, S.; Kolishetti, N.; Lippard, S.J.; Farokhzad, O.C. Targeted delivery of a cisplatin prodrug for safer and more effective prostate cancer therapy in vivo. *Proc. Natl. Acad. Sci. USA* **2011**, *108*, 1850–1855. [CrossRef] [PubMed]
193. Zhuang, Y.Y.; Deng, H.P.; Su, Y.; He, L.; Wang, R.B.; Tong, G.S.; He, D.N.; Zhu, X.Y. Aptamer-functionalized and backbone redox-responsive hyperbranched polymer for targeted drug delivery in cancer therapy. *Biomacromolecules* **2016**, *17*, 2050–2062. [CrossRef] [PubMed]
194. Lao, Y.H.; Phua, K.K.L.; Leong, K.W. Aptamer nanomedicine for cancer therapeutics: Barriers and potential for translation. *ACS Nano* **2015**, *9*, 2235–2254. [CrossRef] [PubMed]
195. Taghavi, S.; Ramezani, M.; Alibolandi, M.; Abnous, K.; Taghdisi, S.M. Chitosan-modified plga nanoparticles tagged with 5tr1 aptamer for in vivo tumor-targeted drug delivery. *Cancer Lett.* **2017**, *400*, 1–8. [CrossRef] [PubMed]
196. Coles, D.J.; Rolfe, B.E.; Boase, N.R.B.; Veedu, R.N.; Thurecht, K.J. Aptamer-targeted hyperbranched polymers: Towards greater specificity for tumours in vivo. *Chem. Commun.* **2013**, *49*, 3836–3838. [CrossRef] [PubMed]

197. Yu, S.R.; Dong, R.J.; Chen, J.X.; Chen, F.; Jiang, W.F.; Zhou, Y.F.; Zhu, X.Y.; Yan, D.Y. Synthesis and self-assembly of arnphiphilic aptamer-functionalized hyperbranched multiarm copolymers for targeted cancer imaging. *Biomacromolecules* **2014**, *15*, 1828–1836. [CrossRef] [PubMed]
198. Xu, W.J.; Siddiqui, I.A.; Nihal, M.; Pilla, S.; Rosenthal, K.; Mukhtar, H.; Gong, S.Q. Aptamer-conjugated and doxorubicin-loaded unimolecular micelles for targeted therapy of prostate cancer. *Biomaterials* **2013**, *34*, 5244–5253. [CrossRef] [PubMed]
199. Torchilin, V.P. Recent advances with liposomes as pharmaceutical carriers. *Nat. Rev. Drug Discov.* **2005**, *4*, 145–160. [CrossRef] [PubMed]
200. Huwyler, J.; Wu, D.; Pardridge, W.M. Brain drug delivery of small molecules using immunoliposomes. *Proc. Natl. Acad. Sci. USA* **1996**, *93*, 14164–14169. [CrossRef] [PubMed]
201. Schnyder, A.; Huwyler, J. Drug transport to brain with targeted liposomes. *NeuroRX* **2005**, *2*, 99–107. [CrossRef] [PubMed]
202. Willis, M.C.; Collins, B.; Zhang, T.; Green, L.S.; Sebesta, D.P.; Bell, C.; Kellogg, E.; Gill, S.C.; Magallanez, A.; Knauer, S.; et al. Liposome anchored vascular endothelial growth factor aptamers. *Bioconjug. Chem.* **1998**, *9*, 573–582. [CrossRef] [PubMed]
203. Ara, M.N.; Matsuda, T.; Hyodo, M.; Sakurai, Y.; Hatakeyama, H.; Ohga, N.; Hida, K.; Harashima, H. An aptamer ligand based liposomal nanocarrier system that targets tumor endothelial cells. *Biomaterials* **2014**, *35*, 7110–7120. [CrossRef] [PubMed]
204. Alshaer, W.; Hillaireau, H.; Vergnaud, J.; Ismail, S.; Fattal, E. Functionalizing liposomes with anti-CD44 aptamer for selective targeting of cancer cells. *Bioconjug. Chem.* **2015**, *26*, 1307–1313. [CrossRef] [PubMed]
205. Plourde, K.; Derbali, R.M.; Desrosiers, A.; Dubath, C.; Vallée-Bélisle, A.; Leblond, J. Aptamer-based liposomes improve specific drug loading and release. *J. Control. Release* **2017**, *251*, 82–91. [CrossRef] [PubMed]
206. Wochner, A.; Menger, M.; Orgel, D.; Cech, B.; Rimmele, M.; Erdmann, V.A.; Glokler, J. A DNA aptamer with high affinity and specificity for therapeutic anthracyclines. *Anal. Biochem.* **2008**, *373*, 34–42. [CrossRef] [PubMed]
207. Barenholz, Y. Doxil®-the first FDA-approved nano-drug: Lessons learned. *J. Control. Release* **2012**, *160*, 117–134. [CrossRef] [PubMed]
208. Kang, S.; Hah, S.S. Improved ligand binding by antibody—Aptamer pincers. *Bioconjug. Chem.* **2014**, *25*, 1421–1427. [CrossRef] [PubMed]
209. Chu, T.C.; Twu, K.Y.; Ellington, A.D.; Levy, M. Aptamer mediated siRNA delivery. *Nucleic Acids Res.* **2006**, *34*, e73. [CrossRef] [PubMed]
210. Wang, R.W.; Zhu, G.Z.; Mei, L.; Xie, Y.; Ma, H.B.; Ye, M.; Qing, F.L.; Tan, W.H. Automated modular synthesis of aptamer-drug conjugates for targeted drug delivery. *J. Am. Chem. Soc.* **2014**, *136*, 2731–2734. [CrossRef] [PubMed]
211. Zhu, G.Z.; Niu, G.; Chen, X.Y. Aptamer-drug conjugates. *Bioconjug. Chem.* **2015**, *26*, 2186–2197. [CrossRef] [PubMed]
212. Huang, Y.-F.; Shangguan, D.; Liu, H.; Phillips, J.A.; Zhang, X.; Chen, Y.; Tan, W. Molecular assembly of an aptamer-drug conjugate for targeted drug delivery to tumor cells. *ChemBioChem* **2009**, *10*, 862–868. [CrossRef] [PubMed]
213. Zhu, G.; Zheng, J.; Song, E.; Donovan, M.; Zhang, K.; Liu, C.; Tan, W. Self-assembled, aptamer-tethered DNA nanotrains for targeted transport of molecular drugs in cancer theranostics. *Proc. Natl. Acad. Sci. USA* **2013**, *110*, 7998–8003. [CrossRef] [PubMed]
214. Shangguan, D.H.; Cao, Z.H.C.; Li, Y.; Tan, W.H. Aptamers evolved from cultured cancer cells reveal molecular differences of cancer cells in patient samples. *Clin. Chem.* **2007**, *53*, 1153–1155. [CrossRef] [PubMed]
215. Mallikaratchy, P. Evolution of complex target SELEX to identify aptamers against mammalian cell-surface antigens. *Molecules* **2017**, *22*, 215. [CrossRef] [PubMed]
216. Zhu, G.; Meng, L.; Ye, M.; Yang, L.; Sefah, K.; O'Donoghue, M.B.; Chen, Y.; Xiong, X.; Huang, J.; Song, E.; et al. Self-assembled aptamer-based drug carriers for bispecific cytotoxicity to cancer cells. *Chem. Asian J.* **2012**, *7*, 1630–1636. [CrossRef] [PubMed]
217. Zhang, P.; Zhao, N.X.; Zeng, Z.H.; Chang, C.C.; Zu, Y.L. Combination of an aptamer probe to CD4 and antibodies for multicolored cell phenotyping. *Am. J. Clin. Pathol.* **2010**, *134*, 586–593. [CrossRef] [PubMed]

218. Jo, N.; Mailhos, C.; Ju, M.H.; Cheung, E.; Bradley, J.; Nishijima, K.; Robinson, G.S.; Adarnis, A.P.; Shima, D.T. Inhibition of platelet-derived growth factor B signaling enhances the efficacy of anti-vascular enclothelial growth factor therapy in multiple models of ocular neovascularization. *Am. J. Pathol.* **2006**, *168*, 2036–2053. [CrossRef] [PubMed]
219. Heo, K.; Min, S.-W.; Sung, H.J.; Kim, H.G.; Kim, H.J.; Kim, Y.H.; Choi, B.K.; Han, S.; Chung, S.; Lee, E.S.; et al. An aptamer-antibody complex (oligobody) as a novel delivery platform for targeted cancer therapies. *J. Control. Release* **2016**, *229*, 1–9. [CrossRef] [PubMed]
220. Liu, Y.C.; Chen, Z.C.; He, A.B.; Zhan, Y.H.; Li, J.F.; Liu, L.; Wu, H.W.; Zhuang, C.L.; Lin, J.H.; Zhang, Q.X.; et al. Targeting cellular mRNAs translation by CRISPR-Cas9. *Sci. Rep.* **2016**, *6*, 29652. [CrossRef] [PubMed]
221. Wang, S.Y.; Su, J.H.; Zhang, F.; Zhuang, X.W. An RNA-aptamer-based two-color CRISPR labeling system. *Sci. Rep.* **2016**, *6*, 26857. [CrossRef] [PubMed]
222. Dassie, J.P.; Giangrande, P.H. Current progress on aptamer-targeted oligonucleotide therapeutics. *Ther. Deliv.* **2013**, *4*, 1527–1546. [CrossRef] [PubMed]
223. Kruspe, S.; Mittelberger, F.; Szameit, K.; Hahn, U. Aptamers as drug delivery vehicles. *Chem. Med. Chem.* **2014**, *9*, 1998–2011. [CrossRef] [PubMed]
224. Kruspe, S.; Giangrande, P. Aptamer-siRNA chimeras: Discovery, progress, and future prospects. *Biomedicines* **2017**, *5*, 45. [CrossRef] [PubMed]
225. McNamara, J.O.; Andrechek, E.R.; Wang, Y.; D Viles, K.; Rempel, R.E.; Gilboa, E.; Sullenger, B.A.; Giangrande, P.H. Cell type-specific delivery of siRNAs with aptamer-siRNA chimeras. *Nat. Biotechnol.* **2006**, *24*, 1005–1015. [CrossRef] [PubMed]
226. Dassie, J.P.; Liu, X.Y.; Thomas, G.S.; Whitaker, R.M.; Thiel, K.W.; Stockdale, K.R.; Meyerholz, D.K.; McCaffrey, A.P.; McNamara, J.O.; Giangrande, P.H. Systemic administration of optimized aptamer-siRNA chimeras promotes regression of PSMA-expressing tumors. *Nat. Biotechnol.* **2009**, *27*, 839–849. [CrossRef] [PubMed]
227. Liu, H.Y.; Yu, X.L.; Liu, H.T.; Wu, D.Q.; She, J.X. Co-targeting EGFR and survivin with a bivalent aptamer-dual siRNA chimera effectively suppresses prostate cancer. *Sci. Rep.* **2016**, *6*, 30346. [CrossRef] [PubMed]
228. Liu, H.Y.; Gao, X.H. A universal protein tag for delivery of siRNA-aptamer chimeras. *Sci. Rep.* **2013**, *3*, 3129. [CrossRef] [PubMed]
229. Jeong, H.; Lee, S.H.; Hwang, Y.; Yoo, H.; Jung, H.; Kim, S.H.; Mok, H. Multivalent aptamer-RNA conjugates for simple and efficient delivery of doxorubicin/siRNA into multidrug-resistant cells. *Macromol. Biosci.* **2017**, *17*, 1600343. [CrossRef] [PubMed]
230. Wilner, S.E.; Wengerter, B.; Maier, K.; Magalhaes, M.D.B.; Del Amo, D.S.; Pai, S.; Opazo, F.; Rizzoli, S.O.; Yan, A.; Levy, M. An RNA alternative to human transferrin: A new tool for targeting human cells. *Mol. Ther. Nucleic Acids* **2012**, *1*, e21. [CrossRef] [PubMed]
231. Breitz, H.B.; Weiden, P.L.; Beaumier, P.L.; Axworthy, D.B.; Seiler, C.; Su, F.M.; Graves, S.; Bryan, K.; Reno, J.M. Clinical optimization of pretargeted radioimmunotherapy with antibody-streptavidin conjugate and Y-90-DOTA-biotin. *J. Nucl. Med.* **2000**, *41*, 131–140. [PubMed]
232. Binzel, D.W.; Shu, Y.; Li, H.; Sun, M.Y.; Zhang, Q.S.; Shu, D.; Guo, B.; Guo, P.X. Specific delivery of miRNA for high efficient inhibition of prostate cancer by RNA nanotechnology. *Mol. Ther.* **2016**, *24*, 1267–1277. [CrossRef] [PubMed]
233. Serganov, A.; Patel, D.J. Ribozymes, riboswitches and beyond: Regulation of gene expression without proteins. *Nat. Rev. Genet.* **2007**, *8*, 776–790. [CrossRef] [PubMed]
234. Romero-Lopez, C.; Barroso-delJesus, A.; Puerta-Fernandez, E.; Berzal-Herranz, A. Interfering with hepatitis C virus ires activity using RNA molecules identified by a novel in vitro selection method. *Biol. Chem.* **2005**, *386*, 183–190. [CrossRef] [PubMed]
235. Romero-Lopez, C.; Diaz-Gonzalez, R.; Barroso-DelJesus, A.; Berzal-Herranz, A. Inhibition of hepatitis C virus replication and internal ribosome entry site-dependent translation by an RNA molecule. *J. Gen. Virol.* **2009**, *90*, 1659–1669. [CrossRef] [PubMed]
236. Romero-Lopez, C.; Lahlali, T.; Berzal-Herranz, B.; Berzal-Herranz, A. Development of optimized inhibitor RNAs allowing multisite-targeting of the HCV genome. *Molecules* **2017**, *22*, 861. [CrossRef] [PubMed]
237. Travascio, P.; Li, Y.F.; Sen, D. DNA-enhanced peroxidase activity of a DNA aptamer-hemin complex. *Chem. Biol.* **1998**, *5*, 505–517. [CrossRef]

238. Golub, E.; Albada, H.B.; Liao, W.C.; Biniuri, Y.; Willner, I. Nucleoapzymes: Hemin/G-quadruplex DNAzyme-aptamer binding site conjugates with superior enzyme-like catalytic functions. *J. Am. Chem. Soc.* **2016**, *138*, 164–172. [CrossRef] [PubMed]
239. Ni, S.; Yao, H.; Wang, L.; Lu, J.; Jiang, F.; Lu, A.; Zhang, G. Chemical modifications of nucleic acid aptamers for therapeutic purposes. *Int. J. Mol. Sci.* **2017**, *18*, 1683. [CrossRef] [PubMed]
240. Diafa, S.; Hollenstein, M. Generation of aptamers with an expanded chemical repertoire. *Molecules* **2015**, *20*, 16643–16671. [CrossRef] [PubMed]
241. Chen, T.; Hongdilokkul, N.; Liu, Z.X.; Thirunavukarasu, D.; Romesberg, F.E. The expanding world of DNA and RNA. *Curr. Opin. Chem. Biol.* **2016**, *34*, 80–87. [CrossRef] [PubMed]
242. Dellafiore, M.A.; Montserrat, J.M.; Iribarren, A.M. Modified nucleoside triphosphates for in vitro selection techniques. *Front. Chem.* **2016**, *4*, 18. [CrossRef] [PubMed]
243. Tolle, F.; Mayer, G. Dressed for success—Applying chemistry to modulate aptamer functionality. *Chem. Sci.* **2013**, *4*, 60–67. [CrossRef]
244. Dunn, M.R.; Jimenez, R.M.; Chaput, J.C. Analysis of aptamer discovery and technology. *Nat. Rev. Chem.* **2017**, *1*, 76. [CrossRef]
245. Gawande, B.N.; Rohloff, J.C.; Carter, J.D.; von Carlowitz, I.; Zhang, C.; Schneider, D.J.; Janjic, N. Selection of DNA aptamers with two modified bases. *Proc. Natl. Acad. Sci. USA* **2017**, *114*, 2898–2903. [CrossRef] [PubMed]
246. Lam, C.H.; Hipolito, C.J.; Hollenstein, M.; Perrin, D.M. A divalent metal-dependent self-cleaving DNAzyme with a tyrosine side chain. *Org. Biomol. Chem.* **2011**, *9*, 6949–6954. [CrossRef] [PubMed]
247. Renders, M.; Miller, E.; Lam, C.H.; Perrin, D.M. Whole cell-SELEX of aptamers with a tyrosine-like side chain against live bacteria. *Org. Biomol. Chem.* **2017**, *15*, 1980–1989. [CrossRef] [PubMed]
248. So, H.-M.; Park, D.-W.; Jeon, E.-K.; Kim, Y.-H.; Kim, B.S.; Lee, C.-K.; Choi, S.Y.; Kim, S.C.; Chang, H.; Lee, J.-O. Detection and Titer estimation of *Escherichia coli* using aptamer-functionalized single-walled carbon-nanotube field-effect transistors. *Small* **2008**, *4*, 197–201. [CrossRef] [PubMed]
249. Minagawa, H.; Onodera, K.; Fujita, H.; Sakamoto, T.; Akitomi, J.; Kaneko, N.; Shiratori, I.; Kuwahara, M.; Horii, K.; Waga, I. Selection, characterization and application of artificial DNA aptamer containing appended bases with sub-nanomolar affinity for a salivary biomarker. *Sci. Rep.* **2017**, *7*, 42716. [CrossRef] [PubMed]
250. Imaizumi, Y.; Kasahara, Y.; Fujita, H.; Kitadume, S.; Ozaki, H.; Endoh, T.; Kuwahara, M.; Sugimoto, N. Efficacy of base-modification on target binding of small molecule DNA aptamers. *J. Am. Chem. Soc.* **2013**, *135*, 9412–9419. [CrossRef] [PubMed]
251. Cho, E.J.; Lee, J.-W.; Ellington, A.D. Applications of aptamers as sensors. *Annu. Rev. Anal. Chem.* **2009**, *2*, 241–264. [CrossRef] [PubMed]
252. Vaish, N.K.; Larralde, R.; Fraley, A.W.; Szostak, J.W.; McLaughlin, L.W. A novel, modification-dependent ATP-binding aptamer selected from an RNA library incorporating a cationic functionality. *Biochemistry* **2003**, *42*, 8842–8851. [CrossRef] [PubMed]
253. Kabza, A.M.; Sczepanski, J.T. An L-RNA aptamer with expanded chemical functionality that inhibits microRNA biogenesis. *ChemBioChem* **2017**, *18*, 1824–1827. [CrossRef] [PubMed]
254. Kong, D.H.; Lei, Y.; Yeung, W.; Hili, R. Enzymatic synthesis of sequence-defined synthetic nucleic acid polymers with diverse functional groups. *Angew. Chem. Int. Ed.* **2016**, *55*, 13164–13168. [CrossRef] [PubMed]
255. Lei, Y.; Kong, D.H.; Hili, R. A high-fidelity codon set for the T4 DNA ligase-catalyzed polymerization of modified oligonucleotides. *ACS Comb. Sci.* **2015**, *17*, 716–721. [CrossRef] [PubMed]
256. Kong, D.; Yeung, W.; Hili, R. In vitro selection of diversely-functionalized aptamers. *J. Am. Chem. Soc.* **2017**, *139*, 13977–13980. [CrossRef] [PubMed]
257. Feldman, A.W.; Romesberg, F.E. In vivo structure–activity relationships and optimization of an unnatural base pair for replication in a semi-synthetic organism. *J. Am. Chem. Soc.* **2017**, *139*, 11427–11433. [CrossRef] [PubMed]
258. Kimoto, M.; Yamashige, R.; Matsunaga, K.-I.; Yokoyama, S.; Hirao, I. Generation of high-affinity DNA aptamers using an expanded genetic alphabet. *Nat. Biotechnol.* **2013**, *31*, 453–457. [CrossRef] [PubMed]
259. Kimoto, M.; Nakamura, M.; Hirao, I. Post-exSELEX stabilization of an unnatural-base DNA aptamer targeting VEGF(165) toward pharmaceutical applications. *Nucleic Acids Res.* **2016**, *44*, 7487–7494. [PubMed]

260. Matsunaga, K.-I.; Kimoto, M.; Hirao, I. High-affinity DNA aptamer generation targeting von willebrand factor A1-domain by genetic alphabet expansion for systematic evolution of ligands by exponential enrichment using two types of libraries composed of five different bases. *J. Am. Chem. Soc.* **2017**, *139*, 324–334. [CrossRef] [PubMed]
261. Hirao, I.; Kawai, G.; Yoshizawa, S.; Nishimura, Y.; Ishido, Y.; Watanabe, K.; Miura, K. Most compact hairpin-turn structure exerted by a short DNA fragment, d(GCGAAGC) in solution—An extraordinarily stable structure resistant to nucleases and heat. *Nucleic Acids Res.* **1994**, *22*, 576–582. [CrossRef] [PubMed]
262. Matsunaga, K.; Kimoto, M.; Hanson, C.; Sanford, M.; Young, H.A.; Hirao, I. Architecture of high-affinity unnatural-base DNA aptamers toward pharmaceutical applications. *Sci. Rep.* **2015**, *5*, 18478. [CrossRef] [PubMed]
263. Hirao, I.; Kimoto, M.; Lee, K.H. DNA aptamer generation by exSELEX using genetic alphabet expansion with a mini-hairpin DNA stabilization method. *Biochimie* **2017**. [CrossRef] [PubMed]
264. Yang, Z.Y.; Chen, F.; Chamberlin, S.G.; Benner, S.A. Expanded genetic alphabets in the polymerase chain reaction. *Angew. Chem. Int. Ed.* **2010**, *49*, 177–180. [CrossRef] [PubMed]
265. Benner, S.A.; Karalkar, N.B.; Hoshika, S.; Laos, R.; Shaw, R.W.; Matsuura, M.; Fajardo, D.; Moussatche, P. Alternative Watson-Crick synthetic genetic systems. *Cold Spring Harb. Perspect. Biol.* **2016**, *8*, a023770. [CrossRef] [PubMed]
266. Sefah, K.; Yang, Z.; Bradley, K.M.; Hoshika, S.; Jiménez, E.; Zhang, L.; Zhu, G.; Shanker, S.; Yu, F.; Turek, D.; et al. In vitro selection with artificial expanded genetic information systems. *Proc. Natl. Acad. Sci. USA* **2014**, *111*, 1449–1454. [CrossRef] [PubMed]
267. Zhang, L.; Yang, Z.; Le Trinh, T.; Teng, I.T.; Wang, S.; Bradley, K.M.; Hoshika, S.; Wu, Q.; Cansiz, S.; Rowold, D.J.; et al. Aptamers against cells overexpressing glypican 3 from expanded genetic systems combined with cell engineering and laboratory evolution. *Angew. Chem. Int. Ed.* **2016**, *55*, 12372–12375. [CrossRef] [PubMed]
268. Biondi, E.; Lane, J.D.; Das, D.; Dasgupta, S.; Piccirilli, J.A.; Hoshika, S.; Bradley, K.M.; Krantz, B.A.; Benner, S.A. Laboratory evolution of artificially expanded DNA gives redesignable aptamers that target the toxic form of anthrax protective antigen. *Nucleic Acids Res.* **2016**, *44*, 9565–9577. [CrossRef] [PubMed]
269. Kikin, O.; D'Antonio, L.; Bagga, P.S. Qgrs mapper: A web-based server for predicting G-quadruplexes in nucleotide sequences. *Nucleic Acids Res.* **2006**, *34*, W676–W682. [CrossRef] [PubMed]
270. Malyshev, D.A.; Dhami, K.; Lavergne, T.; Chen, T.J.; Dai, N.; Foster, J.M.; Correa, I.R.; Romesberg, F.E. A semi-synthetic organism with an expanded genetic alphabet. *Nature* **2014**, *509*, 385–388. [CrossRef] [PubMed]
271. Zhang, Y.; Lamb, B.M.; Feldman, A.W.; Zhou, A.X.; Lavergne, T.; Li, L.; Romesberg, F.E. A semisynthetic organism engineered for the stable expansion of the genetic alphabet. *Proc. Natl. Acad. Sci. USA* **2017**, *114*, 1317–1322. [CrossRef] [PubMed]
272. Rothlisberger, P.; Levi-Acobas, F.; Sarac, I.; Marliere, P.; Herdewijn, P.; Hollenstein, M. On the enzymatic incorporation of an imidazole nucleotide into DNA. *Org. Biomol. Chem.* **2017**, *15*, 4449–4455. [CrossRef] [PubMed]
273. Kaul, C.; Muller, M.; Wagner, M.; Schneider, S.; Carell, T. Reversible bond formation enables the replication and amplification of a crosslinking salen complex as an orthogonal base pair. *Nat. Chem.* **2011**, *3*, 794–800. [CrossRef] [PubMed]
274. Matyasovsky, J.; Perlikova, P.; Malnuit, V.; Pohl, R.; Hocek, M. 2-substituted dATP derivatives as building blocks for polymerase-catalyzed synthesis of DNA modified in the minor groove. *Angew. Chem. Int. Ed.* **2016**, *55*, 15856–15859. [CrossRef] [PubMed]
275. Hollenstein, M. Deoxynucleoside triphosphates bearing histamine, carboxylic acid, and hydroxyl residues—Synthesis and biochemical characterization. *Org. Biomol. Chem.* **2013**, *11*, 5162–5172. [CrossRef] [PubMed]
276. Eremeeva, E.; Abramov, M.; Margamuljana, L.; Herdewijn, P. Base-modified nucleic acids as a powerful tool for synthetic biology and biotechnology. *Chem. Eur. J.* **2017**, *23*, 9560–9576. [CrossRef] [PubMed]
277. Hollenstein, M. Synthesis of deoxynucleoside triphosphates that include proline, urea, or sulfamide groups and their polymerase incorporation into DNA. *Chem. Eur. J.* **2012**, *18*, 13320–13330. [CrossRef] [PubMed]
278. Röthlisberger, P.; Levi-Acobas, F.; Hollenstein, M. New synthetic route to ethynyl-dUTP: A means to avoid formation of acetyl and chloro vinyl base-modified triphosphates that could poison SELEX experiments. *Bioorg. Med. Chem. Lett.* **2017**, *27*, 897–900. [CrossRef] [PubMed]

279. Houlihan, G.; Arangundy-Franklin, S.; Holliger, P. Engineering and application of polymerases for synthetic genetics. *Curr. Opin. Biotechnol.* **2017**, *48*, 168–179. [CrossRef] [PubMed]
280. Chen, T.; Hongdilokkul, N.; Liu, Z.; Adhikary, R.; Tsuen, S.S.; Romesberg, F.E. Evolution of thermophilic DNA polymerases for the recognition and amplification of C2′-modified DNA. *Nat. Chem.* **2016**, *8*, 556–562. [CrossRef] [PubMed]
281. Thirunavukarasu, D.; Chen, T.; Liu, Z.; Hongdilokkul, N.; Romesberg, F.E. Selection of 2′-fluoro-modified aptamers with optimized properties. *J. Am. Chem. Soc.* **2017**, *139*, 2892–2895. [CrossRef] [PubMed]
282. Liu, Z.; Chen, T.; Romesberg, F.E. Evolved polymerases facilitate selection of fully 2′-OMe-modified aptamers. *Chem. Sci.* **2017**. [CrossRef]
283. Pinheiro, V.B.; Holliger, P. The XNA world: Progress towards replication and evolution of synthetic genetic polymers. *Curr. Opin. Chem. Biol.* **2012**, *16*, 245–252. [CrossRef] [PubMed]
284. Ferreira-Bravo, I.A.; Cozens, C.; Holliger, P.; DeStefano, J.J. Selection of 2′-deoxy-2′-fluoroarabinonucleotide (FANA) aptamers that bind HIV-1 reverse transcriptase with picomolar affinity. *Nucleic Acids Res.* **2015**, *43*, 9587–9599.
285. Yu, H.Y.; Zhang, S.; Chaput, J.C. Darwinian evolution of an alternative genetic system provides support for tna as an RNA progenitor. *Nat. Chem.* **2012**, *4*, 183–187. [CrossRef] [PubMed]
286. Diafa, S.; Evéquoz, D.; Leumann, C.J.; Hollenstein, M. Enzymatic synthesis of 7′,5′-bicyclo-DNA oligonucleotides. *Chem. Asian J.* **2017**, *12*, 1347–1352. [CrossRef] [PubMed]
287. Maiti, M.; Maiti, M.; Knies, C.; Dumbre, S.; Lescrinier, E.; Rosemeyer, H.; Ceulemans, A.; Herdewijn, P. Xylonucleic acid: Synthesis, structure, and orthogonal pairing properties. *Nucleic Acids Res.* **2015**, *43*, 7189–7200. [CrossRef] [PubMed]
288. Siegmund, V.; Santner, T.; Micura, R.; Marx, A. Screening mutant libraries of T7 RNA polymerase for candidates with increased acceptance of 2′-modified nucleotides. *Chem. Commun.* **2012**, *48*, 9870–9872. [CrossRef] [PubMed]
289. Inoue, N.; Shionoya, A.; Minakawa, N.; Kawakami, A.; Ogawa, N.; Matsuda, A. Amplification of 4′-thioDNA in the presence of 4′-thio-dTTP and 4′-thio-dCTP, and 4′-thioDNA-directed transcription in vitro and in mammalian cells. *J. Am. Chem. Soc.* **2007**, *129*, 15424–15425. [CrossRef] [PubMed]
290. Kojima, T.; Furukawa, K.; Maruyama, H.; Inoue, N.; Tarashima, N.; Matsuda, A.; Minakawa, N. PCR amplification of 4′-thioDNA using 2′-deoxy-4′-thionucleoside 5′-triphosphates. *ACS Synth. Biol.* **2013**, *2*, 529–536. [CrossRef] [PubMed]
291. Houlihan, G.; Arangundy-Franklin, S.; Holliger, P. Exploring the chemistry of genetic information storage and propagation through polymerase engineering. *Acc. Chem. Res.* **2017**, *50*, 1079–1087. [CrossRef] [PubMed]
292. Ghadessy, F.J.; Ramsay, N.; Boudsocq, F.; Loakes, D.; Brown, A.; Iwai, S.; Vaisman, A.; Woodgate, R.; Holliger, P. Generic expansion of the substrate spectrum of a DNA polymerase by directed evolution. *Nat. Biotechnol.* **2004**, *22*, 755–759. [CrossRef] [PubMed]
293. Higashimoto, Y.; Matsui, T.; Nishino, Y.; Taira, J.; Inoue, H.; Takeuchi, M.; Yamagishi, S. Blockade by phosphorothioate aptamers of advanced glycation end products-induced damage in cultured pericytes and endothelial cells. *Microvasc. Res.* **2013**, *90*, 64–70. [CrossRef] [PubMed]
294. Volk, D.; Lokesh, G. Development of phosphorothioate DNA and DNA thioaptamers. *Biomedicines* **2017**, *5*, 41. [CrossRef] [PubMed]
295. Yang, X.; Zhu, Y.; Wang, C.; Guan, Z.; Zhang, L.; Yang, Z. Alkylation of phosphorothioated thrombin binding aptamers improves the selectivity of inhibition of tumor cell proliferation upon anticoagulation. *Biochim. Biophys. Acta* **2017**, *1861*, 1864–1869. [CrossRef] [PubMed]
296. Padmanabhan, K.; Padmanabhan, K.P.; Ferrara, J.D.; Sadler, J.E.; Tulinsky, A. The structure of α-thrombin inhibited by a 15-mer single-stranded DNA aptamer. *J. Biol. Chem.* **1993**, *268*, 17651–17654. [PubMed]
297. Macaya, R.F.; Schultze, P.; Smith, F.W.; Roe, J.A.; Feigon, J. Thrombin-binding DNA aptamer forms a unimolecular quadruplex structure in solution. *Proc. Natl. Acad. Sci. USA* **1993**, *90*, 3745–3749. [CrossRef] [PubMed]
298. Lato, S.M.; Ozerova, N.D.S.; He, K.Z.; Sergueeva, Z.; Shaw, B.R.; Burke, D.H. Boron-containing aptamers to ATP. *Nucleic Acids Res.* **2002**, *30*, 1401–1407. [CrossRef] [PubMed]
299. Cheng, C.S.; Chen, Y.H.; Lennox, K.A.; Behlke, M.A.; Davidson, B.L. In vivo SELEX for identification of brain-penetrating aptamers. *Mol. Ther. Nucleic Acids* **2013**, *2*, e67. [CrossRef] [PubMed]

300. Monaco, I.; Camorani, S.; Colecchia, D.; Locatelli, E.; Calandro, P.; Oudin, A.; Niclou, S.; Arra, C.; Chiariello, M.; Cerchia, L.; et al. Aptamer functionalization of nanosystems for glioblastoma targeting through the blood-brain barrier. *J. Med. Chem.* **2017**, *60*, 4510–4516. [CrossRef] [PubMed]
301. Temme, J.S.; Drzyzga, M.G.; MacPherson, I.S.; Krauss, I.J. Directed evolution of 2g12-targeted nonamannose glycoclusters by SELMA. *Chem. Eur. J.* **2013**, *19*, 17291–17295. [CrossRef] [PubMed]
302. Larsen, A.C.; Dunn, M.R.; Hatch, A.; Sau, S.P.; Youngbull, C.; Chaput, J.C. A general strategy for expanding polymerase function by droplet microfluidics. *Nat. Commun.* **2016**, *7*, 11235. [CrossRef] [PubMed]
303. MacPherson, I.S.; Temme, J.S.; Krauss, I.J. DNA display of folded RNA libraries enabling RNA-SELEX without reverse transcription. *Chem. Commun.* **2017**, *53*, 2878–2881. [CrossRef] [PubMed]
304. Lai, J.C.; Hong, C.Y. Magnetic-assisted rapid aptamer selection (MARAS) for generating high-affinity DNA aptamer using rotating magnetic fields. *ACS Comb. Sci.* **2014**, *16*, 321–327. [CrossRef] [PubMed]
305. Renders, M.; Miller, E.; Hollenstein, M.; Perrin, D.M. A method for selecting modified DNAzymes without the use of modified DNA as a template in PCR. *Chem. Commun.* **2015**, *51*, 1360–1362. [CrossRef] [PubMed]

International Journal of
*Molecular Sciences*

MDPI

*Review*

# Computational Methods for Modeling Aptamers and Designing Riboswitches

**Sha Gong [1], Yanli Wang [2], Zhen Wang [2] and Wenbing Zhang [2,*]**

[1] Hubei Key Laboratory of Economic Forest Germplasm Improvement and Resources Comprehensive Utilization, Hubei Collaborative Innovation Center for the Characteristic Resources Exploitation of Dabie Mountains, Huanggang Normal University, Huanggang 438000, China; shagong@hgnu.edu.cn

[2] Department of Physics, Wuhan University, Wuhan 430072, China; 13212746736@163.com (Y.W.), zhenwang@whu.edu.cn (Z.W.)

* Correspondence: wbzhang@whu.edu.cn; Tel.: +86-27-6875-2989 (ext. 3225)

Received: 19 October 2017; Accepted: 14 November 2017; Published: 17 November 2017

**Abstract:** Riboswitches, which are located within certain noncoding RNA region perform functions as genetic "switches", regulating when and where genes are expressed in response to certain ligands. Understanding the numerous functions of riboswitches requires computation models to predict structures and structural changes of the aptamer domains. Although aptamers often form a complex structure, computational approaches, such as RNAComposer and Rosetta, have already been applied to model the tertiary (three-dimensional (3D)) structure for several aptamers. As structural changes in aptamers must be achieved within the certain time window for effective regulation, kinetics is another key point for understanding aptamer function in riboswitch-mediated gene regulation. The coarse-grained self-organized polymer (SOP) model using Langevin dynamics simulation has been successfully developed to investigate folding kinetics of aptamers, while their co-transcriptional folding kinetics can be modeled by the helix-based computational method and BarMap approach. Based on the known aptamers, the web server Riboswitch Calculator and other theoretical methods provide a new tool to design synthetic riboswitches. This review will represent an overview of these computational methods for modeling structure and kinetics of riboswitch aptamers and for designing riboswitches.

**Keywords:** riboswitch; aptamer; mRNA structure; gene regulation

## 1. Introduction

Many noncoding RNAs (ncRNAs) have been found to bear important and diverse biological functions in all domains of life, including catalysis, protection of genomes, and regulation of cell activities [1–3]. This diversity in biological functions is attributed to the remarkable structure variety accommodated by RNAs. Riboswitches, which present a fundamental example of ncRNAs, are involved in cellular regulation through vast structural rearrangement in response to the intracellular physical signals, such as metabolites [1,4,5] and ions [6–10]. Among previously validated riboswitches, metabolite-specific riboswitches are the most widespread and the nature of their ligands is well defined in most cases, except for several "riboswitch-like", presumably *cis*-acting, RNA structures for which no ligand has been found yet [11,12]. In order to function, most riboswitches usually consist of two domains: a conserved aptamer domain that is responsible for ligand binding, and an expression platform that converts changes in the aptamer domain into changes in gene expression. In contrast to these riboswitches, the $S_{MK}$ (SAM-III) riboswitch is the one that can use single domain for both ligand binding and gene regulation [13–15]. Aptamer domains, which are typically 35~200 nucleotides in length [16–18], often form a ligand-binding pocket (the aptamer structure) to bind the ligands with high specificity. To date, according to the aptamer structures (Figure 1), more than 30 riboswitch classes

have been found in all three kingdoms of life [19–21]. Due to their specificity and function as genetic regulators, riboswitches represent a novel class of molecular target for developing antibiotics and chemical tools [22]. Thus, a comprehensive understanding of riboswitches is important to facilitate the design for riboswitch-targeted drug, molecular robotics, and new molecular sensors.

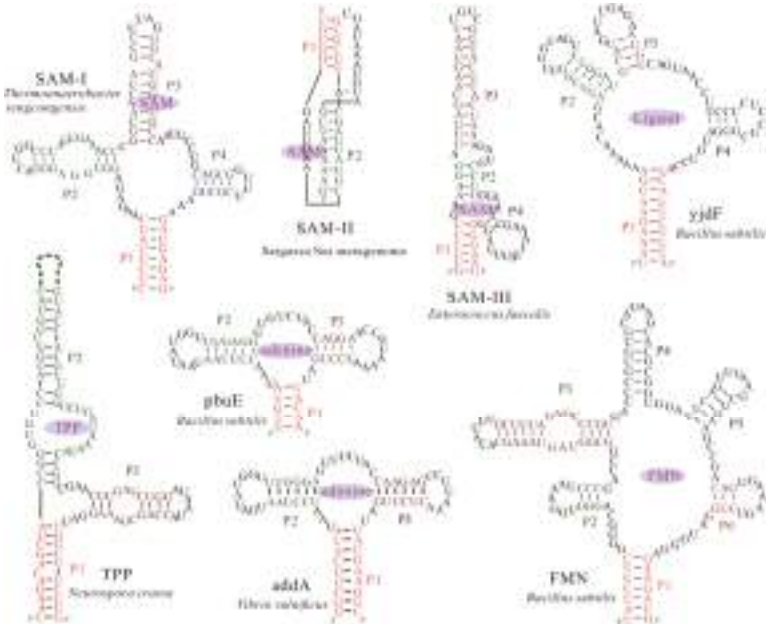


**Figure 1.** Structural models of aptamers from several extensively studied riboswitch candidates. The structures can bind their nature ligands, such as *S*-adenosylmethionine (SAM), thiamine pyrophosphate (TPP), adenine and flavin mononucleotide (FMN), to form a ligand bound conformation. Except the SAM-II riboswitch from the Sargasso Sea metagenome [23,24] and TPP riboswitch aptamer from *Neurospora crassa* [25], other aptamers are from bacteria. Nucleotides within helices P1, P2, P3, P4, P5, and P6 found within the bound aptamers, are colored differently. The dash line denotes the long helix region in the structure of TPP riboswitch aptamer.

The signal-dependent conformational shifts of riboswitches, usually between two distinct functional states, i.e., ligand bound state and unbound state, regulate the downstream gene expression (Figure 2). One of the alternative states serves as the genetic off state (OFF state) by forming an intrinsic terminator hairpin or a repression stem to repress gene expression [26–28]. The other state acts as the genetic on state (ON state), which induces gene expression by preventing the formation of these regulatory elements. Riboswitches can also regulate RNA splicing by controlling the structural flexibility near the relevant splice site [25]. During the regulatory activities, one of the two structures is adopted by riboswitches, depending on whether the aptamer domain can form the pocket and bind its ligand on time or not. Therefore, to investigate the regulation mechanism of these functional ncRNAs, one of the major challenges is the information of the aptamer structure (Figure 2). In contrast to proteins, a much smaller number of RNA structures have been solved by using the traditional experimental methods [29], such as nuclear magnetic resonance (NMR) spectroscopy and X-ray crystallography [15,30]. Sensitive X-ray crystallography must take special care to avoid RNA aggregation and misfolding prior to crystal formation, and NMR experiments easily suffer from poor long-range correlations for RNA. These create a great demand to obtain information of RNA structures

by using theoretical approaches. Up to now, many packages and methods have been developed to predict RNA secondary structure (two-dimensional (2D)) [31–33], as well as the three-dimensional (3D) structure for small RNAs [32–38]. These methods can quickly produce structure for a given RNA based on the input data. Some computational methods, such as RNAComposer and Rosetta [34,35,39], have been successfully applied to modeling 3D structure for several complex aptamers. As classical experimental methods may be limited in applicability to RNA [40], these theoretical approaches are likely to circumvent the bottleneck from experimental methods.

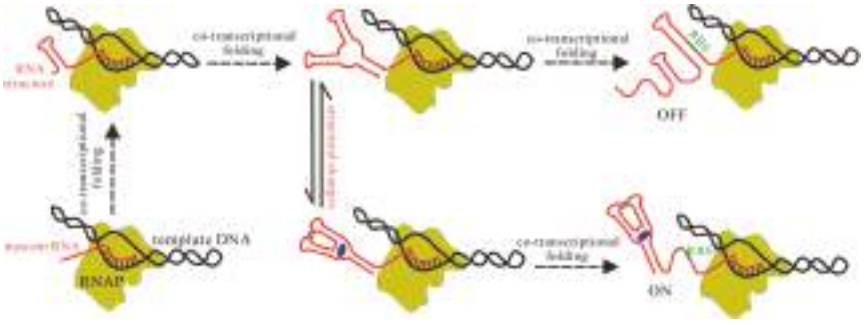


**Figure 2.** Schematic representation of riboswitch behaviors in cells. Nascent chain of the riboswitch and the ligand are colored red and blue respectively. The green line denotes the ribosome binding site (RBS) and RNA polymerase (RNAP) is denoted by yellow-green. The structure, structural changes, and co-transcriptional folding should be investigated for fully understanding the regulation mechanisms of riboswitches.

Another scientific challenge for the elucidation of the riboswitch function is to model aptamer kinetics, which is intrinsic to folding and conformational switching. Traditional molecular dynamics (MD) simulations [41,42], are able to provide a direct link between structure and dynamics. Nonetheless, due to the extreme complexity of force fields, a large number of atoms and a high number of degrees of freedom in RNA molecules, the detailed all of the atom simulations are difficult to produce trajectories in the time frame relevant for function of aptamers, which usually need to undergo large structural changes for purposes. Coarse-grained structural model with a less exhaustive representation is therefore particularly efficient to deal with these problems [43,44]. For example, the folding kinetics of *pbuE* [45], *addA*, and $S_{MK}$ riboswitch aptamers [43,46], have already been studied by using the coarse-grained SOP model. Another efficient alternative based on coarse-grained model is to investigate the kinetics of RNA 2D structure [47,48], which can also capture enough detail to understand the functions of aptamers.

Like protein, which can fold as soon as the N-terminal part emerges from the ribosome (co-translational folding) [49], nascent RNA also folds spontaneously as the nucleotides are synthesized by RNA polymerase in living cells (co-transcriptional folding) [50]. As riboswitches fold co-transcriptionally, folding patterns of the aptamer domain can direct the folding of the downstream expression platform. In fact, since many riboswitches regulate transcription, ligand binding can only occur during transcription for these to control gene expression [26,51–53]. Hence, the co-transcriptional folding kinetics is crucial for understanding the intracellular function of aptamers. Besides the optical-trapping assay and other experimental approaches [28,50,54], the kinetic Monte Carlo (MC) method was used to study the co-transcriptional folding of riboswitches [55], but it only considered the base pairing interactions closed in the native structures. By combining the master equation and the free energy landscape, BarMap and the helix-based computational methods have been applied to modeling the co-transcriptional folding behaviors for several riboswitches [56–60]. The results suggest that the aptamer domain folds into the pocket structure as soon as the nucleotides are transcribed [57,58],

while the riboswitch without a separate aptamer domain is more likely to form an alternative structure instead of the pocket during the transcription [56]. These computation models, which can predict stable and metastable structures, kinetics, and transition states, bridge the gap in understanding the relationship between the structure and biological function of aptamers. Furthermore, computational RNA design has also made a great progress to construct synthetic riboswitches by using different strategies [61,62]. Here, we will provide a collection of these computational methods for modeling the structure and kinetics of aptamers, and for designing riboswitches.

## 2. Computational Method for Predicting Aptamer Structures

Since the structure of RNA determines its biological function, a complete understanding of the aptamer structure is the necessary prerequisite to understand the riboswitch-mediated regulation processes in the cell. RNAs fold into complex structures; the linear ribonucleotide sequence is the determinant of base-pairing interactions (2D structure), which in turn, determines the spatial shape (3D structure). Since most computational methods use the input of 2D structure to produce the RNA 3D structure [29,32,63], the precise prediction of 2D structure becomes more and more important. Early computational approaches for predicting RNA 2D structure (e.g., RNAfold [64]), only find the structure with the lowest free energy for a given RNA. As the functional structure may not be the one with the lowest energy, methods such as *mfold* and RNAsubopt [31,65] are developed to predict a set of low-energy structures. Other prediction methods, such as PPfold and RNAalifold [66,67], are based on evolutionary considerations. For a given aptamer, these methods can quickly produce 2D structure and the free energy. The methods for the modeling structure do not consist of a process that assumes co-transcriptional folding. Recently, RNA 2D structure prediction has been reinforced by incorporating the constraints from the experiments [65].

### 2.1. RNAComposer

RNA 2D structure is a crucial step in the functional characterization, but a thorough understanding of aptamer functions depends critically on the 3D structure, which is the key determinant of their interactions with ions and other molecules in cell. Based on the 2D structure tree graph representation and homology of structural elements, the RNAComposer method (Table 1) was developed to automatically predict the 3D structure for large RNAs [29]. As a knowledge-based method, it uses RNA sequence and 2D structure topology in dot-bracket notation as an input for 3D structure prediction (Figure 3). In this notation [64], unpaired nucleotides and the nucleotides that are involved in base pairs are represented by dots and brackets, respectively; square brackets and curly brackets refer to first-order pseudoknots and higher order structures, respectively. Although the input RNA 2D structure can be obtained by using the methods that are incorporated within the RNAComposer system: RNAfold, RNAstructure, and Contrafold, experimentally adjusted 2D structure is able to largely improve quality of the prediction [39].

The input RNA 2D structure first is divided into stems, loops, and single strands in the program. 3D structure elements corresponding to these fragmentations are searched within the structure elements dictionary, which is tailored from the RNA FRABASE database and consists of a 3D structural element with good structural properties [68]. After the searching process, the 3D elements whose heavy-atom root mean square deviation (RMSD) is lower than 1.0 Å relative to the parent PDB structure, are selected according to the 2D structure topology, sequence similarity, and so on. By merging the selected 3D structure elements, the initial RNA 3D structure is obtained, and then refined by the energy minimization in the torsion angle space and Cartesian atom coordinate space to get the final 3D structure. RNAComposer has been used to accurately build the 3D structure of several complex riboswitch families [39], such as FMN riboswitch aptamer, TPP, and purine riboswitch aptamers. It is offered at two sites: http://rnacomposer.ibch.poznan.pl and http://rnacomposer.cs.put.poznan.pl. By typing the 2D structure of THI riboswitch aptamer in Figure 3 on the website [69], the related 3D structure will be released in PDB formatted file to users within 10 s. RNAComposer is automated,

efficient, especially suited for RNA 3D structure prediction of large RNAs, but it highly depends on the 3D structural elemental dictionary, and the applicability of the method is limited to RNAs with a few complex kink turn motifs.

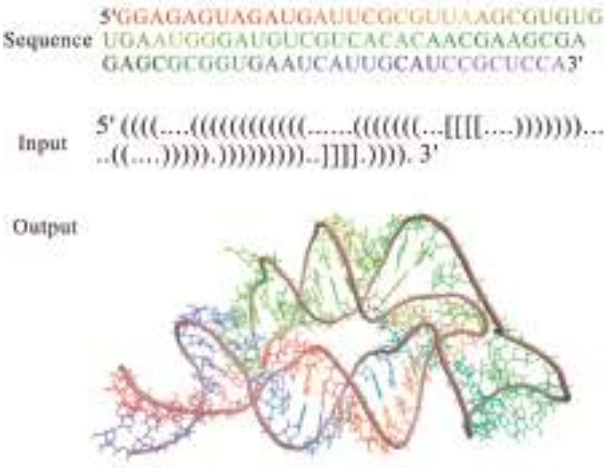


**Figure 3.** Three-dimensional (3D) structure for THF riboswitch aptamer (PDB code: 3SD3) predicted by using RNAComposer program online.

### *2.2. Rosetta and Discrete Molecular Dynamics*

RNAComposer is motif library-based, while Rosetta is a fragment-based method that is available online [35]. In the Rosetta approach, according to the RNA 2D structure and the experimental proximity mapping data, low-resolution models are generated by using Fragment Assembly of RNA (FARNA) [34], where models are assembled using RNA fragments from a crystallographic database via a MC algorithm. The Rosetta all-atom energy function is then used to minimize a small number of the low-resolution models with the lowest Rosetta energy scores. To select a representative set of 3D models, the largest and lowest-energy subsets of models that fall within a certain RMSD threshold of each other are collected to reflect the native fold of the RNA. Taking the aptamer from *Fusobacterium nucleatum* double glycine riboswitch as an example, the Rosetta 3D modeling can give a similar prediction as RMdetect and JAR3D [70–73].

**Table 1.** Methods which have been used for modeling 3D structure for aptamers.

| Methods | Description | Availability | Reference |
|---|---|---|---|
| RNAComposer | A motif library-based method that uses the dictionary tailored from RNA FRABASED database to build initial 3D structure. | Web server | [39] |
| Rosetta | A fragment-based method that uses FARFAR optimizes RNA conformations in the context of a physically realistic energy function. | Local installation | [72] |
| RMdetect | A bioinformatics tool for identifying known 3D structural modules on genomic sequences. | Local installation | [73] |
| JAR3D | Scoring sequences to motif groups based on sequences' ability to form the same pattern of interactions in motif. | Web server | [70] |
| RAGTOP | Predicting RNA topologies by a coarse-grained sampling of 3D graphs guided by statistical knowledge-based potentials. | Not available online | [74] |
| iFoldRNA | Incorporating SHAPE into discrete molecular dynamics to predict RNA structure. | Web server | [75] |

Also, starting from 2D structures, a hierarchical computational approach (RAGTOP) was modified to predict 10 representative riboswitch aptamers with diverse structural features [74], by combining the coarse-grained graph sampling approach [76]. Through integration of computational and experimental

methods, a three-bead coarse-grained model of RNA for discrete molecular dynamics simulation have gotten precise 3D structure predictions for the M-box riboswitch and TPP riboswitch aptamers [77], and for RNA in the range of a few hundred nucleotides [40]. In this coarse-grained model, each RNA nucleotide is represented by three beads corresponding to the base, sugar, and phosphate groups. The potential terms includes bonded, non-bonded interactions, and additional potential terms based on the experimental hydroxyl radical probing data. This method uses RNA sequences and base pairing as inputs to generate structures, and then applies replica exchange simulations with the potential to find a representative structure. Based on this method, the web server iFoldRNA was created for prediction of RNA 3D structure [75].

The 3D structures of aptamers modeled by these approaches suggest that the aptamer domains often form a compact structure involving many complicated tertiary interactions. Since the entire prediction of these approaches depends on the input data, the correct 2D structure is critical for the accurate 3D structure modeling. Experimental data provides powerful constraints to reinforce 2D structure prediction, but these methods currently can only achieve subhelix-resolution accuracy or near-atomic accuracy for RNAs.

## 3. Computation Model to Characterize Structural Changes in Aptamers

A key event in the biological function of riboswitches is the structural change within the aptamer domain. This change can lead to a change of the folding pattern within the expression platform, thereby directly modulating the gene expression. For effective flipping of riboswitches, the structural change of aptamers must be achieved within the certain time window. Therefore, characterizing the structural changes of aptamers is also important for fully understanding their function in the cell. The conventional all atom MD simulation has been widely used to describe the time-dependent motions of biological molecules [78]. However, even though modern parallelization of MD simulation is able to model trajectories on the order of milliseconds, it still fails to address the majority of biological processes, including folding or unfolding of aptamers that occur on much longer timescales (in seconds). In order to model time-dependent structural changes of aptamers, an effective solution is to use a coarse-grained structural model.

### 3.1. The Master Equation Approach

The master equation approach or kinetic MC method based on coarse-grained system [79–81], namely RNA 2D structure, is advantageous for accessing behaviors at long time scales, even minutes or hours [80]. In the master equation approach, structural changes are usually modeled on the RNA energy landscape, which specifies the conformation space and the transition rates between conformations. For a given RNA, the conformation space is sampled by all of the possible 2D structures that are constructed by using the formation or disruption of an entire helix as the elementary step to allow for large structural changes. Their free energies can be calculated using the Turner energy parameters [82,83]. The transition rates between states are obtained based on the free energy landscape analysis [48,80,81]: (1) formation; (2) disruption of a helix; and, (3) helix formation with concomitant partial melting of a competing helix. With these key concepts, the folding process can be described by the master equation:

$$dp_i(t)/dt = \sum_{i \neq i} [k_{j \to i} p_j(t) - k_{i \to j} p_i(t)] \quad (1)$$

where $p_i(t)$ is the population of state $i$ at time $t$ and $k_{i \to j}$ is the transition rate from state $i$ to state $j$. This computational method which integrates RNA 2D structure with the static energy landscape, provides a basic idea to predict the folding kinetics of the Hepatitis delta virus ribozyme and $S_{MK}$ riboswitch [56,80].

### 3.2. Coarse-Grained SOP Model

Besides these approaches, the coarse-grained SOP model using Langevin dynamics simulation can also be used to study the kinetics of RNA molecules by characterizing the folding landscape [43,45,46]. Actually, many complex biological processes, such as unfolding and refolding of various RNA and proteins [44,84,85], are described with great success by using the SOP model. In this coarse-grained model, each nucleotide, as well as the ligand, is represented as a single site. The total potential energy of the bound aptamer is

$$V_{\mathrm{T}} = V_{\mathrm{APT}} + V_{\mathrm{APT-L}} \tag{2}$$

where $V_{\mathrm{APT}}$ is the energy function of the aptamer; and, $V_{\mathrm{APT-L}}$ is the interaction between the ligand and the aptamer. The dynamics of the system can be simulated by using Brownian dynamics or the Langevin equation in the overdamped limit. During the force ramp simulation, the 5′-end of RNA is attached to a spring pulled with a constant speed, while the 3′-end is fixed. The free energy profiles are obtained using

$$G_z = -k_{\mathrm{B}} T \ln P(z) \tag{3}$$

where $k_{\mathrm{B}}$ and $T$ are the Boltzmann constant and temperature, respectively; and, the probability $P(z)$ of the extension between $z$ and $z + dz$, is calculated from the folding trajectories. Based on the theory of mean first-passage times [84], the transition rate between two folding states can be calculated from the time traces of the extension.

The kinetics of the SAM-III and *addA* riboswitch aptamers have been successfully studied with this approach [43,46]. As the crystal structure of *pbuE* riboswitch aptamer is not available, its atomic structure is produced via conformational sampling with MD by substituting the sequence of *pbuE* aptamer into the crystal structure of *addA* aptamer (PDB code: 1Y26), when considering the structural similarity between the two aptamers. But despite this structural similarity, their folding behaviors are different in the pulling simulation [43,45]. In *addA* riboswitch aptamer (Figure 1), the unfolding occurs in the order of $\mathrm{F} \rightarrow \mathrm{P2|P3} \rightarrow \mathrm{P3} \rightarrow \mathrm{U}$, while the unfolding order of *pbuE* aptamer is $\mathrm{F} \rightarrow \mathrm{P2|P3} \rightarrow \mathrm{P2} \rightarrow \mathrm{U}$, where F and U denote the fully folded state and unfolded state, respectively; Pi is the hairpin structure with helix Pi; P2|P3 denotes the state with helices P2 and P3. The different unfolding order of P2 and P3 in the two aptamers suggests that the riboswitches carry out different regulatory activities in bacteria, even though they belong to the same class. Helix P3 in *pbuE* riboswitch is unfolded ahead of helix P2, because of its unstability. This can explain why helix P3 is disrupted in OFF state of *pbuE* riboswitch but keeps folded in that of *addA* riboswitch [28,86]. Due to this greater conformational change in *pbuE* riboswitch, its OFF state can hardly transit to the aptamer structure, implying an irreversible kinetic riboswitch [57]. On the contrary, *addA* riboswitch is able to quickly reach equilibrium between the OFF state and the aptamer structure, which is consistent with a reversible thermodynamic switch [28]. The different unfolding kinetics of the aptamers under force thus can provide the information of their function.

## 4. Methods to Predict the Structure Transitions during Transcription

RNA folding occurs in two different ways [87]: (i) folding after synthesis of the entire RNA molecule (refolding); and, (ii) sequential folding occurs during transcription, namely co-transcriptional folding. In vivo, most RNAs fold co-transcriptionally, due to the sequential nature of RNA synthesis. The sequential folding during transcription is crucial for riboswitches, especially the kinetic riboswitches, to exert their regulation. Since kinetic switches are trapped in one state depending on whether the trigger is present at the time of folding, the mechanism of their function can only be understood in the context of co-transcriptional folding. For example, the full length *pbuE* riboswitch quickly folds to OFF state, which hinders adenine binding, while the aptamer structure that is responsible for ligand binding is not observed [53,57]. However, as nucleotides of the aptamer domain are transcribed first, the sequential folding may allow for the aptamer to form the pocket and bind to the ligand before formation of OFF state during transcription. Thus, the co-transcriptional

folding kinetics of aptamers during transcription plays an important role for understanding their function in living cells.

In the case of co-transcriptional folding, as the RNA chain grows, the whole transcription process can be divided into a series of transcription steps [48,57,59], with each corresponding to adding one nucleotide. RNA folding kinetics within each step is modeled on the energy landscape as a certain RNA chain. But a link between two consecutive steps should be constructed due to the sequential folding in the transcription context. Based on this idea, the BarMap approach and helix-based computational approach have been developed to investigate the folding behaviors of several riboswitches under different transcription conditions [56–58,88].

### 4.1. BarMap

The BarMap approach integrates RNA 2D structure with the dynamic energy landscape to explore co-transcriptional folding kinetics [59]. The main idea of this approach is to model RNA kinetics on individual landscapes, where external triggers are considered as discrete changes. For successive kinetic simulations, a map between states of adjacent landscapes is computed to define the transfer of population densities.

In the case of transcription, the folding is treated as a process on a time-varying landscape in this approach. For each RNA elongation step, an energy landscape is first computed using the barriers program, which can simulate RNA folding kinetics [89,90]. Then, BarMap constructs a map between the landscapes of two successive steps, as shown in Figure 4a. According to this map, the final population at the previous step can be mapped to the initial population on the landscape at the current step. Finally, starting with the first landscape with more than one state, RNA folding kinetics can be simulated by the treekin program [59], which integrates the master equation for arbitrary times through calculating the matrix exponential. The amount of time $t$ on a particular landscape corresponds to the elongation time of the polymerase. Co-transcriptional folding behaviors of RNAs can be obtained from the relationship between the population density and the transcription step that is given by the approach.

The BarMap approach has been used to study the RNA thermometer, RNA refolding during pore translocation, and co-transcriptional folding [59,88]. The effects of transcriptional pause sites, transcription rates and ligand concentrations, can easily be included in the approach by specifying the amount of time $t$ and changing the binding energy added to all of the ligand-competent states, respectively. Using the example of a recently designed theophylline-dependent RS10 riboswitch, the BarMap approach predicts the folding behaviors in good agreement with experimental observations [88].

### 4.2. The Helix-Based Computational Method

In helix-based computation model [60], the folding time window for each RNA elongation step also depends on the time required for RNAP to transcribe the relevant nucleotide. At each step, the population kinetics is calculated in the same manner as the refolding kinetics that are calculated in the master equation approach [48,60]: first, the conformation space is generated and the transition rates are calculated; then, the population relaxation within the folding time window is described with the master equation, where the initial population at the current step is determined by the folding results of the previous step. Based on possible structural changes as the RNA chain is elongated by one nucleotide, a link between the initial population distribution at the current step and the final population distribution at the previous step is constructed in Figure 4b. Like the BarMap approach, the effects of the transcription speed, transcriptional pause, and ligand concentration can be mimicked by modifying the folding time window for each step and the binding energy in this method.

The helix-based computational method has been used to explore the regulation mechanisms of several well-studied riboswitches, such as *pbuE* [57], $S_{MK}$ [56], *metF*, and *yitJ* riboswitches [58]. The results show an excellent agreement of predicted trajectories with that from experiments and other methods [50,55,91]. The folding behavior of *addA* riboswitch aptamer, as shown in Figure 5, suggests that as the chain grows, the nascent RNA chain folds through a series of discrete intermediate

states (from S0 to S5). When the first 25th nucleotide is transcribed, the open RNA chain S0 begins to form structure S1, which is replaced by S2 from step on 32. As the 49th nucleotide is free to form structures, S3 is formed and occupies most of the population till the 59th step. From step on 59, S3 begins to transit to S4. When helix P1 can be nucleated, the chain folds into S5.

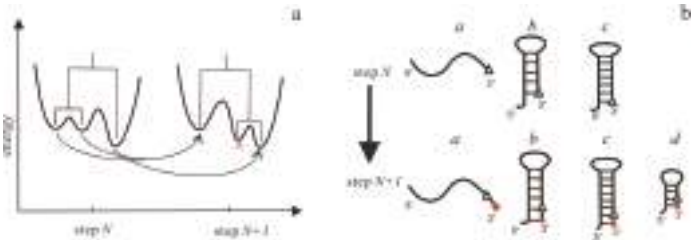

**Figure 4.** Relationship of landscapes in the BarMap approach (**a**) and structures in the helix-based computational method (**b**) between two adjacent steps. In (**a**), there are three types of events in landscapes: (i) A one-to-one correspondence between two minima (right); (ii) A two-to-one correspondence (left); and, (iii) a new local minima (marked by *) appears in the landscape at step $N + 1$. In (**b**), the triangles and red dots denote the newly transcribed nucleotide at step $N$ and $N + 1$, respectively. For structures belonging to the first three types, their initial population at step $N + 1$ "directly inherit" from step $N$, while for type *d*, the initial population of the structure at step $N + 1$ is zero.

This aptamer domain can fold into the pocket S5 as soon as the relevant nucleotides are transcribed (Figure 5a,d), which has also been found in *pbuE* [57], *yitJ*, and *metF* riboswitches [58]. During the refolding process (Figure 5b,e), the entire molecule folds into S5 mainly through structure I and S3. Although the refolding pathway is different from the co-transcriptional folding pathway, the aptamer domain also can form S5 within 0.1 s, implying that the aptamer domain is highly evolved. In contrast to these riboswitch aptamers, the SAM-III riboswitch, which utilizes a single domain to exert functions, quickly folds to ON state instead of the pocket (OFF) structure (as shown in Figure 1) under both the transcription context and the refolding condition (Figure 5) [56]. This thermodynamic switch is not sensitive to co-transcriptional folding kinetics, so it can be understood by the equilibrium properties. The co-transcriptional folding pathway of *addA* aptamer is similar to that of the *pbuE* aptamer [57], possibly because of the conservation within the aptamer domains. For many riboswitches, since the expression platforms are required to form a terminator or a repression stem [1,4], their sequences could be helpful to decipher the different folding intermediates as well.

Previous studies suggest that transcriptional pause plays a key role for riboswitches and other RNAs to exert function [92–95]. The major transcriptional pause sites found within several riboswitches are located immediately after the aptamer domains [51,86,96]. As the time window that is allowed for ligands binding is limited during transcription, the pauses in these regions can give the aptamers extra time to bind to the ligands but prevent the unbound functional states from being formed. Their effects have been assessed by the helix-based computational method and experimental approaches [51,57,58,93]. The results from the helix-based computational method suggest that removing the pause sites leads to a demand for an even higher ligand concentration to trigger the switch [57,58].

The good agreement of the results from these theoretical approaches with the experiments and other methods implies that they provide a reliable tool to understand the function of aptamers in the riboswitch-mediated gene regulation. However, all of these approaches based on 2D structure prediction ignore tertiary interactions and the effects of ions. Although the ligand binding can be mimicked by modifying the binding energy from experiments, the 2D structure model still cannot precisely predict the ligand–RNA interactions. Hence, there is a significant requirement in incorporating these factors to fully understand the function of riboswitches.

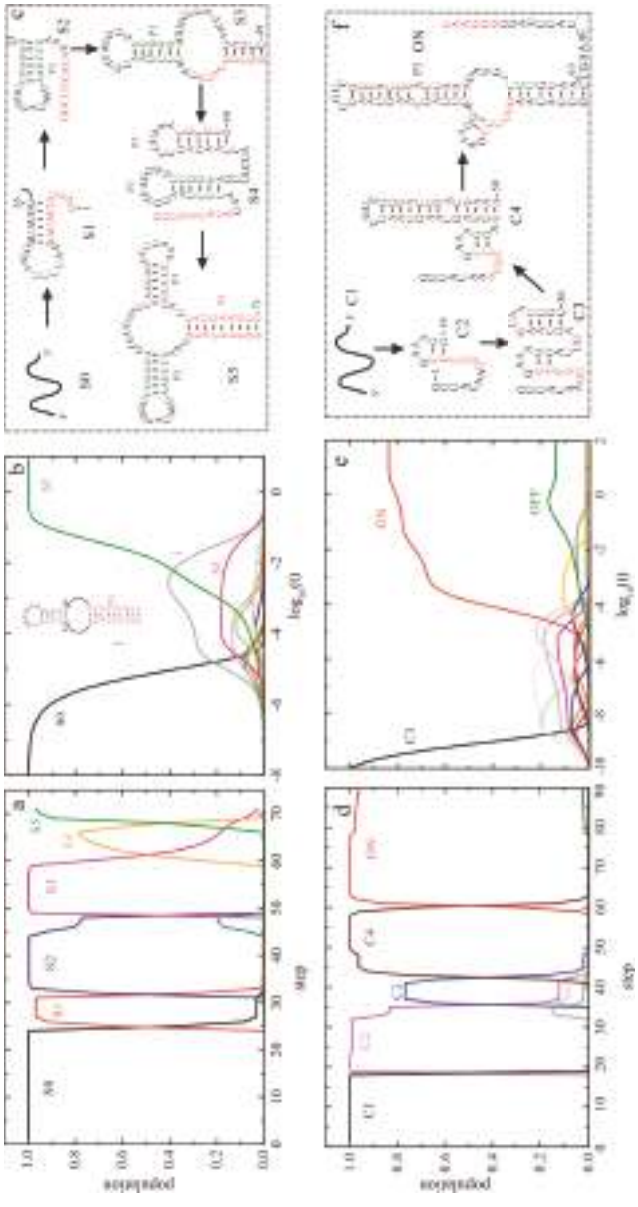


**Figure 5.** The co-transcriptional folding kinetics (**a**,**d**) and refolding kinetics (**b**,**e**) of *addA* riboswitch aptamer (up panel) and $S_{MK}$ riboswitch (bottom panel). The transcription rates for *addA* aptamer and $S_{MK}$ riboswitch are 25 nt/s and 50 nt/s, respectively, and the main intermediate states formed during the transcription are shown in (**c**,**f**). The dash dot lines in (**b**) for *addA* riboswitch aptamer denote the unpaired nucleotides within the large inter-loop. OFF state of $S_{MK}$ riboswitch is the structure that is responsible for SAM binding shown in Figure 1.

## 5. Computation Design for Synthetic Riboswitches

Artificial riboswitches established recently demonstrate that they can be used as a new tool for the drug-regulated expression of viral genes [97]. To design artificial riboswitches or other RNA devices for industrial and medical applications, different computation strategies have been developed over the years [62,98–102]. Based on a biophysical model of translation initiation, a web server called Riboswitch Calculator can be used to design synthetic riboswitches form various RNA aptamers [62]. In this model, a riboswitch is considered as a long mRNA molecule. The interactions of RNA–RNA, RNA–ribosome and ligand–RNA, control the translation initiation rate, which can be calculated as:

$$r = \exp(-\beta \Delta G_{total}) \quad (4)$$

where $\beta$, $\Delta G_{total}$ are the apparent Boltzmann coefficient and total energy change between mRNA and initiating 30S ribosomal subunit. The energies of RNA folding and the ribosome binding to mRNA are calculated using the ViennaRNA suite and RBS Calculator [64,103], respectively.

Riboswitch Calculator provides a useful tool to design translation regulating riboswitches. The four inputs are necessary for the design: the sequence and structural constraint of an aptamer, the ligand binding energy, and the protein coding section. These inputs are used by the optimization algorithm to generate an initial set of riboswitch candidates. Rounds of random mutations, evaluation, selection, and recombination are performed using these candidates. The biophysical model calculations are employed for the fitness evaluation to select the candidates that meet the objective function requirements, such as reaching targeted translation rates in OFF and ON states. The selected candidates will be sent back for the next round to find the riboswitch candidates with the highest fitness.

Transcription regulating riboswitches can also be designed by using the computational method [61]. The design algorithm used the aptamer with the known sequence and secondary structure. When considering the terminators always with a minimal size and the U stretch, sequences with lengths between 6 and 20 nucleotides are randomly generated to create a spacer database. The following step is to generate the sequences that are complementary to the subsequences of the 3′ part of the given aptamer. With these terms, a riboswitch candidate can be created by concatenating the aptamer, a spacer, a complementary sequence, and the U stretch. Using the RNAfold program [64], these candidates are evaluated by the folding simulations to select the elite members. A theophylline-specific riboswitch that is generated by this approach can activate transcription on binding of the target ligand [61].

These computational methods can be applied to constructing synthetic riboswitches, but the evaluation of synthetic riboswitch candidates is based on thermodynamic calculations in both of the approaches. Besides the above approaches, other methods that use different strategies are developed to design RNA devices recently [99–101,104]. It is known that co-transcriptional folding kinetics is fundamental to the action of functional RNAs in cell. However, it is not well incorporated into these methods, possibly because of the complexity of co-transcriptional folding. Although the transcription context may pose a serious challenge in the quest for designing RNA devices, these methods have made a great progress in the development of computational methods for designing RNA devices.

## 6. Conclusions

Since functions of biological molecules are determined by the formed structures, precise structure precondition is crucial to a complete understanding of many RNA-mediated processes, such as the regulation activities of riboswitches. Two domains of riboswitches, namely, the aptamer domain and the expression platform, often share nucleotides. The aptamer domain usually needs to form a unique ligand-binding pocket for specifically binding its ligand, which in turn, locks the conformation of the aptamer domain and directs the folding of the downstream expression platform. However, if the aptamer fails to bind its ligand, part of the nucleotides within the aptamer domain will pair with the nucleotides within the expression platform to form an alternative structure. For the riboswitches

with one single domain, conformational change induced by the ligand binding would result in the formation of the structure that is different from the unbound functional state.

As structural changes within the aptamer domain produce a substantial change in the gene expression, it therefore demands to characterize structure and kinetics of aptamers for a thorough understanding of the riboswitch-mediated regulation. Given the fact that most aptamers have been extensively studied experimentally, yet they are not well characterized in some aspects. In the last several decades, many computational methods have been developed to investigate aptamers. One primary concern for aptamers is to precisely model the structure that is responsible for ligand recognizing and binding. Effective approaches, such as the motif library-based and fragment-based methods, have made significant progress in 3D structure prediction by integrating knowledge-based algorithm with experimental data or physics-based model. However, 3D modeling for aptamers and other large RNAs has not achieved a consistent atomic accuracy and the data may not enable statistical meta-analysis currently. Most of them are not suitable for predicting the 3D structure for highly complex RNAs. Furthermore, RNA chaperones may play a role in RNA folding [87,105,106], which are not considered in the model. High quality 3D structure prediction may require more experimental mapping data and significant human insight to build accurate models. Further advancements may hold great promise for making progress toward the goal.

Another important issue for aptamers comes from describing their great structural changes. Modern parallelization of MD simulation largely improves the computation efficiency, but it still cannot address the structural rearrangements of aptamers that occur on a seconds' timescale. The coarse-grained SOP model and other computational methods have been applied to characterizing the kinetics of several riboswitch aptamers with great success. These demonstrate that the coarse-grained structural model, which enhances the conformation sampling, can be used to study the large scale conformational fluctuations of RNAs.

Also based on the coarse-grained structural model, a number of computational methods, such as RNAkinetics [107], Kinefold [108], and COFOLD [47] are developed to simulate co-transcriptional folding pathways of mRNAs from the early 1980s when key experiments show that structure formation happens co-transcriptionally [109]. In order to investigate the riboswitch-mediated regulation mechanisms, ligand binding should be taken into account. By incorporating the effect of ligand binding, the BarMap package and helix-based computational method have been successfully used to predict the co-transcriptional folding for several riboswitches. The application of these approaches in riboswitches implies that the 2D structure model can capture enough details of their behaviors in living cells.

Since conformational changes in aptamers can be induced by ligands, some other theoretical approaches focus on the prediction about interactions between ligands and aptamers or other features [110–112]. In recent years, computational methods for designing riboswitches have also made excellent progress in synthetic biology. As discussed above, several notable limitations of these computational methods still exist. Continuing developments in computational and hybrid methods are expected to overcome these limitations.

**Acknowledgments:** This work was partly supported by the National Natural Science Foundation of China under Grants No. 31600592 (to Sha Gong), 31270761 and 11574234 (to Wenbing Zhang). It was supported in part from Hubei Key Laboratory of Economic Forest Germplasm Improvement and Resources Comprehensive Utilization, Hubei Collaborative Innovation Center for the Characteristic Resources Exploitation of Dabie Mountains [2017BX08].

**Author Contributions:** Sha Gong, Yanli Wang, Zhen Wang and Wenbing Zhang designed the paper. Sha Gong and Wenbing Zhang wrote the paper. All authors have contributed in the improving of the manuscript, and read and approved its final version.

**Conflicts of Interest:** The authors declare no conflict of interest.

## Abbreviations

| | |
|---|---|
| ncRNA | noncoding RNA |
| SOP | Self-Organized Polymer |
| MC | Monte Carlo |
| FMN | Flavin Mononucleotide |
| SAM | *S*-adenosylmethionine |
| TPP | Thiamine Pyrophosphate |
| NMR | Nuclear Magnetic Resonance |
| MD | Molecular Dynamics |
| RNAP | RNA polymerase |
| RMSD | Root Mean Square Deviation |
| FARNA | Fragment Assembly of RNA |
| RAGTOP | RNA-As-Graph-Topologies |

## References


1. Breaker, R.R. Riboswitches and the RNA world. *Cold Spring Harb. Perspect. Biol.* **2012**, *4*, 1–15. [CrossRef] [PubMed]
2. Winkler, W.C. Riboswitches and the role of noncoding RNAs in bacterial metabolic control. *Curr. Opin. Chem. Biol.* **2005**, *9*, 594–602. [CrossRef] [PubMed]
3. Cech, T.R.; Steitz, J.A. The noncoding RNA revolution—Trashing old rules to forge new ones. *Cell* **2014**, *157*, 77–94. [CrossRef] [PubMed]
4. Chen, J.; Gottesman, S. Riboswitch regulates RNA. *Science* **2014**, *345*, 876–877. [CrossRef] [PubMed]
5. Tucker, B.J.; Breaker, R.R. Riboswitches as versatile gene control elements. *Curr. Opin. Struct. Biol.* **2005**, *15*, 342–348. [CrossRef] [PubMed]
6. Baker, J.L.; Sudarsan, N.; Weinberg, Z.; Roth, A.; Stockbridge, R.B.; Breaker, R.R. Widespread Genetic Switches and Toxicity Resistance Proteins for Fluoride. *Science* **2012**, *335*, 233–235. [CrossRef] [PubMed]
7. Dambach, M.; Sandoval, M.; Updegrove, T.B.; Anantharaman, V.; Aravind, L.; Waters, L.S.; Storz, G. The Ubiquitous yybP-ykoY Riboswitch Is a Manganese-Responsive Regulatory Element. *Mol. Cell* **2015**, *57*, 1099–1109. [CrossRef] [PubMed]
8. Dann, C.E.; Wakeman, C.A.; Sieling, C.L.; Baker, S.C.; Irnov, I.; Winkler, W.C. Structure and Mechanism of a Metal-Sensing Regulatory RNA. *Cell* **2007**, *130*, 878–892. [CrossRef] [PubMed]
9. Price, I.R.; Gaballa, A.; Ding, F.; Helmann, J.D.; Ke, A. $Mn^{2+}$-Sensing Mechanisms of yybP-ykoY Orphan Riboswitches. *Mol. Cell* **2015**, *57*, 1110–1123. [CrossRef] [PubMed]
10. Cromie, M.J.; Shi, Y.; Latifi, T.; Groisman, E.A. An RNA Sensor for Intracellular $Mg^{2+}$. *Cell* **2006**, *125*, 71–84. [CrossRef] [PubMed]
11. Li, S.; Breaker, R.R. Identification of 15 candidate structured noncoding RNA motifs in fungi by comparative genomics. *BMC Genom.* **2017**, *18*, 785. [CrossRef] [PubMed]
12. Weinberg, Z.; Lünse, C.E.; Corbino, K.A.; Ames, T.D.; Nelson, J.W.; Roth, A.; Perkins, K.R.; Sherlock, M.E.; Breaker, R.R. Detection of 224 candidate structured RNAs by comparative analysis of specific subsets of intergenic regions. *Nucleic Acids Res.* **2017**, *45*, 10811–10823. [CrossRef] [PubMed]
13. Fuchs, R.T.; Grundy, F.J.; Henkin, T.M. *S*-adenosylmethionine directly inhibits binding of 30S ribosomal subunits to the SMK box translational riboswitch RNA. *Proc. Natl. Acad. Sci. USA* **2007**, *104*, 4876–4880. [CrossRef] [PubMed]
14. Lu, C.; Smith, A.M.; Ding, F.; Chowdhury, A.; Henkin, T.M.; Ke, A. Variable sequences outside the SAM-binding core critically influence the conformational dynamics of the SAM-III/SMK box riboswitch. *J. Mol. Biol.* **2011**, *409*, 786–799. [CrossRef] [PubMed]
15. Wilson, R.C.; Smith, A.M.; Fuchs, R.T.; Kleckner, I.R.; Henkin, T.M.; Foster, M.P. Tuning riboswitch regulation through conformational selection. *J. Mol. Biol.* **2011**, *405*, 926–938. [CrossRef] [PubMed]
16. DebRoy, S.; Gebbie, M.; Ramesh, A.; Goodson, J.R.; Cruz, M.R.; van Hoof, A.; Winkler, W.C.; Garsin, D.A. A riboswitch-containing sRNA controls gene expression by sequestration of a response regulator. *Science* **2014**, *345*, 937–940. [CrossRef] [PubMed]

17. Rinaldi, A.J.; Lund, P.E.; Blanco, M.R.; Walter, N.G. The Shine-Dalgarno sequence of riboswitch-regulated single mRNAs shows ligand-dependent accessibility bursts. *Nat. Commun.* **2016**, *7*, 8976. [CrossRef] [PubMed]
18. Barrick, J.E.; Breaker, R.R. The distributions, mechanisms, and structures of metabolite-binding riboswitches. *Genome Biol.* **2007**, *8*, R239. [CrossRef] [PubMed]
19. Breaker, R.R. Prospects for Riboswitch Discovery and Analysis. *Mol. Cell* **2011**, *43*, 867–879. [CrossRef] [PubMed]
20. Li, S.; Hwang, X.Y.; Stav, S.; Breaker, R.R. The ydjF riboswitch candidate regulates gene expression by binding diverse azaaromatic compounds. *RNA* **2016**, *22*, 530–541. [CrossRef] [PubMed]
21. Serganov, A.; Nudler, E. A Decade of Riboswitches. *Cell* **2013**, *152*, 17–24. [CrossRef] [PubMed]
22. Deigan, K.E.; FerrÉ-D'AmarÉ, A.R. Riboswitches: Discovery of Drugs That Target Bacterial Gene-Regulatory RNAs. *Acc. Chem. Res.* **2011**, *44*, 1329–1338. [CrossRef] [PubMed]
23. Liberman, J.A.; Wedekind, J.E. Riboswitch structure in the ligand-free state. *Wiley Interdiscip. Rev. RNA* **2012**, *3*, 369–384. [CrossRef] [PubMed]
24. Gilbert, S.D.; Rambo, R.P.; Van Tyne, D.; Batey, R.T. Structure of the SAM-II riboswitch bound to *S*-adenosylmethionine. *Nat. Struct. Mol. Biol.* **2008**, *15*, 177–182. [CrossRef] [PubMed]
25. Cheah, M.T.; Wachter, A.; Sudarsan, N.; Breaker, R.R. Control of alternative RNA splicing and gene expression by eukaryotic riboswitches. *Nature* **2007**, *447*, 497–500. [CrossRef] [PubMed]
26. Mandal, M. A Glycine-Dependent Riboswitch That Uses Cooperative Binding to Control Gene Expression. *Science* **2004**, *306*, 275–279. [CrossRef] [PubMed]
27. Diegelman-Parente, A.; Bevilacqua, P.C. A mechanistic framework for Co-transcriptional folding of the HDV genomic ribozyme in the presence of downstream sequence. *J. Mol. Biol.* **2002**, *324*, 1–16. [CrossRef]
28. Lemay, J.-F.; Desnoyers, G.; Blouin, S.; Heppell, B.; Bastet, L.; St-Pierre, P.; Massé, E.; Lafontaine, D.A. Comparative Study between Transcriptionally- and Translationally-Acting Adenine Riboswitches Reveals Key Differences in Riboswitch Regulatory Mechanisms. *PLoS Genet.* **2011**, *7*, e1001278. [CrossRef] [PubMed]
29. Popenda, M.; Szachniuk, M.; Antczak, M.; Purzycka, K.J.; Lukasiak, P.; Bartol, N.; Blazewicz, J.; Adamiak, R.W. Automated 3D structure composition for large RNAs. *Nucleic Acids Res.* **2012**, *40*, 1–12. [CrossRef] [PubMed]
30. Chen, B.; Zuo, X.; Wang, Y.-X.; Dayie, T.K. Multiple conformations of SAM-II riboswitch detected with SAXS and NMR spectroscopy. *Nucleic Acids Res.* **2012**, *40*, 3117–3130. [CrossRef] [PubMed]
31. Zuker, M. Mfold web server for nucleic acid folding and hybridization prediction. *Nucleic Acids Res.* **2003**, *31*, 3406–3415. [CrossRef] [PubMed]
32. Xu, X.; Zhao, P.; Chen, S.J. Vfold: A web server for RNA structure and folding thermodynamics prediction. *PLoS ONE* **2014**, *9*. [CrossRef] [PubMed]
33. Reuter, J.S.; Mathews, D.H. RNAstructure: Software for RNA secondary structure prediction and analysis. *BMC Bioinform.* **2010**, *11*, 129. [CrossRef] [PubMed]
34. Das, R.; Baker, D. Automated de novo prediction of native-like RNA tertiary structures. *Proc. Natl. Acad. Sci. USA* **2007**, *104*, 14664–14669. [CrossRef] [PubMed]
35. Das, R.; Karanicolas, J.; Baker, D. Atomic accuracy in predicting and designing noncanonical RNA structure. *Nat. Methods* **2010**, *7*, 291–294. [CrossRef] [PubMed]
36. Jonikas, M.A.; Radmer, R.J.; Altman, R.B. Knowledge-based instantiation of full atomic detail into coarse-grain RNA 3D structural models. *Bioinformatics* **2009**, *25*, 3259–3266. [CrossRef] [PubMed]
37. Parisien, M.; Major, F. The MC-Fold and MC-Sym pipeline infers RNA structure from sequence data. *Nature* **2008**, *452*, 51–55. [CrossRef] [PubMed]
38. Shi, Y.-Z.; Wang, F.-H.; Wu, Y.-Y.; Tan, Z.-J. A coarse-grained model with implicit salt for RNAs: Predicting 3D structure, stability and salt effect. *J. Chem. Phys.* **2014**, *141*, 105102. [CrossRef] [PubMed]
39. Purzycka, K.J.; Popenda, M.; Szachniuk, M.; Antczak, M.; Lukasiak, P.; Blazewicz, J.; Adamiak, R.W. Automated 3D RNA Structure Prediction Using the RNAComposer Method for Riboswitches. In *Methods in Enzymology*; Elsevier Inc.: Waltham, MA, USA, 2015; Volume 553, pp. 3–34, ISBN 0076-6879.
40. Ding, F.; Lavender, C.A.; Weeks, K.M.; Dokholyan, N.V. Three-dimensional RNA structure refinement by hydroxyl radical probing. *Nat. Methods* **2012**, *9*, 603–608. [CrossRef] [PubMed]
41. Higgs, P.G. RNA secondary structure: Physical and computational aspects. *Q. Rev. Biophys.* **2000**, *33*, 199–253. [CrossRef] [PubMed]

42. Sharma, M.; Bulusu, G.; Mitra, A. MD simulations of ligand-bound and ligand-free aptamer: Molecular level insights into the binding and switching mechanism of the add A-riboswitch. *RNA* **2009**, *15*, 1673–1692. [CrossRef] [PubMed]
43. Lin, J.-C.; Thirumalai, D. Relative stability of helices determines the folding landscape of adenine riboswitch aptamers. *J. Am. Chem. Soc.* **2008**, *130*, 14080–14081. [CrossRef] [PubMed]
44. Hyeon, C.; Thirumalai, D. Mechanical Unfolding of RNA: From Hairpins to Structures with Internal Multiloops. *Biophys. J.* **2007**, *92*, 731–743. [CrossRef] [PubMed]
45. Lin, J.-C.; Hyeon, C.; Thirumalai, D. Sequence-dependent folding landscapes of adenine riboswitch aptamers. *Phys. Chem. Chem. Phys.* **2014**, *16*, 6376–6382. [CrossRef] [PubMed]
46. Lin, J.-C.C.; Thirumalai, D. Kinetics of allosteric transitions in *S*-adenosylmethionine riboswitch are accurately predicted from the folding landscape. *J. Am. Chem. Soc.* **2013**, *135*, 16641–16650. [CrossRef] [PubMed]
47. Proctor, J.R.; Meyer, I.M. CoFold: An RNA secondary structure prediction method that takes co-transcriptional folding into account. *Nucleic Acids Res.* **2013**, *41*, e102. [CrossRef] [PubMed]
48. Zhao, P.; Zhang, W.-B.; Chen, S.-J. Predicting Secondary Structural Folding Kinetics for Nucleic Acids. *Biophys. J.* **2010**, *98*, 1617–1625. [CrossRef] [PubMed]
49. Holtkamp, W.; Kokic, G.; Jäger, M.; Mittelstaet, J.; Komar, A.A.; Rodnina, M.V. Cotranslational protein folding on the ribosome monitored in real time. *Science* **2015**, *350*, 1104–1107. [CrossRef] [PubMed]
50. Frieda, K.L.; Block, S.M. Direct Observation of Cotranscriptional Folding in an Adenine Riboswitch. *Science* **2012**, *338*, 397–400. [CrossRef] [PubMed]
51. Wickiser, J.K.; Winkler, W.C.; Breaker, R.R.; Crothers, D.M. The Speed of RNA Transcription and Metabolite Binding Kinetics Operate an FMN Riboswitch. *Mol. Cell* **2005**, *18*, 49–60. [CrossRef] [PubMed]
52. Hennelly, S.P.; Novikova, I.V.; Sanbonmatsu, K.Y. The expression platform and the aptamer: Cooperativity between $Mg^{2+}$ and ligand in the SAM-I riboswitch. *Nucleic Acids Res.* **2013**, *41*, 1922–1935. [CrossRef] [PubMed]
53. Lemay, J.-F.; Penedo, J.C.; Tremblay, R.; Lilley, D.M.J.; Lafontaine, D.A. Folding of the Adenine Riboswitch. *Chem. Biol.* **2006**, *13*, 857–868. [CrossRef] [PubMed]
54. Watters, K.E.; Strobel, E.J.; Yu, A.M.; Lis, J.T.; Lucks, J.B. Cotranscriptional folding of a riboswitch at nucleotide resolution. *Nat. Struct. Mol. Biol.* **2016**, *23*, 1124–1131. [CrossRef] [PubMed]
55. Lutz, B.; Faber, M.; Verma, A.; Klumpp, S.; Schug, A. Differences between cotranscriptional and free riboswitch folding. *Nucleic Acids Res.* **2014**, *42*, 2687–2696. [CrossRef] [PubMed]
56. Gong, S.; Wang, Y.; Wang, Z.; Wang, Y.; Zhang, W. Reversible-Switch Mechanism of the SAM-III Riboswitch. *J. Phys. Chem. B* **2016**, *120*, 12305–12311. [CrossRef] [PubMed]
57. Gong, S.; Wang, Y.; Zhang, W. Kinetic regulation mechanism of pbuE riboswitch. *J. Chem. Phys.* **2015**, *142*, 15103. [CrossRef] [PubMed]
58. Gong, S.; Wang, Y.; Zhang, W. The regulation mechanism of yitJ and metF riboswitches. *J. Chem. Phys.* **2015**, *143*, 45103. [CrossRef] [PubMed]
59. Hofacker, I.L.; Flamm, C.; Heine, C.; Wolfinger, M.T.; Scheuermann, G.; Stadler, P.F. BarMap: RNA folding on dynamic energy landscapes. *RNA* **2010**, *16*, 1308–1316. [CrossRef] [PubMed]
60. Zhao, P.; Zhang, W.; Chen, S.-J. Cotranscriptional folding kinetics of ribonucleic acid secondary structures. *J. Chem. Phys.* **2011**, *135*, 245101. [CrossRef] [PubMed]
61. Wachsmuth, M.; Findeiß, S.; Weissheimer, N.; Stadler, P.F.; Mörl, M. De novo design of a synthetic riboswitch that regulates transcription termination. *Nucleic Acids Res.* **2013**, *41*, 2541–2551. [CrossRef] [PubMed]
62. Espah Borujeni, A.; Mishler, D.M.; Wang, J.; Huso, W.; Salis, H.M. Automated physics-based design of synthetic riboswitches from diverse RNA aptamers. *Nucleic Acids Res.* **2016**, *44*, 1–13. [CrossRef] [PubMed]
63. Zhao, Y.; Huang, Y.; Gong, Z.; Wang, Y.; Man, J.; Xiao, Y. Automated and fast building of three-dimensional RNA structures. *Sci. Rep.* **2012**, *2*, 734. [CrossRef] [PubMed]
64. Hofacker, I.L. RNA Secondary Structure Analysis Using the Vienna RNA Package. In *Current Protocols in Bioinformatics*; John Wiley & Sons, Inc.: Hoboken, NJ, USA, 2009; pp. 1–16, ISBN 0471250953.
65. Puton, T.; Kozlowski, L.P.; Rother, K.M.; Bujnicki, J.M. CompaRNA: A server for continuous benchmarking of automated methods for RNA secondary structure prediction. *Nucleic Acids Res.* **2013**, *41*, 4307–4323. [CrossRef] [PubMed]
66. Bernhart, S.H.; Hofacker, I.L.; Will, S.; Gruber, A.R.; Stadler, P.F. RNAalifold: Improved consensus structure prediction for RNA alignments. *BMC Bioinform.* **2008**, *9*, 474. [CrossRef] [PubMed]

67. Sükösd, Z.; Knudsen, B.; Vaerum, M.; Kjems, J.; Andersen, E.S. Multithreaded comparative RNA secondary structure prediction using stochastic context-free grammars. *BMC Bioinform.* **2011**, *12*, 103. [CrossRef] [PubMed]
68. Popenda, M.; Szachniuk, M.; Blazewicz, M.; Wasik, S.; Burke, E.K.; Blazewicz, J.; Adamiak, R.W. RNA FRABASE 2.0: An advanced web-accessible database with the capacity to search the three-dimensional fragments within RNA structures. *BMC Bioinform.* **2010**, *11*, 231. [CrossRef] [PubMed]
69. Miranda-Rios, J.; Navarro, M.; Soberon, M. A conserved RNA structure (thi box) is involved in regulation of thiamin biosynthetic gene expression in bacteria. *Proc. Natl. Acad. Sci. USA* **2001**, *98*, 9736–9741. [CrossRef] [PubMed]
70. Zirbel, C.L.; Roll, J.; Sweeney, B.A.; Petrov, A.I.; Pirrung, M.; Leontis, N.B. Identifying novel sequence variants of RNA 3D motifs. *Nucleic Acids Res.* **2015**, *43*, 7504–7520. [CrossRef] [PubMed]
71. Rahrig, R.R.; Leontis, N.B.; Zirbel, C.L. R3D align: Global pairwise alignment of RNA 3D structures using local superpositions. *Bioinformatics* **2010**, *26*, 2689–2697. [CrossRef] [PubMed]
72. Kladwang, W.; Chou, F.C.; Das, R. Automated RNA structure prediction uncovers a kink-turn linker in double glycine riboswitches. *J. Am. Chem. Soc.* **2012**, *134*, 1404–1407. [CrossRef] [PubMed]
73. Cruz, J.A.; Westhof, E. Sequence-based identification of 3D structural modules in RNA with RMDetect. *Nat. Methods* **2011**, *8*, 513–519. [CrossRef] [PubMed]
74. Kim, N.; Zahran, M.; Schlick, T. Computational Prediction of Riboswitch Tertiary Structures Including Pseudoknots by RAGTOP. In *Methods in Enzymology*; Elsevier Inc.: Waltham, MA, USA, 2015; Volume 553, pp. 115–135, ISBN 1557-7988 (Electronic) 0076-6879.
75. Krokhotin, A.; Houlihan, K.; Dokholyan, N.V. iFoldRNA v2: Folding RNA with constraints. *Bioinformatics* **2015**, *31*, 2891–2893. [CrossRef] [PubMed]
76. Kim, N.; Laing, C.; Elmetwaly, S.; Jung, S.; Curuksu, J.; Schlick, T. Graph-based sampling for approximating global helical topologies of RNA. *Proc. Natl. Acad. Sci. USA* **2014**, *111*, 4079–4084. [CrossRef] [PubMed]
77. Krokhotin, A.; Dokholyan, N. V Computational methods toward accurate RNA structure prediction using coarse-grained and all-atom models. *Methods Enzymol.* **2015**, *553*, 65–89. [CrossRef] [PubMed]
78. Wang, Y.; Gong, S.; Wang, Z.; Zhang, W. The thermodynamics and kinetics of a nucleotide base pair. *J. Chem. Phys.* **2016**, *144*, 115101. [CrossRef] [PubMed]
79. Gusarov, I.; Nudler, E. Control of intrinsic transcription termination by N and NusA: The basic mechanisms. *Cell* **2001**, *107*, 437–449. [CrossRef]
80. Chen, J.; Gong, S.; Wang, Y.; Zhang, W. Kinetic partitioning mechanism of HDV ribozyme folding. *J. Chem. Phys.* **2014**, *140*, 25102. [CrossRef] [PubMed]
81. Chen, J.; Zhang, W. Kinetic analysis of the effects of target structure on siRNA efficiency. *J. Chem. Phys.* **2012**, *137*, 225102. [CrossRef] [PubMed]
82. Xia, T.; SantaLucia, J.; Burkard, M.E.; Kierzek, R.; Schroeder, S.J.; Jiao, X.; Cox, C.; Turner, D.H. Thermodynamic Parameters for an Expanded Nearest-Neighbor Model for Formation of RNA Duplexes with Watson−Crick Base Pairs. *Biochemistry* **1998**, *37*, 14719–14735. [CrossRef] [PubMed]
83. Mathews, D.H.; Sabina, J.; Zuker, M.; Turner, D.H. Expanded sequence dependence of thermodynamic parameters improves prediction of RNA secondary structure. *J. Mol. Biol.* **1999**, *288*, 911–940. [CrossRef] [PubMed]
84. Hyeon, C.; Morrison, G.; Thirumalai, D. Force-dependent hopping rates of RNA hairpins can be estimated from accurate measurement of the folding landscapes. *Proc. Natl. Acad. Sci. USA* **2008**, *105*, 9604–9609. [CrossRef] [PubMed]
85. Hyeon, C.; Dima, R.I.; Thirumalai, D. Pathways and Kinetic Barriers in Mechanical Unfolding and Refolding of RNA and Proteins. *Structure* **2006**, *14*, 1633–1645. [CrossRef] [PubMed]
86. Rieder, R.; Lang, K.; Graber, D.; Micura, R. Ligand-Induced Folding of the Adenosine Deaminase A-Riboswitch and Implications on Riboswitch Translational Control. *ChemBioChem* **2007**, *8*, 896–902. [CrossRef] [PubMed]
87. Schroeder, R.; Grossberger, R.; Pichler, A.; Waldsich, C. RNA folding in vivo. *Curr. Opin. Struct. Biol.* **2002**, *12*, 296–300. [CrossRef]
88. Badelt, S.; Hammer, S.; Flamm, C.; Hofacker, I.L. Thermodynamic and kinetic folding of riboswitches. *Methods Enzymol.* **2015**, *553*, 193–213. [CrossRef] [PubMed]

89. Wolfinger, M.T.; Svrcek-Seiler, W.A.; Flamm, C.; Hofacker, I.L.; Stadler, P.F. Efficient computation of RNA folding dynamics. *J. Phys. A. Math. Gen.* **2004**, *37*, 4731–4741. [CrossRef]
90. Flamm, C.; Hofacker, I.L.; Stadler, P.F.; Wolfinger, M.T. Barrier Trees of Degenerate Landscapes. *Z. Phys. Chem.* **2002**, *216*, 155. [CrossRef]
91. Geis, M.; Flamm, C.; Wolfinger, M.T.; Tanzer, A.; Hofacker, I.L.; Middendorf, M.; Mandl, C.; Stadler, P.F.; Thurner, C. Folding kinetics of large RNAs. *J. Mol. Biol.* **2008**, *379*, 160–173. [CrossRef] [PubMed]
92. Huang, W.; Kim, J.; Jha, S.; Aboul-ela, F. A mechanism for S-adenosyl methionine assisted formation of a riboswitch conformation: A small molecule with a strong arm. *Nucleic Acids Res.* **2009**, *37*, 6528–6539. [CrossRef] [PubMed]
93. Chauvier, A.; Picard-Jean, F.; Berger-Dancause, J.-C.; Bastet, L.; Naghdi, M.R.; Dubé, A.; Turcotte, P.; Perreault, J.; Lafontaine, D.A. Transcriptional pausing at the translation start site operates as a critical checkpoint for riboswitch regulation. *Nat. Commun.* **2017**, *8*, 13892. [CrossRef] [PubMed]
94. Perdrizet II, G.A.; Artsimovitch, I.; Furman, R.; Sosnick, T.R.; Pan, T. Transcriptional pausing coordinates folding of the aptamer domain and the expression platform of a riboswitch. *Proc. Natl. Acad. Sci. USA* **2012**, *109*, 3323–3328. [CrossRef] [PubMed]
95. Hollands, K.; Sevostiyanova, A.; Groisman, E.A. Unusually long-lived pause required for regulation of a Rho-dependent transcription terminator. *Proc. Natl. Acad. Sci. USA* **2014**, *111*, E1999–E2007. [CrossRef] [PubMed]
96. Wong, T.N.; Pan, T. RNA Folding During Transcription: Protocols and Studies. In *Methods in Enzymology*; Elsevier Inc.: San Diego, CA, USA, 2009; Volume 468, pp. 167–193, ISBN 1557-7988 (Electronic)r0076-6879.
97. Ketzer, P.; Kaufmann, J.K.; Engelhardt, S.; Bossow, S.; von Kalle, C.; Hartig, J.S.; Ungerechts, G.; Nettelbeck, D.M. Artificial riboswitches for gene expression and replication control of DNA and RNA viruses. *Proc. Natl. Acad. Sci. USA* **2014**, *111*, E554–E562. [CrossRef] [PubMed]
98. Zhang, F.; Carothers, J.M.; Keasling, J.D. Design of a dynamic sensor-regulator system for production of chemicals and fuels derived from fatty acids. *Nat. Biotechnol.* **2012**, *30*, 354–359. [CrossRef] [PubMed]
99. Carothers, J.M.; Goler, J.A.; Juminaga, D.; Keasling, J.D. Model-Driven Engineering of RNA Devices to Quantitatively Program Gene Expression. *Science* **2011**, *334*, 1716–1719. [CrossRef] [PubMed]
100. Townshend, B.; Kennedy, A.B.; Xiang, J.S.; Smolke, C.D. High-throughput cellular RNA device engineering. *Nat. Methods* **2015**, *12*, 989–994. [CrossRef] [PubMed]
101. Endoh, T.; Sugimoto, N. Rational Design and Tuning of Functional RNA Switch to Control an Allosteric Intermolecular Interaction. *Anal. Chem.* **2015**, *87*, 7628–7635. [CrossRef] [PubMed]
102. Wei, K.Y.; Smolke, C.D. Engineering dynamic cell cycle control with synthetic small molecule-responsive RNA devices. *J. Biol. Eng.* **2015**, *9*, 21. [CrossRef] [PubMed]
103. Espah Borujeni, A.; Channarasappa, A.S.; Salis, H.M. Translation rate is controlled by coupled trade-offs between site accessibility, selective RNA unfolding and sliding at upstream standby sites. *Nucleic Acids Res.* **2014**, *42*, 2646–2659. [CrossRef] [PubMed]
104. McKeague, M.; Wong, R.S.; Smolke, C.D. Opportunities in the design and application of RNA for gene expression control. *Nucleic Acids Res.* **2016**, *44*, 2987–2999. [CrossRef] [PubMed]
105. Zemora, G.; Waldsich, C. RNA folding in living cells. *RNA Biol.* **2010**, *7*, 634–641. [CrossRef] [PubMed]
106. Herschlag, D. RNA Chaperones and the RNA Folding Problem. *J. Biol. Chem.* **1995**, *270*, 20871–20874. [CrossRef] [PubMed]
107. Danilova, L.V.; Pervouchine, D.D.; Favorov, A.V.; Mironov, A.A. RNAKinetics: A web server that models secondary structure kinetics of an elongating RNA. *J. Bioinform. Comput. Biol.* **2006**, *4*, 589–596. [CrossRef] [PubMed]
108. Xayaphoummine, A.; Bucher, T.; Isambert, H. Kinefold web server for RNA/DNA folding path and structure prediction including pseudoknots and knots. *Nucleic Acids Res.* **2005**, *33*, 605–610. [CrossRef] [PubMed]
109. Kramer, F.R.; Mills, D.R. Secondary structure formation during RNA synthesis. *Nucleic Acids Res.* **1981**, *9*, 5109–5124. [CrossRef] [PubMed]
110. Gong, Z.; Zhao, Y.; Chen, C.; Xiao, Y. Role of Ligand Binding in Structural Organization of Add A-riboswitch Aptamer: A Molecular Dynamics Simulation. *J. Biomol. Struct. Dyn.* **2011**, *29*, 403–416. [CrossRef] [PubMed]

111. Philips, A.; Milanowska, K.; Lach, G.; Boniecki, M.; Rother, K.; Bujnicki, J.M. MetalionRNA: Computational predictor of metal-binding sites in RNA structures. *Bioinformatics* **2012**, *28*, 198–205. [CrossRef] [PubMed]
112. Philips, A.; Milanowska, K.; Ach, G.L.; Bujnicki, J.M. LigandRNA: Computational predictor of RNA—Ligand interactions. *RNA* **2013**, 1605–1616. [CrossRef] [PubMed]

International Journal of
*Molecular Sciences*

MDPI

*Review*

# Aptamer Bioinformatics

**Andrew B. Kinghorn, Lewis A. Fraser, Shaolin Liang, Simon Chi-Chin Shiuand Julian A. Tanner ***

School of Biomedical Sciences, Li Ka Shing Faculty of Medicine, The University of Hong Kong, Pokfulam, Hong Kong SAR China; kinghorn@hku.hk (A.B.K.); lewis-fraser@hku.hk (L.A.F.); shaolin2@hku.hk (S.L.); simon156@hku.hk (S.C.-C.S.)

* Correspondence: jatanner@hku.hk; Tel.: +852-3917-9472; Fax: +852-2855-1254

Received: 31 October 2017; Accepted: 20 November 2017; Published: 24 November 2017

**Abstract:** Aptamers are short nucleic acid sequences capable of specific, high-affinity molecular binding. They are isolated via SELEX (Systematic Evolution of Ligands by Exponential Enrichment), an evolutionary process that involves iterative rounds of selection and amplification before sequencing and aptamer characterization. As aptamers are genetic in nature, bioinformatic approaches have been used to improve both aptamers and their selection. This review will discuss the advancements made in several enclaves of aptamer bioinformatics, including simulation of aptamer selection, fragment-based aptamer design, patterning of libraries, identification of lead aptamers from high-throughput sequencing (HTS) data and in silico aptamer optimization.

**Keywords:** aptamer; simulation; in silico selection; molecular dynamics; fragment based design; HTS

## 1. Introduction

Aptamers are short nucleic acid sequences capable of specific, high-affinity molecular binding [1,2]. Aptamers are isolated via SELEX (Systematic Evolution of Ligands by Exponential Enrichment) (Figure 1), an evolutionary process in which successive rounds of selection and amplification are used to enrich an aptamer library for high affinity aptamers. Aptamers are among the simplest of genetic entities, having both genotypic and phenotypic properties and being capable of heredity in an in vitro selection experiment. Their combinatorial complexity poses many questions and problems that are well suited to computational analysis. Many computational approaches have been applied to aptamers, bringing together different disciplines and technologies. This review encompasses a broad range of aptamer bioinformatics approaches including simulation of aptamer selection, aptamer selection by molecular dynamics, patterning of libraries, identification of lead aptamers from high-throughput sequencing (HTS) data, and in silico aptamer optimization. We aim to describe and contrast these methods so that aptamer scientists might make use of the diverse array of bioinformatics resources available.

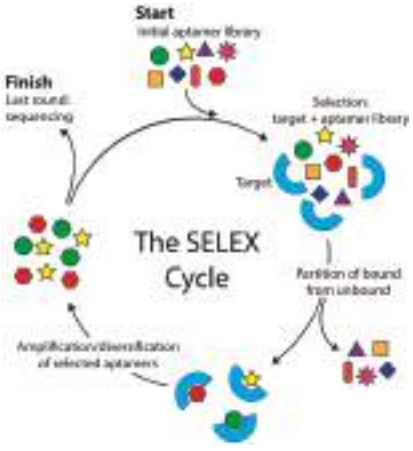


**Figure 1.** The SELEX (Systematic Evolution of Ligands by Exponential Enrichment) cycle. SELEX starts with a random nucleic acid aptamer library which is used to initiate the SELEX cycle (top arrow entering cycle). The library is incubated with the target and the target is washed to remove and discard unbound aptamers (right arrow exiting cycle) before the bound aptamers are eluted and amplified by PCR. The amplified sequences seed the next round of SELEX. Typically, around 12 SELEX cycles are performed before sequencing and aptamer characterization (left arrow exiting cycle).

## 2. Simulation of Aptamer Selection

Aptamer selection is complex. Complexity is found in both the myriad of experimental parameters and the combinatorial complexity of nucleic acid libraries. McKeague et al. performed a statistical analysis of 492 SELEX experiments, investigating experimental parameters such as choice of target, selection template, pH, and temperature [3,4]. Specific parameters were shown to have a significant effect on the dissociation constant of the tightest binding aptamers [4]. This information is valuable to aptamer scientists, but is limited to routinely disclosed experimental parameters. Many useful experimental parameters are not routinely disclosed, such as mutation rate, target concentration per selection cycle, recombination techniques and the inclusion of novel unnatural bases. An exhaustive empirical analysis, involving SELEX with sequencing of every round, is limited further by the combinatorial complexity of nucleic acid libraries, which contain ~$10^{15}$ sequences in an initial aptamer library pool [5]. Empirical analysis of anything close to this number of library members is simply not feasible. To investigate the experimental parameters of aptamer selection, simulation has been used.

In 1991, SELEX was first simulated using a program named SELEXION (Systematic Evolution of Ligands by Exponential Enrichment with Integrated Optimization by Non-linear Analysis) [6]. SELEXION was first used to reconstruct bacteriophage T4 DNA polymerase gp43 SELEX experiments [2]. A library of eight random RNA bases underwent eight rounds of SELEX comprising ligand binding, partitioning, and amplification. Ligand binding was modeled using a kinetic mechanism between target-protein and all aptamer ligands that reach equilibrium, stated by Irvine et al. [6] as follows:

$$(Pf) + (RNAf_i) \underset{k-i}{\overset{k+i}{\rightleftharpoons}} (P : RNA_i) \qquad i = 1, \ldots n,$$

where (*Pf*) was the free protein concentration, ($RNAf_i$) was the free RNA species of $i$ concentration, ($P$: $RNA_i$) was the protein-RNA species $i$ complex concentration, $k + i$ was the rate constant for association of free protein and free RNA species $i$, $k - i$ is the rate constant for dissociation of

protein-RNA species *i* complexes, ($P: RNA_i$) was the protein-RNA species *i* complex concentration, and *n* is the number of RNA sequences with a unique set of rate constants [6]. Partitioning efficiency for the reconstruction was set to 80% of bound aptamers and 0.1% of unbound aptamers. Amplification of partitioned aptamers involved reverse transcription to cDNA and PCR amplification before library generation using transcription. The experimental parameters of the gp43 selection [2] were reconstructed and underwent simulation as a proof of principle for SELEXION [6]. These simulations indicated that the equilibrium mechanism proposed above for SELEX was sufficient to explain the high levels of enrichment after just a few rounds observed in the laboratory experiments. Following the reconstruction simulation of the gp43 selection, several properties were investigated using SELEXION including predicted enrichment under different conditions, optimal protein concentration when dissociation constant ($K_D$) estimates are known, near-optimum protein concentration with no estimate for $K_D$, determination of sufficient protein concentration with no estimate for $K_D$ or background, likelihood of SELEX success, and finally sequence representation in the random library pool [6]. SELEXION took a thorough approach to modeling ligand binding. However, a possible shortcoming would be the determination of aptamer properties such as $K_D$. The binding affinities in terms of $K_D$ were distributed without reference to aptamer sequence. For the reconstruction there were just five unique $K_D$ values for all 65,536 unique aptamers in the initial library.

In 1998, Irvine et al.'s work [6] was extended and the program MultiSELEXION was coded to investigate SELEX against multiple targets [7]. MultiSELEXION allowed the investigation of problems arising from the use of contaminated protein preparations in SELEX, as well as analysis of complex target selections such as Cell-SELEX [8] and in vivo SELEX [9]. It was found that in most cases SELEX is capable of isolating differing ligands against the different targets in a heterogeneous mixture, irre SELEX spective of large variations in target concentrations or aptamer/target affinities. However, a low relative partitioning efficiency for a given target in a mixture gives a greatly reduced rate of selection of high-affinity aptamers [7].

Similarly to Irvine et al. [6] and Vant-Hull et al. [7], Chen et al. devised a SELEX simulation model that uses ligand binding based on equilibrium between target aptamer ligands and was applied to subtractive SELEX [10] as well as SELEX against a complex mixture [11]. This difference highlights and simulates selection pressures in SELEX experiments. Further similarities to Irvine et al. [6] and Vant-Hull et al. [7] included the binding affinities in terms of $K_D$ being distributed without reference to aptamer sequence. Chen et al. used just 10 unique $K_D$ values for all aptamers in the simulations [10].

Wang et al. developed a model that focused on the two SELEX parameters, target concentration and the effect of nonspecific binding [12]. The model represented ligand binding using equilibrium kinetics similarly to Irvine et al. [6] and Vant-Hull et al. [7]. Partitioning was modeled in two ways: without background binding, which was intended to mimic microfluidic selection; and with background binding, which was intended to mimic nitrocellulose filter-based separation. Aptamer binding properties were normally distributed [12] as hypothesized in the literature [13,14]. Wang et al. [12] found that "without background binding" conditions, an increasing amount of target decreases the selection efficiency. Under "with background binding" conditions, there is an optimum target concentration that increases with increasing background binding. Interestingly, under multiple selection rounds and "with background binding" condition the optimum target concentration for achieving maximum enrichment increases with each SELEX round. This is contrary to the generally accepted practice of reducing the target concentration as SELEX progresses. The reason for this trend of increasing optimum target concentration in successive SELEX rounds could be the modeling of background binders. The more target, the greater the number of specifically binding aptamers make it to the next round, therefore the higher the ratio of specific to nonspecific binders and the higher the average $K_D$ value. One aspect that SELEX Wang et al.'s model and many other models do not take into account is the possibility of adaptation in the aptamer pool giving rise to aptamers with increasingly tighter $K_D$ values.

Spill et al. developed a model that simulates Capture-SELEX and includes non-covalent ligand–substrate immobilization [15]. Aptamer–target binding was represented using a hybrid approach whereby an equilibrium constant is combined with a stochastic probability model. Following partitioning, the amplification of selected aptamers was simulated. Of particular interest is that the initial library $K_D$ distribution has a dramatic effect on the outcome of the simulation. Additionally, the impact of distribution noise and the downstream effects on the total target concentration were assessed. The use of a stochastic model and Monte Carlo simulation highlighted sensitivity of SELEX to stochastic variation. Twenty very tight binders are capable of outcompeting $10^{15}$ library members or can be totally lost.

Simulation of SELEX has given insight into how an aptamer scientist might optimize the SELEX protocol. SELEX has both vast complexity in terms of the number of sequences (typically around $10^{15}$), and informational complexity associated with each individual aptamer's sequence, folding, and target binding. The aforementioned simulations have focused on representing the vast complexity of SELEX and neglected the informational complexity of individual aptamer sequences. All binding properties of aptamers are selected randomly or from a distribution with no relevance to the aptamer sequence. For particular questions about SELEX, including the role of adaptation and the occurrence of divergent and convergent evolution, a more thorough binding model is required.

Hoinka et al. coded a program to simulate the aptamer selection process called "AptaSim" [16]. AptaSim aimed at realistically recreating the selection process during SELEX with the intention of investigating the effect of error-prone PCR on aptamer selection. An initial library pool was generated using a first-order Markov Model, previously trained on early SELEX round selection data. The generated aptamer was randomly assigned a copy number and binding affinity within a predefined range. Iterative cycles of capture and amplification were then simulated where the capture probability is related to an aptamer's copy number and binding affinity, and amplification is subject to a specified probability of mutation. The binding model used attributed aptamer affinities at random without relevance of sequence. Additionally, mutated versions of these aptamers retained the original's attributed binding affinity. While AptaSim was an important step forward in simulating selection, enrichment and mutation copy number, AptaSim did not appropriately represent heritability or represent binding affinities correlated between related sequences, which is required for the study of SELEX as a genetic system.

Oh et al. used a string matching function as a binding model to simulate aptamer selection [17]. All aptamers were given a target binding score based on their similarity to a given "optimal aptamer" sequence [17]. This model does include heritability and binding correlation between related sequences. As string matching is not computationally demanding, this approach can be used for very large library sizes, which is more representative of aptamer selection. The drawback of string matching is that only close-range epistasis is possible and by using a one "optimal aptamer" model, the landscape is cone-shaped and would not represent a true aptamer binding landscape.

Wedge et al. used Kauffman's *NK* model [18] to represent ligand–target binding for the simulation of protein-directed evolution [19], a similar field to aptamer selection. The *NK* model is a robust mathematical model that serves as an objective function relating genotypic sequences to phenotypic fitnesses that make up a fitness landscape. Using the *NK* model, strings of informational digits of length $N$ are attributed fitness values equal to the sum of each digits interaction with $K$ other digits. In this way, epistatic and pleiotropic interactions can be modeled. The *NK* model has been used to describe many complex systems such as immunology [20], evolutionary biology [21], and economics [22]. The *NK* model has also been related to aptamers [23]. In Wedge et al.'s [23] work the ligand properties were determined using an *NK* model in which binary strings of length $N = 100$ were used with random epistatic interactions varying from $K = 0$ to 10. The initial library size was 40,000 and during each of the 10 selection rounds, 1 to 4000 of the tightest binding ligands were partitioned. Varying degrees of selection pressure (number of ligands selected each round), mutation rate, and crossover (recombination) were tested and it was found that optimal directed evolution (DE) parameters were

strong selection pressure, a high mutation rate, and that crossover is only valuable when epistasis is low to moderate ($K < 5$). While these results are valuable to the field of protein-directed evolution, the simulation did not mimic properties specific to SELEX.

The *NK* model can effectively represent the target binding of polymeric ligands such as proteins and aptamers. Besides the challenges for biological accuracy in representing base interactions within an aptamer, the classical *NK* model may have limitations in representing some aspects of biological systems. The *NK* model's greatest utility is that epistasis can be tuned using the variable *K*. However, this epistasis is reasonably uniform throughout the sequence. To represent some biological systems, a higher amount of epistasis is desirable. As *K* increases the fitness landscape tends to become more rugged, to the point where it is too chaotic to allow adaptation, a phenomenon is referred to as the "complexity catastrophe" [24].

To overcome the "complexity catastrophe" and use the *NK* model to represent gene regulation, Altenberg [25] developed "selective genome growth" in 1995. Selective genome growth is an evolutionary approach that selects epistatic interaction in such a way to create a highly epistatic landscape that is smoother than classic *NK* landscapes with the same degree of epistatic interaction [25]. Altenberg's selective genome growth *NK* landscape represents gene regulation very well. However, due to the increasing returns of the selection system, an extremely high pleiotropy is attributed to a handful of digits [26]. This highly aggregated pleiotropy is biologically appropriate and accurate for describing gene regulation. However, as each base in an aptamer has a relatively low number of interactions due to its spatial capacity, the highly aggregated pleiotropy is not biologically representative for base interactions within an aptamer.

To overcome this problem Kinghorn and Tanner recently devised the method "selective phenome growth", which generates fitness landscapes with low aggregated pleiotropy that more appropriately represent aptamer binding [26]. The selective phenome growth process involves phenotypic contributors being added to a genotype/phenotype interaction map sequentially in such a way as to increase the fitness of a selected "fit sequence". In this way, a fitness landscape is built around the selected "fittest sequence". The fitness landscapes obtained were compared to empirical aptamer microarray data and were shown to more accurately represent aptamer ligand binding than other theoretical models (Figure 2) [26]. The selective phenome growth model has not yet been utilized in the simulation of SELEX, only described and validated as a model that more accurately represents aptamer binding.

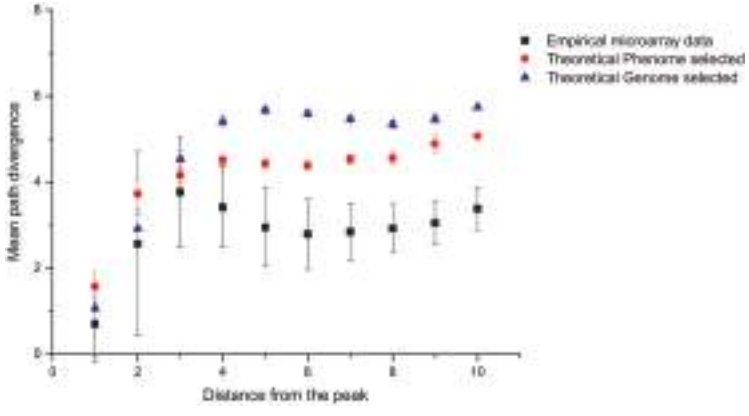


**Figure 2.** Comparison of novel phenome selected model to both genome selected and empirical aptamer microarray binding data. The mean path divergence analysis, a measure of landscape smoothness, shows that the novel phenome selected landscape is more similar to empirical microarray binding data than the previous genome selected landscape model. Figure adapted from Kinghorn et al. [26].

The no-free-lunch theorem states that all search algorithms perform exactly the same when averaged over all possible problems [27]. This infers that any elevated performance in one class of problem is exactly paid for in the performance of another class of problem. If there is discrepancy between a real-life system and a model used to describe it, for example an empirical SELEX experiment and a SELEX simulation, any elevated performance insight found using the simulation is exactly paid for in the performance of the real-life system. This illustrates the need for the simulation model to be as accurate as possible; otherwise optimizations will not translate to empirical SELEX experiments. The area least accurately modeled in SELEX simulations has been the aptamer binding model.

## 3. Aptamer Selection by Molecular Dynamics

Molecular dynamics have applications across biotechnology, including but not limited to protein studies, membrane transport, and drug discovery [28–31]. One particular application is to improve the efficacy of aptamer selections by computationally solving the three-dimensional structures of nucleic acids (NAs) and their targets, and simulating the physical forces involved in NA docking to a target. This is achieved by various N-body simulations that calculate the dynamic forces of the atoms and molecules of a NA within a binding site, in the form of a docking score. Docking scores can be used to identify sequences that bind to a target, defining a novel approach for aptamer discovery. Here, we will discuss studies wherein molecular dynamics has been used to enrich selection pools, optimize existing aptamers, and discover new aptamers.

### *3.1. Whole Aptamer Docking*

For the purpose of this review we have divided in silico techniques into two categories: those that simulate the molecular dynamics of a whole aptamer and its target, and those that fragment an aptamer into discrete units to simulate binding interactions. We will discuss the literature that underpins in silico selections for whole aptamers.

Computationally predicting secondary and tertiary structures of NAs and targets reveals the steric and energetic properties of each structure. These predictions allow researchers to modify their selection pools to have a broader range of three-dimensional structures and NAs with more favorable free energy [32–34], and provides essential information for molecular docking simulations [35]. Many protein-NA structures have been solved experimentally using NMR and X-ray crystallography, for which there are large but limited libraries in the Protein Data Bank (PDB). If the structure has not been solved experimentally, homology modeling webserver services exist for both proteins and NAs [36–39].

In simulating the docking between a target and an aptamer, several non-covalent interactions are assessed including ionic interactions, hydrogen bonds, van der Waal's forces, hydrophobic interactions, base stacking interactions, and shape complementarity [35] (Figure 3A). Algorithms calculate the potential energy between interacting atomic components, known as force fields. For biological systems, the most frequently used MD force field simulations are CHARMM and AMBER [35]. Homology and modeling software for DNA–protein interactions is currently limited [35], as much of the software is based in analyzing protein–protein interactions. A coarse-grained force field has shown how dsDNA interacts with protein structures. Specific interactions are useful but limited in their scope and shape complementarity and internal DNA energy play an important role in simulating protein–DNA docking [40] (Figure 3B).

An initial attempt at in silico selection was proposed by Chushak and Stone. Computationally, they decreased RNA sequence search space in a selection pool by up to five orders of magnitude to enable conjugation of an enriched RNA selection pool to a microarray to improve high-throughput aptamer selections [34]. A three-step enrichment approach was used:

(1) Selection based on secondary structure—a set of criteria were used to identify and eliminate sequences with common simple structural motifs and high-energy unstable RNA sequences, both of which would be unlikely to form aptamers.

(2) Selecting for conformational flexibility—a single RNA sequence can have a large range of three-dimensional conformations; the Rosetta RNA package [41] was used to generate these structures. Then the five lowest energy three-dimensional structures, and therefore those with the greatest conformational flexibility, were selected using the AMBER force field simulation and the generalized Born solvation model [42].

(3) Screening the RNA library with computational docking—a modified docking tool called DOVIS using Autodock v4 [43] was used to simulate interactions between all the generated RNA three-dimensional structures and small molecule targets. Docking was scored based on their calculated affinity for the targets. By selecting for the highest scoring sequences they effectively lowered the RNA pool size from ~$2.5 \times 10^8$ to $5 \times 10^3$. Six known aptamer–ligand complexes were used to validate this approach. Native aptamers were found in within the top 5% of in silico selected structures.

Confirming that molecular dynamic calculations align with experimental evidence provides further evidence that in silico approaches can complement aptamer selections. A software package that uses the CHARMM force field to analyze protein–protein interactions called Discovery Studio uses a docking simulation algorithm called ZDOCK [35,44]. ZDOCK was found to work effectively with short RNA–protein interactions [45] but was found to be ineffective when simulating longer RNA strands [46,47]. When combined with ZRANK, an algorithm that takes into account a range of attractive and repulsive forces, van der Waal's forces, and desolvation, effective simulation of protein–long-strand RNA was achieved [35,48]. Having confirmed the efficacy of this software package in conjunction with aptamer–protein interactions, Chen's research group mutated aptamers of angiopoiten-2 protein (Ang-2), a protein that regulates angiogenesis and is linked with the development and spread of cancer [49,50]. From the mutated strands, they selected three with high scores and tested them experimentally for binding with surface plasmon resonance (SPR). Based on binding affinity and SPR response, they claim one of these novel aptamers (Seq15_12_35, $K_D$ 0.61) has improved binding when compared to a high-affinity Ang-2 aptamer (Seq1, $K_D$ 1.39) found in the literature [48].

Selection can be a lengthy and costly process [51], especially when targeting human proteins for which native proteins may be expensive or commercially unavailable [52]. To lower the cost of selection, it is common to select an aptamer towards a recombinant or non-human version of the equivalent human protein [53]. There is an increased risk that the difference in homology between the native protein and the recombinant/non-human protein will result in selecting for an aptamer that will not bind to the native protein. This is the case for immune-checkpoint blockade receptor TIM3 [54], for which aptamers selected for murine binding aptamers lacked cross-reactivity with the human form. Based on the murine aptamer, Rabal et al. used a three-step bioinformatics process similar to those already discussed, but coupled cluster analysis with their chosen 3D docking algorithm, 3DRPC [55]. Clustering algorithm GROMACS [56] revealed highly populated clusters focused around specific binding sites. In four out of five cases, combining clustering with docking simulation revealed a binding mode and site that were not identified by docking simulation alone. They were able to show the scope of in silico aptamer–protein analysis by identifying a plausible binding site on murine TIM3 and aptamer binding mode that explains the lack of cross-reactivity in murine over human TIM-3 [54].

### 3.2. Fragment-Based Aptamer Design and Docking

Whole aptamer selections require massive computational resources and three-dimensional structures of both nucleotides and target. A fragment-based approach has been argued to simplify the process of in silico aptamer generation [57]. Tseng et al. presented a three-step approach in which they only require structural information of the target, known as the entropic fragment-based approach (EFBA) [57]. They first determined the probability distribution of the first nucleotide binding to the target. They then sequentially added nucleotides to the first, taking into account the probability distributions of the added nucleotide to its neighbors and the target. Finally, they determined a cutoff length based on an entropic criterion (information theory entropy). Once the target–NA complex was saturated and the interactions of the complex were at a global minimum irrespective of nucleotide

additions, the sequence was selected [57] (Figure 3C). They developed the in silico "seed and grow" method by selecting two aptamers. One aptamer bound to the target phosphatidylserine (PS), which previously had no reported aptamer [57]. They have since continued their investigation on the PS binding aptamer with more computational and experimental detail with a view to translation for practical use [58].

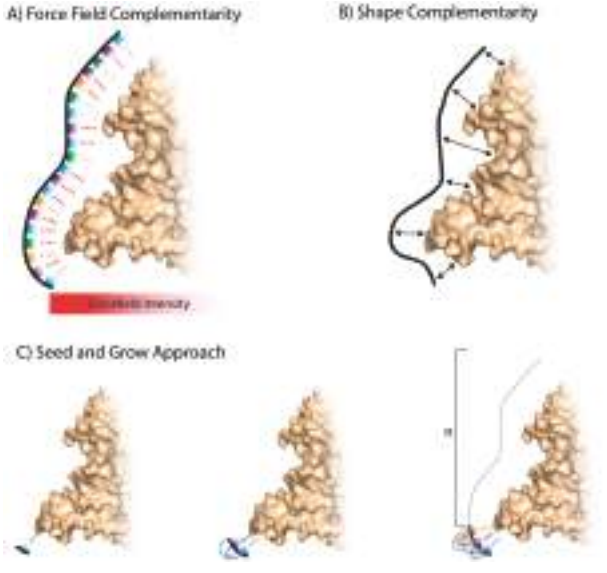


**Figure 3.** Simplified visualization of the molecular dynamics used in aptamer selections. (**A**) Force fields, the algorithmically calculated potential energies between atomic components of a nucleotide sequence and a target, are algorithmically calculated and represented here as a dashed red line. The differential opacity represents the variable favorability of each interaction, which is later translated into a docking score; (**B**) shape complementarity, a simplified representation of the nucleotide sequence interacting with a target based on spatial orientation; (**C**) the seed and grow approach, a fragment-based method. A single nucleotide is matched with a target and single nucleotides are added in sequence. A probability distribution is used to measure the interactions between the target and linked nucleotides. The target in this figure is derived from crystal structure PDB 3ZH2.

## 4. Patterning of Libraries

In a SELEX experiment, typically nanomoles of aptamer library or approximately $10^{15}$ molecules are used. The typical length of a nucleic acid in a library is around 40 bases (total sequence space $4^{40}$), so less than one in 1.2 billionth of the sequence space is covered. Aptamers generally require secondary structure to bind their targets, therefore increasing the occurrence of secondary structure in the library should enhance the success rate when selecting for an aptamer. Here, we will outline several approaches that have been taken to pattern aptamer libraries with secondary structures.

RNA aptamer and ribozyme selection analysis has shown that the presence of distinctive secondary structures, such as a stem–loop, enhances the binding affinity [32,59,60]. Such analysis began by observing the nucleotide distributions. Schultes et al. [61] found that functional RNAs have a tendency to have more purine than pyrimidine. This correlation was studied by functional class and phylogenetic domain. It was found that the G+A and G+U content in archaea, bacteria, and eukaryote functional single-stranded RNA showed a similar positive bias and that the bias was inversely proportional to the sequence length [61]. Knight et al. performed a comparative analysis of distantly related and unrelated sequences using simplex to study all possible composition vectors

(G+A, G+U and G+C) of isoleucine aptamer and hammerhead ribozyme [62]. A library size of $6.23 \times 10^9$ sequences containing 25% U, 15% C, 20% A, and 40% G could maximize the probability of identifying both motifs (99%). This study demonstrated that adjustment of base composition could be used to lower the total number of candidates in a SELEX (Systematic Evolution of Ligands by Exponential Enrichment) experiment.

Computational methods use sequence information to pattern initial libraries, which results in the evolution of more complex structures. For DNA aptamer selection, Ruff et al. patterned their initial library pool with alternating purine and pyrimidine, which was found to increase the formation of stem–loop structures that bind to streptavidin, immunoglobulin E (IgE), and vascular endothelial growth factor (VEGF) [63]. By sequencing pools from each selection round, they compared the selection efficiency for both random and patterned libraries. The patterned library was significantly enriched relative to the unpatterned library at the 10th round. For IgE, after adding restriction endonuclease to digest the tagged sequences, it was found that the enrichment was further significantly increased. The use of a patterned library in SELEX was able to select specific binders for all three molecules with affinity at nanomolar levels better than those selected from random libraries (streptavidin: $K_D$ = 105 nM, IgE: $K_D$ = 26 nM, VEGF: $K_D$ = 45 nM). These results showed that the use of a patterned library could increase the proportion of active aptamer, speed of selection, and affinity of the resultant aptamers [63].

This alternating purine and pyrimidine patterning strategy was enhanced when Martin et al. used a novel computational method to increase the structural complexity of a DNA library (Table 1) [64]. This patterning method reduced the size of the library, allowing the integration of the entire library onto a microarray, for the identification of a thrombin binding aptamer. The initial library was designed with UNAFold software using three major constraints. First, the first nucleotide of the aptamer must pair with the final one. Second, the number of unpaired bases must fluctuate between 10 and 30 for the 50-nucleotide strands. Third, there must be at least two stretches of unpaired nucleotides. This limited the total number of candidates in the library to 50,000 sequences. The selection results showed that the first six to eight bases of the top 15 sequences resembled thrombin binding aptamer and binding was also specific to thrombin. This demonstrated the effectiveness of using a patterned library on a microarray to select for aptamers.

**Table 1.** Library design used by Martin et al. [64].

| Pattern | Library Design |
|---|---|
| 1 | $(RY)_3$-$N_4$-$(RY)_4$-$N_3$-$(RY)_4$-$N_4$-$(RY)_4$-$N_3$-$(RY)_3$ |
| 2 | $(RRYY)_2$-$N_4$-(RRYY)-$N_3$-(RRYY)-$N_4$-(RRYY)-$N_3$-(RRYY)-$N_4$-$(RRYY)_2$ |
| 3 | $(RRYY)_2$-$N_4$-(RRRYYY)-$N_4$-(RRRYYY)-$N_4$-(RRRYYY)-$N_4$-$(RRYY)_2$ |
| 4 | $(RRYY)_2$-$N_4$-$(RY)_3$-$N_4$-$(RY)_3$-$N_4$-$(RY)_3$-$N_4$-$(RRYY)_2$ |

[1] Library designs of different patterns of alternating purine and pyrimidine. Pattern 1 library theoretically has $1.8 \times 10^{19}$ sequences and Pattern 2 has $3 \times 10^{20}$. Pattern 3 has three consecutive purines or pyrimidines, which may allow the formation of quadruplex, while Pattern 4 only allows alternating purines and pyrimidines. R is purine, Y is pyrimidine, and N is a random mixture of purine and pyrimidine. Table adapted from [64].

The 1963 discovery of Hoogsteen base-pairing explains the formation of triplex and quadruplex structures [65,66]. The G-quadruplex structure now holds significant interest due to applications in therapeutics [67,68] and diagnosis [69,70]. A G-quadruplex usually consists of four guanine tracks and a few tetrads [71]. The structural features include a broad surface of π-orbitals above and below the quadruplex that allow hydrophobic binding to targets such as nucleolin [72], hemin [73,74], and light-up fluorogens [75–77].

The binding capacity of G-quadruplex structures was exploited by McManus and Li, who integrated patterning into DNA libraries to select aptamers with quadruplex structures. They patterned the library with the following methods: inclusion of four G-tracts in the library while leaving the rest to be random; simplifying the complicated three-layer G-quadruplex into

a two-layered structure; and four $G_2$ tracts were designed with three domains of random sequences for loop formation [71,78]. The authors first investigated the effective loop length for the folding of a quadruplex by adding three to seven thymidines between the G-tracts and characterizing by circular dichroism (CD). The CD characteristics of different quadruplex configurations are shown in Table 2. When compared to a completely random library, the $G_2$ tract library showed peaks at 265, 280, and 295 nm, indicative of G-quadruplex structures (Figure 4), whilst the random library only showed a single peak at 280 nm. The authors also investigated the melting temperatures of individual libraries with different loop lengths at 295 nm. Libraries with a loop length of 3–6 were suitable for the selection of a single-stranded aptamer as their melting temperature did not change at increased concentrations. However, the melting temperature of a library with a loop length of seven increased with concentration. This indicated that it formed multimolecular quadruplexes because the interaction between large loops of different strands has a more regular structure and is not ideal for SELEX, requiring certain structural flexibility in the library. This pioneering work shows how optimizing DNA library parameters can maximize the possibility of selecting active binders.

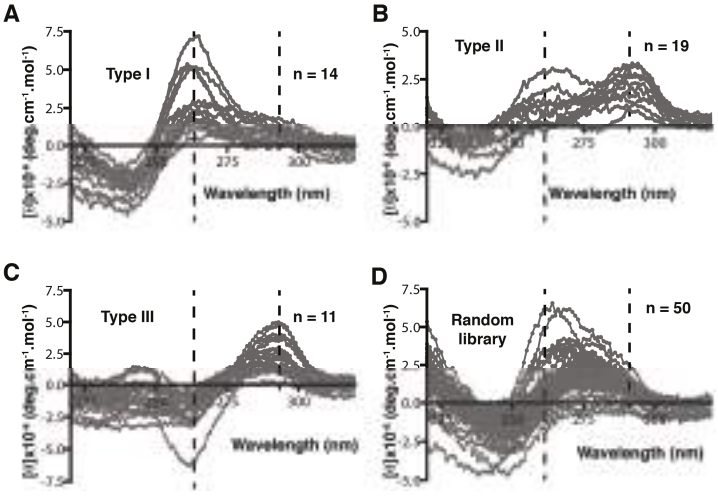


**Figure 4.** Circular dichroism (CD) characteristics of different quadruplexes and random library. (**A**) Parallel quadruplex shows positive peaks at 265 and 295 nm; (**B**) antiparallel quadruplex with glycosidic bond angles of the same orientation shows bimodal spectra as positive peaks at 265 nm and 295 nm of the same intensity; (**C**) antiparallel quadruplex with glycosidic bond angles of opposite orientation—the CD shows a negative peak at 265 nm and a positive peak at 295 nm; (**D**) random library shows a peak at 280 nm but no peaks at 265 nm and 295 nm, indicating the absence of a quadruplex. Figure adapted from McManus and Li [78].

**Table 2.** Major open-source programs for SELEX (Systematic Evolution of Ligands by Exponential Enrichment) HTS (high-throughput sequencing) data analysis.

| Program | Operation System | Language | Clustering Method | Validation Experiment |
|---|---|---|---|---|
| FASTAptamer | Mac/Linux | Perl | Levenshtein distance | HIV-1 Reverse Transcriptase |
| AptaCluster/AptaGUI | Mac/Linux/PC | Java | LSH and k-mer counting | IL-10RA |
| APTANI | Linux | Python | Structure motif-based clustering | Murine IL4Ra |
| AptaTrace | Mac/Linux/PC | C++, Java | Structure motif-based clustering | C-C chemokine receptor |
| PATTERNITY-seq | No details | No details | Levenshtein distance | Annexin-A2 |

In a SELEX experiment, the random library provides low sequence space coverage and low structure space representation. Using stem–loop structures and/or patterned libraries can increase sequence space coverage and improve space representation. Although it is difficult to pinpoint the best method to pattern a library, it is clear that patterned libraries can enhance aptamer selection by reducing the time taken to select an aptamer, increasing the success rate of a selection, and improving the binding affinity of isolated aptamers [63].

## 5. In Silico Aptamer Identification from High-Throughput Sequencing (HTS) Data

### 5.1. The Trend of Using HTS for Improving SELEX

Initially developed for the purpose of tackling the increasing complexity of whole genome sequencing, HTS technologies have continued to evolve and change the landscape in many fields of biomedical research over the last 10 years [79]. Since the development of the first commercialized 454 sequencer, companies such as Illumina, Ion Torrent, and Oxford Nanopore technologies are all increasing sequencer capacity and reducing cost [80]. In the area of aptamer research, deep, high-throughput, and in-parallel DNA sequencing technologies allow the analysis of millions of sequences found in each round of aptamer selection, and thus open a new avenue for identification and optimization of aptamers [81]. HTS data obtained from each round of the selection can not only be used to monitor the dynamic sequence change of aptamer selection to identify the best-performing sequences in early rounds [82–84], but also as a tool for aptamer scientists to further investigate the enrichment principles of SELEX process such as selection efficiency [85], aptamer–target interactions [86], and mutation landscape [16].

Some of the earliest works applying HTS for identification of aptamers were performed by Schroeder's group in 2010. In the study, they applied a genomic RNA library—overlapping sequences constructed via PCR from the *E. coli* genome—to select against an RNA binding protein named Hfq. 454 sequencing was used to obtain sequence data for two of the last round libraries from the genomic selection and, for comparison purposes, the rounds of another selection that omitted the target binding step, to monitor the amplification variants of the genomic SELEX. By analyzing the HTS data, they successfully identified genomic RNA aptamers and discovered that these aptamers are predominant in the antisense transcripts [87,88]. In the same year, Soh's group pioneered DNA aptamer quantitative selection by applying microfluidic and HTS technologies. They performed three rounds of microfluidic device-assisted selection against platelet-derived growth factor BB (PDGF-BB) and sequenced each round of the selection via high-throughput sequencing. More than $1.7 \times 10^7$ sequences from each round of selection were obtained and the enrichment trajectory across different rounds was tracked by analyzing the HTS data. Comparing the sequences obtained from different rounds, they discovered the sequence with the highest affinity did not have the highest copy number in the last round [89]. Schultze et al. [90] confirmed this finding when they discovered that the library convergence in SELEX led to high-performance sequences being outcompeted by weaker-performing sequences that amplify more efficiently during PCR. The best binders tend to enrich rapidly in the very early rounds of selection [90]. Spiga et al. [91] performed HTS and SPR to monitor the binding affinity change and aptamer enrichment for tobramycin selection. They also discovered the most enriched and best binding sequences are visible even after two selection rounds [91]. As the cost of HTS continues to decrease [92], more researchers use it for characterizing multiple selection round libraries to ensure the quality of selected candidates [84,93]. Using the HTS dynamic monitoring method, researchers successfully identified high binding aptamers both for proteins [94] and small molecule targets [91].

### 5.2. Benchmark Toolkit for HTS SELEX Analysis

Besides the cost, one of the major hindrances in early years to generalize HTS methods for aptamer identification was the difficulty of processing large amounts of sequence data. However, multiple open-source/paid bioinformatics tools have been developed specifically for aptamer scientists.

The initial step in processing HTS data from a sequenced SELEX pool is to remove the adapter, barcode, or constant region from the sequences. After this pre-processing, a tool to count the sequence frequency is required. Previously, aptamer research groups used genomic informatics software packages such as Tallymer [95,96] or RazerS [90,97], or designed in-house programs to fulfill the counting requirement [89,98].

Galaxy Project is a platform that provides fundamental bioinformatic tools for bench scientists who may not have a background in bioinformatics. Thiel et al. recently developed workflows based on this Galaxy Project for handling HTS SELEX data to perform pre-processing steps [99,100]. This tool also allows researchers to remove adapter/barcode/primer regions from sequences; identify and remove sequences with mismatches within the primer region; set a variable region length cutoff; and count the number of duplicate reads. Another benefit of the Galaxy workflow is it is "ready to use" and "easy to access" for an open-source, web-based platform. However, the Galaxy web service does not currently provide analysis for motif-based clustering as the platform was designed for general genomic projects.

An easy-to-use, aptamer-specific bioinformatics tool to address the clustering based on primary sequence is FASTAptamer [101]. FASTAptamer consists of a library of modular Perl scripts and is compatible across UNIX-like systems (or a Windows system with a Perl interpreter installed). Count, compare, cluster, enrich, and search are the five major script modules. By using these modules, users can count, normalize, and rank the sequence reads in a FASTQ file and group these sequences into families based on Levenshtein distance, as well as determine the SELEX enrichment across multiple selection rounds [101]. PATTERNITY-seq, developed by Ducongé's group [102], is another package that uses sequence pattern clustering based on Levenshtein distance. They validated this approach by re-analyzing the data from a previously published cell-SELEX against Annexin-A2 [103].

AptaCluster [104] is similar to FASTAptamer but based on the local sensitive hashing (LSH) method, which is capable of comparing sequences with a reduced number of dimensions (Figure 5). Iterative rounds of comparison within groups of aptamers are used to cluster aptamer sequences. By using such a method, the computational time required for AptaCluster is less than FASTAptamer. However, this method cannot be applied as a sequence pool containing various sizes. FASTAptamer and AptaCluster are purely text-based tools, whereas a program called AptaGUI that can be used alongside AptaCluster includes a graphical user interface (GUI) for the dynamic visualization of HTS SELEX data [105]. An alternative to AptaGUI is the paid platform COMPAS, developed by AptaIT GmbH. This also contains GUI for the navigation of the HTS data, but many of the operational details are proprietary and the company program is only available in conjunction with the purchase of their selection service.

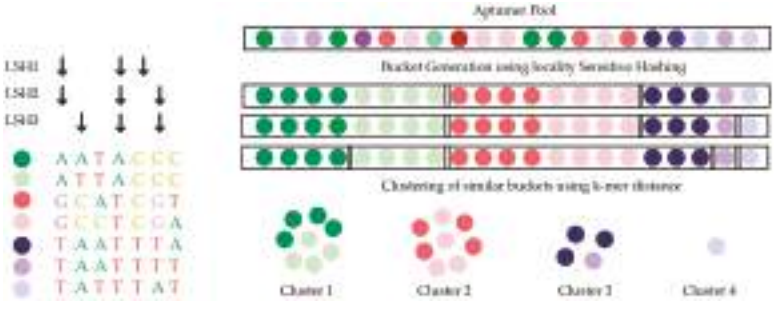


**Figure 5.** Illustration of the AptaCluster algorithm. Each colored sphere represents an individual sequence in the library and the similar colors represent related sequence. AptaCluster clusters the library pool into different sets of similar sequences based on locality sensitive hashing (LSH). The black arrows represent the user-defined number of nucleotide positions, which are sampled to generate input for the hash function. Figure adapted from Honika [16].

### 5.3. Structure Motif Clustering-Based Tools

Most of the previously mentioned bioinformatics tools do not include functions for prediction and clustering of HTS data for structure-based methods. Furthermore, they do not allow elucidation of complex motifs and important pre-processing steps for initial analysis of the data generated during SELEX.

Structure prediction programs such as Mfold [106] have been used to analyze low-throughput sequence data. Mfold predicts the secondary structure of single-stranded nucleic acids by energy minimization. Even though "bulk" servers of Mfold can analyze hundreds of sequences at once, it is, however, difficult to handle structure prediction on the HTS scale.

A recently developed platform for structure motif clustering is AptaTrace [107]. Based on the secondary structure prediction from SFOLD [108,109], AptaTrace applies this information into all of the sequences input to the program. This allows for the prediction of a specific structure for each k-mer in each selection round and ranking by predicted significant structural enrichment. APTANI is a similar program, able to cluster sequence motifs based on secondary structure prediction. It uses RNAsubopt from the Vienna RNA package [110] and predicts using sub-structures, apical loops, bulge loops, and intra-strand loops. This method was validated using a SELEX against IL4Ra. Using APTANI, an aptamer was identified in one round, which previously required five rounds.

The speed of HTS technology adoption has motivated the development of particular tools to assist HTS-based SELEX and identify better aptamer candidates (Table 2). Even though many approaches still lack multiple validations, using HTS to replace conventional sequencing methods for aptamer development is the trend. Recent progress in this field shows the potential for developing an all-in-one bioinformatics tools for aptamer researchers.

## 6. In Silico Aptamer Optimization

Aptamers have been isolated with both high affinity and high specificity for binding to their selected targets [5,111]. SELEX is an efficient method of isolating aptamers; however, following selection an aptamer scientist must always ask "Have I isolated the best possible aptamer sequence?" The library used for SELEX generally has a random region of around 40 bases [4], and typically only a few nanomoles can be used for the initial selection round. This represents a sequence space coverage of one in 80 billion. From this incredibly small sequence space coverage, it is unlikely that one will select the single best aptamer sequence. Sequence adaptation via mutation may account for some sequence space searching; however, as selection for SELEX is relatively low resolution [112], it is difficult to resolve the very best aptamer sequence.

Bioinformatic approaches have been used to improve the affinity of aptamers. As highlighted earlier, due to low selection pressure classical SELEX is unlikely to resolve the very best aptamer sequences. Therefore, each individual aptamer generated using a bioinformatics approach must be individually assayed for binding affinity, which can be labor-intensive and time-consuming. DNA microarrays consist of many features or spots on a glass slide, each feature containing many copies of a unique DNA sequence. This high-throughput technology allows for simultaneous assay of many aptamer sequences via incubation with fluorescent target.

In 2007, Katilius et al. used DNA microarrays to optimize and explore the surrounding sequence space of an aptamer against immunoglobulin E (IgE) [113]. Variations of the aptamer sequence with single, double and a selection of triple point mutations were synthesized onto a DNA microarray and assayed with Alexa Fluor 647 labeled IgE. This mutational analysis highlighted the conserved and unconserved base positions in the aptamer sequence. One aptamer variant showed mild affinity improvement ($K_D$ = 4.1 nM) when compared to the original aptamer sequence ($K_D$ = 4.7 nM) [113].

Platt et al. analyzed the sequence activity relationship of a set of G-quadruplex thrombin binding aptamers using DNA microarray technology [114]. The combinatorial landscape was probed via two methods. The first method investigated two internal loops of the G-quadruplex with 2-3 base random regions (GGGGAGTAGG($X_{2-3}$)GGTGTTGG($X_{2-3}$)GGGGCTCCCC, where X denotes the bases varied).

The second method investigated the hairpin in which the G-quadruplex is nested within a section using pseudo-random variants (($X_8$)GGTT($X_{2–4}$)GGTTGGGG($X_6$), where X denotes the bases varied). Despite this search through sequence space, the tightest binding novel aptamer ($K_D$ = 28 nM) had a lower affinity than the original ThB aptamer ($K_D$ = 26 nM) [114].

Knight et al. combined a DNA aptamer microarray assay with in silico closed-loop aptameric directed evolution (CLADE) to select for aptamers against the natively fluorescent target allophycocyanin (APC) [115]. Five hundred control aptamer and 5500 test pool aptamers of 30 nucleotides were synthesized onto a DNA microarray for each round. The initial test pool for the first round was randomly generated. The test pool aptamers were assayed on the microarray for APC binding and ranked according to binding score. The top four aptamers were then subjected to point mutations and insertion–deletion events to give rise to a new 5500 test pool for synthesis onto a DNA microarray and use in the next round of selection. Nine rounds of CLADE were performed and the resulting aptamers characterized and phylogenetically analyzed. The CLADE strategy was successful with the tightest binding aptamer had a SPR determined $K_D$ value of around 2 nM [115]. Although high-affinity aptamers were isolated, the cost of nine microarrays would be much greater than the cost of an average SELEX experiment.

Expanding upon this work, Rowe et al. used the CLADE approach and tested the three diversification systems: mutation, recombination, and statistical binding prediction [116]. Over five CLADE selection rounds, aptamers were evolved to bind to glucose-6-phosphate dehydrogenase. The tightest binding aptamer was isolated using the recombination diversification system and had a $K_D$ of 245 nM.

In 2012, Nonaka et al. used an in silico system to improve the affinity of the VEap121 aptamer against VEGF [117]. Interestingly, this study did not use DNA microarrays but instead used SPR to assay every individual aptamer. Three rounds of improvement were performed. Each round consisted of adaptation, SPR determination of $K_D$ value, and selection of the five tightest binding aptamers to seed the next round. For the first generation, 10 mutants of VEap121 were generated, each with several mutations, where the guanine bases were conserved to retain the G-quadruplex structure. For the second generation, the five tightest binding aptamers from G1 as determined by SPR were replicated relative to their binding affinity to yield 20 sequences. These were then randomly paired to undergo single-point crossover and two single-base mutations, randomly introduced. For the third generation, the five tightest binding aptamers from both G1 and G2 as determined by SPR were crossed with VEap121 at a random point and two single-point mutations were randomly introduced. This process was repeated three times in order to produce the third generation of 20 sequences. This process produced four aptamers with a tighter binding ($K_D$ = 0.3, 1.5, 1.7 and 2.4 nM) than the original VEap121 aptamer ($K_D$ = 4.7 nM) [117].

In 2016 Kinghorn et al. reported a novel strategy of aptamer affinity maturation by library resampling from SELEX sequence data [118]. This approach relies on the principle that classical SELEX is unlikely to select the best possible aptamer, but is highly likely to select family members of the best possible aptamer. The sequence of the best possible aptamer is hidden within the sequences of its family members. To make use of this aptamer family information, the authors coded the bioinformatic software "Resample", which uses information from a SELEX experiment in terms of an aptamer family motif and any available folding information. This information is used to generate a novel library that consists of every possible aptamer permutation within the aptamer family. This library is focused on a particular area of sequence space, representing it thoroughly while still having a library size small enough to fit onto a DNA microarray for screening (Figure 6). To demonstrate this process, the sequence data from a previous selection against the malarial antigen *Plasmodium falciparum* lactate dehydrogenase (PfLDH) was input into Resample to generate a library of 186,624 novel aptamer sequences within the specified aptamer family. This library was ordered on a DNA microarray that was incubated with 50 nM Alexa Fluor 555 labeled PfLDH (target) and 1 μM Alexa Fluor 647 labeled human lactate dehydrogenase B (counter-target) and washed and scanned to measure both binding affinity and binding specificity for all aptamers. The lead candidates were further characterized

using microscale thermophoresis to show an order of magnitude improvement in binding affinity $K_D$ value. The authors provide Resample as a hosted web service (website available: http://resample.azurewebsites.net) and state that affinity maturation using Resample round should just take two days, excluding microarray shipping time. While many microarray aptamer optimization processes use mutation and recombination, taking many small evolutionary steps to arrive at an optimum, Resample takes all possible selection sequence information and takes a single evolutionary leap to an optimum. In this way, a single Resample diversification round can be used to hone in on the sequence space containing the best possible aptamer sequence [118].

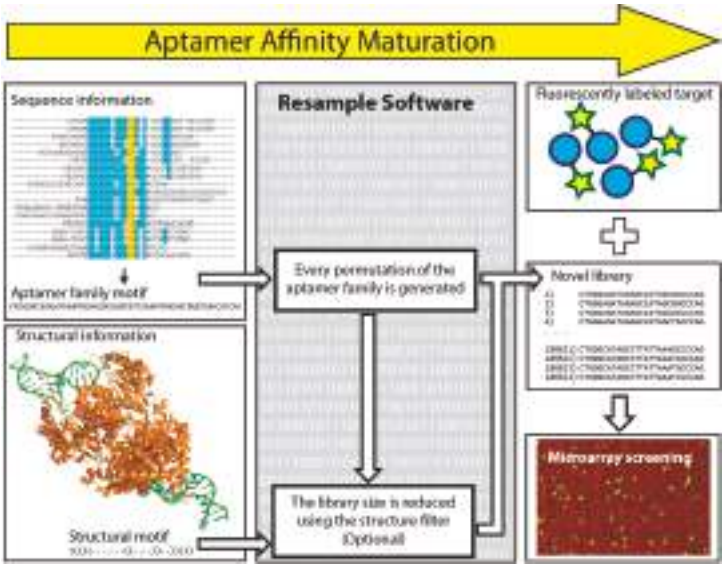


**Figure 6.** The aptamer affinity maturation process. The yellow arrow designates the aptamer affinity maturation process, in which data from a SELEX experiment is utilized by bioinformatic software to Create a novel aptamer library which undergoes a microarray screening process. Sequence information and, if available, folding information (optional) from a SELEX experiment is used as input for the resample software. Resample outputs a novel focused aptamer library that is small enough to fit on a DNA microarray. The microarray is incubated with a fluorescently labeled target before washing and scanning to measure the binding strength of all aptamers. Figure adapted from Kinghorn et al. [118].

## 7. Conclusions and Future Perspectives

Simulation of aptamer selection has given insight into the SELEX process, including the optimum protein/target concentration, the detrimental effect of low relative partitioning efficiency, the effect of background binding, and the stochastic nature of SELEX. The area least accurately modeled in SELEX simulations is aptamer binding. Development of more accurate aptamer binding models and applying them in simulation may lead to new insights into SELEX.

In silico approaches have been used to classify molecular interactions between binding macromolecules into discrete categories. Each categorized interaction is assigned a probability and level of importance, which is translated into a score. By grouping all the scores, it is possible to distinguish a poor binding interaction from a strong interaction. Most programs have been developed for protein–protein interactions, but in recent years useful software has been devised to investigate DNA–target interactions. These in silico tools for both whole aptamer and fragment approaches have aided aptamer scientists in improving their selections and identifying novel high-affinity aptamers.

It is commonly known that the huge number of candidates in a random nucleic acid library cannot be covered by a single SELEX experiment. One of the solutions to reduce that number or increase the coverage of selection is to introduce patterns into the library. In silico methods include defining alternating purine and pyrimidine patterns leading to the increase in occurrence of stem–loop structures or more complicated structures such as quadruplexes. The design could also be combined with in vitro experiments to access the structural diversity of certain patterned libraries by CD and NMR. Such approaches will effectively help to increase the success rate of identifying active binders in the selection process.

HTS technology shows high potential to replace the cloning and Sanger sequencing methods applied in traditional SELEX. By integrating an HTS step into SELEX, researchers can successfully reduce the selection rounds and the need for post-selection experiments to identify optimal aptamer sequences. These advantages of HTS technology encourage the rapid development of aptamer-based bioinformatic tools. There are several software packages and databases customized for aptamer scientists (Table 2) to analyze the large amount of HTS data based on different strategies. It will be useful to consider how best to compare these tools, using the same batch of data with multiple validations from different research groups.

In silico aptamer optimization has not been widely adopted. This may be due to the observation that most studies either achieve only mild affinity improvements or that the optimization method, while successful, is prohibitively expensive. Nonaka et al. achieved binding improvement of an order of magnitude by using a low-cost method, albeit labor-intensive in SPR measurements [117]. Kinghorn et al. achieved binding improvement of an order of magnitude with a low-cost method that can be performed in two days, excluding microarray shipping time [118]. Many aptamer optimization studies are stand-alones without follow-up or verification by other research groups. For the aptamer community to adopt in silico aptamer optimization, replicate studies need to be performed to strengthen and further validate in silico aptamer optimization methods.

Bioinformatic approaches have been used to improve both aptamers and their selection. In this review we have outlined a broad range of aptamer bioinformatics techniques including simulation of aptamer selection, aptamer selection by molecular dynamics, patterning of libraries, identification of lead aptamers from HTS data, and in silico aptamer optimization. Aptamers are particularly suited to bioinformatic techniques and their development and use can benefit aptamer scientific community.

**Acknowledgments:** This work was supported in part by the Hong Kong General Research Fund under grants 17127515 and 17163416 to JAT.

**Author Contributions:** Andrew B. Kinghorn wrote Section 2. Simulation of Aptamer Selection and Section 6. In Silico Aptamer Optimization as well as manuscript editing. Lewis A. Fraser wrote Section 3. Aptamer Selection by Molecular Dynamics as well as manuscript editing. Shaolin Liang wrote Section 5. In Silico Aptamer Identification from High-Throughput Sequencing (HTS) Data as well as manuscript editing. Simon Chi-Chin Shiu wrote Section 4. Patterning of libraries as well as manuscript editing. Julian A. Tanner edited and directed writing of the manuscript.

**Conflicts of Interest:** The authors declare no conflict of interest.

## References

1. Ellington, A.D.; Szostak, J.W. In vitro selection of RNA molecules that bind specific ligands. *Nature* **1990**, *346*, 818–822. [CrossRef] [PubMed]
2. Tuerk, C.; Gold, L. Systematic evolution of ligands by exponential enrichment: RNA ligands to bacteriophage T4 DNA polymerase. *Science* **1990**, *249*, 505–510. [CrossRef] [PubMed]
3. Cruz-Toledo, J.; McKeague, M.; Zhang, X.; Giamberardino, A.; McConnell, E.; Francis, T.; DeRosa, M.C.; Dumontier, M. Aptamer base: A collaborative knowledge base to describe aptamers and SELEX experiments. *Database* **2012**. [CrossRef] [PubMed]
4. McKeague, M.; McConnell, E.M.; Cruz-Toledo, J.; Bernard, E.D.; Pach, A.; Mastronardi, E.; Zhang, X.; Beking, M.; Francis, T.; Giamberardino, A. Analysis of in vitro aptamer selection parameters. *J. Mol. Evol.* **2015**, *81*, 150–161. [CrossRef] [PubMed]

5. Cheung, Y.-W.; Kwok, J.; Law, A.W.; Watt, R.M.; Kotaka, M.; Tanner, J.A. Structural basis for discriminatory recognition of Plasmodium lactate dehydrogenase by a DNA aptamer. *Proc. Natl. Acad. Sci. USA* **2013**, *110*, 15967–15972. [CrossRef] [PubMed]
6. Irvine, D.; Tuerk, C.; Gold, L. SELEXION: Systematic evolution of ligands by exponential enrichment with integrated optimization by non-linear analysis. *J. Mol. Biol.* **1991**, *222*, 739–761. [CrossRef]
7. Vant-Hull, B.; Payano-Baez, A.; Davis, R.H.; Gold, L. The mathematics of SELEX against complex targets. *J. Mol. Biol.* **1998**, *278*, 579–597. [CrossRef] [PubMed]
8. Homann, M.; Göringer, H.U. Combinatorial selection of high affinity RNA ligands to live African trypanosomes. *Nucleic Acids Res.* **1999**, *27*, 2006–2014. [CrossRef] [PubMed]
9. Coulter, L.R.; Landree, M.A.; Cooper, T.A. Identification of a new class of exonic splicing enhancers by in vivo selection. *Mol. Cell. Biol.* **1997**, *17*, 2143–2150. [CrossRef] [PubMed]
10. Chen, C.-K.; Kuo, T.-L.; Chan, P.-C.; Lin, L.-Y. Subtractive SELEX against two heterogeneous target samples: Numerical simulations and analysis. *Comput. Biol. Med.* **2007**, *37*, 750–759. [CrossRef] [PubMed]
11. Chen, C.-K. Complex SELEX against target mixture: Stochastic computer model, simulation, and analysis. *Comput. Meth. Prog. Biol.* **2007**, *87*, 189–200. [CrossRef] [PubMed]
12. Wang, J.; Rudzinski, J.F.; Gong, Q.; Soh, H.T.; Atzberger, P.J. Influence of target concentration and background binding on in vitro selection of affinity reagents. *PLoS ONE* **2012**, *7*, e43940. [CrossRef] [PubMed]
13. Vant-Hull, B.; Gold, L.; Zichi, D.A. Theoretical principles of in vitro selection using combinatorial nucleic acid libraries. *Curr. Protoc. Nucleic Acid Chem.* **2000**. [CrossRef]
14. Zhao, Y.; Granas, D.; Stormo, G.D. Inferring binding energies from selected binding sites. *PLoS Comput. Biol.* **2009**, *5*, e1000590. [CrossRef] [PubMed]
15. Spill, F.; Weinstein, Z.B.; Shemirani, A.I.; Ho, N.; Desai, D.; Zaman, M.H. Controlling uncertainty in aptamer selection. *Proc. Natl. Acad. Sci. USA* **2016**. [CrossRef] [PubMed]
16. Hoinka, J.; Berezhnoy, A.; Dao, P.; Sauna, Z.E.; Gilboa, E.; Przytycka, T.M. Large scale analysis of the mutational landscape in HT-SELEX improves aptamer discovery. *Nucleic Acids Res.* **2015**, *43*, 5699–5707. [CrossRef] [PubMed]
17. Oh, I.S.; Lee, Y.-G.; McKay, R. Simulating chemical evolution. In Proceedings of the IEEE Congress on Evolutionary Computation, New Orleans, LA, USA, 5–8 July 2011; pp. 2717–2724. [CrossRef]
18. Kauffman, S.; Levin, S. Towards a general theory of adaptive walks on rugged landscapes. *J. Theor. Biol.* **1987**, *128*, 11–45. [CrossRef]
19. Wedge, D.C.; Rowe, W.; Kell, D.B.; Knowles, J. In silico modelling of directed evolution: Implications for experimental design and stepwise evolution. *J. Theor. Biol.* **2009**, *257*, 131–141. [CrossRef] [PubMed]
20. Deem, M.W.; Lee, H.Y. Sequence space localization in the immune system response to vaccination and disease. *Phys. Rev. Lett.* **2003**, *91*, 068101. [CrossRef] [PubMed]
21. Hall, M.; Christensen, K.; di Collobiano, S.A.; Jensen, H.J. Time-dependent extinction rate and species abundance in a tangled-nature model of biological evolution. *Phys. Rev. E* **2002**, *66*, 011904. [CrossRef] [PubMed]
22. Kauffman, S.; Macready, W. Technological evolution and adaptive organizations: Ideas from biology may find applications in economics. *Complexity* **1995**, *1*, 26–43. [CrossRef]
23. Klussmann, S. Functional oligonucleotides and their applications. In *The Aptamer Handbook*; John Wiley & Sons: New York, NY, USA, 2006.
24. Kauffman, S.A. *The Origins of Order: Self Organization and Selection in Evolution*; Oxford University Press: Oxford, UK, 1992; pp. 61–100.
25. Altenberg, L. Evolving better representations through selective genome growth. In Proceedings of the First IEEE Conference on IEEE World Congress on Computational Intelligence, Evolutionary Computation, Orlando, FL, USA, 27–29 June 1994; pp. 182–187.
26. Kinghorn, A.B.; Tanner, J.A. Selective Phenome Growth Adapted Model: A Novel Landscape to Represent Aptamer Ligand Binding. *Complexity* **2017**, *2017*, 1–12. [CrossRef]
27. Wolpert, D.H.; Macready, W.G. No free lunch theorems for optimization. *IEEE Trans. Evolut. Comput.* **1997**, *1*, 67–82. [CrossRef]
28. MacKerell, A.D.; Bashford, D.; Bellott, M.; Dunbrack, R.L., Jr.; Evanseck, J.D.; Field, M.J.; Fischer, S.; Gao, J.; Guo, H.; Ha, S. All-atom empirical potential for molecular modeling and dynamics studies of proteins. *J. Phys. Chem. B* **1998**, *102*, 3586–3616. [CrossRef] [PubMed]

29. Durrant, J.D.; McCammon, J.A. Molecular dynamics simulations and drug discovery. *BMC Biol.* **2011**, *9*, 71.
30. MacKerell, A.D.; Nilsson, L. Molecular dynamics simulations of nucleic acid–protein complexes. *Curr. Opin. Struct. Biol.* **2008**, *18*, 194–199. [CrossRef]
31. Gurtovenko, A.A.; Vattulainen, I. Pore formation coupled to ion transport through lipid membranes as induced by transmembrane ionic charge imbalance: Atomistic molecular dynamics study. *J. Am. Chem. Soc.* **2005**, *127*, 17570–17571. [CrossRef] [PubMed]
32. Carothers, J.M.; Oestreich, S.C.; Szostak, J.W. Aptamers selected for higher-affinity binding are not more specific for the target ligand. *J. Am. Chem. Soc.* **2006**, *128*, 7929–7937. [CrossRef] [PubMed]
33. Gevertz, J.; Gan, H.H.; Schlick, T. In vitro RNA random pools are not structurally diverse: A computational analysis. *RNA* **2005**, *11*, 853–863. [CrossRef]
34. Chushak, Y.; Stone, M.O. In silico selection of RNA aptamers. *Nucleic Acids Res.* **2009**, *37*, e87. [CrossRef] [PubMed]
35. Hua, W.P.; Linb, H.T.; Tsaia, J.J.; Chenc, W.Y. Investigating interactions between proteins and nucleic acids by computational approaches. In *Computational Methods with Applications in Bioinformatics Analysis*; World Scientific: Singapore, 2017; p. 98.
36. Arnold, K.; Bordoli, L.; Kopp, J.; Schwede, T. The SWISS-MODEL workspace: A web-based environment for protein structure homology modelling. *Bioinformatics* **2006**, *22*, 195–201. [CrossRef] [PubMed]
37. Kelley, L.A.; Mezulis, S.; Yates, C.M.; Wass, M.N.; Sternberg, M.J. The Phyre2 web portal for protein modeling, prediction and analysis. *Nat. Protoc.* **2015**, *10*, 845–858. [CrossRef] [PubMed]
38. Van Dijk, M.; Bonvin, A.M. 3D-DART: A DNA structure modelling server. *Nucleic Acids Res.* **2009**, *37*, W235–W239. [CrossRef] [PubMed]
39. Popenda, M.; Szachniuk, M.; Antczak, M.; Purzycka, K.J.; Lukasiak, P.; Bartol, N.; Blazewicz, J.; Adamiak, R.W. Automated 3D structure composition for large RNAs. *Nucleic Acids Res.* **2012**, *40*, e112. [CrossRef] [PubMed]
40. Setny, P.; Bahadur, R.P.; Zacharias, M. Protein-DNA docking with a coarse-grained force field. *BMC Bioinform.* **2012**, *13*, 228. [CrossRef] [PubMed]
41. Das, R.; Baker, D. Automated de novo prediction of native-like RNA tertiary structures. *Proc. Natl. Acad. Sci. USA* **2007**, *104*, 14664–14669. [CrossRef] [PubMed]
42. Tsui, V.; Case, D.A. Theory and applications of the generalized Born solvation model in macromolecular simulations. *Biopolymers* **2000**, *56*, 275–291. [CrossRef]
43. Zhang, S.; Kumar, K.; Jiang, X.; Wallqvist, A.; Reifman, J. DOVIS: An implementation for high-throughput virtual screening using AutoDock. *BMC Bioinform.* **2008**, *9*, 126. [CrossRef] [PubMed]
44. Chen, R.; Li, L.; Weng, Z. ZDOCK: An initial-stage protein-docking algorithm. *Proteins* **2003**, *52*, 80–87. [CrossRef] [PubMed]
45. Kumar, J.V.; Chen, W.-Y.; Tsai, J.J.; Hu, W.-P. Molecular simulation methods for selecting thrombin-binding aptamers. In *Information Technology Convergence*; Springer: Dordrecht, The Netherlands, 2013; Volume 253, pp. 743–749.
46. White, R.R.; Shan, S.; Rusconi, C.P.; Shetty, G.; Dewhirst, M.W.; Kontos, C.D.; Sullenger, B.A. Inhibition of rat corneal angiogenesis by a nuclease-resistant RNA aptamer specific for angiopoietin-2. *Proc. Natl. Acad. Sci. USA* **2003**, *100*, 5028–5033. [CrossRef] [PubMed]
47. Sarraf-Yazdi, S.; Mi, J.; Moeller, B.J.; Niu, X.; White, R.R.; Kontos, C.D.; Sullenger, B.A.; Dewhirst, M.W.; Clary, B.M. Inhibition of in vivo tumor angiogenesis and growth via systemic delivery of an angiopoietin 2-specific RNA aptamer. *J. Surg. Res.* **2008**, *146*, 16–23. [CrossRef] [PubMed]
48. Hu, W.-P.; Kumar, J.V.; Huang, C.-J.; Chen, W.-Y. Computational selection of RNA aptamer against angiopoietin-2 and experimental evaluation. *BioMed Res. Int.* **2015**, *2015*, 658712. [CrossRef] [PubMed]
49. Maisonpierre, P.C.; Suri, C.; Jones, P.F.; Bartunkova, S.; Wiegand, S.J.; Radziejewski, C.; Compton, D.; McClain, J.; Aldrich, T.H.; Papadopoulos, N. Angiopoietin-2, a natural antagonist for Tie2 that disrupts in vivo angiogenesis. *Science* **1997**, *277*, 55–60. [CrossRef] [PubMed]
50. Holash, J.; Maisonpierre, P.; Compton, D.; Boland, P.; Alexander, C.; Zagzag, D.; Yancopoulos, G.; Wiegand, S. Vessel cooption, regression, and growth in tumors mediated by angiopoietins and VEGF. *Science* **1999**, *284*, 1994–1998. [CrossRef] [PubMed]
51. Lin, H.; Zhang, W.; Jia, S.; Guan, Z.; Yang, C.J.; Zhu, Z. Microfluidic approaches to rapid and efficient aptamer selection. *Biomicrofluid* **2014**, *8*, 041501. [CrossRef] [PubMed]

52. Shangguan, D.; Bing, T.; Zhang, N. *Cell-SELEX: Aptamer selection against whole cells, in Aptamers Selected by Cell-SELEX for Theranostics*; Springer: Heidelberg, Germany, 2015; pp. 13–33.
53. Mallikaratchy, P. Evolution of Complex Target SELEX to Identify Aptamers against Mammalian Cell-Surface Antigens. *Molecules* **2017**, *22*, 215. [CrossRef] [PubMed]
54. Rabal, O.; Pastor, F.; Villanueva, H.; Soldevilla, M.M.; Hervas-Stubbs, S.; Oyarzabal, J. In Silico Aptamer Docking Studies: From a Retrospective Validation to a Prospective Case Study'TIM3 Aptamers Binding. *Mol. Ther. Nucleic Acids* **2016**, *5*, e376. [CrossRef] [PubMed]
55. Huang, Y.; Liu, S.; Guo, D.; Li, L.; Xiao, Y. A novel protocol for three-dimensional structure prediction of RNA-protein complexes. *Sci. Rep.* **2013**, *3*, 1887. [CrossRef] [PubMed]
56. Berendsen, H.J.; van der Spoel, D.; van Drunen, R. GROMACS: A message-passing parallel molecular dynamics implementation. *Comput. Phys. Commun.* **1995**, *91*, 43–56. [CrossRef]
57. Tseng, C.Y.; Ashrafuzzaman, M.; Mane, J.Y.; Kapty, J.; Mercer, J.R.; Tuszynski, J.A. Entropic Fragment-Based Approach to Aptamer Design. *Chem. Biol. Drug Des.* **2011**, *78*, 1–13. [CrossRef] [PubMed]
58. Ashrafuzzaman, M.; Tseng, C.-Y.; Kapty, J.; Mercer, J.R.; Tuszynski, J.A. A computationally designed DNA aptamer template with specific binding to phosphatidylserine. *Nucleic Acid Ther.* **2013**, *23*, 418–426. [CrossRef]
59. Carothers, J.M.; Oestreich, S.C.; Davis, J.H.; Szostak, J.W. Informational complexity and functional activity of RNA structures. *J. Am. Chem. Soc.* **2004**, *126*, 5130–5137. [CrossRef] [PubMed]
60. Davis, J.H.; Szostak, J.W. Isolation of high-affinity GTP aptamers from partially structured RNA libraries. *Proc. Natl. Acad. Sci. USA* **2002**, *99*, 11616–11621. [CrossRef] [PubMed]
61. Schultes, E.; Hraber, P.T.; LaBean, T.H. Global similarities in nucleotide base composition among disparate functional classes of single-stranded RNA imply adaptive evolutionary convergence. *RNA* **1997**, *3*, 792–806. [PubMed]
62. Knight, R.; De Sterck, H.; Markel, R.; Smit, S.; Oshmyansky, A.; Yarus, M. Abundance of correctly folded RNA motifs in sequence space, calculated on computational grids. *Nucleic Acids Res.* **2005**, *33*, 5924–5935. [CrossRef] [PubMed]
63. Ruff, K.M.; Snyder, T.M.; Liu, D.R. Enhanced functional potential of nucleic acid aptamer libraries patterned to increase secondary structure. *J. Am. Chem. Soc.* **2010**, *132*, 9453–9464. [CrossRef] [PubMed]
64. Martin, J.A.; Mirau, P.A.; Chushak, Y.; Chavez, J.L.; Naik, R.R.; Hagen, J.A.; Kelley-Loughnane, N. Single-Round Patterned DNA Library Microarray Aptamer Lead Identification. *J. Anal. Methods Chem.* **2015**, *2015*, 137489. [CrossRef] [PubMed]
65. Hoogsteen, K. The crystal and molecular structure of a hydrogen-bonded complex between 1-methylthymine and 9-methyladenine. *Acta Crystallogr.* **1963**, *16*, 907–916. [CrossRef]
66. Frank-Kamenetskii, M.D.; Mirkin, S.M. Triplex DNA structures. *Annu. Rev. Biochem.* **1995**, *64*, 65–95. [CrossRef] [PubMed]
67. De Nicola, B.; Lech, C.J.; Heddi, B.; Regmi, S.; Frasson, I.; Perrone, R.; Richter, S.N.; Phan, A.T. Structure and possible function of a G-quadruplex in the long terminal repeat of the proviral HIV-1 genome. *Nucleic Acids Res.* **2016**, *44*, 6442–6451. [CrossRef] [PubMed]
68. Corey, D.R. Telomeres and telomerase: From discovery to clinical trials. *Chem. Biol.* **2009**, *16*, 1219–1223. [CrossRef] [PubMed]
69. Bourdoncle, A.; Estévez Torres, A.; Gosse, C.; Lacroix, L.; Vekhoff, P.; Le Saux, T.; Jullien, L.; Mergny, J.L. Quadruplex-Based Molecular Beacons as Tunable DNA Probes. *J. Am. Chem. Soc.* **2006**, *128*, 11094–11105. [CrossRef] [PubMed]
70. Zhu, J.; Zhang, L.; Li, T.; Dong, S.; Wang, E. Enzyme-free unlabeled DNA logic circuits based on toehold-mediated strand displacement and split G-quadruplex enhanced fluorescence. *Adv. Mater.* **2013**, *25*, 2440–2444. [CrossRef] [PubMed]
71. Webba da Silva, M. Geometric formalism for DNA quadruplex folding. *Chemistry* **2007**, *13*, 9738–9745. [CrossRef] [PubMed]
72. Bates, P.J.; Kahlon, J.B.; Thomas, S.D.; Trent, J.O.; Miller, D.M. Antiproliferative activity of G-rich oligonucleotides correlates with protein binding. *J. Biol. Chem.* **1999**, *274*, 26369–26377. [CrossRef] [PubMed]
73. Travascio, P.; Li, Y.; Sen, D. DNA-enhanced peroxidase activity of a DNA-aptamer-hemin complex. *Chem. Biol.* **1998**, *5*, 505–517. [CrossRef]

74. Sen, D.; Poon, L.C. RNA and DNA complexes with hemin [Fe(III) heme] are efficient peroxidases and peroxygenases: How do they do it and what does it mean? *Crit. Rev. Biochem. Mol. Biol.* **2011**, *46*, 478–492. [CrossRef] [PubMed]
75. Baugh, C.; Grate, D.; Wilson, C. 2.8 Å crystal structure of the malachite green aptamer11Edited by J. A. Doudna. *J. Mol. Biol.* **2000**, *301*, 117–128. [CrossRef] [PubMed]
76. Warner, K.D.; Chen, M.C.; Song, W.; Strack, R.L.; Thorn, A.; Jaffrey, S.R.; Ferre-D'Amare, A.R. Structural basis for activity of highly efficient RNA mimics of green fluorescent protein. *Nat. Struct. Mol. Biol.* **2014**, *21*, 658–663. [CrossRef] [PubMed]
77. Trachman, R.J., 3rd; Demeshkina, N.A.; Lau, M.W.L.; Panchapakesan, S.S.S.; Jeng, S.C.Y.; Unrau, P.J.; Ferre-D'Amare, A.R. Structural basis for high-affinity fluorophore binding and activation by RNA Mango. *Nat. Chem. Biol.* **2017**, *13*, 807–813. [CrossRef] [PubMed]
78. McManus, S.A.; Li, Y. Assessing the amount of quadruplex structures present within G(2)-tract synthetic random-sequence DNA libraries. *PLoS ONE* **2013**, *8*, e64131. [CrossRef] [PubMed]
79. Goodwin, S.; McPherson, J.D.; McCombie, W.R. Coming of age: Ten years of next-generation sequencing technologies. *Nat. Rev. Genet.* **2016**, *17*, 333–351. [CrossRef] [PubMed]
80. Marian, A.J. Sequencing your genome: What does it mean? *Methodist Debakey Cardiovasc. J.* **2014**, *10*, 3–6. [CrossRef] [PubMed]
81. Blind, M.; Blank, M. Aptamer selection technology and recent advances. *Mol. Ther. Nucleic Acids* **2015**, *4*, e223. [CrossRef] [PubMed]
82. Berezhnoy, A.; Stewart, C.A.; McNamara, J.O.; Thiel, W.; Giangrande, P.; Trinchieri, G.; Gilboa, E. Isolation and optimization of murine IL-10 receptor blocking oligonucleotide aptamers using high-throughput sequencing. *Mol. Ther.* **2012**, *20*, 1242–1250. [CrossRef] [PubMed]
83. Thiel, W.H.; Bair, T.; Peek, A.S.; Liu, X.; Dassie, J.; Stockdale, K.R.; Behlke, M.A.; Miller, F.J., Jr.; Giangrande, P.H. Rapid identification of cell-specific, internalizing RNA aptamers with bioinformatics analyses of a cell-based aptamer selection. *PLoS ONE* **2012**, *7*, e43836. [CrossRef] [PubMed]
84. Valenzano, S.; De Girolamo, A.; DeRosa, M.C.; McKeague, M.; Schena, R.; Catucci, L.; Pascale, M. Screening and Identification of DNA Aptamers to Tyramine Using in Vitro Selection and High-Throughput Sequencing. *ACS Comb. Sci.* **2016**, *18*, 302–313. [CrossRef] [PubMed]
85. Takahashi, M.; Wu, X.; Ho, M.; Chomchan, P.; Rossi, J.J.; Burnett, J.C.; Zhou, J. High throughput sequencing analysis of RNA libraries reveals the influences of initial library and PCR methods on SELEX efficiency. *Sci. Rep.* **2016**, *6*, 33697. [CrossRef] [PubMed]
86. Dupont, D.M.; Larsen, N.; Jensen, J.K.; Andreasen, P.A.; Kjems, J. Characterisation of aptamer-target interactions by branched selection and high-throughput sequencing of SELEX pools. *Nucleic Acids Res.* **2015**, *43*, e139. [CrossRef] [PubMed]
87. Zimmermann, B.; Gesell, T.; Chen, D.; Lorenz, C.; Schroeder, R. Monitoring genomic sequences during SELEX using high-throughput sequencing: Neutral SELEX. *PLoS ONE* **2010**, *5*, e9169. [CrossRef] [PubMed]
88. Lorenz, C.; Gesell, T.; Zimmermann, B.; Schoeberl, U.; Bilusic, I.; Rajkowitsch, L.; Waldsich, C.; von Haeseler, A.; Schroeder, R. Genomic SELEX for Hfq-binding RNAs identifies genomic aptamers predominantly in antisense transcripts. *Nucleic Acids Res.* **2010**, *38*, 3794–3808. [CrossRef] [PubMed]
89. Cho, M.; Xiao, Y.; Nie, J.; Stewart, R.; Csordas, A.T.; Oh, S.S.; Thomson, J.A.; Soh, H.T. Quantitative selection of DNA aptamers through microfluidic selection and high-throughput sequencing. *Proc. Natl. Acad. Sci. USA* **2010**, *107*, 15373–15378. [CrossRef] [PubMed]
90. Schütze, T.; Wilhelm, B.; Greiner, N.; Braun, H.; Peter, F.; Mörl, M.; Erdmann, V.A.; Lehrach, H.; Konthur, Z.; Menger, M. Probing the SELEX process with next-generation sequencing. *PLoS ONE* **2011**, *6*, e29604.
91. Spiga, F.M.; Maietta, P.; Guiducci, C. More DNA-Aptamers for Small Drugs: A Capture-SELEX Coupled with Surface Plasmon Resonance and High-Throughput Sequencing. *ACS Comb. Sci.* **2015**, *17*, 326–333. [CrossRef] [PubMed]
92. Gotrik, M.R.; Feagin, T.A.; Csordas, A.T.; Nakamoto, M.A.; Soh, H.T. Advancements in Aptamer Discovery Technologies. *Acc. Chem. Res.* **2016**, *49*, 1903–1910. [CrossRef] [PubMed]
93. Ditzler, M.A.; Lange, M.J.; Bose, D.; Bottoms, C.A.; Virkler, K.F.; Sawyer, A.W.; Whatley, A.S.; Spollen, W.; Givan, S.A.; Burke, D.H. High-throughput sequence analysis reveals structural diversity and improved potency among RNA inhibitors of HIV reverse transcriptase. *Nucleic Acids Res.* **2013**, *41*, 1873–1884. [CrossRef] [PubMed]

94. Scoville, D.J.; Uhm, T.K.; Shallcross, J.A.; Whelan, R.J. Selection of DNA Aptamers for Ovarian Cancer Biomarker CA125 Using One-Pot SELEX and High-Throughput Sequencing. *J. Nucleic Acids* **2017**, *2017*, 9879135. [CrossRef] [PubMed]
95. Hoon, S.; Zhou, B.; Janda, K.D.; Brenner, S.; Scolnick, J. Aptamer selection by high-throughput sequencing and informatic analysis. *Biotechniques* **2011**, *51*, 413–416. [CrossRef] [PubMed]
96. Kurtz, S.; Narechania, A.; Stein, J.C.; Ware, D. A new method to compute K-mer frequencies and its application to annotate large repetitive plant genomes. *BMC Genom.* **2008**, *9*, 517. [CrossRef] [PubMed]
97. Weese, D.; Emde, A.K.; Rausch, T.; Doring, A.; Reinert, K. RazerS–fast read mapping with sensitivity control. *Genome Res.* **2009**, *19*, 1646–1654. [CrossRef] [PubMed]
98. Jing, M.; Bowser, M.T. Tracking the emergence of high affinity aptamers for rhVEGF165 during capillary electrophoresis-systematic evolution of ligands by exponential enrichment using high throughput sequencing. *Anal. Chem.* **2013**, *85*, 10761–10770. [CrossRef] [PubMed]
99. Thiel, W.H.; Giangrande, P.H. Analyzing HT-SELEX data with the Galaxy Project tools—A web based bioinformatics platform for biomedical research. *Methods* **2016**, *97*, 3–10. [CrossRef] [PubMed]
100. Thiel, W.H. Galaxy Workflows for Web-based Bioinformatics Analysis of Aptamer High-throughput Sequencing Data. *Mol. Ther. Nucleic Acids* **2016**, *5*, e345. [CrossRef] [PubMed]
101. Alam, K.K.; Chang, J.L.; Burke, D.H. FASTAptamer: A Bioinformatic Toolkit for High-throughput Sequence Analysis of Combinatorial Selections. *Mol. Ther. Nucleic Acids.* **2015**, *4*, e230. [CrossRef] [PubMed]
102. Ducongé, F. Improvement of aptamers using PATTERNITY-seq (high-throughput analysis of sequence patterns and paternity relationship between them). In Proceedings of the the Aptamer Bordeaux Conference, Bordeaux, France, 24–25 June 2016.
103. Nguyen Quang, N.; Perret, G.; Duconge, F. Applications of High-Throughput Sequencing for In Vitro Selection and Characterization of Aptamers. *Pharmaceuticals* **2016**, *9*, 76. [CrossRef] [PubMed]
104. Hoinka, J.; Berezhnoy, A.; Sauna, Z.E.; Gilboa, E.; Przytycka, T.M. AptaCluster—A Method to Cluster HT-SELEX Aptamer Pools and Lessons from its Application. *Res. Comput. Mol. Biol.* **2014**, *8394*, 115–128. [PubMed]
105. Hoinka, J.; Dao, P.; Przytycka, T.M. AptaGUI-A Graphical User Interface for the Efficient Analysis of HT-SELEX Data. *Mol. Ther. Nucleic Acids.* **2015**, *4*, e257. [CrossRef] [PubMed]
106. Zuker, M. Mfold web server for nucleic acid folding and hybridization prediction. *Nucleic Acids Res.* **2003**, *31*, 3406–3415. [CrossRef] [PubMed]
107. Dao, P.; Hoinka, J.; Takahashi, M.; Zhou, J.; Ho, M.; Wang, Y.; Costa, F.; Rossi, J.J.; Backofen, R.; Burnett, J. AptaTRACE Elucidates RNA Sequence-Structure Motifs from Selection Trends in HT-SELEX Experiments. *Cell Syst.* **2016**, *3*, 62–70. [CrossRef] [PubMed]
108. Ding, Y.; Chan, C.Y.; Lawrence, C.E. S fold web server for statistical folding and rational design of nucleic acids. *Nucleic Acids Res.* **2004**, *32*, W135–W141. [CrossRef] [PubMed]
109. Chan, C.Y.; Lawrence, C.E.; Ding, Y. Structure clustering features on the S fold Web server. *Bioinformatics* **2005**, *21*, 3926–3928. [CrossRef] [PubMed]
110. Hofacker, I.L. RNA secondary structure analysis using the Vienna RNA package. In *Current Protoc Bioinformatics*; John Wiley & Sons, Inc.: Hoboken, NJ, USA, 2009.
111. Wang, J.; Gong, Q.; Maheshwari, N.; Eisenstein, M.; Arcila, M.L.; Kosik, K.S.; Soh, H.T. Particle Display: A Quantitative Screening Method for Generating High-Affinity Aptamers. *Angew. Chem. Int. Ed.* **2014**, *53*, 4796–4801. [CrossRef] [PubMed]
112. Bowser, M.T. SELEX: Just another separation? *Analyst* **2005**, *130*, 128–130. [CrossRef] [PubMed]
113. Katilius, E.; Flores, C.; Woodbury, N.W. Exploring the sequence space of a DNA aptamer using microarrays. *Nucleic Acids Res.* **2007**, *35*, 7626–7635. [CrossRef] [PubMed]
114. Platt, M.; Rowe, W.; Knowles, J.; Day, P.J.; Kell, D.B. Analysis of aptamer sequence activity relationships. *Integr. Biol.* **2009**, *1*, 116–122. [CrossRef] [PubMed]
115. Knight, C.G.; Platt, M.; Rowe, W.; Wedge, D.C.; Khan, F.; Day, P.J.; McShea, A.; Knowles, J.; Kell, D.B. Array-based evolution of DNA aptamers allows modelling of an explicit sequence-fitness landscape. *Nucleic Acids Res.* **2009**, *37*, e6. [CrossRef] [PubMed]
116. Rowe, W.; Platt, M.; Wedge, D.C.; Day, P.J.; Kell, D.B.; Knowles, J. Convergent evolution to an aptamer observed in small populations on DNA microarrays. *Phys. Biol.* **2010**, *7*, 036007. [CrossRef] [PubMed]

117. Nonaka, Y.; Yoshida, W.; Abe, K.; Ferri, S.; Schulze, H.; Bachmann, T.T.; Ikebukuro, K. Affinity improvement of a VEGF aptamer by in silico maturation for a sensitive VEGF-detection system. *Anal. Chem.* **2012**, *85*, 1132–1137. [CrossRef] [PubMed]
118. Kinghorn, A.B.; Dirkzwager, R.M.; Liang, S.; Cheung, Y.-W.; Fraser, L.A.; Shiu, S.C.-C.; Tang, M.S.; Tanner, J.A. Aptamer Affinity Maturation by Resampling and Microarray Selection. *Anal. Chem.* **2016**, *88*, 6981–6985. [CrossRef] [PubMed]

International Journal of
*Molecular Sciences*

MDPI

*Review*

# Aptamers and Glioblastoma: Their Potential Use for Imaging and Therapeutic Applications

**Emma M. Hays, Wei Duan and Sarah Shigdar ***

Centre for Molecular and Medical Research, School of Medicine, Deakin University, 75 Pigdons Road, Waurn Ponds, Victoria 3216, Australia; ehays@deakin.edu.au (E.M.H.); wei.duan@deakin.edu.au (W.D.)
* Correspondence: sarah.shigdar@deakin.edu.au; Tel.: +61-3-5227-2846

Received: 1 November 2017; Accepted: 27 November 2017; Published: 30 November 2017

**Abstract:** Glioblastoma is a highly aggressive primary brain tumour, renowned for its infiltrative growth and varied genetic profiles. The current treatment options are insufficient, and their off-target effects greatly reduce patient quality of life. The major challenge in improving glioblastoma diagnosis and treatment involves the development of a targeted imaging and drug delivery platform, capable of circumventing the blood brain barrier and specifically targeting glioblastoma tumours. The unique properties of aptamers demonstrate their capability of bridging the gap to the development of successful diagnosis and treatment options, where antibodies have previously failed. Aptamers possess many characteristics that make them an ideal novel imaging and therapeutic agent for the treatment of glioblastoma and other brain malignancies, and are likely to provide patients with a better standard of care and improved quality of life. Their target sensitivity, selective nature, ease of modification and low immunogenicity make them an ideal drug-delivery platform. This review article summarises the aptamers previously generated against glioblastoma cells or its identified biomarkers, and their potential application in diagnosis and therapeutic targeting of glioblastoma tumours.

**Keywords:** glioblastoma; aptamers; SELEX; cancer; targeted therapies; imaging; diagnosis; biomarkers; blood brain barrier

## 1. Introduction

Glioblastoma or grade IV glioma is a highly malignant primary brain tumour with a particularly poor median survival duration of 14 months [1]. Whilst the incidence rate of glioblastoma currently stands markedly low at 3.2 per 100,000 population, its five-year survival rate is below 6% [2]. These tumours can arise spontaneously from glial cells, or can develop from the progression of a lower grade glioma and are defined as primary or secondary glioblastomas, respectively (see Figure 1) [3]. Histological features of glioblastoma include increased cellularity and angiogenesis, vascular proliferation, hemorrhage, necrosis, and cystic regions throughout the tumours [4,5]. Cell populations within these tumours tend to vary greatly, with the presence of both small, undifferentiated cells and large cells with multiple nuclei reported [4].

According to the World Health Organization, glioblastomas are grouped into three categories based on isocitrase dehydrogenase (IDH) status: glioblastoma IDH-wildtype, which is designated as primary or to have originated de novo; glioblastoma IDH-mutant, which is identified as a secondary tumour, arising from a lower grade glioma; and glioblastoma not otherwise specified (NOS) for tumours when IDH evaluation cannot be performed [6]. An estimated 90% of glioblastoma arise de novo, with the remaining 10% developing from a lower grade glioma [7]. Mutations of IDH lead to hypermethylation of histones and DNA, altering gene expression, promoting the activation of oncogenes and blocking tumour suppressing mechanisms [8]. A variety of genetic mutations are implicated in glioblastoma development including the *epidermal growth factor receptor* (*EGFR*), *human epidermal growth factor receptor two* (*ERBB2*), *isocitrase dehydrogenase one* (*IDH1*), *neurofibromin one* (*NF1*),

*phosphoinositide three-kinase* (*PI3K*), *phosphatase and tensin homolog* (*PTEN*), *retinoblastoma protein* (*RB1*) and *tumour suppressor p53* (*TP53*) [9]. The gene expression patterns can be used to further categorise glioblastomas into four sub-categories: proneural; neural; mesenchymal; and classical [10].

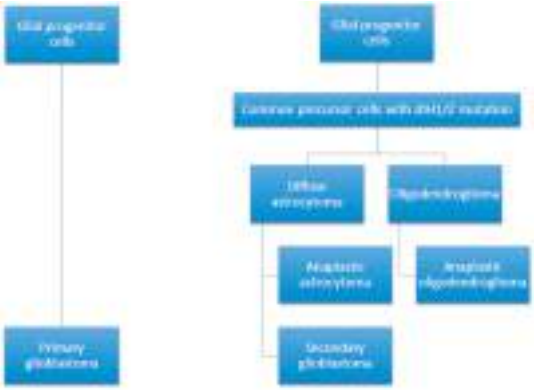

**Figure 1.** Glioblastomas can develop through two different pathways; arising as a primary malignancy; or through the progression of a lower grade glioma [11].

The classical subtype is associated with amplification of chromosome 7 teamed with loss of chromosome 10, EGFRoverexpression and mutations. Mesenchymal glioblastomas maintain a high expression of *CH13L1*, *MET*, and genes associated with tumour necrosis factor and nuclear factor-κB pathways, along with mutations and deletions of NF1. The proneural subclass parallels secondary glioblastoma and lower-grade glioma with mutations in *IDH1* and *TP53*, and modification of platelet-derived growth factor receptor A (PDGFR-A) [10]. Finally, neural glioblastomas are similar to normal brain tissue; however, they do overexpress EGFR [10,12].The current treatment modality includes surgery, radiotherapy, and chemotherapy with the DNA-alkylating agent temozolomide [1,13]. Surgery is performed to debulk the tumour thereby reducing mass effect symptoms in the patient, while also allowing for the collection of tissue specimens for histologic analysis [14]. Glioblastomas are renowned for their heterogeneity and infiltrative growth; complete surgical resection is near impossible as a result, and further complicated by the inability to differentiate the tumour from normal brain tissue [15]. Radiation and chemotherapy form the next line of treatment, aiming to destroy the cancer cells that were missed or could not be removed during surgery [1]. Temozolomide is a DNA-alkylating agent capable of inducing single- and double-stranded breaks in DNA, resulting in senescence and cell death [16]. Whilst surgery and the addition of temozolomide during and post-radiotherapy has led to an increase in patient survival times, they are responsible for various adverse effects and poor quality of life in patients [13,17]. In addition, chemo-resistance and glioblastoma recurrence are inevitable for the majority of patients, highlighting the necessity of improved treatment options [16,18]. One of the greatest challenges facing modern medicine is the development of tumour targeting molecules, capable of specifically binding to their target with no adverse effects to normal cells and tissues within the body. Whilst the discovery and subsequent development of antibodies have become an integral part of scientific research, disease diagnosis and therapies, these molecules possess undesired characteristics and many pose significant risks to patients, limiting their clinical efficacy [19,20]. Antibody generation occurs in vivo, in both a time consuming and costly process, with incidences of great batch-to-batch variability [21]. The high cost of the complicated antibody production process limits their clinical use, particularly as large doses are needed for effective responses in patients [22]. Their large size hinders their ability to reach the desired targets due to poor tissue penetration, and can be irreversibly denatured by small changes in temperature, thereby limiting their shelf life and transport options [23]. Attempts have been made to humanize antibodies; however, complement-dependent

toxicity (CDC), antibody-dependent cellular cytotoxicity (ADCC), and cytokine storms still occur in patients [24–26]. Despite these known issues, antibodies remain in development and clinical trials, while the development of alternatives with improved safety profiles are being investigated [27,28]. Targeted peptides and aptamers may bridge the gaps of diagnostic and therapeutic applications that are currently unfilled by antibodies; however, targeted peptides have been reviewed extensively elsewhere (see [29–31]) and fall beyond the scope of this review article. Targeted therapies will pave the way for personalized cancer medicine, ensuring patients receive treatment based on their tumour's gene expression profiles, for effective treatment against glioblastoma and other currently incurable conditions.

Further understanding of the altered and uncontrolled signaling pathways in glioblastoma has potential to aid in the development of targeted treatments against the disease. Gene amplification and overexpression of the EGFR protein and its mutant variant EGFRvIII contributes to glioblastoma tumorigenesis and has been the target for new therapeutics [32,33]. Tyrosine kinase inhibitors of EGFR block downstream signaling pathways by inhibiting ATP binding to the intracellular domain, thereby impeding with responses leading to cell growth, invasion, and angiogenesis [34]. The use of the EGFR tyrosine kinase inhibitors erlotinib and gefitinib have been evaluated in numerous clinical trials, alone and in combination with standard glioblastoma treatment, with minimal effect on patient survival [35–38]. Monoclonal antibodies have also been investigated for the treatment of glioblastoma. In particular, bevacizumab was generated to inhibit vascular endothelial growth factor (VEGF) in order to prevent angiogenesis, survival and migration of glioblastoma tumour cells [39]. Two large phase III trials determined that the use of bevacizumab did not lead to increased survival compared to standard treatment, despite this, it has remained in use to treat recurrent glioblastoma when temozolomide rechallenge fails [40–42]. The unsuccessful development and clinical translation of more effective treatments for glioblastoma are hindered by the restrictive nature of the blood brain barrier.

The blood brain barrier's role is to control the passage of molecules and cells into the brain, in order to protect this vital organ [43]. Tight junctions formed by a uniform monolayer of endothelial cells maintain an almost impermeable barrier, increasing the difficulty of conveying chemotherapeutics into the brain [44]. Great efforts have been made to develop mechanisms capable of delivering therapeutic agents across this barrier, including both invasive and non-invasive strategies. The proposed invasive strategies include temporary disruption of the blood brain barrier and intrathecal drug delivery [45–48]. A temporary disruption of the barrier can be achieved using focused ultrasound and its interaction with microbubbles to alter the structure of the endothelial layer [49]. However, this technique can lead to necrosis in the target tissue area, vasculitis, and seizures [50]. Intrathecal drug delivery introduces therapeutics via direct injection into the cerebrospinal fluid [48]. While this is a simple method of bypassing the blood brain barrier, the drugs are often filtered from the cerebrospinal fluid before they reach the targeted area, and the use of a catheter often results in infection [47,51]. A less invasive method involves chemically altering drugs, potentially by the addition of a lipid-like structure, or modifying the drug to suit specific receptors, where it would be converted within the target organ to the active state [52]. Modifying drugs may result in considerable changes from the parental drug, in turn altering the pharmacodynamics and biological efficacy [44]. Finally, biological delivery systems can be used to increase the uptake of drugs by transporters that would normally be used for essential nutrients [53].

The presence of transport molecules on the surface of the blood brain barrier have recently proven to be an effective mechanism to utilise for the delivery of substances into the brain via receptor-mediated endocytosis. Yu and colleagues successfully utilised the transferrin receptor to transport an antibody across the endothelial layer into the brain itself [54]. On the contrary, the use of antibodies is associated with an immune response, therefore the development of a novel targeting agent similar to antibodies is required for the safe treatment of brain malignancies [55]. The recent development of a bi-functional aptamer capable of transcytosing across the blood brain barrier aided

by the transferrin receptor in vivo, can be conjugated to a glioblastoma targeting aptamer (Figure 2), and potentially improve its treatment modality [56].

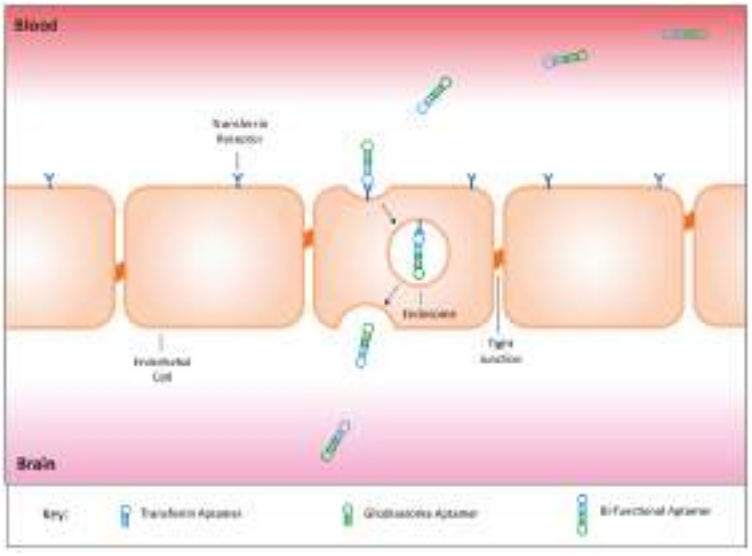


**Figure 2.** The fusion of a transferrin aptamer with a glioblastoma targeting aptamer would create a bi-functional aptamer capable of crossing the blood brain barrier to target glioblastoma tumour tissues specifically. This targeted mechanism may be utilised for the safe delivery of both imaging and therapeutic agents, sparing healthy cells throughout the body and the surrounding brain tissues from off-target effects.

## 2. Aptamers

Aptamers, also referred to as 'chemical antibodies' are single stranded oligonucleotides capable of binding to a target via shape recognition, in a similar fashion to antibodies [57]. Aptamers are generated against specific targets via the process of the systematic evolution of ligands by exponential enrichment (SELEX) and their sequence can be modified to optimise binding affinity and selectivity (see Figure 3) [58–61]. The selection of aptamers occurs in vitro, as does their subsequent manufacture, leading to little to no variation between batches, low immunogenicity, and are a considerably smaller size than antibodies, further increasing their ease of tissue penetration [62]. The enhanced binding properties of aptamers can saturate the available binding sites on the tumour surface, and therefore lead to improved imaging signals and intratumoural delivery of therapeutic agents, comparative to antibodies [22,63]. Chemotherapeutic agents can be attached to aptamers in order to deliver them to tumour cells, thereby reducing unwanted off-target effects, a particularly important factor for the development of new therapeutic agents for brain tumours [57]. Specificity of aptamer binding highlights their suitability for tumour imaging and targeted drug delivery, particularly in an organ as important as the brain. The attachment of imaging agents to aptamers has previously been achieved, and may lead to the development of more effective tumour imaging strategies for both histologic analysis of tissues as well as determining tumour location within the patient [64–67]. The use of aptamers for both imaging and therapeutic delivery have been reviewed extensively elsewhere [68–71].

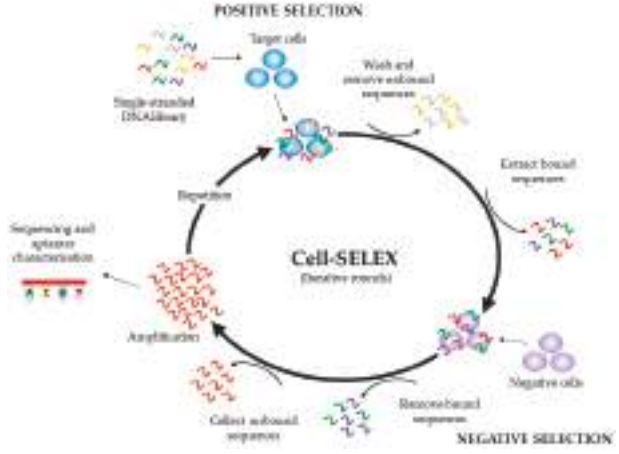


**Figure 3.** Schematic representation of a Cell-SELEX (systematic evolution of ligands by exponential enrichment) protocol. Initially, a single-stranded DNA library is incubated with the target cells. The cells are washed to remove the unbound sequences, and the bound sequences are collected, prior to incubation with negative (control) cells. The bound sequences are removed and discarded, whilst the unbound sequences are amplified and used to begin the next round of SELEX. This cycle is repeated a number of times, before the pool is sequenced and characterised. The bold arrows denote one iterative round of SELEX, with the small arrows depicting the different steps of the protocol: incubation of the single-stranded DNA library with the target cells; washing and removal of the unbound sequences, incubation with negative cells; removal of bound sequences; collection of bound sequences; amplification and cycle repetition prior to sequencing and aptamer characterization.

## 3. Glioblastoma Targeting Aptamers

To date, a multitude of aptamers have been generated against cell membrane proteins expressed on glioblastoma cells (see Tables 1 and 2). These aptamers have potential to be used to identify new biomarkers, and to specifically deliver imaging or therapeutic agents to revolutionise glioblastoma diagnosis and treatment (see Figure 4).

**Table 1.** Glioblastoma aptamers and their SELEX methods.

| Aptamer | Target | SELEX Method | Positive Selection | Negative Selection | Reference(s) |
|---|---|---|---|---|---|
| **A3, A4** | Unknown | Differential cell-SELEX | CD133+ TIC | CD133− cells; human neural progenitor cells | [72] |
| **TTA1** | Tenascin-C | Crossover-SELEX | U251 cells; human Tenascin-C | No negative selection | [66,73] |
| **GBI-10** | Tenascin-C | Cell-SELEX | U251 cells | No negative selection | [74,75] |
| **Gint4.T** | PDGFRβ | Cell-SELEX | U87MG cells | No negative selection | [76,77] |
| **GL21.T** | Axl | Differential cell-SELEX | U87MG cells | T98G cells | [77–80] |
| **U2** | EGFRvIII | Differential cell-SELEX | U87MG-EGFRvIII cells | U87MG cells | [81] |
| **Aptamer 32** | EGFRvIII | Differential cell-SELEX | U87MG-EGFRvIII cells | U87MG cells | [82–84] |
| **E07** | EGFR; EGFRvIII | Protein-SELEX | Human EGFR | No negative selection | [85–87] |
| **GMT 3–9** | Unknown | Differential cell-SELEX | A172 cells | No negative selection | [88] |
| **GBM128, GBM131** | Unknown | Differential cell-SELEX | U118-MG cells | SVGp12 cells | [89] |

**Table 2.** Aptamers generated against potential biomarkers for glioblastoma targeting.

| Aptamer | Target | SELEX Method | Positive Selection | Negative Selection | Reference(s) |
|---|---|---|---|---|---|
| **CD133-A15, CD133-B19** | CD133 | Differential cell-SELEX | HEK293T-CD133 cells | HEK293T cells | [90] |
| **CL4** | EGFR; EGFRvIII | Differential cell-SELEX | A549 cells | H460 cells | [91–93] |

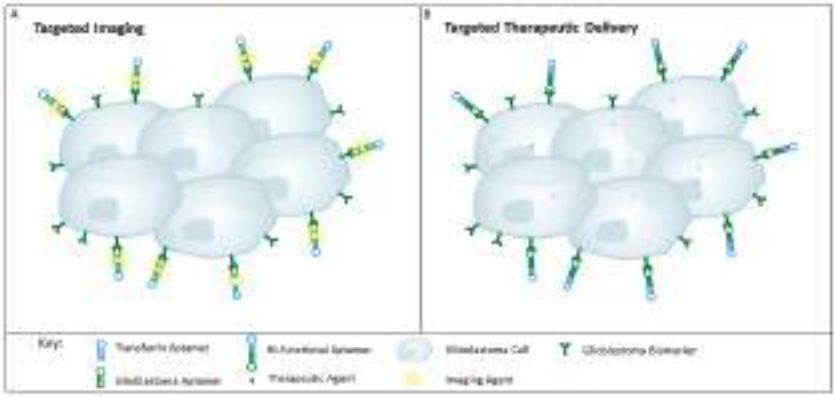


**Figure 4.** Schematic representation of aptamers for targeting glioblastoma tissue. (**A**) Targeted delivery of imaging agents to glioblastomas with the use of a bi-functional aptamer conjugated with an imaging agent such as radionuclides, may improve tumour detection; (**B**) Therapeutic agents can be conjugated to the bi-functional aptamer for the specific delivery to the glioblastoma cells, thereby reducing unwanted off-target effects and sparing the healthy surrounding tissues and throughout the rest of the body.

### *3.1. Aptamers Targeting Tumour Intitiating Cells*

A relatively new concept in cancer biology is the discovery of tumour initiating cells (TIC), referred to as cancer stem cells, thought to be a driving force in tumour development and therapeutic resistance [94]. While a population of TIC in glioblastomas can be identified by the glycoprotein CD133, some CD133-negative cells in these tumours have the ability to self-renew, thus this marker may not be indicative of all stem cells within glioblastoma tumours [95]. It should be noted that the CD133 receptor, usually detected with the AC133 epitope monoclonal antibody, can become truncated, thereby hindering the antibody's access to its binding region and leading to false-negative CD133 expression results in cancer cell populations [96]. As such, CD133 expression should be confirmed with multiple techniques. Despite these controversies, CD133 is still an attractive therapeutic target that requires further investigation due to its presence within these tumours.

To develop aptamers against CD133, Shigdar et al. utilised differential cell-SELEX with HEK293T-CD133 transfected cells and normal HEK293T cells as a negative control, to ensure the aptamers were binding to the desired epitope [90]. The generation of RNA containing 2′-F-pyrimidine aptamers capable of binding to CD133 was confirmed using both CD133 positive, and negative cell lines, via flow cytometry and confocal microscopy. The CD133-A15 aptamer binds to the AC133 epitope, similar to that of the standard antibody used for this receptor's detection. In contrast, CD133-B19 does not bind to the AC133 epitope and therefore has potential to be used to detect cancer stem cells within glioblastoma tumours, as well as potentially deliver therapeutics to these target cells.

Differential cell-SELEX was also utilised to generate the aptamers A3 and A4 against glioblastoma TIC, by using cells extracted from human glioblastoma tissue xenografts [72]. The collected cells were sorted based on CD133 expression and used for positive and negative selection in all SELEX rounds, with the addition of human neural progenitor cells as an extra counter selection step to

promote binding to a cancer surface marker. This selection process developed aptamers capable of specific binding and uptake to glioblastoma TIC, generating a potential method for their detection and treatment. Further characterisation of the identified aptamers is required to determine their molecular targets and determine their efficacy as diagnostic or therapeutic delivery agents.

### 3.2. Aptamers Targeting Tenascin-C

Tenascin-C is a large glycoprotein found in the extracellular matrix [73]. While normal adult tissues have little or no expression, higher levels are present during foetal development, wound healing, atherosclerosis, psoriasis, and tumour growth [97,98]. The high levels of tenascin-C expression in tumours is associated with angiogenesis, and may be an effective biomarker for diagnosis and treatment [73].

The aptamer TTA1 was developed via a crossover-SELEX protocol with U251 glioblastoma cells and purified human tenascin-C [73]. This aptamer was generated with RNA containing 2′-F-pyrimidine to induce resistance to nucleases in the blood, and was truncated prior to further modifications to improve aptamer stability and half-life with the substitution of 2′-$OCH_3$ purines, the addition of a thymidine cap at the 3′ end, and a 5′ amine as a conjugation site. In vitro testing determined the aptamer to bind to human tenascin-C with high affinity, with a 20-fold reduction in affinity to the mouse protein. The addition of the conjugate site on TTA1 enables the attachment of various molecules, ensuring its adaptability for various clinical applications. $^{99m}$Tc radiolabelled-TTA1 administered intravenously to nude mice successfully targeted tumour xenografts of U251 glioblastoma cells and MDA-MB-435 breast cancer cells, and its rapid clearance from the blood and uptake into the tumours indicates TTA1 as a viable tumour imaging modality [66]. It should be noted that there are limitations with the use of animals as human disease models, as xenografts do not wholly replicate the disease that occurs in humans [99]. The use of cultured cells in xenografts can lead to tumours with genetic profiles differing greatly from patient tumours and therefore do not always accurately represent treatment outcomes in patients. The use of xenograft models for glioblastoma tumours completely fails to replicate the cancer's microenvironment, and indeed the ability of these aptamers to cross the blood brain barrier, as these xenografts are heterotopic. Despite these drawbacks, animal models still provide important information for translational drug development prior to experimental clinical trials, and give great insight into efficacy of newly developed imaging agents. It is vital that the TTA1 aptamer is tested in healthy animal models to determine if it is capable of specifically targeting tumour tissue and also asses its ability to cross the blood brain barrier. If TTA1 is not able to do so, this aptamer may be attached to a transferrin aptamer to ensure its successful transition into the brain. TTA1 must also be tested in animal models that provide a relevant clinical representation of glioblastoma, to ensure its effectiveness as both a diagnostic and therapeutic delivery agent.

Another aptamer capable of specifically binding to tenascin-C is GBI-10, a DNA aptamer generated against U251 glioblastoma cells. Radiolabeling GBI-10 with positron emission tomography (PET) isotopes, $^{18}$F and $^{64}$Cu, developed aptamers capable of imaging tenascin-C within U87MG glioblastoma and MDA-MB-435 breast cancer xenografts in mice [74]. The aptamer's rapid clearance hindered intratumoural uptake; although these properties are ideal for PET imaging agents, they would need to be modified for effective therapeutic delivery in in vivo systems. To improve GBI-10's stability and affinity, D-/L-isonucleotides and 2′-dI phosphoramidite were incorporated into the aptamer structure, and successfully increased the binding affinity to U251 cells in vitro [75]. Aptamer binding affinity and serum stability are vital characteristics that determine their efficacy as diagnostic or drug-delivery platforms. Modifications to aptamers to improve their half-life and targeting ability may be vital to ensure their success in clinical applications. Further testing is warranted in more appropriate glioblastoma animal models to prove GBI-10's capability to specifically target glioblastoma tissues in a clinically relevant in vivo system.

### 3.3. Aptamers Targeting Platelet Derived Growth Factor Receptor β

Overexpression and mutations of the platelet derived growth factor receptor (PDGFR) are associated with gliomagenesis and tumour progression [100]. In glioblastoma, deregulation of the PDGFR signaling cascade and overexpression of this receptor is frequently displayed, indicating it as a potential therapeutic target [101].

Cell-SELEX was employed to develop a 2′-F-pyrimidine containing RNA aptamer capable of recognising platelet derived growth factor receptor β (PDGFRβ) [76]. This aptamer, Gint4.T, was determined to internalise into the U87MG glioblastoma cells, indicating its ability to be developed as a targeted delivery platform of therapeutics to the tumour tissues. Binding of this aptamer to the PDGFRβ was found to interfere with the receptor's signaling cascade by preventing phosphorylation of the tyrosine kinase domains, thereby reducing cell proliferation and migration both in vitro and in athymic CD-1 nude mice tumour xenografts in vivo. To prove Gint4.T's success as a therapeutic delivery platform, this aptamer was conjugated with anti-microRNA-10b to counteract expression of the oncogenic microRNA-10b seen in glioblastoma cancer stem cells, and induced cellular differentiation, thereby preventing tumoursphere growth and development when combined with GL21.T conjugated with microRNA-37 [77]. Interestingly, Gint4.T was capable of crossing the blood brain barrier in a physiologically relevant in vitro model previously developed by Kumar and associates (see [102]), likely via receptor mediated transcytosis, although this is yet to be replicated in an in vivo model. The ability of this aptamer to cross the blood brain barrier and specifically target glioblastoma cancer stem cells may lead to an effective therapeutic against this normally evasive cell population, thereby improving prognosis and increasing survival times for glioblastoma patients.

### 3.4. Aptamers Targeting Axl

Axl is a receptor tyrosine kinase commonly overexpressed in glioblastomas and other systemic tumours, associated with cancer cell survival, angiogenesis, proliferation, invasion, and motility [103–105]. The GL21.T aptamer is capable of binding and inhibiting Axl signaling, and may serve as a novel therapeutic agent to control tumour cell growth and invasion driven by this oncogenic protein [78]. This aptamer reduced migration and invasion of A549 lung cancer cells and U87MG glioblastoma cells in vitro and in athymic CD-1 nude mice xenografts in vivo. As previously mentioned, GL21.T conjugated with microRNA-37 used in combination with microRNA-10b-conjugated Gint4.T, transformed tumourspheres into adherent-like cells, inhibiting their ability to grow in spheroid form [77]. GL21.T was also able to traverse the in vitro blood brain barrier model, if this aptamer is capable of crossing this barrier in vivo, it could potentially be developed as a therapeutic targeting agent in the clinical setting. However, previous attempts to inhibit PDGFR in clinical trials have failed due to tumour resistance and pathway compensatory mechanisms [79,80]. Therefore, GL21.T should be used as a therapeutic delivery platform, and used in combination with other targeted therapies to ensure complete tumour eradication.

### 3.5. Aptamers Targeting the Epidermal Growth Factor Receptor

EGFR is involved with important cellular functions including cell growth, differentiation, survival, and migration, and deregulation of its signaling cascade is a driving force of glioblastoma tumorigenesis [32,106]. An aptamer capable of targeting EGFR and the mutant variant EGFRvIII would serve to be an ideal candidate for use in glioblastoma therapy, as their overexpression and mutation are prevalent in the majority of glioblastoma tumours [32].

An anti-EGFR RNA aptamer, CL4, capable of binding to both the wildtype and mutant variant has previously been generated via differential cell-SELEX with lung cancer cell lines [91]. Upon binding to the target receptor, CL4 prevented tyrosine-phosphorylation in a time-dependent manner, decreasing cell viability, proliferation, migration, and invasion in vitro [91,92]. Whilst minimal in vivo work has been undertaken with CL4, promising results from a triple-negative breast cancer xenograft model

in athymic CD-1 nude mice determined this aptamer was capable of reducing tumour size, without inducing toxicity in the treated mice [93]. CL4 displays a therapeutic effect against EGFR activation; however, EGFR inhibitors have failed to prove success as monotherapies for glioblastoma, as such, CL4 should be used as a shuttle for therapeutic or diagnostic agents to these tumours in order to have clinical success [107].

Differential cell-SELEX developed an aptamer, U2, with U87MG cells expressing EGFRvIII or wildtype EGFR as positive and negative selectors, respectively [81]. This aptamer's high affinity for the membrane receptors indicated its potential use as a diagnostic agent. Therefore, U2 was radiolabelled with $^{188}$Re to investigate its ability to function as a molecular probe in EGFRvIII expressing glioblastoma xenografts in male BALB/c nude mice. This aptamer successfully accumulated in the target tumours, highlighting its potential to be used as an effective glioblastoma imaging tool. There is little evidence to date that suggests U2 can penetrate the blood brain barrier in these mice, as such, conjugation with a transferrin receptor aptamer would ensure effective transport into the brain, though this would need to be extensively investigated both in vitro and in vivo. Tan et al. created aptamer 32 via differential cell-SELEX, utilising U87MG-EGFRvIII cells as the target for aptamer selection and U87MG cells as a negative control [82]. Binding assays were performed to evaluate aptamer specificity, with aptamer 32 showing binding to the U87MG-EGFRvIII target cells, and no binding to U87MG cells or the kidney cell line HEK293. Pull-down assays and confocal microscopy concluded the aptamer's target was EGFRvIII, and the aptamer was translocated to the nucleus of target cells, indicating its potential to be used for the targeted delivery of therapeutics within glioblastoma tumours. A follow-on study conjugated c-Met small interfering RNA (siRNA) to aptamer 32, and successfully delivered the siRNA to target U87MG-EGFRvIII cells, inhibiting the target gene's expression and cell proliferation whilst inducing apoptosis [83]. Conjugation of aptamer 32 to quantum dots could verify the expression of EGFRvIII in various glioblastoma tissues, the presence of this receptor was confirmed with immunohistochemistry [84]. This novel imaging probe was also capable of crossing the blood brain barrier in vivo, and accumulated in tumour tissues within the brains of male nude mice. Analysis of mouse body weight and major organs determined that the quantum dot-aptamer conjugates did not induce toxicity in the animals, further highlighting this aptamer's potential for use in the clinical setting. Overall, these results indicate aptamer 32 as a candidate tumour imaging probe and as a therapeutic delivery platform for the treatment of glioblastoma, though further investigation is required to determine aptamer 32's mechanism of crossing the blood brain barrier, and to further determine its stability and specificity to glioblastoma tumours within the brain.

An alternative SELEX method was employed to develop a 2′-F-pyrimidine containing RNA aptamer against human EGFR protein [85]. This aptamer, E07, was determined to competitively bind to both the wildtype and mutant variant three of EGFR, hindering ligand binding and autophosphorylation of these receptors in vitro. E07 has since been utilised to successfully capture and isolate circulating tumour cells with the use of biochips in vitro, with potential to be used for cancer diagnosis and evaluation of metastasis in patients [86,87].

### *3.6. Targeting Nucleolin with a Guanine-Rich Oligonucleotide*

Nucleolin is associated with ribosome biogenesis, and the overexpression of this protein in cancer cells is linked to cell division, angiogenesis and inhibiting apoptosis, and therefore, is a viable target for delivery of therapeutic agents to glioblastomas, or other forms of cancer [108,109]. The development and use of guanine-rich oligonucleotides (GRO) stems from their intriguing biological properties, notably, their enhanced uptake that could aid in the delivery of therapeutic agents to target tissues, although they are known to display non-specific effects [110,111]. AS1411 is a GRO, utilised for its antiproliferative effects and nucleolin targeting ability in vitro [112]. The efficacy of AS1411 as a cancer therapy was replicated in vivo, as intraperitoneal injections were able to significantly reduce pancreatic cancer xenograft growth in mice. In terms of using AS1411 as a treatment for glioblastoma, Luo et al. successfully delivered AS1411-conjugated paclitaxel nanoconjugates to U87MG-PMT48 orthotopic

glioblastoma xenografts in BALB/c nude mice, significantly increasing the median survival time for the treated mice [113]. Despite these promising results, the clinical translation of AS1411 was not so successful, with evaluation as a therapeutic in a phase II trial for metastatic renal cell carcinoma, only one patient out of 35 responded to the treatment [114]. Rigorous evaluation of AS1411 as a glioblastoma treatment in physiologically relevant in vitro and in vivo models is vital to ensure successful transition into clinical trials, and the potential off-target uptake must be evaluated if AS1411 is to be used for targeted drug delivery in the future.

### 3.7. Glioblastoma Aptamers with Unknown Targets

Cell-SELEX can be advantageous for aptamer development as whole cells have a myriad of surface markers that aptamers could bind to, many which remain unidentified. Therefore, aptamers can be generated against unknown surface markers that can later be identified, improving our knowledge of glioblastoma and other cancers.

Cell-SELEX was employed to develop DNA aptamers using the A172 glioblastoma cell line [88]. The sequenced aptamers GMT 3, GMT 4, GMT 5, GMT 8, and GMT 9 bound to glioblastoma cells with high affinity, and were further characterised to determine if binding was specific to glioblastoma cell lines. GMT 4 and 8 bound to the CEM leukemia cells and breast cancer cells GMBJ1, indicating that these cells share a surface marker recognised by these aptamers. Whilst these aptamers did bind to the glioblastoma cells, they had increased affinities to one of each leukemic and breast cancer cell line by more than two-fold. As such, these aptamers may have potential for use as a targeted imaging or therapeutic delivery strategy in these cancers as well. Treatment with proteinase K and trypsin was performed to determine if the aptamer binding targets were membrane proteins. All aptamers lost binding affinity after proteinase K treatment, indicating all of the aptamers likely bind to proteins. Trypsin application lead to a slight decrease in GMT 3 and 5 binding, demonstrating their targets are resistant to trypsin cleavage. These results show that negative selection is vital to cell-SELEX to identify aptamers specific to a tumour type, and to date, no publications have indicated the targets of these aptamers.

Differential cell-SELEX generated aptamers GBM128 and 131 using U118-MG cells for positive selection and astroglial cells SVGp12 for negative selection [89]. These aptamers were found to bind to the U118-MG glioblastoma cells in vitro, and did not recognise the astroglial cell line used in the SELEX process. Further testing with paraffin embedded tissues determined these aptamer's ability to bind to glioblastoma and glioma tissues, with no binding observed in the astroglial tissues. Whilst these aptamers could not differentiate between glioblastoma and other glioma tumours, they did not bind to normal brain tissue, indicating their potential use in glioma diagnosis. Further investigation is required to determine the aptamers' targets and prove their efficacy for glioma diagnosis.

### 3.8. Circumventing the Blood Brain Barrier

Whilst there are a number of aptamers that have been generated against cancer cells or their surface markers, the majority have only been investigated in vitro. Although the results show good selectivity, specificity, and efficacy, the challenge will be to see if these aptamers can cross the blood brain barrier in clinical models. One way of rescuing these aptamers, should they fail, is to use a transferrin receptor aptamer for receptor-mediated transcytosis in order to give these aptamers access to the brain. This mechanism has been successfully utilised by Macdonald et al. with a bi-functional aptamer capable of transcytosing through an in vitro blood brain barrier model, and also confirmed to reach the brain of a healthy mouse model following intravenous injection [56]. The conjugation of aptamers seen in the previous paper serves as a proof of concept that combining a cancer-targeting aptamer to a transferrin receptor aptamer, can develop a bi-functional aptamer capable of transcytosing through the blood brain barrier, to specifically target tumours within the brain.

## 4. Conclusions

Brain cancers, particularly glioblastomas, have very poor five-year survival rates and there is an urgent need to develop new therapeutic strategies with superior mechanisms of action to the current available therapies. The issue of getting new therapies across the blood brain barrier has been investigated in a number of studies, and there are now several strategies available to actively transport therapeutics through the barrier in order to reach the cancer cells within the brain. Whilst some of these transport mechanisms are unlikely to provide the patient with a better standard of care and improved quality of life, there are some with potential to revolutionise the treatment of glioblastoma, and other brain disorders.

Aptamers possess many characteristics that make them an ideal novel therapeutic agent for the treatment of glioblastoma and other brain malignancies. Their target sensitivity, selective nature, ease of modification and low immunogenicity make them an ideal drug-delivery platform. The development and optimisation of aptamers capable of transcytosing through the blood brain barrier to specifically deliver imaging and chemotherapeutic agents to glioblastoma tissues have potential to revolutionise brain tumour treatment.

In conclusion, aptamers show great promise as novel agents for tumour detection and treatment, although ongoing investigations are required to ensure their effective clinical translation. The research performed to date indicates aptamers are an innovative diagnostic and therapeutic platform for glioblastomas. Furthermore, these novel nucleic acids are improving our understanding of cancer and glioblastoma biology.

**Acknowledgments:** We would like to thank the Australian Government for the support through an Australian Government Research Training Program Scholarship.

**Author Contributions:** Emma M. Hays, Wei Duan, and Sarah Shigdar conceived the idea, Emma Hays performed the literature search. Emma M. Hays and Sarah Shigdar wrote the manuscript, and Wei Duan and Sarah Shigdar edited the manuscript.

**Conflicts of Interest:** The authors declare no conflict of interest.

## Abbreviations

| | |
|---|---|
| ADCC | Antibody-dependent cellular cytotoxicity |
| ATP | Adenosine triphosphate |
| CDC | Complement-dependent cytotoxicity |
| DNA | Deoxyribose nucleic acid |
| EGFR | Epidermal growth factor receptor |
| EGFRvIII | Epidermal growth factor receptor variant three |
| ERBB2 | Human epidermal growth factor receptor two |
| NF1 | Neurofibromin one |
| NOS | Not otherwise specified |
| PDGFRA | Platelet derived growth factor receptor A |
| PDGFRβ | Platelet derived growth factor receptor β |
| PI3K | Phosphoinositide three-kinase |
| PTEN | Phosphatase and tensin homolog |
| SELEX | Systematic evolution of ligands by exponential enrichment |
| PET | Positron emission tomography |
| RB1 | Retinoblastoma protein |
| RNA | Ribonucleic acid |
| siRNA | Small interfering RNA |
| TIC | Tumour initiating cells |
| TP53 | Tumour suppressor p53 |
| VEGF | Vascular endothelial growth factor |

## References


1. Hanif, F.; Muzaffar, K.; Perveen, K.; Malhi, S.M.; Simjee, S.U. Glioblastoma multiforme: A review of its epidemiology and pathogenesis through clinical presentation and treatment. *Asian Pac. J. Cancer Prev.* **2017**, *18*, 3–9. [PubMed]
2. Ostrom, Q.T.; Gittleman, H.; Xu, J.; Kromer, C.; Wolinsky, Y.; Kruchko, C.; Barnholtz-Sloan, J.S. Cbtrus statistical report: Primary brain and other central nervous system tumors diagnosed in the united states in 2009–2013. *Neuro Oncol.* **2016**, *18*, v1–v75. [CrossRef] [PubMed]
3. Cohen, A.L.; Holmen, S.L.; Colman, H. Idh1 and Idh2 mutations in gliomas. *Curr. Neurol. Neurosci. Rep.* **2013**, *13*, 345. [CrossRef] [PubMed]
4. Smith, C.; Ironside, J.W. Diagnosis and pathogenesis of gliomas. *Curr. Diagn. Pathol.* **2007**, *13*, 180–192. [CrossRef]
5. Louis, D.N.; Ohgaki, H.; Wiestler, O.D.; Cavenee, W.K. *Who Classification of Tumours of the Central Nervous System*, 4th ed.; IARC Press: Lyon, France, 2016.
6. Louis, D.N.; Perry, A.; Reifenberger, G.; von Deimling, D.; Figarella-Branger, W.; Cavenee, K.; Ohgaki, H.; Wiestler, O.D.; Kleihues, P.; Ellison, D.W. The 2016 world health organization classification of tumors of the central nervous system: A summary. *Acta Neuropathol.* **2016**, *131*, 803–820. [CrossRef] [PubMed]
7. Ohgaki, H.; Kleihues, P. Genetic pathways to primary and secondary glioblastoma. *Am. J. Pathol.* **2007**, *170*, 1445–1453. [CrossRef] [PubMed]
8. Molenaar, R.J.; Radivoyevitch, T.; Maciejewski, J.P.; van Noorden, C.J.F.; Bleeker, F.E. The driver and passenger effects of isocitrate dehydrogenase 1 and 2 mutations in oncogenesis and survival prolongation. *Biochim. Biophys. Acta Rev. Cancer* **2014**, *1846*, 326–341. [CrossRef] [PubMed]
9. Liu, A.; Hou, C.; Chen, H.; Zong, X.; Zong, P. Genetics and epigenetics of glioblastoma: Applications and overall incidence of Idh1 mutation. *Front. Oncol.* **2016**, *6*, 16. [CrossRef] [PubMed]
10. Szopa, W.; Burley, T.A.; Kramer-Marek, G.; Kaspera, W. Diagnostic and therapeutic biomarkers in glioblastoma: Current status and future perspectives. *BioMed Res. Int.* **2017**, *2017*. [CrossRef] [PubMed]
11. Ohgaki, H.; Kleihues, P. The definition of primary and secondary glioblastoma. *Clin. Cancer Res.* **2013**, *19*, 764–772. [CrossRef] [PubMed]
12. Eder, K.; Kalman, B. Molecular heterogeneity of glioblastoma and its clinical relevance. *Pathol. Oncol. Res.* **2014**, *20*, 777–787. [CrossRef] [PubMed]
13. Stupp, R.; Mason, W.P.; van den Bent, M.J.; Weller, M.; Fisher, B.; Taphoorn, M.J.B.; Belanger, K.; Brandes, A.A.; Marosi, C.; Bogdahn, U.; et al. Mirimanoff radiotherapy plus concomitant and adjuvant temozolomide for glioblastoma. *N. Engl. J. Med.* **2005**, *352*, 987–996. [CrossRef] [PubMed]
14. Oppenlander, M.E.; Wolf, A.B.; Snyder, L.A.; Bina, R.; Wilson, J.R.; Coons, S.W.; Ashby, L.S.; Brachman, D.; Nakaji, P.; Porter, R.W.; et al. An extent of resection threshold for recurrent glioblastoma and its risk for neurological morbidity. *J. Neurosurg.* **2014**, *120*, 846–853. [CrossRef] [PubMed]
15. Urbanska, K.; Sokolowska, J.; Szmidt, M.; Sysa, P. Glioblastoma multiforme—An overview. *Contemp. Oncol.* **2014**, *18*, 307–312.
16. Thomas, R.P.; Recht, L.; Nagpal, S. Advances in the management of glioblastoma: The role of temozolomide and mgmt testing. *Clin. Pharmacol.* **2013**, *5*, 1–9. [PubMed]
17. Jakola, A.S.; Gulati, S.; Weber, C.; Unsgard, G.; Solheim, O. Postoperative Deterioration in health related quality of life as predictor for survival in patients with glioblastoma: A prospective study. *PLoS ONE* **2011**, *6*, e28592. [CrossRef] [PubMed]
18. Omuro, A.; DeAngelis, L.M. Glioblastoma and other malignant gliomas: A clinical review. *JAMA* **2013**, *310*, 1842–1850. [CrossRef] [PubMed]
19. Silverstein, A.M. Paul Ehrlich's passion: The origins of his receptor immunology. *Cell. Immunol.* **1999**, *194*, 213–221. [CrossRef] [PubMed]
20. Carvalho, S.; Levi-Schaffer, F.; Sela, M.; Yarden, Y. Immunotherapy of cancer: From monoclonal to oligoclonal cocktails of anti-cancer antibodies: Iuphar review 18. *Br. J. Pharmacol.* **2016**, *173*, 1407–1424. [CrossRef] [PubMed]
21. Baker, M. Reproducibility crisis: Blame it on the antibodies. *Nature* **2015**, *521*, 274–276. [CrossRef] [PubMed]
22. Chames, P.; van Regenmortel, M.; Weiss, E.; Baty, D. Therapeutic antibodies: Successes, limitations and hopes for the future. *Br. J. Pharmacol.* **2009**, *157*, 220–233. [CrossRef] [PubMed]

23. Radom, F.; Jurek, P.M.; Mazurek, M.P.; Otlewski, J.; Jeleń, F. Aptamers: Molecules of great potential. *Biotechnol. Adv.* **2013**, *31*, 1260–1274. [CrossRef] [PubMed]
24. Maggi, E.; Vultaggio, A.; Matucci, A. Acute infusion reactions induced by monoclonal antibody therapy. *Expert Rev. Clin. Immunol.* **2011**, *7*, 55–63. [CrossRef] [PubMed]
25. Suntharalingam, G.; Perry, M.R.; Ward, S.; Brett, S.J.; Castello-Cortes, A.; Brunner, M.D.; Panoskaltsis, N. Cytokine storm in a phase 1 trial of the Anti-CD28 monoclonal antibody Tgn1412. *N. Engl. J. Med.* **2006**, *355*, 1018–1028. [CrossRef] [PubMed]
26. Descotes, J. Immunotoxicity of monoclonal antibodies. *mABs* **2009**, *1*, 104–111. [CrossRef] [PubMed]
27. Gan, H.K.; van den Bent, M.; Lassman, A.B.; Reardon, D.A.; Scott, A.M. Antibody–drug conjugates in glioblastoma therapy: The right drugs to the right cells. *Nat. Rev. Clin. Oncol.* **2017**, *14*, 695. [CrossRef] [PubMed]
28. Reichert, J.M. Antibodies to Watch in 2017. *mABs* **2017**, *9*, 167–181. [CrossRef] [PubMed]
29. Sarafraz-Yazdi, E.; Pincus, M.R.; Michl, J. Tumor-targeting peptides and small molecules as anti-cancer agents to overcome drug resistance. *Curr. Med. Chem.* **2014**, *21*, 1618–1630. [CrossRef] [PubMed]
30. Le Joncour, V.; Laakkonen, P. Seek & destroy, use of targeting peptides for cancer detection and drug delivery. *Bioorg. Med. Chem.* **2017**. [CrossRef]
31. Mousavizadeh, A.; Jabbari, A.; Akrami, M.; Bardania, H. Cell targeting peptides as smart ligands for targeting of therapeutic or diagnostic agents: A systematic review. *Colloids Surf. B Biointerfaces* **2017**, *158*, 507–517. [CrossRef] [PubMed]
32. Gan, H.K.; Cvrljevic, A.N.; Johns, T.G. The epidermal growth factor receptor variant III (EGFRvIII): Where wild things are altered. *FEBS J.* **2013**, *280*, 5350–5370. [CrossRef] [PubMed]
33. Xu, H.; Zong, H.; Ma, C.; Ming, X.; Shang, M.; Li, K.; He, X.; Du, H.; Cao, L. Epidermal growth factor receptor in glioblastoma. *Oncol. Lett.* **2017**, *14*, 512–516. [CrossRef] [PubMed]
34. Raymond, E.; Faivre, S.; Armand, J.P. Epidermal growth factor receptor tyrosine kinase as a target for anticancer therapy. *Drugs* **2000**, *60*, 15–23. [CrossRef] [PubMed]
35. Prados, M.D.; Chang, S.M.; Butowski, N.; DeBoer, R.; Parvataneni, R.; Carliner, H.; Kabuubi, P.; Ayers-Ringler, J.; Rabbitt, J.; Page, M.; et al. Phase II study of erlotinib plus temozolomide during and after radiation therapy in patients with newly diagnosed glioblastoma multiforme or gliosarcoma. *J. Clin. Oncol.* **2009**, *27*, 579–584. [CrossRef] [PubMed]
36. Van den Bent, M.J.; Brandes, A.A.; Rampling, R.; Kouwenhoven, M.C.; Kros, J.M.; Carpentier, A.F.; Clement, P.M.; Frenay, M.; Campone, M.; Baurain, J.F.; et al. Randomized phase II trial of erlotinib versus temozolomide or carmustine in recurrent glioblastoma: Eortc brain tumor group study. *J. Clin. Oncol.* **2009**, *27*, 1268–1274. [CrossRef] [PubMed]
37. Rich, J.N.; Reardon, D.A.; Peery, T.; Dowell, J.M.; Quinn, J.A.; Penne, K.L.; Wikstrand, C.J.; van Duyn, L.B.; Dancey, J.E.; McLendon, R.E.; et al. Phase II trial of gefitinib in recurrent glioblastoma. *J. Clin. Oncol.* **2004**, *22*, 133–142. [CrossRef] [PubMed]
38. Franceschi, E.; Cavallo, G.; Lonardi, S.; Magrini, E.; Tosoni, A.; Grosso, D.; Scopece, L.; Blatt, V.; Urbini, B.; Pession, A.; et al. Gefitinib in patients with progressive high-grade gliomas: A multicentre phase II study by gruppo italiano cooperativo di neuro-oncologia (GICNO). *Br. J. Cancer* **2007**, *96*, 1047–1051. [CrossRef] [PubMed]
39. Narita, Y. Drug review: Safety and efficacy of bevacizumab for glioblastoma and other brain tumors. *Jpn. J. Clin. Oncol.* **2013**, *43*, 587–595. [CrossRef] [PubMed]
40. Gilbert, M.R.; Dignam, J.J.; Armstrong, T.S.; Wefel, J.S.; Blumenthal, D.T.; Vogelbaum, M.A.; Colman, H.; Chakravarti, A.; Pugh, S.; Won, M.; et al. A randomized trial of bevacizumab for newly diagnosed glioblastoma. *N. Engl. J. Med.* **2014**, *370*, 699–708. [CrossRef] [PubMed]
41. Chinot, O.L.; Wick, W.; Mason, W.; Henriksson, R.; Saran, F.; Nishikawa, R.; Carpentier, A.F.; Hoang-Xuan, K.; Kavan, P.; Cernea, D.; et al. Bevacizumab plus radiotherapy-temozolomide for newly diagnosed glioblastoma. *N. Engl. J. Med.* **2014**, *370*, 709–722. [CrossRef] [PubMed]
42. Tipping, M.; Eickhoff, J.; Robins, H.I. Clinical outcomes in recurrent glioblastoma with bevacizumab therapy: An analysis of the literature. *J. Clin. Neurosci.* **2017**, *44*, 101–106. [CrossRef] [PubMed]
43. Abbott, N.J. Blood-brain barrier structure and function and the challenges for CNS drug delivery. *J. Inherit. Metab. Dis.* **2013**, *36*, 437–449. [CrossRef] [PubMed]

44. Gabathuler, R. Approaches to transport therapeutic drugs across the blood-brain barrier to treat brain diseases. *Neurobiol. Dis.* **2010**, *37*, 48–57. [CrossRef] [PubMed]
45. Patel, M.M.; Goyal, B.R.; Bhadada, S.V.; Bhatt, J.S.; Amin, A.F. Getting into the brain: Approaches to enhance brain drug delivery. *CNS Drugs* **2009**, *23*, 35–58. [CrossRef] [PubMed]
46. Baseri, B.; Choi, J.J.; Tung, Y.S.; Konofagou, E.E. Multi-modality safety assessment of blood-brain barrier opening using focused ultrasound and definity microbubbles: A short-term study. *Ultrasound Med. Biol.* **2010**, *36*, 1445–1459. [CrossRef] [PubMed]
47. Calias, P.; Banks, W.A.; Begley, D.; Scarpa, M.; Dickson, P. Intrathecal delivery of protein therapeutics to the brain: A critical reassessment. *Pharmacol. Ther.* **2014**, *144*, 114–122. [CrossRef] [PubMed]
48. Benjamin, S.B.; Kohman, R.E.; Feldman, R.E.; Ramanlal, S.; Han, X. Permeabilization of the blood-brain barrier via mucosal engrafting: Implications for drug delivery to the brain. *PLoS ONE* **2013**, *8*, e61694.
49. Sheikov, N.; McDannold, N.; Vykhodtseva, N.; Jolesz, F.; Hynynen, K. Cellular mechanisms of the blood-brain barrier opening induced by ultrasound in presence of microbubbles. *Ultrasound Med. Biol.* **2004**, *30*, 979–989. [CrossRef] [PubMed]
50. Miyake, M.M.; Bleier, B.S. The blood-brain barrier and nasal drug delivery to the central nervous system. *Am. J. Rhinol. Allergy* **2015**, *29*, 124–127. [CrossRef] [PubMed]
51. Aprili, D.; Bandschapp, O.; Rochlitz, C.; Urwyler, A.; Ruppen, W. Serious complications associated with external intrathecal catheters used in cancer pain patients: A systematic review and meta-analysis. *Anesthesiology* **2009**, *111*, 1346–1355. [CrossRef] [PubMed]
52. Chen, Y.; Dalwadi, G.; Benson, H.A. Drug delivery across the blood-brain barrier. *Curr. Drug Deliv.* **2004**, *1*, 361–376. [CrossRef] [PubMed]
53. Jones, A.R.; Shusta, E.V. Blood-brain barrier transport of therapeutics via receptor-mediation. *Pharm. Res.* **2007**, *24*, 1759–1771. [CrossRef] [PubMed]
54. Yu, Y.J.; Zhang, Y.; Kenrick, M.; Hoyte, K.; Luk, W.; Lu, Y.; Atwal, J.; Elliott, J.M.; Prabhu, S.; Watts, R.J.; et al. Boosting brain uptake of a therapeutic antibody by reducing its affinity for a transcytosis target. *Sci. Transl. Med.* **2011**, *3*, 84ra44. [CrossRef] [PubMed]
55. Pestourie, C.; Tavitian, B.; Duconge, F. Aptamers against extracellular targets for in vivo applications. *Biochimie* **2005**, *87*, 921–930. [CrossRef] [PubMed]
56. Macdonald, J.; Henri, J.; Goodman, L.; Xiang, D.; Duan, W.; Shigdar, S. Development of a bifunctional aptamer targeting the transferrin receptor and epithelial cell adhesion molecule (EPCAM) for the treatment of brain cancer metastases. *ACS Chem. Neurosci.* **2017**, *8*, 777–784. [CrossRef] [PubMed]
57. Yang, Y.; Yang, D.; Schluesener, H.J.; Zhang, Z. Advances in SELEX and application of aptamers in the central nervous system. *Biomol. Eng.* **2007**, *24*, 583–592. [CrossRef] [PubMed]
58. Tuerk, C.; Gold, L. Systematic evolution of ligands by exponential enrichment: RNA ligands to bacteriophage T4 DNA polymerase. *Science* **1990**, *249*, 505–510. [CrossRef] [PubMed]
59. Ellington, A.D.; Szostak, J.W. In vitro selection of RNA molecules that bind specific ligands. *Nature* **1990**, *346*, 818–822. [CrossRef] [PubMed]
60. Hasegawa, H.; Savory, N.; Abe, K.; Ikebukuro, K. Methods for improving aptamer binding affinity. *Molecules* **2016**, *21*, 421. [CrossRef] [PubMed]
61. Sefah, K.; Shangguan, D.; Xiong, X.; O'Donoghue, M.B.; Tan, W. Development of DNA aptamers using cell-SELEX. *Nat. Protoc.* **2010**, *5*, 1169–1185. [CrossRef] [PubMed]
62. Bunka, D.H.J.; Stockley, P.G. Aptamers come of age—At last. *Nat. Rev. Microbiol.* **2006**, *4*, 588–596. [CrossRef] [PubMed]
63. Hicke, B.J.; Stephens, A.W. Escort aptamers: A delivery service for diagnosis and therapy. *J. Clin. Investig.* **2000**, *106*, 923–928. [CrossRef] [PubMed]
64. Dougherty, C.A.; Cai, W.; Hong, H. Applications of aptamers in targeted imaging: State of the art. *Curr. Top. Med. Chem.* **2015**, *15*, 1138–1152. [CrossRef] [PubMed]
65. Keshtkar, M.; Shahbazi-Gahrouei, D.; Khoshfetrat, S.M.; Mehrgardi, M.A.; Aghaei, M. Aptamer-conjugated magnetic nanoparticles as targeted magnetic resonance imaging contrast agent for breast cancer. *J. Med. Signals Sens.* **2016**, *6*, 243–247. [PubMed]
66. Hicke, B.J.; Stephens, A.W.; Gould, T.; Chang, Y.F.; Lynott, C.K.; Heil, J.; Borkowski, S.; Hilger, C.S.; Cook, G.; Warren, S.; et al. Tumor targeting by an aptamer. *J. Nucl. Med.* **2006**, *47*, 668–678. [PubMed]

67. Rockey, W.M.; Huang, L.; Kloepping, K.C.; Baumhover, N.J.; Giangrande, P.H.; Schultz, M.K. Synthesis and radiolabeling of chelator-RNA aptamer bioconjugates with copper-64 for targeted molecular imaging. *Bioorg. Med. Chem.* **2011**, *19*, 4080–4090. [CrossRef] [PubMed]
68. Shigdar, S. What potential do aptamers hold in therapeutic delivery? *Ther. Deliv.* **2017**, *8*, 53–55. [CrossRef] [PubMed]
69. Chandola, C.; Kalme, S.; Casteleijn, M.G.; Urtti, A.; Neerathilingam, M. Application of aptamers in diagnostics, drug-delivery and imaging. *J. Biosci.* **2016**, *41*, 535–561. [CrossRef] [PubMed]
70. Keefe, A.D.; Pai, S.; Ellington, A. Aptamers as therapeutics. *Nat. Rev. Drug Discov.* **2010**, *9*, 537–550. [CrossRef] [PubMed]
71. Gijs, M.; Aerts, A.; Impens, N.; Baatout, S.; Luxen, A. Aptamers as radiopharmaceuticals for nuclear imaging and therapy. *Nucl. Med. Biol.* **2016**, *43*, 253–271. [CrossRef] [PubMed]
72. Kim, Y.; Wu, Q.; Hamerlik, P.; Hitomi, M.; Sloan, A.E.; Barnett, G.H.; Weil, R.J.; Leahy, P.; Hjelmeland, A.B.; Rich, J.N. Aptamer identification of brain tumor-initiating cells. *Cancer Res.* **2013**, *73*, 4923–4936. [CrossRef] [PubMed]
73. Hicke, B.J.; Marion, C.; Chang, Y.F.; Gould, T.; Lynott, C.K.; Parma, D.; Schmidt, P.G.; Warren, S. Tenascin-C Aptamers are generated using tumor cells and purified protein. *J. Biol. Chem.* **2001**, *276*, 48644–48654. [CrossRef] [PubMed]
74. Jacobson, O.; Yan, X.; Niu, G.; Weiss, I.D.; Ma, Y.; Szajek, L.P.; Shen, B.; Kiesewetter, D.O.; Chen, X. Pet imaging of tenascin-C with a radiolabeled single-stranded DNA aptamer. *J. Nucl. Med.* **2015**, *56*, 616–621. [CrossRef] [PubMed]
75. Li, K.; Deng, J.; Jin, H.; Yang, X.; Fan, X.; Li, L.; Zhao, Y.; Guan, Z.; Wu, Y.; Zhang, L.; et al. Chemical modification improves the stability of the DNA aptamer GBI-10 and its affinity towards tenascin-c. *Org. Biomol. Chem.* **2017**, *15*, 1174–1182. [CrossRef] [PubMed]
76. Camorani, S.; Esposito, C.L.; Rienzo, A.; Catuogno, S.; Iaboni, M.; Condorelli, G.; de Franciscis, V.; Cerchia, L. Inhibition of receptor signaling and of glioblastoma-derived tumor growth by a novel PDGFRβ aptamer. *Mol. Ther.* **2014**, *22*, 828–841. [CrossRef] [PubMed]
77. Esposito, C.L.; Nuzzo, S.; Kumar, S.A.; Rienzo, A.; Lawrence, C.L.; Pallini, R.; Shaw, L.; Alder, J.E.; Ricci-Vitiani, L.; Catuogno, S.; et al. A combined microrna-based targeted therapeutic approach to eradicate glioblastoma stem-like cells. *J. Control Release* **2016**, *238*, 43–57. [CrossRef] [PubMed]
78. Cerchia, L.; Esposito, C.L.; Camorani, S.; Rienzo, A.; Stasio, L.; Insabato, L.; Affuso, A.; de Franciscis, V. Targeting Axl with an high-affinity inhibitory aptamer. *Mol. Ther.* **2012**, *20*, 2291–2303. [CrossRef] [PubMed]
79. Jayson, G.C.; Parker, G.J.; Mullamitha, S.; Valle, J.W.; Saunders, M.; Broughton, L.; Lawrance, J.; Carrington, B.; Roberts, C.; Issa, B.; et al. Blockade of platelet-derived growth factor receptor-β by CDP860, a humanized, pegylated DI-FAB', leads to fluid accumulation and is associated with increased tumor vascularized volume. *J. Clin. Oncol.* **2005**, *23*, 973–981. [CrossRef] [PubMed]
80. Chee, C.E.; Krishnamurthi, S.; Nock, C.J.; Meropol, N.J.; Gibbons, J.; Fu, P.F.; Bokar, J.; Teston, L.; O'Brien, T.; Gudena, V.; et al. Phase II study of dasatinib (BMS-354825) in patients with metastatic adenocarcinoma of the pancreas. *Oncologist* **2013**, *18*, 1091–1092. [CrossRef] [PubMed]
81. Wu, X.; Liang, H.; Tan, Y.; Yuan, C.; Li, S.; Li, X.; Li, G.; Shi, Y.; Zhang, X. Cell-SELEX aptamer for highly specific radionuclide molecular imaging of glioblastoma in vivo. *PLoS ONE* **2014**, *9*, e90752. [CrossRef] [PubMed]
82. Tan, Y.; Shi, Y.S.; Wu, X.D.; Liang, H.Y.; Gao, Y.B.; Li, S.J.; Zhang, X.M.; Wang, F.; Gao, T.M. DNA aptamers that target human glioblastoma multiforme cells overexpressing epidermal growth factor receptor variant iii in vitro. *Acta Pharmacol. Sin.* **2013**, *34*, 1491–1498. [CrossRef] [PubMed]
83. Zhang, X.; Liang, H.; Tan, Y.; Wu, X.; Li, S.; Shi, Y. A U87-EGFRvIII cell-specific aptamer mediates small interfering RNA delivery. *Biomed. Rep.* **2014**, *2*, 495–499. [CrossRef] [PubMed]
84. Tang, J.; Huang, N.; Zhang, X.; Zhou, T.; Tan, Y.; Pi, J.; Pi, L.; Cheng, S.; Zheng, H.; Cheng, Y. Aptamer-conjugated pegylated quantum dots targeting epidermal growth factor receptor variant III for fluorescence imaging of glioma. *Int. J. Nanomed.* **2017**, *12*, 3899–3911. [CrossRef] [PubMed]
85. Li, N.; Nguyen, H.H.; Byrom, M.; Ellington, A.D. Inhibition of cell proliferation by an anti-EGFR aptamer. *PLoS ONE* **2011**, *6*, e20299. [CrossRef] [PubMed]

86. Wan, Y.; Liu, Y.; Allen, P.B.; Asghar, W.; Mahmood, M.A.I.; Tan, J.; Duhon, H.; Kim, Y.; Ellington, A.D.; Iqbal, S.M. Capture, isolation and release of cancer cells with aptamer-functionalized glass bead array. *Lab Chip* **2012**, *12*, 4693–4701. [CrossRef] [PubMed]
87. Wan, Y.; Mahmood, M.A.I.; Li, N.; Allen, P.B.; Kim, Y.; Bachoo, R.; Ellington, A.D.; Iqbal, S.M. Nanotextured substrates with immobilized aptamers for cancer cell isolation and cytology. *Cancer* **2012**, *118*, 1145–1154. [CrossRef] [PubMed]
88. Bayrac, A.T.; Sefah, K.; Parekh, P.; Bayrac, C.; Gulbakan, B.; Oktem, H.A.; Tan, W. In vitro selection of dna aptamers to glioblastoma multiforme. *ACS Chem. Neurosci.* **2011**, *2*, 175–181. [CrossRef] [PubMed]
89. Kang, D.; Wang, J.; Zhang, W.; Song, Y.; Li, X.; Zou, Y.; Zhu, M.; Zhu, Z.; Chen, F.; Yang, C.J. Selection of DNA aptamers against glioblastoma cells with high affinity and specificity. *PLoS ONE* **2012**, *7*, e42731. [CrossRef] [PubMed]
90. Shigdar, S.; Qiao, L.; Zhou, S.F.; Xiang, D.; Wang, T.; Li, Y.; Lim, L.Y.; Kong, L.; Li, L.; Duan, W. RNA aptamers targeting cancer stem cell marker CD133. *Cancer Lett.* **2013**, *330*, 84–95. [CrossRef] [PubMed]
91. Esposito, C.L.; Passaro, D.; Longobardo, I.; Condorelli, G.; Marotta, P.; Affuso, A.; de Franciscis, V.; Cerchia, L. A neutralizing RNA aptamer against EGFR causes selective apoptotic cell death. *PLoS ONE* **2011**, *6*, e24071. [CrossRef] [PubMed]
92. Camorani, S.; Crescenzi, E.; Colecchia, D.; Carpentieri, A.; Amoresano, A.; Fedele, M.; Chiariello, M.; Cerchia, L. Aptamer targeting EGFRvIII mutant hampers its constitutive autophosphorylation and affects migration, invasion and proliferation of glioblastoma cells. *Oncotarget* **2015**, *6*, 37570–37587. [CrossRef] [PubMed]
93. Camorani, S.; Crescenzi, E.; Gramanzini, M.; Fedele, M.; Zannetti, A.; Cerchia, L. Aptamer-mediated impairment of EGFR-integrin Avβ3 complex inhibits vasculogenic mimicry and growth of triple-negative breast cancers. *Sci. Rep.* **2017**, *7*, 46659. [CrossRef] [PubMed]
94. Singh, S.K.; Hawkins, C.; Clarke, I.D.; Squire, J.A.; Bayani, J.; Hide, T.; Henkelman, R.M.; Cusimano, M.D.; Dirks, P.B. Identification of human brain tumour initiating cells. *Nature* **2004**, *432*, 396–401. [CrossRef] [PubMed]
95. Brescia, P.; Ortensi, B.; Fornasari, L.; Levi, D.; Broggi, G.; Pelicci, G. CD133 is essential for glioblastoma stem cell maintenance. *Stem Cells* **2013**, *31*, 857–869. [CrossRef] [PubMed]
96. Schmohl, J.U.; Vallera, D.A. CD133, selectively targeting the root of cancer. *Toxins* **2016**, *8*, 165. [CrossRef] [PubMed]
97. Erickson, H.P.; Bourdon, M.A. Tenascin: An extracellular matrix protein prominent in specialized embryonic tissues and tumors. *Annu. Rev. Cell Biol.* **1989**, *5*, 71–92. [CrossRef] [PubMed]
98. Tiitta, O.; Virtanen, I.; Sipponen, P.; Gould, V. Tenascin expression in inflammatory, dysplastic and neoplastic lesions of the human stomach. *Virchows Arch.* **1994**, *425*, 369–374. [CrossRef] [PubMed]
99. Denayer, T.; Stöhr, T.; van Roy, M. Animal models in translational medicine: Validation and prediction. *New Horiz. Transl. Med.* **2014**, *2*, 5–11. [CrossRef]
100. Östman, A. PDGF receptors-mediators of autocrine tumor growth and regulators of tumor vasculature and stroma. *Cytokine Growth Factor Rev.* **2004**, *15*, 275–286. [CrossRef] [PubMed]
101. Kim, Y.; Kim, E.; Wu, Q.; Guryanova, O.; Hitomi, M.; Lathia, J.D.; Serwanski, D.; Sloan, A.E.; Weil, R.J.; Lee, J.; et al. Platelet-derived growth factor receptors differentially inform intertumoral and intratumoral heterogeneity. *Genes Dev.* **2012**, *26*, 1247–1262. [CrossRef] [PubMed]
102. Kumar, S.; Shaw, L.; Lawrence, C.; Lea, R.; Alder, J. P50developing a physiologically relevant blood brain barrier model for the study of drug disposition in glioma. *Neuro Oncol.* **2014**, *16*, vi8. [CrossRef]
103. Shieh, Y.-S.; Lai, C.-Y.; Kao, Y.-R.; Shiah, S.-G.; Chu, Y.-W.; Lee, H.-S.; Wu, C.-W. Expression of Axl in lung adenocarcinoma and correlation with tumor progression. *Neoplasia* **2005**, *7*, 1058–1064. [PubMed]
104. Zhang, Y.X.; Knyazev, P.G.; Cheburkin, Y.V.; Sharma, K.; Knyazev, Y.P.; Orfi, L.; Szabadkai, I.; Daub, H.; Keri, G.; Ullrich, A. Axl is a potential target for therapeutic intervention in breast cancer progression. *Cancer Res.* **2008**, *68*, 1905–1915. [CrossRef] [PubMed]
105. Hutterer, M.; Knyazev, P.; Abate, A.; Reschke, M.; Maier, H.; Stefanova, N.; Knyazeva, T.; Barbieri, V.; Reindl, M.; Muigg, A.; et al. Axl and *growth arrest-specific gene 6* are frequently overexpressed in human gliomas and predict poor prognosis in patients with glioblastoma multiforme. *Clin. Cancer Res.* **2008**, *14*, 130–138. [CrossRef] [PubMed]

106. Voldborg, B.R.; Damstrup, L.; Spang-Thomsen, M.; Poulsen, H.S. Epidermal growth factor receptor (EGFR) and EGFR mutations, function and possible role in clinical trials. *Ann. Oncol.* **1997**, *8*, 1197–1206. [CrossRef] [PubMed]
107. Padfield, E.; Ellis, H.P.; Kurian, K.M. Current therapeutic advances targeting EGFR and EGFRvIII in glioblastoma. *Front Oncol.* **2015**, *5*, 5. [CrossRef] [PubMed]
108. Ginisty, H.; Sicard, H.; Roger, B.; Bouvet, P. Structure and functions of nucleolin. *J. Cell Sci.* **1999**, *112 Pt 6*, 761–772. [PubMed]
109. Berger, C.M.; Gaume, X.; Bouvet, P. The roles of nucleolin subcellular localization in cancer. *Biochimie* **2015**, *113*, 78–85. [CrossRef] [PubMed]
110. Wu, C.C.N.; Castro, J.E.; Motta, M.; Cottam, H.B.; Kyburz, D.; Kipps, T.J.; Corr, M.; Carson, D.A. Selection of oligonucleotide aptamers with enhanced uptake and activation of human leukemia B cells. *Hum. Gene Ther.* **2003**, *14*, 849. [CrossRef] [PubMed]
111. Stein, C.A. The experimental use of antisense oligonucleotides: A guide for the perplexed. *J. Clin. Investig.* **2001**, *108*, 641–644. [CrossRef] [PubMed]
112. Bates, P.J.; Laber, D.A.; Miller, D.M.; Thomas, S.D.; Trent, J.O. Discovery and development of the G-rich oligonucleotide AS1411 as a novel treatment for cancer. *Exp. Mol. Pathol.* **2009**, *86*, 151–164. [CrossRef] [PubMed]
113. Luo, Z.; Yan, Z.; Jin, K.; Pang, Q.; Jiang, T.; Lu, H.; Liu, X.; Pang, Z.; Yu, L.; Jiang, X. Precise glioblastoma targeting by AS1411 aptamer-functionalized poly (L-γ-glutamylglutamine)-paclitaxel nanoconjugates. *J. Colloid Interface Sci.* **2017**, *490*, 783–796. [CrossRef] [PubMed]
114. Rosenberg, J.E.; Bambury, R.M.; van Allen, E.M.; Drabkin, H.A.; Lara, P.N., Jr.; Harzstark, A.L.; Wagle, N.; Figlin, R.A.; Smith, G.W.; Garraway, L.A.; et al. A phase II trial of AS1411 (a novel nucleolin-targeted DNA aptamer) in metastatic renal cell carcinoma. *Investig. New Drugs* **2014**, *32*, 178–187. [CrossRef] [PubMed]


International Journal of
*Molecular Sciences*

MDPI

*Review*

# Charomers—Interleukin-6 Receptor Specific Aptamers for Cellular Internalization and Targeted Drug Delivery

**Ulrich Hahn**

Chemistry Department, Institute for Biochemistry and Molecular Biology, MIN-Faculty, Universität Hamburg, Martin-Luther-King-Platz 6, D-20146 Hamburg, Germany; uli.hahn@uni-hamburg.de; Tel.: +49-177-213-4297

Received: 28 September 2017; Accepted: 24 November 2017; Published: 6 December 2017

**Abstract:** Interleukin-6 (IL-6) is a key player in inflammation and the main factor for the induction of acute phase protein biosynthesis. Further to its central role in many aspects of the immune system, IL-6 regulates a variety of homeostatic processes. To interfere with IL-6 dependent diseases, such as various autoimmune diseases or certain cancers like multiple myeloma or hepatocellular carcinoma associated with chronic inflammation, it might be a sensible strategy to target human IL-6 receptor (hIL-6R) presenting cells with aptamers. We therefore have selected and characterized different DNA and RNA aptamers specifically binding IL-6R. These IL-6R aptamers, however, do not interfere with the IL-6 signaling pathway but are internalized with the receptor and thus can serve as vehicles for the delivery of different cargo molecules like therapeutics. We succeeded in the construction of a chlorin e6 derivatized aptamer to be delivered for targeted photodynamic therapy (PDT). Furthermore, we were able to synthesize an aptamer intrinsically comprising the cytostatic 5-Fluoro-2′-deoxy-uridine for targeted chemotherapy. The α6β4 integrin specific DNA aptamer IDA, also selected in our laboratory is internalized, too. All these aptamers can serve as vehicles for targeted drug delivery into cells. We call them charomers—in memory of Charon, the ferryman in Greek mythology, who ferried the deceased into the underworld.

**Keywords:** aptamers; charomers; targeted drug delivery; targeted chemotherapy; photodynamic therapy; interleukin-6 receptor

## 1. Introduction

The multifunctional cytokine interleukin-6 (IL-6) consists of 183 amino acids and is in case of e.g., a skin lesion secreted by violated cells to signal this violation to recipient cells, thus inducing an inflammation followed by the healing process. The IL-6 signal is recognized by a highly specific IL-6 receptor (IL-6R) which is presented at the surfaces of certain cells. At least two further molecules of the nearly ubiquitously occurring glycosylated transmembrane protein gp130 are needed to result in the active complex for initiating signal transduction from outside the cell, finally into the nucleus to regulate corresponding gene expression (for review see [1–3]). One prerequisite of many receptors is their ability to exhibit a mechanism for desensitizing. IL-6R achieves this by internalization.

IL-6 mediated signal transduction is involved in many disease processes and is thus of high medical relevance. In some cases, one might wish to have a tool at hand to interrupt this signaling pathway. Candidates therefore are antibodies or even better, aptamers. Highlighting advantages and disadvantages of aptamers can be omitted in a special issue on aptamers and thus we can step directly into the projects which should be described here.

Our original plan, initiated by Stefan Rose-John, was to select aptamers specific for IL-6R aiming at getting a tool at hand to block IL-6 mediated signal transduction. Attempts to select aptamers with

high specificity for IL-6R were successful for canonical and modified RNA (dissociation constants from 20 nM to 55 nM [4–6]) as well as for DNA aptamers (dissociation constant 490 nM [7]).

All these aptamers, however, did not inhibit IL-6 signaling at all but most RNA aptamers were internalized and thus could function as vehicles for cargo delivery into target cells.

Another kind of cell surface proteins chosen as targets for the selection of aptamers in our laboratory was α6β4 integrin. This is presented by epithelial cells, Schwann cells, keratinocytes and endothelial cells [8,9]. The α6β4 integrin can bind to laminin, which leads to the assembly of hemidesmosomes followed by stable adhesion via connecting the intracellular keratin cytoskeleton to the basement membrane [10,11]. The selected α6β4 integrin specific aptamer IDA was also internalized.

In addition to the aptamers discussed so far, a number of others have been selected and characterized that can also be used to shuttle a variety of drugs, liposomes and (nano) particles into cells. Among those are aptamers targeting prostate-specific membrane antigen (PSMA) [12] which served for the directed delivery of an appropriate siRNA where it was connected to [13]. Aptamers specific for mucin-1 [14], nucleolin [15] transferrin receptor [16] or αvβ integrin [17]—just to list some as representatives—served as vehicles for different kinds of drug delivery approaches.

We have recently presented an overview on aptamers to be used as drug delivery vehicles [18,19]; readers are also referred to excellent reviews of the systemic administration of aptamer-based therapeutics by Burnett and Rossi [20] and Catuogno et al. [21], Sun et al. [22], Gilboa et al. [23], Jiang et al. [24] and not least, recently by Kruspe and Giangrande [25,26].

For all those internalized aptamers exhibiting the capability for cargo delivery I here would like to introduce the term "charomers".

In this brief review, however, solely aptamers selected in our laboratory and suitable as charomers will be dealt with in the following.

## 2. Interleukin-6-Recetor (IL-6R) Specific Aptamers

### *2.1. G-Quadruplex Forming Interleukin-6 Receptor (IL-6R) Specific Dimeric RNA Aptamers of 19 or 34 Nucleotides*

#### 2.1.1. AIR-3A—An Aptamer Specific for IL-6R and Consisting of RNA

The first IL-6R specific aptamers selected in our laboratory consisted of RNA. Sequencing of the enriched pool revealed six individual clones all comprising a very similar consensus sequence (Figure 1; [4]).

**Figure 1.** Alignment of interleukin-6 receptor (IL-6R) aptamer sequences from enriched pools. Consensus sequence is given below (conserved Gs in **blue** and conserved Cs and Us in **green**); H encodes A, C, or U and W encodes A or U, respectively. Flanking primer binding sites or constant regions of starting pool are omitted.

Minimal variants of each of these clones presenting each individual consensus motif were synthesized and analyzed for their capacity to bind IL-6R. AIR-3A (an aptamer specific for IL-6R and consisting of RNA; Figure 2) turned out to be the best candidate and was thus used for all further investigations [4]. Its high G-content was a strong hint of a G-quadruplex topology of this aptamer. Biophysical analyses like circular dichroism spectroscopy (CD) and UV-melting studies proved that AIR-3A adopted a parallel G-quadruplex structure (Figure 3).

| | |
|---|---|
| **AIR-3A** | **5′-GGGGAGGCUGUGGUGAGGG-3′** |
| **G17U** | **5′-GGGGAGGCUGUGGUGAUGG-3′** |
| **G18U** | **5′-GGGGAGGCUGUGGUGAGUG-3′** |
| **G17U/G18U** | **5′-GGGGAGGCUGUGGUGAUUG-3′** |

**Figure 2.** Nucleotide sequence of AIR-3A, the minimized active version of the IL-6R specific RNA aptamer AIR-3 and inactive AIR-3A variants; replaced nucleotides in red. A dissociation constant of about 20 nM was determined if AIR-3A was incubated with recombinant soluble human receptor (shIL-6R) in filter retention assays [4]. If the aptamer was incubated with IL-6R-presenting bone marrow-derived pro-B (BaF3) cells, the $K_d$ turned out to be about 2 nM [27]. Variants with one (G17U or G18U) or two Gs replaced by Us (G17U/G18U), respectively, did not bind to any target at all.

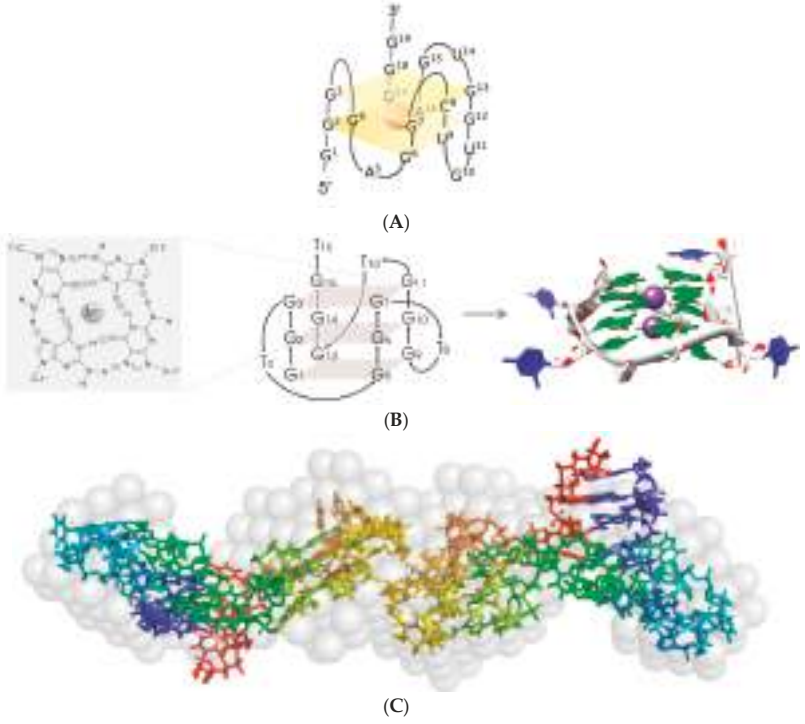

(**A**)

(**B**)

(**C**)

**Figure 3.** Aptamers AIR-3A, AID-1 as well as RAID3 all exhibit a G-quadruplex structure; the RNA aptamers AIR-3A and RAID3 were shown to dimerize. Circular dichroism (CD) spectroscopic investigations and UV-melting analyses revealed a G-quadruplex structure for both the RNA aptamers AIR-3A (**A**) [4] and RAID3 (**C**) [6], as well as for the DNA aptamer AID-1 (**B**) [7]. Balls in B represent structure stabilizing metal ions; gray semitransparent spheres in C symbolize a model deduced from synchrotron-based small-angle X-ray scattering (SAXS) analyses which could be superimposed with an ab initio model of an aptamer dimer.

#### 2.1.2. RAID3—An RNA Aptamer for Interleukin-6 receptor Domain 3

Another IL-6R specific 34 nt long RNA aptamer selected in our laboratory was RAID3 (RNA Aptamer for Interleukin-6 receptor Domain 3) [6]. It also exhibited a G-quadruplex structure and, most remarkably, could post-selectively be modified by replacing all pyrimidines by their 2′-fluoro analogs, resulting in the aptamer RAID3 2′-F-Py. Both mentioned aptamers did not show significant differences in their target binding ability ($K_d$ about 50 nM both). RAID3 2′-F-Py, however, exhibited an exceptional stability over a period of two days in Dulbecco's modified Eagle's medium supplemented with 10% fetal bovine serum (DMEM 10% FBS) at 37 °C. Not to forget that even the unmodified aptamer, RAID3, had a relatively long half-life of up to five minutes under the same conditions [6].

### *2.2. AIR-3A and RAID3 Are Internalized by IL-6R Presenting Cells and thus Charomers Allowing Their Usage as Vehicles for Targeted Drug Delivery*

AIR-3A and also RAID3 both turned out not to interfere with IL-6 initiated signal transduction. IL-6R, however, was internalized [28] as are many other receptors or cell surface proteins. Therefore, it was obvious to assume that a considerably tight binding ligand might be internalized too, together with the receptor. This could be demonstrated for some of the IL-6R specific RNA aptamers selected in our laboratory (Figure 4 and [4,6]).

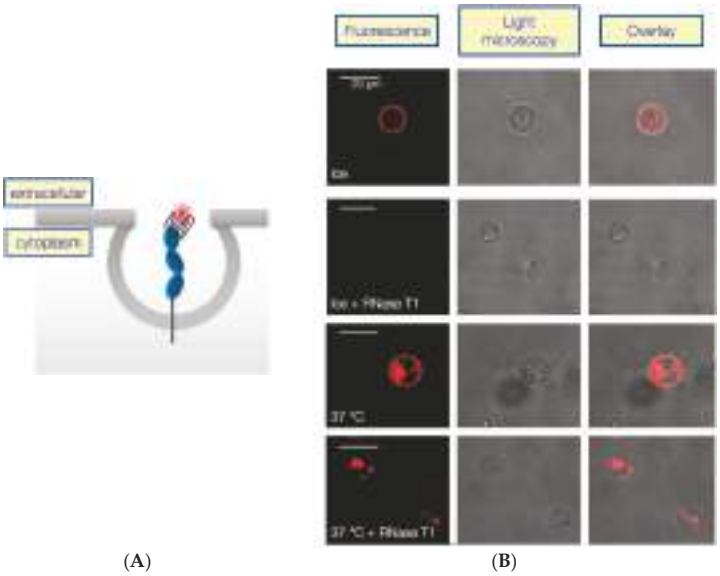


(**A**) (**B**)

**Figure 4.** Fluorescently labeled aptamer AIR-3A is internalized by IL-6R presenting BAF/gp130/IL6R/TNF cells. (**A**) Schematic presentation of internalization process of G-quadruplex forming fluorescently labeled aptamer bound to the receptor IL-6R and (**B**) confocal laser scanning and light microscopy of IL-6R presenting cells after 30 min incubation with Atto645N-labeled AIR-3A at 37 °C and on ice (control, as internalization does not occur at 0 °C). Another control included an incubation with G specific ribonuclease (RNase) T1 which degraded surface bound RNA aptamers [4].

In Greek mythology, a ferryman named Charon ferried the dead from the world to the underworld. In memory of this ferryman and in honor of one of the first cloning vectors based on the bacteriophage lambda—which was invented by Blattner et al. in 1977 and named "Charon phages" [29]—and in search of an acronym, we named our internalized and drug delivering aptamers "charomers".

### *2.3. Charomer Mediated Targeted Photodynamic Therapy (PDT)*

Chlorin e6 (c-e6) is a photoactivatable agent that generates singlet oxygen upon irradiation (Figure 5A). It is approved for ex vivo and in vivo application and thus very well suited for photodynamic therapy (PDT [30–33]). If pure c-e6 is applied to target cells it is non-specifically internalized and intracellularly accumulated. We have covalently linked c-e6 to the 3′-terminus of the IL-6R specific RNA aptamer AIR-3A which was then incubated with IL-6R presenting cells for appropriate times. After illumination of treated cells with light of 660 nm cell vitality dropped considerably under 50% and apoptosis increased significantly [34].

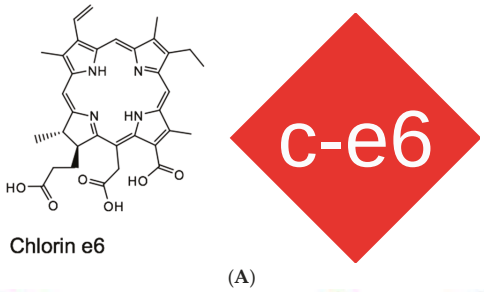


(**A**)

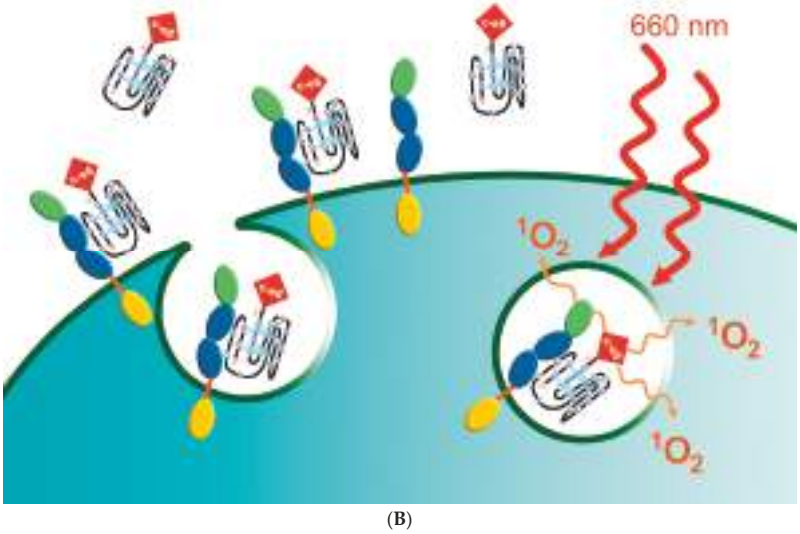


(**B**)

**Figure 5.** Chlorin e6 (c-e6) derivatized charomer AIR-3A-ce6 was internalized by IL-6R presenting cells leading to their destruction after illumination with appropriate light [34]. Schematic drawing of the aptamer mediated targeted photodynamic therapy (PDT). C-e6 (**A**) was covalently linked to the IL-6R specific aptamer (here schematically depicted as a G-quadruplex structured molecule); (**B**) This aptamer derivative was incubated with appropriate cells which did not survive after illumination with light of 660 nm wavelength (**red** waved lines) which is absorbed by ce-6 leading to the generation of singlet oxygen ($^1O_2$, **orange** waved lines) [34]; different colored ellipses of receptors symbolize different domains, extracellular domains in blue and green, intracellular part yellow.

### *2.4. Charomer Mediated Targeted Chemotherapy*

The base analogue 5-fluorouracil (5-FU; Figure 6A) is a warts therapeutic [35] and known since 60 years as chemo therapeutic or cancer drug [36,37]. It is also used in different kinds of application

forms [38]. We have enzymatically incorporated 5-fluoro-2′-deoxyuridine (5-FdU; Figure 6B) into aptamer AIR-3, the initially selected IL-6R specific "long version" of AIR-3A (Figures 1 and 2). AIR-3 was chosen as it exhibits significantly more Us than AIR-3A (Figures 1 and 6C). The resulting aptamer, AIR-3-FdU, still bound IL-6R with a dissociation constant of about 150 nM and IL-6R presenting BaF3 hIL-6R cells with a remarkable $K_d$ of about 20 nM [27]. Furthermore, when incubated with target cells AIR-3-FdU also was internalized, finally resulting in a decrease of cell proliferation to about 75%.

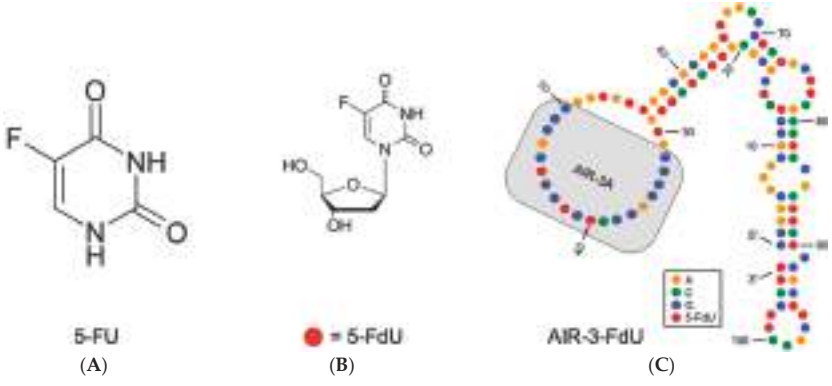


**Figure 6.** Charomer AIR-3-FdU, a tool for directed cancer drug delivery [27]. Shown are structures of 5-fluorouracil (5-FU; (**A**)), 5-fluoro-2′-deoxyuridine (5-FdU; (**B**)) and AIR-3-FdU (**C**) a derivative of the IL-6R specific RNA aptamer AIR-3 with each U replaced by 5-FdU (red dots); AIR-3-FdU structure is deduced from a model predicted for the originally selected aptamer AIR-3A with the software Mfold [39]; grey area emphasizes the minimized aptamer version AIR-3A.

To re-emphasize it, AIR-3-FdU could be readily synthesized in an enzymatic one step reaction. It specifically bound to a cell surface receptor which then most likely was transferred to the lysosome. When the aptamer then was degraded by intracellular nucleases, the active drug 5-FdU was released exclusively within the target cells [27]. Thus, the aptamer did act as a prodrug as it fulfilled two main prerequisites of a drug delivery system: specific cell targeting and controlled release of the drug triggered by an endogenous stimulus. As this prodrug also could be enzymatically reverse transcribed into DNA, which then served as template for the synthesis of new prodrug molecules, it thus also functioned as its own gene.

### *2.5. Structural Investigations of IL-6R Aptamers*

Remarkably, all IL-6R specific aptamers selected in our laboratory—regardless whether consisting of DNA or RNA—at least partly comprise a G-quadruplex structure (Figure 3; [4–7,40]). One might get the impression that this structural motive is a prerequisite for a nucleic acid aptamer for binding to IL-6R [40]. This is especially striking in case of the SELEX-selected IL-6R specific only 16 nt long DNA aptamer $d(GGGT)_4$ whose RNA counterpart $r(GGGU)_4$ also behaves very similar with respect to IL-6R binding and inhibition of HIV-1 integrase and HIV-1 infection [7].

Further structural investigations of the different aptamers discussed here included small-angle X-ray scattering (SAXS) analyses, structure probing, electrophoretic mobility shift assays and microscale thermophoresis [6,40]. In all cases the investigated aptamers were shown to form dimers (Figure 3).

## 3. Integrin α6β4 Specific DNA Aptamer IDA—Another Charomer

In another project in our laboratory we selected IDA, a 77 nt long integrin α6β4 specific DNA aptamer [41]. The initial motivation for the selection of IDA was to get a tool at hand to inhibit α6β4 integrin mediated cell-cell-interactions. Especially as this particular interaction can constitute

a pivotal step in transendothelial migration during metastasis formation [8,11,42,43]. This aptamer actually binds its target ($K_d$ about 140 nM) and also blocks the integrin-laminin-interaction but it is also internalized very effectively. Under appropriate conditions 98% of fluorescently labelled aptamer was internalized within 10 min (Figure 7; [41]).

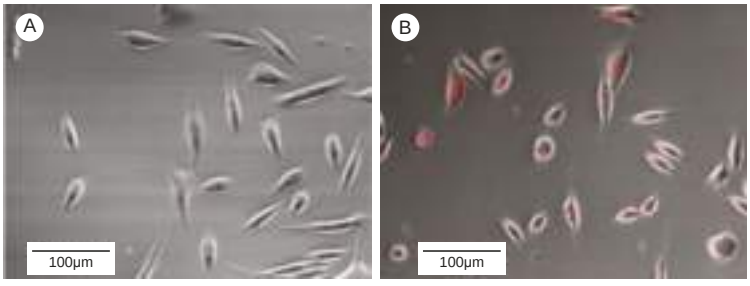


**Figure 7.** Fluorescently labeled aptamer IDA is internalized by integrin presenting PC-3 cells. Cells were incubated with fluorescently labelled non-specific DNA (**A**) and aptamer IDA (**B**) as described [41]. Scanning microscopic analysis after treating both samples with DNase showed clearly labelled molecules inside cells.

## 4. Conclusions

The nucleic acid charomers described here are targeting two different cell surface transmembrane proteins exhibiting different functions. The initial motivation for selecting these aptamers was to get tools at hand to inhibit the best-known functions of their targets—receiving signals from other cells or mediating unfavorable cellular interactions. As the targeted proteins are not solely presented but also internalized by the producing cells, it was not surprising that the mentioned and quite strongly binding nucleic acid aptamers were concurrently internalized, too. The possibility to fuse different kinds of cargo molecules [25,44] or even larger particles [21,45,46] with these internalized aptamers makes them charomers.

The inhibitory efficiency of the charomers reported here may not yet be very satisfactory but they can be precursors of a potentially very helpful new class of therapeutics and possibly their effect could be enhanced by the combination of several different charomers, covalently linked to each other or just in an appropriate mixture. Also attempts to improve stability and pharmacokinetic of the charomers might increase their utility. One can think about many different possibilities of new selection strategies or chemical modifications [6,47,48]. Lastly, the applicability in the living organism has to be demonstrated.

And now one final idea. If one imagines how many nucleic acid molecules can be found in the environment (early described by Karl and Bailiff [49]) one easily can imagine that not only a few of them will find their way from the environment into a cell just due to an accidentally sufficient affinity to a surface protein which is internalized. Maybe this is another noteworthy passway for gene exchange across species barriers.

**Acknowledgments:** I am grateful to Cindy Meyer, Florian Mittelberger, Sven Kruspe, Katharina Redder (née Berg) and Eileen Waldmann (née Magbanua) for providing and helping with Figures.

**Conflicts of Interest:** The author declares no conflicts of interest.

## References

1. Schaper, F.; Rose-John, S. Interleukin-6: Biology, signaling and strategies of blockade. *Cytokine Growth Factor Rev.* **2015**, *26*, 475–487. [CrossRef] [PubMed]

2. Garbers, C.; Aparicio-Siegmund, S.; Rose-John, S. The IL-6/gp130/STAT3 signaling axis: Recent advances towards specific inhibition. *Curr. Opin. Immunol.* **2015**, *34*, 75–82. [CrossRef] [PubMed]
3. Rothaug, M.; Becker-Pauly, C.; Rose-John, S. The role of interleukin-6 signaling in nervous tissue. *Biochim. Biophys. Acta* **2016**, *1863*, 1218–1227. [CrossRef] [PubMed]
4. Meyer, C.; Eydeler, K.; Magbanua, E.; Zivkovic, T.; Piganeau, N.; Lorenzen, I.; Grotzinger, J.; Mayer, G.; Rose-John, S.; Hahn, U. Interleukin-6 receptor specific RNA aptamers for cargo delivery into target cells. *RNA Biol.* **2012**, *9*, 57–65. [CrossRef] [PubMed]
5. Meyer, C.; Berg, K.; Eydeler-Haeder, K.; Lorenzen, I.; Grotzinger, J.; Rose-John, S.; Hahn, U. Stabilized Interleukin-6 receptor binding RNA aptamers. *RNA Biol.* **2014**, *11*, 57–65. [CrossRef] [PubMed]
6. Mittelberger, F.; Meyer, C.; Waetzig, G.H.; Zacharias, M.; Valentini, E.; Svergun, D.I.; Berg, K.; Lorenzen, I.; Grotzinger, J.; Rose-John, S.; et al. RAID3—An interleukin-6 receptor-binding aptamer with post-selective modification-resistant affinity. *RNA Biol.* **2015**, *12*, 1043–1053. [CrossRef] [PubMed]
7. Magbanua, E.; Zivkovic, T.; Hansen, B.; Beschorner, N.; Meyer, C.; Lorenzen, I.; Grotzinger, J.; Hauber, J.; Torda, A.E.; Mayer, G.; et al. d(GGGT) 4 and r(GGGU) 4 are both HIV-1 inhibitors and interleukin-6 receptor aptamers. *RNA Biol.* **2013**, *10*, 216–227. [CrossRef] [PubMed]
8. Stewart, R.L.; O'Connor, K.L. Clinical significance of the integrin α6β4 in human malignancies. *Lab. Investig.* **2015**, *95*, 976–986. [CrossRef] [PubMed]
9. Mercurio, A.M.; Rabinovitz, I.; Shaw, L.M. The α6β4 integrin and epithelial cell migration. *Curr. Opin. Cell Biol.* **2001**, *13*, 541–545. [CrossRef]
10. Litjens, S.H.; de Pereda, J.M.; Sonnenberg, A. Current insights into the formation and breakdown of hemidesmosomes. *Trends Cell Biol.* **2006**, *16*, 376–383. [CrossRef] [PubMed]
11. Giancotti, F.G. Targeting integrin β4 for cancer and anti-angiogenic therapy. *Trends Pharmacol. Sci.* **2007**, *28*, 506–511. [CrossRef] [PubMed]
12. Lupold, S.E.; Hicke, B.J.; Lin, Y.; Coffey, D.S. Identification and characterization of nuclease-stabilized RNA molecules that bind human prostate cancer cells via the prostate-specific membrane antigen. *Cancer Res.* **2002**, *62*, 4029–4033. [PubMed]
13. Bagalkot, V.; Gao, X. siRNA-aptamer chimeras on nanoparticles: Preserving targeting functionality for effective gene silencing. *ACS Nano* **2011**, *5*, 8131–8139. [CrossRef] [PubMed]
14. Ferreira, C.S.; Matthews, C.S.; Missailidis, S. DNA aptamers that bind to MUC1 tumour marker: Design and characterization of MUC1-binding single-stranded DNA aptamers. *Tumour Biol.* **2006**, *27*, 289–301. [CrossRef] [PubMed]
15. Bates, P.J.; Kahlon, J.B.; Thomas, S.D.; Trent, J.O.; Miller, D.M. Antiproliferative activity of G-rich oligonucleotides correlates with protein binding. *J. Biol. Chem.* **1999**, *274*, 26369–26377. [CrossRef] [PubMed]
16. Wilner, S.E.; Wengerter, B.; Maier, K.; de Lourdes Borba Magalhaes, M.; Del Amo, D.S.; Pai, S.; Opazo, F.; Rizzoli, S.O.; Yan, A.; Levy, M. An RNA alternative to human transferrin: A new tool for targeting human cells. *Mol. Ther. Nucleic Acids* **2012**, *1*, e21. [CrossRef] [PubMed]
17. Mi, J.; Zhang, X.; Giangrande, P.H.; McNamara, J.O., 2nd; Nimjee, S.M.; Sarraf-Yazdi, S.; Sullenger, B.A.; Clary, B.M. Targeted inhibition of αvβ3 integrin with an RNA aptamer impairs endothelial cell growth and survival. *Biochem. Biophys. Res. Commun.* **2005**, *338*, 956–963. [CrossRef] [PubMed]
18. Kruspe, S.; Mittelberger, F.; Szameit, K.; Hahn, U. Aptamers as drug delivery vehicles. *ChemMedChem* **2014**, *9*, 1998–2011. [CrossRef] [PubMed]
19. Meyer, C.; Hahn, U.; Rentmeister, A. Cell-specific aptamers as emerging therapeutics. *J. Nucleic Acids* **2011**, *2011*. [CrossRef] [PubMed]
20. Burnett, J.C.; Rossi, J.J. RNA-based therapeutics: Current progress and future prospects. *Chem. Biol.* **2012**, *19*, 60–71. [CrossRef] [PubMed]
21. Catuogno, S.; Esposito, C.L.; de Franciscis, V. Aptamer-mediated targeted delivery of therapeutics: An update. *Pharmaceuticals* **2016**, *9*, 69. [CrossRef] [PubMed]
22. Sun, H.; Zhu, X.; Lu, P.Y.; Rosato, R.R.; Tan, W.; Zu, Y. Oligonucleotide aptamers: New tools for targeted cancer therapy. *Mol. Ther. Nucleic Acids* **2014**, *3*, e182. [CrossRef] [PubMed]
23. Gilboa, E.; Berezhnoy, A.; Schrand, B. Reducing toxicity of immune therapy using aptamer-targeted drug delivery. *Cancer Immunol. Res.* **2015**, *3*, 1195–1200. [CrossRef] [PubMed]

24. Jiang, F.; Liu, B.; Lu, J.; Li, F.; Li, D.; Liang, C.; Dang, L.; Liu, J.; He, B.; Badshah, S.A.; et al. Progress and challenges in developing aptamer-functionalized targeted drug delivery systems. *Int. J. Mol. Sci.* **2015**, *16*, 23784–23822. [CrossRef] [PubMed]
25. Kruspe, S.; Giangrande, P.H. Aptamer-siRNA chimeras: Discovery, progress, and future prospects. *Biomedicines* **2017**, *5*, 45. [CrossRef] [PubMed]
26. Kruspe, S.; Giangrande, P.H. Design and preparation of aptamer-siRNA chimeras (AsiCs) for targeted cancer therapy. *Methods Mol. Biol.* **2017**, *1632*, 175–186. [PubMed]
27. Kruspe, S.; Hahn, U. An aptamer intrinsically comprising 5-fluoro-2′-deoxyuridine for targeted chemotherapy. *Angew. Chem. Int. Ed. Engl.* **2014**, *53*, 10541–10544. [CrossRef] [PubMed]
28. Fujimoto, K.; Ida, H.; Hirota, Y.; Ishigai, M.; Amano, J.; Tanaka, Y. Intracellular dynamics and fate of a humanized anti-interleukin-6 receptor monoclonal antibody, tocilizumab. *Mol. Pharmacol.* **2015**, *88*, 660–675. [CrossRef] [PubMed]
29. Blattner, F.R.; Williams, B.G.; Blechl, A.E.; Denniston-Thompson, K.; Faber, H.E.; Furlong, L.; Grunwald, D.J.; Kiefer, D.O.; Moore, D.D.; Schumm, J.W.; et al. Charon phages: Safer derivatives of bacteriophage lambda for DNA cloning. *Science* **1977**, *196*, 161–169. [CrossRef] [PubMed]
30. Li, Y.; Yu, Y.; Kang, L.; Lu, Y. Effects of chlorin e6-mediated photodynamic therapy on human colon cancer SW480 cells. *Int. J. Clin. Exp. Med.* **2014**, *7*, 4867–4876. [PubMed]
31. Yoon, I.; Li, J.Z.; Shim, Y.K. Advance in photosensitizers and light delivery for photodynamic therapy. *Clin. Endosc.* **2013**, *46*, 7–23. [CrossRef] [PubMed]
32. Agostinis, P.; Berg, K.; Cengel, K.A.; Foster, T.H.; Girotti, A.W.; Gollnick, S.O.; Hahn, S.M.; Hamblin, M.R.; Juzeniene, A.; Kessel, D.; et al. Photodynamic therapy of cancer: An update. *CA Cancer J. Clin.* **2011**, *61*, 250–281. [CrossRef] [PubMed]
33. Choudhary, S.; Nouri, K.; Elsaie, M.L. Photodynamic therapy in dermatology: A review. *Lasers Med. Sci.* **2009**, *24*, 971–980. [CrossRef] [PubMed]
34. Kruspe, S.; Meyer, C.; Hahn, U. Chlorin e6 conjugated interleukin-6 receptor aptamers selectively kill target cells upon irradiation. *Mol. Ther. Nucleic Acids* **2014**, *3*, e143. [CrossRef] [PubMed]
35. Salk, R.S.; Grogan, K.A.; Chang, T.J. Topical 5% 5-fluorouracil cream in the treatment of plantar warts: A prospective, randomized, and controlled clinical study. *J. Drugs Dermatol.* **2006**, *5*, 418–424. [PubMed]
36. Heidelberger, C.; Chaudhuri, N.K.; Danneberg, P.; Mooren, D.; Griesbach, L.; Duschinsky, R.; Schnitzer, R.J.; Pleven, E.; Scheiner, J. Fluorinated pyrimidines, a new class of tumour-inhibitory compounds. *Nature* **1957**, *179*, 663–666. [CrossRef] [PubMed]
37. Longley, D.B.; Harkin, D.P.; Johnston, P.G. 5-fluorouracil: Mechanisms of action and clinical strategies. *Nat. Rev. Cancer* **2003**, *3*, 330–338. [CrossRef] [PubMed]
38. Goette, D.K. Topical chemotherapy with 5-fluorouracil. A review. *J. Am. Acad Dermatol.* **1981**, *4*, 633–649. [CrossRef]
39. Zuker, M. Mfold web server for nucleic acid folding and hybridization prediction. *Nucleic Acids Res.* **2003**, *31*, 3406–3415. [CrossRef] [PubMed]
40. Szameit, K.; Berg, K.; Kruspe, S.; Valentini, E.; Magbanua, E.; Kwiatkowski, M.; Chauvot de Beauchene, I.; Krichel, B.; Schamoni, K.; Uetrecht, C.; et al. Structure and target interaction of a G-quadruplex RNA-aptamer. *RNA Biol.* **2016**, *13*, 973–987. [CrossRef] [PubMed]
41. Berg, K.; Lange, T.; Mittelberger, F.; Schumacher, U.; Hahn, U. Selection and characterization of an α6β4 Integrin blocking DNA Aptamer. *Mol. Ther. Nucleic Acids* **2016**, *5*, e294. [CrossRef] [PubMed]
42. Guo, W.; Giancotti, F.G. Integrin signalling during tumour progression. *Nat. Rev. Mol. Cell Biol.* **2004**, *5*, 816–826. [CrossRef] [PubMed]
43. Nikolopoulos, S.N.; Blaikie, P.; Yoshioka, T.; Guo, W.; Giancotti, F.G. Integrin β4 signaling promotes tumor angiogenesis. *Cancer Cell* **2004**, *6*, 471–483. [CrossRef] [PubMed]
44. Zhou, J.; Rossi, J.J. Cell-specific aptamer-mediated targeted drug delivery. *Oligonucleotides* **2011**, *21*, 1–10. [CrossRef] [PubMed]
45. Chen, Z.; Tai, Z.; Gu, F.; Hu, C.; Zhu, Q.; Gao, S. Aptamer-mediated delivery of docetaxel to prostate cancer through polymeric nanoparticles for enhancement of antitumor efficacy. *Eur. J. Pharm. Biopharm.* **2016**, *107*, 130–141. [CrossRef] [PubMed]

46. Prisner, L.; Bohn, N.; Hahn, U.; Mews, A. Size dependent targeted delivery of gold nanoparticles modified with the IL-6R-specific aptamer AIR-3A to IL-6R-carrying cells. *Nanoscale* **2017**, *9*, 14486–14498. [CrossRef] [PubMed]
47. Wang, R.E.; Wu, H.; Niu, Y.; Cai, J. Improving the stability of aptamers by chemical modification. *Curr. Med. Chem.* **2011**, *18*, 4126–4138. [CrossRef] [PubMed]
48. Tolle, F.; Brandle, G.M.; Matzner, D.; Mayer, G. A Versatile approach towards nucleobase-modified aptamers. *Angew. Chem. Int. Ed. Engl.* **2015**, *54*, 10971–10974. [CrossRef] [PubMed]
49. Karl, D.M.; Bailiff, M.D. The measurement and distribution of dissolved nucleic acids in aquatic environments. *Limnol. Oceanogr.* **1989**, *34*, 543–558. [CrossRef]

International Journal of
*Molecular Sciences*

MDPI

*Review*

# Light-Up RNA Aptamers and Their Cognate Fluorogens: From Their Development to Their Applications

**Farah Bouhedda †, Alexis Autour † and Michael Ryckelynck ***

Architecture et Réactivité de l'ARN, CNRS, Université de Strasbourg, UPR 9002, F-67000 Strasbourg, France; f.bouhedda@ibmc-cnrs.unistra.fr (F.B.), a.autour@ibmc-cnrs.unistra.fr (A.A.)
* Correspondence: m.ryckelynck@unistra.fr; Tel.: +33-(0)3-8841-7055
† These authors contributed equally to this work.

Received: 29 November 2017; Accepted: 15 December 2017; Published: 23 December 2017

**Abstract:** An RNA-based fluorogenic module consists of a light-up RNA aptamer able to specifically interact with a fluorogen to form a fluorescent complex. Over the past decade, significant efforts have been devoted to the development of such modules, which now cover the whole visible spectrum, as well as to their engineering to serve in a wide range of applications. In this review, we summarize the different strategies used to develop each partner (the fluorogen and the light-up RNA aptamer) prior to giving an overview of their applications that range from live-cell RNA imaging to the set-up of high-throughput drug screening pipelines. We then conclude with a critical discussion on the current limitations of these modules and how combining in vitro selection with screening approaches may help develop even better molecules.

**Keywords:** light-up aptamer; fluorogen; fluorogenic dye; fluorescence; RNA; in vitro evolution; gene expression monitoring; live-cell imaging; biosensing

## 1. Introduction

Quoting the famous idiom: "seeing is believing", which makes imaging and spectroscopic technologies very popular in life sciences to detect and track molecules. Among the different visualization strategies, fluorescence is the most attractive and widely used, mainly because it is safe, sensitive and it offers the possibility of analyzing multiple colors at the same time, with a long shelf life of the fluorophores when properly stored. Among the different fluorescent probes, those acquiring their fluorescence only in permissive conditions (e.g., presence of a target molecule) and hereafter defined as being fluorogenic are the most useful. These probes exhibit only a weak fluorescence in non-permissive conditions, making washing steps dispensable, and permitting the monitoring of dynamic processes in time course experiments. A plethora of such fluorogenic molecules has been developed for applications as diverse as ions and small molecules sensing, pH monitoring or environment viscosity assessment [1,2]. Moreover, significant efforts have been devoted to the development of fluorogenic tools dedicated to RNA and protein, two biological polymers particularly relevant to cellular activity. Historically, these molecules were first detected using fluorescently labeled and extracellularly supplied specific probes such as antibodies and oligonucleotides [3]. Recent developments allow these strategies to reach single-molecule sensitivity, but the requirement of fixing cells represents a major drawback that could be overcome using genetically encoded fluorescent reporters.

The discovery of the naturally fluorescing Green Fluorescent Protein (GFP) from the jellyfish *Aequorea victoria* [4] had a profound impact on protein imaging field and paved the way for major breakthroughs. Indeed, this first genetically encoded probe post-translationally acquires its fluorescence through an autocatalytic cyclization involving three amino acids (Serine, Tyrosine,

and Glycine) independently of any cell factor [5,6], making it usable in any cell type. Moreover, simple point mutations can shift the excitation/emission spectra of the protein toward the blue [7] or the red [8] regions of the visible spectrum. These great properties, shared with many other fluorescent proteins (FPs), make them highly versatile (see [9] for a comprehensive review) and very attractive for biotechnological applications. However, the strict requirement of molecular oxygen for the maturation of their fluorophore also limits FPs application in some circumstances and led to the development of alternative labeling strategies in which a fluorescent dye labels the protein of interest via a peptide (e.g., tetracystein peptide labeled by the Fluorescein Arsenical Helix binder FlAsH [10]) or a whole domain (e.g., SNAP-tag labeled by dye conjugated to a benzylguanine group [11]) appended to the target protein [12].

In contrast to proteins, no naturally fluorescent RNA has been discovered yet, making the development of RNA-based genetically encoded fluorescent reporters less straightforward than their protein counterparts. A first live-cell compatible strategy pioneered by Bertrand et al. [13] consists of inserting tandem repeats of elements recognized by an RNA-binding protein (RBP) into the RNA to image. Then, co-expressing this construct with an RBP-GFP fusion protein allows the direct labeling of the target RNA with the GFP. Moreover, the use of a split form of the GFP allows converting the otherwise always fluorescent GFP into a fluorogenic system in which fluorescence is expected only upon RBP-GFP/target RNA interaction [14]. Whereas this approach proved to be efficient for live-cell monitoring of large messenger RNAs [15], it may be more challenging for smaller RNAs (e.g., regulatory RNAs). Indeed, the insertion of a large number (20–30) of RBP binding sites into a small target RNA as well as its later decoration by RBP-GFPs leads to a significant increase of RNA size that could interfere with its biological function, making a size reduction of the labels a high priority. As was the case for protein labels, significant size reduction can be obtained by exchanging the bulky GFP for a smaller fluorescent synthetic dye. Constructs in which tandem repeats of RNA aptamers (i.e., small nucleic acid folds able to specifically recognize a target molecule) specific to a dye can be inserted into the target RNA, and the labeling can be obtained by placing cells in culture medium containing a membrane permeable dye. Aptamers binding specifically to fluorescent dyes such as sulforhodamine, fluorescein [16] or modified cyanines [17] can be used in arrays [17,18]. However, since the dye emits fluorescence even in its free unbound form, such approach may suffer from significant background fluorescence, limiting its application spectrum. Nevertheless, this limitation can be overcome by exchanging the fluorescent dye for a fluorogenic one. In this view, a seminal work by Tsien's group showed that, not only an RNA aptamer can specifically interact with a target molecule, but this interaction can also strongly increase the fluorescence of compounds such as Malachite green, making such aptamer/dye couple fluorogenic [19]. This discovery was all the more astonishing that the Malachite green-binding aptamer was not originally selected to function as a light-up aptamer but rather to mediate site-specific inactivation of target RNAs [20]. Since then, a variety of fluorogenic dyes and their cognate RNAs have been developed [21] (Table 1). This short review will be primarily focused on the main design strategies of each partner (the dye and the RNA) prior to giving a rapid overview of their application scope ranging from in vivo live-cell RNA imaging to in vitro small molecule biosensing. For a more general view of the current technologies available to image RNA, the reader is redirected to other reviews [22–25].

**Table 1.** Main RNA-based fluorogenic modules and their properties.

| Fluorogen | Light-Up Aptamer | $K_D$ (nM) | Ex./Em. (nm) | ε [1] ($M^{-1}$/cm) | $\Phi^{complex}$ [2] | Brightness [3] | Relative Brightness [4] | Ref. |
|---|---|---|---|---|---|---|---|---|
| GFP | / | / | 395/508 | 21,000 | 0.770 | 16.20 | 0.60 | [26] |
| eGFP | / | / | 490/508 | 39,200 | 0.680 | 26.60 | 1.00 | [26] |
| OTB | DiR2s-Apt | 662 | 380/421 | 73,000 | 0.510 | 37.23 | 1.40 | [27] |
| Hoescht | Apt II-mini3-4 c | 35 | 345/470 | n.a. | 0.260 | n.a. | n.a. | [28] |
| DFHBI | Spinach | 540 | 469/501 | 24,300 | 0.720 | 17.50 | 0.65 | [29] |
| DFHBI-1T | Spinach2 | 560 | 482/505 | 31,000 | 0.940 | 29.10 | 1.10 | [30] |
| DFHBI-1T | Broccoli | 360 | 472/507 | 29,600 | 0.940 | 27.80 | 1.04 | [31] |
| DFHBI-2T | Spinach2 | 1300 | 500/523 | 29,000 | 0.120 | 3.48 | 0.10 | [30] |
| RG-DN | DNB | 4480 | 507/534 | 37,350 | 0.320 | 11.90 | 0.44 | [32] |
| TO-1 | Mango | 3 | 510/535 | 77,500 | 0.140 | 10.85 | 0.40 | [33] |
| DFHO | Corn | 70 | 505/545 | 29,000 | 0.250 | 7.25 | 0.27 | [34] |
| CY3-BHQ1 | BHQ apt (A1) | n.a. | 520/565 | n.a. | n.a. | n.a. | n.a. | [35] |
| DFHO | Red-Broccoli | 206 | 518/582 | 35,000 | 0.340 | 11.90 | 0.44 | [34] |
| TMR-DN | DNB | 350 | 555/582 | 47,150 | 0.900 | 42.43 | 1.60 | [32] |
| SR-DN | DNB | 800 | 572/591 | 50,250 | 0.980 | 49.24 | 1.80 | [32] |
| DIR | DIR apt | 86 | 600/646 | 134,000 | 0.260 | 34.80 | 1.30 | [36] |
| Mal. Green | MG aptamer | 117 | 630/650 | 150,000 | 0.187 | 28.00 | 1.05 | [19] |
| DIR-pro | DIR2s-Apt | 252 | 600/658 | 164,000 | 0.330 | 54.12 | 2.00 | [27] |
| TO-3 | Mango | 6–8 | 637/658 | 9300 | n.a. | n.a. | n.a. | [33] |
| Patent Blue | SRB apt | 23 | n.a./665 | n.a. | 0.034 | n.a. | n.a. | [19] |

[1] Absorption coefficient (ε); [2] Quantum yield of the complex ($\Phi^{complex}$); [3] Brightness calculated as Brightness = ($\varepsilon \times \Phi^{complex}$)/1000; [4] Brightness expressed relative to eGFP. n.a.: not available. RNA modules were ordered according to their fluorescence emission wavelength.

## 2. Development of RNA-Based Fluorogenic Modules

RNA-based fluorogenic modules are made of two components: a fluorogenic dye (later called fluorogen) and a specific light-up RNA aptamer. In an ideal case, such module should feature five essential properties. (i) The module should be as bright as possible to ensure sensitive detection, ideally down to single molecule resolution. Therefore, the dye should have an elevated absorption coefficient (ε) and its interaction with the RNA should place it in a conformation and an environment maximizing its quantum yield ($\Phi^{bound}$) that should be as close as possible to 1. (ii) In its free form, the fluorogen should display the lowest possible quantum yield ($\Phi^{free}$) to minimize background fluorescence. Consequently, a good fluorogenic module is expected to have the highest possible fluorescence enhancement (calculated as the ratio of $\Phi^{bound}$ over $\Phi^{free}$). (iii) The RNA–dye interaction should be highly specific and bio-orthogonal (i.e., cell compounds or reagents of the assay should not interfere with the interaction). (iv) Moreover, the interaction should occur with a high affinity (dissociation constant $K_D$ in the nM range or less) to make using low concentration of the dye possible and to keep fluorescence background as low as possible, which allows getting high contrast [37]. (v) Finally, the module should be as photostable as possible to allow prolonged data acquisition. Since both components of the module affect all these parameters (with the exception of the second one that is only affected by the dye), the proper development of an RNA-based fluorogenic module is not a trivial task and both the dye and the RNA should be developed while trying to stay as close as possible to the ideal scenario depicted above.

### *2.1. Fluorogenic Dye Engineering*

The fluorogen plays a key role in the functionality of a fluorogenic module by contributing to both its brightness and its photostability. Moreover, for live-cell applications, additional parameters such as membrane permeability and the lack of toxicity of the dye should also be considered. The fluorogenicity of a dye can be obtained in various ways encompassing but not limited to charge (or proton) transfer, conformational change, isomerization or even dye aggregation [38]. Several of these principles having been used for the development of RNA-based fluorogenic modules.

Many compounds are known to become highly fluorescent upon interaction with nucleic acids [39]. Among them, ethidium bromide [40] and Hoechst 33258 [41] are environment sensitive dyes characterized by a poor fluorescence in aqueous solution. However, upon binding to a DNA molecule (respectively by intercalation between base pairs or binding in the DNA minor groove at AT-rich region), the dye is placed into a non-polar environment that strongly increases its fluorescence (Figure 1a). The non-specific DNA binding capacity of these dyes can lead to significant unwanted background fluorescence when used in cell-based assay. However, this property can be suppressed by decorating the dye with additional chemical functions. For instance, substituting Hoechst 33258 with bulky groups allowed designing derivatives no longer capable of non-specific DNA binding, but preserving their fluorogenic capacity and becoming fluorescent only upon specific interaction with DNA and RNA aptamers [28,42] (Table 1).

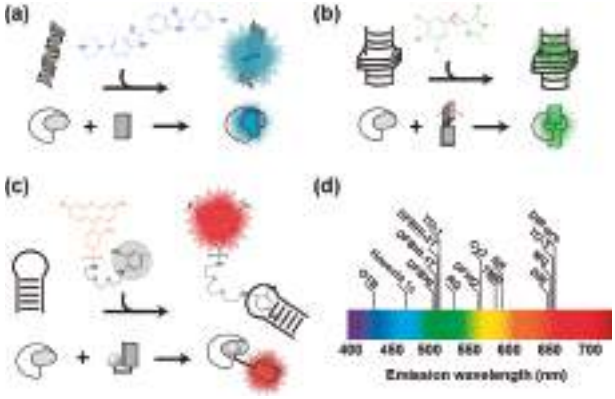


**Figure 1.** Main conception strategies of fluorogens. (**a**) Environment sensitive fluorogens. Molecules such as Hoescht 33258 (formula in blue) emit blue fluorescence upon association with DNA minor groove. Modifying the fluorogen with bulky groups allows aborting this non-specific DNA binding capacity, while preserving the fluorogenic capacity that can be now specifically activated by the cognate aptamer [35]. (**b**) Molecular rotor fluorogens. DFHBI (formula in green) [29] eliminates excitation energy by molecular movements (red arrows). However, upon association to the cognate aptamer, movements are restricted and fluorogen energy is eliminated by fluorescence emission. (**c**) Quenched fluorogens. Sulforhodamine B (formula in red) fluorescence is quenched by a conjugated dinitroaniline (formula in black and shaded in gray) [32]. However, the fluorescence is restored upon the specific recognition of the quencher (or the fluorophore moiety in other systems) by an aptamer. In every example, RNA aptamer is represented by the croissant-shaped object and the fluorogen by the rectangles. (**d**) Distribution of fluorogen emission wavelength along the visible spectrum.

Fluorogenicity can also result from intramolecular movements allowing for non-radiative relaxation of the dye upon excitation (Figure 1b). Such compounds, hereafter called molecular rotors, are poorly fluorescent in their unbound form in a fluid environment. However, fluorescence can be restored by restricting intramolecular movements either by strongly increasing medium viscosity, or upon specific interaction with a nucleic acid. Triphenylmethane dyes (e.g., Malachite Green (MG) and Patent Blue, Table 1) were the first class of compounds for which specific RNA light-up aptamers were identified [19,20]. Among them, MG shows an impressive ~2400-fold fluorescence enhancement when bound to its cognate RNA aptamer [19]. Nevertheless, MG light irradiation is known to elicit the generation of free radical leading to subsequent RNA cleavage [20], making this approach potentially toxic for living cells [34,43,44]. Moreover, MG was also found to be able to generate significant background fluorescence within mammalian cell [45] and bacteria [46], further limiting the use of this system. Unsymmetrical fluorogenic cyanines constitute a second attractive class of

fluorogenic molecular rotors composed of two different heterocycles connected by a methine bridge subjected to twisting in fluid solution [47,48]. Thiazole Orange (TO) is a good representative of these dyes, but it is also characterized by a significant non-specific DNA binding capacity [49,50]. However, as with Hoechst 33258, modifying the dye makes it possible to strongly attenuate this adverse effect. Indeed, using a large dimethylindole heterocycle and substituting the quinolone ring with a propylsulfonate group led to Dimethyl Indole Red (DIR), a TO derivative displaying a strongly reduced non-specific interaction with nucleic acids [36]. Alternatively, adding an acetate group on the benzothiazole moiety led to TO-1, a TO derivative also displaying a reduced affinity for DNA [33]. Moreover, a specific RNA aptamer was developed for each TO derivative (Table 1). In addition to their elevated absorption coefficient, cyanines are attractive molecules from a spectral point of view since their excitation/emission spectra can be easily modulated by changing the length of the methine bridge. Indeed, simply lengthening this bridge by two carbons converted the green emitting TO-1 into a red-emitting TO-3 [33]. Despite these promising properties, one can also foresee that current cyanine-derived dyes may suffer a potential limitation regarding cell-permeability. Indeed, the charged (e.g., acetate and sulfonate [27]) and bulky polar groups (e.g., PEG-biotin [33]) used to prevent non-specific binding, may also affect the capacity of the dyes to freely cross the cell membrane. Nevertheless, transiently caging these groups (e.g., by protecting carboxylic group as acetoxymethyl (AM) esters) may improve their membrane permeability. A last class of molecular rotors is made of GFP-mimicking dyes, a set of synthetic fluorogens that mimic the fluorophore of the GFP formed upon the cyclization of the Ser-Tyr-Gly tripeptide. Many derivatives of these fluorogens have been synthesized and used to develop a variety of sensors (see [51] for a recent review). Among them, the 3,5-difluoro-4-hydroxybenzylidene imidazolinone (DFHBI, Table 1) was developed by Jaffrey's group in 2011 together with a specific light-up aptamer [29]. Among other interesting features, DFHBI displays a ~1000 fluorescence enhancement in the presence of specific binding aptamers, it is non-toxic and has good cell permeability. Further substituting the imidazolinone cycle with a trifluoroethyl or a pentafluorophenyl group allowed obtaining DFHBI-1T [30] and DFHBI-PFP [45], two dyes with improved brightness and spectral properties. Whereas these GFP-mimicking dyes emit in the green region of the spectrum, the recent development of the DsRed-mimicking dye 3,5-difluoro-4-hydroxybenzylidene imidazolinone-2-oxime (DFHO, [34]) and others [52] also makes possible imaging nucleic acids in the orange-red region of the spectrum.

Finally, fluorogenic dyes can be obtained by appending a quenching group to a fluorescent organic dye (Figure 1c). In its free off-state, the fluorescence of the dye is quenched by a mechanism of photoinduced electron transfer (PET, [53,54]), Förster resonance energy transfer (FRET, [35]) or contact-mediated quenching [32,55]. However, the presence of an aptamer specifically recognizing either the dye [16,55] or the quencher [32,35,53] moiety allows for retrieving the fluorescence of the dye and the emission of a bright fluorescence (Table 1).

All together, these different strategies allowed designing a variety of fluorogens with fluorescence emission spanning most of the visible spectrum (Figure 1d) and brightness sometimes exceeding that of the broadly used GFP (Table 1).

### 2.2. Isolation of Fluorogenic RNA Aptamers

Once a fluorogen has been designed, the molecule can be used as target for the isolation and the optimization of a specific light-up RNA aptamer using two conceptually different approaches: (i) a selection strictly speaking during which an RNA pool is challenged to interact with the dye and only the best binders are recovered; or (ii) a screening approach where the light-up capacity of each molecule is analyzed and only the most fluorogenic ones are recovered.

#### 2.2.1. Aptamers Selection Based on Binding Capacity

Historically, RNA (or DNA) aptamers are isolated using the Systematic Evolution of Ligands by EXponential enrichment (SELEX) approach [56,57], a set of technologies particularly well suited for

the identification of nucleic acid specifically recognizing virtually any type of target, ranging from ions to more complex proteins [58]. Conceptually, SELEX works by performing iterative rounds of selection to exponentially enrich an RNA (or DNA) library in molecules able to bind a target molecule. Moreover, SELEX possesses the attractive capacity of handling large sequence diversity ($10^{12}$ to $10^{15}$ sequences) in a single experiment.

Depending on target size and physicochemical properties, several variations of SELEX have been introduced. However, all the new light-up RNA aptamers isolated so far were obtained through the same selection scheme (Figure 2). The success of such selection relies mainly on the proper design of the starting library as well as the partition mode used during the selection process. The starting DNA gene library is usually obtained by inserting a randomized region of ~50 nucleotides or more between two constants regions. Moreover, early work on the selection of aptamers targeting small molecules showed that interrupting the randomized region with a short constant hairpin may increase the success rate of a selection process [59] and, interestingly, the use of such discontinuous randomized libraries allowed isolating some of the best fluorogenic aptamers described so far [27,29,31,36]. The selection process is then initiated by transcribing the DNA gene library into an RNA pool prior the selection step where target-binding RNAs are partitioned away from the non-binding ones. To do so, the RNA pool is usually incubated with beads (e.g., streptavidin-conjugated agarose or magnetic beads) displaying the fluorogenic dye attached via a PEG linker. After several washing steps, the retained RNAs are eluted and reverse transcribed into cDNAs. These cDNAs can be later PCR-amplified and used to prime a new round of selection. Gradually increasing the wash stringency (e.g., increase the number and/or the duration of the wash) during the selection process allows favoring the selection of aptamers with the highest affinity for the dye while the poorer binders are counter selected. Moreover, the choice of the elution mode may also significantly affect the properties of the selected molecules. For instance, immobilized RNAs can be eluted using an excess of free dye. Such a general selection scheme led to the isolation of several fluorogenic RNAs such as the Malachite Green-binding aptamer [20], the DFHBI-binding aptamer Spinach [29], the DFHO-binding aptamer Corn [34] and the Dimethylindole Red-binding aptamer [27,36]. However, even though competition-based elution may favor the isolation of aptamers having great specificity for the dye moiety, they also suffer the major drawback that variants with low dissociation constant, so very high affinity, might likely be counter selected and lost. This may partly explain why these aptamers have a moderate affinity ($K_D$ ~ 0.1–1 μM) for their cognate dyes. This limitation could be overcome by changing the elution mode. For instance, the insertion of a disulfide bond within the linker between the dye and the bead, allows for the elution of dye/RNA complexes by adding dithiothreitol [32]. Alternatively, retained RNAs can be recovered by eluting them under denaturing conditions (e.g., heating, addition of urea, formamide, NaOH, etc.) as used for the selection of Hoechst-binding aptamer [28] and TO-1-binding Mango RNA aptamer [33]. Combined with drastic washing conditions (ionic strength reduction and addition of free competitive dye in the washing buffer), denaturing elution allowed the isolation of Mango RNA, a fluorogenic aptamer forming a fluorescent complex with the thiazole orange derivative TO-1-biotin characterized by a $K_D$ in the nM range, the highest affinity described so far for a fluorogenic module (Table 1). Nevertheless, one should note that RNAs isolated by non-competitive elution might also display affinity not only for the dye moiety but also accessory elements. This is well exemplified by Mango RNA that recognizes the TO-1-biotin not only via its thiazole orange moiety, but also displays some affinity for the PEG linker and the terminal biotin [60].

Upon isolation, fluorogenic aptamers can be further optimized by truncation and rational design. For instance, rationally inserting a few mutations in the Spinach aptamer resulted in Spinach2, a DFHBI-binding aptamer with improved folding properties [61]. However, some beneficial mutations may be difficult to predict and improving these aptamers may require individually testing many mutants. Moreover, an intrinsic limitation of SELEX is linked to the way selections are performed. Indeed, in this format, molecules are selected for their capacity to bind a fluorogen rather than for their

capacity to trigger its fluorescence. Therefore, screening approaches, in which molecules are directly analyzed for their fluorogenic capacity, represent an attractive complement to SELEX.

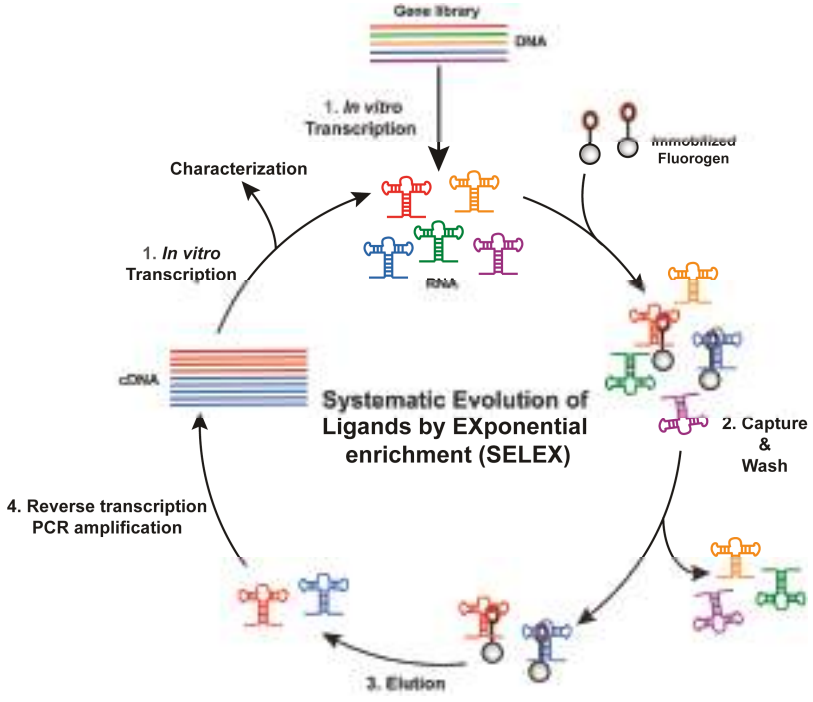


**Figure 2.** General overview of an in vitro selection using Systematic Evolution of Ligands by EXponential enrichment (SELEX). Each round proceeds in four main steps. A gene library is in vitro transcribed (Step 1) and mixed with beads displaying the fluorogen. Poor binders are eliminated by wash of variable stringency (selection pressure, Step 2) prior to recovering binding RNAs during the elution step (Step 3). Finally, RNAs are converted into cDNAs (Step 4), later used to prime a new round of selection.

### 2.2.2. Aptamers Isolation Based on Their Fluorogenic Capacity

Screening a light-up aptamer gene library requires isolating each gene prior to its expression into RNA followed by the assessment of its light-up capacity. In a first scheme, the library can be inserted into an expression plasmid later used to transform bacterial cells that will express light-up aptamers [31,62]. Bacteria can then be screened in two ways. First, they can be plated onto a solid medium supplemented with the fluorogen and allowed to grow until forming colonies [62]. The plates are then observed under fluorogen exciting light and the most fluorescent clones are recovered (Figure 3a). Even though it is simple and direct, such approach suffers from a limited throughput (a few thousand clones per day) and exploring large libraries can rapidly become time consuming, tedious and expensive. Alternatively, upon gene expression the cells can be incubated with the fluorogen prior to being screened using a Fluorescence-Activated Cell Sorter (FACS) (Figure 3b) [31], which substantially increases the analytical throughput (up to several million genes analyzed per day). However, even though it is more accurate, these screening approaches explore a much smaller fraction of the sequence space than SELEX does. Therefore, preferred methods combine library pre-enrichment by SELEX followed by ultrahigh-throughput screening using FACS. Such a tandem procedure was already used to obtain different light-up aptamers such as Broccoli [31], a new DFHBI-binding molecules [63]

and Corn [34]. These in vivo approaches offer the great advantage of directly assaying the performance of the aptamers in the cellular context, and in doing so to select those RNAs with optimal in vivo performances. However, they also suffer two major drawbacks: (i) the absolute need of using a cell-permeable fluorogen (a property dispensable for in vitro applications); and (ii) the applicable selection pressures are limited to those compatible with living cells (e.g., presence of potassium, physiological pH and temperature). Moreover, in the case of FACS, since the analysis is performed at single cell level, the screening may also face cell-to-cell expression variability and requires the co-expression of an internal fluorescent standard (e.g., GFP and mCherry).

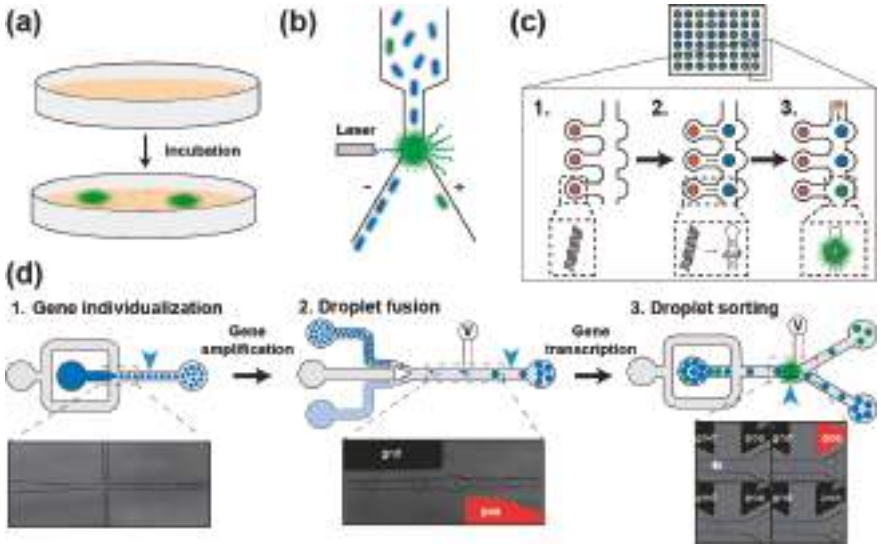


**Figure 3.** Main screening strategies for isolating light-up RNA aptamers. (**a**) Colony screening [31,62]. SELEX-enriched gene library is cloned and expressed in bacteria plated on a solid medium supplemented with the fluorogen. Upon incubation, colonies expressing light-up aptamers are identified by fluorescence emission (green shadow) when illuminated with fluorogen excitation wavelength. (**b**) FACS-based bacteria screening [31]. SELEX-enriched gene library is cloned and expressed in bacteria incubated in the presence of the fluorogen. Bacteria fluorescence is then analyzed on a FACS using a laser exciting the fluorogen. Fluorescence emitting bacteria (green shadow) are then deflected and sorted from the rest of the population. (**c**) Miniaturized in vitro screening using large integration scale microfluidic devices [64]. DNA coding for each variant is first spotted (red dots, Step 1) onto a surface prior to assembling the microfluidic chip. Then, each DNA cluster is transcribed in RNA later captured on a second spot of the chip (blue spot, Step 2). Finally, flowing the fluorogen into the microfluidic channels (Step 3) allows the detection of light-up aptamers (green spot). Quantifying the fluorescence emitted by each construct at various concentrations of fluorogen allows the determination of parameters such as the brightness and the dissociation constant ($K_D$). (**d**) Droplet-based microfluidic in vitro screening workflow [65]. A gene library is diluted into a PCR mixture (in dark blue) prior to individualizing the molecules into picoliter-sized water-in-oil droplets carried by an oil phase (in gray, Step 1). Upon off-chip PCR amplification, small and amplified DNA-containing droplets (dark blue) are synchronized and fused with larger droplets containing an in vitro transcription mixture supplemented with the fluorogen (light blue, Step 2). Upon an incubation step allowing for in vitro transcription to take place, the fluorescence of each droplet is analyzed and those droplets containing a light-up aptamer (in green) are sorted from the rest of the population (in blue). Both fusion and sorting events are triggered by the application of an electric field to built-in positive (pos, shown in red) and ground (gnd, shown in black) electrodes.

Most of the cell-based screening limitations can be overcome by switching to an in vitro expression approach. Performing such screening in microtiter plate can rapidly become very expensive, making the miniaturization of the process using microfluidics highly desirable [66]. A first level of miniaturization can be achieved by using a large-scale integration microfluidic device made of 640 independent one-nanoliter chambers, each containing several copies of the DNA coding for the variant to assay (Figure 3c) [64]. Then, genes are in vitro transcribed into RNA, which are later individually assayed for fluorogenic capacity. Moreover, the possibility of varying ligand concentration during the experiment allows the extraction of thermodynamic parameters of each variant in an automated way. However, the low throughput of the method (640 chambers per run) mainly restricts its use for refinement purposes. Further substantial throughput increase and cost reduction can be achieved by transposing the screening to droplet-based microfluidics [65,67] (Figure 3d). In this format, DNA molecules of a library are diluted into a PCR mixture and individualized at very high throughputs (several thousands of droplets generated per second) in small two-picoliter water-in-oil droplets. Upon thermocycling, each small droplet is fused to a larger 18-picoliter droplet containing an in vitro transcription mixture supplemented with the fluorogen. Finally, upon a last incubation, the fluorescence of each droplet is profiled and the most fluorescent ones (so those containing the best light-up aptamers) are sorted. Using this approach, we recently isolated iSpinach, a variant of the Spinach light-up aptamer optimized for in vitro applications (far less salt-sensitive, brighter and more thermo-stable) [65]. The isolation of this variant was made possible by the great control over the reaction conditions and the possibility of applying strong selection pressures difficult to apply in cell-based screening (e.g., warming and complete replacement of potassium ions by sodium). Therefore, droplet-based microfluidics screening is a viable and efficient way of isolating optimized light-up aptamers for in vitro application. Finally, further automation of the process could be obtained by integrating a Next Generation Sequencing analysis at the end of the process.

### *2.3. Features of the Best Characterized RNA-Based Fluorogenic Modules*

Among the variety of RNA-based fluorogenic modules developed so far (Table 1), those involving MG, fluorescent protein mimicking dyes (e.g., DFHBI and DFHO) and TO-1 are the best characterized, especially from a structural point of view. Interestingly, even though each of these RNAs adopts a distinct folding, they all possess a fluorogen-binding pocket comprising an extended planar platform made of at least one base quadruple onto which the fluorogen is accommodated in a near planar conformation competent for efficient fluorescence emission (see [68] for a recent critical review on the topic). Whereas the MG-binding aptamer platform is made of mixed base quadruple [69], the platform of all the other light-up aptamers is made from a stack of two or more G-quartets stabilized by potassium ions [60,70–73], indicating that such platform might be a consensus solution to fluorogens binding. However, beside this consensus platform, the rest of the fluorogen-binding pocket as well as the recognition strategy vary from one aptamer to the other. Indeed, for instance, MG-binding pocket acquires its structure only upon dye binding. On the other hand, in Spinach and its derivatives, the DFHBI intercalates between the platform and a base triple whilst additional contacts are established with lateral bases [70–72]. This pocket is formed prior to dye binding and was found to accommodate other dyes [74] limiting the possibility of using these aptamers concomitantly to other ones in multiplex experiments. Moreover, the pocket does not strongly constrain the dye that is free to rapidly isomerize upon illumination followed by a rapid exchange with a non-isomerized fluorogen to restore the fluorescent module [75]. DFHBI-based fluorogenic modules are therefore poorly photostable under continuous-wave illumination and are better imaged using a pulsed mode illumination scheme. This behavior challenges the accurate monitoring of some biological phenomena (e.g., RNA movement in the cell). Moreover, even though no crystal structure has been solved yet for Broccoli (another DFHBI-binding aptamer), the strong sequence homologies as well as photophysical behavior shared with Spinach suggest that both aptamers are very likely to possess an identical fluorogen-binding pocket [76]. Recently, the structure of Corn RNA in complex with DFHO has been resolved [73] and

revealed that, surprisingly, the fluorogen-binding pocket does not lie into a single RNA molecule but instead is formed by the interface of two interacting protomers of identical sequence, each made of four base quadruples and six adenine residues asymmetrically oriented. This preformed binding pocket can specifically accommodate a single DFHO and not only triggers its fluorescence but it also constitutes a highly protective environment preserving the dye from photobleaching over a long period of time [34]. Consequently, even though Corn/DFHO module is dimmer than the other systems, its strong photostability makes it well suited for the prolonged imaging of RNAs in live cells. Finally, the crystal structure of RNA Mango in complex with TO-1 helped explain in part the origin of the elevated affinity in the complex. Indeed, like the other aptamers, Mango possesses a planar platform made of G-quartets and interacts not only with the cyanine moiety but also with the PEG linker and the biotin group of the fluorogen [60]. Interestingly, both heterocycles of the cynanine are not coplanar but instead they make a 45 °C angle, suggesting that brighter mutants of the aptamer that would accommodate the cyanine more coplanarly could, in principle, be isolated by functional screening (a work currently in progress in our lab).

Up to now, RNA-based fluorogenic modules involving quenched fluorogen have been less characterized. However, even though these modules display a lower affinity than the aforementioned ones (Table 1), they have the great advantage of using very bright and photostable organic dyes as fluorogenic moiety (i.e., symmetrical cynanines [35,77], Sulforhodamines [55] or Rhodamine Green [32]), making them attractive for future developments.

## 3. Applications of RNA-Based Fluorogenic Modules

The development of RNA-based fluorogenic modules was initially motivated by the need for genetically encoded tools to monitor gene expression and regulation at the RNA level. However, the great flexibility and the ease to engineer these RNA molecules rapidly led to the development of new sets of fluorogenic reporters with applications both in vivo and in vitro (Figure 4).

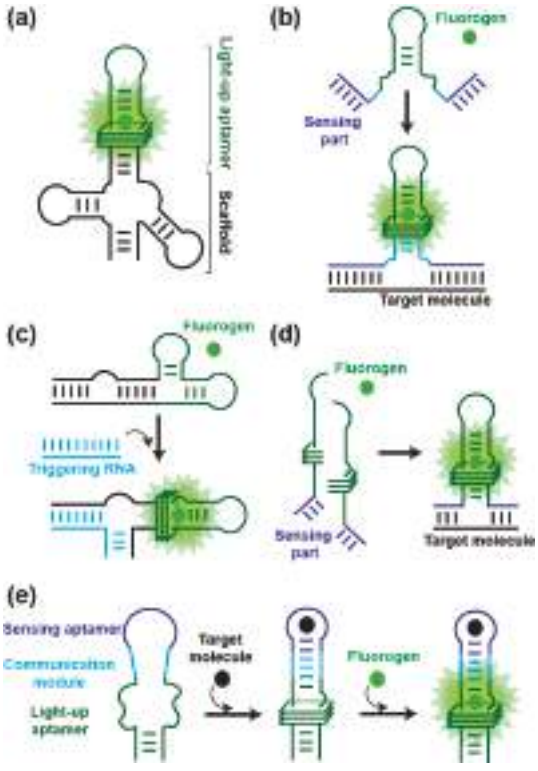


**Figure 4.** Light-up aptamers engineering and uses thereof. (**a**) Light-up RNA aptamers can be embedded into a scaffold RNA (here a tRNA) to improve folding efficiency and resistance to RNases [29,61]. The construct can either be directly expressed from an independent promoter or inserted into the sequence of a target mRNA. (**b**) Light-up aptamer sensing a target RNA in trans [77,78]. A key helix (light blue) of the light-up aptamer is engineered to weaken the structure of the RNA and destabilized the fluorogen-binding site. Furthermore, sequences complementary to the target nucleic acid (acting as a sensing part) are appended to both ends of the molecule (dark blue). Upon binding to the target molecule (in black), the structure of the light-up moiety is stabilized and its fluorogen-binding capacity is restored, leading to fluorescence emission (green shadow). (**c**) Light-up aptamer sensing a target RNA in trans via strand displacement [79–81]. Sequences are appended to both ends of the light-up aptamer and induce an alternative folding preventing the interaction of the aptamer with the fluorogen. However, the binding of the target RNA to the construct induces a conformational change restoring the structure of the light-up aptamer moiety and its fluorogen-binding capacity, leading to fluorescence emission (green shadow). (**d**) Sensing target nucleic acids using split light-up aptamers [82,83]. The aptamer is split into two halves, each possessing a sequence complementary to the target nucleic acid (acting as a sensing part, in dark blue). Whereas both halves cannot form a functional aptamer in the absence of the target nucleic acid, the presence of the latter drives the productive association of both molecules into a functional light-up aptamer able to emit fluorescence. (**e**) Allosteric light-up RNA aptamer [84,85]. The light-up aptamer is engineered to weaken the structure of the RNA and destabilize the fluorogen-binding site. Moreover, the sequence of a sensing aptamer (in dark blue) is inserted into that of the light-up aptamer via a communication module (in light blue). Upon the interaction of the sensing aptamer with a target molecule (e.g., a metabolite or a protein), the structure of the light-up aptamer is stabilized and its fluorogen-binding capacity is restored. Note that all the examples are shown with the Spinach aptamer, but these concepts can be extended to any other light-up aptamer.

### 3.1. Live-Cell Imaging of Biomolecules

#### 3.1.1. Live-Cell RNA Imaging

Direct expression of light-up RNA aptamers in cells can be challenging due to their degradation by cell nucleases. Therefore, the molecules are usually expressed inserted into a second RNA such as a transfer RNA (tRNA) [29,86] or a three-way junction [87] acting as a scaffold to both protect the aptamer from rapid degradation and assist its folding (Figure 4a). Expressing such constructs from a strong promoter (e.g., T7 RNA polymerase promoter in *E. coli*, 5S promoter in mammalian cells) allows the expression of abundant non-coding RNAs to be monitored in prokaryotes [29,32,55] and eukaryotes [29,31,34]. Moreover, recent publications reported on the possibility to insert Spinach-derived aptamers into the variable region of bacterial tRNAs [88], within an apical loop of the bacterial 16S ribosomal RNA [89] or in metazoan tRNA introns [90] while preserving the natural functionality of the carrier molecules. Being able to image these non-coding RNAs not only informs on their own expression but it can also be used to diagnose the whole associated pathway (e.g., Pol III transcription, translation, etc.). Spinach was also found suited for imaging messenger RNAs in organisms as diverse as bacteria [91–93], yeast [94], mammalian cells [61], viruses [95–97] and algae [98]. The limited brightness and poor photostability of Spinach and its derivatives initially limited its use to the imaging of mRNAs either aggregated [61] or labeled with tandem repeats of up to 64 copies of the aptamer [93]. However, an improved understanding the photophysics of DFHBI inactivation allowed devising pulsed excitation-based imaging procedures making it possible to monitor Spinach-labeled RNAs over a much longer period of time [75] and enabling imaging much less abundant mRNAs [93]. Furthermore, using spinning disk confocal microscopy and post-acquisition image analysis algorithms it was possible to track the nuclear export of yeast mRNA labeled with a single copy of Spinach [94]. Interestingly, these studies also revealed that inserting the light-up aptamer into the 3′ untranslated region of the mRNA did not affect the fate (i.e., localization, translation or stability) of the labeled molecule.

Direct insertion of light-up aptamers into target RNAs is mainly limited by the laborious genetics required for modifying the locus of each target gene. This limitation can nevertheless be overcome by using in trans-acting fluorogenic modules that are destabilized forms of the light-up aptamer [77,78] (Figure 4b). In this approach, the aptamer is engineered at two levels. First, a helix of the aptamer is truncated to weaken the structure of the RNA and abolish its capacity to interact with the fluorogen. Second, sequences complementary to the target RNA are appended at both extremities of the helix. Upon binding to the target RNA, the structure of the aptamer is stabilized and its capacity to bind and activate the fluorogen is restored. Provided an unstructured region is accessible in the target RNA, this approach can be used to image both mRNA [77,78] and small non-coding RNA [99]. Moreover, embedding the aptamer into a scaffold RNA and triggering its activation by a strand-displacement mechanism respectively improve the stability of the fluorogenic module and increase signal amplitude [80,81] (Figure 4c). Further improvement in detection specificity and signal amplitude can be obtained by using split aptamers [82,83] (Figure 4d). Recently, a split version of the Broccoli light-up aptamer was also generated and embedded into an AND logic gate for sensing the simultaneous presence of two target RNAs in vivo [100].

#### 3.1.2. Live-Cell Imaging of Metabolites and Proteins

Its great structural flexibility enables RNA to fold into aptamers able to specifically recognize virtually any type of molecule. Moreover, if the interaction between the aptamer and its target leads to a structural remodeling or even the stabilization of RNA structure, then such aptamer can be used for the conception of an allosteric biosensor in which a sensing module is connected to a reporting module via a communication module (Figure 4e). Briefly, the structure of the reporting module (a ribozyme or a light-up aptamer) is destabilized which keeps its function (e.g., RNA cleavage or fluorescence emission) in an off state. However, the presence of the target analyte induces a structural

change (or stabilization) of the sensing aptamer that is transmitted to the reporting module via the communication module. The structure of the reporting RNA is in turn stabilized and its function restored. This strategy was originally pioneered using ribozymes as reporting modules [101] and early work with MG aptamer allowed establishing the proof-of-concept experiment using light-up aptamers as reporter [84]. Since then, Spinach RNA-based fluorogenic biosensors have been developed to specifically report on the presence of metabolites such as FMN [84], cyclic-di-GMP [85,102–104], cyclic-di-AMP [105], cyclic AMP-GMP [106,107], cyclic-AMP [108], S-adenosylmethionine (SAM) [109], S-adenosyl-L-homocysteine (SAH) [110], Thiamine Pyrophosphate (TPP) [111] and neurotransmitter precursors [112]. The majority of these biosensors are built using riboswitch-derived aptamers. Indeed, since these molecules have naturally evolved to switch RNA structure in cellular environment, these aptamers possess the required structural flexibility and are able to efficiently discriminate their cognate target from closely related analogues contained in the cell. Finally, even though they were less used, allosteric biosensors can also be developed for protein detection [113]. With such biosensor in hands it is then possible to precisely detect and quantify a target molecule in a dynamic way and with single cell resolution. This allows the dynamics of a biological pathway to be monitored, but also to characterize the enzymes involved in this pathway, paving the way for drug discovery applications [105–107].

Whereas both sensing and reporting modules have key roles in the proper function of allosteric fluorogenic biosensors, the communication module is probably the most critical element, as it drives the information from one aptamer to the other. Usually, a communication module is rationally designed based on thermodynamic considerations since such module would be extremely challenging to isolate using a SELEX approach. However, the recent advances in high-throughput screening technologies introduced above offer a new way of rapidly identifying optimal communication modules. For instance, a large-scale integration microfluidic device was used to systematically screen a library of 94 different Spinach-based glycine biosensor containing different communication modules while measuring their response to various glycine concentrations [114]. Therefore, a single experiment allows accessing both the fluorescence amplitude of many biosensors as well as their affinity for the glycine and their dynamic range. Consequently, assisting the development of new biosensors by high-throughput screening technologies should both accelerate their development and improve their performances. Finally, one should note that a communication might be dispensable if one simply wants to develop an aptamer-based protein-targeting fluorescent probe. In that case, the binding aptamer can be directly connected to a light-up aptamer as recently exemplified by the use of a fluorogenic cyanine-binding aptamer fused with a VEGF-binding aptamer [27].

### 3.2. In Vitro Applications

The possibility of detecting RNA via fluorogenic assays opened a whole bunch of applications in vitro. First, inserting the sequence of a light-up aptamer into that of another RNA allows monitoring in real-time the in vitro transcription of the construct [35,115] and, doing so, to compute its transcription rate while decorrelating it from the translation rate of an encoded protein. This is of particular importance in experiments aiming at engineering genetic circuits, especially for generating artificial cells [116–118]. Being able to monitor transcription activity in an automatable way makes also possible to set-up high-throughput microtiter plate-based screening of drugs targeting RNA polymerase activity [115]. Drug screening actually represents a second important set of applications of light-up aptamers in vitro. For instance, the fluorogenic function of the RNA can be transiently inactivated by modifying (e.g., methylating) a key nucleotide to convert the aptamer into a fluorogenic substrate of a modification-removing enzyme such as demethylases, a class of enzymes involved in several diseases [119]. Monitoring reaction product apparition by the mean of the fluorogenic allosteric biosensors introduced above [110,120,121] represents an alternative way of assaying enzyme activity. In any case, these different strategies can easily be transposed to microtiter plate format to set-up a

high-throughput screening workflow [115,119,120] and even an ultrahigh-throughput one by using droplet-based microfluidics [121].

The great ability to predict to some extent the folding of an RNA sequence makes possible the design of molecular circuits composed of two or several RNA (or DNA) elements trapped by folding to keep the circuit silent [122,123]. However, in the presence of one or several target molecules, sensing elements undergo structural rearrangements activating the circuit to compute the information and eventually reports the presence of the targets via engineered light-up aptamer [79,83,124]. Whereas simple circuit made of a split light-up aptamer directly sensing the target molecule would lead to a signal stoichiometric to the input [124], the implementation of an enzyme-free amplification loop [122,123,125] is expected to significantly increase the sensitivity of these assays.

Split and full-length light-up aptamers can also be used to devise in vitro procedures aimed at assisting catalytic RNAs engineering [126,127], tracking RNA-based molecular complexes as well as monitoring the formation of supramolecular assemblies such as those used in RNA nanotechnology [128–131] directly through fluorescence emission measurements. Moreover, the proper size and integrity of light-up-labeled RNAs can also be verified by gel electrophoresis followed by specific staining of the target RNAs by the fluorogen directly in the gel [87,131]. Finally, light-up aptamers inserted into a target RNA can serve as handles to specifically fish-out the labeled RNA and its associated partners in native conditions by incubating a reaction mixture (e.g., a cell lysate) with a biotinylated fluorogen and purifying the resulting complex on a streptavidin-conjugated resin [132].

## 4. Conclusions

Over the past decade, significant efforts were devoted to the development of new RNA-based fluorogenic modules leading to a toolbox of modules covering the whole visible spectrum (Table 1). Many of these modules are significantly brighter than the widely used GFP and, conversely to their protein counterparts, they do not require oxygen since no maturation step is needed. Therefore, labeling target RNAs with light-up aptamers is not only subjected to a low fluorescent background, but RNAs can also be monitored in conditions in which fluorescent proteins could not be used (e.g., anaerobiosis [104]). Besides direct RNA imaging in vivo, RNA-based fluorogenic modules also found a wide range of applications as briefly reviewed in this article and it is very likely that many new ones shall be developed in a near future (see below).

Interestingly, even though current modules are already pretty efficient and permitted multiple questions to be answered, none of them completely fulfills all the criteria enounced in Section 2 of this review, suggesting that there is still room for improvement in terms of sensitivity and robustness. Indeed, most of the current light-up aptamers were obtained by SELEX using moderate selection pressures and have dissociation constant (so affinity) for the fluorogen of tens of nM or more. Thus far, Mango is the only RNA displaying a very high affinity for its fluorogen ($K_D$ of a few nM), likely resulting from the use of very stringent wash and elution conditions. Therefore, applying the same concept to other systems could yield modules with much higher affinity. This would reduce the amount of dye in the assays and lead to a gain in sensitivity by improving the contrast of the experiment [37]. Moreover, since SELEX-derived RNAs were selected for their capacity to bind the fluorogen rather than their capacity to generate fluorescent complexes, it is likely that the fluorescence of most of the current modules may still be sub-optimal. Indeed, our own experience with Spinach [65] and Mango (on-going work in our lab) RNAs shows that revisiting these aptamers by a screening approach may significantly increase their light-up capacity. Such improvement could result from an increased brightness but also from a higher photostability. Indeed, both properties rely not only on the fluorogen itself but also on capacity of the RNA to properly accommodate it and protect it from unwanted photoisomerization and photobleaching. This last point was recently exemplified by Corn, an RNA isolated by SELEX in tandem with FACS screenings, that forms with DFHO a complex displaying an extraordinary high photostability [34]. This photostability likely results from a caging of the fluorogen preventing its rapid isomerization [73]. This property is clearly contributed

by the RNA since lighting-up DFHO with Broccoli did not yield a significant photostability [34]. Therefore, we anticipate that future selection schemes combining conventional SELEX with an (ultra)high-throughput functional screening (e.g., FACS or microfluidic-based screening) together with next-generation sequencing could lead to the efficient discovery of light-up aptamers with superior turn-on and photostabilizing properties. This new generation of molecules should further enlarge the already wide application range of RNA-based fluorogenic modules. For example, they would allow labeling target RNAs with a limited number of aptamer repeats (ideally a single one) to make possible single molecule resolution, thus enabling the tracking of low abundant RNA molecules, for instance using super-resolution microscopy [133]. New generations of fluorogenic modules would not only allow highly sensitive gene expression monitoring, but they could also serve to set-up new drug screening pipelines as well as a variety of analytical platforms such as microarrays developed to sense target molecules with size ranging from ions (recently exemplified by the capacity of Spinach to specifically sense lead [134]) to more complex protein using allosteric biosensors such as those introduce in this review. Finally, whereas this review was focused on RNA aptamers, DNA light-up aptamers were also reported [28,52] and one should consider the possibility of applying the concepts exposed throughout this review to the development of new DNA-based sensors.

**Acknowledgments:** We thank Redmond Smyth for his help in manuscript proofreading. This work has been published under the framework of the LabExNetRNA (ANR-10-LABX-0036_NETRNA) and benefits from a funding from the state managed by the French National Research Agency as part of the Investments for the Future Program. It also received the financial support of the Agence Nationale de la Recherche (ANR-16-CE11-0010-01) and was supported by the Université de Strasbourg and the Centre National de la Recherche Scientifique.

**Author Contributions:** All authors analyzed the literature and wrote the paper. Farah Bouhedda and Alexis Autour equally contributed to this work.

**Conflicts of Interest:** The authors declare no conflict of interest.

## Abbreviations

| | |
|---|---|
| Cy3-BHQ1 | Cyanine 3-Black Hole Quencher 1 |
| DIR | Dimethyl Indole Red |
| DFHBI | 3,5-difluoro-4-hydroxybenzylidene imidazolinone |
| DFHBI-1(2)T | 3,5-difluoro-4-hydroxybenzylidene imidazolinone 1 (2) trifluoroethyl |
| DFHO | 3,5-difluoro-4-hydroxybenzylidene imidazolinone-2-oxime |
| FACS | Fluorescence Activated Cell Sorter |
| GFP | Green Fluorescent Protein |
| MG | Malachite Green |
| OTB | Oxazole Thiazole Blue |
| RG-DN | Rhodamine Green-DiNitroaniline |
| SELEX | Systematic Evolution of Ligands by EXponential enrichment |
| SR-DN | Sulforhodamine-DiNitroaniline |
| TMR-DN | Tertamethyl rhodamine-DiNitroaniline |
| TO-1 (3) | Thiazole Orange 1 (3) |

## References

1. Schaferling, M. The art of fluorescence imaging with chemical sensors. *Angew. Chem.* **2012**, *51*, 3532–3554. [CrossRef] [PubMed]
2. Wong, J.K.; Todd, M.H.; Rutledge, P.J. Recent advances in macrocyclic fluorescent probes for ion sensing. *Molecules* **2017**, *22*, 200. [CrossRef] [PubMed]
3. Cui, C.; Shu, W.; Li, P. Fluorescence in situ hybridization: Cell-based genetic diagnostic and research applications. *Front. Cell Dev. Biol.* **2016**, *4*, 89. [CrossRef] [PubMed]
4. Shimomura, O.; Johnson, F.H.; Saiga, Y. Extraction, purification and properties of aequorin, a bioluminescent protein from the luminous hydromedusan, Aequorea. *J. Cell. Comp. Physiol.* **1962**, *59*, 223–239. [CrossRef] [PubMed]

5. Cody, C.W.; Prasher, D.C.; Westler, W.M.; Prendergast, F.G.; Ward, W.W. Chemical structure of the hexapeptide chromophore of the Aequorea green-fluorescent protein. *Biochemistry* **1993**, *32*, 1212–1218. [CrossRef] [PubMed]
6. Chalfie, M.; Tu, Y.; Euskirchen, G.; Ward, W.W.; Prasher, D.C. Green fluorescent protein as a marker for gene expression. *Science* **1994**, *263*, 802–805. [CrossRef] [PubMed]
7. Heim, R.; Prasher, D.C.; Tsien, R.Y. Wavelength mutations and posttranslational autoxidation of green fluorescent protein. *Proc. Natl. Acad. Sci. USA* **1994**, *91*, 12501–12504. [CrossRef] [PubMed]
8. Ormo, M.; Cubitt, A.B.; Kallio, K.; Gross, L.A.; Tsien, R.Y.; Remington, S.J. Crystal structure of the Aequorea victoria green fluorescent protein. *Science* **1996**, *273*, 1392–1395. [CrossRef] [PubMed]
9. Chudakov, D.M.; Matz, M.V.; Lukyanov, S.; Lukyanov, K.A. Fluorescent proteins and their applications in imaging living cells and tissues. *Physiol. Rev.* **2010**, *90*, 1103–1163. [CrossRef] [PubMed]
10. Griffin, B.A.; Adams, S.R.; Tsien, R.Y. Specific covalent labeling of recombinant protein molecules inside live cells. *Science* **1998**, *281*, 269–272. [CrossRef] [PubMed]
11. Correa, I.R., Jr. Live-cell reporters for fluorescence imaging. *Curr. Opin. Chem. Biol.* **2014**, *20*, 36–45. [CrossRef] [PubMed]
12. Li, C.; Tebo, A.G.; Gautier, A. Fluorogenic labeling strategies for biological imaging. *Int. J. Mol. Sci.* **2017**, *18*, 1473. [CrossRef] [PubMed]
13. Bertrand, E.; Chartrand, P.; Schaefer, M.; Shenoy, S.M.; Singer, R.H.; Long, R.M. Localization of *ASH1* mRNA particles in living yeast. *Mol. Cell* **1998**, *2*, 437–445. [CrossRef]
14. Wu, B.; Chen, J.; Singer, R.H. Background free imaging of single mRNAs in live cells using split fluorescent proteins. *Sci. Rep.* **2014**, *4*, 3615. [CrossRef] [PubMed]
15. Buxbaum, A.R.; Haimovich, G.; Singer, R.H. In the right place at the right time: Visualizing and understanding mRNA localization. *Nat. Rev. Mol. Cell Biol.* **2015**, *16*, 95–109. [CrossRef] [PubMed]
16. Holeman, L.A.; Robinson, S.L.; Szostak, J.W.; Wilson, C. Isolation and characterization of fluorophore-binding RNA aptamers. *Fold. Des.* **1998**, *3*, 423–431. [CrossRef]
17. Shin, I.; Ray, J.; Gupta, V.; Ilgu, M.; Beasley, J.; Bendickson, L.; Mehanovic, S.; Kraus, G.A.; Nilsen-Hamilton, M. Live-cell imaging of pol II promoter activity to monitor gene expression with RNA IMAGEtag reporters. *Nucleic Acids Res.* **2014**, *42*, e90. [CrossRef] [PubMed]
18. Eydeler, K.; Magbanua, E.; Werner, A.; Ziegelmuller, P.; Hahn, U. Fluorophore binding aptamers as a tool for RNA visualization. *Biophys. J.* **2009**, *96*, 3703–3707. [CrossRef] [PubMed]
19. Babendure, J.R.; Adams, S.R.; Tsien, R.Y. Aptamers switch on fluorescence of triphenylmethane dyes. *J. Am. Chem. Soc.* **2003**, *125*, 14716–14717. [CrossRef] [PubMed]
20. Grate, D.; Wilson, C. Laser-mediated, site-specific inactivation of RNA transcripts. *Proc. Natl. Acad. Sci. USA* **1999**, *96*, 6131–6136. [CrossRef] [PubMed]
21. Ouellet, J. RNA fluorescence with light-up aptamers. *Front. Chem.* **2016**, *4*, 29. [CrossRef] [PubMed]
22. Rath, A.K.; Rentmeister, A. Genetically encoded tools for RNA imaging in living cells. *Curr. Opin. Biotechnol.* **2015**, *31*, 42–49. [CrossRef] [PubMed]
23. Pauff, S.; Withers, J.M.; McKean, I.J.; Mackay, S.P.; Burley, G.A. Synthetic biological approaches for RNA labelling and imaging: Design principles and future opportunities. *Curr. Opin. Biotechnol.* **2017**, *48*, 153–158. [CrossRef] [PubMed]
24. Schneider, A.F.; Hackenberger, C.P. Fluorescent labelling in living cells. *Curr. Opin. Biotechnol.* **2017**, *48*, 61–68. [CrossRef] [PubMed]
25. Van Gijtenbeek, L.A.; Kok, J. Illuminating messengers: An update and outlook on RNA visualization in bacteria. *Front. Microbiol.* **2017**, *8*, 1161. [CrossRef] [PubMed]
26. Heim, R.; Cubitt, A.B.; Tsien, R.Y. Improved green fluorescence. *Nature* **1995**, *373*, 663–664. [CrossRef] [PubMed]
27. Tan, X.; Constantin, T.P.; Sloane, K.L.; Waggoner, A.S.; Bruchez, M.P.; Armitage, B.A. Fluoromodules consisting of a promiscuous RNA aptamer and red or blue fluorogenic cyanine dyes: Selection, characterization, and bioimaging. *J. Am. Chem. Soc.* **2017**, *139*, 9001–9009. [CrossRef] [PubMed]
28. Sando, S.; Narita, A.; Hayami, M.; Aoyama, Y. Transcription monitoring using fused RNA with a dye-binding light-up aptamer as a tag: A blue fluorescent RNA. *Chem. Commun.* **2008**, *44*, 3858–3860. [CrossRef] [PubMed]
29. Paige, J.S.; Wu, K.Y.; Jaffrey, S.R. RNA mimics of green fluorescent protein. *Science* **2011**, *333*, 642–646. [CrossRef] [PubMed]

30. Song, W.; Strack, R.L.; Svensen, N.; Jaffrey, S.R. Plug-and-play fluorophores extend the spectral properties of Spinach. *J. Am. Chem. Soc.* **2014**, *136*, 1198–1201. [CrossRef] [PubMed]
31. Filonov, G.S.; Moon, J.D.; Svensen, N.; Jaffrey, S.R. Broccoli: Rapid selection of an RNA mimic of green fluorescent protein by fluorescence-based selection and directed evolution. *J. Am. Chem. Soc.* **2014**, *136*, 16299–16308. [CrossRef] [PubMed]
32. Arora, A.; Sunbul, M.; Jaschke, A. Dual-colour imaging of RNAs using quencher- and fluorophore-binding aptamers. *Nucleic Acids Res.* **2015**, *43*, e144. [CrossRef] [PubMed]
33. Dolgosheina, E.V.; Jeng, S.C.; Panchapakesan, S.S.; Cojocaru, R.; Chen, P.S.; Wilson, P.D.; Hawkins, N.; Wiggins, P.A.; Unrau, P.J. RNA Mango aptamer-fluorophore: A bright, high-affinity complex for RNA labeling and tracking. *ACS Chem. Biol.* **2014**, *9*, 2412–2420. [CrossRef] [PubMed]
34. Song, W.; Filonov, G.S.; Kim, H.; Hirsch, M.; Li, X.; Moon, J.D.; Jaffrey, S.R. Imaging RNA polymerase III transcription using a photostable RNA-fluorophore complex. *Nat. Chem. Biol.* **2017**, *13*, 1187–1194. [CrossRef] [PubMed]
35. Murata, A.; Sato, S.; Kawazoe, Y.; Uesugi, M. Small-molecule fluorescent probes for specific RNA targets. *Chem. Commun.* **2011**, *47*, 4712–4714. [CrossRef] [PubMed]
36. Constantin, T.P.; Silva, G.L.; Robertson, K.L.; Hamilton, T.P.; Fague, K.; Waggoner, A.S.; Armitage, B.A. Synthesis of new fluorogenic cyanine dyes and incorporation into RNA fluoromodules. *Org. Lett.* **2008**, *10*, 1561–1564. [CrossRef] [PubMed]
37. Dolgosheina, E.V.; Unrau, P.J. Fluorophore-binding RNA aptamers and their applications. *Wiley Interdiscip. Rev. RNA* **2016**, *7*, 843–851. [CrossRef] [PubMed]
38. Klymchenko, A.S. Solvatochromic and fluorogenic dyes as environment-sensitive probes: Design and biological applications. *Acc. Chem. Res.* **2017**, *50*, 366–375. [CrossRef] [PubMed]
39. Lǒber, G. The fluorescence of dye-nucleic acid complexes. *J. Lumin.* **1981**, *22*, 221–265. [CrossRef]
40. Olmsted, J., 3rd; Kearns, D.R. Mechanism of ethidium bromide fluorescence enhancement on binding to nucleic acids. *Biochemistry* **1977**, *16*, 3647–3654. [CrossRef] [PubMed]
41. Jin, R.; Breslauer, K.J. Characterization of the minor groove environment in a drug-DNA complex: Bisbenzimide bound to the poly[d(AT)].Poly[d(AT)]duplex. *Proc. Natl. Acad. Sci. USA* **1988**, *85*, 8939–8942. [CrossRef] [PubMed]
42. Sando, S.; Narita, A.; Aoyama, Y. Light-up hoechst-DNA aptamer pair: Generation of an aptamer-selective fluorophore from a conventional DNA-staining dye. *Chembiochem* **2007**, *8*, 1795–1803. [CrossRef] [PubMed]
43. Kraus, G.A.; Jeon, I.; Nilsen-Hamilton, M.; Awad, A.M.; Banerjee, J.; Parvin, B. Fluorinated analogs of malachite green: Synthesis and toxicity. *Molecules* **2008**, *13*, 986–994. [CrossRef] [PubMed]
44. Lux, J.; Pena, E.J.; Bolze, F.; Heinlein, M.; Nicoud, J.F. Malachite green derivatives for two-photon RNA detection. *Chembiochem* **2012**, *13*, 1206–1213. [CrossRef] [PubMed]
45. Ilgu, M.; Ray, J.; Bendickson, L.; Wang, T.; Geraskin, I.M.; Kraus, G.A.; Nilsen-Hamilton, M. Light-up and FRET aptamer reporters; evaluating their applications for imaging transcription in eukaryotic cells. *Methods* **2016**, *98*, 26–33. [CrossRef] [PubMed]
46. Saurabh, S.; Perez, A.M.; Comerci, C.J.; Shapiro, L.; Moerner, W.E. Super-resolution imaging of live bacteria cells using a genetically directed, highly photostable fluoromodule. *J. Am. Chem. Soc.* **2016**, *138*, 10398–10401. [CrossRef] [PubMed]
47. Silva, G.L.; Ediz, V.; Yaron, D.; Armitage, B.A. Experimental and computational investigation of unsymmetrical cyanine dyes: Understanding torsionally responsive fluorogenic dyes. *J. Am. Chem. Soc.* **2007**, *129*, 5710–5718. [CrossRef] [PubMed]
48. Armitage, B.A. Cyanine dye–nucleic acid interactions. In *Heterocyclic Polymethine Dyes: Synthesis, Properties and Applications*; Strekowski, L., Ed.; Springer: Berlin/Heidelberg, Germany, 2008; pp. 11–29.
49. Lee, L.G.; Chen, C.H.; Chiu, L.A. Thiazole orange: A new dye for reticulocyte analysis. *Cytometry* **1986**, *7*, 508–517. [CrossRef] [PubMed]
50. Nygren, J.; Svanvik, N.; Kubista, M. The interactions between the fluorescent dye thiazole orange and DNA. *Biopolymers* **1998**, *46*, 39–51. [CrossRef]
51. Walker, C.L.; Lukyanov, K.A.; Yampolsky, I.V.; Mishin, A.S.; Bommarius, A.S.; Duraj-Thatte, A.M.; Azizi, B.; Tolbert, L.M.; Solntsev, K.M. Fluorescence imaging using synthetic GFP chromophores. *Curr. Opin. Chem. Biol.* **2015**, *27*, 64–74. [CrossRef] [PubMed]

52. Feng, G.; Luo, C.; Yi, H.; Yuan, L.; Lin, B.; Luo, X.; Hu, X.; Wang, H.; Lei, C.; Nie, Z.; et al. DNA mimics of red fluorescent proteins (RFP) based on G-quadruplex-confined synthetic RFP chromophores. *Nucleic Acids Res.* **2017**, *45*, 10380–10392. [CrossRef] [PubMed]
53. Sparano, B.A.; Koide, K. A strategy for the development of small-molecule-based sensors that strongly fluoresce when bound to a specific RNA. *J. Am. Chem. Soc.* **2005**, *127*, 14954–14955. [CrossRef] [PubMed]
54. Sparano, B.A.; Koide, K. Fluorescent sensors for specific RNA: A general paradigm using chemistry and combinatorial biology. *J. Am. Chem. Soc.* **2007**, *129*, 4785–4794. [CrossRef] [PubMed]
55. Sunbul, M.; Jaschke, A. Contact-mediated quenching for RNA imaging in bacteria with a fluorophore-binding aptamer. *Angew. Chem.* **2013**, *52*, 13401–13404. [CrossRef] [PubMed]
56. Ellington, A.D.; Szostak, J.W. In vitro selection of RNA molecules that bind specific ligands. *Nature* **1990**, *346*, 818–822. [CrossRef] [PubMed]
57. Tuerk, C.; Gold, L. Systematic evolution of ligands by exponential enrichment: RNA ligands to bacteriophage T4 DNA polymerase. *Science* **1990**, *249*, 505–510. [CrossRef] [PubMed]
58. Stoltenburg, R.; Reinemann, C.; Strehlitz, B. Selex—A (r)evolutionary method to generate high-affinity nucleic acid ligands. *Biomol. Eng.* **2007**, *24*, 381–403. [CrossRef] [PubMed]
59. Davis, J.H.; Szostak, J.W. Isolation of high-affinity GTP aptamers from partially structured RNA libraries. *Proc. Natl. Acad. Sci. USA* **2002**, *99*, 11616–11621. [CrossRef] [PubMed]
60. Trachman, R.J., 3rd; Demeshkina, N.A.; Lau, M.W.L.; Panchapakesan, S.S.S.; Jeng, S.C.Y.; Unrau, P.J.; Ferre-D'Amare, A.R. Structural basis for high-affinity fluorophore binding and activation by RNA Mango. *Nat. Chem. Biol.* **2017**, *13*, 807–813. [CrossRef] [PubMed]
61. Strack, R.L.; Disney, M.D.; Jaffrey, S.R. A superfolding Spinach2 reveals the dynamic nature of trinucleotide repeat-containing RNA. *Nat. Methods* **2013**, *10*, 1219–1224. [CrossRef] [PubMed]
62. Lee, J.; Lee, K.H.; Jeon, J.; Dragulescu-Andrasi, A.; Xiao, F.; Rao, J. Combining SELEX screening and rational design to develop light-up fluorophore-RNA aptamer pairs for RNA tagging. *ACS Chem. Biol.* **2010**, *5*, 1065–1074. [CrossRef] [PubMed]
63. Zou, J.; Huang, X.; Wu, L.; Chen, G.; Dong, J.; Cui, X.; Tang, Z. Selection of intracellularly functional RNA mimics of green fluorescent protein using fluorescence-activated cell sorting. *J. Mol. Evol.* **2015**, *81*, 172–178. [CrossRef] [PubMed]
64. Ketterer, S.; Fuchs, D.; Weber, W.; Meier, M. Systematic reconstruction of binding and stability landscapes of the fluorogenic aptamer Spinach. *Nucleic Acids Res.* **2015**, *43*, 9564–9572. [CrossRef] [PubMed]
65. Autour, A.; Westhof, E.; Ryckelynck, M. iSpinach: A fluorogenic RNA aptamer optimized for in vitro applications. *Nucleic Acids Res.* **2016**, *44*, 2491–2500. [CrossRef] [PubMed]
66. Autour, A.; Ryckelynck, M. Ultrahigh-throughput improvement and discovery of enzymes using droplet-based microfluidic screening. *Micromachines* **2017**, *8*, 128. [CrossRef]
67. Ryckelynck, M.; Baudrey, S.; Rick, C.; Marin, A.; Coldren, F.; Westhof, E.; Griffiths, A.D. Using droplet-based microfluidics to improve the catalytic properties of RNA under multiple-turnover conditions. *RNA* **2015**, *21*, 458–469. [CrossRef] [PubMed]
68. Trachman, R.J., 3rd; Truong, L.; Ferre-D'Amare, A.R. Structural principles of fluorescent RNA aptamers. *Trends Pharmacol.Sci.* **2017**, *38*, 928–939. [CrossRef] [PubMed]
69. Baugh, C.; Grate, D.; Wilson, C. 2.8 a crystal structure of the malachite green aptamer. *J. Mol. Biol.* **2000**, *301*, 117–128. [CrossRef] [PubMed]
70. Huang, H.; Suslov, N.B.; Li, N.S.; Shelke, S.A.; Evans, M.E.; Koldobskaya, Y.; Rice, P.A.; Piccirilli, J.A. A G-quadruplex-containing RNA activates fluorescence in a GFP-like fluorophore. *Nat. Chem. Biol.* **2014**, *10*, 686–691. [CrossRef] [PubMed]
71. Warner, K.D.; Chen, M.C.; Song, W.; Strack, R.L.; Thorn, A.; Jaffrey, S.R.; Ferre-D'Amare, A.R. Structural basis for activity of highly efficient RNA mimics of green fluorescent protein. *Nat. Struct. Mol. Biol.* **2014**, *21*, 658–663. [CrossRef] [PubMed]
72. Fernandez-Millan, P.; Autour, A.; Ennifar, E.; Westhof, E.; Ryckelynck, M. Crystal structure and fluorescence properties of the iSpinach aptamer in complex with dfhbi. *RNA* **2017**, *23*, 1788–1795. [CrossRef] [PubMed]
73. Warner, K.D.; Sjekloca, L.; Song, W.; Filonov, G.S.; Jaffrey, S.R.; Ferre-D'Amare, A.R. A homodimer interface without base pairs in an RNA mimic of red fluorescent protein. *Nat. Chem. Biol.* **2017**, *13*, 1195–1201. [CrossRef] [PubMed]

74. Jeng, S.C.; Chan, H.H.; Booy, E.P.; McKenna, S.A.; Unrau, P.J. Fluorophore ligand binding and complex stabilization of the RNA Mango and RNA Spinach aptamers. *RNA* **2016**, *22*, 1884–1892. [CrossRef] [PubMed]
75. Han, K.Y.; Leslie, B.J.; Fei, J.; Zhang, J.; Ha, T. Understanding the photophysics of the Spinach-DFHBI RNA aptamer-fluorogen complex to improve live-cell RNA imaging. *J. Am. Chem. Soc.* **2013**, *135*, 19033–19038. [CrossRef] [PubMed]
76. Ageely, E.A.; Kartje, Z.J.; Rohilla, K.J.; Barkau, C.L.; Gagnon, K.T. Quadruplex-flanking stem structures modulate the stability and metal ion preferences of RNA mimics of GFP. *ACS Chem. Biol.* **2016**, *11*, 2398–2406. [CrossRef] [PubMed]
77. Sato, S.; Watanabe, M.; Katsuda, Y.; Murata, A.; Wang, D.O.; Uesugi, M. Live-cell imaging of endogenous mRNAs with a small molecule. *Angew. Chem.* **2015**, *54*, 1855–1858. [CrossRef] [PubMed]
78. Ong, W.Q.; Citron, Y.R.; Sekine, S.; Huang, B. Live cell imaging of endogenous mRNA using RNA-based fluorescence "turn-on" probe. *ACS Chem. Biol.* **2017**, *12*, 200–205. [CrossRef] [PubMed]
79. Bhadra, S.; Ellington, A.D. A Spinach molecular beacon triggered by strand displacement. *RNA* **2014**, *20*, 1183–1194. [CrossRef] [PubMed]
80. Huang, K.; Doyle, F.; Wurz, Z.E.; Tenenbaum, S.A.; Hammond, R.K.; Caplan, J.L.; Meyers, B.C. Fastmir: An RNA-based sensor for in vitro quantification and live-cell localization of small RNAs. *Nucleic Acids Res.* **2017**, *45*, e130. [CrossRef] [PubMed]
81. Ying, Z.M.; Wu, Z.; Tu, B.; Tan, W.; Jiang, J.H. Genetically encoded fluorescent RNA sensor for ratiometric imaging of microRNA in living tumor cells. *J. Am. Chem. Soc.* **2017**, *139*, 9779–9782. [CrossRef] [PubMed]
82. Kolpashchikov, D.M. Binary malachite green aptamer for fluorescent detection of nucleic acids. *J. Am. Chem. Soc.* **2005**, *127*, 12442–12443. [CrossRef] [PubMed]
83. Kikuchi, N.; Kolpashchikov, D.M. A universal split Spinach aptamer (USSA) for nucleic acid analysis and DNA computation. *Chem. Commun.* **2017**, *53*, 4977–4980. [CrossRef] [PubMed]
84. Stojanovic, M.N.; Kolpashchikov, D.M. Modular aptameric sensors. *J. Am. Chem. Soc.* **2004**, *126*, 9266–9270. [CrossRef] [PubMed]
85. Kellenberger, C.A.; Wilson, S.C.; Sales-Lee, J.; Hammond, M.C. RNA-based fluorescent biosensors for live cell imaging of second messengers cyclic di-GMP and cyclic AMP-GMP. *J. Am. Chem. Soc.* **2013**, *135*, 4906–4909. [CrossRef] [PubMed]
86. Ponchon, L.; Dardel, F. Recombinant RNA technology: The tRNA scaffold. *Nat. Methods* **2007**, *4*, 571–576. [CrossRef] [PubMed]
87. Filonov, G.S.; Kam, C.W.; Song, W.; Jaffrey, S.R. In-gel imaging of RNA processing using Broccoli reveals optimal aptamer expression strategies. *Chem. Biol.* **2015**, *22*, 649–660. [CrossRef] [PubMed]
88. Masuda, I.; Igarashi, T.; Sakaguchi, R.; Nitharwal, R.G.; Takase, R.; Han, K.Y.; Leslie, B.J.; Liu, C.; Gamper, H.; Ha, T.; et al. A genetically encoded fluorescent tRNA is active in live-cell protein synthesis. *Nucleic Acids Res.* **2017**, *45*, 4081–4093. [CrossRef] [PubMed]
89. Okuda, M.; Fourmy, D.; Yoshizawa, S. Use of baby Spinach and Broccoli for imaging of structured cellular RNAs. *Nucleic Acids Res.* **2017**, *45*, 1404–1415. [CrossRef] [PubMed]
90. Lu, Z.; Filonov, G.S.; Noto, J.J.; Schmidt, C.A.; Hatkevich, T.L.; Wen, Y.; Jaffrey, S.R.; Matera, A.G. Metazoan tRNA introns generate stable circular RNAs in vivo. *RNA* **2015**, *21*, 1554–1565. [CrossRef] [PubMed]
91. Pothoulakis, G.; Ceroni, F.; Reeve, B.; Ellis, T. The Spinach RNA aptamer as a characterization tool for synthetic biology. *ACS Synth. Biol.* **2013**, *3*, 182–187. [CrossRef] [PubMed]
92. Ellefson, J.W.; Meyer, A.J.; Hughes, R.A.; Cannon, J.R.; Brodbelt, J.S.; Ellington, A.D. Directed evolution of genetic parts and circuits by compartmentalized partnered replication. *Nat. Biotechnol.* **2014**, *32*, 97–101. [CrossRef] [PubMed]
93. Zhang, J.; Fei, J.; Leslie, B.J.; Han, K.Y.; Kuhlman, T.E.; Ha, T. Tandem Spinach array for mRNA imaging in living bacterial cells. *Sci. Rep.* **2015**, *5*, 17295. [CrossRef] [PubMed]
94. Guet, D.; Burns, L.T.; Maji, S.; Boulanger, J.; Hersen, P.; Wente, S.R.; Salamero, J.; Dargemont, C. Combining Spinach-tagged RNA and gene localization to image gene expression in live yeast. *Nat. Commun.* **2015**, *6*, 8882. [CrossRef] [PubMed]
95. Tsvetkova, I.B.; Yi, G.; Yi, Y.; Kao, C.C.; Dragnea, B.G. Segmented GFP-like aptamer probes for functional imaging of viral genome trafficking. *Virus Res.* **2015**, *210*, 291–297. [CrossRef] [PubMed]
96. Burch, B.D.; Garrido, C.; Margolis, D.M. Detection of human immunodeficiency virus RNAs in living cells using Spinach RNA aptamers. *Virus Res.* **2017**, *228*, 141–146. [CrossRef] [PubMed]

97. Nilaratanakul, V.; Hauer, D.A.; Griffin, D.E. Development and characterization of sindbis virus with encoded fluorescent RNA aptamer Spinach2 for imaging of replication and immune-mediated changes in intracellular viral RNA. *J. Gen. Virol.* **2017**, *98*, 992–1003. [CrossRef] [PubMed]
98. Guzman-Zapata, D.; Dominguez-Anaya, Y.; Macedo-Osorio, K.S.; Tovar-Aguilar, A.; Castrejon-Flores, J.L.; Duran-Figueroa, N.V.; Badillo-Corona, J.A. mRNA imaging in the chloroplast of chlamydomonas reinhardtii using the light-up aptamer Spinach. *J. Biotechnol.* **2017**, *251*, 186–188. [CrossRef] [PubMed]
99. Aw, S.S.; Tang, M.X.; Teo, Y.N.; Cohen, S.M. A conformation-induced fluorescence method for microRNA detection. *Nucleic Acids Res.* **2016**, *44*, e92. [CrossRef] [PubMed]
100. Alam, K.K.; Tawiah, K.D.; Lichte, M.F.; Porciani, D.; Burke, D.H. A fluorescent split aptamer for visualizing RNA-RNA assembly in vivo. *ACS Synth. Biol.* **2017**, *6*, 1710–1721. [CrossRef] [PubMed]
101. Breaker, R.R. Engineered allosteric ribozymes as biosensor components. *Curr. Opin. Biotechnol.* **2002**, *13*, 31–39. [CrossRef]
102. Nakayama, S.; Luo, Y.; Zhou, J.; Dayie, T.K.; Sintim, H.O. Nanomolar fluorescent detection of c-di-GMP using a modular aptamer strategy. *Chem. Commun.* **2012**, *48*, 9059–9061. [CrossRef] [PubMed]
103. Inuzuka, S.; Matsumura, S.; Ikawa, Y. Optimization of RNA-based c-di-GMP fluorescent sensors through tuning their structural modules. *J. Biosci. Bioeng.* **2016**, *122*, 183–187. [CrossRef] [PubMed]
104. Wang, X.C.; Wilson, S.C.; Hammond, M.C. Next-generation RNA-based fluorescent biosensors enable anaerobic detection of cyclic di-GMP. *Nucleic Acids Res.* **2016**, *44*, e139. [CrossRef] [PubMed]
105. Kellenberger, C.A.; Chen, C.; Whiteley, A.T.; Portnoy, D.A.; Hammond, M.C. RNA-based fluorescent biosensors for live cell imaging of second messenger cyclic di-AMP. *J. Am. Chem. Soc.* **2015**, *137*, 6432–6435. [CrossRef] [PubMed]
106. Kellenberger, C.A.; Wilson, S.C.; Hickey, S.F.; Gonzalez, T.L.; Su, Y.; Hallberg, Z.F.; Brewer, T.F.; Iavarone, A.T.; Carlson, H.K.; Hsieh, Y.F.; et al. Gemm-I riboswitches from geobacter sense the bacterial second messenger cyclic AMP-GMP. *Proc. Natl. Acad. Sci. USA* **2015**, *112*, 5383–5388. [CrossRef] [PubMed]
107. Hallberg, Z.F.; Wang, X.C.; Wright, T.A.; Nan, B.; Ad, O.; Yeo, J.; Hammond, M.C. Hybrid promiscuous (hypr) ggdef enzymes produce cyclic AMP-GMP (3′, 3′-cgamp). *Proc. Natl. Acad. Sci. USA* **2016**, *113*, 1790–1795. [CrossRef] [PubMed]
108. Sharma, S.; Zaveri, A.; Visweswariah, S.S.; Krishnan, Y. A fluorescent nucleic acid nanodevice quantitatively images elevated cyclic adenosine monophosphate in membrane-bound compartments. *Small* **2014**, *10*, 4276–4280. [CrossRef] [PubMed]
109. Paige, J.S.; Nguyen-Duc, T.; Song, W.; Jaffrey, S.R. Fluorescence imaging of cellular metabolites with RNA. *Science* **2012**, *335*, 1194. [CrossRef] [PubMed]
110. Su, Y.; Hickey, S.F.; Keyser, S.G.; Hammond, M.C. In vitro and in vivo enzyme activity screening via RNA-based fluorescent biosensors for *S*-adenosyl-L-homocysteine (SAH). *J. Am. Chem. Soc.* **2016**, *138*, 7040–7047. [CrossRef] [PubMed]
111. You, M.; Litke, J.L.; Jaffrey, S.R. Imaging metabolite dynamics in living cells using a Spinach-based riboswitch. *Proc. Natl. Acad. Sci. USA* **2015**, *112*, E2756–E2765. [CrossRef] [PubMed]
112. Porter, E.B.; Polaski, J.T.; Morck, M.M.; Batey, R.T. Recurrent RNA motifs as scaffolds for genetically encodable small-molecule biosensors. *Nat. Chem. Biol.* **2017**, *13*, 295–301. [CrossRef] [PubMed]
113. Song, W.; Strack, R.L.; Jaffrey, S.R. Imaging bacterial protein expression using genetically encoded RNA sensors. *Nat. Methods* **2013**, *10*, 873–875. [CrossRef] [PubMed]
114. Ketterer, S.; Gladis, L.; Kozica, A.; Meier, M. Engineering and characterization of fluorogenic glycine riboswitches. *Nucleic Acids Res.* **2016**, *44*, 5983–5992. [CrossRef] [PubMed]
115. Hofer, K.; Langejurgen, L.V.; Jaschke, A. Universal aptamer-based real-time monitoring of enzymatic RNA synthesis. *J. Am. Chem. Soc.* **2013**, *135*, 13692–13694. [CrossRef] [PubMed]
116. Van Nies, P.; Nourian, Z.; Kok, M.; van Wijk, R.; Moeskops, J.; Westerlaken, I.; Poolman, J.M.; Eelkema, R.; van Esch, J.H.; Kuruma, Y.; et al. Unbiased tracking of the progression of mRNA and protein synthesis in bulk and in liposome-confined reactions. *Chembiochem* **2013**, *14*, 1963–1966. [CrossRef] [PubMed]
117. Chizzolini, F.; Forlin, M.; Cecchi, D.; Mansy, S.S. Gene position more strongly influences cell-free protein expression from operons than T7 transcriptional promoter strength. *ACS Synth. Biol.* **2014**, *3*, 363–371. [CrossRef] [PubMed]
118. Chizzolini, F.; Forlin, M.; Yeh Martin, N.; Berloffa, G.; Cecchi, D.; Mansy, S.S. Cell-free translation is more variable than transcription. *ACS Synth. Biol.* **2017**, *6*, 638–647. [CrossRef] [PubMed]

119. Svensen, N.; Jaffrey, S.R. Fluorescent RNA aptamers as a tool to study RNA-modifying enzymes. *Cell Chem. Biol.* **2016**, *23*, 415–425. [CrossRef] [PubMed]
120. Bose, D.; Su, Y.; Marcus, A.; Raulet, D.H.; Hammond, M.C. An RNA-based fluorescent biosensor for high-throughput analysis of the cGAS-cGAMP-sting pathway. *Cell Chem. Biol.* **2016**, *23*, 1539–1549. [CrossRef] [PubMed]
121. Abatemarco, J.; Sarhan, M.F.; Wagner, J.M.; Lin, J.L.; Liu, L.; Hassouneh, W.; Yuan, S.F.; Alper, H.S.; Abate, A.R. RNA-aptamers-in-droplets (RAPID) high-throughput screening for secretory phenotypes. *Nat. Commun.* **2017**, *8*, 332. [CrossRef] [PubMed]
122. Li, B.; Ellington, A.D.; Chen, X. Rational, modular adaptation of enzyme-free DNA circuits to multiple detection methods. *Nucleic Acids Res.* **2011**, *39*, e110. [CrossRef] [PubMed]
123. Bhadra, S.; Ellington, A.D. Design and application of cotranscriptional non-enzymatic RNA circuits and signal transducers. *Nucleic Acids Res.* **2014**, *42*, e58. [CrossRef] [PubMed]
124. Rogers, T.A.; Andrews, G.E.; Jaeger, L.; Grabow, W.W. Fluorescent monitoring of RNA assembly and processing using the split-Spinach aptamer. *ACS Synth. Biol.* **2015**, *4*, 162–166. [CrossRef] [PubMed]
125. Akter, F.; Yokobayashi, Y. RNA signal amplifier circuit with integrated fluorescence output. *ACS Synth. Biol.* **2015**, *4*, 655–658. [CrossRef] [PubMed]
126. Auslander, S.; Fuchs, D.; Hurlemann, S.; Auslander, D.; Fussenegger, M. Engineering a ribozyme cleavage-induced split fluorescent aptamer complementation assay. *Nucleic Acids Res.* **2016**, *44*, e94. [CrossRef] [PubMed]
127. Furukawa, A.; Tanaka, T.; Furuta, H.; Matsumura, S.; Ikawa, Y. Use of a fluorescent aptamer RNA as an exonic sequence to analyze self-splicing ability of agroup I intron from structured RNAs. *Biology* **2016**, *5*, 43. [CrossRef] [PubMed]
128. Afonin, K.A.; Danilov, E.O.; Novikova, I.V.; Leontis, N.B. TokenRNA: A new type of sequence-specific, label-free fluorescent biosensor for folded RNA molecules. *Chembiochem* **2008**, *9*, 1902–1905. [CrossRef] [PubMed]
129. Shu, D.; Shu, Y.; Haque, F.; Abdelmawla, S.; Guo, P. Thermodynamically stable RNA three-way junction for constructing multifunctional nanoparticles for delivery of therapeutics. *Nat. Nanotechnol.* **2011**, *6*, 658–667. [CrossRef] [PubMed]
130. Reif, R.; Haque, F.; Guo, P. Fluorogenic RNA nanoparticles for monitoring RNA folding and degradation in real time in living cells. *Nucleic Acid Ther.* **2012**, *22*, 428–437. [PubMed]
131. Shu, D.; Khisamutdinov, E.F.; Zhang, L.; Guo, P. Programmable folding of fusion RNA in vivo and in vitro driven by pRNA 3WJ motif of phi29 DNA packaging motor. *Nucleic Acids Res.* **2014**, *42*, e10. [CrossRef] [PubMed]
132. Panchapakesan, S.S.S.; Ferguson, M.L.; Hayden, E.J.; Chen, X.; Hoskins, A.A.; Unrau, P.J. Ribonucleoprotein purification and characterization using RNA Mango. *RNA* **2017**, *23*, 1592–1599. [CrossRef] [PubMed]
133. You, M.; Jaffrey, S.R. Structure and mechanism of RNA mimics of green fluorescent protein. *Annu. Rev. Biophys.* **2015**, *44*, 187–206. [CrossRef] [PubMed]
134. DasGupta, S.; Shelke, S.A.; Li, N.S.; Piccirilli, J.A. Spinach RNA aptamer detects lead(II) with high selectivity. *Chem. Commun.* **2015**, *51*, 9034–9037. [CrossRef] [PubMed]


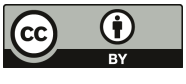

International Journal of
*Molecular Sciences*

MDPI

*Review*

# Key Aspects of Nucleic Acid Library Design for in Vitro Selection

**Maria A. Vorobyeva [1,*], Anna S. Davydova [1], Pavel E. Vorobjev [1,2], Dmitrii V. Pyshnyi [1,2] and Alya G. Venyaminova [1]**

[1] Institute of Chemical Biology and Fundamental Medicine, Siberian Division of Russian Academy of Sciences, Lavrentiev Ave., 8, 630090 Novosibirsk, Russia; anna.davydova@niboch.nsc.ru (A.S.D.); vorobyev@niboch.nsc.ru (P.E.V.); pyshnyi@niboch.nsc.ru (D.V.P.); ven@niboch.nsc.ru (A.G.V.)
[2] Department of Natural Sciences, Novosibirsk State University, Pirogova St., 2, 630090 Novosibirsk, Russia
* Correspondence: maria.vorobjeva@gmail.com; Tel.: +7-383-363-5129

Received: 1 November 2017; Accepted: 2 February 2018; Published: 5 February 2018

**Abstract:** Nucleic acid aptamers capable of selectively recognizing their target molecules have nowadays been established as powerful and tunable tools for biospecific applications, be it therapeutics, drug delivery systems or biosensors. It is now generally acknowledged that in vitro selection enables one to generate aptamers to almost any target of interest. However, the success of selection and the affinity of the resulting aptamers depend to a large extent on the nature and design of an initial random nucleic acid library. In this review, we summarize and discuss the most important features of the design of nucleic acid libraries for in vitro selection such as the nature of the library (DNA, RNA or modified nucleotides), the length of a randomized region and the presence of fixed sequences. We also compare and contrast different randomization strategies and consider computer methods of library design and some other aspects.

**Keywords:** SELEX; aptamers; design of nucleic acid libraries

## 1. Introduction

Nucleic Acid (NA) aptamers [1] are a special class of nucleic acid molecules capable of tight and specific binding with certain molecular or supramolecular targets, thanks to characteristic spatial structures. The range of their targets is enormously wide. Nowadays, NA aptamers have been generated to metal ions (e.g., mercury [2] and lead [3]), small organic molecules (e.g., theophylline [4] and cocaine [5]), larger molecules (e.g., fluorophores [6,7] and porphyrins [8]), peptides and proteins (e.g., hormones [9,10], enzymes [11,12], antibodies [13] and cell surface proteins [14]) and liposomes [15]. These are just a few examples selected from a large diversity of NA aptamers. Nucleic acid aptamers were selected from the NA libraries by means of the method of Selective Evolution of Ligands by Exponential enrichment (SELEX) [16,17]. SELEX technology incorporates a variety of related methods for selecting functional nucleic acids with the desired properties, including also catalytic nucleic acids and riboswitches [18,19]. A selection process could also be aimed at finding genomic sequences or expressible NAs with an affinity to a specific molecule, e.g., to reveal the sequence specificity of NA-enzyme interactions [20,21]. In this review, we focus particularly on NA aptamers.

The main characteristics of NA aptamers are defined by their chemical nature. As nucleic acids, these molecules possess a significant negative charge and are susceptible to nuclease hydrolysis, and surrounding conditions (pH, ionic strength and the presence of certain ions) can influence the stability of their secondary structure. Binding with a target molecule, the aptamer can change the properties of the target, e.g., inhibit the enzymatic activity [11] or alter the characteristics of fluorescent dyes [22].

The molecular recognition function specifies the areas of possible applications of NA aptamers. An ability to inhibit pathogenic proteins affords an opportunity to employ aptamers as therapeutics [22–25]. Aptamers specific to certain cell-surface receptors, which are able to induce an internalization process, could be used as vehicles for cell-targeted drug delivery [26]. Aptamers are anticipated to compete with therapeutic monoclonal antibodies since the chemical synthesis of nucleic acids is far simpler and more cost-effective than obtaining humanized antibodies (although the SELEX process itself could become rather laborious). A set of chemical modifications is available to improve the nuclease resistance and pharmacokinetics of NA aptamers [27]. It is also worth noting that aptamers have the benefit of having a low immunogenicity typical for most oligonucleotides.

Bioanalytics represents probably the broadest application area of nucleic acid aptamers. In principle, every aptamer can be considered as a recognizing module for a certain molecule. It is no wonder that such a vast diversity of aptamer-based biosensors (also known as "aptasensors") has been created (see [28–31] for a review).

The main success criteria for any given aptamer include binding affinity, nuclease resistance and convenience of chemical synthesis. All these properties are largely defined by the particular nucleic acid library employed for SELEX. Therefore, the choice of library design has a great impact on the overall efficiency of the selection. When generating the initial library, a researcher should keep in mind the properties of the target (such as in capture SELEX for small molecules [32]) and the end use of an aptamer (whether nuclease resistance is necessary or not) [27,33]. The importance of covering a maximal sequence space (a multi-dimensional space of different sequences of a certain length), the necessity of introducing a particular sequence or structural element should also be taken into account. In some cases, additional effort is needed to obtain a library that enables the generation of aptamers to SELEX-inaccessible (somewhat similar to non-immunogenic) targets [34,35]. Thus, at the beginning of the study, one has to fill out a kind of checklist of the key issues to choose the most suitable library design (Figure 1). The main aspects regarding the design of the initial libraries for aptamer selection and the basic trends in library design will be reviewed and discussed below.

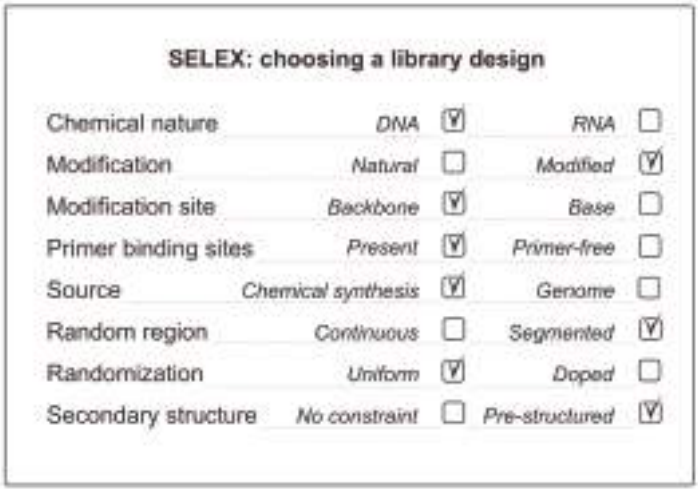


**Figure 1.** An example checklist for an NA library design with the key issues to be considered.

## 2. General Issues of Initial Library Design

### 2.1. DNA or RNA?

All SELEX studies can be generally divided into two groups. In the first group, the choice of the type of nucleic acid library is predetermined by the task of the study such as for the in vitro selection of ribozymes, riboswitches, DNAzymes or genomic SELEX studies. Experiments on the isolation of RNA aptamers or artificial riboswitches intended to be expressed in cells also relate to this group. The second group includes SELEX studies on aptamers that will be further employed for research, therapeutic or bioanalytical purposes. In this case, a researcher can deliberately choose the type of sugar-phosphate backbone.

The first decade in the development of SELEX technology was marked by a dominance of RNA aptamers [36,37]. This was possibly due to the common opinion that only RNA molecules could form functional motifs [38]. At the very beginning of the SELEX era, Ellington and Szostak demonstrated the ability of single-stranded DNA to fold into functional spatial structures [39]. Nevertheless, until 2007, about 70% of all experiments in the field related to RNA aptamers [36]. The distribution became quite the opposite in 2008–2013: DNA aptamers now occupy 70% of SELEX studies, and no significant differences were found in the distributions of the lowest $K_D$ values [36]. DNA and RNA aptamers generated for a number of small-molecule targets have demonstrated similar affinities [40].

Thus, neither the RNA nor DNA libraries provide any systemic preferences for the isolation of affine aptamers [36]. Such preferences can clearly be attributed to some modified nucleic acids, e.g., Slow Off-rate Modified Aptamers (SOMAmers), which will be discussed below. The particular conditions of an aptamer's application also influence the choice of a sugar-phosphate backbone. An enhanced nuclease resistance could require the use of backbone chemical modifications, which will be briefly described in the next section. According to [37], the number of aptamers isolated from non-natural nucleic acid libraries increased significantly in 2011–2015.

### 2.2. Backbone Modifications of NA Libraries

A number of popular applications of in vitro selected aptamers—such as the design of new therapeutics or engineering of drug delivery systems and biosensors—assumes their use in biological media containing different nucleases. Both DNA and RNA aptamers are susceptible to nuclease degradation. To protect them, a large set of chemical modifications of the sugar-phosphate backbone has been developed. However, any post-selective chemical modification of individual aptamers can affect binding affinity, so the modification pattern should be optimized in every particular case, which is rather laborious and time-consuming. Therefore, it seems reasonable to introduce modified nucleotides into the initial library to select molecules that are both affine and nuclease-resistant. One of the most important criteria for such pre-SELEX modifications is the compatibility of modified nucleotides with all enzyme reactions involved in a selection protocol. A number of chemical modifications meeting this requirement are now available (see the reviews in [27,35,41–43]), including ribose (2′-$NH_2$, 2′-F, 2′-O-Me, 4′-S-, LNA (locked nucleic acids), TNA (threose nucleic acid), FANA (fluoroarabino nucleic acid) and HNA (1,5-anhydro hexitol nucleic acid)) and internucleoside phosphate (boranophosphate or phosphorothioate) modifications (Figure 2). Among them, 2′-modifications are clearly at the top of the list. The first SELEX-compatible 2′-modification was the replacement of ribose 2′-OH by an amino group [44]. However, this type of modification was then quite rarely used, owing to problems with the chemical synthesis of 2′-$NH_2$-modified aptamers and the negative impact of the 2′-amino group on the ribose conformation [35]. In contrast, the 2′-F modification of pyrimidine nucleotides, which was proposed almost at the same time, gained outstanding popularity since it provided sufficient nuclease resistance, did not dramatically affect the RNA spatial structure and could be introduced by even using a non-modified T7 RNA polymerase under optimized conditions [45]. To apply any other

SELEX-compatible modifications as mentioned above, one should use mutant versions of polymerase enzymes (see [41,46,47] for reviews).

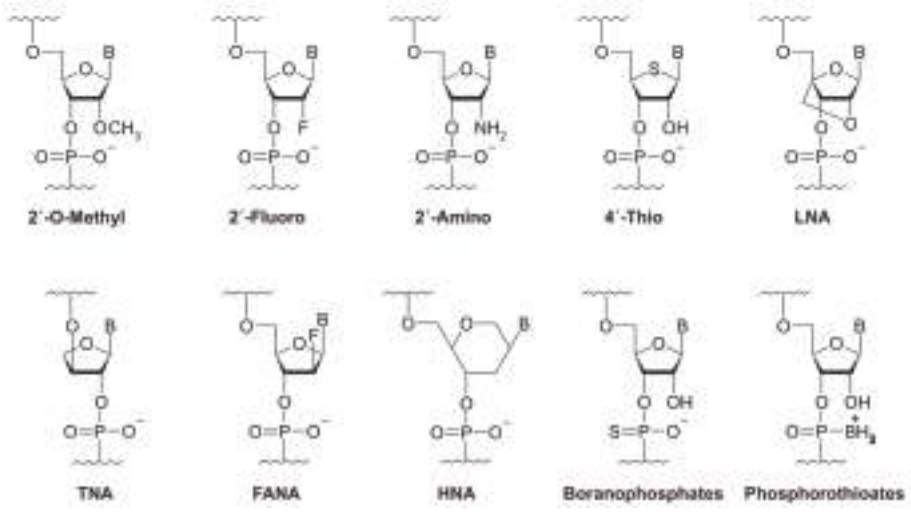


**Figure 2.** Sugar-phosphate backbone modifications compatible with a SELEX procedure. LNA: locked nucleic acids; TNA: threose nucleic acid; FANA: fluoroarabino nucleic acid; and HNA: 1,5-anhydro hexitol nucleic acid.

### *2.3. The Length of the Random Region*

When choosing the length of the random region, a researcher should consider both the sequence space and structural diversity. In the general case, the maximum possible sequence space for a random sequence of N nucleotides comprises a total of $4^N$ possible sequences. Therefore, for those quantities of libraries that can be routinely obtained and handled, a maximal theoretical diversity can only be reached for random regions shorter than 28 nt ($7 \times 10^{16}$ sequences $\approx$ 0.1 μmol corresponds to a fully-represented library) [48]. Longer libraries are unable to extensively cover the sequence space. On the other hand, longer sequences can fold into more complex structures that may be needed to form a target-binding domain. Thus, a balance should be kept between the diversity of the sequences and the desired complexity of the spatial structures formed by these sequences. For in vitro selection of aptamers, 30–50-nt randomized regions are the most abundant [49].

With regard to the minimal sequence diversity to provide a sufficient selection, a value of $10^{11}$ is often used (see [50]), based on SELEX publications from the early 1990s [1,51,52]. It should be noted that all these works deal with RNA SELEX to small-molecule targets, so the question arises as to whether such estimation is applicable for all possible types of targets and libraries.

Aside from the theoretical considerations, from a practical point of view, the length of the library is governed by: (1) the convenience and cost of its chemical synthesis; (2) the possibility of PCR (polymerase chain reaction) artifact formation in the course of an amplification of long libraries; and (3) future applications of the selected aptamers. When an aptamer is further used for practical applications, a shorter length of the oligonucleotide chain is always better. To minimize the length of an individual aptamer, a series of its truncated variants has to be synthesized and tested to choose the minimal one retaining target binding affinity. To avoid this resource-consuming procedure, Thiel et al. [50] employed a short 51-nt library with a randomized region as short as 20 nt and demonstrated that this length was sufficient to generate high-affinity 2′-F-RNA aptamers to protein targets.

### *2.4. Primer-Binding Sites and Primer-Free SELEX*

Traditional SELEX protocols, which are still prevalent today, imply the use of two fixed sequences flanking the randomized region for primer annealing during amplification (Figure 3a). As a rule, primer-binding sites (PBS) are about 20 nt in length. According to the statistical analysis performed in [49], their length does not correlate with the length of a randomized region. The sequences of primer-binding sites are designed to meet several general requirements, particularly to avoid PCR artifacts emerging from self-association or secondary structure formation and to ensure efficient polymerase extension. In the case of RNA SELEX, the 5′-primer contains a promoter sequence for T7 RNA polymerase. A detailed guide to the design of the primer-binding sites can be found in [53]. Some examples of starting SELEX libraries and primers are given in the Table 1.

**Table 1.** Examples of starting libraries for SELEX. SOMAmers, Slow Off-rate Modified Aptamers.

| Type | Starting Libraries and Primers (5′->3′) | Ref. |
|---|---|---|
| Classical SELEX | | |
| DNA | Library:<br>GGGAGACAAGAATAAACGCTCAA-N40-TTCGACAGGAGGCTCACAACAGGC<br>5′-primer: GGGAGACAAGAATAAACGCTCAA<br>3′-primer: GCCTGTTGTGAGCCTCCTGTCGAA | [45] |
| RNA, 2′-F-pyrimidine (Py) modified RNA, 2′-$NH_2$ Py modified RNA | Library:<br>GGGAGACAAGAAUAAACGCUCAA-N40-UUCGACAGGAGGCUCACAACAGGC<br>ssDNA template:<br>GCCTGTTGTGAGCCTCCTTGTCGAA-N40-TTGAGCGTTTATTCTTGTCTCCC<br>5′-primer: TAATACGACTCACTATAGGGAGACAAGAATAAACGCTCAA [1]<br>3′-primer: GCCTGTTGTGAGCCTCCTGTCGAA | [45] |
| 2′-O-Me RNA | Library:<br>GGGAGAGAGGAACGUUCUCG-N30-GGAUCGUUACGACUAGCAUCGAUG<br>ssDNA template:<br>CATCGATGCTAGTCGTAACGATCC-N30-CGAGAACGTTCTCTCTCCCTATAGTGA<br>GTCGTATTA<br>5′-primer: TAATACGACTCACTATAGGGAGAGGAGAGAAACGTTCTCG<br>3′-primer: CATCGATGCTAGTCGTAACGATCC | [54] |
| dRmY (2′-deoxy purine ribonucleotides, 2′-O-$CH_3$ Py ribonucleotides) | Library:<br>GGGAGAGGAGAAGGUUCUAC-N30-GCGUGUCGAUCGAUCGAUCGAUG<br>ssDNA template:<br>CATCGATCGATCGATCGACAGCG-N30-GTAGAACGTTCTCTCCTCTCCCTATAGTGA<br>GTCGTATTA<br>5′-primer: TAATACGACTCACTATAGGGAGAGGAGAGAAACGTTCTAC<br>3′-primer: CATCGATCGATCGATCGACAGC | [55] |
| SOMAmers | Library: GATGTGAGTGTGTGACGAG-N40-CACAGAGAAGAAACAAGACC,<br>random region containing 5-(*N*-benzylcarboxamide)-2′-deoxyuridine (Bn-dU) or<br>5-[*N*-(1-naphthylmethyl)carboxamide]-2′-deoxyuridine (Nap-dU) in place of dT<br>5′-primer: GATGTGAGTGTGTGACGAG<br>3′-primer: GGTCTTGTTTCTTCTCTGTG | [56] |
| Capture SELEX | | |
| DNA | Library:<br>ATACCAGCTTATTCAATT-N10-TGAGGCTCGATC-N40-AGATAGTAAGTGCAATCT<br>Capture oligonucleotide: Bio-GTC-$(CH_2CH_2O)_6$-GATCGAGCCTCA or<br>GATCGAGCCTCA-$(CH_2CH_2O)_6$-GTC-Bio<br>5′-primer: ATACCAGCTTATTCAATT<br>3′-primer: AGATTGCACTTACTATCT | [57] |
| Pre-structured libraries | | |
| RNA | Library:<br>GGAGGCGCCAACTGAATGAA-N26-CUGCUUCGGCAG-N26-UCCGUAACUAGUUCG<br>CGUCAC<br>ssDNA template:<br>GTGACGCGACTAGTTACGGA-N26-CTGCCGAAGCAG-N26-TTCATTCAGTTGGCGCCT<br>CCTATAGTGAGTCGTATTACAT<br>5′-primer: ATGTAATACGACTCACTATAGGAGGCGCCAACTGAATGAA<br>3′-primer: GTGACGCGACTAGTTACGGA | [58] |

[1] Hereinafter in the table, the T7 promoter sequence is underlined.

Ideally, aptamer sequences generated by in vitro selection should bind their targets by means of spatial structures formed only by nucleotides from a random region. For most aptamers, this is indeed the case: the analysis of >2000 sequences from the Aptamer Database revealed that for a majority of aptamers, their secondary structure was independent of primer-binding sites [49]. However,

there was a number of outliers (examples in [59–61]). Taking this into account, primer-binding sites cannot be simply cut off to minimize the length of the sequence during aptamer truncation, and additional minimization studies are needed. Moreover, during the SELEX, primer-binding sites could interact with sequences in the random region, hampering their target binding and/or amplification (for more details, see [62] and the references therein).

These problems stimulated a search for SELEX approaches that minimize the influence of primer-binding sites on the sequence and structure of selected aptamers (schematically depicted in Figure 3). For instance, Shtatland et al. [61] showed that fixed regions of a genomic RNA library (with *Escherichia coli* (*E. coli*) genome fragments as a random region) interacted with a random region, which resulted in a large number of experimental artifacts. After the traditional SELEX from this library on MS2 bacteriophage capsid protein, about 90% of the generated sequences were represented by artifacts (not found in the *E. coli* genome). The authors proposed two alternative selection strategies to neutralize the negative impact of constant regions: primer-annealing genomic SELEX and primer-switching genomic SELEX. In the primer-annealing genomic SELEX protocol, prior to selection, the RNA library was hybridized with two oligonucleotides complementary to the primer-binding sites (Figure 3b). This approach provided 60% of the artifacts in the obtained clones. During the course of primer-switching genomic SELEX, several rounds of classical SELEX were performed, followed by a replacement of primer-binding sites and subsequent classical or primer-annealing SELEX. To replace the flanking regions, the purified library was digested by the FokI restrictase (restriction sites were introduced 9–13 nt from the random region); the sticky ends were extended to blunt ends by a Klenow reaction; then, new primer-binding sites were ligated to the library. This approach enabled the authors to decrease the fraction of unwanted products down to 10%.

Ouellet et al. successfully adapted the primer-annealing SELEX protocol for completely random libraries [62,63]. Blocking oligonucleotides annealed with primer-binding sites eliminated their negative impact in several selections on therapeutically-important targets.

The approach proposed by Shtatland et al. was further developed for the genomic SELEX on the bacteriophage Ff gene 5 protein [64]. The authors hypothesized that constant nucleotides remaining in the library after an enzymatic digestion could also influence the course of selection. In their version of primer-free genomic SELEX, the Fok1 restriction site at the 5′-end was combined with a ribose linkage at the 3′-end of the library (Figure 3c). Enzymatic digestion followed by alkaline treatment provided a genomic insert free of any constant nucleotides. To regenerate the primer-binding sites for amplification at every SELEX round, the authors employed thermal cycles of hybridization-extension using the initial genomic library as a template.

Pan et al. [65–67] employed the possibility of using the second strand as a template for completely randomized libraries. The authors developed two similar approaches for primer-free SELEX, which allowed the use of DNA libraries with only two constant nucleotides or even without constant positions (Figure 3d). The first approach was based on the introduction of Nt.BbvCI and Nt.BstNBI restriction sites into the initial dsDNA library. These enzymes recognize dsDNA, but cleave only one strand. A subsequent digestion of the library resulted in the formation of 32-nt ssDNA (0 + 30 + 2), which was used for in vitro selection. The second DNA strand remained uncleaved and acted as a template for the ligation of primer-binding sites prior to amplification. The second protocol provides a completely primer-less DNA library. In this case, the authors supplied the initial DNA library with Nt.BstNBI and BspMI restriction sites. Digestion by both restrictases provided the 30-nt ssDNA library (0 + 30 + 0), while the treatment only by Nt.BstNBI gave an uncleaved second strand, which also acted as a ligation template.

The possibility of using primer-free SELEX for completely randomized RNA libraries was also shown in [68]. The authors developed a tailored SELEX approach, implying the use of primers/adapters added previously by ligation and removed within the amplification processes (Figure 3e). A randomized 40-nt region was flanked by two short constant sequences (4 and 6 nt) for annealing the adapter oligonucleotides, so the total length of the aptamers generated by this method

was as low as 50 nt. Further development of the method led to the design of the dual RNA library [69]. An introduction of both T3 and T7 RNA promoters (Figure 3f) allowed the generation of two different RNA libraries. The transcription carried out by a T3 RNA polymerase provided a long "traditional" RNA library with 34-nt random regions and conventional primer binding sites. Alternatively, the use of T7 RNA polymerase obtained an RNA library for tailored SELEX, with the same N34 region flanked by two short fixed sequences forming a stem that excluded their involvement in active functional structures. The design of primer-binding sequences complementary to each other was also employed in [70]. It is noteworthy that such stem-forming flanking sequences could, in some cases, hamper the selection of aptamers [71].

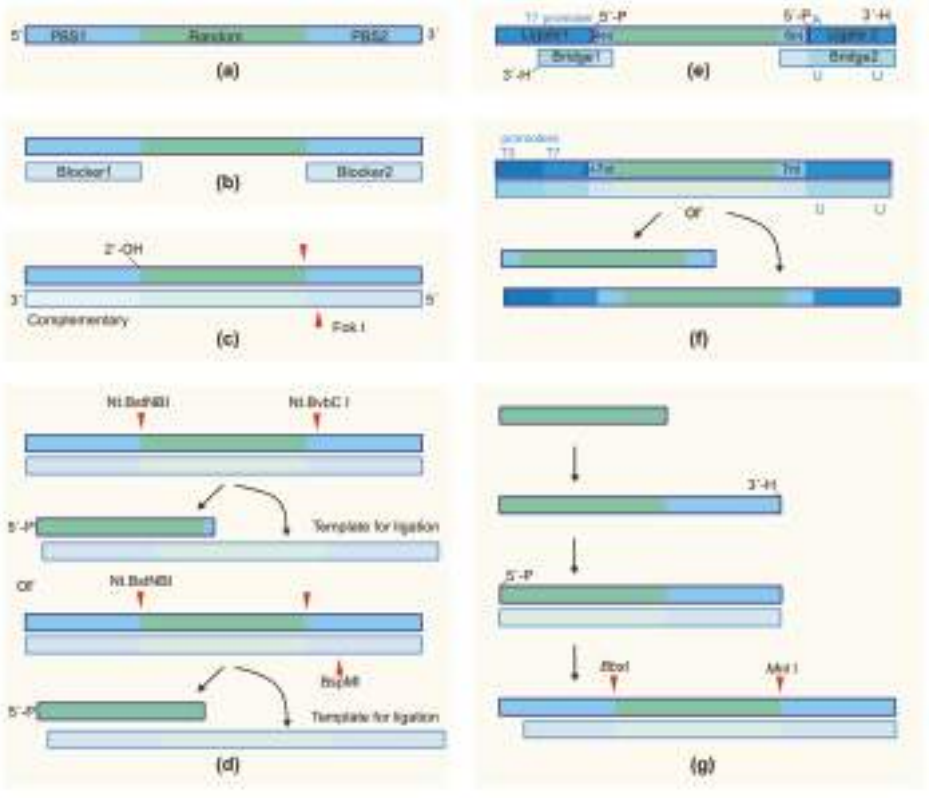


**Figure 3.** Different variants of design for NA libraries for a primer-free SELEX. (**a**) A conventional NA library; (**b**) blocked primer-binding sites for primer-annealing SELEX [62]; (**c**) the design of primer-binding sites for primer-free genomic SELEX [64]; (**d**) the design of a DNA library for primer-free SELEX from a completely randomized library [65]; (**e**) the RNA library for a tailored SELEX in a complex with auxiliary oligonucleotides [68]; (**f**) the DNA template for a dual-RNA library suitable for both conventional and tailored SELEX [69]; (**g**) DNA libraries lacking any constant nucleotides for the primer-free SELEX protocol of Lai et al. [72]. PBS: primer binding site, 2′-OH-ribonucleotide, 3′-H-dideoxynucleotide.

Another protocol for primer-free SELEX was developed by Lai et al. [72,73] for a totally randomized 30-nt DNA library aimed at selecting aptamers for HIV RT (Figure 3g). To amplify the library after target binding, the authors proposed the use of a non-template ligation of the 3′-primer-binding fragment containing the MnlI site by the thermostable RNA ligase at 60 °C.

These ligation conditions are supposed to lower the possibility of secondary structure formation and increase the efficiency of ligation as compared to the conventional T4 RNA ligase. The ligation of the 5′-primer-binding site as a duplex containing the BbsI site was performed by the T4 DNA ligase.

A drastic approach to avoid the use of primer-binding sites was recently proposed by Tsao et al. [74]. The Rotating Magnetic Field Magnetic-Assisted Rapid Aptamer Selection (RO-MARAS) method enables the one-step generation of high affinity aptamers, which relies on the sophisticated, but efficient, procedure of pool isolation. The protocol included an incubation of the starting library, free of any constant nucleotides, with a target protein immobilized on the surface of magnetic beads. This was followed by the employment of a rotating magnetic field to select the most tightly bound molecules. Notably, the amplification of the enriched library before sequencing required a very complex scheme to add primer-binding sites.

To summarize, a number of different initial libraries and selection schemes are now available to generate the aptamers lacking primer-binding sites. We would like to emphasize that the absence of fixed flanking sequences provides the important advantages of (1) decreasing the probability of SELEX artifacts; and (2) shortening the overall length of the aptamer sequence. At the same time, all primer-free SELEX protocols rely on the additional stages of ligation and restrictase digestion. Insufficient ligation, or deletion of restriction sites during PCR amplification could result in a loss of some potential binders, which can be considered as the pitfall of primer-free selection.

### *2.5. NA Libraries Containing Additional Constant Sequences*

It should be mentioned that primer-binding sites are not the only possible constant regions of the library having an auxiliary role. NA libraries can also be supplied by additional constant sequences necessary for the immobilization within a capture SELEX approach. This approach, first proposed by Nutiu et al. [75,76] for the selection of structure-switching aptamers specific to ATP (adenosine triphosphate) or GTP (guanosine triphosphate), relies on the annealing of the so-called docking sequence within a library to the complementary capture oligonucleotide bound to a carrier through biotin–streptavidin interactions (Figure 4). In this way, prior to selection, the initial library is immobilized on a carrier, and target binding causes a structural rearrangement, which results in duplex dissociation and passing of the library to the solution. Therefore, the pool without target binding affinity remains immobilized and can be easily separated from the enriched one. Aptamers selected by this method gain the ability of structure-switching, which can be employed for engineering analytical systems (e.g., fluorescent beacons) for the detection of target molecules. A capture SELEX method turned out to be particularly suitable for selecting aptamers on small-molecule targets such as antibiotics, toxins, drugs or food contaminants (see the reviews in [32,77]). The problem of separating bound and unbound pools becomes crucial for these selections. After target binding, a change of the properties of NA molecules is not significant enough to isolate the complexes from unbound molecules in solution. Otherwise, the immobilization of small molecule targets masks potential binding sites and also increases the probability of selecting aptamers with an affinity to the target-carrier conjugate, but not to the target itself. Capture SELEX enables the selection of the target in its native state in solution, while employing the advantages of resin-based isolation. Some shortcomings of the method are connected with subsequent applications of structure-switching aptamers: during their binding with a target in solution, a rearrangement of the structure could be different from that of immobilized aptamers, which can influence binding affinity [32].

The design of a docking sequence for capture SELEX, namely the length and nucleotide composition, should provide both strong immobilization before target binding and sufficient dissociation afterwards [57]. As a rule, it is a heterosequence of 12–18 deoxynucleotides (see, e.g., Table 1) placed within the random region (as in [57,78,79]), or extending one of the primer-binding sites (as described in [80–83]). Currently, the capture SELEX strategy is generally employed for DNA selection, but also suits RNA libraries. For example, Morse et al. [84] isolated RNA beacon aptamers specific to tobramycin; interestingly, in this case, only a 6-nt capture deoxy oligomer was used for immobilization of the library.

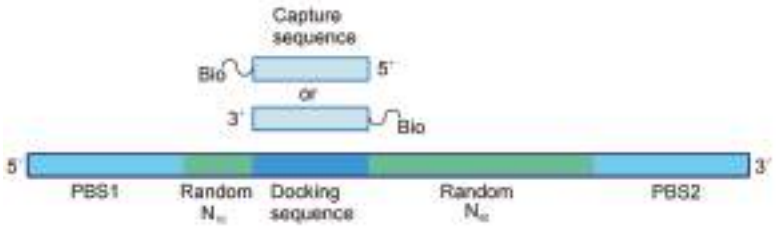


**Figure 4.** A general scheme of library design for a capture SELEX.

*2.6. NA Libraries for a Genomic SELEX*

Genomic SELEX is employed to screen sequences within a certain genome for aptamers or regulator sequences, which interact with proteins or other ligands [85], such as DNA sequences recognized by transcription factors [86], or RNA sites bound by splicing factors [87]. Initial libraries consist of genomic DNA fragments, and the motifs obtained by this method are called "genomic aptamers" [88].

Genomic SELEX libraries are derived from the genomic DNA of a given organism by means of random priming and transcription. This allows the representation of all possible genomic aptamers within a library. The first strand of a genomic DNA library is usually synthesized by the Klenow fragment in the presence of the random primer supplied by a fixed sequence at the 5′-end. After the reaction, the excess primer is thoroughly removed. The second strand is synthesized by the same method. As a result, a set of genomic sequences is obtained, flanked by constant regions. At this step, fragments of a certain length can be isolated, e.g., by electrophoretic separation. If RNA transcription is required, the T7 promotor sequence is introduced by means of PCR with the corresponding primers.

The benefits of the genomic SELEX approach over the conventional one include the use of much more restricted sequence space and the increased probability of selecting a biologically-relevant aptamer. Since the initial library is obtained from genomic DNA, RNA selection can be performed regardless of the expression level, thus making it possible to isolate RNA motifs with a low expression level, or those expressible only at certain stages of a cell cycle. Unfortunately, non-expressible RNAs can also be obtained [85].

## 3. The Design of Initial NA Libraries for More Affine Aptamers

One of the most important issues in the design of nucleic acids libraries is the maximal selection efficiency, i.e., the highest probability of selecting tight-binding aptamers. In contrast to proteins, nucleic acids possess a very limited repertoire of functional groups. Consequently, high binding affinity is reached by combining the diversity of spatial structures with the available functional groups. Otherwise, a toolkit of functionalities can be artificially expanded by adding extra chemical modifications. Below, we discuss both of these possibilities.

*3.1. Expanding the Chemical Repertoire of NA Libraries*

A more obvious (but definitely not simpler) way to generate higher-affinity aptamers is to use additional functional groups, thereby making nucleic acid aptamers more similar to proteins.

Expanding the chemical repertoire of NA libraries enables a selection of either better binders or aptamers directed to target epitopes inaccessible for unmodified pools. Additional chemical functions are generally introduced into heterocyclic bases (thoroughly reviewed in [35]).

SomaLogic, one of the world's leading companies in the development of aptamers, has created so-called SOMAmers, or Slow Off-rate Modified Aptamers. SOMAmers are selected from base-modified nucleic acids libraries [56,89–93] (see Table 1 for example sequences of the library and primers). Heterocyclic base modifications introduce protein-like functionalities, which provide

a unique aptamer-target complex stability and even make it possible to select aptamers for previously inaccessible targets. Novel hydrophobic base modifications for DNA libraries have also been recently proposed by Chudinov et al. [94].

Heterocyclic base modification can also expand the genetic alphabet of nucleic acid libraries. The use of an extra artificial base pair Ds:Px (Figure 5) in the starting library was proposed by Kimoto et al. [95] to select VEGF-165 (vascular endothelial growth factor) binding aptamers. The selected aptamers, which contained several artificial base pairs, possessed 100-fold higher binding affinity as compared to the non-modified analogs. Sefah et al. [96] supplemented four natural bases with non-natural nucleosides Z and P (Figure 5) to generate DNA aptamers binding to liver cancer cells with nanomolar affinities.

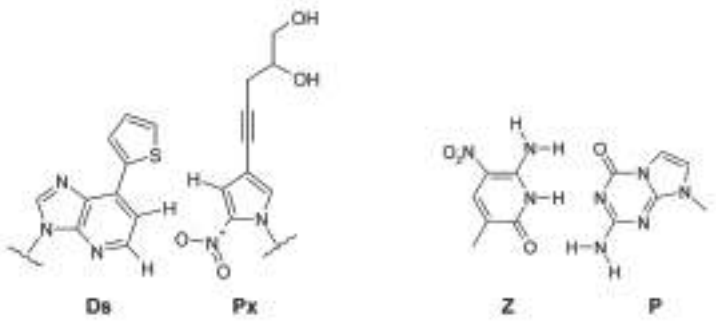


**Figure 5.** Chemical structures of artificial base pairs Ds:Px [95] and Z:P [96].

Click-SELEX represents a relatively new method for introducing chemical modifications into NA libraries. In this case, thymidine residues within a DNA library are replaced by C5-ethynyl-2′-deoxyuridine, followed by the Cu(I)-catalyzed cycloaddition of the azide component. The modified library is then employed in the modified SELMA (SELection with Modified Aptamers) protocol for different targets [97–102]. For example, this method was used to generate glycan-conjugated aptamers. Interestingly, in this case, the DNA aptamer served as a scaffold to provide an optimal tertiary structure and flexibility for the glycoclusters, which were then used as vaccine components.

Notably, expanding the chemical repertoire of NA libraries requires base-modified nucleotide monomers and mutant polymerases, as well as more complex SELEX protocols. That is probably why such a promising strategy has not yet become routine.

### *3.2. Structural Repertoire of Nucleic Acid Libraries*

#### 3.2.1. Uniformly Randomized Libraries

According to a widely-held point of view, all four nucleotides have to be uniformly represented in the random region of the library. An equal distribution is considered to provide the maximal sequence diversity, thus increasing the probability of selecting highly affine aptamers [103,104].

Currently, protocols for chemical synthesis have been developed to provide equal nucleotide distribution in the random region, which consider the different reactivities of corresponding phosphoramidites (see [53]). Methods of high-throughput sequencing and specially-developed program packages enable the estimation of the smoothness of the randomization in terms of nucleotides or short sequences, e.g., hexanucleotides [103,105]. In the latter case, a Gaussian profile is characteristic for the balanced library.

Unfortunately, today, only a few studies devoted to the impact of nucleotide composition on the structure of the library have been published. For example, the computer analysis of the structure

distribution for random regions of RNA libraries revealed that for the 40-nt region, a shift to G and C (30% each) led to the predominant formation of structures with more stems when compared to the same A + U shift [106]. At the same time, for the 100-nt random region, such bias in nucleotide composition was not significant and did not markedly change the distribution of secondary structures.

On the other hand, several experiments on RNA SELEX from smoothly-randomized starting libraries have shown that the selection progress is accompanied by an accumulation of pyrimidine-rich sequences and the loss of adenosine [50,104], both for targeted and non-targeted selections. The loss of adenosine was observed for all adenosine-containing dinucleoside pairs. This corresponded to a decrease in the overall minimum free energy of the RNA library, which resulted in RNA sequences with higher predicted structural stability [50]. Therefore, a slight bias in the initial library, especially a pyrimidine bias, can be considered as acceptable, since over the course of selection, the nucleotide distribution will inevitably shift.

#### 3.2.2. Doped and Segmented NA Libraries

When a starting library is designed to improve the properties of existing aptamers by determining their target binding sites or for a functional analysis of natural RNA, the task is not a total randomization, but a delicate varying of particular nucleotides within a certain sequence. To solve this problem, one should choose doped or segmented NA libraries.

In their pioneering work, Bartel et al. [107] generated a doped library on the basis of the viral RNA element of the Rev protein of human immunodeficiency virus 1 (HIV-1) to identify the binding site for the protein. The 66-nt fragment of Rev-responsive element (RRE) was generated in such a way that point mutations were introduced uniformly throughout the sequence at a rate of 30% with 5% deletions (which meant that every position contained 65% of a wild-type nucleotide, 10% of each other nucleotide and 5% deletions). An example of the use of doping strategy to explore the secondary structure of the aptamer and determine its conservative positions is given in [108]. The authors doped the sequence of the aptamer specific to the ricin A-chain (generated by the conventional SELEX) at a 15% mutation rate. The doping strategy also helps to improve the affinity of the aptamer. Burke et al. [106,109] employed it for a secondary SELEX of pseudoknot aptamers for an HIV reverse transcriptase: truncated aptamer motifs found by the primary SELEX were doped at a 30% mutation rate (70% of the wild-type base and 10% of each of the other bases).

Nevertheless, how can we choose the mutation rate suitable for a particular task and sequence? To answer this question, Knight et al. [110] performed a comprehensive theoretical analysis of doped selections and developed an algorithm to select the length of the doped sequence and mutation rate depending on a given task. To search for sequences close to the wild-type, the authors recommended a low mutation rate (about 5%). If the structure space had to be extended, the mutation rate increased up to 30–50%. The concrete values for the doping scheme could be calculated by the developed method.

Apart from the doping of certain positions, segmental randomization is employed to specify the sequence or optimize the structure of an aptamer. For this, certain parts of the sequence are replaced by randomized stretches of the appropriate length. In principle, the segmental randomization can be considered as a special case of a doped randomization with a mutation rate of 75%. Usually, segments represent rather short sequences placed within certain elements of the secondary structure or other wild-type context [53]. A contrary example is given in [60], where core RNA aptamer sequences were flanked by 40- and 45-nt random regions to improve the aptamer analogs of green fluorescent protein. Longer segments provide larger structural diversity, which increases the probability of generating a better binder.

#### 3.2.3. Nonhomologous Recombination as an Alternative to the Doping Strategy

Bittker et al. [111] proposed an entirely different approach of varying the existing aptamer sequences to find conservative regions, identify binding sites or improve the affinity: a nonhomologous random recombination (NRR). This method enables variation of the length of the library, deletion

of inactive fragments and alternation of the mutual location of different motifs. For this purpose, a sequential scheme of enzymatic synthesis of NRR libraries was developed (Figure 6), starting from the treatment of the dsDNA library by DNase I and T4 DNA polymerase, which gives a mixture of blunt-ended DNA fragments. During the recombination step, DNA fragments were treated with the T4 DNA ligase under conditions favoring intermolecular ligation. The presence of an additional 5′-phosphorylated hairpin DNA containing a restriction site enabled both introducing the fixed PBS to the ends of the library and regulating the length of the recombined molecules (by varying the stoichiometry of the hairpin). Digestion of the resulted circular DNAs gave a pool of dsDNA molecules with defined sequences at both ends.

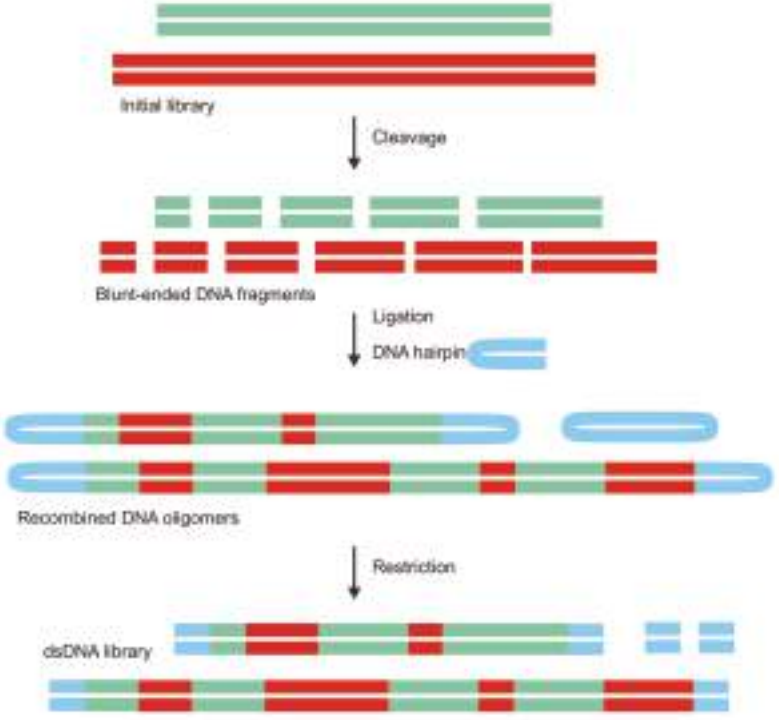


**Figure 6.** A scheme of the nonhomologous random recombination method [111].

When the NRR approach had been applied to a model partly-enriched aptamer library, the authors observed that NRR-derived aptamers accumulated several copies of the active motif. Therefore, the NRR strategy was considered as a more effective alternative for error-prone PCR or site-directed mutagenesis. This strategy might also be used instead of a synthesis of doped libraries. Although the NRR protocol seems to be more complex, the synthesis of the NRR library, otherwise, does not require a sophisticated doping scheme for chemical synthesis and enables almost unlimited exploration of the sequence space. We presume that the NRR strategy could also bring benefits when used as a basic SELEX protocol starting from an unselected random pool.

#### 3.2.4. Nucleic Acid Libraries with Pre-Defined Secondary Structures

The design of starting libraries can also be performed in the framework of a paradigm that does not follow uniform randomization. An alternative concept arises from the facts that

the number of productive structures providing the selection of effective binders is limited and the maximal accessible diversity of sequences folds in a restricted set of spatial structures (see [48] for a review). A computer analysis of uniformly-randomized libraries of different lengths (20–100 nt) [106] revealed that a limited set of secondary structures corresponded to every library. It was found that the complexity of the structures increased with the length of the library, and every length was characterized by three predominating structural motifs.

Thus, instead of a "smooth" randomization, it could be more beneficial to introduce secondary structure motifs into an initial library. A pioneering work in the field was published by Davis and Szostak [58]. Integrating structural data for aptamers that had been known at the time, the authors observed a common element for all structures: a stem-loop, which appeared to act as a structural anchor for recognition loops. Based on this knowledge, they designed an RNA library containing an 8-nt stem-loop motif placed in the middle of the random region (Figure 7a, Table 1). An equal mix of this pre-structured library with a conventionally-randomized one was employed in the SELEX of GTP-binding aptamers. All resulting aptamers contained the hairpin insert, thus proving the efficiency of the strategy. To further establish the proof-of-principle, the authors demonstrated that more complex structures provided more active RNAs (by examples of GTP-binding aptamers and ligase ribozymes) [112]. Notably, the hairpin motif derived in [58] was then successfully employed by other researchers to generate aptamers for different small-molecule targets [113,114].

Secondary structure elements can also be successfully introduced into DNA libraries. To form a hydrophobic pocket for steroid binding, Yang et al. [115] designed a DNA library containing a three-way junction structure with a total of eight randomized positions (Figure 7b). The same motif was also used in [116] to select structure-switchable aptamer beacons for the steroid hormone dehydroisoandrosterone 3-sulfate (Figure 7c).

Attempts were also made to design DNA libraries in a manner that provided a preferential formation of G-quadruplex structures. To generate hemin-binding G-quadruplex structures, Zhu et al. [117] created DNA libraries containing 25–45% of guanosine in the random region. The selection was successful, but the authors noted that G-rich sequences were harder to amplify by PCR, which may lead to a loss of the best binders.

Ruff et al. [118] developed a general approach for the design of pre-structured DNA libraries, also using a doping strategy. A structured DNA library with 60-nt random regions contained an RY pattern (alternating purines (R) and pyrimidines (Y)) that favors stem formation. To increase the frequency and diversity of loops and other non-stem structures within the patterned library, RY sequences alternated with stretches of 3–4 random nucleotides. Moreover, every position in the RY sites was slightly doped by nucleosides of another type: every R contained 45% A and G and 5% C and T, and vice versa for Y. The authors performed competitive selections from the mix of unpatterned and patterned libraries for three different target proteins (streptavidin, VEGF and IgE). The results proved that namely a combination of RY fragments and doping provided the selection of the highest affinity aptamers.

During the last decade, several approaches to in silico optimization of starting libraries have been developed to lower the fraction of poorly-structured (and thus low-affinity) sequences. Chushak et al. [119] developed a protocol for the computer optimization of RNA libraries prior to the selection of aptamers for small molecules. The algorithm included two main steps. First, the secondary structures of all possible sequences of a given length were analyzed. Based on secondary structure data for existing aptamers, the authors derived a set of criteria that allowed selecting an affective binder. At Step 2, 3D structures were built for all sequences meeting these criteria, followed by molecular docking with a given target molecule that resulted in a minimal free energy rating. Such high-throughput virtual screening enabled them to reduce a library of $2.5 \times 10^8$ sequences to $10^3$–$10^4$ sequences suitable for the experimental screening and verification.

The concepts of doped and partly-structured RNA libraries complemented each other in the method developed by Kim et al. [120]. The approach included the use of a definite set of starting

sequences and certain mutation rates in certain positions within a random region (mixing matrixes). To generate these two key sets of parameters, the authors employed graph theory and matrix analysis, respectively. Starting RNA pools obtained by the proposed algorithms ensured the selection of better binders when compared to the uniformly-randomized pools. The authors also developed the web server RAGPOOLS (RNA-As-Graph-Pools) for designing and analyzing structured pools for SELEX (http://rubin2.biomath.nyu.edu/home.html) [121,122]. It is worth noting that the synthesis of the initial pool according to the mixing matrix (i.e., with an individual mutation rate for every doped position) may be laborious and time-consuming.

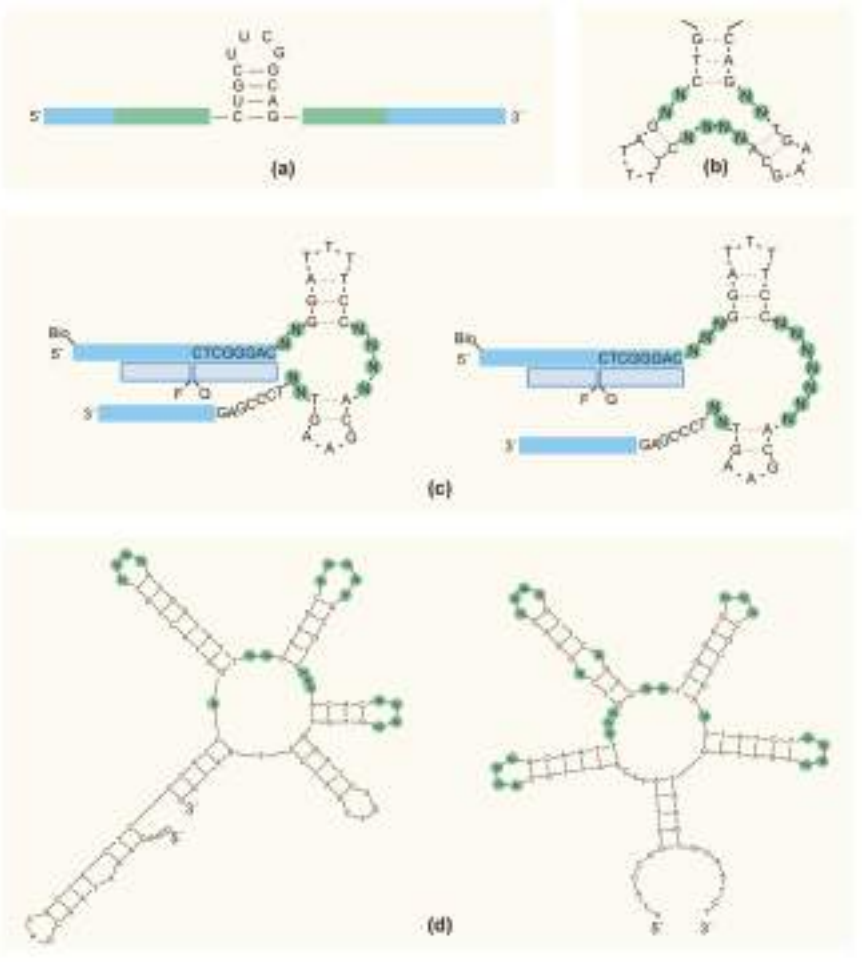


**Figure 7.** Partially-structured NA libraries. (**a**) The pre-structured RNA library with the stem-loop scaffold engineered in [58]; (**b**) the DNA library with three-way junction scaffolds for a steroid binding engineered in [115]; (**c**) DNA libraries with three-way junction scaffolds for a selection of steroid-binding DNA beacon aptamers [116]; and (**d**) highly structured RNA libraries engineered by the random filtering (left) and genetic filtering (right) approaches [123].

Luo et al. [123] developed two computational methods to generate starting DNA libraries with increased structural diversity: random filtering and genetic filtering. The random filtering

approach is based on the secondary structure analysis of all sequences in the library and isolating those containing five-way junctions as the most structured elements. Then, for every such sequence, a set of mutant versions is generated with all four possible nucleotides at all positions not involved in base pairing. Random filtering thus pre-enriches the starting library with highly-structured motifs, hence increasing the probability of generating better binders. The genetic filtering approach aims to create a library with a desired distribution (either uniform or not) of all secondary structure elements (one-way, two-way, three-way, four-way and five-way junction). First, all secondary structures are analyzed for a library of a given length and the primer-binding sites. The authors recommended using 24 random positions for the pool design to provide complete sequence coverage. After secondary structure analysis, the pool is assigned a fitness score that indicates its proximity to the desired distribution of the structure elements. New generations of pool designs are obtained by selecting designs from previous generations with better (i.e., smaller) fitness scores and applying mutation, copy and crossover procedures. Typically, 500–3000 generations are needed for the best pool design. Examples of starting pools developed by random filtering and genetic filtering methods are given in Figure 7d. The pool with a uniform structure distribution was tested in a wet SELEX experiment aimed at finding ATP-binding DNA aptamers. Notably, the resulting aptamers possessed five-way junction structures, and their binding affinities were close to those for previously published aptamers from a conventionally-designed library. The authors concluded that although complexity alone could not guarantee better target binding, higher complexity structures possessed the potential to yield better aptamers. They also emphasized the importance of structural diversity, and not only structural complexity in the starting pool.

To sum up this section, the use of NA libraries with pre-designed secondary structures is a very promising strategy, which has been strongly underestimated until now. The inherent ability of nucleic acids to form complex spatial structures is used here to its full extent. A pre-structured library can be designed in silico considering the properties of a given molecular target. Once generated, the pre-structured initial library is further used in a routine SELEX protocol without any additional stages, modified nucleotides or unusual polymerases. However, it may be suggested that a combination of base-functionalized monomers with a pre-defined secondary structure would provide even more efficient starting libraries.

## 4. Conclusions

Nucleic acid aptamers generated by SELEX technology have proven themselves as highly selective and high-affinity, biospecific molecules for a number of applications. Aptamers are now considered as "chemical antibodies" with the advantages of chemical synthesis, long shelf-life and the ability to be built into almost any system of interest. In principle, aptamers can be selected for nearly any molecular or supramolecular target. However, to generate an efficient aptamer for a certain target, one should choose the most suitable SELEX protocol, and the most important issue in this case is the proper choice of an initial library. The design of a library is governed by the different parameters of a particular system such as the need for nuclease resistance, hydrophobicity, the molecular weight of a target molecule, etc. A classic design of a starting library, which still remains the most popular, uses a uniformly-randomized region flanked by two fixed primer-binding sequences. These universal "traditional" libraries are suitable for any SELEX target, from small molecules to proteins. Nevertheless, a number of alternative strategies has recently been developed. Primer-binding sites can be deleted to exclude their impact on the course of selection and to shorten the resulting aptamers. Different primer-free selection strategies have proven successful for protein targets. On the contrary, to generate an aptamer for a small-molecule target, it could be better to use the capture-SELEX technique, where the library is resin-immobilized through an additional docking sequence and the target retains its native structure. The smart design of random region enables the enrichment of a library with complex spatial structures favorable for the selection of tightly-binding motifs. The shape of the random region can be adjusted to fit the structure of the given molecule (or a class of molecules), so the "smart

randomization" strategy might be recommended for any target. A chemical repertoire of initial NA libraries can also be expanded to generate better binders and to obtain aptamers for previously "SELEX-inaccessible" targets.

To summarize, a large variety of different approaches for library design is now available. A conscious choice from this diversity and the development of novel approaches to design the initial NA libraries would guarantee the generation of high-affinity aptamers for any desired ligand.

**Acknowledgments:** The work was supported by the Russian Science Foundation (Grant No. 16-14-10296).

**Author Contributions:** Mariya A. Vorobyeva and Anna S. Davydova wrote the manuscript, and Pavel E. Vorobjev generated the figures and wrote the manuscript. Dmitrii V. Pyshnyi conceived of the review topic and performed general revision of the manuscript. Alya G. Venyaminova performed general revision and editing of the manuscript. All authors read and approved the final manuscript.

**Conflicts of Interest:** The authors declare no conflict of interest. The founding sponsors had no role in the design of the study; in the collection, analyses or interpretation of data; in the writing of the manuscript; nor in the decision to publish the results.

## Abbreviations

| | |
|---|---|
| SELEX | Selective Evolution of Ligands by Exponential enrichment |
| NA | Nucleic Acid(s) |
| PBS | Primer-Binding Site(s) |
| PCR | Polymerase Chain Reaction |
| Pu, or R | Purine nucleotide |
| Py, or Y | Pyrimidine nucleotide |

## References

1. Ellington, A.D.; Szostak, J.W. In vitro selection of RNA molecules that bind specific ligands. *Nature* **1990**, *346*, 818–822. [CrossRef] [PubMed]
2. Ono, A.; Togashi, H. Highly selective oligonucleotide-based sensor for mercury (II) in aqueous solutions. *Angew. Chem. Int. Ed.* **2004**, *43*, 4300–4302. [CrossRef] [PubMed]
3. Ye, B.-F.; Zhao, Y.-J.; Cheng, Y.; Li, T.-T.; Xie, Z.-Y.; Zhao, X.-W.; Gu, Z.-Z. Colorimetric photonic hydrogel aptasensor for the screening of heavy metal ions. *Nanoscale* **2012**, *4*, 5998–6003. [CrossRef] [PubMed]
4. Jenison, R.D.; Gill, S.C.; Pardi, A.; Polisky, B. High-resolution molecular discrimination by RNA. *Science* **1994**, *263*, 1425–1429. [CrossRef] [PubMed]
5. Stojanovic, M.N.; de Prada, P.; Landry, D.W. Aptamer-based folding fluorescent sensor for cocaine. *J. Am. Chem. Soc.* **2001**, *123*, 4928–4931. [CrossRef] [PubMed]
6. Holeman, L.A.; Robinson, S.L.; Szostak, J.W.; Wilson, C. Isolation and characterization of fluorophore-binding RNA aptamers. *Fold. Des.* **1998**, *3*, 423–431. [CrossRef]
7. Grate, D.; Wilson, C. Laser-mediated, site-specific inactivation of RNA transcripts. *Proc. Natl. Acad. Sci. USA* **1999**, *96*, 6131–6136. [CrossRef] [PubMed]
8. Li, Y.; Geyer, R.; Sen, D. Recognition of anionic porphyrins by DNA aptamers. *Biochemistry* **1996**, *35*, 6911–6922. [CrossRef] [PubMed]
9. Leva, S.; Lichte, A.; Burmeister, J.; Muhn, P.; Jahnke, B.; Fesser, D.; Erfurth, J.; Burgstaller, P.; Klussmann, S. GnRH Binding RNA and DNA spiegelmers: A novel approach toward GnRH antagonism. *Chem. Biol.* **2002**, *9*, 351–359. [CrossRef]
10. Yoshida, W.; Mochizuki, E.; Takase, M.; Hasegawa, H.; Morita, Y.; Yamazaki, H.; Sode, K.; Ikebukuro, K. Selection of DNA aptamers against insulin and construction of an aptameric enzyme subunit for insulin sensing. *Biosens. Bioelectron.* **2009**, *24*, 1116–1120. [CrossRef] [PubMed]
11. Dupont, D.M.; Andersen, L.M.; Botkjaer, K.A.; Andreasen, P.A. Nucleic acid aptamers against proteases. *Curr. Med. Chem.* **2011**, *18*, 4139–4151. [CrossRef] [PubMed]
12. Cerchia, L.; De Franciscis, V. Nucleic acid aptamers against protein kinases. *Curr. Med. Chem.* **2011**, *18*, 4152–4158. [CrossRef] [PubMed]

13. Missailidis, S. Targeting of antibodies using aptamers. *Methods Mol. Biol.* **2004**, *248*, 547–555. [CrossRef] [PubMed]
14. Chen, M.; Yu, Y.; Jiang, F.; Zhou, J.; Li, Y.; Liang, C.; Dang, L.; Lu, A.; Zhang, G. Development of cell-SELEX technology and its application in cancer diagnosis and therapy. *Int. J. Mol. Sci.* **2016**, *17*, 2079. [CrossRef] [PubMed]
15. Khvorova, A.; Kwak, Y.G.; Tamkun, M.; Majerfeld, I.; Yarus, M. RNAs that bind and change the permeability of phospholipid membranes. *Proc. Natl. Acad. Sci. USA* **1999**, *96*, 10649–10654. [CrossRef] [PubMed]
16. Darmostuk, M.; Rimpelová, S.; Gbelcová, H.; Ruml, T. Current approaches in SELEX: An update to aptamer selection technology. *Biotechnol. Adv.* **2015**, *33*, 1141–1161. [CrossRef] [PubMed]
17. Tuerk, C.; Gold, L. Systematic evolution of ligands by exponential enrichment: RNA ligands to bacteriophage T4 DNA polymerase. *Science* **1990**, *249*, 505–510. [CrossRef] [PubMed]
18. Tremblay, R.; Mulhbacher, J.; Blouin, S.; Penedo, J.C.; Lafontaine, D.A. Natural functional nucleic acids: Ribozymes and riboswitches. In *Functional Nucleic Acids for Analytical Applications*; Yingfu, L., Yi, L., Eds.; Springer: New York, NY, USA, 2009; pp. 11–46. ISBN 978-0-387-73711-9.
19. Silverman, S.K. Artificial functional nucleic acids: Aptamers, ribozymes, and deoxyribozymes identified by in vitro selection. In *Functional Nucleic Acids for Analytical Applications*; Yingfu, L., Yi, L., Eds.; Springer: New York, NY, USA, 2009; pp. 47–108. ISBN 978-0-387-73711-9.
20. Blackwell, T.K.; Weintraub, H. Differences and similarities in DNA-binding preferences of MyoD and E2A protein complexes revealed by binding site selection. *Science* **1990**, *250*, 1104–1110. [CrossRef] [PubMed]
21. Jacoby, K.; Lambert, A.R.; Scharenberg, A.M. Characterization of homing endonuclease binding and cleavage specificities using yeast surface display SELEX (YSD-SELEX). *Nucleic Acids Res.* **2017**, *45*, e11. [CrossRef] [PubMed]
22. Babendure, J.R.; Adams, S.R.; Tsien, R.Y. Aptamers switch on fluorescence of triphenylmethane dyes. *J. Am. Chem. Soc.* **2003**, *125*, 14716–14717. [CrossRef] [PubMed]
23. Nakamura, Y. Aptamers as therapeutic middle molecules. *Biochimie* **2017**. [CrossRef] [PubMed]
24. Parashar, A. Aptamers in therapeutics. *J. Clin. Diagn. Res.* **2016**, *10*, BE01–BE06. [CrossRef] [PubMed]
25. Poolsup, S.; Kim, C.Y. Therapeutic applications of synthetic nucleic acid aptamers. *Curr. Opin. Biotechnol.* **2017**, *48*, 180–186. [CrossRef] [PubMed]
26. Catuogno, S.; Esposito, C.L.; de Franciscis, V. Aptamer-mediated targeted delivery of therapeutics: An update. *Pharmaceuticals* **2016**, *9*, 69. [CrossRef] [PubMed]
27. Ni, S.; Yao, H.; Wang, L.; Lu, J.; Jiang, F.; Lu, A.; Zhang, G. Chemical modifications of nucleic acid aptamers for therapeutic purposes. *Int. J. Mol. Sci.* **2017**, *18*, 1683. [CrossRef] [PubMed]
28. Ilgu, M.; Nilsen-Hamilton, M. Aptamers in analytics. *Analyst* **2016**, *141*, 1551–1568. [CrossRef] [PubMed]
29. Seo, H.B.; Gu, M.B. Aptamer-based sandwich-type biosensors. *J. Biol. Eng.* **2017**, *11*, 11. [CrossRef] [PubMed]
30. Vorobyeva, M.; Vorobjev, P.; Venyaminova, A. Multivalent aptamers: Versatile tools for diagnostic and therapeutic applications. *Molecules* **2016**, *21*, 1613. [CrossRef] [PubMed]
31. Zhang, H.; Zhou, L.; Zhu, Z.; Yang, C. Recent progress in aptamer-based functional probes for bioanalysis and biomedicine. *Chem. A Eur. J.* **2016**, *22*, 9886–9900. [CrossRef] [PubMed]
32. Ruscito, A.; DeRosa, M.C. Small-molecule binding aptamers: Selection strategies, characterization, and applications. *Front. Chem.* **2016**, *4*, 1–14. [CrossRef] [PubMed]
33. Volk, D.E.; Lokesh, G.L.R. Development of Phosphorothioate DNA and DNA thioaptamers. *Biomedicines* **2017**, *5*, 41. [CrossRef] [PubMed]
34. Chen, T.; Hongdilokkul, N.; Liu, Z.; Thirunavukarasu, D.; Romesberg, F.E. The expanding world of DNA and RNA. *Curr. Opin. Chem. Biol.* **2016**, *34*, 80–87. [CrossRef] [PubMed]
35. Lipi, F.; Chen, S.; Chakravarthy, M.; Rakesh, S.; Veedu, R.N. In vitro evolution of chemically-modified nucleic acid aptamers: Pros and cons, and comprehensive selection strategies. *RNA Biol.* **2016**, *13*, 1232–1245. [CrossRef] [PubMed]
36. McKeague, M.; McConnell, E.M.; Cruz-Toledo, J.; Bernard, E.D.; Pach, A.; Mastronardi, E.; Zhang, X.; Beking, M.; Francis, T.; Giamberardino, A.; et al. Analysis of In Vitro Aptamer Selection Parameters. *J. Mol. Evol.* **2015**, *81*, 150–161. [CrossRef] [PubMed]
37. Dunn, M.R.; Jimenez, R.M.; Chaput, J.C. Analysis of aptamer discovery and technology. *Nat. Rev. Chem.* **2017**, *1*, 76. [CrossRef]
38. Gilbert, W. The RNA world. *Nature* **1986**, *319*, 618. [CrossRef]

39. Ellington, A.; Szostak, J. Selection in vitro of single-stranded DNA molecules that fold into specific ligand-binding structures. *Nature* **1992**, *355*, 850–852. [CrossRef] [PubMed]
40. McKeague, M.; Derosa, M.C. Challenges and opportunities for small molecule aptamer development. *J. Nucleic Acids* **2012**, *2012*, 748913. [CrossRef] [PubMed]
41. Lapa, S.A.; Chudinov, A.V.; Timofeev, E.N. The Toolbox for Modified Aptamers. *Mol. Biotechnol.* **2016**, *58*, 79–92. [CrossRef] [PubMed]
42. Meek, K.N.; Rangel, A.E.; Heemstra, J.M. Enhancing aptamer function and stability via in vitro selection using modified nucleic acids. *Methods* **2016**, *106*, 29–36. [CrossRef] [PubMed]
43. Diafa, S.; Hollenstein, M. Generation of aptamers with an expanded chemical repertoire. *Molecules* **2015**, *20*, 16643–16671. [CrossRef] [PubMed]
44. Lin, Y.; Qiu, Q.; Gill, S.C.; Jayasena, S.D. Modified RNA sequence pools for in vitro selection. *Nucleic Acids Res.* **1994**, *22*, 5229–5234. [CrossRef] [PubMed]
45. Fitzwater, T.; Polisky, B. A SELEX primer. *Meth. Enzym.* **1996**, *267*, 275–301. [PubMed]
46. Lauridsen, L.H.; Rothnagel, J.A.; Veedu, R.N. Enzymatic recognition of 2′-modified ribonucleoside 5′-triphosphates: Towards the evolution of versatile aptamers. *ChemBioChem* **2012**, *13*, 19–25. [CrossRef] [PubMed]
47. Stovall, G.M.; BedenBaugh, R.; Singh, S.; Meyer, A.; Hatala, P.; Ellington, A.D.; Hall, B. In vitro selection using modified or unnatural nucleotides. *Curr. Protoc. Nucleic Acid Chem.* **2014**, *56*, 9.6.1–9.6.33. [PubMed]
48. Pobanz, K.; Luptak, A. Improving the odds: Influence of starting pools on in vitro selection outcomes. *Methods* **2016**, *106*, 14–20. [CrossRef] [PubMed]
49. Cowperthwaite, M.C.; Ellington, A.D. Bioinformatic analysis of the contribution of primer sequences to aptamer structures. *J. Mol. Evol.* **2008**, *67*, 95–102. [CrossRef] [PubMed]
50. Thiel, W.H.; Bair, T.; Wyatt Thiel, K.; Dassie, J.P.; Rockey, W.M.; Howell, C.A.; Liu, X.Y.; Dupuy, A.J.; Huang, L.; Owczarzy, R.; et al. Nucleotide Bias Observed with a Short SELEX RNA Aptamer Library. *Nucleic Acid Ther.* **2011**, *21*, 253–263. [CrossRef] [PubMed]
51. Famulok, M.; Szostak, J.W. Stereospecific Recognition of Tryptophan Agarose by in Vitro Selected RNA. *J. Am. Chem. Soc.* **1992**, *114*, 3990–3991. [CrossRef]
52. Sassanfar, M.; Szostak, J.W. An RNA motif that binds ATP. *Nature* **1993**, *364*, 550–553. [CrossRef] [PubMed]
53. Hall, B.; Micheletti, J.M.; Satya, P.; Ogle, K.; Pollard, J.; Ellington, A.D. Design, synthesis, and amplification of DNA pools for in vitro selection. *Curr. Protoc. Mol. Biol.* **2009**, *88*. [CrossRef]
54. Burmeister, P.E.; Lewis, S.D.; Silva, R.F.; Preiss, J.R.; Horwitz, L.R.; Pendergrast, P.S.; McCauley, T.G.; Kurz, J.C.; Epstein, D.M.; Wilson, C.; et al. Direct In Vitro Selection of a 2′-*O*-Methyl Aptamer to VEGF. *Chem. Biol.* **2005**, *12*, 25–33. [CrossRef] [PubMed]
55. Burmeister, P.E.; Wang, C.; Killough, J.R.; Lewis, S.D.; Horwitz, L.R.; Ferguson, A.; Thompson, K.M.; Pendergrast, P.S.; McCauley, T.G.; Kurz, M.; et al. 2′-Deoxy purine, 2′-*O*-methyl pyrimidine (dRmY) aptamers as candidate therapeutics. *Oligonucleotides* **2006**, *16*, 337–351. [CrossRef] [PubMed]
56. Gupta, S.; Hirota, M.; Waugh, S.M.; Murakami, I.; Suzuki, T.; Muraguchi, M.; Shibamori, M.; Ishikawa, Y.; Jarvis, T.C.; Carter, J.D.; et al. Chemically modified DNA aptamers bind interleukin-6 with high affinity and inhibit signaling by blocking its interaction with interleukin-6 receptor. *J. Biol. Chem.* **2014**, *289*, 8706–8719. [CrossRef] [PubMed]
57. Stoltenburg, R.; Nikolaus, N.; Strehlitz, B. Capture-SELEX: Selection of DNA aptamers for aminoglycoside antibiotics. *J. Anal. Methods Chem.* **2012**, *2012*, 415697. [CrossRef] [PubMed]
58. Davis, J.H.; Szostak, J.W. Isolation of high-affinity GTP aptamers from partially structured RNA libraries. *Proc. Natl. Acad. Sci. USA* **2002**, *99*, 11616–11621. [CrossRef] [PubMed]
59. Wiegand, T.W.; Williams, P.B.; Dreskin, S.C.; Jouvin, M.H.; Kinet, J.P.; Tasset, D. High-affinity oligonucleotide ligands to human IgE inhibit binding to Fc epsilon receptor I. *J. Immunol.* **1996**, *157*, 221–230. [PubMed]
60. Shui, B.; Ozer, A.; Zipfel, W.; Sahu, N.; Singh, A.; Lis, J.T.; Shi, H.; Kotlikoff, M.I. RNA aptamers that functionally interact with green fluorescent protein and its derivatives. *Nucleic Acids Res.* **2012**, *40*. [CrossRef] [PubMed]
61. Shtatland, T.; Gill, S.C.; Javornik, B.E.; Johansson, H.E.; Singer, B.S.; Uhlenbeck, O.C.; Zichi, D. A; Gold, L. Interactions of Escherichia coli RNA with bacteriophage MS2 coat protein: Genomic SELEX. *Nucleic Acids Res.* **2000**, *28*, E93. [CrossRef] [PubMed]

62. Ouellet, E.; Foley, J.H.; Conway, E.M.; Haynes, C. Hi-Fi SELEX: A high-fidelity digital-PCR based therapeutic aptamer discovery platform. *Biotechnol. Bioeng.* **2015**, *112*, 1506–1522. [CrossRef] [PubMed]
63. Ouellet, E.; Lagally, E.T.; Cheung, K.C.; Haynes, C.A. A simple method for eliminating fixed-region interference of aptamer binding during SELEX. *Biotechnol. Bioeng.* **2014**, *111*, 2265–2279. [CrossRef] [PubMed]
64. Wen, J.-D.; Gray, D.M. Selection of genomic sequences that bind tightly to Ff gene 5 protein: Primer-free genomic SELEX. *Nucleic Acids Res.* **2004**, *32*, e182. [CrossRef] [PubMed]
65. Pan, W.; Xin, P.; Patrick, S.; Dean, S.; Keating, C.; Clawson, G. Primer-Free Aptamer Selection Using A Random DNA Library. *J. Vis. Exp.* **2010**, *629*, 369–385. [CrossRef]
66. Pan, W.; Xin, P.; Clawson, G.A. Minimal primer and primer-free SELEX protocols for selection of aptamers from random DNA libraries. *Biotechniques* **2008**, *44*, 351–360. [CrossRef] [PubMed]
67. Pan, W.; Clawson, G.A. Primer-free aptamer selection using a random DNA library. *Meth. Mol. Biol.* **2010**, *629*, 367–383. [CrossRef]
68. Vater, A.; Jarosch, F.; Buchner, K.; Klussmann, S. Short bioactive Spiegelmers to migraine-associated calcitonin gene-related peptide rapidly identified by a novel approach: Tailored-SELEX. *Nucleic Acids Res.* **2003**, *31*, e130. [CrossRef] [PubMed]
69. Jarosch, F.; Buchner, K.; Klussmann, S. In vitro selection using a dual RNA library that allows primerless selection. *Nucleic Acids Res.* **2006**, *34*, e86. [CrossRef] [PubMed]
70. Skrypina, N.A.; Savochkina, L.P.; Beabealashvilli, R.S. In vitro selection of single-stranded DNA aptamers that bind human pro-urokinase. *Nucleosides Nucleotides Nucleic Acids* **2004**, *23*, 891. [CrossRef] [PubMed]
71. Legiewicz, M.; Lozupone, C.; Knight, R.; Yarus, M. Size, constant sequences, and optimal selection. *RNA* **2005**, *11*, 1701–1709. [CrossRef] [PubMed]
72. Lai, Y.T.; DeStefano, J.J. A primer-free method that selects high-affinity single-stranded DNA aptamers using thermostable RNA ligase. *Anal. Biochem.* **2011**, *414*, 246–253. [CrossRef] [PubMed]
73. Lai, Y.-T.; DeStefano, J.J. DNA aptamers to human immunodeficiency virus reverse transcriptase selected by a primer-free SELEX method: Characterization and comparison with other aptamers. *Nucleic Acid Ther.* **2012**, *22*, 162–176. [CrossRef] [PubMed]
74. Tsao, S.-M.; Lai, J.-C.; Horng, H.-E.; Liu, T.-C.; Hong, C.-Y. Generation of aptamers from a primer-free randomized ssDNA library using magnetic-assisted rapid aptamer selection. *Sci. Rep.* **2017**, *7*, 45478. [CrossRef] [PubMed]
75. Nutiu, R.; Li, Y. In vitro selection of structure-switching signaling aptamers. *Angew. Chem. Int. Ed.* **2005**, *44*, 1061–1065. [CrossRef] [PubMed]
76. Nutiu, R.; Li, Y. Structure-switching signaling aptamers. *J. Am. Chem. Soc.* **2003**, *125*, 4771–4778. [CrossRef] [PubMed]
77. Pfeiffer, F.; Mayer, G. Selection and biosensor application of aptamers for small molecules. *Front. Chem.* **2016**, *4*, 25. [CrossRef] [PubMed]
78. Nikolaus, N.; Strehlitz, B. DNA-aptamers binding aminoglycoside antibiotics. *Sensors* **2014**, *14*, 3737–3755. [CrossRef] [PubMed]
79. Paniel, N.; Istambouli, G.; Triki, A.; Lozano, C.; Barthelmebs, L.; Noguer, T. Selection of DNA aptamers against penicillin G using Capture-SELEX for the development of an impedimetric sensor. *Talanta* **2017**, *162*, 232–240. [CrossRef] [PubMed]
80. Zhang, A.; Chang, D.; Zhang, Z.; Li, F.; Li, W.; Wang, X.; Li, Y.; Hua, Q. In vitro selection of DNA aptamers that binds geniposide. *Molecules* **2017**, *22*, 383. [CrossRef] [PubMed]
81. Martin, J.A.; Smith, J.E.; Warren, M.; Chávez, J.L.; Hagen, J.A.; Kelley-Loughnane, N. A method for selecting structure-switching aptamers applied to a colorimetric gold nanoparticle assay. *J. Vis. Exp.* **2015**, e52545. [CrossRef] [PubMed]
82. Spiga, F.M.; Maietta, P.; Guiducci, C. More DNA-aptamers for small drugs: A capture-SELEX coupled with surface plasmon resonance and high-throughput sequencing. *ACS Comb. Sci.* **2015**, *17*, 326–333. [CrossRef] [PubMed]
83. Rajendran, M.; Ellington, A.D. Selection of fluorescent aptamer beacons that light up in the presence of zinc. *Anal. Bioanal. Chem.* **2008**, *390*, 1067–1075. [CrossRef] [PubMed]
84. Morse, D.P. Direct selection of RNA beacon aptamers. *Biochem. Biophys. Res. Commun.* **2007**, *359*, 94–101. [CrossRef] [PubMed]

85. Boots, J.L.; Matylla-Kulinska, K.; Zywicki, M.; Zimmermann, B.; Schroeder, R. Genomic SELEX. In *Handbook of RNA Biochemistry: Second, Completely Revised and Enlarged Edition*; Hartmann, R. K., Bindereif, A., Schön, A., Westhof, E., Eds.; Wiley-VCH Verlag GmbH & Co: Weinheim, Germany, 2014; pp. 1185–1206. ISBN 9783527327645.
86. Ogasawara, H.; Hasegawa, A.; Kanda, E.; Miki, T.; Yamamoto, K.; Ishihama, A. Genomic SELEX search for target promoters under the control of the PhoQP-RstBA signal relay cascade. *J. Bacteriol.* **2007**, *189*, 4791–4799. [CrossRef] [PubMed]
87. Kim, S.; Shi, H.; Lee, D.K.; Lis, J.T. Specific SR protein-dependent splicing substrates identified through genomic SELEX. *Nucleic Acids Res.* **2003**, *31*, 1955–1961. [CrossRef] [PubMed]
88. Zimmermann, B.; Bilusic, I.; Lorenz, C.; Schroeder, R. Genomic SELEX: A discovery tool for genomic aptamers. *Methods* **2010**, *52*, 125–132. [CrossRef] [PubMed]
89. Davies, D.R.; Gelinas, A.D.; Zhang, C.; Rohloff, J.C.; Carter, J.D.; O'Connell, D.; Waugh, S.M.; Wolk, S.K.; Mayfield, W.S.; Burgin, A.B.; et al. Unique motifs and hydrophobic interactions shape the binding of modified DNA ligands to protein targets. *Proc. Natl. Acad. Sci. USA* **2012**, *109*, 19971–19976. [CrossRef] [PubMed]
90. Gawande, B.N.; Rohloff, J.C.; Carter, J.D.; von Carlowitz, I.; Zhang, C.; Schneider, D.J.; Janjic, N. Selection of DNA aptamers with two modified bases. *Proc. Natl. Acad. Sci. USA* **2017**, *114*, 2898–2903. [CrossRef] [PubMed]
91. Gold, L.; Ayers, D.; Bertino, J.; Bock, C.; Bock, A.; Brody, E.N.; Carter, J.; Dalby, A.B.; Eaton, B.E.; Fitzwater, T.; Flather, D.; et al. Aptamer-based multiplexed proteomic technology for biomarker discovery. *PLoS ONE* **2010**, *5*, e15004. [CrossRef] [PubMed]
92. Naduvile Veedu, R.; AlShamaileh, H. Next generation nucleic acid aptamers with two base modified nucleotides improve the binding affinity and potency. *ChemBioChem* **2017**, *9*, 9–12. [CrossRef]
93. Ochsner, U.A.; Katilius, E.; Janjic, N. Detection of Clostridium difficile toxins A, B and binary toxin with slow off-rate modified aptamers. *Diagn. Microbiol. Infect. Dis.* **2013**, *76*, 278–285. [CrossRef] [PubMed]
94. Chudinov, A.V.; Kiseleva, Y.Y.; Kuznetsov, V.E.; Shershov, V.E.; Spitsyn, M.A.; Guseinov, T.O.; Lapa, S.A.; Timofeev, E.N.; Archakov, A.I.; Lisitsa, A.V.; et al. Structural and functional analysis of biopolymers and their complexes: Enzymatic synthesis of high-modified DNA. *Mol. Biol.* **2017**, *51*, 474–482. [CrossRef]
95. Kimoto, M.; Yamashige, R.; Matsunaga, K.; Yokoyama, S.; Hirao, I. Generation of high-affinity DNA aptamers using an expanded genetic alphabet. *Nat. Biotechnol.* **2013**, *31*, 453–457. [CrossRef] [PubMed]
96. Sefah, K.; Yang, Z.; Bradley, K.M.; Hoshika, S.; Jimenez, E.; Zhang, L.; Zhu, G.; Shanker, S.; Yu, F.; Turek, D.; et al. In vitro selection with artificial expanded genetic information systems. *Proc. Natl. Acad. Sci. USA* **2014**, *111*, 1449–1454. [CrossRef] [PubMed]
97. Horiya, S.; Macpherson, I.S.; Krauss, I.J. Recent Strategies Targeting HIV Glycans in Vaccine Design Satoru. *Nat. Chem. Biol.* **2015**, *10*, 990–999. [CrossRef] [PubMed]
98. Temme, J.S.; Krauss, I.J. SELMA: Selection with modified aptamers. *Curr. Protoc. Chem. Biol.* **2015**, *7*, 73–92. [CrossRef] [PubMed]
99. Temme, J.S.; MacPherson, I.S.; Decourcey, J.F.; Krauss, I.J. High temperature SELMA: Evolution of DNA-supported oligomannose clusters which are tightly recognized by HIV bnAb 2G12. *J. Am. Chem. Soc.* **2014**, *136*, 1726–1729. [CrossRef] [PubMed]
100. Tolle, F.; Brändle, G.M.; Matzner, D.; Mayer, G. A Versatile Approach Towards Nucleobase-Modified Aptamers. *Angew. Chem. Int. Ed.* **2015**, *54*, 10971–10974. [CrossRef] [PubMed]
101. Warner, W.A.; Sanchez, R.; Dawoodian, A.; Li, E.; Momand, J. Multivalent glycocluster design through directed evolution. *Angew. Chem. Int. Ed.* **2013**, *80*, 631–637. [CrossRef]
102. Warner, W.A.; Sanchez, R.; Dawoodian, A.; Li, E.; Momand, J. Directed Evolution of 2G12-Targeted Nonamannose Glycoclusters by SELMA. *Chemistry* **2013**, *19*, 17291–17295. [CrossRef]
103. Blind, M.; Blank, M. Aptamer Selection Technology and Recent Advances. *Mol. Ther. Acids* **2015**, *4*, e223. [CrossRef] [PubMed]
104. Takahashi, M.; Wu, X.; Ho, M.; Chomchan, P.; Rossi, J.J.; Burnett, J.C.; Zhou, J. High throughput sequencing analysis of RNA libraries reveals the influences of initial library and PCR methods on SELEX efficiency. *Sci. Rep.* **2016**, *6*, 33697. [CrossRef] [PubMed]
105. Blank, M. Next-Generation Analysis of Deep Sequencing Data: Bringing Light into the Black Box of SELEX Experiments. *Methods* **2016**, *1380*, 85–95. [CrossRef]

106. Gevertz, J.; Gan, H.H.; Schlick, T. In vitro RNA random pools are not structurally diverse: A computational analysis. *RNA* **2005**, *11*, 853–863. [CrossRef] [PubMed]
107. Bartel, D.P.; Zapp, M.L.; Green, M.R.; Szostak, J.W. HIV-1 Rev regulation involves recognition of non-Watson-Crick base pairs in viral RNA. *Cell* **1991**, *67*, 529–536. [CrossRef]
108. Hesselberth, J.R.; Miller, D.; Robertus, J.; Ellington, A.D. In vitro selection of RNA molecules that inhibit the activity of ricin A-chain. *J. Biol. Chem.* **2000**, *275*, 4937–4942. [CrossRef] [PubMed]
109. Burke, D.H.; Scates, L.; Andrews, K.; Gold, L. Bent pseudoknots and novel RNA inhibitors of type 1 human immunodeficiency virus (HIV-1) reverse transcriptase. *J. Mol. Biol.* **1996**, *264*, 650–666. [CrossRef] [PubMed]
110. Knight, R.; Yarus, M. Analyzing partially randomized nucleic acid pools: Straight dope on doping. *Nucleic Acids Res.* **2003**, *31*, e30. [CrossRef] [PubMed]
111. Bittker, J.A.; Le, B.V.; Liu, D.R. Nucleic acid evolution and minimization by nonhomologous random recombination. *Nat. Biotechnol.* **2002**, *20*, 1024–1029. [CrossRef] [PubMed]
112. Carothers, J.M.; Oestreich, S.C.; Davis, J.H.; Szostak, J.W. Informational complexity and functional activity of RNA structures. *Science* **2004**, *126*, 5130–5137. [CrossRef] [PubMed]
113. Paige, G.F.; Wu, K.; Jaffrey, S.R. RNA mimics of green fluorescent protein. *Science* **2011**, *333*, 642–646. [CrossRef] [PubMed]
114. Xu, J.; Carrocci, T.J.; Hoskins, A.A. Evolution and characterization of a benzylguanine-binding RNA aptamer. *Chem. Commun.* **2016**, 549–552. [CrossRef] [PubMed]
115. Yang, K.A.; Pei, R.; Stefanovic, D.; Stojanovic, M.N. Optimizing cross-reactivity with evolutionary search for sensors. *J. Am. Chem. Soc.* **2012**, *134*, 1642–1647. [CrossRef] [PubMed]
116. Trevino, S.G.; Levy, M. High-throughput bead-based identification of structure-switching aptamer beacons. *ChemBioChem* **2014**, *15*, 1877–1881. [CrossRef] [PubMed]
117. Zhu, L.; Li, C.; Zhu, Z.; Liu, D.; Zou, Y.; Wang, C.; Fu, H.; Yang, C.J. In vitro selection of highly efficient G-quadruplex-based DNAzymes. *Anal. Chem.* **2012**, *84*, 8383–8390. [CrossRef] [PubMed]
118. Ruff, K.M.; Snyder, T.M.; Liu, D.R. Enhanced functional potential of nucleic acid aptamer libraries patterned to increase secondary structure. *J. Am. Chem. Soc.* **2010**, *132*, 9453–9464. [CrossRef] [PubMed]
119. Chushak, Y.; Stone, M.O. In silico selection of RNA aptamers. *Nucleic Acids Res.* **2009**, *37*, e87. [CrossRef] [PubMed]
120. Kim, N.; Gan, H.H.; Schlick, T. A computational proposal for designing structured RNA pools for in vitro selection of RNAs. *RNA* **2007**, *13*, 478–492. [CrossRef] [PubMed]
121. Kim, N.; Shin, J.S.; Elmetwaly, S.; Gan, H.H.; Schlick, T. RagPools: RNA-As-Graph-Pools-a web server for assisting the design of structured RNA pools for in vitro selection. *Bioinformatics* **2007**, *23*, 2959–2960. [CrossRef] [PubMed]
122. RAGPOOLS (RNA-As-Graph-Pools)—A Web Server. Available online: http://rubin2.biomath.nyu.edu/home.html (accessed on 27 October 2017).
123. Luo, X.; McKeague, M.; Pitre, S.; Dumontier, M.; Green, J.; Golshani, A.; Derosa, M.C.; Dehne, F. Computational approaches toward the design of pools for the in vitro selection of complex aptamers. *RNA* **2010**, *16*, 2252–2262. [CrossRef] [PubMed]


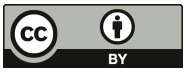

International Journal of
*Molecular Sciences*

MDPI

*Review*

# Aptamers Selected for Recognizing Amyloid β-Protein—A Case for Cautious Optimism

**Farid Rahimi**

Division of Biomedical Science and Biochemistry, Research School of Biology, The Australian National University, Canberra, ACT 2601, Australia; farid.rahimi@anu.edu.au or z2170549@zmail.unsw.edu.au; Tel.: +61-2-6125-2851

Received: 5 February 2018; Accepted: 22 February 2018; Published: 27 February 2018

**Abstract:** Aptamers are versatile oligonucleotide ligands used for molecular recognition of diverse targets. However, application of aptamers to the field of amyloid β-protein (Aβ) has been limited so far. Aβ is an intrinsically disordered protein that exists in a dynamic conformational equilibrium, presenting time-dependent ensembles of short-lived, metastable structures and assemblies that have been generally difficult to isolate and characterize. Moreover, despite understanding of potential physiological roles of Aβ, this peptide has been linked to the pathogenesis of Alzheimer disease, and its pathogenic roles remain controversial. Accumulated scientific evidence thus far highlights undesirable or nonspecific interactions between selected aptamers and different Aβ assemblies likely due to the metastable nature of Aβ or inherent affinity of RNA oligonucleotides to β-sheet-rich fibrillar structures of amyloidogenic proteins. Accordingly, lessons drawn from Aβ–aptamer studies emphasize that purity and uniformity of the protein target and rigorous characterization of aptamers' specificity are important for realizing and garnering the full potential of aptamers selected for recognizing Aβ or other intrinsically disordered proteins. This review summarizes studies of aptamers selected for recognizing different Aβ assemblies and highlights controversies, difficulties, and limitations of such studies.

**Keywords:** Alzheimer disease; amyloid β-protein; antibodies; cross-reactions; nucleotide aptamers; oligonucleotide ligands; systematic evolution of ligands by exponential enrichment; specificity; therapeutics

## 1. Introduction

Specifically detecting or recognizing targets of interest—by molecular recognition—is fundamental in many medical and scientific applications. Conventionally, antibodies have been used for detecting antigenic targets, which may include large proteins, small peptides, polysaccharides, lipids, or nucleic acids. Antibodies have been essential for diagnostic or routine clinical assays and immunotherapeutic applications, and in important techniques such as immunohistochemistry, immunoprecipitation, enzyme-linked immunosorbent assay (ELISA), and western blotting. Besides antibodies, however, nucleotide aptamers (oligonucleotide ligands) have emerged since 1990 and progressed rapidly as alternative molecular-recognition tools, offering many useful and novel scientific applications [1–6]. So far, US Food and Drug Administration (FDA) has approved one aptamer drug, Macugen® or generically pegaptanib (Pfizer Pharmaceuticals Group, New York, NY, USA) [7,8], and reportedly, some additional ten aptamers have undergone clinical trials for treating various conditions, including macular degeneration, coagulation, cancer, and inflammation [5,6]. The continually increasing number of reports on aptamers published since the initial 1990 publications [9–12] also vouches for the rapid progress of aptamer science. Searching the MEDLINE database through PubMed for the phrase "aptamer or aptamers" returns 328 reports published in the first decade of aptamer research. The same search returns 9459 reports collectively from 2001 to the end of December 2017 (Figure 1). (Related to aptamers, spiegelmers also are synthetic ligand-binding oligonucleotides, but spiegelmers comprise non-natural L-nucleotides [13]).

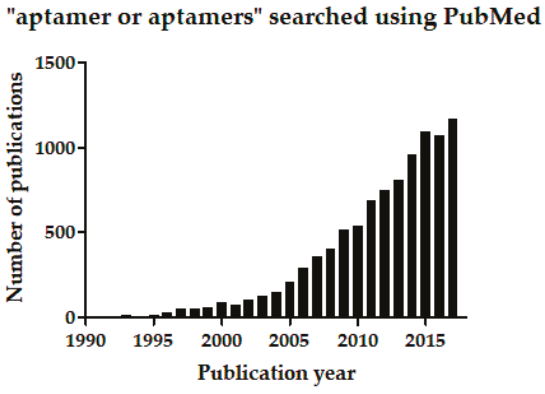


**Figure 1.** The phrase "aptamer or aptamers" was used as the search term on Pubmed. The number of publications are plotted per publication year.

Importantly, aptamers offer additional advantages that antibodies do not (aptamer advantages and disadvantages have been extensively compared to those of antibodies elsewhere [5]). For example, aptamers effectively cause low or no immunogenicity and can be "selected" for many diverse molecules, including toxic compounds, for which generating antibodies in vivo would likely be impossible. Individual aptamers always interact with a single "aptatope", whereas antibodies could be monoclonal or polyclonal. Moreover, an aptamer's selectivity and specificity for a particular target's aptatope can potentially be tested during the aptamer-selection process in vitro. An antibody's target specificity, however, cannot be ensured because antibodies are generated in vivo, and their capability to distinguish between specific antigenic and less structured epitopes (e.g., polyclonal antibodies) or between conformational epitopes (e.g., monoclonal antibodies) and their closely related molecular structures is determined post facto.

Conformational specificity of antibodies or that of aptamers becomes particularly crucial for targeting intrinsically disordered proteins (IDPs). Many amyloidogenic proteins belong to IDPs [14–16]. IDPs are heterogeneous proteins that exist in a dynamic conformational equilibrium under physiological conditions and present a time-dependent ensemble of short-lived structures that are likely difficult to isolate or stabilize. This conformational behavior, as well as homooligomerization and fibrillization, characterize amyloid β-protein (Aβ) [17,18], a metastable, amyloidogenic IDP that is controversially linked to pathogenesis of Alzheimer disease (AD). Some antibodies generated against a certain assembly of Aβ reportedly cross-react with other assemblies of this peptide. Similarly, polyclonal antibodies generated against oligomeric or fibrillar Aβ may cross-react with structurally similar assemblies of other IDPs unrelated to Aβ [19,20]. Therefore, specificities of some Aβ antibodies have been unconvincing and disputed [21,22], and studies using such disputed antibodies should be revisited and interpreted carefully. Akin to reports using controversial antibodies or studies using insufficiently characterized antibodies against Aβ, collective evidence on aptamers selected for reacting with Aβ highlights undesirable or unexpected interactions despite implementing strict selection experiments. Such studies should also be reconsidered and reviewed carefully.

This review discusses controversies and methodological limitations of using and characterizing aptamers selected for recognizing, mainly, Aβ, while alluding to some other relevant studies of Aβ-unrelated IDPs. To set the scene and before summarizing aptamer studies relevant to Aβ (in Section 4), I briefly introduce this peptide in Section 2 and write about aptamers and the systematic evolution of ligands by exponential enrichment (SELEX) in Section 3. In Section 5, I highlight the shortcomings of sodium dodecyl sulfate–polyacrylamide gel electrophoresis (SDS–PAGE) in

characterizing Aβ assemblies and in assessing aptamer/antibody specificities for such assemblies. Finally, I sum up with contextual conclusions.

## 2. Amyloid β-Protein and Alzheimer Disease

Aβ is produced mainly as Aβ40 or Aβ42 (respectively comprising 40 or 42 amino acid residues) from the amyloid β-protein precursor (APP), when APP is sequentially cleaved by β-secretase and γ-secretase [23,24]. Aβ is produced in its monomeric form as a normal, physiologically relevant peptide [25–34], but it has been studied profusely in pathogenic, protein-misfolding contexts underlying AD. Aβ's normal functions and its cytotoxic effects may be regulated by its local concentration; for example, picomolar amounts of synthetic Aβ42 reportedly enhance long-term potentiation and hippocampus-dependent memory in mice, whereas nanomolar levels of the same peptide yield the opposite effects [31]. Long-term potentiation is an electrophysiological paradigm for learning and memory composition, but its role in this capacity has been debated [35]. The above concentration-dependent effects are not unique to Aβ function in the brain. As an aside, S100B, a calcium-binding protein abundant in the brain and implicated in AD pathogenesis [36,37], exerts neurotrophic or neurotoxic effects at nanomolar or micromolar concentrations, respectively [38].

Aβ's pathogenic premises in AD have been based on the classical amyloid cascade hypothesis [39] and its contemporary, revised version [40–42]. The classical amyloid cascade hypothesis posited that overproduction and deposition of Aβ fibrils in amyloid plaques, the pathological hallmarks of AD, cause AD and that formation of neurofibrillary tangles (the other AD hallmark), cell loss, vascular damage, and dementia are direct results of Aβ deposition [39]. The contemporary/revised version of the amyloid cascade hypothesis—the oligomer cascade hypothesis [43]—gives primacy to the neurotoxic and synaptotoxic effects of soluble, prefibrillar oligomeric Aβ assemblies in AD pathogenesis [42]. Therefore, many trials have attempted to target Aβ for therapeutic or diagnostic purposes [44,45]. However, the two cascade hypotheses have been consistently debated and challenged [46–49]. Furthermore, since the original observations that Aβ is a major component of plaques in AD-afflicted brains [50–54], and that the plaques contain fibrillar, β-sheet-rich Aβ [55,56], and since introduction of the revised hypothesis [40,41], diverse but elusive structural assemblies of Aβ have been described and studied profusely in vitro [43,57–60], adding to the complexity of Aβ-oligomer literature. These assemblies have been studied or described structurally, functionally, or both, but their interrelationships, and more importantly, their relevance to AD pathogenesis and progression are still enigmatic [57,60] particularly because their undisputed identification or characterization in vivo has been challenging [47].

Importantly, the AD plaque core contains not only Aβ—as thought [61–63]—but also other potential products of APP processing [22,64], other proteinaceous and nonproteinaceous components, including glycosaminoglycan, collagen, lipids, metal ions, reactive oxygen species, inflammatory proteins, and nucleic acids [65–77]. These observations suggest that diverse detrimental mechanisms, other than or additional to misfolding or deposition of Aβ, may underlie AD pathogenesis or progression. These mechanisms include disruption of cellular metabolism [78,79], deregulation of synapse structure and function [80], membrane damage [81], ionic imbalance [82], oxidative stress [83], inflammatory stress [84–86], and apoptotic [78] or other cytotoxic effects. Aβ by itself is unlikely to be underlying AD pathogenesis or progression. This is corroborated by the failure or discontinuation of some high-profile clinical trials designed based on the amyloid cascade hypothesis [47], repudiating the notion that Aβ is central to AD pathogenesis. It is likely that targeting of Aβ by some means may disrupt its physiological roles and may not be effective therapeutically in humans [47]. Although this may be an unresolved controversy, the physiological roles of Aβ should be considered when designing Aβ-targeting therapeutics.

## 3. Aptamers and Systematic Evolution of Ligands by Exponential Enrichment

Aptamers for a target are selected from a pool of random nucleotides by a combinatorial, in vitro molecular-evolution technique termed—SELEX [9,10,12]. Two groups first used SELEX to select highly avid and specific RNA aptamers for particular targets, including organic dyes [10] and bacteriophage T4 DNA polymerase [12,87]. Since then, aptamers have been selected for a variety of targets, including metal ions [88], organic molecules [89], amino acids [90–92], viral nucleic acid components [93–96], peptides [97], proteins [5,6,98], drugs [99–101], macromolecules [102–105], cells [106,107], and pathogens [108–113].

SELEX is an iterative process that enables selecting and amplifying a specific property (e.g., avid binding for aptamers, or enzymatic activity for ribozymes or DNAzymes) from a large pool of oligonucleotide sequences, similar to a miniature Darwinian evolution [6,114]. A typical SELEX experiment includes repeated rounds of (1) incubating a library of random oligonucleotide sequences (~$10^{13}$–$10^{15}$ unique sequence in a naïve, unselected pool) with a target molecule; (2) separating target-bound sequences from unbound sequences; (3) dissociating the oligonucleotide–target complexes; and (4) amplifying, identifying, and sequencing the resultant, selected oligonucleotide pool, which contains potentially specific and avid aptamers for the target [114]. Repeated rounds of SELEX are driven by affinity to the target and by competition amongst random sequences. Preselection (negative SELEX) and counter-SELEX (subtractive SELEX) can be interspersed between certain rounds of SELEX respectively to remove sequences that nonspecifically bind to the partitioning matrix or those that bind to molecules closely similar to the actual target [114]. The final oligonucleotide pool becomes enriched with a relatively small number of sequences that, in case of aptamers, bind the target avidly and hopefully specifically. (In case of ribozymes and DNAzymes, sequences with desired catalytic activities are enriched [115,116].) The resultant aptamers can be amplified by polymerase chain reaction (PCR), products of which can then be cloned and sequenced to identify the best binding sequences. Finally, binding affinities, specificities, and cross-reactivity of aptamers are determined [117], and post-SELEX modifications are applied to improve affinity, specificity, stability, pharmacokinetics, or bioavailability of aptamers [114,118].

Since its inception [10,12,87], many variations of SELEX have been developed and used, achieving targeted and specific outcomes [119,120], and SELEX has been optimized and extended to isolation of RNA, single-stranded DNA, or modified versions thereof.

The discriminatory power and specificity of aptamers in some cases are surprisingly high. Aptamers reportedly can discriminate targets based on subtle chemical differences e.g., presence or absence of a methyl/hydroxyl group or chirality (*R* vs. *S* enantiomer). For example, a theophylline-specific aptamer distinguishes it from caffeine—which differs from theophylline by only one methyl group—at least ten-fold more efficiently than an antibody generated for this purpose [121]. Similarly, an enantioselective, modified DNA aptamer could distinguish (*R*)-thalidomide from (*S*)-thalidomide [122]. Such high levels of aptamer specificity result from the selective pressure achieved by counter-SELEX (subtractive SELEX) [121].

Selecting highly specific aptamers is not always achievable, however. For example, in some cases of cell-SELEX, which uses whole cells for selection, the resultant aptamers recognize both membrane proteins and membrane lipids [123]. As discussed in more detail later, selecting for targeting IDPs may also result in aptamers that cross-react with different structures of a targeted protein. Although determining aptamer specificity is a crucial step in characterizing aptamers, aptamer characterization has rarely been fully considered, especially for aptamers selected for cell-membrane targets [123] and for IDPs such as prion proteins (PrP) [124] or Aβ [125–127]. In the following two sections, I discuss why characterizing aptamer specificity is important in research into Aβ and, by extension, other IDPs.

## 4. Aptamers and Aβ

Aptamer studies using IDPs and amyloidogenic proteins so far show a general tendency for aptamers (and unselected, naïve oligonucleotide libraries) to preferentially bind to β-sheet-rich

fibrillar amyloid assemblies despite selection against prefibrillar/nonfibrillar assemblies. For example, several groups have reported aptamers that bind PrP sequences [124,128–134]. An RNA aptamer selected for the recombinant bovine PrP reportedly recognized bovine PrP-β [134]—a soluble, oligomeric, β-sheet-rich conformational variant of full-length PrP that forms amyloid fibrils [135]. Bunka et al. generated aptamers for monomeric and several forms of fibrillar β2-microglobulin [136]. These aptamers were found to bind also fibrils of other amyloidogenic proteins, including apomyoglobin, Aβ40, transthyretin, or lysozyme, in addition to those of β2-microglobulin [136]. In the latter study, the naïve library also apparently reacted with long, straight fibrils of β2-microglobulin with half the strength of the selected aptamers [136]. Aptamers for α-synuclein have been reported and shown to bind strongly to α-synuclein oligomers but weakly to its fibrils [137,138]. Similar outcomes have been obtained in the context of Aβ as discussed in detail below.

The first study that described RNA aptamers for Aβ used a chemically synthesized monomeric Aβ40 preparation with an additional engineered N-terminal cysteine as SELEX target. This preparation was immobilized on a thiopropyl-activated Sepharose 6B matrix by disulfide bonding [125]. Importantly, because Aβ tends to aggregate rapidly, the authors coupled the Aβ40 preparation to Sepharose using 60% 1,1,1,3,3,3-hexafluoro-2-propanol (HFIP) in 10 mM Tris-HCl, pH 7.7, to keep Aβ40 disaggregated and soluble. (HFIP is used to dissociate self-assembling amyloid proteins [139,140].) The authors used a random 70-nucleotide RNA library (~$10^{15}$ sequences) plus the flanking 5′ and 3′ primer sites. The library was first precleared (negative SELEX) using unloaded Sepharose and then incubated with Sepharose-bound Aβ40 at 4 μM on the resin. After washing the unbound RNA pool, the bound RNA was eluted with Aβ40 by dithiothreitol reduction of the disulfide bond. RNA was extracted, reverse transcribed to DNA, and amplified by PCR. After eight rounds of selection, ~140 binding sequences were eluted. The aptamers were then characterized by affinity chromatography to measure their dissociation constants, which ranged from 29 to 48 nM. Surprisingly, the selected aptamers did not bind soluble Aβ40 as tested by counter-elution using soluble Aβ40 and by mobility-shift assays. The aptamers showed unexpected binding to fibrillar assemblies of Aβ40 as observed by streptavidin–biotin conjugation, gold labeling, and electron microscopy. The authors concluded that Aβ40 may have aggregated on the matrix despite their using HFIP during Aβ40 conjugation to Sepharose [125], and thus selected aptamers bound fibrils nonspecifically.

As another example of aptamers selected for Aβ preparations, aptamers reported by Takahashi et al. so far are the only ones displaying binding affinity to an oligomeric "model" of Aβ40 [126]. The library pool in their study was incubated with Aβ40 conjugated to colloidal gold nanoparticles (10 nm diameter) acting as an "Aβ oligomer model," which was described previously [20]. Two aptamers, N2 and E2, could bind this Aβ40 preparation when incubated at 4 °C and recognized Aβ40 in solution by fluorescence anisotropy. $K_d$ values calculated from fluorescence anisotropy studies ranged from 11 to 22 μM. However, upon aptamer binding saturation with ~50 μM Aβ40, fluorescence anisotropy showed a change of 0.006–0.008 units which may well fall within the noise of such experiments (as discussed elsewhere [141]) despite the authors' argument that this change may have resulted from the small mass of Aβ40. Thus, the reported $K_d$ values remain questionable.

Conjugating Aβ40 to gold nanoparticles was first used to imitate spherical oligomers as antigen for generating the oligomer-specific antibody A11 [20]. A11 was found to react specifically with certain oligomeric preparations of Aβ40 and Aβ42 but not soluble, low-molecular-weight Aβ or fibrillar Aβ preparations [20]. Low-molecular-weight Aβ preparations comprise soluble, monomeric Aβ in dynamic equilibrium with low-order Aβ homooligomers [142]. Although arranging Aβ40 monomers on the surface of gold nanoparticles likely mimics high-order Aβ assemblies, and N2 and E2 aptamers likely preferably bound these structures, the ultimate proof of specificity is to exclude cross-reactivity of N2 or E2 aptamers with Aβ fibrils or fibrillar assemblies of other amyloidogenic proteins because of reported cross-reactivity of some "oligomer-specific" antibodies and "oligomer-specific" aptamers with fibrillar amyloid structures [21]. N2 and E2 were not tested for their cross-reactivity with fibrillar assemblies of Aβ or of other amyloidogenic proteins. They were not tested against other oligomeric

preparations of Aβ or oligomeric preparations of other IDPs either. Similar to the case of N2 and E2, the aptamer M5-15, selected for the amyloidogenic protein, α-synuclein, reportedly reacted with monomeric and oligomeric forms of the target protein, but its cross-reactivity with α-synuclein fibrils was not tested [138].

Although N2 and E2 aptamers were not tested for their cross-reactivity with fibrillar assemblies of Aβ40 or Aβ42, they reportedly inhibited Aβ fibrillization as observed by ELISA using the 6E10 antibody [126]. (6E10 is a monoclonal antibody raised against residues 1–17 of human Aβ [143–145]). However, the reported ELISA results are surprising because of the following two caveats. First, at the initial time point, 6E10 ELISA did not detect the Aβ preparation either in the absence or in presence of the two aptamers, contradicting the fact that 6E10 reportedly reacts with random-coil (or statistical-coil) Aβ monomers [19,146]. Thus, at the initial time points, the sample without aptamers should have presented an ELISA signal at least as intense as that with the fibrillar preparation without added aptamers. Secondly, the authors did not exclude the possibility that the aptamers could compete with 6E10 binding to Aβ under the ELISA conditions. Thus, ELISA results may merely indicate low binding of the 6E10 antibody to the protein–aptamer mixture because of potential competition between aptamer and 6E10 for binding to fibrillar Aβ. Nevertheless, Aβ fibrils were not detected by electron microscopy in the presence of the aptamers; authors reported oligomers, protofibrils, and amorphous aggregates as potential products of fibril disintegration in the presence of aptamers [126]. Whether the abovementioned nonfibrillar Aβ assemblies were cytotoxic or not was not tested. Thus, the full reactivity/specificity spectrum and functions of these aptamers are yet to be confirmed.

Three years later, the N2 aptamer was reported as a conjugate to poly(lactic-*co*-glycolic acid)–coated curcumin (PLGA–curcumin) nanoparticles [147]. Aptamer–PLGA–curcumin nanoparticles were not cytotoxic, taken up by cells, and found to bind Aβ42 fibrils and disintegrate them [147]. Whether the fibril-disintegration products under such experimental conditions were cytotoxic or not was not tested, but the authors concluded that the fibril-degrading effect of curcumin was unaffected by conjugation of the aptamer to the PLGA–curcumin nanoparticles. The authors postulated that the resultant smaller amyloid fragments could easily be cleared by phagocytosis [147]. Interestingly, a recently published review [148] cites the above study, "... the N2 aptamer conjugated to curcumin-polymer nanoparticles enhanced binding to, and disaggregated, amyloid plaques, which were then cleared by phagocytosis", misleading the reader by misreporting that actual "amyloid plaques" were used and "phagocytosis assays" were done in the original study [147]. Taking both studies [126,147] together, it is unclear whether the N2 aptamer or curcumin or both could bind Aβ42 fibrils (not plaques as mentioned [148], which are the in vivo hallmarks of AD) and degrade them because both activities were seemingly attributed to curcumin and N2. Importantly, curcumin along with resveratrol and epigallocatechin-3-gallate (reviewed [149]) have been dubbed as pan-assay-interfering compounds [150,151], and conclusions made about these three polyphenols in the AD literature in relation to their effects on Aβ should be reassessed carefully [152].

We asked why aptamers selected for monomeric or prefibrillar assemblies of amyloidogenic proteins recognized their polymeric, fibrillar forms. Could specific aptamers for monomeric and/or oligomeric forms of an amyloidogenic protein ever be obtained? What are the implications of fibril reactivity of RNA or DNA aptamers? To answer these questions, we performed SELEX to obtain aptamers that could potentially recognize the covalently stabilized trimeric Aβ40 [153], which were produced by using photo-induced crosslinking of unmodified proteins (PICUP) [154,155], extracted from gels subjected to SDS–PAGE, and purified by removing SDS [156]. We also used a mixture of low-molecular-weight oligomeric Aβ40, which was generated by PICUP but not exposed to SDS at all, in later experiments. (The significance of SDS effects on Aβ preparations is discussed below).

I summarize the main findings of that study: (1) aptamers selected for purified, covalently stabilized trimeric Aβ40 failed to react with purified Aβ40 trimers or with the low-molecular-weight mixture of prefibrillar Aβ40 assemblies, but they reacted with Aβ40 or Aβ42 fibrils, as confirmed by dot blotting. (2) Aptamers selected for recognizing trimeric Aβ40 reacted not only with Aβ

fibrils, but also with fibrils of other amyloidogenic proteins, including calcitonin, islet amyloid polypeptide (IAPP), insulin, lysozyme, and prion$_{106–126}$. (3) Our aptamers reacted with fibrils of the tested amyloidogenic proteins similarly to β aptamers selected for Aβ40 previously [125] and reused/retested for imaging Aβ plaques [127]. (4) To exclude the possibility of SDS contamination in our trimeric Aβ40 preparation, we used a PICUP-generated mixture of low-molecular-weight Aβ40 preparation, which was not subjected to SDS–PAGE. As discussed below, SDS is known to accelerate Aβ self-assembly and β-sheet formation [157]. In these series of SELEX experiments, we included two counter-SELEX cycles against Aβ40 fibrils after the fourth and fifth SELEX cycles. The RNA pool obtained after the fifth SELEX cycle reacted with fibrils of Aβ and fibrils of the other tested amyloidogenic proteins similarly to our aptamers [153] and β aptamers selected previously [125]. This finding indicated that counter-selection against Aβ40 fibrils could not effectively remove aptamer reactivity with fibrils. (5) Because of this finding, we performed another SELEX cycle with several counter-SELEX experiments using Aβ40 fibrils aiming to obtain an RNA pool devoid of fibril-binding sequences. However, five consecutive rounds of counter-SELEX using excess Aβ40 fibrils failed to reduce the binding of the RNA pool to Aβ40 fibrils. (6) Because of the persistent and apparently non-specific binding of RNA aptamers to amyloid fibrils, and because counter-SELEX using Aβ40 fibrils failed to abrogate aptamer binding to amyloid fibrils, we assessed our naïve RNA library and a G-biased RNA library for their reactivity with amyloid fibrils. We used the biased library with reduced G ratio (A:C:G:T = 30%:30%:10%:30%) because our sequencing and motif analyses showed high G content in selected aptamers. We found that both naïve RNA libraries reacted with fibrillar assemblies of the same proteins akin to all the selected aptamers we tested [153]. (7) The selected aptamers—and the naïve library—could track progression of β-sheet formation and fibrillization in Aβ40 and insulin with ~16-fold higher sensitively than the thioflavin T fluorescence assay, which is commonly used to assess fibril formation by many amyloidogenic proteins [158,159]. (8) HFIP-treated lysozyme and IAPP contained sufficient β-sheet content as inferred from their recognition by the tested aptamers and the naïve library. Our observation of non-specific reactivity with fibrils of selected and tested aptamers, which is reminiscent of similar findings in previous studies [62,125,134,136], suggest that aptamers (and naïve libraries of oligonucleotides) likely recognize potentially common aptatopes [62,153,160].

Studies that selected aptamers for recognizing Aβ assemblies are summarized in Table 1.

**Table 1.** Aptamers selected for interacting with different amyloid β-protein (Aβ) preparations.

| Aptamer Type | Target | SELEX Method | Aptamer Reactivity | Reference |
|---|---|---|---|---|
| RNA, β aptamers, e.g., β55 | Synthetic Aβ40 with an engineered N-terminal cysteine | Chromatographic separation using Sepharose 6B matrix carrying the target | No interaction with monomeric, soluble Aβ40, but reactive with Aβ40 fibrils | [125] |
| RNA aptamers E1, E2, N1, G2 etc. | Aβ40 conjugated to gold nanoparticles as a model of Aβ oligomers | RNA pool was exposed to target, separation was by centrifugation, and three different elution strategies used | Aβ40 oligomer model and apparently monomeric Aβ40 | [126] |
| RNA aptamers, KM and previously reported β aptamers | PICUP-generated and purified trimeric Aβ40, and a PICUP-generated mixture of low-molecular-weight Aβ40 oligomers | Filter-binding assay used for separation | Aβ fibrils and fibrils of other exemplary amyloidogenic proteins | [153,160] |

SELES, systematic evolution of ligands by exponential enrichment; Aβ, amyloid β-protein; PICUP, photo-induced crosslinking of unmodified proteins.

Farrar et al. [127] used the β55 aptamer, which was published [125] and retested [153] previously, for ex vivo imaging of frozen sections of human AD brain fixed in paraformaldehyde, while including the corresponding reverse sequence of β55 as control. The authors performed in vivo multiphoton microscopy using the APP–PS1 transgenic mouse model of AD [161] to visualize plaques [127]. Biotinylated β55 reportedly stained many more plaques than its reverse sequence, and β55 staining localized with thioflavin-S signal, confirming staining of amyloid plaques

ex vivo [127], and by inference confirming binding to Aβ fibrils as shown by previous studies [125,160]. Fluorescein-conjugated β55 stained amyloid plaques and amyloid angiopathic lesions in brains of APP–PS1 mice visualized by multiphoton microscopy [127]. In localization staining experiments, β55 and methoxy-X04 stained the dense core of the plaques, whereas β55 additionally stained a diffuse halo surrounding the plaque cores [127]. (Methoxy-X04 is a derivative of Congo Red and it has been used previously for optical imaging of AD mouse models [162]. Congo Red is used to stain and detect amyloid depositions in tissues. Upon binding to amyloid structures, Congo Red yields a unique blue–green birefringence under a cross-polarized light microscope [159].) Farrar et al. [127] concluded that β55 may have bound smaller aggregates, including oligomers, of Aβ peripheral to the dense plaques based on their observation that β55 apparently bound low-molecular-weight oligomers of Aβ40 and Aβ42 on SDS–PAGE gels, and similar observation reported by Koffie et al. [163], showing a "halo of oligomers" surrounding the plaques detected by a so-called "conformation-specific" NAB61 antibody [164]. However, Farrar et al. [127] did not test nor compared the sensitivity of methoxy-X04 with that of β55 for binding small, early, β-sheet-containing fibrillar aggregates of Aβ. Possibly, methoxy-X04 could not sensitively detect the small β-sheet-containing fibrillar Aβ similarly to thioflavin T, which failed to detect early, sparse Aβ40 and insulin fibrils, but RNA aptamers detected early fibrillar assemblies of Aβ40 and insulin containing β-sheet structure [153]. Implications of β55 aptamer binding to SDS-fractionated Aβ species and Farrar's conclusions about β55's ability to detect oligomeric Aβ species around Aβ plaques are discussed in more detail in the following section.

## 5. SDS–PAGE, Aptamers, Antibodies, and "Halos of Oligomers"

Along with silver staining, Coomassie staining, western blotting, or mass spectrometry, SDS–PAGE has been used to identify proteins and examine protein oligomerization, size distribution, or protein–protein interactions. However, SDS (288.38 $g \cdot mol^{-1}$) does not affect all proteins identically [165] because different proteins, different conformations of a protein [166], or fragments of certain proteins [167] may not bind SDS at stoichiometric amounts (though SDS generally binds different proteins at an approximately constant mass–mass ratio—1.4 g SDS per gram of polypeptide [159]). Furthermore, in certain cases, SDS induces or stabilizes—rather than disrupting—secondary or quaternary structures [166,168,169]. In some other cases, SDS may induce homo-oligomerization or conversely dissociate protein complexes [169–172]. For example, both human and rat α-synuclein show aberrant electrophoretic mobility and SDS–PAGE-induced high-molecular-mass components, which do not exist in the samples when analyzed by size-exclusion chromatography [173].

Aβ is an amphipathic protein that forms "SDS-stable oligomers" [174,175]. In fact, SDS-induced aggregation of Aβ has facilitated extraction of Aβ from brain homogenates [176]. Aβ42-derived "globulomers" are in vitro model oligomeric species produced by incubating Aβ42 with 0.2% SDS [177,178]. Aβ aggregates rapidly after being treated with SDS and forms high-molecular-mass assemblies [157]. During electrophoresis of Aβ40, its SDS-induced aggregates dissociate and only a monomeric component is observed by staining, whereas electrophoresis of Aβ42 yields apparently trimeric and tetrameric components as observed previously [179,180]. In addition, essentially identical monomer–trimer–tetramer components appear when different Aβ42 preparations, including monomeric, oligomeric, or fibrillar Aβ42, are subjected to SDS–PAGE [181], demonstrating that SDS treatment, and electrophoresis in the presence of SDS—rather than the initial assembly state—determines Aβ42's apparent PAGE mobility. After treatment in a urea-containing SDS–PAGE system, Aβ and its truncated versions defy the mass–mobility relationships, because Aβ–SDS interaction likely does not relate to the number of constituent amino acids but to the sum of hydrophobicity indices [167]. An exemplary study of Aβ40 dimers stabilized by an intermolecular disulfide bridge showed the same SDS–PAGE profile before and after formation of β-sheet-rich Aβ protofibrils [182]. Watt et al. compared SDS–PAGE, the xMAP® multiplex immunoassay (Luminex, Madison, WI, USA) and surface-enhanced laser desorption/ionization time-of-flight mass spectrometry when examining Aβ extracted from human cortical tissues [183]. Their mass-spectrometry experiments

could not detect oligomers, while monomeric and dimeric Aβ components appeared through SDS–PAGE; surprisingly, the apparent monomeric and dimeric Aβ levels increased with increasing SDS concentrations in the sample buffer [183]. Thus, electrophoretic separation and detection of monomeric or oligomeric assemblies in an Aβ preparation do not necessarily prove that such components exist in the sample before SDS–PAGE.

The shortcomings of SDS–PAGE have been highlighted in many studies of Aβ [21,60,157,159,179,181,183] and α-synuclein [173] and is gradually being appreciated in the AD field. Meanwhile, interpretations of findings about elusive Aβ oligomers has come under scrutiny and disputed to such an extent that the foundations of the oligomer cascade hypothesis have been shaken. Accordingly, a relatively recent study has critically evaluated the use of SDS–PAGE, claiming that the concept of Aβ oligomers has disserved decades of research into AD [184]. This study used ion mobility coupled with electrospray-ionization mass spectrometry (ESI–IM–MS), challenging the biophysical paradigms dominating the Aβ field based on SDS–PAGE and PICUP analyses of prefibrillar assemblies of Aβ. When coupled with MS, ion-mobility spectrometry, which distinguishes ions according to both their mass-to-charge ratio and their three-dimensional structures, is a useful analytical technique for examining covalent or non-covalent protein structures in complex mixtures. Ion-mobility spectrometry–mass spectrometer (IMS–MS) can resolve molecules of identical mass-to-charge ratios with differing collision cross-sections (e.g., different assembly states or conformations) and/or differing charge states [159]. Pujol-Pina et al. used PICUP-stabilized Aβ oligomers and showed that the Aβ42 pentamer–hexamer components observed by SDS–PAGE following PICUP are methodological artifacts [184]. The authors removed the SDS–PAGE step from analyzing PICUP-generated, cross-linked Aβ40 and Aβ42 preparations and, instead, used size-exclusion chromatography and ESI–IM–MS. Since initial PICUP–SDS–PAGE observations, Aβ40 and Aβ42 were thought to oligomerize and aggregate through distinct pathways [154,179]; that is, Aβ42 was thought to aggregate through formation of "paranuclei"—the pentamer–hexamer subunits—and distinctly from Aβ40, which was thought to aggregate through dimer–trimer–tetramer subunits. By excluding SDS–PAGE, ESI–IM–MS showed no differences in the oligomer-size distribution between cross-linked or uncross-linked Aβ40 and Aβ42, suggesting that Aβ40 and Aβ42 predominantly and similarly initiate oligomerization and aggregation through dimer–trimer subunits [184]. The implications of the ESI–IM–MS findings controverts the conclusions that C-terminal length of Aβ was the most important structural determinant in early oligomerization, and the side-chains of Ile41 and Ala42 in Aβ42 were important both for effective formation of paranuclei and for their self-association [179,185]. It was discussed previously that differences in toxicity between Aβ40 and Aβ42 [186] correlate with PICUP–SDS–PAGE observations that paranuclei are produced by Aβ42 only, confirming the correlation of the latter to AD pathogenesis.

As another example, the elaborate study by Koffie et al., which used ultrathin array tomography and immunofluorescence, claimed that senile plaques in brains of AD model mice are surrounded by "haloes of oligomeric Aβ" [163]. This conclusion was mainly based on immunoreactivity of NAB61, which apparently reacted with oligomeric Aβ assemblies fractionated by SDS–PAGE [164]. The original paper, which described this antibody as a "Conformation-selective Monoclonal Antibody," ironically reported that NAB61 also recognized synthetic Aβ fibrils by electron microscopy, as presented in its small Figure 4B panel [164]. Considering these caveats, one may rightly question the major conclusions drawn by Koffie et al. [163], and the same interpretative analogies repeated and drawn by Farrar et al. [127]. The former used NAB61 and the latter β55 and claimed that the antibody and aptamer were specific for SDS–PAGE-fractionated oligomeric Aβ and, in this capacity, detected Aβ oligomers around plaques, ignoring the shortcomings of SDS–PAGE (firstly) and the fact that β55 and NAB61 *both* cross-react with fibrillar Aβ assemblies besides SDS-fractionated Aβ species (secondly). Similar cross-reactivity was apparent in antibodies that were produced and characterized after iterative immunization of beagles [187] with an aggregated Aβ preparation [188]. Thus, the conclusions by Farrar et al. [127] about staining small oligomers haloing the dense plaques as observed by β55 must

be reexamined in light of the collective literature regarding (1) SDS–PAGE analysis of Aβ; (2) NAB61 reactivity with Aβ assemblies; (3) plaque immunohistochemistry; (4) and sensitivity of the aptamer binding compared to methoxy-X04 (or thioflavin T/S) binding to Aβ fibrils—and plaques.

To sum up, despite its wide use and resolution, SDS–PAGE and western blotting are not reliable methods for determining oligomer sizes or assembly states of certain IDPs, e.g., α-synuclein and Aβ oligomers. As such, SDS–PAGE is not suitable for assessing the specificity or selectivity of aptamers (or antibodies) for Aβ preparations. Considering SDS–PAGE's shortcomings is important for characterizing the reactivity and specificity of aptamers or antibodies generated against Aβ species (see [127,163,164]) because SDS-induced oligomers in an Aβ preparation are not necessarily structurally the same as those potentially present in the absence of SDS [184].

## 6. Conclusions

The conclusions from this review are manifold.

- The handful of reports published since 2002 on aptamers developed for targeting Aβ have led to important and instructive findings. RNA and DNA aptamers and random nucleotide libraries used for selecting aptamers are found to react inherently and nonspecifically with fibrillar Aβ preparations and exemplary amyloid assemblies [21,153,160]. Most likely, the aptamer-targeted common aptatope in these cases is the backbone of the proteins in a cross-β structure because this protein structure reportedly facilitates retention of RNAs and RNA-binding proteins into special ribonucleoprotein complexes, including stress granules and RNA-processing organelles [189]. The inherent and persistent tendency of RNA aptamers to bind amyloid fibrils (or vice versa) may explain entrapment of RNA in the senile plaques and neurofibrillary tangles [73–75], the two pathological hallmarks of AD brains. Moreover, amyloid fibrils and oligonucleotides act as polyelectrolytes and interact by electrostatic forces [190]. These β-sheet-mediated, polyelectrolytic, protein–oligonucleotide interactions were thought to be vital for support, stability, compartmentalization, protection, and resistance to degradation in the harsh environments of the antediluvian, prebiotic world [191], indicating an ancient phenomenon. Interaction of RNA aptamers with amyloid fibrils have implications for the previous and future studies of aptamers selected for amyloidogenic proteins and conclusions drawn from such studies.
- Attributing oligomer specificity to an aptamer based on results obtained by SDS–PAGE fractionation of Aβ preparations disregards the collected evidence on the unsuitability of SDS–PAGE for analyzing and size estimation of amyloidogenic protein assemblies.
- Attributing oligomer specificity to an aptamer (or an antibody) that evidently binds fibrillar structures of amyloidogenic proteins (see [127,163]) is erroneous and misleading; thus, binding specificities of such aptamers in tissue sections do not represent their true specificities and enhances the illusion about presence of Aβ oligomers in tissue sections.
- Implications of SDS–PAGE are extendable to studies whereby prefibrillar amyloid assemblies were extracted and studied in vitro [192–199] or PICUP-stabilized oligomers were studied to establish the biophysical paradigms of Aβ oligomerization [179,184,185].
- Finally, I hope this review could encourage the aptamer–amyloid–Alzheimer researchers, the relevant funding bodies, these fields' peer-reviewers, and the fields' young scholars to scrutinize and study the relevant literature deeply before enthusing [148,200–202] about aptamers in the context of Aβ research. Let us not generate an aptamer field akin to the muddled assortment of antibodies promoted in AD research [21,22].

**Acknowledgments:** The author acknowledges the helpful comments by Susan Howitt, Division of Biomedical Science and Biochemistry, Research School of Biology, The Australian National University.

**Conflicts of Interest:** The author declares no conflict of interest.

## Abbreviations

| | |
|---|---|
| Aβ | amyloid β-protein |
| AD | Alzheimer disease |
| APP | amyloid β-protein precursor |
| ELISA | enzyme-linked immunosorbent assay |
| ESI–IM–MS | ion mobility coupled with electrospray-ionization mass spectrometry |
| HFIP | 1,1,1,3,3,3-hexafluoro-2-propanol |
| IAPP | islet amyloid polypeptide |
| IDPs | intrinsically disordered proteins |
| IM–MS | ion-mobility spectrometry–mass spectrometery |
| PCR | polymerase chain reaction |
| PICUP | photo-induced crosslinking of unmodified proteins |
| PLGA | poly(lactic-*co*-glycolic acid) |
| PrP | prion proteins |
| SDS–PAGE | sodium dodecyl sulfate–polyacrylamide gel electrophoresis |
| SELEX | systematic evolution of ligands by exponential enrichment |

## References


1. Jayasena, S.D. Aptamers: An emerging class of molecules that rival antibodies in diagnostics. *Clin. Chem.* **1999**, *45*, 1628–1650. [PubMed]
2. Famulok, M.; Mayer, G. Aptamers as tools in molecular biology and immunology. *Curr. Top. Microbiol. Immunol.* **1999**, *243*, 123–136. [PubMed]
3. Tan, W.; Wang, H.; Chen, Y.; Zhang, X.; Zhu, H.; Yang, C.; Yang, R.; Liu, C. Molecular aptamers for drug delivery. *Trends Biotechnol.* **2011**, *29*, 634–640. [CrossRef] [PubMed]
4. Ni, X.; Castanares, M.; Mukherjee, A.; Lupold, S.E. Nucleic acid aptamers: Clinical applications and promising new horizons. *Curr. Med. Chem.* **2011**, *18*, 4206–4214. [CrossRef] [PubMed]
5. Zhou, J.; Rossi, J. Aptamers as targeted therapeutics: Current potential and challenges. *Nat. Rev. Drug Discov.* **2017**, *16*, 181–202. [CrossRef] [PubMed]
6. Zhuo, Z.; Yu, Y.; Wang, M.; Li, J.; Zhang, Z.; Liu, J.; Wu, X.; Lu, A.; Zhang, G.; Zhang, B. Recent advances in SELEX technology and aptamer applications in biomedicine. *Int. J. Mol. Sci.* **2017**, *18*. [CrossRef] [PubMed]
7. Siddiqui, M.A.; Keating, G.M. Pegaptanib: In exudative age-related macular degeneration. *Drugs* **2005**, *65*, 1571–1577; discussion 1578–1579. [CrossRef] [PubMed]
8. Ng, E.W.; Shima, D.T.; Calias, P.; Cunningham, E.T., Jr.; Guyer, D.R.; Adamis, A.P. Pegaptanib, a targeted anti-VEGF aptamer for ocular vascular disease. *Nat. Rev. Drug Discov.* **2006**, *5*, 123–132. [CrossRef] [PubMed]
9. Oliphant, A.R.; Brandl, C.J.; Struhl, K. Defining the sequence specificity of DNA-binding proteins by selecting binding sites from random-sequence oligonucleotides: Analysis of yeast GCN4 protein. *Mol. Cell. Biol.* **1989**, *9*, 2944–2949. [CrossRef] [PubMed]
10. Ellington, A.D.; Szostak, J.W. In vitro selection of RNA molecules that bind specific ligands. *Nature* **1990**, *346*, 818–822. [CrossRef] [PubMed]
11. Robertson, D.L.; Joyce, G.F. Selection in vitro of an RNA enzyme that specifically cleaves single-stranded DNA. *Nature* **1990**, *344*, 467–468. [CrossRef] [PubMed]
12. Tuerk, C.; Gold, L. Systematic evolution of ligands by exponential enrichment: RNA ligands to bacteriophage T4 DNA polymerase. *Science* **1990**, *249*, 505–510. [CrossRef] [PubMed]
13. Vater, A.; Klussmann, S. Turning mirror-image oligonucleotides into drugs: The evolution of Spiegelmer® therapeutics. *Drug Discov. Today* **2015**, *20*, 147–155. [CrossRef] [PubMed]
14. Uversky, V.N. Targeting intrinsically disordered proteins in neurodegenerative and protein dysfunction diseases: Another illustration of the $D^2$ concept. *Expert Rev. Proteom.* **2010**, *7*, 543–564. [CrossRef] [PubMed]
15. Ambadipudi, S.; Zweckstetter, M. Targeting intrinsically disordered proteins in rational drug discovery. *Expert Opin. Drug Discov.* **2016**, *11*, 65–77. [CrossRef] [PubMed]
16. Basu, S.; Bahadur, R.P. A structural perspective of RNA recognition by intrinsically disordered proteins. *Cell. Mol. Life Sci.* **2016**, *73*, 4075–4084. [CrossRef] [PubMed]

17. Korsak, M.; Kozyreva, T. Beta Amyloid hallmarks: From intrinsically disordered proteins to Alzheimer's disease. *Adv. Exp. Med. Biol.* **2015**, *870*, 401–421. [CrossRef] [PubMed]
18. Hoshino, M. Fibril formation from the amyloid-β peptide is governed by a dynamic equilibrium involving association and dissociation of the monomer. *Biophys. Rev.* **2017**, *9*, 9–16. [CrossRef] [PubMed]
19. Kayed, R.; Head, E.; Sarsoza, F.; Saing, T.; Cotman, C.W.; Necula, M.; Margol, L.; Wu, J.; Breydo, L.; Thompson, J.L.; et al. Fibril specific, conformation dependent antibodies recognize a generic epitope common to amyloid fibrils and fibrillar oligomers that is absent in prefibrillar oligomers. *Mol. Neurodegener.* **2007**, *2*, 18. [CrossRef] [PubMed]
20. Kayed, R.; Head, E.; Thompson, J.L.; McIntire, T.M.; Milton, S.C.; Cotman, C.W.; Glabe, C.G. Common structure of soluble amyloid oligomers implies common mechanism of pathogenesis. *Science* **2003**, *300*, 486–489. [CrossRef] [PubMed]
21. Rahimi, F.; Bitan, G. Overview of fibrillar and oligomeric assemblies of amyloidogenic proteins. In *Non-Fibrillar Amyloidogenic Protein Assemblies—Common Cytotoxins Underlying Degenerative Diseases*; Rahimi, F., Bitan, G., Eds.; Springer: Dordrecht, The Netherlands, 2012; pp. 1–36, ISBN 978-9-40-072773-1.
22. Hunter, S.; Brayne, C. Do anti-amyloid beta protein antibody cross reactivities confound Alzheimer disease research? *J. Negat. Results Biomed.* **2017**, *16*, 1. [CrossRef] [PubMed]
23. Esler, W.P.; Wolfe, M.S. A portrait of Alzheimer secretases—New features and familiar faces. *Science* **2001**, *293*, 1449–1454. [CrossRef] [PubMed]
24. Martins, R.N.; Robinson, P.J.; Chleboun, J.O.; Beyreuther, K.; Masters, C.L. The molecular pathology of amyloid deposition in Alzheimer's disease. *Mol. Neurobiol.* **1991**, *5*, 389–398. [CrossRef] [PubMed]
25. Haass, C.; Hung, A.Y.; Schlossmacher, M.G.; Oltersdorf, T.; Teplow, D.B.; Selkoe, D.J. Normal cellular processing of the β-amyloid precursor protein results in the secretion of the amyloid β peptide and related molecules. *Ann. N. Y. Acad. Sci.* **1993**, *695*, 109–116. [CrossRef] [PubMed]
26. Parihar, M.S.; Brewer, G.J. Amyloid-β as a modulator of synaptic plasticity. *J. Alzheimers Dis.* **2010**, *22*, 741–763. [CrossRef] [PubMed]
27. Puzzo, D.; Arancio, O. Amyloid-β peptide: Dr. Jekyll or Mr. Hyde? *J. Alzheimers Dis.* **2013**, *33*, S111–S120. [CrossRef] [PubMed]
28. Carrillo-Mora, P.; Luna, R.; Colín-Barenque, L. Amyloid beta: Multiple mechanisms of toxicity and only some protective effects? *Oxid. Med. Cell. Longev.* **2014**, *2014*, 795375. [CrossRef] [PubMed]
29. Dawkins, E.; Small, D.H. Insights into the physiological function of the β-amyloid precursor protein: Beyond Alzheimer's disease. *J. Neurochem.* **2014**, *129*, 756–769. [CrossRef] [PubMed]
30. Martorana, A.; Di Lorenzo, F.; Belli, L.; Sancesario, G.; Toniolo, S.; Sallustio, F.; Sancesario, G.M.; Koch, G. Cerebrospinal fluid $A\beta_{42}$ levels: When physiological become pathological state. *CNS Neurosci. Ther.* **2015**, *21*, 921–925. [CrossRef] [PubMed]
31. Fedele, E.; Rivera, D.; Marengo, B.; Pronzato, M.A.; Ricciarelli, R. Amyloid β: Walking on the dark side of the moon. *Mech. Ageing Dev.* **2015**, *152*, 1–4. [CrossRef] [PubMed]
32. Gupta, A.; Goyal, R. Amyloid beta plaque: A culprit for neurodegeneration. *Acta Neurol. Belg.* **2016**, *116*, 445–450. [CrossRef] [PubMed]
33. Chen, G.F.; Xu, T.H.; Yan, Y.; Zhou, Y.R.; Jiang, Y.; Melcher, K.; Xu, H.E. Amyloid beta: Structure, biology and structure-based therapeutic development. *Acta Pharmacol. Sin.* **2017**, *38*, 1205–1235. [CrossRef] [PubMed]
34. Alkasir, R.; Li, J.; Li, X.; Jin, M.; Zhu, B. Human gut microbiota: The links with dementia development. *Protein Cell* **2017**, *8*, 90–102. [CrossRef] [PubMed]
35. Dudai, Y. Molecular bases of long-term memories: A question of persistence. *Curr. Opin. Neurobiol.* **2002**, *12*, 211–216. [CrossRef]
36. Mrak, R.E.; Griffin, W.S. The role of activated astrocytes and of the neurotrophic cytokine S100B in the pathogenesis of Alzheimer's disease. *Neurobiol. Aging* **2001**, *22*, 915–922. [CrossRef]
37. Wilcock, D.M.; Griffin, W.S. Down's syndrome, neuroinflammation, and Alzheimer neuropathogenesis. *J. Neuroinflamm.* **2013**, *10*, 84. [CrossRef] [PubMed]
38. Donato, R. S100: A multigenic family of calcium-modulated proteins of the EF-hand type with intracellular and extracellular functional roles. *Int. J. Biochem. Cell Biol.* **2001**, *33*, 637–668. [CrossRef]
39. Hardy, J.A.; Higgins, G.A. Alzheimer's disease: The amyloid cascade hypothesis. *Science* **1992**, *256*, 184–185. [CrossRef] [PubMed]
40. Hardy, J. Testing times for the "amyloid cascade hypothesis". *Neurobiol. Aging* **2002**, *23*, 1073–1074. [CrossRef]

41. Selkoe, D.J.; American College of Physicians; American Physiological Society. Alzheimer disease: Mechanistic understanding predicts novel therapies. *Ann. Intern. Med.* **2004**, *140*, 627–638. [CrossRef] [PubMed]
42. Haass, C.; Selkoe, D.J. Soluble protein oligomers in neurodegeneration: Lessons from the Alzheimer's amyloid β-peptide. *Nat. Rev. Mol. Cell Biol.* **2007**, *8*, 101–112. [CrossRef] [PubMed]
43. Hayden, E.Y.; Teplow, D.B. Amyloid β-protein oligomers and Alzheimer's disease. *Alzheimers Res. Ther.* **2013**, *5*, 60. [CrossRef] [PubMed]
44. van Dyck, C.H. Anti-amyloid-β monoclonal antibodies for Alzheimer's disease: Pitfalls and promise. *Biol. Psychiatry* **2017**. [CrossRef] [PubMed]
45. Hung, S.Y.; Fu, W.M. Drug candidates in clinical trials for Alzheimer's disease. *J. Biomed. Sci.* **2017**, *24*, 47. [CrossRef] [PubMed]
46. Clark, I.A.; Vissel, B. Amyloid β: One of three danger-associated molecules that are secondary inducers of the proinflammatory cytokines that mediate Alzheimer's disease. *Br. J. Pharmacol.* **2015**, *172*, 3714–3727. [CrossRef] [PubMed]
47. Morris, G.P.; Clark, I.A.; Vissel, B. Inconsistencies and controversies surrounding the amyloid hypothesis of Alzheimer's disease. *Acta Neuropathol. Commun.* **2014**, *2*, 135. [CrossRef] [PubMed]
48. Clark, I.A.; Alleva, L.M.; Vissel, B. The roles of TNF in brain dysfunction and disease. *Pharmacol. Ther.* **2010**, *128*, 519–548. [CrossRef] [PubMed]
49. Clark, I.A.; Vissel, B. Excess cerebral TNF causing glutamate excitotoxicity rationalizes treatment of neurodegenerative diseases and neurogenic pain by anti-TNF agents. *J. Neuroinflamm.* **2016**, *13*, 236. [CrossRef] [PubMed]
50. Glenner, G.G.; Wong, C.W. Alzheimer's disease and Down's syndrome: Sharing of a unique cerebrovascular amyloid fibril protein. *Biochem. Biophys. Res. Commun.* **1984**, *122*, 1131–1135. [CrossRef]
51. Glenner, G.G.; Wong, C.W. Alzheimer's disease: Initial report of the purification and characterization of a novel cerebrovascular amyloid protein. *Biochem. Biophys. Res. Commun.* **1984**, *120*, 885–890. [CrossRef]
52. Glenner, G.G.; Wong, C.W.; Quaranta, V.; Eanes, E.D. The amyloid deposits in Alzheimer's disease: Their nature and pathogenesis. *Appl. Pathol.* **1984**, *2*, 357–369. [PubMed]
53. Masters, C.L.; Multhaup, G.; Simms, G.; Pottgiesser, J.; Martins, R.N.; Beyreuther, K. Neuronal origin of a cerebral amyloid: Neurofibrillary tangles of Alzheimer's disease contain the same protein as the amyloid of plaque cores and blood vessels. *EMBO J.* **1985**, *4*, 2757–2763. [PubMed]
54. Masters, C.L.; Simms, G.; Weinman, N.A.; Multhaup, G.; McDonald, B.L.; Beyreuther, K. Amyloid plaque core protein in Alzheimer disease and Down syndrome. *Proc. Natl. Acad. Sci. USA* **1985**, *82*, 4245–4249. [CrossRef] [PubMed]
55. Narang, H.K. High-resolution electron microscopic analysis of the amyloid fibril in Alzheimer's disease. *J Neuropathol. Exp. Neurol.* **1980**, *39*, 621–631. [CrossRef] [PubMed]
56. Merz, P.A.; Wisniewski, H.M.; Somerville, R.A.; Bobin, S.A.; Masters, C.L.; Iqbal, K. Ultrastructural morphology of amyloid fibrils from neuritic and amyloid plaques. *Acta Neuropathol.* **1983**, *60*, 113–124. [CrossRef] [PubMed]
57. Rahimi, F.; Shanmugam, A.; Bitan, G. Structure–function relationships of pre-fibrillar protein assemblies in Alzheimer's disease and related disorders. *Curr. Alzheimer Res.* **2008**, *5*, 319–341. [CrossRef] [PubMed]
58. Roychaudhuri, R.; Yang, M.; Hoshi, M.M.; Teplow, D.B. Amyloid β-protein assembly and Alzheimer disease. *J. Biol. Chem.* **2009**, *284*, 4749–4753. [CrossRef] [PubMed]
59. Benilova, I.; Karran, E.; De Strooper, B. The toxic Aβ oligomer and Alzheimer's disease: An emperor in need of clothes. *Nat. Neurosci.* **2012**, *15*, 349–357. [CrossRef] [PubMed]
60. Rahimi, F.; Bitan, G. Methods for studying and structure–function relationships of non-fibrillar protein assemblies in Alzheimer's disease and related disorders. In *Advances in Alzheimer Research*; Lahiri, D.K., Ed.; Bentham Science Publishers: Sharjah, United Arab Emirates, 2014; Volume 2, pp. 291–374, ISBN 978-1-60-805853-2.
61. Söderberg, L.; Bogdanovic, N.; Axelsson, B.; Winblad, B.; Näslund, J.; Tjernberg, L.O. Analysis of single Alzheimer solid plaque cores by laser capture microscopy and nanoelectrospray/tandem mass spectrometry. *Biochemistry* **2006**, *45*, 9849–9856. [CrossRef] [PubMed]
62. Mitkevich, O.V.; Kochneva-Pervukhova, N.V.; Surina, E.R.; Benevolensky, S.V.; Kushnirov, V.V.; Ter-Avanesyan, M.D. DNA aptamers detecting generic amyloid epitopes. *Prion* **2012**, *6*, 400–406. [CrossRef] [PubMed]

63. Rüfenacht, P.; Güntert, A.; Bohrmann, B.; Ducret, A.; Döbeli, H. Quantification of the Aβ peptide in Alzheimer's plaques by laser dissection microscopy combined with mass spectrometry. *J. Mass Spectrom.* **2005**, *40*, 193–201. [CrossRef] [PubMed]
64. Wirths, O.; Walter, S.; Kraus, I.; Klafki, H.W.; Stazi, M.; Oberstein, T.J.; Ghiso, J.; Wiltfang, J.; Bayer, T.A.; Weggen, S. N-truncated $A\beta_{4-x}$ peptides in sporadic Alzheimer's disease cases and transgenic Alzheimer mouse models. *Alzheimers Res. Ther.* **2017**, *9*, 80. [CrossRef] [PubMed]
65. Panchal, M.; Gaudin, M.; Lazar, A.N.; Salvati, E.; Rivals, I.; Ayciriex, S.; Dauphinot, L.; Dargere, D.; Auzeil, N.; Masserini, M.; et al. Ceramides and sphingomyelinases in senile plaques. *Neurobiol. Dis.* **2014**, *65*, 193–201. [CrossRef] [PubMed]
66. Panchal, M.; Loeper, J.; Cossec, J.C.; Perruchini, C.; Lazar, A.; Pompon, D.; Duyckaerts, C. Enrichment of cholesterol in microdissected Alzheimer's disease senile plaques as assessed by mass spectrometry. *J. Lipid Res.* **2010**, *51*, 598–605. [CrossRef] [PubMed]
67. Alexandrescu, A.T. Amyloid accomplices and enforcers. *Protein Sci.* **2005**, *14*, 1–12. [CrossRef] [PubMed]
68. Liao, L.; Cheng, D.; Wang, J.; Duong, D.M.; Losik, T.G.; Gearing, M.; Rees, H.D.; Lah, J.J.; Levey, A.I.; Peng, J. Proteomic characterization of postmortem amyloid plaques isolated by laser capture microdissection. *J. Biol. Chem.* **2004**, *279*, 37061–37068. [CrossRef] [PubMed]
69. Hadley, K.C.; Rakhit, R.; Guo, H.; Sun, Y.; Jonkman, J.E.; McLaurin, J.; Hazrati, L.N.; Emili, A.; Chakrabartty, A. Determining composition of micron-scale protein deposits in neurodegenerative disease by spatially targeted optical microproteomics. *eLife* **2015**, *4*. [CrossRef] [PubMed]
70. Shepherd, C.E.; Goyette, J.; Utter, V.; Rahimi, F.; Yang, Z.; Geczy, C.L.; Halliday, G.M. Inflammatory S100A9 and S100A12 proteins in Alzheimer's disease. *Neurobiol. Aging* **2006**, *27*, 1554–1563. [CrossRef] [PubMed]
71. Sokolova, A.; Hill, M.D.; Rahimi, F.; Warden, L.A.; Halliday, G.M.; Shepherd, C.E. Monocyte chemoattractant protein-1 plays a dominant role in the chronic inflammation observed in Alzheimer's disease. *Brain Pathol.* **2009**, *19*, 392–398. [CrossRef] [PubMed]
72. Atwood, C.S.; Martins, R.N.; Smith, M.A.; Perry, G. Senile plaque composition and posttranslational modification of amyloid-β peptide and associated proteins. *Peptides* **2002**, *23*, 1343–1350. [CrossRef]
73. Ginsberg, S.D.; Galvin, J.E.; Chiu, T.S.; Lee, V.M.; Masliah, E.; Trojanowski, J.Q. RNA sequestration to pathological lesions of neurodegenerative diseases. *Acta Neuropathol.* **1998**, *96*, 487–494. [CrossRef] [PubMed]
74. Ginsberg, S.D.; Crino, P.B.; Hemby, S.E.; Weingarten, J.A.; Lee, V.M.; Eberwine, J.H.; Trojanowski, J.Q. Predominance of neuronal mRNAs in individual Alzheimer's disease senile plaques. *Ann. Neurol.* **1999**, *45*, 174–181. [CrossRef]
75. Marcinkiewicz, M. βAPP and furin mRNA concentrates in immature senile plaques in the brain of Alzheimer patients. *J. Neuropathol. Exp. Neurol.* **2002**, *61*, 815–829. [CrossRef] [PubMed]
76. Hirschfield, G.M.; Hawkins, P.N. Amyloidosis: New strategies for treatment. *Int. J. Biochem. Cell Biol.* **2003**, *35*, 1608–1613. [CrossRef]
77. Drummond, E.; Nayak, S.; Faustin, A.; Pires, G.; Hickman, R.A.; Askenazi, M.; Cohen, M.; Haldiman, T.; Kim, C.; Han, X.; et al. Proteomic differences in amyloid plaques in rapidly progressive and sporadic Alzheimer's disease. *Acta Neuropathol.* **2017**, *133*, 933–954. [CrossRef] [PubMed]
78. Gerakis, Y.; Hetz, C. Emerging roles of ER stress in the etiology and pathogenesis of Alzheimer's disease. *FEBS J.* **2017**. [CrossRef] [PubMed]
79. Gibas, K.J. The starving brain: Overfed meets undernourished in the pathology of mild cognitive impairment (MCI) and Alzheimer's disease (AD). *Neurochem. Int.* **2017**, *110*, 57–68. [CrossRef] [PubMed]
80. Yang, Q.; Song, D.; Qing, H. Neural changes in Alzheimer's disease from circuit to molecule: Perspective of optogenetics. *Neurosci. Biobehav. Rev.* **2017**, *79*, 110–118. [CrossRef] [PubMed]
81. De Groot, N.S.; Burgas, M.T. Is membrane homeostasis the missing link between inflammation and neurodegenerative diseases? *Cell. Mol. Life Sci.* **2015**, *72*, 4795–4805. [CrossRef] [PubMed]
82. Budimir, A. Metal ions, Alzheimer's disease and chelation therapy. *Acta Pharm.* **2011**, *61*, 1–14. [CrossRef] [PubMed]
83. Petrou, A.L.; Terzidaki, A. A meta-analysis and review examining a possible role for oxidative stress and singlet oxygen in diverse diseases. *Biochem. J.* **2017**, *474*, 2713–2731. [CrossRef] [PubMed]
84. Bagyinszky, E.; Giau, V.V.; Shim, K.; Suk, K.; An, S.S.A.; Kim, S. Role of inflammatory molecules in the Alzheimer's disease progression and diagnosis. *J. Neurol. Sci.* **2017**, *376*, 242–254. [CrossRef] [PubMed]

85. Rojas-Gutierrez, E.; Muñoz-Arenas, G.; Treviño, S.; Espinosa, B.; Chavez, R.; Rojas, K.; Flores, G.; Díaz, A.; Guevara, J. Alzheimer's disease and metabolic syndrome: A link from oxidative stress and inflammation to neurodegeneration. *Synapse* **2017**. [CrossRef] [PubMed]
86. Santos, L.E.; Ferreira, S.T. Crosstalk between endoplasmic reticulum stress and brain inflammation in Alzheimer's disease. *Neuropharmacology* **2017**. [CrossRef] [PubMed]
87. Tuerk, C.; Eddy, S.; Parma, D.; Gold, L. Autogenous translational operator recognized by bacteriophage T4 DNA polymerase. *J. Mol. Biol.* **1990**, *213*, 749–761. [CrossRef]
88. Wrzesinski, J.; Jóźwiakowski, S.K. Structural basis for recognition of $Co^{2+}$ by RNA aptamers. *FEBS J.* **2008**, *275*, 1651–1662. [CrossRef] [PubMed]
89. Kim, Y.S.; Niazi, J.H.; Chae, Y.J.; Ko, U.R.; Gu, M.B. Aptamers-in-liposomes for selective and multiplexed capture of small organic compounds. *Macromol. Rapid Commun.* **2011**, *32*, 1169–1173. [CrossRef] [PubMed]
90. Yang, X.; Bing, T.; Mei, H.; Fang, C.; Cao, Z.; Shangguan, D. Characterization and application of a DNA aptamer binding to L-tryptophan. *Analyst* **2011**, *136*, 577–585. [CrossRef] [PubMed]
91. Kuwahara, M.; Ohsawa, K.; Kasamatsu, T.; Shoji, A.; Sawai, H.; Ozaki, H. Screening of a glutamic acid-binding aptamer from arginine-modified DNA library. *Nucleic Acids Symp. Ser.* **2005**, 81–82. [CrossRef] [PubMed]
92. Ames, T.D.; Breaker, R.R. Bacterial aptamers that selectively bind glutamine. *RNA Biol.* **2011**, *8*, 82–89. [CrossRef] [PubMed]
93. Darfeuille, F.; Hansen, J.B.; Orum, H.; Di Primo, C.; Toulmé, J.J. LNA/DNA chimeric oligomers mimic RNA aptamers targeted to the TAR RNA element of HIV-1. *Nucleic Acids Res.* **2004**, *32*, 3101–3107. [CrossRef] [PubMed]
94. Lebars, I.; Richard, T.; Di Primo, C.; Toulmé, J.J. NMR structure of a kissing complex formed between the TAR RNA element of HIV-1 and a LNA-modified aptamer. *Nucleic Acids Res.* **2007**, *35*, 6103–6114. [CrossRef] [PubMed]
95. Lebars, I.; Richard, T.; Di Primo, C.; Toulmé, J.J. LNA derivatives of a kissing aptamer targeted to the trans-activating responsive RNA element of HIV-1. *Blood Cells Mol. Dis.* **2007**, *38*, 204–209. [CrossRef] [PubMed]
96. Sekkai, D.; Dausse, E.; Di Primo, C.; Darfeuille, F.; Boiziau, C.; Toulmé, J.J. In vitro selection of DNA aptamers against the HIV-1 TAR RNA hairpin. *Antisense Nucleic Acid Drug Dev.* **2002**, *12*, 265–274. [CrossRef] [PubMed]
97. Bruno, J.G.; Carrillo, M.P.; Phillips, T. Development of DNA aptamers to a foot-and-mouth disease peptide for competitive FRET-based detection. *J. Biomol. Tech.* **2008**, *19*, 109–115. [PubMed]
98. Ashrafuzzaman, M. Aptamers as both drugs and drug-carriers. *BioMed Res. Int.* **2014**, *2014*, 697923. [CrossRef] [PubMed]
99. Du, Y.; Chen, C.; Yin, J.; Li, B.; Zhou, M.; Dong, S.; Wang, E. Solid-state probe based electrochemical aptasensor for cocaine: A potentially convenient, sensitive, repeatable, and integrated sensing platform for drugs. *Anal. Chem.* **2010**, *82*, 1556–1563. [CrossRef] [PubMed]
100. Du, Y.; Chen, C.; Zhou, M.; Dong, S.; Wang, E. Microfluidic electrochemical aptameric assay integrated on-chip: A potentially convenient sensing platform for the amplified and multiplex analysis of small molecules. *Anal. Chem.* **2011**, *83*, 1523–1529. [CrossRef] [PubMed]
101. Kawano, R.; Osaki, T.; Sasaki, H.; Takinoue, M.; Yoshizawa, S.; Takeuchi, S. Rapid detection of a cocaine-binding aptamer using biological nanopores on a chip. *J. Am. Chem. Soc.* **2011**, *133*, 8474–8477. [CrossRef] [PubMed]
102. Boese, B.J.; Breaker, R.R. In vitro selection and characterization of cellulose-binding DNA aptamers. *Nucleic Acids Res.* **2007**, *35*, 6378–6388. [CrossRef] [PubMed]
103. Boese, B.J.; Corbino, K.; Breaker, R.R. In vitro selection and characterization of cellulose-binding RNA aptamers using isothermal amplification. *Nucleosides Nucleotides Nucleic Acids* **2008**, *27*, 949–966. [CrossRef] [PubMed]
104. Kim, J.P.; Kwon, I.K.; Sim, S.J. The strategy of signal amplification for ultrasensitive detection of hIgE based on aptamer-modified poly(di-acetylene) supramolecules. *Biosens. Bioelectron.* **2011**, *26*, 4823–4827. [CrossRef] [PubMed]
105. Kim, J.P.; Park, C.H.; Sim, S.J. Aptamer biosensors for label-free colorimetric detection of human IgE based on polydiacetylene (PDA) supramolecules. *J. Nanosci. Nanotechnol.* **2011**, *11*, 4269–4274. [CrossRef] [PubMed]

106. Strahm, Y.; Flueckiger, A.; Billinger, M.; Meier, P.; Mettler, D.; Weisser, S.; Schaffner, T.; Hess, O. Endothelial-cell-binding aptamer for coating of intracoronary stents. *J. Invasive Cardiol.* **2010**, *22*, 481–487. [PubMed]
107. Thiel, K.W.; Hernandez, L.I.; Dassie, J.P.; Thiel, W.H.; Liu, X.; Stockdale, K.R.; Rothman, A.M.; Hernandez, F.J.; McNamara, J.O., II; Giangrande, P.H. Delivery of chemo-sensitizing siRNAs to HER2$^{+}$-breast cancer cells using RNA aptamers. *Nucleic Acids Res.* **2012**, *40*, 6319–6337. [CrossRef] [PubMed]
108. Thiel, K.W.; Giangrande, P.H. Therapeutic applications of DNA and RNA aptamers. *Oligonucleotides* **2009**, *19*, 209–222. [CrossRef] [PubMed]
109. Jyoti, A.; Vajpayee, P.; Singh, G.; Patel, C.B.; Gupta, K.C.; Shanker, R. Identification of environmental reservoirs of nontyphoidal salmonellosis: Aptamer-assisted bioconcentration and subsequent detection of *Salmonella* Typhimurium by quantitative polymerase chain reaction. *Environ. Sci. Technol.* **2011**, *45*, 8996–9002. [CrossRef] [PubMed]
110. Cui, Z.Q.; Ren, Q.; Wei, H.P.; Chen, Z.; Deng, J.Y.; Zhang, Z.P.; Zhang, X.E. Quantum dot–aptamer nanoprobes for recognizing and labeling influenza A virus particles. *Nanoscale* **2011**, *3*, 2454–2457. [CrossRef] [PubMed]
111. Ellenbecker, M.; Sears, L.; Li, P.; Lanchy, J.M.; Lodmell, J.S. Characterization of RNA aptamers directed against the nucleocapsid protein of Rift Valley fever virus. *Antiviral Res.* **2012**, *93*, 330–339. [CrossRef] [PubMed]
112. Feng, H.; Beck, J.; Nassal, M.; Hu, K.H. A SELEX-screened aptamer of human hepatitis B virus RNA encapsidation signal suppresses viral replication. *PLoS ONE* **2011**, *6*, e27862. [CrossRef] [PubMed]
113. Park, S.Y.; Kim, S.; Yoon, H.; Kim, K.B.; Kalme, S.S.; Oh, S.; Song, C.S.; Kim, D.E. Selection of an antiviral RNA aptamer against hemagglutinin of the subtype H5 avian influenza virus. *Nucleic Acid Ther.* **2011**, *21*, 395–402. [CrossRef] [PubMed]
114. Stoltenburg, R.; Reinemann, C.; Strehlitz, B. SELEX—A (r)evolutionary method to generate high-affinity nucleic acid ligands. *Biomol. Eng.* **2007**, *24*, 381–403. [CrossRef] [PubMed]
115. Diafa, S.; Hollenstein, M. Generation of aptamers with an expanded chemical repertoire. *Molecules* **2015**, *20*, 16643–16671. [CrossRef] [PubMed]
116. Hollenstein, M. DNA catalysis: The chemical repertoire of DNAzymes. *Molecules* **2015**, *20*, 20777–20804. [CrossRef] [PubMed]
117. Tan, S.Y.; Acquah, C.; Sidhu, A.; Ongkudon, C.M.; Yon, L.S.; Danquah, M.K. SELEX modifications and bioanalytical techniques for aptamer–target binding characterization. *Crit. Rev. Anal. Chem.* **2016**, *46*, 521–537. [CrossRef] [PubMed]
118. Gao, S.; Zheng, X.; Jiao, B.; Wang, L. Post-SELEX optimization of aptamers. *Anal. Bioanal. Chem.* **2016**, *408*, 4567–4573. [CrossRef] [PubMed]
119. Huang, Z.; Wen, W.; Wu, A.; Niu, L. Chemically modified, α-amino-3-hydroxy-5-methyl-4-isoxazole (AMPA) receptor RNA aptamers designed for in vivo use. *ACS Chem. Neurosci.* **2017**, *8*, 2437–2445. [CrossRef] [PubMed]
120. Pfeiffer, F.; Rosenthal, M.; Siegl, J.; Ewers, J.; Mayer, G. Customised nucleic acid libraries for enhanced aptamer selection and performance. *Curr. Opin. Biotechnol.* **2017**, *48*, 111–118. [CrossRef] [PubMed]
121. Jenison, R.D.; Gill, S.C.; Pardi, A.; Polisky, B. High-resolution molecular discrimination by RNA. *Science* **1994**, *263*, 1425–1429. [CrossRef] [PubMed]
122. Shoji, A.; Kuwahara, M.; Ozaki, H.; Sawai, H. Modified DNA aptamer that binds the (*R*)-isomer of a thalidomide derivative with high enantioselectivity. *J. Am. Chem. Soc.* **2007**, *129*, 1456–1464. [CrossRef] [PubMed]
123. Janas, T.; Janas, T. The selection of aptamers specific for membrane molecular targets. *Cell. Mol. Biol. Lett.* **2011**, *16*, 25–39. [CrossRef] [PubMed]
124. Macedo, B.; Cordeiro, Y. Unraveling prion protein interactions with aptamers and other PrP-binding nucleic acids. *Int. J. Mol. Sci.* **2017**, *18*. [CrossRef]
125. Ylera, F.; Lurz, R.; Erdmann, V.A.; Fürste, J.P. Selection of RNA aptamers to the Alzheimer's disease amyloid peptide. *Biochem. Biophys. Res. Commun.* **2002**, *290*, 1583–1588. [CrossRef] [PubMed]
126. Takahashi, T.; Tada, K.; Mihara, H. RNA aptamers selected against amyloid β-peptide (Aβ) inhibit the aggregation of Aβ. *Mol. Biosyst.* **2009**, *5*, 986–991. [CrossRef] [PubMed]
127. Farrar, C.T.; William, C.M.; Hudry, E.; Hashimoto, T.; Hyman, B.T. RNA aptamer probes as optical imaging agents for the detection of amyloid plaques. *PLoS ONE* **2014**, *9*, e89901. [CrossRef] [PubMed]

128. Weiss, S.; Proske, D.; Neumann, M.; Groschup, M.H.; Kretzschmar, H.A.; Famulok, M.; Winnacker, E.L. RNA aptamers specifically interact with the prion protein PrP. *J. Virol.* **1997**, *71*, 8790–8797. [PubMed]
129. Rhie, A.; Kirby, L.; Sayer, N.; Wellesley, R.; Disterer, P.; Sylvester, I.; Gill, A.; Hope, J.; James, W.; Tahiri-Alaoui, A. Characterization of 2′-fluoro-RNA aptamers that bind preferentially to disease-associated conformations of prion protein and inhibit conversion. *J. Biol. Chem.* **2003**, *278*, 39697–39705. [CrossRef] [PubMed]
130. Takemura, K.; Wang, P.; Vorberg, I.; Surewicz, W.; Priola, S.A.; Kanthasamy, A.; Pottathil, R.; Chen, S.G.; Sreevatsan, S. DNA aptamers that bind to $PrP^{C}$ and not $PrP^{Sc}$ show sequence and structure specificity. *Exp. Biol. Med.* **2006**, *231*, 204–214. [CrossRef]
131. Bibby, D.F.; Gill, A.C.; Kirby, L.; Farquhar, C.F.; Bruce, M.E.; Garson, J.A. Application of a novel in vitro selection technique to isolate and characterise high affinity DNA aptamers binding mammalian prion proteins. *J. Virol. Methods* **2008**, *151*, 107–115. [CrossRef] [PubMed]
132. King, D.J.; Safar, J.G.; Legname, G.; Prusiner, S.B. Thioaptamer interactions with prion proteins: Sequence-specific and non-specific binding sites. *J. Mol. Biol.* **2007**, *369*, 1001–1014. [CrossRef] [PubMed]
133. Proske, D.; Gilch, S.; Wopfner, F.; Schätzl, H.M.; Winnacker, E.L.; Famulok, M. Prion-protein-specific aptamer reduces $PrP^{Sc}$ formation. *ChemBioChem* **2002**, *3*, 717–725. [CrossRef]
134. Murakami, K.; Nishikawa, F.; Noda, K.; Yokoyama, T.; Nishikawa, S. Anti-bovine prion protein RNA aptamer containing tandem GGA repeat interacts both with recombinant bovine prion protein and its β isoform with high affinity. *Prion* **2008**, *2*, 73–80. [CrossRef] [PubMed]
135. Lührs, T.; Zahn, R.; Wüthrich, K. Amyloid formation by recombinant full-length prion proteins in phospholipid bicelle solutions. *J. Mol. Biol.* **2006**, *357*, 833–841. [CrossRef] [PubMed]
136. Bunka, D.H.; Mantle, B.J.; Morten, I.J.; Tennent, G.A.; Radford, S.E.; Stockley, P.G. Production and characterization of RNA aptamers specific for amyloid fibril epitopes. *J. Biol. Chem.* **2007**, *282*, 34500–34509. [CrossRef] [PubMed]
137. Tsukakoshi, K.; Abe, K.; Sode, K.; Ikebukuro, K. Selection of DNA aptamers that recognize α-synuclein oligomers using a competitive screening method. *Anal. Chem.* **2012**, *84*, 5542–5547. [CrossRef] [PubMed]
138. Tsukakoshi, K.; Harada, R.; Sode, K.; Ikebukuro, K. Screening of DNA aptamer which binds to α-synuclein. *Biotechnol. Lett.* **2010**, *32*, 643–648. [CrossRef] [PubMed]
139. Burdick, D.; Soreghan, B.; Kwon, M.; Kosmoski, J.; Knauer, M.; Henschen, A.; Yates, J.; Cotman, C.; Glabe, C. Assembly and aggregation properties of synthetic Alzheimer's A4/β amyloid peptide analogs. *J. Biol. Chem.* **1992**, *267*, 546–554. [PubMed]
140. Stine, W.B.; Jungbauer, L.; Yu, C.; LaDu, M.J. Preparing synthetic Aβ in different aggregation states. *Methods Mol. Biol.* **2011**, *670*, 13–32. [CrossRef] [PubMed]
141. Mahood, R.A. Selection of RNA Aptamers and Their Recognition of Amyloid Assemblies. Ph.D. Thesis, The University of Leeds, Leeds, UK, 2015.
142. Teplow, D.B. Preparation of amyloid β-protein for structural and functional studies. *Methods Enzymol.* **2006**, *413*, 20–33. [CrossRef] [PubMed]
143. Kim, K.S.; Miller, D.L.; Sapienza, V.J.; Chen, C.M.J.; Bai, C.; Grundke-Iqbal, I.; Currie, J.R.; Wisniewski, H.M. Production and characterization of monoclonal antibodies reactive to synthetic cerebrovascular amyloid peptide. *Neurosci. Res. Commun.* **1988**, *2*, 121–130.
144. Kim, K.S.; Wen, G.Y.; Bancher, C.; Chen, C.M.J.; Sapienza, V.J.; Hong, H.; Wisniewski, H.M. Detection and quantitation of amyloid β-peptide with two monoclonal antibodies. *Neurosci. Res. Commun.* **1990**, *7*, 113–122.
145. Pirttilä, T.; Kim, K.S.; Mehta, P.D.; Frey, H.; Wisniewski, H.M. Soluble amyloid β-protein in the cerebrospinal fluid from patients with Alzheimer's disease, vascular dementia and controls. *J. Neurol. Sci.* **1994**, *127*, 90–95. [CrossRef]
146. Necula, M.; Kayed, R.; Milton, S.; Glabe, C.G. Small molecule inhibitors of aggregation indicate that amyloid β oligomerization and fibrillization pathways are independent and distinct. *J. Biol. Chem.* **2007**, *282*, 10311–10324. [CrossRef] [PubMed]
147. Mathew, A.; Aravind, A.; Brahatheeswaran, D.; Fukuda, T.; Nagaoka, Y.; Hasumura, T.; Iwai, S.; Morimoto, H.; Yoshida, Y.; Maekawa, T.; et al. Amyloid-binding aptamer conjugated curcumin—PLGA nanoparticle for potential use in Alzheimer's disease. *BioNanoScience* **2012**, *2*, 83–93. [CrossRef]
148. Chakravarthy, M.; Chen, S.; Dodd, P.R.; Veedu, R.N. Nucleic acid-based theranostics for tackling Alzheimer's disease. *Theranostics* **2017**, *7*, 3933–3947. [CrossRef] [PubMed]

149. Rahimi, F.; Li, H.; Sinha, S.; Bitan, G. Modulators of Amyloid β-Protein (Aβ) Self-Assembly. In *Developing Therapeutics for Alzheimer's Diseas*; Wolfe, M.S., Ed.; Academic Press: Boston, MA, USA, 2016; pp. 97–191, ISBN 978-0-12-802173-6.
150. Baell, J.; Walters, M.A. Chemical con artists foil drug discovery. *Nature* **2014**, *513*, 481–483. [CrossRef] [PubMed]
151. Nelson, K.M.; Dahlin, J.L.; Bisson, J.; Graham, J.; Pauli, G.F.; Walters, M.A. The essential medicinal chemistry of curcumin. *J. Med. Chem.* **2017**, *60*, 1620–1637. [CrossRef] [PubMed]
152. Bahadori, F.; Demiray, M. A realistic view on "the essential medicinal chemistry of curcumin". *ACS Med. Chem. Lett.* **2017**, *8*, 893–896. [CrossRef] [PubMed]
153. Rahimi, F.; Murakami, K.; Summers, J.L.; Chen, C.H.B.; Bitan, G. RNA aptamers generated against oligomeric Aβ40 recognize common amyloid aptatopes with low specificity but high sensitivity. *PLoS ONE* **2009**, *4*, e7694. [CrossRef] [PubMed]
154. Bitan, G.; Lomakin, A.; Teplow, D.B. Amyloid β-protein oligomerization: Prenucleation interactions revealed by photo-induced cross-linking of unmodified proteins. *J. Biol. Chem.* **2001**, *276*, 35176–35184. [CrossRef] [PubMed]
155. Rahimi, F.; Maiti, P.; Bitan, G. Photo-induced cross-linking of unmodified proteins (PICUP) applied to amyloidogenic peptides. *J. Vis. Exp.* **2009**. [CrossRef] [PubMed]
156. Rosensweig, C.; Ono, K.; Murakami, K.; Lowenstein, D.K.; Bitan, G.; Teplow, D.B. Preparation of stable amyloid β-protein oligomers of defined assembly order. *Methods Mol. Biol.* **2012**, *849*, 23–31. [CrossRef] [PubMed]
157. Bitan, G.; Fradinger, E.A.; Spring, S.M.; Teplow, D.B. Neurotoxic protein oligomers—What you see is not always what you get. *Amyloid* **2005**, *12*, 88–95. [CrossRef] [PubMed]
158. LeVine, H., 3rd. Quantification of β-sheet amyloid fibril structures with thioflavin T. *Methods Enzymol.* **1999**, *309*, 274–284. [PubMed]
159. Li, H.; Rahimi, F.; Sinha, S.; Maiti, P.; Bitan, G.; Murakami, K. Amyloids and Protein Aggregation—Analytical Methods. In *Encyclopedia of Analytical Chemistry*; John Wiley & Sons, Ltd.: Hoboken, NJ, USA, 2009, ISBN 9780470027318.
160. Rahimi, F.; Bitan, G. Selection of aptamers for amyloid β-protein, the causative agent of Alzheimer's disease. *J. Vis. Exp.* **2010**. [CrossRef] [PubMed]
161. Jankowsky, J.L.; Fadale, D.J.; Anderson, J.; Xu, G.M.; Gonzales, V.; Jenkins, N.A.; Copeland, N.G.; Lee, M.K.; Younkin, L.H.; Wagner, S.L.; et al. Mutant presenilins specifically elevate the levels of the 42 residue β-amyloid peptide in vivo: Evidence for augmentation of a 42-specific γ secretase. *Hum. Mol. Genet.* **2004**, *13*, 159–170. [CrossRef] [PubMed]
162. Klunk, W.E.; Bacskai, B.J.; Mathis, C.A.; Kajdasz, S.T.; McLellan, M.E.; Frosch, M.P.; Debnath, M.L.; Holt, D.P.; Wang, Y.; Hyman, B.T. Imaging Aβ plaques in living transgenic mice with multiphoton microscopy and methoxy-X04, a systemically administered Congo red derivative. *J. Neuropathol. Exp. Neurol.* **2002**, *61*, 797–805. [CrossRef] [PubMed]
163. Koffie, R.M.; Meyer-Luehmann, M.; Hashimoto, T.; Adams, K.W.; Mielke, M.L.; Garcia-Alloza, M.; Micheva, K.D.; Smith, S.J.; Kim, M.L.; Lee, V.M.; et al. Oligomeric amyloid β associates with postsynaptic densities and correlates with excitatory synapse loss near senile plaques. *Proc. Natl. Acad. Sci. USA* **2009**, *106*, 4012–4017. [CrossRef] [PubMed]
164. Lee, E.B.; Leng, L.Z.; Zhang, B.; Kwong, L.; Trojanowski, J.Q.; Abel, T.; Lee, V.M. Targeting amyloid-β peptide (Aβ) oligomers by passive immunization with a conformation-selective monoclonal antibody improves learning and memory in Aβ precursor protein (APP) transgenic mice. *J. Biol. Chem.* **2006**, *281*, 4292–4299. [CrossRef] [PubMed]
165. Gudiksen, K.L.; Gitlin, I.; Whitesides, G.M. Differentiation of proteins based on characteristic patterns of association and denaturation in solutions of SDS. *Proc. Natl. Acad. Sci. USA* **2006**, *103*, 7968–7972. [CrossRef] [PubMed]
166. Leffers, K.W.; Schell, J.; Jansen, K.; Lucassen, R.; Kaimann, T.; Nagel-Steger, L.; Tatzelt, J.; Riesner, D. The structural transition of the prion protein into its pathogenic conformation is induced by unmasking hydrophobic sites. *J. Mol. Biol.* **2004**, *344*, 839–853. [CrossRef] [PubMed]

167. Kawooya, J.K.; Emmons, T.L.; Gonzalez-DeWhitt, P.A.; Camp, M.C.; D'Andrea, S.C. Electrophoretic mobility of Alzheimer's amyloid-β peptides in urea-sodium dodecyl sulfate-polyacrylamide gel electrophoresis. *Anal. Biochem.* **2003**, *323*, 103–113. [CrossRef] [PubMed]
168. Montserret, R.; McLeish, M.J.; Böckmann, A.; Geourjon, C.; Penin, F. Involvement of electrostatic interactions in the mechanism of peptide folding induced by sodium dodecyl sulfate binding. *Biochemistry* **2000**, *39*, 8362–8373. [CrossRef] [PubMed]
169. Yamamoto, S.; Hasegawa, K.; Yamaguchi, I.; Tsutsumi, S.; Kardos, J.; Goto, Y.; Gejyo, F.; Naiki, H. Low concentrations of sodium dodecyl sulfate induce the extension of $\beta_2$-microglobulin-related amyloid fibrils at a neutral pH. *Biochemistry* **2004**, *43*, 11075–11082. [CrossRef] [PubMed]
170. Rangachari, V.; Moore, B.D.; Reed, D.K.; Sonoda, L.K.; Bridges, A.W.; Conboy, E.; Hartigan, D.; Rosenberry, T.L. Amyloid-β(1–42) rapidly forms protofibrils and oligomers by distinct pathways in low concentrations of sodium dodecylsulfate. *Biochemistry* **2007**, *46*, 12451–12462. [CrossRef] [PubMed]
171. Rangachari, V.; Reed, D.K.; Moore, B.D.; Rosenberry, T.L. Secondary structure and interfacial aggregation of amyloid-β(1–40) on sodium dodecyl sulfate micelles. *Biochemistry* **2006**, *45*, 8639–8648. [CrossRef] [PubMed]
172. Piening, N.; Weber, P.; Högen, T.; Beekes, M.; Kretzschmar, H.; Giese, A. Photo-induced crosslinking of prion protein oligomers and prions. *Amyloid* **2006**, *13*, 67–77. [CrossRef] [PubMed]
173. Moussa, C.E.; Wersinger, C.; Rusnak, M.; Tomita, Y.; Sidhu, A. Abnormal migration of human wild-type α-synuclein upon gel electrophoresis. *Neurosci. Lett.* **2004**, *371*, 239–243. [CrossRef] [PubMed]
174. Podlisny, M.B.; Ostaszewski, B.L.; Squazzo, S.L.; Koo, E.H.; Rydell, R.E.; Teplow, D.B.; Selkoe, D.J. Aggregation of secreted amyloid β-protein into sodium dodecyl sulfate-stable oligomers in cell culture. *J. Biol. Chem.* **1995**, *270*, 9564–9570. [CrossRef] [PubMed]
175. Walsh, D.M.; Hartley, D.M.; Kusumoto, Y.; Fezoui, Y.; Condron, M.M.; Lomakin, A.; Benedek, G.B.; Selkoe, D.J.; Teplow, D.B. Amyloid β-protein fibrillogenesis. Structure and biological activity of protofibrillar intermediates. *J. Biol. Chem.* **1999**, *274*, 25945–25952. [CrossRef] [PubMed]
176. Mori, H.; Takio, K.; Ogawara, M.; Selkoe, D.J. Mass spectrometry of purified amyloid β protein in Alzheimer's disease. *J. Biol. Chem.* **1992**, *267*, 17082–17086. [PubMed]
177. Yu, L.; Edalji, R.; Harlan, J.E.; Holzman, T.F.; Lopez, A.P.; Labkovsky, B.; Hillen, H.; Barghorn, S.; Ebert, U.; Richardson, P.L.; et al. Structural characterization of a soluble amyloid β-peptide oligomer. *Biochemistry* **2009**, *48*, 1870–1877. [CrossRef] [PubMed]
178. Barghorn, S.; Nimmrich, V.; Striebinger, A.; Krantz, C.; Keller, P.; Janson, B.; Bahr, M.; Schmidt, M.; Bitner, R.S.; Harlan, J.; et al. Globular amyloid β-peptide$_{1-42}$ oligomer—A homogenous and stable neuropathological protein in Alzheimer's disease. *J. Neurochem.* **2005**, *95*, 834–847. [CrossRef] [PubMed]
179. Bitan, G.; Kirkitadze, M.D.; Lomakin, A.; Vollers, S.S.; Benedek, G.B.; Teplow, D.B. Amyloid β-protein (Aβ) assembly: Aβ40 and Aβ42 oligomerize through distinct pathways. *Proc. Natl. Acad. Sci. USA* **2003**, *100*, 330–335. [CrossRef] [PubMed]
180. Bitan, G.; Tarus, B.; Vollers, S.S.; Lashuel, H.A.; Condron, M.M.; Straub, J.E.; Teplow, D.B. A molecular switch in amyloid assembly: Met$^{35}$ and amyloid β-protein oligomerization. *J. Am. Chem. Soc.* **2003**, *125*, 15359–15365. [CrossRef] [PubMed]
181. Hepler, R.W.; Grimm, K.M.; Nahas, D.D.; Breese, R.; Dodson, E.C.; Acton, P.; Keller, P.M.; Yeager, M.; Wang, H.; Shughrue, P.; et al. Solution state characterization of amyloid β-derived diffusible ligands. *Biochemistry* **2006**, *45*, 15157–15167. [CrossRef] [PubMed]
182. O'Nuallain, B.; Freir, D.B.; Nicoll, A.J.; Risse, E.; Ferguson, N.; Herron, C.E.; Collinge, J.; Walsh, D.M. Amyloid β-protein dimers rapidly form stable synaptotoxic protofibrils. *J. Neurosci.* **2010**, *30*, 14411–14419. [CrossRef] [PubMed]
183. Watt, A.D.; Perez, K.A.; Rembach, A.; Sherrat, N.A.; Hung, L.W.; Johanssen, T.; McLean, C.A.; Kok, W.M.; Hutton, C.A.; Fodero-Tavoletti, M.; et al. Oligomers, fact or artefact? SDS-PAGE induces dimerization of β-amyloid in human brain samples. *Acta Neuropathol.* **2013**, *125*, 549–564. [CrossRef] [PubMed]
184. Pujol-Pina, R.; Vilaprinyó-Pascual, S.; Mazzucato, R.; Arcella, A.; Vilaseca, M.; Orozco, M.; Carulla, N. SDS-PAGE analysis of Aβ oligomers is disserving research into Alzheimer s disease: Appealing for ESI-IM-MS. *Sci. Rep.* **2015**, *5*, 14809. [CrossRef] [PubMed]
185. Bitan, G.; Vollers, S.S.; Teplow, D.B. Elucidation of primary structure elements controlling early amyloid β-protein oligomerization. *J. Biol. Chem.* **2003**, *278*, 34882–34889. [CrossRef] [PubMed]

186. Dahlgren, K.N.; Manelli, A.M.; Stine, W.B., Jr.; Baker, L.K.; Krafft, G.A.; LaDu, M.J. Oligomeric and fibrillar species of amyloid-β peptides differentially affect neuronal viability. *J. Biol. Chem.* **2002**, *277*, 32046–32053. [CrossRef] [PubMed]
187. Vasilevko, V.; Pop, V.; Kim, H.J.; Saing, T.; Glabe, C.C.; Milton, S.; Barrett, E.G.; Cotman, C.W.; Cribbs, D.H.; Head, E. Linear and conformation specific antibodies in aged beagles after prolonged vaccination with aggregated Abeta. *Neurobiol. Dis.* **2010**, *39*, 301–310. [CrossRef] [PubMed]
188. Head, E.; Pop, V.; Vasilevko, V.; Hill, M.; Saing, T.; Sarsoza, F.; Nistor, M.; Christie, L.A.; Milton, S.; Glabe, C.; et al. A two-year study with fibrillar β-amyloid (Aβ) immunization in aged canines: Effects on cognitive function and brain Aβ. *J. Neurosci.* **2008**, *28*, 3555–3566. [CrossRef] [PubMed]
189. Galzitskaya, O.V. Repeats are one of the main characteristics of RNA-binding proteins with prion-like domains. *Mol. Biosyst.* **2015**, *11*, 2210–2218. [CrossRef] [PubMed]
190. Calamai, M.; Kumita, J.R.; Mifsud, J.; Parrini, C.; Ramazzotti, M.; Ramponi, G.; Taddei, N.; Chiti, F.; Dobson, C.M. Nature and significance of the interactions between amyloid fibrils and biological polyelectrolytes. *Biochemistry* **2006**, *45*, 12806–12815. [CrossRef] [PubMed]
191. Maury, C.P. The emerging concept of functional amyloid. *J. Intern. Med.* **2009**, *265*, 329–334. [CrossRef] [PubMed]
192. Sharon, R.; Bar-Joseph, I.; Frosch, M.P.; Walsh, D.M.; Hamilton, J.A.; Selkoe, D.J. The formation of highly soluble oligomers of α-synuclein is regulated by fatty acids and enhanced in Parkinson's disease. *Neuron* **2003**, *37*, 583–595. [CrossRef]
193. Lesné, S.; Koh, M.T.; Kotilinek, L.; Kayed, R.; Glabe, C.G.; Yang, A.; Gallagher, M.; Ashe, K.H. A specific amyloid-β protein assembly in the brain impairs memory. *Nature* **2006**, *440*, 352–357. [CrossRef] [PubMed]
194. Klucken, J.; Ingelsson, M.; Shin, Y.; Irizarry, M.C.; Hedley-Whyte, E.T.; Frosch, M.; Growdon, J.; McLean, P.; Hyman, B.T. Clinical and biochemical correlates of insoluble α-synuclein in dementia with Lewy bodies. *Acta Neuropathol.* **2006**, *111*, 101–108. [CrossRef] [PubMed]
195. Shankar, G.M.; Bloodgood, B.L.; Townsend, M.; Walsh, D.M.; Selkoe, D.J.; Sabatini, B.L. Natural oligomers of the Alzheimer amyloid-β protein induce reversible synapse loss by modulating an NMDA-type glutamate receptor-dependent signaling pathway. *J. Neurosci.* **2007**, *27*, 2866–2875. [CrossRef] [PubMed]
196. Shankar, G.M.; Li, S.; Mehta, T.H.; Garcia-Munoz, A.; Shepardson, N.E.; Smith, I.; Brett, F.M.; Farrell, M.A.; Rowan, M.J.; Lemere, C.A.; et al. Amyloid-β protein dimers isolated directly from Alzheimer's brains impair synaptic plasticity and memory. *Nat. Med.* **2008**, *14*, 837–842. [CrossRef] [PubMed]
197. Paleologou, K.E.; Kragh, C.L.; Mann, D.M.; Salem, S.A.; Al-Shami, R.; Allsop, D.; Hassan, A.H.; Jensen, P.H.; El-Agnaf, O.M. Detection of elevated levels of soluble α-synuclein oligomers in post-mortem brain extracts from patients with dementia with Lewy bodies. *Brain* **2009**, *132*, 1093–1101. [CrossRef] [PubMed]
198. Head, E.; Pop, V.; Sarsoza, F.; Kayed, R.; Beckett, T.L.; Studzinski, C.M.; Tomic, J.L.; Glabe, C.G.; Murphy, M.P. Amyloid-β peptide and oligomers in the brain and cerebrospinal fluid of aged canines. *J. Alzheimers Dis.* **2010**, *20*, 637–646. [CrossRef] [PubMed]
199. Ono, K.; Condron, M.M.; Teplow, D.B. Structure–neurotoxicity relationships of amyloid β-protein oligomers. *Proc. Natl. Acad. Sci. USA* **2009**, *106*, 14745–14750. [CrossRef] [PubMed]
200. Qu, J.; Yu, S.; Zheng, Y.; Zheng, Y.; Yang, H.; Zhang, J. Aptamer and its applications in neurodegenerative diseases. *Cell. Mol. Life Sci.* **2017**, *74*, 683–695. [CrossRef] [PubMed]
201. Röthlisberger, P.; Gasse, C.; Hollenstein, M. Nucleic acid aptamers: Emerging applications in medical imaging, nanotechnology, neurosciences, and drug delivery. *Int. J. Mol. Sci.* **2017**, *18*, 2430. [CrossRef] [PubMed]
202. Sriramoju, B.; Kanwar, R.; Veedu, R.N.; Kanwar, J.R. Aptamer-targeted oligonucleotide theranostics: A smarter approach for brain delivery and the treatment of neurological diseases. *Curr. Top. Med. Chem.* **2015**, *15*, 1115–1124. [CrossRef] [PubMed]


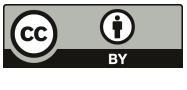

International Journal of
*Molecular Sciences*

MDPI

*Article*

# Selection, Characterization and Interaction Studies of a DNA Aptamer for the Detection of *Bifidobacterium bifidum*

**Lujun Hu [1], Linlin Wang [1], Wenwei Lu [1,2], Jianxin Zhao [1,2], Hao Zhang [1,2] and Wei Chen [1,2,3,*]**

1 State Key Laboratory of Food Science and Technology, School of Food Science and Technology, Jiangnan University, Wuxi 214122, China; 7130112038@vip.jiangnan.edu.cn (L.H.); wanglllynn09@163.com (L.W.); luwenwei@jiangnan.edu.cn (W.L.); jxzhao@jiangnan.edu.cn (J.Z.); zhanghao@jiangnan.edu.cn (H.Z.)
2 International Joint Research Center for Probiotics & Gut Health, Jiangnan University, Wuxi 214122, China
3 Beijing Innovation Centre of Food Nutrition and Human Health, Beijing Technology and Business University, Beijing 100048, China
* Correspondence: chenwei66@jiangnan.edu.cn; Tel.: +86-510-8591-2155

Academic Editor: Julian Alexander Tanner
Received: 7 March 2017; Accepted: 18 April 2017; Published: 25 April 2017

**Abstract:** A whole-bacterium-based SELEX (Systematic Evolution of Ligands by Exponential Enrichment) procedure was adopted in this study for the selection of an ssDNA aptamer that binds to *Bifidobacterium bifidum*. After 12 rounds of selection targeted against *B. bifidum*, 30 sequences were obtained and divided into seven families according to primary sequence homology and similarity of secondary structure. Four FAM (fluorescein amidite) labeled aptamer sequences from different families were selected for further characterization by flow cytometric analysis. The results reveal that the aptamer sequence CCFM641-5 demonstrated high-affinity and specificity for *B. bifidum* compared with the other sequences tested, and the estimated $K_d$ value was 10.69 ± 0.89 nM. Additionally, sequence truncation experiments of the aptamer CCFM641-5 led to the conclusion that the 5′-primer and 3′-primer binding sites were essential for aptamer-target binding. In addition, the possible component of the target *B. bifidum*, bound by the aptamer CCFM641-5, was identified as a membrane protein by treatment with proteinase. Furthermore, to prove the potential application of the aptamer CCFM641-5, a colorimetric bioassay of the sandwich-type structure was used to detect *B. bifidum*. The assay had a linear range of $10^4$ to $10^7$ cfu/mL ($R^2$ = 0.9834). Therefore, the colorimetric bioassay appears to be a promising method for the detection of *B. bifidum* based on the aptamer CCFM641-5.

**Keywords:** *Bifidobacterium bifidum*; aptamer; SELEX; sequence truncation; colorimetric bioassay

## 1. Introduction

Aptamers are highly structured single-stranded oligonucleotides obtained from an in vitro evolution process called Systematic Evolution of Ligands by Exponential Enrichment (SELEX) according to their binding abilities to target molecules [1,2]. Compared with traditional antibodies, aptamers have many advantages such as low molecular weight, ease of synthesis and modifications, and comparable stability during long-term storage [3–5]. Whole-bacterium SELEX was specifically developed to separate aptamers against live bacteria, and it is a particularly promising selection strategy for the identification of bacteria. Bacterium-based aptamer selection methods have been implemented to select ssDNA aptamers against many bacteria, including *Campylobacter jejuni*, *Escherichia coli*, *Lactobacillus acidophilus*, *Mycobacterium tuberculosis*, *Vibrio parahemolyticus*, *Streptococcus pyogenes*, and *Staphylococcus aureus* without previous knowledge of a specific target molecule [6–12].

Many studies have found that *Bifidobacterium bifidum* has the potential to prevent inflammatory bowel disease and necrotizing enterocolitis, reduce cholesterol activity, treat infantile eczema, modulate the host innate immune response, show preventive potential for diarrheal disease in infants, and exert a key role in the evolution and maturation of the immune system of the host [13–19]. *B. bifidum* has also been granted QPS (quality and presumption of safety) status by the European Food Safety Authority. Thus, *B. bifidum* is often used in probiotic products along with other lactic acid bacteria [20–22], and identification of *B. bifidum* is vital for its industrial use. The conventional approaches for the identification of *B. bifidum* are laborious and time-consuming. There is thus a need of developing alternative methods for the identification of *B. bifidum*. Many molecular methods have been developed for the identification of *B. bifidum* [23–26], but they increase the analysis cost in that they require specialized instruments and highly trained personnel [24,27,28]. Therefore, aptamers may be an alternative method for the detection of *B. bifidum*.

Enzyme linked aptamer assay (ELAA), a variant of the classical ELISA (enzyme linked immunosorbent assay) uses aptamers instead of antibodies [29,30], and uses an enzyme as the signal readout element and an aptamer as the recognition element. ELAA can realize high-throughput with a 96-well microplate and is convenient because the signal readout requires only simple instruments (or even no instruments, when read with the naked eye). Therefore, ELAA has been used in many bioanalytical applications for target-specific detection of some substances such as *M. tuberculosis*, ochratoxin A, cocaine and thrombin [31–34]. However, ELAA has not been reported in the detection of *B. bifidum*.

In this study, we used an improved whole-bacterium SELEX strategy to select an ssDNA aptamer specific for *B. bifidum*. In addition, truncation experiments were carried out to narrow down the sequence region of the potential aptamers essentially for their binding abilities to the target *B. bifidum*. In addition, *B. bifidum* was treated with proteinases to determine whether the targets of the aptamer were the membrane proteins on the cell surface of *B. bifidum*. Furthermore, to confirm the potential application of the candidate aptamer, we developed a colorimetric assay that was a high-throughput, sensitive and specific method for the detection of *B. bifidum*.

## 2. Results and Discussion

### *2.1. SELEX Optimization*

To separate aptamers that specifically recognize *B. bifidum*, we gradually increased the selective pressure by increasing bovine serum albumin (BSA) and tRNA from a 10-fold molar excess of each in the starting round of selection to a maximum 120-fold molar excess in the 12th round, and by increasing the number of washes (from twice for the first six cycles to three times for the last six cycles). In addition, the suspended cell solutions were transferred to fresh microcentrifuge tubes to remove sequences that bound to the tube walls between each incubation and elution step. Counter-selection against a mixture of unrelated *Bifidobacterium* species, including *B. longum*, *B. animalis*, *B. breve*, and *B. adolescentis*, was employed in the 9th and 11th rounds. In addition, 2.5 μL DMSO (dimethyl sulfoxide) was chosen for the total volume of 50 μL during the PCR amplification of SELEX.

### *2.2. Determination of Affinity and Specificity*

Fluorescently labeled aptamer sequences were incubated with *B. bifidum* and tested via flow cytometric analysis. After the 12th round of selection, 30 sequences were obtained after the aptamer pools were cloned and sequenced. These sequences were then grouped into seven families according to the homology of the DNA sequences and the similarity of the secondary structure (data shown in Table S1 and Figure S1 in the Supplemental Materials). Four sequences were selected for further screening on the basis of their repetitiveness, predicted secondary structure and free energy of formation (Table 1).

**Table 1.** Tested aptamer sequences [a].

| Name | Sequence (5′ → 3′) |
|---|---|
| CCFM641-2 | GCCTGGCCAGGTGCCCCGATATAGCGACGCCTTGCCCGGC |
| CCFM641-4 | GCCCCGGACGGCGGGAAGCCTCGTACCCCCCGTGAGCGGC |
| CCFM641-5 | TGCGTGAGCGGTAGCCCCGTACGACCCACTGTGGTTGGGC |
| CCFM641-12 | GTCACACCGGCCGTCTCCGGTGTGGGACGCCCGCTGTGGC |

[a] The primer sequences are AGCAGCACAGAGGTCAGATG at the 5′ end and CCTATGCGTGCTACCGTGAA at the 3′ end.

The results displayed in Figure 1 demonstrated that CCFM641-5 showed a stronger binding affinity for *B. bifidum* than the other three aptamers. To further evaluate the binding ability of the aptamer CCFM641-5 to the target *B. bifidum*, we performed binding assays by varying the concentrations of the aptamer (from 0 to 100 nM) and using a constant number of cells ($10^8$ cells) for each assay. Saturation curves were fit from these data and the dissociation constant $K_d$ values were determined via nonlinear regression analysis. The dissociation constant $K_d$ between CCFM641-5 and *B. bifidum* was calculated to be 10.69 ± 0.89 nM. Therefore, aptamer CCFM641-5 was chosen for the specificity detection. The predicted secondary structure and binding saturation curve of aptamer CCFM641-5 for *B. bifidum* are shown in Figure 2.

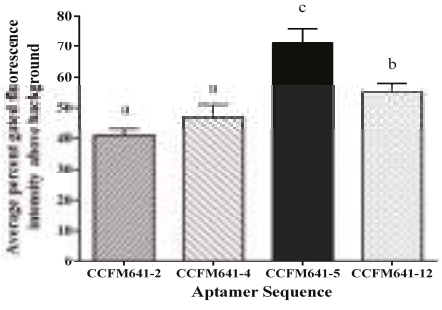


**Figure 1.** Binding affinity of aptamers for *B. bifidum*. The 5′-FAM-labeled individual aptamers were incubated with *B. bifidum* at 37 °C for 45 min (as described in the text). The values of aptamer binding represent the mean ± SD of three independent experiments. Bars with different letters are significantly different ($p < 0.05$).

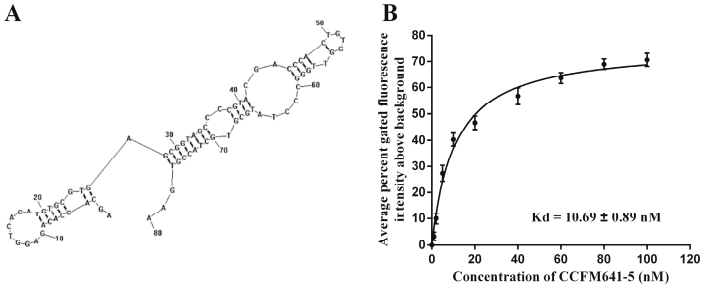


**Figure 2.** The secondary structure and binding ability of aptamer CCFM641-5 against *B. bifidum*. (**A**) The secondary structure of aptamer CCFM641-5. The secondary structure was predicted using RNAstructure 3.0. (**B**) The binding saturation curve of aptamer CCFM641-5 with *B. bifidum*. A nonlinear regression curve was fit according to the data from flow cytometric analysis using GraphPad Prism 5.0. The values of aptamer binding and $K_d$ represent the mean ± SD of three independent experiments.

To determine the specificity of the candidate aptamer CCFM641-5 for the target *B. bifidum*, the FAM (fluorescein amidite) labeled aptamer CCFM641-5 was also tested against a variety of other bacterial species, including *B. longum*, *B. animalis*, *B. breve*, *B. adolescentis* and *L. plantarum*. As shown in Figure 3, the aptamer CCFM641-5 displayed preferential binding ability to *B. bifidum* over the other bacteria tested. In addition, the results from qPCR shown in Figure S2 demonstrated that CCFM641-5 displayed a stronger binding ability to *B. bifidum* than the other bacterial species. Taken together, this preferential binding demonstrated the excellent specificity of the aptamer CCFM641-5 for *B. bifidum*.

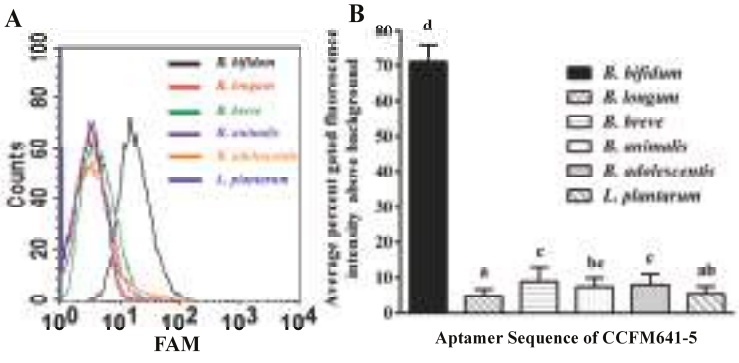


**Figure 3.** Characterization of the specificity of aptamer CCFM641-5 for *B. bifidum*. Selected aptamer sequence CCFM641-5 preferentially bound to *B. bifidum* over other species of bacteria. (**A**) Flow cytometric analysis of aptamer CCFM641-5 binding for different species of bacteria which are shown with differently colored curves; (**B**) Histogram of the percent gated fluorescence intensity above background for aptamer CCFM641-5. The values of aptamer binding represent the mean ± SD of three independent experiments. Bars with different letters are significantly different ($p < 0.05$).

### *2.3. Aptamer Truncations and Their Effects on the Binding Ability to B. bifidum*

In general, not all nucleic acids of the aptamers are necessary for binding affinity between the aptamers and the targets [35]. To determine the minimal sequence necessary for binding affinity between *B. bifidum* and the aptamer CCFM641-5, the aptamer was truncated to narrow down the sequence region responsible for target binding affinity. Either specific primer binding site at the ends of aptamer CCFM641-5 (CCFM641-5F and CCFM641-5R) or both sites (CCFM641-5FR) were removed (Table 2). As displayed in Figure 4, all the aptamer variants bound to *B. bifidum* with a lower binding affinity compared to the full-length aptamer CCFM641-5. Taken together, the results indicate that the 3′-primer and 5′-primer binding sites of aptamer CCFM641-5 are important for its binding affinity for *B. bifidum*, even if the aptamer affinity is still largely preserved for the 5′ truncation.

**Table 2.** Full-length aptamer CCFM641-5 and truncated aptamer variants [a].

| Name | Sequence (5′ → 3′) |
|---|---|
| CCFM641-5 | AGCAGCACAGAGGTCAGATGTGCGTGAGCGGTAGCCCCGTACGACCCACTGTGGTTGG GCCCTATGCGTGCTACCGTGAA |
| CCFM641-5F | TGCGTGAGCGGTAGCCCCGTACGACCCACTGTGGTTGGGC CCTATGCGTGCTACCGTGAA |
| CCFM641-5R | AGCAGCACAGAGGTCAGATGTGCGTGAGCGGTAGCCCCGTACGACCCACTGTGGTTGGGC |
| CCFM641-5FR | TGCGTGAGCGGTAGCCCCGTACGACCCACTGTGGTTGGGC |

[a] The underlined sequences AGCAGCACAGAGGTCAGATG and CCTATGCGTGCTACCGTGAA are the primer binding sites.

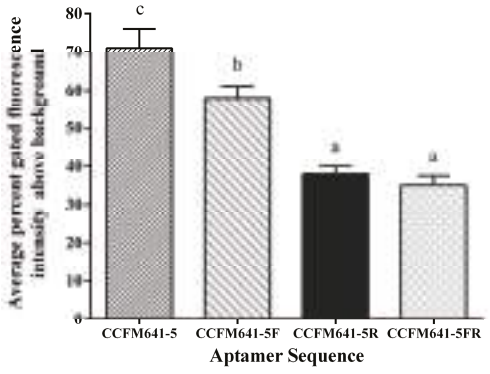


**Figure 4.** Binding abilities of the truncated aptamer variants to *B. bifidum* compared to the full-length aptamer CCFM641-5. The values of aptamer binding represent the mean ± SD of three independent experiments. Bars with different letters are significantly different ($p < 0.05$).

### *2.4. Proteinase Treatment for Bacteria*

To evaluate that the targets of the aptamer are membrane proteins on the *B. bifidum* cell surface, we treated *B. bifidum* with proteinases including trypsin and proteinase K for a short time before adding the aptamer CCFM641-5 to these treated bacteria. As revealed in Figure 5, after the bacteria were treated with trypsin or proteinase K for 2 and 10 min, respectively, in phosphate-buffere saline (PBS, pH 7.2) at 37 °C, aptamer CCFM641-5 lowered its binding ability to *B. bifidum*. It can be deduced that the binding entities of aptamer CCFM641-5 had been broken by the proteinases, suggesting that the target molecules are in fact membrane proteins.

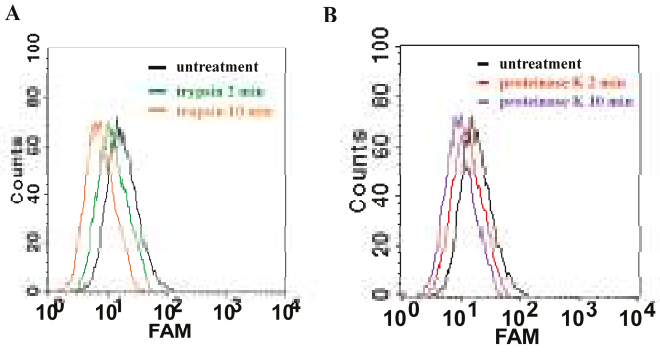


**Figure 5.** Binding assays of aptamer CCFM641-5 to trypsin-treated or proteinase K-treated *B. bifidum*. (**A**) Flow cytometric analysis of aptamer CCFM641-5 binding affinity for trypsin-treated *B. bifidum*; (**B**) Flow cytometric analysis of aptamer CCFM641-5 binding ability to proteinase K-treated *B. bifidum*.

### *2.5. Colorimetric Detection of B. bifidum*

In this study, the candidate aptamer CCFM641-5 was used not only to capture but also to detect *B. bifidum* in the configuration of the colorimetric assay. In the assay, a sandwich-type structure of aptamer/target/aptamer was established. To evaluate the specificity of this method, one blank sample and five samples including *B. bifidum*, *B. longum*, *B. animalis*, *B. breve* and *B. adolescentis* were measured. The assays of all samples were carried out under the same conditions, and the concentrations of all bacteria were between $10^3$ and $10^8$ cfu/mL. As shown in Figure 6, the optical density (OD) values

at 450 nm of the blank sample and the four bacteria other than *B. bifidum* did not change when the concentrations of bacteria were increased, whereas the OD values at 450 nm of *B. bifidum* increased as concentrations of the bacteria increased. Particularly, the results shown in Figure 7 displayed a good linear relationship between the amounts of *B. bifidum* ranging from $10^4$ to $10^7$ cfu/mL and the OD values at 450 nm, with a regression coefficient of 0.9834. The limit of detection of the proposed method was estimated to be $10^4$ cfu/mL at a signal to noise ratio of 3.

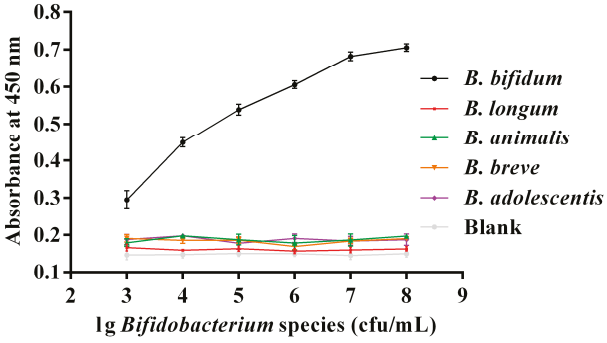


**Figure 6.** The absorbance at 450 nm measured for different species of bifidobacteria at concentrations ranging from $10^3$ to $10^8$ cfu/mL. The absorbance at 450 nm represents the mean ± SD of three independent experiments.

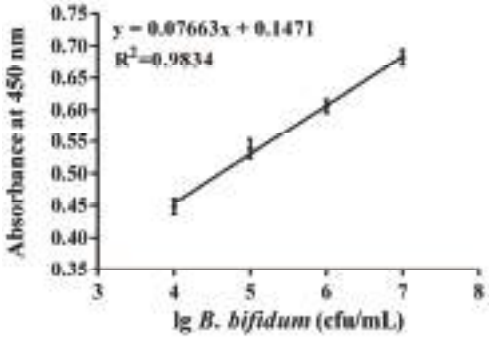


**Figure 7.** The calibration curve between the concentrations of *B. bifidum* and the intensity of the signals. The OD values were determined by the microplate reader at 450 nm wavelength. The absorbance at 450 nm represents the mean ± SD of three independent experiments.

## 3. Materials and Methods

### *3.1. Reagents and Apparatus*

*B. bifidum* ATCC 29521 was adopted as the target for whole-bacterium SELEX. Other *Bifidobacterium* species used in the study included: *B. longum* ATCC 15697, *B. breve* ATCC 15700, *B. animalis* JCM 11658, and *B. adolescentis* ATCC 15705, which were supplied by the American Type Culture Collection (ATCC) or the Japan Collection of Microorganisms (JCM). All of the *Bifidobacterium* species were grown in de Man–Rogosa–Sharpe (MRS) broth with 0.05% of L-cysteine hydrochloride monohydrate at 37 °C. *L. plantarum* ST-III (CGMCC No. 0847) used in this study was cultured in MRS broth at 37 °C (Merck KGaA, Darmstadt, Germany). All bacterial strains were cultured to the logarithmic phase under anaerobic conditions.

The starting ssDNA library and the PCR primers used for PCR amplifications were supplied by Integrated DNA Technologies (IDT, Coralville, IA, USA); tRNA, DMSO and streptavidin-HRP (horseradish peroxidase) were purchased from Sigma (St. Louis, MO, USA); BSA and all PCR chemicals were ordered from Invitrogen China (Shanghai, China); trypsin and proteinase K were purchased from TaKaRa (TaKaRa, Dalian, China); and DNA-BIND 96-well plates were obtained from Corning (Corning, New York, NY, USA). Water was filtered with a Milli-Q water purification system (Millipore, Bedford, MA, USA). All reagents were of analytical grade. Purification treatments were carried out with an Eppendorf 5424R centrifuge. PCR amplification was carried out in a Bio-Rad T 100 Thermal Cycler (Bio-Rad Laboratories, Hercules, CA, USA).

### *3.2. DNA Library and PCR Amplification*

The 80-nt ssDNA library consisted of a central random region of 40 nucleotides, where equimolar amounts of A, G, C and T are available at each position, flanked by two constant primer binding sequences, and the ssDNA library was synthesized with the following sequence: 5′-AGCAGCACAGAGGTCAGATG-N40-CCTATGCGTGCTACCGTGAA-3′. The ssDNA library and following aptamer pools were amplified with sense (5′-AGCAGCACAGAGGTCAGATG-3′) and antisense primer (5′-TTCACGGTAGCACGCATAGG-3′).

The PCR amplification mixture was as follows: 1× PCR amplification buffer, 10 μM forward and reverse primer, 25 mM dNTPs, 5 U/μL of Taq DNA polymerase, 2 μL of the template and 2.5 μL of DMSO in a total volume of 50 μL. PCR amplification was initiated with pre-denaturation at 95 °C for 6 min, followed by 25 cycles with 30 s denaturation at 95 °C, 30 s hybridization at 69 °C, 20 s extension at 72 °C, and finally elongation for 5 min at 72 °C.

PCR amplification products were detected by 8% nondenaturing polyacrylamide gel electrophoresis (PAGE) in 1× TBE buffer (90 mM Tris/89 mM boric acid/2.0 mM EDTA, pH 8.0) (Bio-Rad Protean III, Hercules, CA, USA) at 200 V for 25 min. The polyacrylamide gels were then stained with ethidium bromide, destained with gel running buffer solution, and photographed under UV light. A Qiagen MinElute PCR Purification Kit was used to purify all PCR amplification products (Qiagen Inc., Valencia, CA, USA).

### *3.3. Aptamer Selection*

The SELEX procedure for aptamer selection was implemented using the method described previously with some modifications [8,36]. *B. bifidum* was grown in liquid culture media and collected when it reached the logarithmic phase. The cell mixtures were centrifuged at 5000× *g* and 4 °C for 5 min and washed twice with 500 μL PBS at room temperature. The original ssDNA library/pool was heat denatured at 95 °C for 10 min and rapidly chilled for 10 min in an ice bath before incubation. *B. bifidum* cells totaling $10^8$ cfu/mL were incubated with 2 nmol of the ssDNA library for the initial round or 100 pmol of the aptamer pool for subsequent rounds (600 μL for the initial round, 350 μL for subsequent rounds). An excess of tRNA and BSA were put into the incubation buffer. All incubations were implemented in PBS at 37 °C for 45 min with slight agitation. The cells were centrifuged as described above before washing three times in PBS with 0.05% BSA. The cells were then resuspended with 100 μL of 1× PCR reaction buffer, heat denatured at 95 °C for 10 min, snap cooled for 10 min in an ice bath, and extracted by centrifugation as described above, and the supernatant was used as the template for PCR amplification to acquire the ssDNA pool for the following round of selection.

The ssDNA pool from the 12th round of selection was amplified and then cloned using the TOPO TA Cloning Kit (Invitrogen, Shanghai, China). Individual colonies were picked randomly and their inserts were sequenced. DNAMAN software was adopted to analyze the aptamer sequences and RNAstructure 3.0 was used for predicting a secondary structure for each sequence [10,12,37].

### 3.4. Flow-Cytometric Analysis

A FACSCalibur flow cytometer with a PowerMacG4 workstation and CellQuest Pro software (BD Biosciences, San Jose, CA, USA) was employed to assess the binding ability of the individual aptamer sequences to different species of bacteria (*B. bifidum*, *B. breve* , *B. longum*, *B. animalis*, *B. adolescentis*, and *L. plantarum*) in separate experiments. The aptamers were labeled with FAM fluorophore at the 5′ end. In the binding assays, $10^8$ cells were incubated with the fluorescently labeled aptamer pool (100 nM) at 37 °C for 45 min with slight agitation. The cells were then washed in PBS, collected by centrifugation, and resuspended in PBS for prompt flow cytometric assays. Forward scatter, side scatter, and fluorescence intensity were measured, and the gated fluorescence intensity above the background (cells with no aptamers) was quantified. BD CellQuest Pro software was adopted to analyze data from the FACSCalibur and to create histogram overlays. Binding dissociation constant $K_d$ values were obtained from the binding curves created with GraphPad Prism 5.0 software by varying the aptamer concentration (0 to 100 nM) with a fixed number of cells ($10^8$ cells).

### 3.5. Aptamer CCFM641-5 Binding Assays by Quantitative PCR (qPCR)

To further determine binding affinities of aptamer CCFM641-5 for different bacterial species, qPCR was performed as previously described with some modifications [7]. In the binding assays, $10^7$ bacterial cells were incubated with the aptamer (50 nM) at 37 °C for 45 min with slight agitation. The cells were then washed in PBS, collected by centrifugation, and resuspended with 50 μL of 1× PCR reaction buffer. The ssDNA aptamers recovered in the supernatant were used as the template for quantification by SYBR Green-based qPCR using a CFX96 real-time PCR detection system (Bio-Rad Laboratories, Hercules, CA, USA). All qPCR amplifications were carried out in 20 μL volume using 96-well plates in triplicate.

### 3.6. Aptamer Truncation

Truncation experiments were performed to determine whether all nucleotides of the aptamer sequence CCFM641-5 are necessary [38,39]. The specific primer binding sites of the aptamers were first removed. If DNA aptamer variants possessed high binding affinity for *B. bifidum*, the aptamer variants were then truncated from the 5′ end or 3′ end. In the experiment, the truncated aptamer variants were FAM-labeled at the 5′ end and tested for their binding abilities to *B. bifidum* with flow cytometric assays as described above.

### 3.7. Proteinase Treatment for Bacteria

The procedure used in this study was based on a previously published method [9,40] with some modifications, listed as follows. *B. bifidum* ($10^8$ cells) was collected by centrifugation, washed twice with PBS and incubated with 1 mL of 0.25% trypsin or 0.1 mg/mL proteinase K in PBS at 37 °C for 2 and 10 min. After incubation, the mixture was washed with PBS, and the treated bacteria were incubated with FAM-labeled aptamer for further binding assays as described above in flow-cytometric analysis.

### 3.8. Colorimetric Bioassay on the Basis of the Selected Aptamer

A colorimetric sandwich-type assay for the detection of *B. bifidum* was developed by ELAA. First, the amino-modified candidate aptamer was dissolved in binding buffer (0.01 mol/L PBS) and 100 μL of diluted aptamer (40 pmol/well) was added into each well of the DNA-BIND 96-well plate for incubation at 37 °C for 1 h. The wells were washed three times with washing buffer (0.01 mol/L PBS with 0.05% Tween-20) to remove unbound aptamer. The microplate wells were then blocked with blocking buffer (0.01 mol/L PBS with 3% BSA) for 1 h at 37 °C to prevent the appearance of nonspecific adsorption.

Then, a series of different concentrations of *B. bifidum* cells were added into each well for incubation at 37 °C for 45 min and the biotinylated aptamer and streptavidin-HRP were mixed

at 37 °C for 30 min at the same time. After the microtiter plates were washed three times with the washing buffer, and 100 μL samples of the above biotinylated aptamer and streptavidin-HRP complexes were added to each well for reaction for 45 min at 37 °C. After washing, 200 μL TMB–$H_2O_2$ (tetramethyl benzidine-hydrogen peroxide) working solutions were added into each well for reaction without direct light exposure. After incubating for 15 min, the reaction was terminated with 50 μL 2 M $H_2SO_4$, and the OD at 450 nm was measured with the microplate reader.

## 4. Conclusions

This study is the first report of the use of whole-bacterium SELEX to identify ssDNA aptamers that are specific for *B. bifidum*. The results show that the aptamer CCFM641-5 bound tightly to *B. bifidum* with a $K_d$ value in the nanomolar range, and could bind *B. bifidum* specifically over other bacterial species. According to the results of the present study, we demonstrate that the DNA aptamer CCFM641-5 can be used to capture and detect *B. bifidum*. Thus, the work described in this study testified the ability of this method to screen a good aptamer probe for the detection of *B. bifidum* and has the potential to contribute greatly to the development of the detection of *B. bifidum*.

In addition, the results from the experiments with aptamer truncations indicated that the 3′-primer and 5′-primer binding sites were important for an optimal binding affinity of the aptamer CCFM641-5 for *B. bifidum*. The experiments with proteinase treatment suggest that the component bound by the aptamer CCFM641-5 is likely protein on the *B. bifidum* cell surface.

Furthermore, we developed a colorimetric assay to detect *B. bifidum* which did not rely on expensive instrumentation, but on the basis of the aptamer CCFM641-5. The method is sensitive and specific and could be adopted to detect *B. bifidum* cells at concentrations as low as $10^4$ cfu/mL. Therefore, the colorimetric bioassay based on the aptamer CCFM641-5 is a promising method for the detection of *B. bifidum*.

**Supplementary Materials:** Supplementary materials can be found at www.mdpi.com/1422-0067/18/5/883/s1.

**Acknowledgments:** This work was supported by the Program of National Natural Science Foundation for the Youth of China (No. 31501454).

**Author Contributions:** Lujun Hu and Wei Chen conceived and designed the experiments; Lujun Hu and Linlin Wang performed the experiments; Lujun Hu and Wei Chen analyzed the data; Wenwei Lu, Jianxin Zhao and Hao Zhang contributed reagents/materials/analysis tools; and Lujun Hu and Wei Chen wrote the paper.

**Conflicts of Interest:** The authors declare no conflicts of interest.

## References

1. Tuerk, C.; Gold, L. Systematic evolution of ligands by exponential enrichment: RNA ligands to bacteriophage T4 DNA polymerase. *Science* **1990**, *249*, 505–510. [CrossRef] [PubMed]
2. Ellington, A.D.; Szostak, J.W. In vitro selection of RNA molecules that bind specific ligands. *Nature* **1990**, *346*, 818–822. [CrossRef] [PubMed]
3. Chen, M.; Yu, Y.; Jiang, F.; Zhou, J.; Li, Y.; Liang, C.; Dang, L.; Lu, A.; Zhang, G. Development of Cell-SELEX technology and its application in cancer diagnosis and therapy. *Int. J. Mol. Sci.* **2016**, *17*, 2079. [CrossRef] [PubMed]
4. Famulok, M.; Hartig, J.S.; Mayer, G. Functional aptamers and aptazymes in biotechnology, diagnostics, and therapy. *Chem. Rev.* **2007**, *107*, 3715–3743. [CrossRef] [PubMed]
5. Navani, N.K.; Li, Y. Nucleic acid aptamers and enzymes as sensors. *Curr. Opin. Chem. Biol.* **2006**, *10*, 272–281. [CrossRef] [PubMed]
6. Dwivedi, H.P.; Smiley, R.D.; Jaykus, L.A. Selection and characterization of DNA aptamers with binding selectivity to *Campylobacter jejuni* using whole-cell SELEX. *Appl. Microbiol. Biotechnol.* **2010**, *87*, 2323–2334. [CrossRef] [PubMed]
7. Marton, S.; Cleto, F.; Krieger, M.A.; Cardoso, J. Isolation of an aptamer that binds specifically to *E. coli*. *PLoS ONE* **2016**, *11*, e0153637. [CrossRef] [PubMed]

8. Hamula, C.L.A.; Zhang, H.; Guan, L.L.; Li, X.F.; Le, X.C. Selection of aptamers against live bacterial cells. *Anal. Chem.* **2008**, *80*, 7812–7819. [CrossRef] [PubMed]
9. Chen, F.; Zhou, J.; Luo, F.L.; Mohammed, A.B.; Zhang, X.L. Aptamer from whole-bacterium SELEX as new therapeutic reagent against virulent *Mycobacterium tuberculosis*. *Biochem. Biophys. Res. Commun.* **2007**, *357*, 743–748. [CrossRef] [PubMed]
10. Duan, N.; Wu, S.; Chen, X.; Huang, Y.; Wang, Z. Selection and identification of a DNA aptamer targeted to *Vibrio parahemolyticus*. *J. Agric. Food Chem.* **2012**, *60*, 4034–4038. [CrossRef] [PubMed]
11. Hamula, C.L.A.; Le, X.C.; Li, X.F. DNA aptamers binding to multiple prevalent M-types of *Streptococcus pyogenes*. *Anal. Chem.* **2011**, *83*, 3640–3647. [CrossRef] [PubMed]
12. Cao, X.; Li, S.; Chen, L.; Ding, H.; Xu, H.; Huang, Y.; Li, J.; Liu, N.; Cao, W.; Zhu, Y.; Shen, B.; Shao, N. Combining use of a panel of ssDNA aptamers in the detection of *Staphylococcus aureus*. *Nucleic Acids Res.* **2009**, *37*, 4621–4628. [CrossRef] [PubMed]
13. Kim, N.; Kunisawa, J.; Kweon, M.N.; Ji, G.E.; Kiyono, H. Oral feeding of *Bifidobacterium bifidum* (BGN4) prevents $CD4^+$ $CD45RB^{high}$ T cell-mediated inflammatory bowel disease by inhibition of disordered T cell activation. *Clin. Immunol.* **2007**, *123*, 30–39. [CrossRef] [PubMed]
14. Repa, A.; Thanhaeuser, M.; Endress, D.; Weber, M.; Kreissl, A.; Binder, C.; Berger, A.; Haiden, N. Probiotics (*Lactobacillus acidophilus* and *Bifidobacterium bifidum*) prevent NEC in VLBW infants fed breast milk but not formula. *Pediatr. Res.* **2015**, *77*, 381–388. [CrossRef] [PubMed]
15. Zanotti, I.; Turroni, F.; Piemontese, A.; Mancabelli, L.; Milani, C.; Viappiani, A.; Prevedini, G.; Sanchez, B.; Margolles, A.; Elviri, L.; et al. Evidence for cholesterol-lowering activity by *Bifidobacterium bifidum* PRL2010 through gut microbiota modulation. *Appl. Microbiol. Biotechnol.* **2015**, *99*, 6813–6829. [CrossRef] [PubMed]
16. Lin, R.J.; Qiu, L.H.; Guan, R.Z.; Hu, S.J.; Liu, Y.Y.; Wang, G.J. Protective effect of probiotics in the treatment of infantile eczema. *Exp. Ther. Med.* **2015**, *9*, 1593–1596. [CrossRef] [PubMed]
17. Turroni, F.; Taverniti, V.; Ruas-Madiedo, P.; Duranti, S.; Guglielmetti, S.; Lugli, G.A.; Gioiosa, L.; Palanza, P.; Margolles, A.; van Sinderen, D.; et al. *Bifidobacterium bifidum* PRL2010 modulates the host innate immune response. *Appl. Environ. Microbiol.* **2014**, *80*, 730–740. [CrossRef] [PubMed]
18. Saavedra, J.M.; Bauman, N.A.; Oung, I.; Perman, J.A.; Yolken, R.H. Feeding of *Bifidobacterium bifidum* and *Streptococcus thermophilus* to infants in hospital for prevention of diarrhoea and shedding of rotavirus. *Lancet* **1994**, *344*, 1046–1049. [CrossRef]
19. López, P.; González-Rodríguez, I.; Gueimonde, M.; Margolles, A.; Suárez, A. Immune response to *Bifidobacterium bifidum* strains support Treg/Th17 plasticity. *PLoS ONE* **2011**, *6*, e24776. [CrossRef] [PubMed]
20. Theunissen, J.; Britz, T.J.; Torriani, S.; Witthuhn, R.C. Identification of probiotic microorganisms in South African products using PCR-based DGGE analysis. *Int. J. Food Microbiol.* **2005**, *98*, 11–21. [CrossRef] [PubMed]
21. Mazzola, G.; Aloisio, I.; Biavati, B.; Di Gioia, D. Development of a synbiotic product for newborns and infants. *LWT-Food Sci. Technol.* **2015**, *64*, 727–734. [CrossRef]
22. Stanton, C.; Gardiner, G.; Meehan, H.; Collins, K.; Fitzgerald, G.; Lynch, P.B.; Ross, R.P. Market potential for probiotics. *Am. J. Clin. Nutr.* **2001**, *73*, 476–483.
23. Dinoto, A.; Marques, T.M.; Sakamoto, K.; Fukiya, S.; Watanabe, J.; Ito, S.; Yokota, A. Population dynamics of *Bifidobacterium* species in human feces during raffinose administration monitored by fluorescence in situ hybridization-flow cytometry. *Appl. Environ. Microbiol.* **2006**, *72*, 7739–7747. [CrossRef] [PubMed]
24. Matsuki, T.; Watanabe, K.; Fujimoto, J.; Kado, Y.; Takada, T.; Matsumoto, K.; Tanaka, R. Quantitative PCR with 16S rRNA-gene-targeted species-specific primers for analysis of human intestinal bifidobacteria. *Appl. Environ. Microbiol.* **2004**, *70*, 167–173. [CrossRef] [PubMed]
25. Mullié, C.; Odou, M.F.; Singer, E.; Romond, M.B.; Izard, D. Multiplex PCR using 16S rRNA gene-targeted primers for the identifcation of bifidobacteria from human origin. *FEMS Microbiol. Lett.* **2003**, *222*, 129–136. [CrossRef]
26. Vincent, D.; Roy, D.; Mondou, F.; Déry, C. Characterization of bifidobacteria by random DNA amplification. *Int. J. Food Microbiol.* **1998**, *43*, 185–193. [CrossRef]
27. Torres-Chavolla, E.; Alocilja, E.C. Aptasensors for detection of microbial and viral pathogens. *Biosens. Bioelectron.* **2009**, *24*, 3175–3182. [CrossRef] [PubMed]

28. Langendijk, P.S.; Schut, F.; Jansen, G.J.; Raangs, G.C.; Kamphuis, G.R.; Wilkinson, M.H.; Welling, G.W. Quantitative fluorescence in situ hybridization of *Bifidobacterium* spp. with genus-specific 16S rRNA-targeted probes and its application in fecal samples. *Appl. Environ. Microbiol.* **1995**, *61*, 3069–3075. [PubMed]
29. Ikebukuro, K.; Kiyohara, C.; Sode, K. Novel electrochemical sensor system for protein using the aptamers in sandwich manner. *Biosens. Bioelectron.* **2005**, *20*, 2168–2172. [CrossRef] [PubMed]
30. Zhao, J.; Zhang, Y.; Li, H.; Wen, Y.; Fan, X.; Lin, F.; Tan, L.; Yao, S. Ultrasensitive electrochemical aptasensor for thrombin based on the amplification of aptamer–AuNPs–HRP conjugates. *Biosens. Bioelectron.* **2011**, *26*, 2297–2303. [CrossRef] [PubMed]
31. Aimaiti, R.; Qin, L.; Cao, T.; Yang, H.; Wang, J.; Lu, J.; Huang, X.; Hu, Z. Identification and application of ssDNA aptamers against $H_{37}$Rv in the detection of *Mycobacterium tuberculosis*. *Appl. Microbiol. Biotechnol.* **2015**, *99*, 9073–9083. [CrossRef] [PubMed]
32. Barthelmebs, L.; Jonca, J.; Hayat, A.; Prieto-Simon, B.; Marty, J.L. Enzyme-Linked Aptamer Assays (ELAAs), based on a competition format for a rapid and sensitive detection of Ochratoxin A in wine. *Food Control* **2011**, *22*, 737–743. [CrossRef]
33. Nie, J.; Deng, Y.; Deng, Q.P.; Zhang, D.W.; Zhou, Y.L.; Zhang, X.X. A self-assemble aptamer fragment/target complex based high-throughput colorimetric aptasensor using enzyme linked aptamer assay. *Talanta* **2013**, *106*, 309–314. [CrossRef] [PubMed]
34. Park, J.H.; Cho, Y.S.; Kang, S.; Lee, E.J.; Lee, G.H.; Hah, S.S. A colorimetric sandwich-type assay for sensitive thrombin detection based on enzyme-linked aptamer assay. *Anal. Biochem.* **2014**, *462*, 10–12. [CrossRef] [PubMed]
35. Jayasena, S.D. Aptamers: An emerging class of molecules that rival antibodies in diagnostics. *Clin. Chem.* **1999**, *45*, 1628–1650. [PubMed]
36. Liu, G.; Yu, X.; Xue, F.; Chen, W.; Ye, Y.; Yang, X.; Lian, Y.; Yan, Y.; Zong, K. Screening and preliminary application of a DNA aptamer for rapid detection of Salmonella O8. *Microchim. Acta* **2012**, *178*, 237–244. [CrossRef]
37. Reuter, J.S.; Mathews, D.H. RNAstructure: Software for RNA secondary structure prediction and analysis. *BMC Bioinform.* **2010**, *11*, 129. [CrossRef] [PubMed]
38. Shangguan, D.; Tang, Z.; Mallikaratchy, P.; Xiao, Z.; Tan, W. Optimization and modifications of aptamers selected from live cancer cell lines. *ChemBioChem* **2007**, *8*, 603–606. [CrossRef] [PubMed]
39. Stoltenburg, R.; Schubert, T.; Strehlitz, B. In vitro selection and interaction studies of a DNA aptamer targeting protein A. *PLoS ONE* **2015**, *10*, e0134403. [CrossRef] [PubMed]
40. Shangguan, D.; Li, Y.; Tang, Z.; Cao, Z.C.; Chen, H.W.; Mallikaratchy, P.; Sefah, K.; Yang, C.J.; Tan, W. Aptamers evolved from live cells as effective molecular probes for cancer study. *Proc. Natl. Acad. Sci. USA* **2006**, *103*, 11838–11843. [CrossRef] [PubMed]


International Journal of
*Molecular Sciences*

MDPI

*Article*

# Development of An Impedimetric Aptasensor for the Detection of *Staphylococcus aureus*

**Peggy Reich [1,*], Regina Stoltenburg [2], Beate Strehlitz [3], Dieter Frense [1] and Dieter Beckmann [1]**

1 Institut für Bioprozess- und Analysenmesstechnik e.V., 37308 Heilbad Heiligenstadt, Germany; Dieter.Frense@iba-heiligenstadt.de (D.F.); Dieter.Beckmann@iba-heiligenstadt.de (D.B.)
2 UFZ – Helmholtz Centre for Environmental Research, 06120 Halle, Germany; regina.stoltenburg@ufz.de
3 UFZ – Helmholtz Centre for Environmental Research, 04318 Leipzig, Germany; beate.strehlitz@ufz.de
* Correspondence: ReichPeggy@gmail.com; Tel.: +49-176-4362-4901

Received: 31 October 2017; Accepted: 15 November 2017; Published: 21 November 2017

**Abstract:** In combination with electrochemical impedance spectroscopy, aptamer-based biosensors are a powerful tool for fast analytical devices. Herein, we present an impedimetric aptasensor for the detection of the human pathogen *Staphylococcus aureus*. The used aptamer targets protein A, a surface bound virulence factor of *S. aureus*. The thiol-modified protein A-binding aptamer was co-immobilized with 6-mercapto-1-hexanol onto gold electrodes by self-assembly. Optimization of the ratio of aptamer to 6-mercapto-1-hexanol resulted in an average density of $1.01 \pm 0.44 \times 10^{13}$ aptamer molecules per $cm^2$. As shown with quartz crystal microbalance experiments, the immobilized aptamer retained its functionality to bind recombinant protein A. Our impedimetric biosensor is based on the principle that binding of target molecules to the immobilized aptamer decreases the electron transfer between electrode and ferri-/ferrocyanide in solution, which is measured as an increase of impedance. Microscale thermophoresis measurements showed that addition of the redox probe ferri-/ferrocyanide has no influence on the binding of aptamer and its target. We demonstrated that upon incubation with various concentrations of *S. aureus*, the charge-transfer resistance increased proportionally. The developed biosensor showed a limit of detection of 10 $CFU \cdot mL^{-1}$ and results were available within 10 minutes. The biosensor is highly selective, distinguishing non-target bacteria such as *Escherichia coli* and *Staphylococcus epidermidis*. This work highlights the immense potential of impedimetric aptasensors for future biosensing applications.

**Keywords:** aptamer; staphylococcal protein A; label-free; biosensing techniques; rapid detection; self-assembly; limit of detection; protein binding; ferri-/ferrocyanide; gold electrode

## 1. Introduction

*Staphylococcus aureus* is a major pathogen for humans. It is a common cause of infections, from minor ones such as abscesses and sinusitis to life-threatening diseases such as bacteremia, endocarditis and sepsis [1]. Its antibiotic-resistant strains, e.g., methicillin-resistant *S. aureus* (MRSA) are a serious problem in healthcare [2]. Besides being the origin of hospital-acquired infections, *S. aureus* produces seven different toxins that cause food poisoning [3–5]. It is generally accepted, that $10^5$ cells per g of food produce sufficient enterotoxins to cause food poisoning [6].

Since the relevance of this pathogen was discovered, many approaches in the development of rapid detection methods for infection control were investigated, as reviewed by Law et al. [7] and Zhao et al. [8]. According to these reviews, traditional methods, such as plate counts using selective agar, convince with their simplicity, low costs and high accuracy but take 4 to 6 days to yield results. Nevertheless, they are still regarded as the gold standard. One promising alternative method is polymerase chain reaction (PCR). The commercially available Xpert MRSA assay (Cepheid

International, Sunnyvale, CA, USA) for example requires 2 h from DNA extraction to assay result [9]. However, complex sample preparation by trained staff is needed.

According to Zhao et al., the most rapid detection methods are based on biosensor technology. Biosensors are devices, which use biological components as recognition elements to provide specific affinity to the desired target. The recognition element is coupled to a transducer, which transforms the biological into an electrical signal [10]. To be commercially successful, a biosensor has to meet several requirements, e.g., low cost, fast response and high sensitivity. Therefore, despite its complexity, many researchers recognize the high potential of electrochemical impedance spectroscopy (EIS).

EIS is a fast label-free technique to measure the properties of electrode surfaces and bulk electrolytes. Owed to the progress in engineering and electronics during the last decades, high performance miniaturized impedance instruments are available for a relatively low budget [11]. EIS was used successfully for biosensors with various recognition elements [12,13]. For example, Bekir et al., developed an electrochemical immunosensor using antibodies against *S. aureus* [14]. They report a detection limit of 10 CFU·mL$^{-1}$ of *S. aureus*, exploiting the impedance change of the electrode surface caused by the affinity reaction of the immobilized antibodies.

To overcome the limitations of antibodies, such as high manufacturing costs, instability to high temperatures and short shelf life, aptasensors employ aptamers as recognition element [15]. Aptamers are synthetic, single-stranded nucleic acid molecules that can fold into complex three-dimensional structures allowing them to bind targets based on structure recognition with high affinity and specificity. They are selected using the SELEX procedure (systematic evolution of ligands by exponential enrichment), an iterative in vitro selection and amplification method [16].

Electrochemical aptasensors were reviewed by Willner et al. [17]: besides the well-known thrombin aptamer [18], other impedimetric aptasensors emerged ranging from the detection of potassium ions [19] and small molecules, such as ethanolamine [20], to whole cells, e.g., *Salmonella typhimurium* [21]. Shahdordizadeh et al., provided a review of recent advances in optical and electrochemical aptasensors for the detection of *S. aureus* [22]. They report on aptamers selected against staphylococcal toxins, staphylococcal teichoic acid, staphylococcal protein A and *S. aureus* as whole bacteria. The indirect detection of *S. aureus* via aptamers targeting the toxins excreted by the pathogen are limited due to the difficulty in correlation of the sensor signal to the presence of viable microorganisms. Therefore, direct detection is favored. In the field of optical aptasensors, fluorescence is most prominent, but also one colorimetric aptasensor was developed [23]. Using dielectrophoretic enrichment and fluorescent nanoparticles, Shangguan and coworkers developed an optical aptasensor with a limit of detection (LoD) of 93 CFU·mL$^{-1}$ and an assay time of 2 h [24]. By the use of upconversion nanoparticles, the fluorescence intensity was increased and Duan et al., gained a LoD of 8 CFU·mL$^{-1}$ [25]. Chang et al., developed an optical aptasensor for the single cell detection of *S. aureus* within 1.5 h [26]. The detection principle is based on resonance light scattering of modified gold nanoparticles. Optical sensors have the disadvantage that complex biological samples often interfere with the detection process. Furthermore, electrochemical methods are appreciated for their fast response time, higher sensitivity, low-cost fabrication, simple automation and lower sample volumes. In their review, Shahdordizadeh et al., described five electrochemical aptasensors for the detection of *S. aureus* [22]: Two are based on potentiometry with LoDs of 800 CFU·mL$^{-1}$ [27] and single cell detection [28]. Another used voltammetry to reach a LoD of 1 CFU·mL$^{-1}$ [29] and Lian et al., combined interdigital electrodes (IDE) with quartz crystal sensor to detect the bacteria as low as 12 CFU·mL$^{-1}$ [30]. Jia et al., used a glassy carbon electrode with aptamer modified gold nanoparticles to impedimetric detect a lower limit of 10 CFU·mL$^{-1}$ within 60 min [31].

All mentioned optical and electrochemical aptasensors used different aptamers, but have in common, that the aptamers were selected in a Cell-SELEX, wherein whole cells were used as target for aptamer generation. Although purposive, this has the disadvantage that it stays unknown, which part of the cell surface is targeted by the aptamer. Thus, it is also unknown, which *S. aureus* strains can be bound by these aptamers. *S. aureus* is known for its ability to adapt its genetics quickly to new

environments. Nevertheless, the conserved sequence of the immune-evasive factor protein A shows only one mutation in 70 months [32]. The surface bound protein A enhances *S. aureus*' adhesion to wounds by binding to the von Willebrand factor (vWF) and prevents phagocytosis by binding to the Fc region of various immunoglobulins [33]. Protein A is bound to peptidoglycans on the cell wall of *S. aureus* and not found on other bacteria. Therefore, protein A is an excellent target for the detection of *S. aureus* cells. Also in PCR methods, the *spA* gene, encoding protein A, is used to distinguish between *S. aureus* and other bacteria.

A DNA aptamer targeting staphylococcal protein A was selected by the FluMag-SELEX procedure in 2015 [34,35]. This aptamer development aimed to detect intact bacterial cells of *S. aureus* via the protein A bound to its cell surface. Binding characteristics of the aptamer to protein A were studied intensively by different methods such as bead-based fluorescent binding assay, surface plasmon resonance (SPR), microscale thermophoresis (MST), and enzyme-linked oligonucleotide assay (ELONA) [35,36].

The structural features of an aptamer play a major role in biosensor development. In case of the protein A-binding aptamer, a combination of two structural elements is important for its functionality: First, an intact and free 5′-end, folding into an imperfect stem-loop motif, is crucial for binding to protein A. Second, the aptamer folds into a parallel G-quadruplex structure as demonstrated by circular dichroism spectroscopy [36].

In the present study, we developed a biosensor detecting *Staphylococcus aureus* by its surface bound protein A, which is highly conserved and only found on *S. aureus*. The protein A-binding aptamer served as biological recognition element. In combination with electrochemical impedance spectroscopy as measurement method, rapid and label-free detection was achieved. By immobilization of thiol-modified aptamer on gold electrodes by self-assembly, binding of *S. aureus* was detected in a flow-through chamber with a three-electrode setup in buffer solution containing ferri-/ferrocyanide. Upon binding of *S. aureus*, the impedance increased due to the hindrance of the electron transfer between ferri-/ferrocyanide and the electrode surface (Figure 1). Herein, we elucidate the development of an impedimetric aptasensor and present novel insights on the use of aptamer-based electrochemical biosensors for the rapid and selective detection of *S. aureus*.

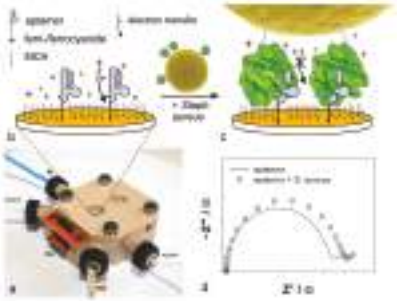

**Figure 1.** Flow-through measurement chamber and measurement principle. (**a**) Flow-through measurement chamber with liquid inlet and outlet (arrows) and a 3-electrode setup including a golden working electrode (Au), a platinum counter electrode (Pt) and a reference electrode (Ref); (**b**) Working electrode modified with aptamer (violet) and 6-mercapto-1-hexanol (MCH) in a buffer containing the redox probe ferri-/ferrocyanide (red stars); (**c**) Upon binding of protein A (green) on the surface of *S. aureus* (yellow) to the immobilized aptamer (violet), the impedance increased due to the hindrance of electron transfer (curved arrow) between ferri-/ferrocyanide (red stars) in solution and gold electrode surface (orange); (**d**) Characteristic Nyquist-plot of impedance spectra before and after incubation with *S. aureus* (based on data from measurements); Z′: real part of impedance and Z″: imaginary part of impedance.

## 2. Results and Discussion

### *2.1. Functionalization of the Gold Electrodes*

Affinity of the protein A-binding aptamer (PAA) to its target has been intensively studied by Stoltenburg et al., using SPR-based measurements with the Biacore X100 [35]. They applied both, the protein A and PAA, respectively as biotinylated receptor, which was immobilized on a streptavidin-coated sensor surface. In the development of the impedimetric sensor, we modified the aptamer with C6-Spacer and thiol for immobilization via self-assembly. To enable high densities of the protein A-binding aptamer (PAA) on the surface, we used the co-immobilization strategy, described by Keighley et al. [37]. They found that in the presence of 6-mercapto-1-hexanol (MCH), oligonucleotides stand upright on the surface rather than lying down, thus, occupy less space and allow a higher density. For optimization studies of our sensor surface, we investigated the influence of different ratios of aptamer to total thiol (PAA + MCH) using chronocoulometry as described by Steel et al. [38]. They stated, that the reduction of hexaammineruthenium (III) chloride (RuHex), measured by chronocoulometry, is proportional to the number of oligonucleotides on the surface. Figure 2 shows the results of chronocoulometry measurements on co-immobilized PAA modified gold electrodes in 40 mM Tris buffer containing 200 µM RuHex. The highest density of PAA ($2.41 \pm 0.39 \times 10^{12}$ PAA/cm$^2$) was reached with a ratio of 1:5 (1 µM PAA and 4 µM MCH), thus, this ratio was used for further experiments.

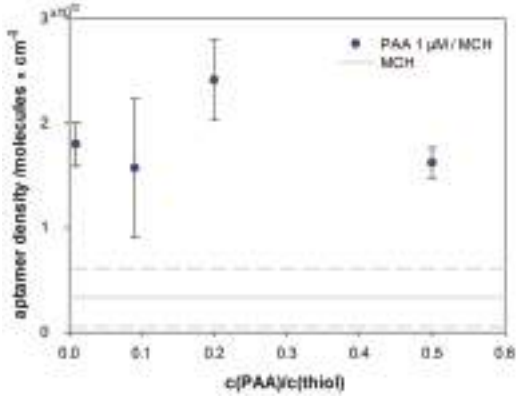


**Figure 2.** Aptamer density on the electrode surface depending on the protein A-binding aptamer (PAA)/6-mercapto-1-hexanol (MCH) molar ratio upon immobilization based on four experiments for each ratio; the grey lines show the average density and standard deviation determined for a MCH monolayer.

To ensure successful immobilization and aptamer functionality, we performed analysis using a quartz crystal microbalance as described in Section 3.3. In Figure 3a is shown the mass increase upon PAA immobilization, calculated accordingly from the measured frequency change. The formation of a self-assembled monolayer comprises two steps. The first is the initial attachment, which takes a few seconds, seen in the significant mass increase immediately after introduction of aptamer-solution in Figure 3a. The second step is the arrangement to an ordered monolayer, which takes more than 8 h [39]. Hence, to ensure an ordered monolayer, the electrode was incubated for at least 15 h. As seen in Figure 3a, upon PAA immobilization the mass increased by 500 ng/cm$^2$. Backfilling of gaps with MCH increased the mass slightly (~20 ng/cm$^2$). In comparison, an electrode covered with a pure MCH monolayer showed a mass increase of only 89 ng/cm$^2$. The difference between both provided the mass change due to immobilized PAA. Although immobilized aptamers hamper the formation of an entire layer of MCH, the error is negligible, because the aptamer mass is 142 times higher than the mass of a MCH-molecule. The average mass increase of immobilized PAA was $320 \pm 139$ ng/cm$^2$ (standard

deviation obtained from three experiments). This correlates to $1.01 \pm 0.44 \times 10^{13}$ aptamers/cm$^2$. The aptamer density determined with chronocoulometry ($2.41 \pm 0.39 \times 10^{12}$ PAA/cm$^2$) is 4 times smaller than measured with QCM. This is due to the difference in the measurement techniques and surfaces. In the QCM measurements, not only the mass of the immobilized molecules, but also the adsorbed water and ions as well as the rigidity of the immobilized layer influence the resonance frequency [40]. Also, the different surfaces—a quartz crystal covered with gold and chrome as adhesion layer versus a glass test slide covered with gold and titanium as adhesion layer—contribute to the differences in surface coverage. Although their roughness, <1 nm RMS (= rough mean square) and $376 \pm 74$ pm RMS respectively, do not diverge significantly. However, both methods confirm successful immobilization and that a high density of aptamers was achieved.

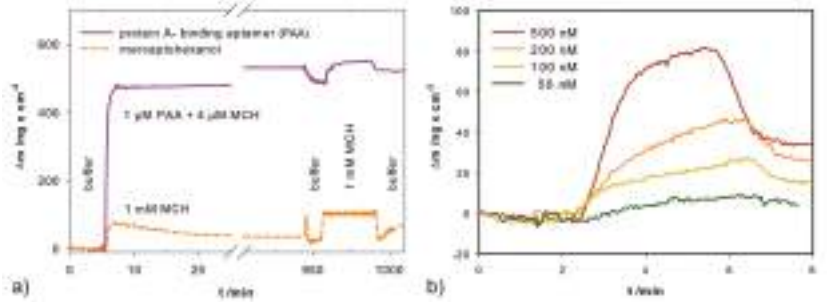


**Figure 3.** Quartz crystal microbalance measurements: (**a**) mass change $\Delta m$ versus time of gold covered quartz crystals incubated with aptamer/6-mercapto-1-hexanol (MCH) (violet solid line) or MCH (orange dashed line) and subsequently blocked with 1 mM MCH; (**b**) $\Delta m$ versus time of an aptamer-modified crystal incubated with different concentrations of protein A.

In general, high densities are desired to obtain a higher protein capture capacity resulting in higher sensitivity, but too high densities may lead to steric hindrance preventing correct aptamer folding and binding of target [41]. Assuming an even distribution, the obtained density results in an area of $9.9 \times 10^{-14}$ cm$^2$ per aptamer. Assuming an aptamer occupies a squared area, the mean distance between two aptamers is 3.15 nm. Due to dimerization and the formation of quadruplexes [36], the true mean distance of the aptamers is likely >3.15 nm. According to Erickson et al., the partial specific volume of a protein can be calculated from its molecular mass [42]. For the recombinant protein A with a molecular mass of 45 kDa, this volume is 54.54 nm$^3$. Assuming protein A has the simplest shape, a sphere, its minimal diameter is 4.71 nm. Therefore, we assumed that the space around an aptamer (>6.3 nm) was sufficient for the binding of protein A.

To prove the functional binding of protein A to the immobilized PAA, we observed the mass change of modified electrodes upon incubation with protein A (Figure 3b). Concentrations of protein A in the range of 100 to 500 nM resulted in signals of 20 to 40 ng/cm$^2$, which correlates to $2.68 \times 10^{11}$ and $5.35 \times 10^{11}$ molecules/cm$^2$ respectively. Thus, we showed that the immobilized aptamer retained its functionality in binding protein A.

Figure 4 represents the impedance measurements during aptamer immobilization. It shows the Nyquist plots of a blank electrode and an aptamer-modified electrode. The impedance increased significantly after PAA immobilization.

### *2.2. Influence of Ferri-/Ferrocyanide*

In faradaic impedimetric measurements, a redox probe for the transfer of electrons from the working electrode to the counter electrode is necessary. The ferri-/ferrocyanide couple is often used due to its fast electron transfer rate ($2 \times 10^{-2}$ cm/s) [43]. For biosensor development, it is important to

examine, if the redox couple inhibits the affinity of the receptor to its target. To examine the influence of ferri-/ferrocyanide on binding of protein A to PAA, microscale thermophoresis (MST) experiments were performed. MST is a powerful technique to detect biomolecular interaction by quantifying directed movement of molecules along an induced microscopic temperature gradient. It is highly sensitive to changes in hydration shell, charge and size and therefore capable to detect many kinds of biomolecular interactions while both reaction partners remain in solution and no immobilization is required.

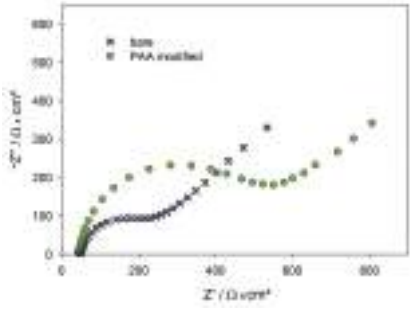

**Figure 4.** Nyquist plot of the impedance spectra of a blank gold electrode (black crosses) and a PAA/MCH-modified gold electrode (green circles); PAA = protein A-binding aptamer, MCH = 6-mercapto-1-hexanol.

In summary, we successfully immobilized PAA via self-assembly with a high density, whereas it retained its functionality of binding protein A.

Figure 5a shows characteristic curves of a MST experiment for a low and a high protein A concentration. The MST fluorescence signal was lower for the high protein A concentration, indicating that in solution, the aptamer-protein A-complex behaved differently than the free aptamer. Binding curves (Figure 5b) in buffer with and without 2 mM ferri-/ferrocyanide were measured as described in Section 3.4. Fitting to the Hill Equation (1) was performed to extract more information from the binding curves:

$$fraction\ bound = \frac{\Delta S}{\Delta S_{\max}} = \frac{[T]^h}{K_D + [T]^h} \quad (1)$$

where $\Delta S$ = signal change, $\Delta S_{max}$ = maximal signal change, $h$ = Hill coefficient, $K_D$ = apparent binding constant, $[T]$ = target concentration (e.g., protein A).

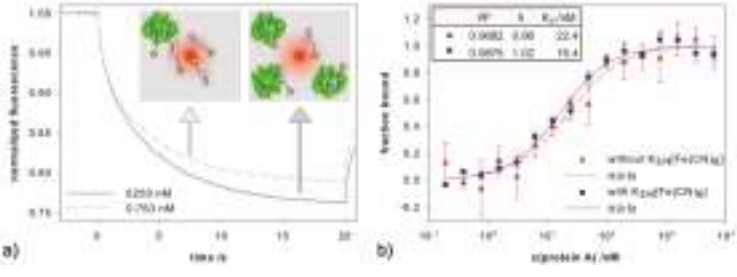

**Figure 5.** (**a**) Microscale thermophoresis (MST) curves for a low (0.763 nM, dashed line) and a high (6250 nM, solid line) protein A concentration with 38.5 nM labeled PAA (MST power 40%, LED power 100%); (**b**) Binding curves of recombinant protein A with aptamer in absence (red triangles) and presence (blue circles) of 2 mM ferri-/ferrocyanide measured in triplicates—the lines represent the Hill fit.

The determined $K_D$ values in absence and presence of ferri-/ferrocyanide were 22.4 ± 5.8 nM and 16.4 ± 2.5 nM respectively. There is no statistically significant difference between the two curves (paired *t*-test, $p = 0.255$). Thus, we conclude, that ferri-/ferrocyanide has no significant influence on the binding of PAA and protein A.

The $K_D$ value obtained by MST measurements in this work, 22.4 nM, differs from the value reported by Stoltenburg et al., 94.7 nM [35]. To investigate if this difference is due to the labeling-procedure or -site, MST measurements were repeated by 2bind GmbH (Regensburg, Germany). A similar analysis setup was applied using the maleimide-fluorophore on the 5′- and 3′-thiol-tagged PAA. The obtained $K_D$ values were 115.6 nM and 110.8 nM, respectively. Hence, we concluded, that the binding behavior was not affected by the labeling site of the aptamer, for both partners in solution. However, the most distinct difference in the experiments was the concentration of Tween 20 (0.05% used by 2bind GmbH compared to 0.005% used in our first measurement), but the data of both experiments revealed no adhesion to the used capillaries. Thus, the variations in the $K_D$ values in MST measurements are attributed to differences in buffer composition, amplified by the handling of very small volumes (10 µL).

### 2.3. Detection of Protein A by Impedance Spectroscopy

The gold electrodes modified with PAA were mounted in the flow-through chamber (see Figure 1) and exposed to different concentrations of protein A (2–700 nM). Impedance spectra were recorded in FeBB as described in Section 3.5. Every protein A concentration was measured in triplicates, i.e., on three different electrodes. Figure 6a shows the impedance spectra of PAA modified electrodes before and after exposure to 7–700 nM protein A. After incubation with protein A the impedance increased proportionally to the concentration of protein A.

To extract the relevant parameters, the impedance spectra were fitted to the modified Randles circuit (see Figure 6a), wherein $R_{sol}$ is the solution resistance, *CPE* is the constant phase element for the double layer at the electrode surface, $R_{ct}$ is the charge-transfer resistance (due to the interaction of ferri-/ferrocyanide with the electrode), and *W* is the Warburg impedance representing the diffusion of ions to the electrode surface. The fitting results are summarized in Table 1. As seen in Figure 6a and Table 1, the fits (lines) show good agreement with the experimental data (markers).

In Figure 6b, the fit parameter changes over all measured protein A concentrations are plotted. The charge transfer resistance $R_{ct}$ showed a maximum increase of 33%, whereas the other parameters changed less than 4%, verifying that the charge transfer was influenced significantly by the binding of protein A. Thus $R_{ct}$ was chosen as the significant parameter for further analysis.

The change of the extracted $R_{ct}$ versus the logarithmic protein A concentration is plotted in Figure 6c. While only a slight increase of $R_{ct}$ up to 10 nM protein A was observed, an exponential increase in $R_{ct}$ from 10 nM to 100 nM was measured. Finally, above 100 nM protein A $R_{ct}$ reached saturation. The resulting sigmoidal curve was fitted to the Hill Equation (2):

$$\Delta R_{ct} = \frac{\Delta R_{ct\_max} \times [T]^h}{K_D + [T]^h} \quad (2)$$

where $\Delta R_{ct}$ = change of the charge transfer resistance, $\Delta R_{ct\_max}$ = maximal change, $h$ = Hill coefficient, $K_D$ = apparent binding constant, $[T]$ = target concentration (e.g., protein A).

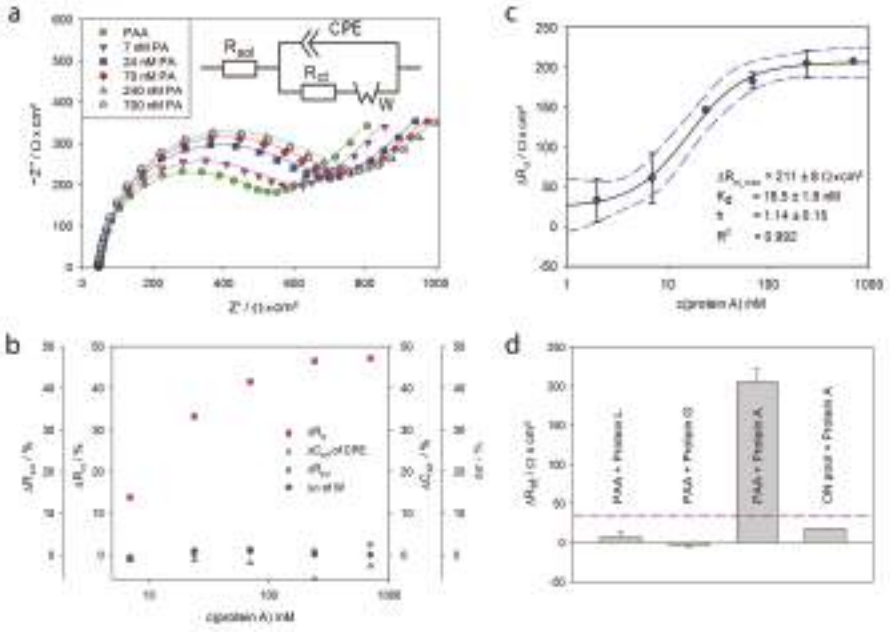


**Figure 6.** Electrochemical impedance spectroscopy measurements with protein A: (**a**) Nyquist plot of a PAA-modified electrode before (green circles) and after incubation with 7–700 nM protein A measured in FeBB—the fits to the equivalent circuit are shown as lines—modified Randles circuit with $R_{sol}$: solution resistance, *CPE*: constant phase element, $R_{ct}$: charge-transfer resistance and *W*: Warburg impedance; (**b**) the percentage change of the different fit parameters for all protein A concentrations, $C_{eff}$: the effective capacitance was calculated from the *CPE* under the assumption of a parallel distribution of time constants on the electrode surface as described in [44], σ is the parameter for the Warburg element; (**c**) binding curve: Change of the extracted charge transfer resistance $\Delta R_{ct}$ of aptamer-modified electrodes upon incubation of protein A measured in triplicate—dashed blue lines mark the 95% confidence interval; (**d**) unspecific signals: Extracted $\Delta R_{ct}$ of 1 µM protein G, protein L and protein A on PAA-modified electrodes as well as 1 µM protein A on electrodes modified with random oligonucleotides measured in triplicate—the dashed line represents the LoD.

**Table 1.** Results from the fitting of impedance data to the modified Randles circuit—SD = standard deviation, $X/\sqrt{N}$ = error of fitting normalized to the number of data points.

| c(Protein A) /nM | $R_{sol}$ /Ω·cm² | SD | CPE /µF·s$^{(\alpha-1)}$ | SD | α | $R_{ct}$ /Ω·cm² | SD | σ /Ω·s$^{-1/2}$ | SD | $X/\sqrt{N}$ |
|---|---|---|---|---|---|---|---|---|---|---|
| 7 | 44.4 | 0.2 | 0.362 | 0.005 | 0.95 | 505.3 | 0.5 | 5769 | 2 | 0.0122 |
| 24 | 46.2 | 0.1 | 0.375 | 0.004 | 0.94 | 593.3 | 0.5 | 5847 | 2 | 0.0124 |
| 70 | 45.4 | 0.1 | 0.359 | 0.004 | 0.95 | 627.9 | 0.5 | 5861 | 2 | 0.0120 |
| 240 | 46.1 | 0.1 | 0.341 | 0.004 | 0.95 | 647.3 | 0.5 | 5834 | 2 | 0.0105 |
| 700 | 45.3 | 0.1 | 0.361 | 0.004 | 0.95 | 657.2 | 0.5 | 5811 | 2 | 0.0118 |

Thereby, an apparent $K_D$ value of 18.5 ± 1.8 nM and Hill coefficient *h* of 1.14 ± 0.15 were obtained. The Hill coefficient *h* is slightly higher than 1, indicating a cooperative binding. Stoltenburg et al., already reported avidity effects [35]. They performed competitive experiments with protein A and immunoglobulin, which suggested that the protein A binding site for PAA overlaps with the known binding sites for immunoglobulin [45]. Hence, we can conclude that protein A provides more than

one binding site for this aptamer. Reflective Interferometric Fourier Transform Spectroscopy (RIFTS) measurements of protein A binding to PAA, immobilized on porous silicon, resulted in an even higher $h$ of 2.61 ± 0.69 [46]. Unlike the herein used planar gold electrodes, the rough and porous silicon surface increases the chance for aptamers being close enough to bind to the same protein A. Both observations substantiate the mentioned avidity affects.

Table 2 summarizes the apparent $K_D$ values obtained with the same aptamer by different detection methods and setups. Affinities were found in the low nanomolar to micromolar range.

**Table 2.** Apparent dissociation constant, $K_D$, determined with different analysis methods for the protein A-binding aptamer—MST = microscale thermophoresis, SPR = surface plasmon resonance, ELONA = enzyme-linked oligonucleotide assay, EIS = electrochemical impedance spectroscopy, RIFTS = reflective interferometric Fourier transform spectroscopy.

| Analysis Method | Aptamer | Aptamer Modification | Protein A | $K_D$/nM | | | Reference |
|---|---|---|---|---|---|---|---|
| MST | free | 5′-fluorescence | free | 94.7 | ± | 64.6 | [35] |
| MST | free | 5′-fluorescence | free | 115.6 | ± | 26.9 | this work |
| MST | free | 3′-fluorescence | free | 110.8 | ± | 42.3 | this work |
| MST | free | 3′-fluorescence | free | 22.4 | ± | 5.8 | this work |
| SPR | free | 5′-fluorescence | immobilized | 1920.0 | ± | 250.0 | [35] |
| SPR | immobilized | 3′-biotin | free | 287.0 | ± | 16.2 | [35] |
| ELONA | free | 5′-biotin | immobilized | 23.7 | ± | 2.0 | [36] |
| ELONA | free | 3′-biotin | immobilized | 11.3 | ± | 1.4 | [36] |
| EIS | immobilized | 3′-thiol | free | 18.5 | ± | 1.8 | this work |
| RIFTS | immobilized | 3′-amino | free | 13980.0 | ± | 1540.0 | [46] |

Table 2 shows that each of these methods is capable of protein A detection utilizing PAA as receptor in a bioanalytical setup. It suggests that in the same analysis setup by the use of different designs, the measurement range can be adapted for the desired application. As shown in the example in the SPR experiments, immobilization of the aptamer instead of protein A, decreased the $K_D$ almost by 14%. We want to emphasize that the $K_D$ values are strongly dependent on the analysis method and setup used. Therefore, the performance of a biosensor cannot be judged based on the $K_D$ value alone. Every method has to be evaluated for its purpose considering advantages and limitations. i.e., the strengths of EIS as detection method are fast, robust, label-free and non-destructive measurements.

Repeated measurements of PAA-modified electrodes in FeBB resulted in a standard deviation $s$ of 11.10 Ω·cm$^2$ of the $R_{ct}$ value. As the limit of detection (LoD) is defined as the lowest target concentration at which the signal is higher than 3·$s$, a LoD of 2.99 ± 0.73 nM was determined using the approximated Hill equation.

Non-specific binding often presents a major challenge in biosensor development. Herein, we investigated the binding of the functionally similar proteins G and L to the aptamer-modified gold electrodes and observed that they neither bind to the surface nor to the aptamer (Figure 6d). Furthermore, the binding of protein A to an electrode, modified with random oligonucleotides, was determined to be 14.8 ± 0.1 Ω·cm$^2$ (Figure 4d), which is significantly below LoD (3·$s$).

### *2.4. Detection of Staphylococcus aureus by Impedance Spectroscopy*

Besides binding to the defined target protein A, the aptamer was also evaluated for its ability to recognize and bind to intact bacterial cells of *S. aureus*, expressing protein A on the cell surface [36]. Therefore, we performed experiments with our developed impedimetric biosensor and live *S. aureus* cells.

The gold electrodes modified with PAA were exposed to different concentrations of *S. aureus* (1 to $10^9$ CFU·mL$^{-1}$). Figure 7a shows impedance spectra of a PAA modified electrode before and after exposure to *S. aureus*, recorded in FeBB. After incubation with *S. aureus*, the impedance increased proportionally to the cell concentration of *S. aureus*. To extract the relevant parameters, the impedance spectra were fitted to the modified Randles circuit (Figure 7a), which describes the phenomena

occurring between the electrodes influencing the flow of current. As presented in Figure 7a and Table 3, the fits (lines) show good agreement with the experimental data (markers).

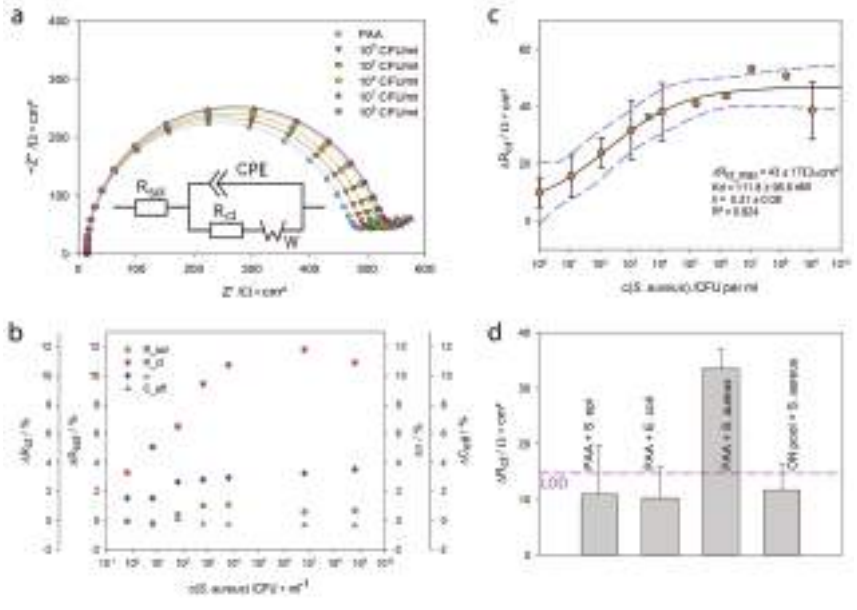


**Figure 7.** Electrochemical impedance spectroscopy (EIS) with *S. aureus* (**a**) Nyquist plot of a PAA-modified electrode before (cyan circles) and after incubation with 1 to $10^9$ CFU·mL$^{-1}$ measured in FeBB—the fits to the equivalent circuit are shown as lines modified Randles circuit with $R_{sol}$: solution resistance, *CPE*: constant phase element, $R_{ct}$: charge-transfer resistance and *W*: Warburg impedance; (**b**) percentage change of the different fit parameters for all *S. aureus* concentrations, $C_{eff}$: the effective capacitance was calculated from the CPE under the assumption of a parallel distribution of time constants on the electrode surface as described in [45], $\sigma$ is the parameter for the Warburg element; (**c**) binding curve: Change of the extracted charge transfer resistance $\Delta R_{ct}$ of aptamer-modified electrodes upon incubation of 1 to $10^9$ CFU·mL$^{-1}$ *S. aureus* measured in triplicate—dashed blue lines mark the 95% confidence interval, green cross marks a sample of unknown concentration; (**d**) unspecific signals: $10^6$ CFU·mL$^{-1}$ of *Staphylococcus epidermidis*, *Escherichia coli* and *Staphylococcus aureus* on PAA-modified electrodes as well as $10^6$ CFU·mL$^{-1}$ *S. aureus* on electrodes modified with random oligonucleotides measured in triplicate—the dashed line represents the LoD.

**Table 3.** Results from the fitting of impedance data to the modified Randles circuit—SD = standard deviation, $X/\sqrt{N}$ = error of fitting normalized to the number of data points.

| c(*S. aureus*) /CFU·mL$^{-1}$ | $R_{sol}$ /Ω·cm$^2$ | SD | CPE /μF·s$^{(\alpha-1)}$ | SD | α | $R_{ct}$ /Ω·cm$^2$ | SD | σ /Ω·s$^{-1/2}$ | SD | $X/\sqrt{N}$ |
|---|---|---|---|---|---|---|---|---|---|---|
| 1E+01 | 14.8 | 0.1 | 1.230 | 0.02 | 0.99 | 459.8 | 0.3 | 310 | 3 | 0.0084 |
| 1E+02 | 14.8 | 0.1 | 1.232 | 0.02 | 0.99 | 467.8 | 0.3 | 311 | 3 | 0.0092 |
| 1E+03 | 14.9 | 0.1 | 1.229 | 0.02 | 0.99 | 474.7 | 0.3 | 312 | 3 | 0.0088 |
| 1E+04 | 15.0 | 0.1 | 1.224 | 0.02 | 0.99 | 485.7 | 0.3 | 315 | 3 | 0.0086 |
| 1E+05 | 15.0 | 0.1 | 1.232 | 0.02 | 0.99 | 492.2 | 0.3 | 312 | 3 | 0.0098 |
| 1E+08 | 14.9 | 0.1 | 1.231 | 0.02 | 0.99 | 497.9 | 0.3 | 312 | 3 | 0.0098 |
| 1E+10 | 14.9 | 0.1 | 1.226 | 0.02 | 0.99 | 491.8 | 0.3 | 317 | 3 | 0.0094 |

Figure 7b displays the fit parameter change for all measured bacteria concentrations. Only $R_{ct}$ showed a significant increase of 12%, while the Warburg diffusion increased ~4% and $R_{sol}$ as well as $C_{eff}$

changed <2%. This suggests that the bound *S. aureus* influences the electron transfer between electrode and the buffer containing ferri-/ferrocyanide. The $R_{ct}$ parameter was chosen for further analysis.

In Figure 7c, the change of the extracted $R_{ct}$ upon incubation with various *S. aureus* concentrations is plotted. Measurements were taken in triplicates, i.e., three electrodes were exposed to each *S. aureus* concentration. The standard deviation of these three measurements is shown as error bars. A diluted sample with 10 *S. aureus* cells per mL resulted in an average $R_{ct}$ change of 35 Ohm. A sample with $10^5$ cells per mL led to saturation of the sensor surface and the maximum change of 100 Ohm. The fit to the Hill Equation (1) resulted in an apparent $K_D$ value of 111 ± 96 CFU·mL$^{-1}$ and $h$ of 0.31 ± 0.08. A measurement with a sample of unknown concentration showed good accordance to the data (green cross). With the approximated Hill equation a bacteria concentration of 5721 ± 2813 CFU·mL$^{-1}$ was determined. Counting the sample under the microscope resulted in a value of 4150 CFU·mL$^{-1}$. The high standard deviation could be minimized by a higher amount of repetitions.

Whereas experiments with protein A resulted in a Hill coefficient slightly higher than 1, indicative for cooperative binding, biosensing experiments with whole cells resulted in a $h$ significantly lower than 1, indicating negative cooperativity. This may be due to the size of *S. aureus* cells (~1 µm) and the spacing of protein A molecules on their surface not allowing for several aptamers to bind the same protein A. Another explanation may be the reduced flexibility of the cell surface bound protein A and therefore decreased accessibility of further binding sites for aptamers in the vicinity.

Repeated impedance measurements of a single PAA-modified electrode in FeBB resulted in a standard deviation of $s(R_{ct})$ = 4.88 Ω·cm$^2$. This corresponds to a calculated LoD of 10 CFU·mL$^{-1}$.

A comparison between previously reported *S. aureus* detection assays and the herein demonstrated biosensor is shown in Table 4. In summary, the achieved LoD is comparable to previous reports; however, our biosensor excels in simplicity, automation, low cost and rapid results.

**Table 4.** Comparison of several detection methods for *Staphylococcus aureus* (SA = *S. aureus* aptamer, LoD = limit of detection).

| Detection Principle | Recognition Element | Assay Time | LoD/CFU·mL$^{-1}$ | Reference |
|---|---|---|---|---|
| polymerase chain reaction | ssDNA | 2 h | 10 | [47] |
| EIS immunosensor | anti-*S. aureus*-antibody | Not stated | 10 | [14] |
| resonance light scattering | SA 17 & SA 61 [26] | 1.5 h | 1 | [26] |
| EIS | SA 43 [48] | 1 h | 10 | [31] |
| fluorescent nanoparticles | SA 31 [48] | 2 h | 93 | [24] |
| EIS | PA2#8[S1–58] [35] | 10 min | 10 | this work |

Lastly, we investigated the binding of protein A-deficient bacteria, such as *Staphylococcus epidermidis* and *Escherichia coli* to aptamer-modified gold electrodes and observed no cross-reactivity (Figure 7d). Similar results were found, if *S. aureus* was applied to electrodes modified with random oligonucleotides. Additionally, the binding of *S. aureus* ($10^6$ CFU·mL$^{-1}$) to a blank electrode and electrodes modified with a 6-mercapto-1-hexanol (MCH) monolayer, resulted in a negligible average $R_{ct}$ change of 10.2 ± 2.2 Ω·cm$^2$ [49], a value below LoD (3·$s$).

These results are in agreement with results of Stoltenburg et al., reporting that protein A-deficient *S. aureus* strains and gram-negative bacteria, such as *E. coli*, were excluded from aptamer binding [36].

For the practical applicability of our sensor, we recommend that samples shall be extracted into tryptic soy broth or similar media and then diluted 1:100 in BB. The BB contains ions which are required for proper aptamer folding and thus binding to protein A. Simple sample preparation, such as a centrifugation step, showed improved results [49]. The influence of complex sample matrices, such as milk, on the performance of the developed sensor, still has to be examined.

For the food industry, detection of enterotoxins is more crucial than whole cell detection. However, *S. aureus* produces more than 7 different toxins, which all can cause illness. While an

existing international standard operation [ISO 19020:2017] describes the screening of staphylococcal enterotoxins SEA, SEB, SECs, SED and SEE, others are excluded (SEG, SHE, SEI, SER, SES and SET). Extraction of the enterotoxins encompasses complex sample preparation, which requires fully equipped food testing laboratories. Furthermore, only enterotoxin assays with low detection limits, such as 0.05 ng/g food, fulfill the requirements [50].

Thus, the predominant approach, especially for small manufacturers, is the detection of *S. aureus* contamination. This approach, based on the Bacteriological Analytical Manual [51], requires culturing on selective agar plates for 2 days. Counting the colony forming units per g food in respect to the processing time is a good indicator for toxin formation. Our sensor could significantly reduce the time required for this approach.

In respect to clinical application, our sensor could improve tests by the rapid identification of bacteria type prior to antibiotic susceptibility testing and thus reduce the costs for isolating patients. Due to the microfluidic setup and the non-destructive impedance measurement, the combination with additional assays and steps will be realizable without great expense.

## 3. Materials and Methods

### *3.1. Reagents*

The protein A-binding aptamer PA#2/8 (76 nt) was originally selected by Stoltenburg et al., using the FluMag-SELEX process [34]. A 3′-truncated variant of the full-length aptamer, PA#2/8[S1-58] (58 nt), was applied in the current study: 5′-ATACCAGCTTATTCAATTAGCAACATGAGGGGGAT AGAGGGGGTGGGTTCTCTCGGCT-3′ [35]. This variant is herein referred to as PAA. A pool of randomized oligonucleotides (58 nt) was used as negative control (ON pool). Both were synthesized by Microsynth AG (Balgach, Switzerland), modified with C6-spacer and a thiol at the 3′-end, and purified with polyacrylamide gel electrophoresis.

Recombinant protein A (expressed in *Escherichia coli*, P7837) and 6-mercapto-1-hexanol (MCH, 99%) were purchased from Sigma-Aldrich Chemie GmbH (Taufkirchen, Germany). *Staphylococcus aureus* (DSM 20231), *Staphylococcus epidermidis* (DSM 3269) and *Escherichia coli* (DSM 498) were purchased from Leibniz Institut DSMZ GmbH (Braunschweig, Germany). Potassium-hexacyanoferrate (II) and (III) ($K_{3/4}[Fe(CN)_6]$) were purchased from Merck Chemicals GmbH (Darmstadt, Germany). Recombinant protein G and protein L (21193 and 21189) were purchased from Pierce Biotechnology (Rockford, USA). Tris-(2-carboxyethyl)-phosphine-hydrochloride (TCEP) was purchased from Carl Roth GmbH + Co. KG (Karlsruhe, Germany). All reagents were of analytical grade and used without further purification. All working solutions were prepared in water purified with a Milli-Q Type-1-system (EMD Millipore Corporation, Billerica, MA, USA; 18 MΩ·cm).

For the aptamer experiments, the binding buffer (BB) as for aptamer selection [35] was used. It consisted of 100 mM NaCl, 20 mM Tris, 10 mM $MgCl_2$, 5 mM KCl, 1 mM $CaCl_2$ (adjusted with HCl to a pH of 7.6) and was autoclaved, sterile filtered before further use. Protein A was directly dissolved and diluted in BBT, BB containing 0.005% Tween 20, to reduce unspecific binding to surfaces. *S. aureus*, *S. epidermidis* and *E. coli* cells were cultured in tryptic soy broth (TSB) and washed twice in BB. A fraction was dyed with SYTO and counted in a cell chamber of 0.02 mm depth. Washed cell suspensions were diluted to desired concentration in BB. For electrochemical measurements, 2 mM of $K_{3/4}[Fe(CN)_6]$ (equimolar) were added to BB (FeBB).

### *3.2. Preparation of Electrodes*

The thiol-modified PAA was preconditioned with TCEP (200 μM/μM thiol) for 20 min to reduce disulfides and heated to 95 °C in BB for 5 min to enable proper folding.

The gold electrodes and gold covered quartz crystals were exposed to ultraviolet light for 5 min and subsequently incubated in hot alkaline piranha solution (5:1:1 water:$NH_3$:$H_2O_2$; CAUTION: this acidic mixture reacts violently with organic solvents and must be handled with care!) in an ultrasonic

bath for 5 min. After rigorous rinsing with ultrapure water, the electrodes were dried in nitrogen and immediately covered by 1 μM preconditioned PAA and 4 μM MCH in BB followed by incubation at room temperature overnight. Next day, the surface was washed intensively with BB and exposed to 1 mM MCH for 30 min, followed by another wash with BB. The modified electrodes were stored in BB until use.

### 3.3. QCM Measurements

A quartz crystal microbalance (QCM, Q-Sense Analyzer E4, Biolin Scientific Holding AB, Stockholm, Sweden) was used for verification of aptamer immobilization and binding of protein A to immobilized aptamers. For measurements, the gold covered quartz crystals (QSX301, resonance frequency 4.95 MHz ± 50 kHz, Biolin Scientific) were cleaned as described above and mounted into the flow module QFM401. First, a baseline in BB was established, and then the chamber was flushed with a solution of 1 μM preconditioned PAA and 4 μM MCH in BB and incubated overnight while the frequency change was continuously measured. The temperature was held at 21 °C. The next day, the crystal was incubated with 1 mM MCH for 30 min and washed with BB. The modified crystals were incubated for 4 min with different concentrations of protein A (50–500 nM). Unbound protein A was washed away with BB. The relative frequency change—difference of frequency change measured in BB before and after incubation with aptamer or protein A—was used to determine the mass change by the Sauerbrey equation [52]. Thereby, most of the influences of viscosity and density of the fluids on the measurements were compensated.

### 3.4. MST Measurements

To determine the influence of ferri-/ferrocyanide on aptamer-target-binding, microscale thermophoresis (MST) measurements were performed with the Monolith NT.115 (NanoTemper Technologies GmbH, Munich, Germany) and standard capillaries. The fluorescence dye NT-547 was bound to the thiol group of PAA using the labeling kit MO-L005 Monolith™ by NanoTemper. A fluorophore-per-aptamer-ratio of 0.5 was determined by measuring the absorbance at 260 and 546 nm with a nanophotometer™ (Implen GmbH, Munich, Germany). The MST power was set to 40% and the LED power was set to 100% (no bleaching was observed). 38.5 nM labeled aptamer (77 nM in total, including the unlabeled aptamer) were incubated with 0.2 nM to 6.25 μM recombinant protein A. The analyses were performed in BBT at 25 °C. Normalization of the fluorescence signal and fitting to the Hill equation were performed using the software MO Affinity Analysis v2.1.3 (NanoTemper). To investigate if the labeling procedure or labeling site influences the aptamer affinity, additional MST measurements were conducted by commercial analysis service of 2bind GmbH (Regensburg, Germany). The same labeling procedure as described above was applied to the 3′- and 5′-end, and 30 nM labeled PAA with 0.354 nM to 11.6 μM protein A in BB with 0.05% Tween 20 were used.

### 3.5. EIS Measurements

Electrochemical impedance spectroscopy (EIS) measurements were performed using the SP-300 potentiostat/galvanostat with impedance analyzer (Bio-Logic Science Instruments SAS, Claix, France). A custom flow-through chamber (Figure 1) made of polyether-ether-ketone was designed and manufactured. Flow-through was realized by a peristaltic pump (IPC-16, Ismatec, Cole-Parmer GmbH, Wertheim, Germany) and a Teflon tube of 0.5 mm inner diameter. The fluid chamber with a volume of 100 μL was covered with glass. It consists of a three-electrode system with a working electrode cut from gold coated test slides (TA134-(Ti/Au), EMF Corporation, Ithaca, NY, USA), a Pt-black wire as counter electrode and a leak-free Ag/AgCl reference electrode (LF-1 Ø1 mm, Innovative Instruments Inc., Tampa, FL, USA). The electrochemical active area ($A_{true}$) of the working electrode was determined by cyclic voltammetry in 0.5 M $H_2SO_4$ with 100 mV/s from 0.2 to 1.5 V. By integration of the reduction peak at ~800 mV, the required charge for reduction of a gold oxide monolayer was obtained (215 μC). Division by the theoretical value, 482 μC/cm$^2$, calculated by [53], resulted in $A_{true}$ = 0.444 ± 0.039 cm$^2$.

The geometric surface area $A_{geo}$ was 0.246 cm$^2$ and thus, the roughness factor $R = A_{true}/A_{geo}$ was 1.8. The flow-through chamber and the solutions were kept in a temperature cabinet at 21 °C while the pump and impedance analyzer were positioned outside.

EIS measurements were performed with the aptamer-modified gold electrode mounted in the flow-through measurement chamber (Figure 1). Different concentrations of protein A (2–700 nM), 6 mL of each, were pumped (50 µL/s) through the chamber and incubated for 5 min while flow-through was paused. Then 6 mL FeBB was pumped (50 µL/s) through the system. Finally, the impedance was measured from 1 Hz to 200 kHz with 7 logarithmic spaced frequencies per decade. The sinusoidal alternating voltage with an amplitude of 10 mV was applied at the equilibrium potential of ferri-/ferrocyanide ($E_{eq}$ ~140 mV). The impedance measurement was repeated four times while the average of the last three cycles was used for fitting and analysis. Fitting was performed with the simplex algorithm implemented in EC-Lab®software (v11.00, Bio-Logic Science Instruments SAS, Claix, France). The same procedure was applied to control samples, protein G and L, of which 1 µM were used and bacteria cell suspensions.

## 4. Conclusions

This study provides the proof of principle for an impedimetric biosensor for the rapid detection of *S. aureus*, based on the protein A-binding aptamer. Successful co-immobilization of protein A-binding aptamers and 6-mercapto-1-hexanol on gold electrodes resulted in an average density of $1.01 \pm 0.44 \times 10^{13}$ aptamers per cm$^2$. The immobilization density can be influenced by the ratio of aptamer to 6-mercapto-1-hexanol (MCH) as shown with chronocoulometry. We showed with MST measurements that ferri-/ferrocyanide, necessary as redox couple for faradaic impedance measurements, has no significant influence on the binding of the aptamer to its target. The biosensor displayed sensitive binding to protein A with a $K_D$ of 18.5 ± 1.8 nM and a LoD of 3 nM. Our results also showed the excellent selectivity of the developed sensor, with signals below LoD upon exposure to high concentrations of the functionally similar proteins G and L.

When exposed to live *S. aureus* cells, our developed aptamer-based biosensor showed a $K_D$ of $111 \pm 96$ CFU·mL$^{-1}$ and a LoD of 10 CFU·mL$^{-1}$, which is in good agreement with other reported assays or sensors. Our results also prove the high selectivity of the aptamer, distinguishing between *S. aureus* and protein A- deficient bacteria, such as *E. coli* and *S. epidermidis*.

For application in a clinical setting, an additional step for the evaluation of the different detectable *S. aureus* strains and their possible antibiotic resistance (e.g., by PCR) may have to be considered. Furthermore, the influence of different ionic strength buffers and sample matrices on the biosensor performance have to be investigated closely.

This work demonstrated that the protein A-binding aptamer can be used as recognition element in impedimetric aptasensors for successful, rapid, sensitive and selective detection of *S. aureus* in buffer. It contributes to the deeper understanding of impedimetric aptasensors and their development. We provided a fundamental base for inexpensive and robust biosensing, utilizing aptamer receptors. The advantages of using gold electrodes are their robustness, enabling regeneration and subsequent reuse of the biosensor. The simplicity of our design enables easy reproduction and the developed microfluidic system can be easily automated. Furthermore, combination with electrode patterning may enable the parallel measurement of multiple analytes when functionalized with different aptamers, in the future.

**Acknowledgments:** We want to thank Tobias Pflüger for his excellent experimental assistance with MST experiments. Our special thanks go to Katharina Urmann for her help in reviewing the manuscript.

**Author Contributions:** Peggy Reich designed the experimental concept, performed experiments and data analysis. Dieter Frense helped with experiments. Regina Stoltenburg and Beate Strehlitz helped profoundly with advice and consultation and provided the aptamer, Dieter Beckmann supervised the project. Peggy Reich wrote the manuscript with help of Regina Stoltenburg and Beate Strehlitz. All authors reviewed the manuscript.

**Conflicts of Interest:** The authors declare no conflict of interest.

## Abbreviations

| | |
|---|---|
| BB | Binding buffer |
| BBT | Binding buffer and 0.005% Tween 20 |
| CFU | Colony-forming unit |
| *CPE* | Constant phase element |
| DNA | Deoxyribonucleic acid |
| EIS | Electrochemical impedance spectroscopy |
| ELONA | Enzyme-linked oligonucleotide assay |
| FeBB | Binding buffer and 2 mM equimolar ferri-/ferrocyanide |
| *h* | Hill coefficient |
| $K_D$ | Apparent binding constant |
| kDa | kiloDalton |
| LoD | Limit of detection |
| MCH | Mercaptohexanol |
| MDPI | Multidisciplinary Digital Publishing Institute |
| MRSA | Methicillin-resistant *Staphylococcus aureus* |
| MST | Microscale thermophoresis |
| ON pool | Random oligonucleotide pool |
| PAA | Protein A-binding Aptamer |
| PCR | Polymerase chain reaction |
| QCM | Quartz crystal microbalance |
| $R_{ct}/\Delta R_{ct}$ | Charge transfer resistance/change of charge transfer resistance |
| RIFTS | Reflective interferometric fourier transform spectroscopy |
| RMS | Rough mean square |
| $R_{sol}$ | Solution resistance |
| RuHex | hexaammineruthenium(III) chloride |
| SELEX | Systematic Evolution of Ligands by Exponential Enrichment |
| spA | Gene encoding protein A |
| SPR | Surface plasmon resonance spectroscopy |
| SD | Standard deviation |
| TSB | Tryptic soy broth |
| vWF | Von Willebrand factor |
| *W* | Warburg element |

## References

1. Tong, S.Y.; Davis, J.S.; Eichenberger, E.; Holland, T.L.; Fowler, V.G., Jr. *Staphylococcus aureus* infections: Epidemiology, pathophysiology, clinical manifestations, and management. *Clin. Microbiol. Rev.* **2015**, *28*, 603–661. [CrossRef] [PubMed]
2. Carroll, K.C. Rapid diagnostics for methicillin-resistant *Staphylococcus aureus*: Current status. *Mol. Diagn. Ther.* **2008**, *12*, 15–24. [CrossRef] [PubMed]
3. Jin, W.; Yamada, K. Staphylococcal enterotoxins in processed dairy products A2. In *Food Hygiene and Toxicology in Ready to Eat Foods*; Kotzekidou, P., Ed.; Academic Press: San Diego, CA, USA, 2016; pp. 241–258.
4. Hibnick, H.E.; Bergdoll, M.S. Staphylococcal enterotoxin. II. Chemistry. *Arch. Biochem. Biophys.* **1959**, *85*, 70–73. [CrossRef]
5. DeDent, A.C.; McAdow, M.; Schneewind, O. Distribution of protein A on the surface of *Staphylococcus aureus*. *J. Bacteriol.* **2007**, *189*, 4473–4484. [CrossRef] [PubMed]
6. Schelin, J.; Wallin-Carlquist, N.; Cohn, M.T.; Lindqvist, R.; Barker, G.C.; Radstrom, P. The formation of *Staphylococcus aureus* enterotoxin in food environments and advances in risk assessment. *Virulence* **2011**, *2*, 580–592. [CrossRef] [PubMed]
7. Law, J.W.; Ab Mutalib, N.S.; Chan, K.G.; Lee, L.H. Rapid methods for the detection of foodborne bacterial pathogens: Principles, applications, advantages and limitations. *Front. Microbiol.* **2014**, *5*, 770. [CrossRef] [PubMed]

8. Zhao, X.; Wei, C.; Zhong, J.; Jin, S. Research advance in rapid detection of foodborne *Staphylococcus aureus*. *Biotechnol. Biotechnol. Equip.* **2016**, *30*, 827–833. [CrossRef]
9. Oh, A.C.; Lee, J.K.; Lee, H.N.; Hong, Y.J.; Chang, Y.H.; Hong, S.I.; Kim, D.H. Clinical utility of the Xpert MRSA assay for early detection of methicillin-resistant *Staphylococcus aureus*. *Mol. Med. Rep.* **2013**, *7*, 11–15. [CrossRef] [PubMed]
10. Mohanty, S.P.; Kougianos, E. Biosensors: A tutorial review. *IEEE Potentials* **2006**, *25*, 35–40. [CrossRef]
11. Hoja, J.; Lentka, G. A family of new generation miniaturized impedance analyzers for technical object diagnostics. *Metrol. Meas. Syst.* **2013**, *20*. [CrossRef]
12. Lisdat, F.; Schafer, D. The use of electrochemical impedance spectroscopy for biosensing. *Anal. Bioanal. Chem.* **2008**, *391*, 1555–1567. [CrossRef] [PubMed]
13. Bahadir, E.B.; Sezginturk, M.K. A review on impedimetric biosensors. *Artif. Cells Nanomed. Biotechnol.* **2016**, *44*, 248–262. [CrossRef] [PubMed]
14. Bekir, K.; Barhoumi, H.; Braiek, M.; Chrouda, A.; Zine, N.; Abid, N.; Maaref, A.; Bakhrouf, A.; Ouada, H.B.; Jaffrezic-Renault, N.; et al. Electrochemical impedance immunosensor for rapid detection of stressed pathogenic *Staphylococcus aureus* bacteria. *Environ. Sci. Pollut. Res. Int.* **2015**, *22*, 15796–15803. [CrossRef] [PubMed]
15. O'Sullivan, C.K. Aptasensors—The future of biosensing? *Anal. Bioanal. Chem.* **2002**, *372*, 44–48. [CrossRef] [PubMed]
16. Gopinath, S.C. Methods developed for SELEX. *Anal. Bioanal. Chem.* **2007**, *387*, 171–182. [CrossRef] [PubMed]
17. Willner, I.; Zayats, M. Electronic aptamer-based sensors. *Angew. Chem. Int. Ed. Engl.* **2007**, *46*, 6408–6418. [CrossRef] [PubMed]
18. Radi, A.E.; Acero Sanchez, J.L.; Baldrich, E.; O'Sullivan, C.K. Reusable impedimetric aptasensor. *Anal. Chem.* **2005**, *77*. [CrossRef] [PubMed]
19. Zhu, B.; Booth, M.A.; Woo, H.Y.; Hodgkiss, J.M.; Travas-Sejdic, J. Label-Free, electrochemical quantitation of potassium ions from femtomolar levels. *Chem. Asian. J.* **2015**, *10*, 2169–2175. [CrossRef] [PubMed]
20. Liang, G.; Man, Y.; Jin, X.; Pan, L.; Liu, X. Aptamer-based biosensor for label-free detection of ethanolamine by electrochemical impedance spectroscopy. *Anal. Chim. Acta.* **2016**, *936*, 222–228. [CrossRef] [PubMed]
21. Labib, M.; Zamay, A.S.; Kolovskaya, O.S.; Reshetneva, I.T.; Zamay, G.S.; Kibbee, R.J.; Sattar, S.A.; Zamay, T.N.; Berezovski, M.V. Aptamer-based viability impedimetric sensor for bacteria. *Anal. Chem.* **2012**, *84*, 8966–8969. [CrossRef] [PubMed]
22. Shahdordizadeh, M.; Taghdisi, S.M.; Ansari, N.; Langroodi, F.A.; Abnous, K.; Ramezani, M. Aptamer based biosensors for detection of *Staphylococcus aureus*. *Sens. Actuators B Chem.* **2017**, *241*, 619–635. [CrossRef]
23. Yuan, J.; Wu, S.; Duan, N.; Ma, X.; Xia, Y.; Chen, J.; Ding, Z.; Wang, Z. A sensitive gold nanoparticle-based colorimetric aptasensor for *Staphylococcus aureus*. *Talanta* **2014**, *127*, 163–168. [CrossRef] [PubMed]
24. Shangguan, J.; Li, Y.; He, D.; He, X.; Wang, K.; Zou, Z.; Shi, H. A combination of positive dielectrophoresis driven on-line enrichment and aptamer-fluorescent silica nanoparticle label for rapid and sensitive detection of *Staphylococcus aureus*. *Analyst* **2015**, *140*, 4489–4497. [CrossRef] [PubMed]
25. Duan, N.; Wu, S.; Zhu, C.; Ma, X.; Wang, Z.; Yu, Y.; Jiang, Y. Dual-color upconversion fluorescence and aptamer-functionalized magnetic nanoparticles-based bioassay for the simultaneous detection of *Salmonella typhimurium* and *Staphylococcus aureus*. *Anal. Chim. Acta* **2012**, *723*, 1–6. [CrossRef] [PubMed]
26. Chang, Y.C.; Yang, C.Y.; Sun, R.L.; Cheng, Y.F.; Kao, W.C.; Yang, P.C. Rapid single cell detection of *Staphylococcus aureus* by aptamer-conjugated gold nanoparticles. *Sci. Rep.* **2013**, *3*. [CrossRef] [PubMed]
27. Zelada-Guillen, G.A.; Sebastian-Avila, J.L.; Blondeau, P.; Riu, J.; Rius, F.X. Label-free detection of *Staphylococcus aureus* in skin using real-time potentiometric biosensors based on carbon nanotubes and aptamers. *Biosens. Bioelectron.* **2012**, *31*, 226–232. [CrossRef] [PubMed]
28. Hernandez, R.; Valles, C.; Benito, A.M.; Maser, W.K.; Rius, F.X.; Riu, J. Graphene-based potentiometric biosensor for the immediate detection of living bacteria. *Biosens. Bioelectron.* **2014**, *54*, 553–557. [CrossRef] [PubMed]
29. Abbaspour, A.; Norouz-Sarvestani, F.; Noori, A.; Soltani, N. Aptamer-conjugated silver nanoparticles for electrochemical dual-aptamer-based sandwich detection of *Staphylococcus aureus*. *Biosens. Bioelectron.* **2015**, *68*. [CrossRef] [PubMed]

30. Lian, Y.; He, F.; Wang, H.; Tong, F. A new aptamer/graphene interdigitated gold electrode piezoelectric sensor for rapid and specific detection of *Staphylococcus aureus*. *Biosens. Bioelectron.* **2015**, *65*, 314–319. [CrossRef] [PubMed]
31. Jia, F.; Duan, N.; Wu, S.; Ma, X.; Xia, Y.; Wang, Z.; Wei, X. Impedimetric aptasensor for *Staphylococcus aureus* based on nanocomposite prepared from reduced graphene oxide and gold nanoparticles. *Microchim. Acta* **2014**, *181*, 967–974. [CrossRef]
32. Kahl, B.C.; Mellmann, A.; Deiwick, S.; Peters, G.; Harmsen, D. Variation of the polymorphic region X of the protein A gene during persistent airway infection of cystic fibrosis patients reflects two independent mechanisms of genetic change in *Staphylococcus aureus*. *J. Clin. Microbiol.* **2005**, *43*, 502–505. [CrossRef] [PubMed]
33. O'Seaghdha, M.; van Schooten, C.J.; Kerrigan, S.W.; Emsley, J.; Silverman, G.J.; Cox, D.; Lenting, P.J.; Foster, T.J. *Staphylococcus aureus* protein A binding to von Willebrand factor A1 domain is mediated by conserved IgG binding regions. *FEBS J.* **2006**, *273*, 4831–4841. [CrossRef] [PubMed]
34. Stoltenburg, R.; Reinemann, C.; Strehlitz, B. FluMag-SELEX as an advantageous method for DNA aptamer selection. *Anal. Bioanal. Chem.* **2005**, *383*, 83–91. [CrossRef] [PubMed]
35. Stoltenburg, R.; Schubert, T.; Strehlitz, B. In vitro selection and interaction studies of a DNA aptamer targeting protein A. *PLoS ONE* **2015**, *10*. [CrossRef] [PubMed]
36. Stoltenburg, R.; Krafcikova, P.; Viglasky, V.; Strehlitz, B. G-quadruplex aptamer targeting protein A and its capability to detect *Staphylococcus aureus* demonstrated by ELONA. *Sci. Rep.* **2016**, *6*, 33812. [CrossRef] [PubMed]
37. Keighley, S.D.; Li, P.; Estrela, P.; Migliorato, P. Optimization of DNA immobilization on gold electrodes for label-free detection by electrochemical impedance spectroscopy. *Biosens. Bioelectron.* **2008**, *23*, 1291–1297. [CrossRef] [PubMed]
38. Steel, A.B.; Herne, T.M.; Tarlov, M.J. Electrochemical quantitation of DNA immobilized on gold. *Anal. Chem.* **1998**, *70*, 4670–4677. [CrossRef] [PubMed]
39. Debono, R.F.; Loucks, G.D.; Manna, D.D.; Krull, U.J. Self-assembly of short and long-chain *n*-alkyl thiols onto gold surfaces: A real-time study using surface plasmon resonance techniques. *Can. J. Chem.* **1996**, *74*, 677–688. [CrossRef]
40. Martin, S.J.; Granstaff, V.E.; Frye, G.C. Characterization of a quartz crystal microbalance with simultaneous mass and liquid loading. *Anal. Chem.* **2002**, *63*, 2272–2281. [CrossRef]
41. Urmann, K.; Modrejewski, J.; Scheper, T.; Walter Johanna, G. Aptamer-modified nanomaterials: Principles and applications. *BioNanoMaterials* **2017**, *18*. [CrossRef]
42. Erickson, H.P. Size and shape of protein molecules at the nanometer level determined by sedimentation, gel filtration, and electron microscopy. *Biol. Proced. Online* **2009**, *11*, 32–51. [CrossRef] [PubMed]
43. Angell, D.H.; Dickinson, T. The kinetics of the ferrous/ferric and ferro/ferricyanide reactions at platinum and gold electrodes. *J. Electroanal. Chem. Interfacial Electrochem.* **1972**, *35*, 55–72. [CrossRef]
44. Hirschorn, B.; Orazem, M.E.; Tribollet, B.; Vivier, V.; Frateur, I.; Musiani, M. Determination of effective capacitance and film thickness from constant-phase-element parameters. *Electrochim. Acta* **2010**, *55*, 6218–6227. [CrossRef]
45. Sjödahl, J. Structural studies on the four repetitive Fc-binding regions in protein A from *Staphylococcus aureus*. *Eur. J. Biochem.* **1977**, *78*, 471–490. [CrossRef] [PubMed]
46. Urmann, K.; Reich, P.; Walter, J.G.; Beckmann, D.; Segal, E.; Scheper, T. Rapid and label-free detection of protein A by aptamer-tethered porous silicon nanostructures. *J. Biotechnol.* **2017**, *257*, 171–177. [CrossRef] [PubMed]
47. Banada, P.P.; Chakravorty, S.; Shah, D.; Burday, M.; Mazzella, F.M.; Alland, D. Highly sensitive detection of *Staphylococcus aureus* directly from patient blood. *PLoS ONE* **2012**, *7*, e31126. [CrossRef] [PubMed]
48. Cao, X.; Li, S.; Chen, L.; Ding, H.; Xu, H.; Huang, Y.; Li, J.; Liu, N.; Cao, W.; Zhu, Y.; et al. Combining use of a panel of ssDNA aptamers in the detection of *Staphylococcus aureus*. *Nucleic Acids Res.* **2009**, *37*, 4621–4628. [CrossRef] [PubMed]
49. Reich, P. Entwicklung eines impedimetrischen Aptasensor zur Detektion von *Staphylococcus aureus*. Ph.D. Thesis, Leibniz Universität Hannover, Hannover, Germany, 2017. in preparation.

50. Tallent, S.M.; Bennett, R.W.; Hait, J.M. Chapter 13 B Staphylococcal Enterotoxins Detection Methods. 2017. U.S. Food and Drug Administration. Available online: https://www.fda.gov/Food/FoodScienceResearch/LaboratoryMethods/ucm564359.htm (accessed on 13 November 2017).
51. Bennett, R.W.; Lancette, G.A. Chapter 12 *Staphylococcus aureus*. 2016; U.S. Food and Drug Administration. Available online: https://www.fda.gov/Food/FoodScienceResearch/LaboratoryMethods/ucm071429.htm (accessed on 13 November 2017).
52. Sauerbrey, G. Verwendung von Schwingquarzen zur Wägung dünner Schichten und zur Mikrowägung. *Zeitschrift für Physik* **1959**, *155*, 206–222. [CrossRef]
53. Oesch, U.; Janata, J. Electrochemical study of gold electrodes with anodic oxide films—I. Formation and reduction behaviour of anodic oxides on gold. *Electrochim. Acta* **1983**, *28*, 1237–1246. [CrossRef]


International Journal of
*Molecular Sciences*

MDPI

*Article*

# In Vitro Selection of a Single-Stranded DNA Molecular Recognition Element against the Pesticide Fipronil and Sensitive Detection in River Water

**Ka L. Hong [1,*] and Letha J. Sooter [2]**

[1] Department of Pharmaceutical Sciences, Nesbitt School of Pharmacy, Wilkes University, 84 W. South Street, Wilkes-Barre, PA 18766, USA
[2] Independent Researcher, Pittsburgh, PA 15234, USA; lethasooter@rocketmail.com
* Correspondence: kalok.hong@wilkes.edu; Tel.: +1-570-408-4296

Received: 31 October 2017; Accepted: 25 December 2017; Published: 28 December 2017

**Abstract:** Fipronil is a commonly used insecticide that has been shown to have environmental and human health risks. The current standard methods of detection for fipronil and its metabolites, such as GC-MS, are time consuming and labor intensive. In this study, a variant of systematic evolution of ligands by exponential enrichment (SELEX), was utilized to identify the first single-stranded DNA (ssDNA) molecular recognition element (MRE) that binds to fipronil with high affinity ($K_d$ = 48 ± 8 nM). The selected MRE displayed low cross binding activity on various environmentally relevant, structurally unrelated herbicides and pesticides, in addition to broad-spectrum binding activity on major metabolites of fipronil and a structurally similar pesticide in prepared river samples. Additionally, a proof-of-principle fluorescent detection assay was developed by using the selected ssDNA MRE as a signal-reporting element, with a limit of detection of 105 nM in a prepared river water sample.

**Keywords:** SELEX; in vitro selection; aptamer; molecular recognition element (MRE); fipronil; pesticide; insecticide; ELISA; Decoy-SELEX

## 1. Introduction

Fipronil has been a widely used phenlpyrazole insecticide in the United States since it was first introduced in the late 1990s [1]. Fipronil inhibits gamma-aminobutyric acid (GABA) gated chloride channels and causes continuous excitation of the central nervous system, which ultimately leads to insect death [2]. Fipronil is often used as an alternative to organophosphate pesticides in many settings, including residential, commercial, and agricultural, due to its selectivity on insect GABA receptors [3]. There was a ten-fold increase in fipronil sales in California from 2000 to 2005 [4]. A report by Simon-Delso et al. indicates that fipronil currently accounts for approximately 10% of the global pesticide market [5].

Fipronil has become a widespread environmental contaminant because of its wide applications. In the United States from 2002 to 2011, fipronil was detected in urban streams up to 63% of the time, and 15 to 20% of the time in agricultural and mixed land [3]. Additionally, measured concentrations of fipronil exceed the aquatic-life benchmark in 70% of urban streams and more than 20% of agricultural and mixed land streams in this timeframe [3]. The chronic benchmarks for fish species and aquatic invertebrates are 6.6 μg/L and 9.8 μg/L, respectively [6]. It has also been shown to contaminate drinking water sources in Vietnam [7]. Worldwide exposure of humans and ecosystems to fipronil has been clearly observed.

The presence of fipronil in urban streams has been reported. It suggested that fipronil is highly toxic to many steam invertebrates, with a mean 96-h viability inhibition $EC_{50}$ values as low as 32.5 ng/L

for *Chironomus dilutus* [8]. In addition to the toxicity in aquatic invertebrates, fipronil is highly toxic to many fish species, with a reported 96-h $LC_{50}$ level as low as 0.246 mg/L for rainbow trout and 0.083 mg/L for bluegill sunfish [1]. It also has a tremendous detrimental effect on non-target insects, such as honey-bees [9]. Although fipronil binds more selectively to insect GABA receptors than mammal GABA receptors, a long term toxicity study showed it increased thyroid follicular cell tumors in rats [10,11]. The U.S. Environmental Protection Agency has therefore classified fipronil as a possible human carcinogen [10]. Even though there has been an overall increase in the knowledge of how fipronil is impacting the environment and human health, a large knowledge gap still exists in terms of its long term environmental fate in various media, such as soils and agricultural products [12]. Thus, it is important to monitor the exposure levels of fipronil in the environment.

Currently, the detection of fipronil levels in environmental and biological samples are mostly dependent on chromatographic methods, such as gas and/or liquid chromatography coupled with mass spectrometry [13–16]. These methods are sensitive, but costly, and time and labor intensive. There have been reported uses of antibody-based enzyme-linked immunosorbent assays (ELISA) to detect total fipronil levels in human blood samples and artificially contaminated tap water samples [17–19]. However, there are inherent limitations in antibody-based assays. They are difficult or non-reusable, expensive to produce, and may suffer from batch-to-batch variations [20,21]. There is a clear need to develop a low-cost, rapid, reusable means to detect fipronil. One possible way to achieve this is by identifying a single-stranded DNA (ssDNA) molecular recognition element (MRE) that specifically binds to fipronil.

The process, systematic evolution of ligands by exponential enrichment (SELEX) can be utilized to identify such a specific binding element [22]. This in vitro selection process involves repeated cycles of incubation of a target with a library of up to $10^{15}$ different molecules, followed by partitioning of binders and non-binders under increasing selective pressure.

This study utilized a stringent variation of the SELEX process previously described by Hong et al. to select a ssDNA MRE with high binding affinity toward fipronil [23]. This Decoy-SELEX variant emphasizes on introducing multiple, lengthy negative selection rounds to direct the enriched library away from binding to structurally similar molecules and molecules that are likely to co-exist in the same environment [23–26]. In this study, major metabolites of fipronil, commonly used herbicides and pesticides (atrazine, malathion and propanil), and a closely related pesticide, ethiprole have been used as negative targets. Bovine serum albumin (BSA) was chosen to be one of the negative targets, as it is a common blocking agent. In addition, the selected ssDNA MRE was also incorporated into a proof-of-principle fluorescence assay for the detection of fipronil in prepared river water at nanomolar concentrations.

## 2. Results and Discussion

### *2.1. Identification of Fipronil Specific ssDNA MRE*

Twelve rounds of SELEX were carried out to identify ssDNA MREs specific to fipronil (Figure 1, Table 1). Thirty eight, thirty three, thirty three, and thirty five of post round 3, 6, 9, and 12 library clones were sequenced and analyzed for consensus sequence families, respectively. Round 12 sequences were also subjected to Mfold analysis for secondary structures with associated Gibbs free energy values (ΔG) (indicating stability). One candidate sequence, designated R12.51 appeared to be highly conserved in multiple sequence families. The random region of R12. 51 shares 30%, 32% and 38% identity with the random regions of R12.43, R12.20 and R12.17 respectively (Figure 2).

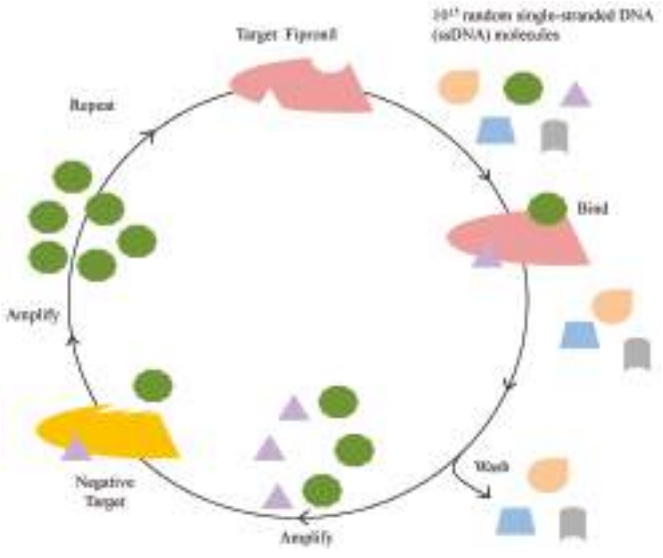


**Figure 1.** Illustration of the in vitro selection process. The in vitro selection process begins with up to $10^{15}$ different ssDNA molecules (represented by various small, colored shapes) and incubation with the target of interest, fipronil. Molecules that bind to fipronil are amplified and subjected to incubation with negative targets. Those that do not bind to negative targets are isolated and amplified. This completes one round of an in vitro selection cycle.

**Table 1.** Systematic evolution of ligands by exponential enrichments (SELEX) scheme for fipronil-specific molecular recognition element (MRE) selection.

| Round | Positive Selection | Time | Negative Selection | Time |
|---|---|---|---|---|
| 1 | Immobilized Target (IT) | 48 h | Immobilizing substrate (IS) | 24 h |
| 2 | IT | 22 h | Immobilized Negative Target (INT) Fipronil Sulfide | 24 h |
| 3 | IT | 16 h | INT Fipronil Desulfinyl | 24 h |
| 4 | IT | 11 h | INT Fipronil Sulfone | 24 h |
| 5 | IT | 6.5 h | INT Ethiprole | 24 h |
| 6 | IT | 3 h | IT/ 1 mM of BSA Free Elution (FE) | 3 h/ 24 h |
| 7 | IT/ Competitive Elution with 500 μM free Fipronil | 3 h/ 1 h | IT/ 1 μM of Atrazine FE/1 μM of Propanil FE | 3 h/ 24 h/ 24 h |
| 8 | IT/ Competitive Elution with 500 μM free Fipronil | 1 h/ 30 min | IT/ 1 μM of Fipronil Sulfone FE/ 1 μM of Fipronil Desulfinyl FE | 3 h/ 24 h/ 24 h |
| 9 | IT/ Competitive Elution with 100 μM free Fipronil | 15 min/ 5 min | IT/ 1 μM of Fipronil Sulfide FE | 15 min/ 15 min |
| 10 | IT/ Competitive Elution with 10 μM free Fipronil | 1 min/ 1 min | IT/ 1 μM of Ethiprole Free Elution | 1 min/ 1 min |
| 11 | IT/ Competitive Elution with 1 μM free Fipronil | Immediate/ Immediate | IT/ 1 mM of BSA FE/ 1 μM of Malathion FE | 1 min/ 6 h/ 30 min |
| 12 | IT/ Competitive Elution with 100 nM free Fipronil | Immediate/ Immediate | - | |

In vitro selection performed for identifying fipronil-specific MRE. Immobilized target (IT) is fipronil conjugated to magnetic beads. Immobilized negative target (INT) is negative targets conjugated to magnetic beads. BSA is the abbreviation for bovine serum albumin. FE is the abbreviation for free elution. Times listed are incubation times in hours (h), minutes (min) or immediate (few seconds).

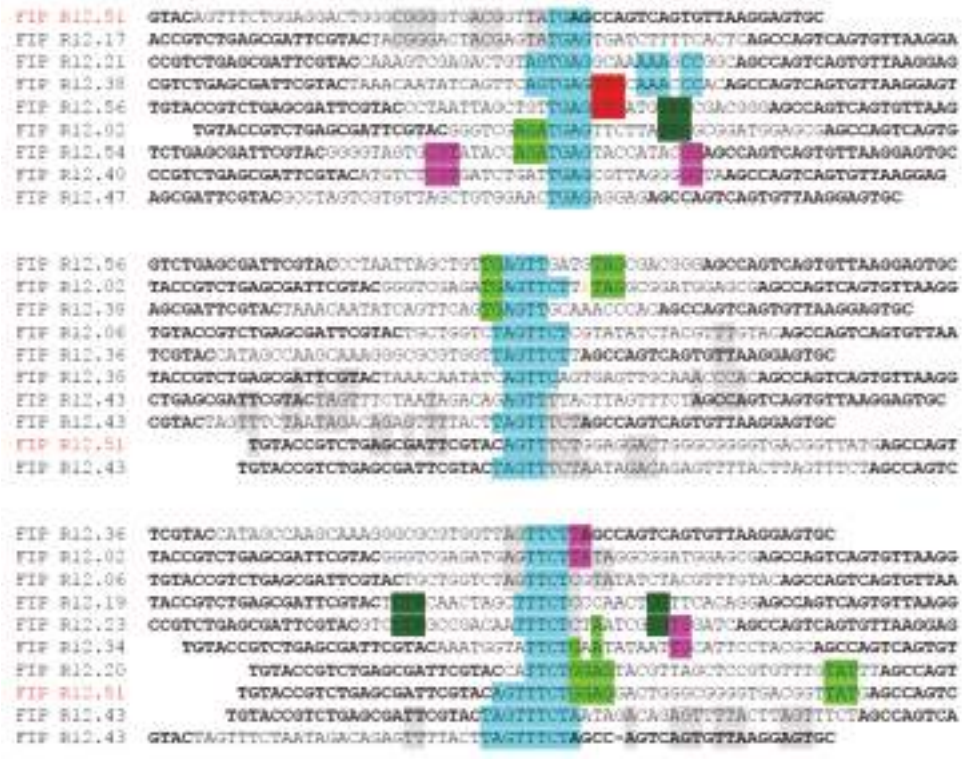

**Figure 2.** Representative sequence families of the round 12 library. Partial constant regions are shown in bold letters. The variable regions are shown in regular letters. R12.51 candidate MRE represented in multiple sequence families, and shared similarity with other sequences in their corresponding families. The turquoise color indicates the center for alignment in each family and other colors represent sequence similarity of each sequence.

The Mfold DNA folding web-server predicts secondary structures of ssDNA sequences with given temperatures, sodium ion and magnesium ion concentrations [27]. The Mfold predicted stem–loop features of R12.51 were comprised of the random region and the constant regions, and had a Gibbs free energy of −9.28 kcal/mol (Figure 3). Previous studies demonstrated the constant region participates in binding events, and therefore may not be ignored when analyzing candidate MRE sequences and predicted secondary structures [28–32]. Based on these criteria, R12.51 was chosen as the candidate MRE for characterization studies.

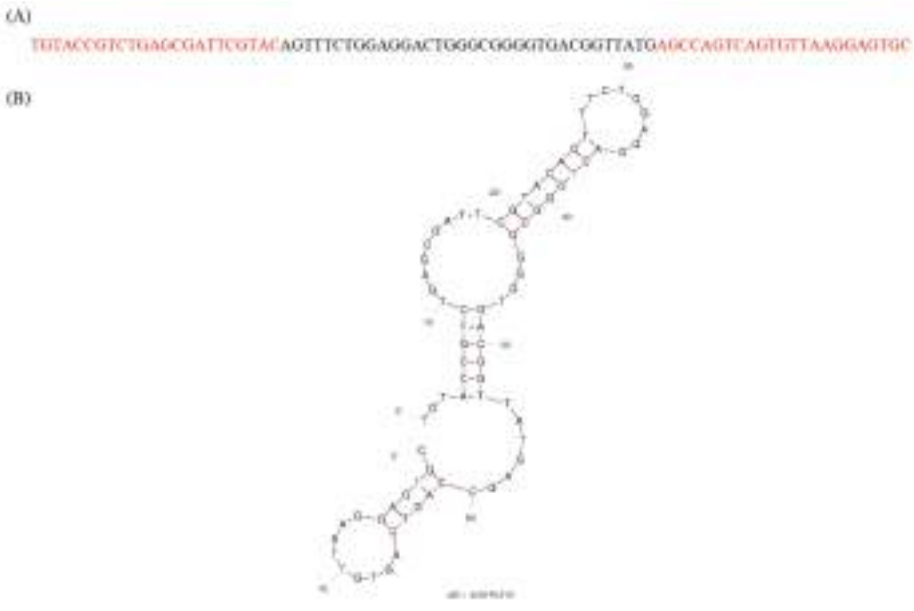


**Figure 3.** Secondary structure and sequence of R12.51 candidate ssDNA MRE. (**A**) ssDNA sequence of candidate fipronil MRE R12.51. The red portions indicate the constant regions for primer attachment, and the black portion indicates the variable region; (**B**) Mfold prediction of R12.51 secondary structure [27].

### 2.2. *Affinity and Specifcity of Fipronil-Specific ssDNA MRE in Selection Buffer and Buffered River Water*

Four independent fluorescent saturation binding assays were conducted to determine the affinity of the R12.51 candidate sequence. Concentrations of the candidate sequence in the low nM to 10 μM range were assayed. The equilibrium dissociation constant ($K_d$) from the four binding assays were 55 ± 14 nM, 35 ± 9 nM, 38 ± 12 nM and 64 ± 12 nM. The average equilibrium dissociation constant ($K_d$) was 48 ± 8 nM (Figure 4). This plate-based fluorescence saturation binding assay method was modified from a previously reported bead-based assay [24–26]. The equilibrium dissociation constant obtained for R12.51 is comparable to other small molecule binding ssDNA MREs identified with other variants of SELEX [33–35]. This high affinity further validates the stringency of this SELEX scheme [36,37].

The cross-binding activity of R12.51 on negative targets used in the selection was also determined. This assay was modified from a previously described bead-based assay [24–26]. The data is presented relative to binding between R12.51 and fipronil as has been previously described [24,25,36,37]. The ssDNA MRE preferentially binds to fipronil, compared to atrazine ($p$ = 0.030), propanil ($p$ = 0.005), and malathion ($p$ = 0.039) in buffer conditions (Table 2). The binding between fipronil, fipronil metabolites and ethiprole are not significantly different in buffer conditions. It is likely due to their high degrees of structural similarity. This suggests R12.51 potentially binds to the core chemical structure that is shared among fipronil, fipronil metabolites and ethiprole. A relatively high concentration of the negative targets (1 μM) were used in the selection buffer cross-binding assays, as the same concentration was introduced during the selection process (Table 1).

(A)

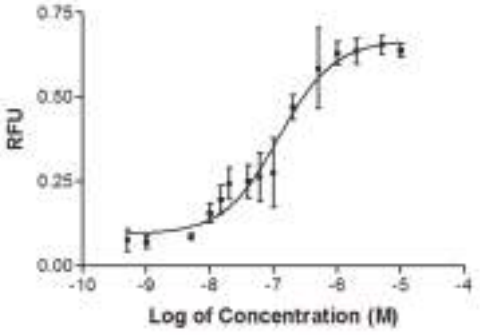


(B)

| Representative $K_d$ | Std Error |
|---|---|
| 64 nM | 12 nM |

**Figure 4.** Fluorescent equilibrium binding assay of R12.51. (**A**) Representative saturation binding curve of R12.51 with nonlinear regression sigmoidal curve best fit. Concentration data was transformed by logarithmic scale. Normalized average fluorescence from triplicate samples were presented. Error bars are representative of $\pm 1\times$ standard deviations. The goodness of fit ($R^2$) was 0.87; (**B**) Representative equilibrium dissociation constant with standard error for the presented R12.51 binding assay.

**Table 2.** Cross-reactivity data of R12.51 ssDNA MRE in selection buffer.

| Target | Normalized Average Fluorescence | Standard Deviation | *p*-Value | Selective Ratio |
|---|---|---|---|---|
| Fipronil | 2.413 | 0.194 | - | - |
| Fipronil Sulfone | 2.248 | 0.388 | 0.279 | 1.07 |
| Fipronil Sulfide | 2.726 | 0.460 | 0.169 | 0.89 |
| Fipronil Desulfinyl | 2.088 | 0.623 | 0.219 | 1.16 |
| Ethiprole | 2.185 | 0.217 | 0.124 | 1.10 |
| Atrazine | 1.963 | 0.227 | 0.030 | 1.23 |
| Propanil | 1.587 | 0.243 | 0.005 | 1.52 |
| Malathion | 2.048 | 0.184 | 0.039 | 1.18 |
| BSA | 8.687 | 0.360 | $5.99 \times 10^{-6}$ | 0.28 |
| Selection Buffer (No Targets) | 0.247 | 0.214 | $1.02 \times 10^{-4}$ | 9.74 |

For each negative target (1 μM), normalized average fluorescence is given with $1\times$ standard deviation. Each set of experiments was performed in triplicate. A one tailed student's *t*-test was performed to calculate the *p*-value between fipronil and the cross-binding targets. The selectivity ratio represents the normalized average fluorescence for fipronil divided by the normalized average fluoresce for the cross-binding target, indicating R12.51's level of preference for fipronil compared to the cross-binding target.

Interestingly, the cross-binding activity of R12.51 in a river water/buffer mix is noticeably different than in selection buffer alone (Table 3). A lower environmentally relevant concentration of negative targets was examined. The ssDNA MRE binds to fipronil significantly higher than it does to atrazine, propanil, and malathion in a river water/buffer mixed condition. While there are statistically significant differences in the binding selectivity ratios between fipronil, fipronil metabolites and ethiprole, the differences are small. It is to be noted that the river water/buffer mix alone did not elute a detectable level of R12.51 bound to immobilized fipronil. The difference between cross-binding profiles of selection buffer and the river water/ buffer mix is likely due to the water hardness found in the sampled river [38]. It is known that divalent cations such as $Ca^{2+}$ and $Mg^{2+}$ can greatly stabilize

the secondary structures of nucleic acid MREs [39]. Hard-water containing a sufficient amount of these divalent cations potentially stabilizes the secondary structure of R12.51 when it binds to fipronil. The selectivity ratios between fipronil and structurally related compounds remain relatively unchanged in both binding conditions. This is again likely due to the close structural similarity between these compounds. It is to be noted that all the fipronil metabolites used in this study are environmentally relevant degradation products of fipronil [40]. This property of broad-spectrum binding to fipronil metabolites is desirable in an environmental biosensor.

**Table 3.** Cross-reactivity data of R12.51 ssDNA MRE in river water/buffer mix.

| Target | Normalized Average Fluorescence | Standard Deviation | *p*-Value | Selective Ratio |
|---|---|---|---|---|
| Fipronil | 3.863 | 0.090 | - | - |
| Fipronil Sulfone | 2.863 | 0.180 | $4.98 \times 10^{-4}$ | 1.34 |
| Fipronil Sulfide | 4.333 | 0.944 | $2.19 \times 10^{-1}$ | 0.89 |
| Fipronil Desulfinyl | 2.902 | 0.245 | $15.5 \times 10^{-3}$ | 1.33 |
| Ethiprole | 3.157 | 0.148 | $1.06 \times 10^{-3}$ | 1.22 |
| Atrazine | 0.804 | 0.302 | $3.66 \times 10^{-5}$ | 4.80 |
| Propanil | 0.764 | 0.509 | $2.44 \times 10^{-4}$ | 5.05 |
| Malathion | 0.725 | 0.355 | $5.98 \times 10^{-5}$ | 5.32 |
| BSA | 20.41 | 1.118 | $6.95 \times 10^{-6}$ | 0.19 |
| River water/Buffer Mix (No Targets) | −0.549 | 1.779 | $6.37 \times 10^{-3}$ | −7.035 |

For each negative target (200 nM), normalized average fluorescence is given with 1× standard deviation. Each set of experiments was performed in triplicate. A one tailed student's *t*-test was performed to calculate the *p*-value between fipronil and cross-binding targets. The selectivity ratio represents the normalized average fluorescence for fipronil divided by the normalized average fluoresce for the cross-binding target, indicating R12.51's level of preference for fipronil compared to the cross-binding target.

Binding of R12.51 to BSA is strong in both binding conditions. This may be due to the large globular nature of the protein and its non-specific interaction with single-stranded DNA. This non-specific interaction appears to be difficult to reduce, despite of having two rounds of negative selection against BSA. High levels of non-specific binding between a small molecule specific ssDNA MRE and BSA was also observed in a previous study [26]. The same library utilized in this study, designated RMW.N34 has been studied in two other protein-targeted in vitro selection projects [36,37]. A phenomenon was observed from these studies in regards to the binding selectivity of the library molecules subjected to the Decoy-SELEX variant. It is possible that the binding selectivity of the library is enriched during early rounds of the selection process based on the molecular sizes of the target/or negative targets. In this study, BSA was first introduced after six rounds of enrichment. It is possible that the library was already enriched to a degree that a majority of the library molecules had non-specific binding to globular protein. This therefore suggests that early rounds of negative selection against globular proteins may be advantageous in magnetic bead-based small molecule SELEX schemes.

### *2.3. Biosensing Application of Fipronil-Specific MRE in River Water*

The broad-spectrum binding profile of R12.51 and its high selectivity in conditioned river water allowed the investigation of its potential application as a biosensing tool. A plate-based biosensing platform using R12.51 as the reporter element was developed. Filtered river water/buffer mix was spiked to contain concentrations of 0, 5, 10, 25, 50, 100, 200, and 500 nM of fipronil. The spiked samples were incubated with FAM-labelled MRE bound to immobilized fipronil. The amount of MRE eluted with spiked sample was retrieved and the fluorescence signal was recorded on a plate reader. The calibration curve of fluorescence intensity and a linear correlation ($R^2$ = 0.9025) between the value of normalized fluorescence and fipronil concentration were generated (Figure 5). The limit of detection (LOD) was calculated to be 105 nM based on the method previously described by Armbruster et al. [41].

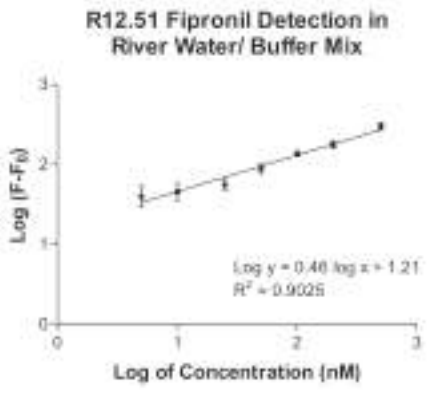


**Figure 5.** The calibration curve of fluorescence intensity with increasing concentrations of fipronil spiked in river water/buffer mix. Data is transformed by logarithmic scale. Normalized average fluorescence from triplicate samples are presented. $F_0$ and F are values of normalized fluorescence intensities without and with fipronil. Buffer: 1× selection buffer. Error bars are representative of ±1× standard deviations.

There were two publications and one patent of fipronil detection immunoassays in the literature at the time this study was written [17,19,42]. In the study by Vasylieva et al., the author tested the cross reactivity of two candidate fipronil binding antibodies to structurally related compounds in complex biological and environmental matrices. Both candidate antibodies displayed a moderate to high levels of cross reactivity to fipronil metabolites, fipronil sulfide, fipronil sulfone, fipronil desulfinyl and ethiprole, that were also tested in the current study [19]. This showed that traditional antibodies also have a limited ability to differentiate the minor structural differences between fipronil and its metabolites. The reported $IC_{50}$ values of the immunoassays were in the low microgram per liter range [19]. Although the LOD of the detection assay in this study was approximately ten-fold higher than environmentally relevant fipronil concentration, this may be enhanced with various signal enhancers, such as quantum dots, gold nanoparticles and horse radish peroxidase-conjugated ssDNA MREs in future biosensor development [43–45]. It is important to note that this study showed the identification of a fipronil binding element without the use of a hapten or animals. It also identified the first ssDNA MRE with high binding affinity to fipronil and structurally related compounds. One intrinsic limitation of R12.51 is its strong non-specific binding to BSA. This suggests additional sample preparation, such as push filtering, would be needed to remove protein contaminants that are likely to non-specifically bind to R12.51. In sum, the ability of candidate R12.51 to be applied in a proof-of-principle detection assay in environmental matrix has been demonstrated, which has the potential to be further developed into a ssDNA MRE based biosensor [46].

## 3. Materials and Methods

### *3.1. In Vitro Selection for Fipronil-Specific MREs*

In brief, the selection began with a ssDNA library with up to $10^{15}$ different molecules. This library was previously designed by the Sooter Laboratory at WVU, and designated RMW.N34 [25]. The library consists of two 23-base constant regions for primer attachment during polymerase chain reaction (PCR), flanked by a 34-base random region, and it was commercially synthesized (Eurofins MWG Operon; Huntsville, AL, USA). Twelve rounds of SELEX were performed to identify ssDNA molecules that bound to fipronil (Table 1, Figure 6).

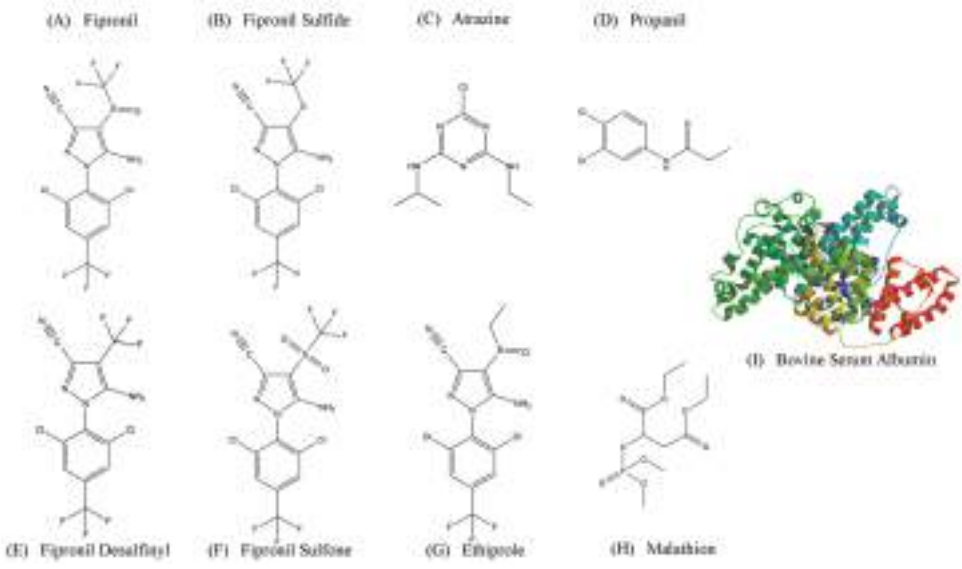


**Figure 6.** Chemical structures of targets used in the SELEX process and cross-binding assays. (**A**) Structure of the pesticide and target of selection fipronil; (**B**,**E**,**F**) Structures of fipronil metabolite; (**G**) Structures of ethiprole: chemically similar to fipronil; (**C**,**D**,**H**) Structures of atrazine, propanil and malathion: herbicides and pesticides commonly found in similar environments as fipronil. (**I**) Bovine serum albumin (PDB 4F5S, 66.5 kDa) [47].

Fipronil (AccuStandard; New Haven, CT, USA) at a concentration of 42 µM in phosphate buffer saline (PBS)/20% acetone was covalently immobilized to carboxylic acid-coated magnetic beads (immobilizing substrate) (Dynabeads M-270 Carboxylic Acid, Life Technologies; Grand Island, NY, USA) via an amidation reaction using *N*-hydroxysulfonyl succinimide (sulfo-NHS) (Pierce; Rockford, IL, USA) and 1-ethyl-3-(3-dimethylaminopropyl) (EDC) (Pierce; Rockford, IL, USA) according to manufacturer's protocol. After the conjugation reaction, beads were washed with phosphate buffer solution three times to remove unreacted fipronil. Unreacted carboxyl groups on the beads were quenched with 1× selection buffer (100 mM sodium chloride, 20 mM Tris-HCl, and 2 mM magnesium chloride). This provided the immobilized target (IT).

For positive rounds, 6.7 µL of IT was incubated with the ssDNA library in 500 µL of selection buffer (100 mM sodium chloride, 20 mM Tris-HCl, and 2 mM magnesium chloride; 1× selection buffer, SB) at room temperature with slow rotation. IT-bound ssDNA molecules were retrieved from the solution by magnetic separation, washed three times with 500 µL of 1× selection buffer, and resuspended in 100 µL of 1× selection buffer. This served as the PCR amplification template. The PCR conditions were as follows: bound ssDNA, 400 nM forward and biotinylated reverse RMW.N34 primers (Eurofins MWG Operon; Huntsville, AL, USA) (forward primer sequence: 5′-TGTACCGTCTGAGCGATTCGTAC-3′, biotinylated reverse primer sequence: 5′-Biotin-GCACTCCTTAACACTGACTGGCT-3′), 250 µM deoxynucleotide triphosphates, 1× GoTaq Reaction Buffer (Promega; Madison, WI, USA), 3.5 units *Taq*, and MilliQ pure water. Thermal cycling conditions were as follows: denature at 95 °C for 5 min, cycle at 95 °C for 1 min, 63 °C for 45 s, and 72 °C for 1 min; and final extension temperature at 72 °C for 7 min [24–26]. Large scale 4 mL PCR was carried out after each positive and negative selection round. This selection procedure for immobilized fipronil was performed for Rounds 1–6, each with decreasing incubation time.

PCR product with amplified dsDNA was purified with the IBI purification kit (IBI Scientific; Peosta, IA, USA) according to manufacturer's protocol. Post-purification process includes single strand separation and ethanol precipitation of the forward strand DNA. These procedures were performed identically to as previously described [24–26].

For negative selection rounds, metabolites of fipronil (AccuStandard; New Haven, CT, USA), ethiprole (Sigma; St. Louis, MO, USA), and BSA were conjugated to carboxylic acid-coated magnetic beads as described above and served as immobilized negative targets. The selection process for negative Rounds 2–6 were performed similarly to positive Rounds 1–6, but unbound ssDNA molecules were instead retrieved and amplified.

Free fipronil was introduced in Round 7 positive and used for competitive elution. Competitive elution with the free target was performed to ensure the library does not bind to the immobilizing substrate, or the target only when it is immobilized. The incubation process was performed as positive Rounds 1–6, but free fipronil at a concentration of 500 μM in 1× selection buffer/0.5% methanol was used to elute ssDNA molecules bound to IT. The solution containing ssDNA bound to free fipronil was retrieved, and served as PCR template. The process was performed for positive Rounds 7–12, each with decreasing incubation time and free fipronil concentrations. For negative Rounds 7–11, similar competitive elutions were performed with free negative targets in solution. However, beads were retained, resuspended in selection buffer, and ssDNA bound to IT were amplified by PCR.

### 3.2. Cloning and Sequencing of the Fipronil-Binding MREs

The ssDNA library of post Rounds 3 negative, 6 negative, 9 negative and 12 positive, were cloned into competent *E. coli* cells, and plasmid DNA was extracted and analyzed for the enrichment of consensus binding sequences. These procedures were performed identically to as previously described [24–26]. A total of thirty to sixty randomly selected sequences from each listed round was analyzed.

### 3.3. Fipronil-Binding MREs Binding Assays in Selection Buffer

One candidate sequence designated as R12.51 from the round 12 sequences was selected for further characterization. The Mfold DNA web server was used for R12.51 secondary structure prediction with parameter settings at the ionic conditions of 1× selection buffer at 25 °C [27]. R12.51 was commercially synthesized with a 5′ FAM modification for the use of fluorescence saturation plate-based binding assay (Eurofins MWG Operon; Huntsville, AL, USA).

Fluorescence saturation plated-based binding assay was modified from previously described bead-based binding assays [24–26]. Concentrations of 0, 10, 20, 40, 60, 100, 500, and 1000 nM MRE were used in saturation binding assays. A 100 μL sample of 10 μM Fipronil in phosphate buffer solution was added to wells of a maleic anhydride activated 96-well microplate (Pierce; Rockford, IL, USA) and incubated with shaking at room temperature overnight. Following this preparation, each well was then blocked and washed with 200 μL of 1× selection buffer for 3 times, 10 min for each wash. FAM-labeled MRE of each concentration in a 100 μL total volume of 1× selection buffer was incubated with each well for five minutes. Unbound MRE was removed and each well was washed five times with 200 μL of 1× selection buffer, then 0.1 M of sodium hydroxide was added to each well to elute bound MRE. Eluted ssDNA was placed in a 96-well microplate and measured in a FLx800 microplate reader with excitation at 490 nm and emission at 520 nm (Biotek US, Winooski, VT, USA). All fluorescent readings on the plate were normalized to 100 μL of a 1 nM FAM-MRE in selection buffer with 0.1 M of sodium hydroxide. For each concentration set, a negative control was performed with wells containing no fipronil. Each set of concentrations were performed in triplicate. Three independent assays were performed as described above. GraphPad Prism 3 (GraphPad Software; La Jolla, CA, USA) was utilized to analyze the data and determine the dissociation constant ($K_d$) of the MRE using nonlinear regression analysis and fit as previously described [24–26] Additional binding assay with concentrations of 0.5, 1, 5, 10, 15, 20, 40, 60, 100, 500, 1000, 2000, 5000, and 10,000 nM MRE were used. Assay was performed as

described above. GraphPad Prism 3 was utilized to analyze the data and determine the dissociation constant ($K_d$) of the MRE using nonlinear regression analysis and fit as described above, and the goodness of fit was determined with nonlinear regression sigmoidal analysis.

To determine the binding of R12.51 to negative targets used in the selection, fipronil was immobilized and microplate wells were washed and blocked exactly as described above. A 100 µL sample of 500 nM FAM-labeled MRE was added to each well for five minutes. Unbound MRE was removed and each well was washed as described above. Then, each well was incubated with 100 µL of 1 µM of the following in 1× selection buffer: fipronil sulfone, fipronil sulfide, fipronil desulfinyl, ethiprole, atrazine, propanil, malathion, BSA and in 1× selection buffer only. An incubation without MRE added and with fipronil as the eluent served as a normalization control. Each eluent solution was first incubated with the immobilized target for fifteen minutes, and then recovered. As described above, the solution was placed in a 96-well plate and the fluorescence was measured. Data were normalized to an internal fluorescent standard of 1nM FAM-labeled MRE and then the no-MRE control was subtracted as previously described [24–26]. Each set of specific binding studies were performed in triplicate. Data was averaged and standard deviation was calculated. A one-tailed student *t*-test was used to determine the statistical significance in difference of the means ($p < 0.05$).

### 3.4. Fipronil Cross-Binding Assay in River Water

To determine the binding of R12.51 to negative targets in river water, the experiment was performed similar to cross-binding assays performed in 1× selection buffer with minor modifications. River water was collected from the Susquehanna River at GPS coordinates 41°15′03.0″ N 75°53′04.8″ W. River water was first decanted to remove visible debris. It was then push-filtered through a 0.2 micron filter paper. An equal volume of 2× selection buffer was mixed with the prepared river water. Fipronil and all the negative targets were prepared in river water/buffer mix at 200 nM. Procedures and data analysis were performed as described in Section 3.3.

### 3.5. Fipronil Detection Assay in River Water

A proof-of-principle plate-based detection assay utilizing R12.51 was developed and modified from a previously described assay [48]. Fipronil was immobilized and microplate wells were washed and blocked exactly as described in Section 3.3. A 100 µL sample of 500 nM FAM-labeled MRE was added to each well for five minutes. Unbound MRE was removed and each well was washed as described above. Concentrations of 0, 5, 10, 25, 50, 100, 200, and 500 nM fipronil were used in detection assays. Varying concentrations of fipronil were spiked into the river water/buffer mix and subsequently added to each prepared well for fifteen minutes. The solution of each well was retrieved and fluorescence measurements were recorded as described in Section 3.3. Negative controls were wells without FAM-MRE and wells without immobilized fipronil. Three parallel experiments were performed. GraphPad Prism 3 was utilized to analyze the data and determine the $R^2$ value with linear regression analysis. The limit of detection (LOD) was calculated as described by Armbruster et al. [41].

## 4. Conclusions

This study utilized a variant of SELEX methodology to identify a novel, broad-spectrum molecular recognition element that binds strongly to fipronil, its major metabolites and a structurally related pesticide. The MRE binds with a nanomolar equilibrium dissociation constant and is selective over structurally unrelated herbicides and pesticides that are found in the same environments as fipronil. Additionally, a proof-of-principle, plate-based fluorescent detection assay was developed and successfully used to detect fipronil in artificially contaminated river water samples. The results show the potential of utilizing this ssDNA MRE in biosensing applications, such as those described by Madianos et al. [46].

**Acknowledgments:** This work was supported by National Science Foundation Cooperative Agreements (NSF-1003907 and NSF-0554328), Department of Defense Cooperative Agreement (W911NF-09-2-0044), West Virginia University and Wilkes University, Department of Pharmaceutical Sciences. The authors would like to thank Ryan M. Williams for providing SELEX experiment training to Ka L. Hong.

**Author Contributions:** Ka L. Hong planned and performed experiments, analyzed data, provided the resources for the experiments, and wrote the manuscript. Letha J. Sooter designed the project, planned experiments, analyzed data, provided the resources for the experiments, and wrote the manuscript.

**Conflicts of Interest:** The authors declare no conflict of interest.

## Abbreviations

| | |
|---|---|
| MRE | Molecular Recognition Element |
| BSA | Bovine Serum Albumin |
| IS | Immobilizing Substrate |
| IT | Immobilized Target |
| LOD | Limit of Detection |

## References

1. U.S. Environmental Protection Agency, Office of Prevention. *New-Pesticide Fact. Sheet—Fipronil*; Pesticides and Toxic Substances, Office of Pesticide Programs, U.S. Government Printing Office: Washington, DC, USA, 1996; pp. 1–10.
2. Caboni, P.; Sammelson, R.E.; Casida, J.E. Phenylpyrazole insecticide photochemistry, metabolism, and gabaergic action: Ethiprole compared with fipronil. *J. Agric. Food Chem.* **2003**, *51*, 7055–7061. [CrossRef] [PubMed]
3. Stone, W.W.; Gilliom, R.J.; Ryberg, K.R. Pesticides in U.S. Streams and rivers: Occurrence and trends during 1992–2011. *Environ. Sci. Technol.* **2014**, *48*, 11025–11030. [CrossRef] [PubMed]
4. Moran, K.D. *Urban Use of the Insecticide Fipronil—Water Quality Implications*; TDC Environmental: San Mateo, CA, USA, 2007; pp. 1–14.
5. Simon-Delso, N.; Amaral-Rogers, V.; Belzunces, L.P.; Bonmatin, J.M.; Chagnon, M.; Downs, C.; Furlan, L.; Gibbons, D.W.; Giorio, C.; Girolami, V.; et al. Systemic insecticides (neonicotinoids and fipronil): Trends, uses, mode of action and metabolites. *Environ. Sci. Pollut. Res. Int.* **2015**, *22*, 5–34. [CrossRef] [PubMed]
6. Aquatic Life Benchmarks and Ecological Risk Assessments for Registered Pesticides. Available online: https://www.epa.gov/pesticide-science-and-assessing-pesticide-risks/aquatic-life-benchmarks-and-ecological-risk#benchmarks (accessed on 30 October 2017).
7. Chau, N.D.; Sebesvari, Z.; Amelung, W.; Renaud, F.G. Pesticide pollution of multiple drinking water sources in the mekong delta, vietnam: Evidence from two provinces. *Environ. Sci. Pollut. Res. Int.* **2015**, *22*, 9042–9058. [CrossRef] [PubMed]
8. Weston, D.P.; Lydy, M.J. Toxicity of the insecticide fipronil and its degradates to benthic macroinvertebrates of urban streams. *Environ. Sci. Technol.* **2014**, *48*, 1290–1297. [CrossRef] [PubMed]
9. Bonmatin, J.M.; Giorio, C.; Girolami, V.; Goulson, D.; Kreutzweiser, D.P.; Krupke, C.; Liess, M.; Long, E.; Marzaro, M.; Mitchell, E.A.; et al. Environmental fate and exposure; neonicotinoids and fipronil. *Environ. Sci. Pollut. Res. Int.* **2015**, *22*, 35–67. [CrossRef] [PubMed]
10. U.S. Environmental Protection Agency, Healthy Effects Division. *Fipronil: Third Reevaluation—Report of the Hazard Identification Assessment Review Committee*; U.S. Government Printing Office: Washington, DC, USA, 2000; pp. 1–24.
11. Li, P.; Akk, G. The insecticide fipronil and its metabolite fipronil sulphone inhibit the rat $\alpha1\beta2\gamma2l$ GABAA receptor. *Br. J. Pharmacol.* **2008**, *155*, 783–794. [CrossRef] [PubMed]
12. Van der Sluijs, J.P.; Amaral-Rogers, V.; Belzunces, L.P.; van Bijleveld Lexmond, M.F.; Bonmatin, J.M.; Chagnon, M.; Downs, C.A.; Furlan, L.; Gibbons, D.W.; Giorio, C.; et al. Conclusions of the worldwide integrated assessment on the risks of neonicotinoids and fipronil to biodiversity and ecosystem functioning. *Environ. Sci. Pollut. Res. Int.* **2015**, *22*, 148–154. [CrossRef] [PubMed]

13. Bichon, E.; Richard, C.A.; Le Bizec, B. Development and validation of a method for fipronil residue determination in ovine plasma using 96-well plate solid-phase extraction and gas chromatography-tandem mass spectrometry. *J. Chromatogr. A* **2008**, *1201*, 91–99. [CrossRef] [PubMed]
14. Duhan, A.; Kumari, B.; Duhan, S. Determination of residues of fipronil and its metabolites in cauliflower by using gas chromatography-tandem mass spectrometry. *Bull. Environ. Contam. Toxicol.* **2015**, *94*, 260–266. [CrossRef] [PubMed]
15. Jimenez, J.J.; Bernal, J.L.; del Nozal, M.J.; Martin, M.T.; Mayo, R. Sample preparation methods to analyze fipronil in honey by gas chromatography with electron-capture and mass spectrometric detection. *J. Chromatogr. A* **2008**, *1187*, 40–45. [CrossRef] [PubMed]
16. Lacroix, M.Z.; Puel, S.; Toutain, P.L.; Viguie, C. Quantification of fipronil and its metabolite fipronil sulfone in rat plasma over a wide range of concentrations by LC/UV/MS. *J. Chromatogr. B Anal. Technol. Biomed. Life Sci.* **2010**, *878*, 1934–1938. [CrossRef] [PubMed]
17. Liu, X.; Yan, C.; Dong, J.; Yu, X.; Xu, D. Poly- and monoclonal antibody-based elisas for fipronil. *J. Agric. Food Chem.* **2007**, *55*, 226–230. [CrossRef] [PubMed]
18. Mohamed, F.; Senarathna, L.; Percy, A.; Abeyewardene, M.; Eaglesham, G.; Cheng, R.; Azher, S.; Hittarage, A.; Dissanayake, W.; Sheriff, M.H.; et al. Acute human self-poisoning with the *N*-phenylpyrazole insecticide fipronil—A GABAA-gated chloride channel blocker. *J. Toxicol. Clin. Toxicol.* **2004**, *42*, 955–963. [CrossRef] [PubMed]
19. Vasylieva, N.; Ahn, K.C.; Barnych, B.; Gee, S.J.; Hammock, B.D. Development of an immunoassay for the detection of the phenylpyrazole insecticide fipronil. *Environ. Sci. Technol.* **2015**, *49*, 10038–10047. [CrossRef] [PubMed]
20. Bordeaux, J.; Welsh, A.; Agarwal, S.; Killiam, E.; Baquero, M.; Hanna, J.; Anagnostou, V.; Rimm, D. Antibody validation. *Biotechniques* **2010**, *48*, 197–209. [CrossRef] [PubMed]
21. Mairal, T.; Ozalp, V.C.; Lozano Sanchez, P.; Mir, M.; Katakis, I.; O'Sullivan, C.K. Aptamers: Molecular tools for analytical applications. *Anal. Bioanal. Chem.* **2008**, *390*, 989–1007. [CrossRef] [PubMed]
22. Tuerk, C.; Gold, L. Systematic evolution of ligands by exponential enrichment: RNA ligands to bacteriophage T4 DNA polymerase. *Science* **1990**, *249*, 505–510. [CrossRef] [PubMed]
23. Hong, K.L.; Yancey, K.; Battistella, L.; Williams, R.M.; Hickey, K.M.; Bostick, C.D.; Gannett, P.M.; Sooter, L.J. Selection of single-stranded DNA molecular recognition elements against exotoxin a using a novel decoy-selex method and sensitive detection of exotoxin a in human serum. *BioMed Res. Int.* **2015**, *2015*, 417641. [CrossRef] [PubMed]
24. Williams, R.M.; Kulick, A.R.; Yedlapalli, S.; Battistella, L.; Hajiran, C.J.; Sooter, L.J. In vitro selection of a single-stranded DNA molecular recognition element specific for bromacil. *J. Nucleic Acids* **2014**, *2014*, 102968. [CrossRef] [PubMed]
25. Williams, R.M.; Crihfield, C.L.; Gattu, S.; Holland, L.A.; Sooter, L.J. In vitro selection of a single-stranded DNA molecular recognition element against atrazine. *Int. J. Mol. Sci.* **2014**, *15*, 14332–14347. [CrossRef] [PubMed]
26. Williams, R.M.; Maher, E.; Sooter, L.J. In vitro selection of a single-stranded DNA molecular recognition element for the pesticide malathion. *Comb. Chem. High Throughput Screen.* **2014**, *17*, 694–702. [CrossRef] [PubMed]
27. Zuker, M. Mfold web server for nucleic acid folding and hybridization prediction. *Nucleic Acids Res.* **2003**, *31*, 3406–3415. [CrossRef] [PubMed]
28. Connell, G.J.; Illangesekare, M.; Yarus, M. Three small ribooligonucleotides with specific arginine sites. *Biochemistry* **1993**, *32*, 5497–5502. [CrossRef] [PubMed]
29. Ellington, A.D.; Khrapov, M.; Shaw, C.A. The scene of a frozen accident. *RNA* **2000**, *6*, 485–498. [CrossRef] [PubMed]
30. Hall, B.; Hesselberth, J.R.; Ellington, A.D. Computational selection of nucleic acid biosensors via a slip structure model. *Biosens. Bioelectron.* **2007**, *22*, 1939–1947. [CrossRef] [PubMed]
31. Lozupone, C.; Changayil, S.; Majerfeld, I.; Yarus, M. Selection of the simplest RNA that binds isoleucine. *RNA* **2003**, *9*, 1315–1322. [CrossRef] [PubMed]
32. Majerfeld, I.; Yarus, M. Isoleucine: RNA sites with associated coding sequences. *RNA* **1998**, *4*, 471–478. [PubMed]

33. Alsager, O.A.; Kumar, S.; Willmott, G.R.; McNatty, K.P.; Hodgkiss, J.M. Small molecule detection in solution via the size contraction response of aptamer functionalized nanoparticles. *Biosens. Bioelectron.* **2014**, *57*, 262–268. [CrossRef] [PubMed]
34. Mehta, J.; Rouah-Martin, E.; van Dorst, B.; Maes, B.; Herrebout, W.; Scippo, M.L.; Dardenne, F.; Blust, R.; Robbens, J. Selection and characterization of PCB-binding DNA aptamers. *Anal. Chem.* **2012**, *84*, 1669–1676. [CrossRef] [PubMed]
35. Nguyen, V.T.; Kwon, Y.S.; Kim, J.H.; Gu, M.B. Multiple go-selex for efficient screening of flexible aptamers. *Chem. Commun.* **2014**, *50*, 10513–10516. [CrossRef] [PubMed]
36. Hong, K.L.; Battistella, L.; Salva, A.D.; Williams, R.M.; Sooter, L.J. In vitro selection of single-stranded DNA molecular recognition elements against *S. aureus* α toxin and sensitive detection in human serum. *Int. J. Mol. Sci.* **2015**, *16*, 2794–2809. [CrossRef] [PubMed]
37. Hong, K.L.; Maher, E.; Williams, R.M.; Sooter, L.J. In vitro selection of a single-stranded DNA molecular recognition element against clostridium difficile toxin B and sensitive detection in human fecal matter. *J. Nucleic Acids* **2015**, *2015*, 808495. [CrossRef] [PubMed]
38. Department of Environmental Protection, Commonwealth of Pennsylvania. *2012–2013 Susquehanna River Sampling and Assessment Report*; Commonwealth of Pennsylvania: Harrisburg, PA, USA, 2014; pp. 1–147.
39. Miyakawa, S.; Nomura, Y.; Sakamoto, T.; Yamaguchi, Y.; Kato, K.; Yamazaki, S.; Nakamura, Y. Structural and molecular basis for hyperspecificity of RNA aptamer to human immunoglobulin G. *RNA* **2008**, *14*, 1154–1163. [CrossRef] [PubMed]
40. Tingle, C.C.; Rother, J.A.; Dewhurst, C.F.; Lauer, S.; King, W.J. Fipronil: Environmental fate, ecotoxicology, and human health concerns. *Rev. Environ. Contam. Toxicol.* **2003**, *176*, 1–66. [PubMed]
41. Armbruster, D.A.; Pry, T. Limit of blank, limit of detection and limit of quantitation. *Clin. Biochem. Rev.* **2008**, *29*, S49–S52. [PubMed]
42. Miyake, S.; Uchigashima, M.; Kadowaki, A. Kit for Measurement of Termite Insecticide Active Ingredient by Immunoassay Method. U.S. Patent 8,323,904 B2, 4 December 2012.
43. Fan, L.; Zhao, G.; Shi, H.; Liu, M.; Li, Z. A highly selective electrochemical impedance spectroscopy-based aptasensor for sensitive detection of acetamiprid. *Biosens. Bioelectron.* **2013**, *43*, 12–18. [CrossRef] [PubMed]
44. Wang, L.; Chen, W.; Ma, W.; Liu, L.; Ma, W.; Zhao, Y.; Zhu, Y.; Xu, L.; Kuang, H.; Xu, C. Fluorescent strip sensor for rapid determination of toxins. *Chem. Commun.* **2011**, *47*, 1574–1576. [CrossRef] [PubMed]
45. Barthelmebs, L.; Jonca, J.; Hayat, A.; Prieto-Simon, B.; Marty, J.-L. Enzyme-linked aptamer assays (ELAAs), based on a competition format for a rapid and sensitive detection of ochratoxin a in wine. *Food Control* **2011**, *22*, 737–743. [CrossRef]
46. Madianos, L.; Tsekenis, G.; Skotadis, E.; Patsiouras, L.; Tsoukalas, D. A highly sensitive impedimetric aptasensor for the selective detection of acetamiprid and atrazine based on microwires formed by platinum nanoparticles. *Biosens. Bioelectron.* **2018**, *101*, 268–274. [CrossRef] [PubMed]
47. Bujacz, A. Structures of bovine, equine and leporine serum albumin. *Acta Crystallogr. Sect. D Biol. Crystallogr.* **2012**, *68*, 1278–1289. [CrossRef] [PubMed]
48. De-Los-Santos-Álvarez, N.; Lobo-Castañón, M.J.; Miranda-Ordieres, A.J.; Tuñón-Blanco, P. Modified-RNA aptamer-based sensor for competitive impedimetric assay of neomycin B. *J. Am. Chem. Soc.* **2007**, *129*, 3808–3809. [CrossRef] [PubMed]


International Journal of
*Molecular Sciences*

MDPI

*Article*

# Selection and Characterization of a DNA Aptamer Specifically Targeting Human HECT Ubiquitin Ligase WWP1

**Wesley O. Tucker, Andrew B. Kinghorn, Lewis A. Fraser, Yee-Wai Cheung and Julian A. Tanner ***

School of Biomedical Sciences, Li Ka Shing Faculty of Medicine, The University of Hong Kong, 21 Sassoon Road, Hong Kong, China; wtucker@hku.hk (W.O.T.); kinghorn@hku.hk (A.B.K.); lewis-fraser@hku.hk (L.A.F.); cheungw@hku.hk (Y.-W.C.)

* Correspondence: jatanner@hku.hk; Tel.: +852-3917-9472

Received: 5 January 2018; Accepted: 2 March 2018; Published: 7 March 2018

**Abstract:** Nucleic acid aptamers hold promise as therapeutic tools for specific, tailored inhibition of protein targets with several advantages when compared to small molecules or antibodies. Nuclear WW domain containing E3 ubiquitin ligase 1 (WWP1) ubiquitin ligase poly-ubiquitinates Runt-related transcription factor 2 (Runx2), a key transcription factor associated with osteoblast differentiation. Since WWP1 and an adapter known as Schnurri-3 are negative regulators of osteoblast function, the disruption of this complex has the potential to increase bone deposition for osteoporosis therapy. Here, we develop new DNA aptamers that bind and inhibit WWP1 then investigate efficacy in an osteoblastic cell culture. DNA aptamers were selected against three different truncations of the HECT domain of WWP1. Aptamers which bind specifically to a C-lobe HECT domain truncation were observed to enrich during the selection procedure. One particular DNA aptamer termed C3A was further evaluated for its ability to bind WWP1 and inhibit its ubiquitination activity. C3A showed a low μM binding affinity to WWP1 and was observed to be a non-competitive inhibitor of WWP1 HECT ubiquitin ligase activity. When SaOS-2 osteoblastic cells were treated with C3A, partial localization to the nucleus was observed. The C3A aptamer was also demonstrated to specifically promote extracellular mineralization in cell culture experiments. The C3A aptamer has potential for further development as a novel osteoporosis therapeutic strategy. Our results demonstrate that aptamer-mediated inhibition of protein ubiquitination can be a novel therapeutic strategy.

**Keywords:** aptamer; SELEX; ubiquitin ligase; WWP1; targeted drug delivery

## 1. Introduction

In mammalian bone, the osteoblast is exclusively responsible for the deposition of bone matrix in the form of hydroxyapatite crystals together with various structural proteins [1]. The osteoblast lineage is largely controlled by Runx2 (Runt–related transcription factor 2/CBFA1/PEBP2αA), often considered the "master regulator" of osteoblast differentiation [2]. The importance of Runx2 is illustrated by observations that Runx2 null mice cannot produce mineralized bone due to a lack of early stage osteoblasts [3]. The Nedd4 family HECT ('Homologous to the E6-AP Carboxyl Terminus') domain E3 ligase WWP1, in complex with an adapter Schnurri-3 (Shn3), ubiquitinates Runx2 thus leading to its degradation and reduction of osteoblast-mediated bone matrix synthesis [2]. WWP1 and Shn3 proteins negatively regulate Runx2 at the protein level, hence are promising targets to stimulate osteoblast differentiation, and by extension, higher bone mass in osteoporosis patients [4,5]. Human WWP1 was discovered in 1997 and contains an independently active HECT domain (Homologous to the E6-AP carboxyl terminus) which has its crystal structure solved [6–8]. WWP1 is structurally

and functionally characterized, is readily "expressible" in *E. coli*, and inhibition of WWP1 to maintain Runx2 levels is a promising therapeutic strategy to stimulate osteoblast function.

Nucleic acid aptamers are short, single-stranded nucleic acid chains evolved to bind specifically to a given target. Riboswitches can be considered as natural non-coding RNA aptamers which regulate gene expression upon binding a metabolic target [9]. Since 1990, aptamers have been created in the laboratory using a process known as Systematic Evolution of Ligands by Exponential Enrichment (SELEX) [10,11]. First, a large pool of random sequences (~$10^{15}$) is exposed to a target, washed to exclude non-binding species, and eluted to recover binding species. Second, the pool is PCR amplified by having included 3′ and 5′ primer binding regions. Finally, the sequences are enriched by repeating the process successively while introducing increased stringency (i.e., more rigorous washing conditions and counter-selections of related targets). The SELEX iterations are continued until enriched pools of homologous sequences are revealed, which then hold the potential to be tightly binding and specific [10,11]. Aptamers often bind to their targets with $K_D$ values in the μM to nM range with aptamer affinity maturation developed to increase affinity and specificity [12]. Aptamers have secondary structure including hairpins, loops, pseudoknots, triplexes, and quadruplexes [13–15]. SELEX can be applied to a wide variety of targets ranging from small molecules to cells [16,17]. Due to these complexities and features, aptamers are sometimes compared and contrasted with both antibodies and small molecules for use as therapeutics [18,19], diagnostics [20–22], and laboratory tools [23]. Importantly, recent work has demonstrated methods that lower the cost of single stranded oligonucleotide synthesis by several orders of magnitude [24].

Aptamers have traditionally focused on extracellular targets. However, polynucleotides such as aptamers can enter the intracellular space by either: (1) extraneous means such as liposomes, polymers, viruses, microinjection, electroporation, particle bombardment, calcium phosphate precipitation and ultrasound, or by (2) inherent mechanisms such as endocytosis or pinocytosis [25–28]. Using cationic reagents, aptamers can be transfected as is commonly practiced with plasmids. Naked DNA, without the company of reagents, does enter the cell to some degree in spite of electrostatic repulsion, as was demonstrated when internalized plasmids were found to express proteins [29]. Uptake depends both on temperature and oligonucleotide length [30]. It has also been found that two putative cell surface receptors are specific to oligonucleotides generally [31]. More recently, aptamers have been conjugated to moieties to bind an internalizing receptor, or may be selected to bind the internalizing receptor themselves [26,32]. Approximately 19,000 DNA molecules can be internalized by one cell once cationic lipoplexes have fused with the anionic plasma membrane [33]. Aptamers can also be transcribed directly in the cell, this type of aptamer has been coined an "intramer" [34–36].

Previously, our group selected aptamers which bind and inhibit the activity of the extracellular protein sclerostin, which is a known negative regulator of bone formation [19]. Here, we investigate an alternative intracellular strategy where the intracellular protein WWP1 is targeted with a DNA aptamer. Herein we select and characterize DNA aptamers against the HECT domain of WWP1. We investigate aptamer binding to its target, specific inhibition of its function, observe localization, and evaluate efficacy in SaOS-2 osteoblastic cells.

## 2. Results

### *2.1. Strategy to Select DNA Aptamers against HECT Domain of WWP1*

As it is not possible to express the full length WWP1 protein in *E. coli*, truncations of the smaller yet active HECT domain were used as the targets for aptamer selection. The HECT domain has two lobes: the N-lobe is involved in E2 binding and the C-lobe is important in ubiquitination [8]. Rotation around a hinge between the two lobes is critical to WWP1 ubiquitin ligation activity [8], hence the HECT domain is central to WWP1 function.

As shown in Figure 1A, we expressed and purified three WWP1 truncations for use as targets in our aptamer selections: the entire HECT domain, the N-lobe of the HECT domain and the C-lobe of the HECT domain.

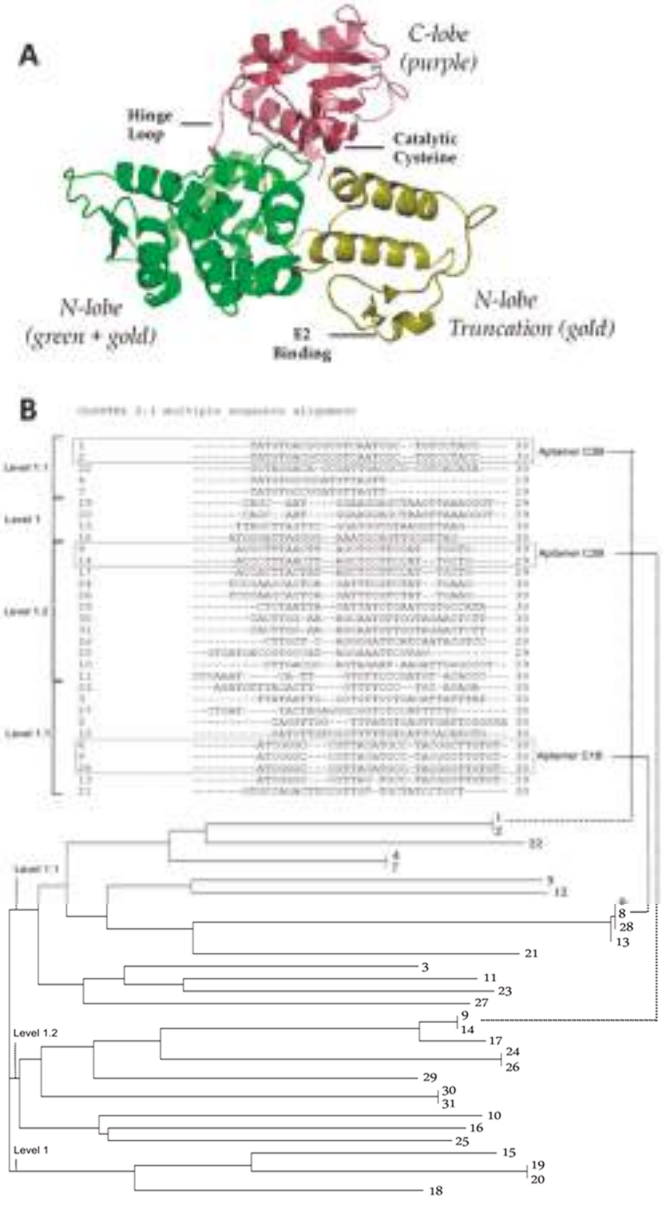


**Figure 1.** Structure of WWP1 HECT domain target and selected pool. (**A**) WWP1 HECT structure as generated by pyMOL with functionally important regions labeled; (**B**) Variable regions of the enriched pool for C-lobe with the three most abundant groups of identical sequences are boxed (C1–C3 where B indicates without constant regions), and phylogenetic tree of sequenced aptamers showing inter familial relationships.

To begin, we used the entire HECT domain for the first 8 rounds of DNA aptamer selection. Important to its inhibition, HECT domain requires a flexible hinge loop, the binding of an E2 adapter, and a catalytic cysteine residue for activity (Figure 1A). We then proceeded to lobe-specific selections to target particular functional regions more specifically. To further increase specificity as well as stringency, C-lobe selections included N-lobe counter selections, N-lobe selections included C-lobe counter selections, and HECT selections included ubiquitin as a general protein counter selection. During the sequencing of pools throughout the process, the C-lobe pools proved to enrich promisingly, while HECT and N-lobe selections did not enrich. This indicated that DNA aptamers had been selected in the initial rounds that likely bind to the C-lobe of the HECT domain.

We performed 4 further SELEX lobe-specific rounds (after the 8 round HECT domain pre-enrichment). Cloning and sequencing identified 31 aptamer sequences against the C-lobe truncation (Figure 1B), annotated as C#A when constant region is included and C#B without. The relationships between the variable regions is somewhat scattered—C3 is more closely related to C1 while C2 is completely unrelated. These three sequences were chosen to move forward in the project due to their higher copy number in sequencing data.

To compare the predicted secondary structures of the three aptamers, mFold software (version 2.3, The RNA Institute, State University of New York at Albany, Albany, NY, USA) was used (Figure 2). The structure of the variable region mirrors that of its full-length counterpart for aptamer C1, but not for C2 and C3; possibly indicating that full length is required for C2 and C3 binding (Figure 2). Experiments were therefore carried out subsequently with constant regions included (indicated by the A suffix).

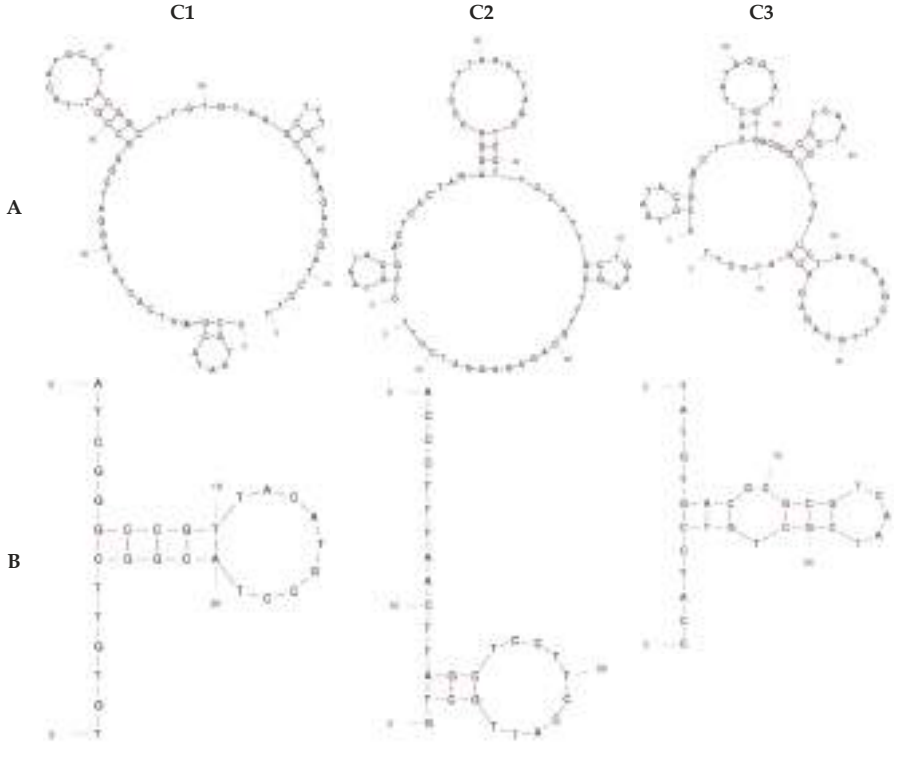


**Figure 2.** Predicted 2D secondary structures for C-lobe aptamers using mFold software comparing full length (**A**) with variable region (**B**) simulated at 150 mM NaCl and 25 °C.

### *2.2. Determination of Binding Affinity of DNA Aptamers Binding to HECT Domain*

We next investigated the relative affinity of the DNA aptamers for the protein target relative to control. To demonstrate qualitative binding of the C-lobe aptamers to our recombinant HECT, Electrophoretic Mobility Shift Assay (EMSA) was employed (Figure 3). EMSA is a hallmark method for characterization of protein-nucleic acid binding. However, EMSA has shortcomings such as complexes differing in stability depending on the gel medium and secondary binding confusing the magnitude of the binding of interest. Thus, we view EMSA here as a relative and semi-quantitative characterization of binding. The full-length aptamers C1A–C3A (the A indicating inclusion of the constant flanking region) were incubated with a range of HECT concentrations then analyzed by PAGE electrophoresis (Figure 3A), and the resultant band intensities were plotted (Figure 3B). Aptamer bound to protein remains at the top of the gel, while free aptamer migrates normally. Of the three C-lobe aptamers, C3A showed the strongest binding affinity. We observed that C3A shows a multimeric band above its monomer band also, which may imply a multimer in equilibrium with the monomer (74 bp). A $K_D$ roughly in the low μM range was estimated for aptamer C3A, while other C-lobe aptamers and controls did not produce an inflection point with which to base a determination but with clearly weaker binding. Therefore, in later experiments we focused on aptamer C3A as the most promising of the three aptamer candidates.

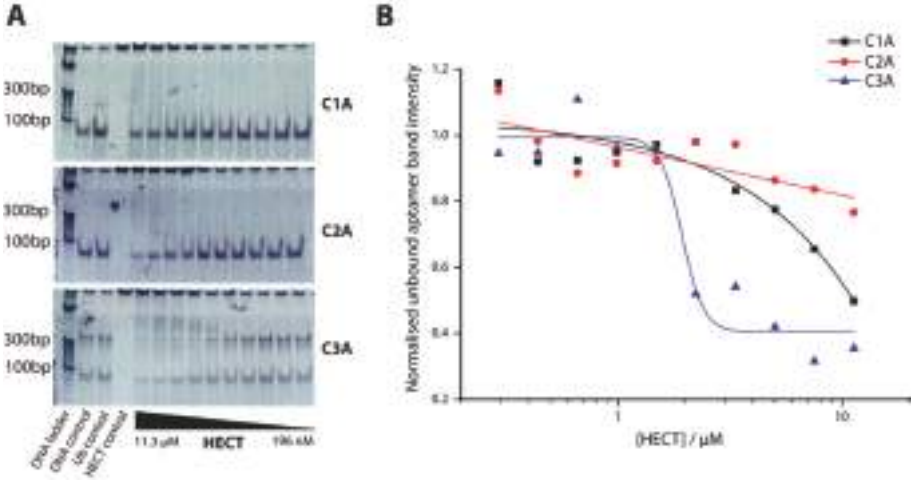


**Figure 3.** Determination of $K_D$ for aptamers using electrophoretic mobility shift assay (EMSA) for aptamers C1A, C2A, and C3A. (**A**) 10% PAGE gels showing bound (upper bands) versus unbound (lower bands) aptamer; (**B**) Plot of HECT concentration versus normalized band intensity (unbound) with a one-site binding fit from representative data in Figure 3A.

### *2.3. Determination of C-Lobe DNA Aptamer-Mediated Inhibition of Ubiquitination Activity of HECT Domain*

The HECT domain's ability to self-ubiquitinate with the requirement of an E1 and E2 protein in vitro provides an approach to observe the kinetics of HECT domain activity. When the HECT domain is ubiquitinated, the HECT domain-ubiquitin conjugate is observed by SDS-PAGE appearing several kilodaltons above HECT and can be used for quantitation (Figure 4C). We used this assay to generate Michaelis-Menten curves between aptamers C1A–C3A which implicates aptamer C3A as the strongest inhibitor of the three (Figure 4A).

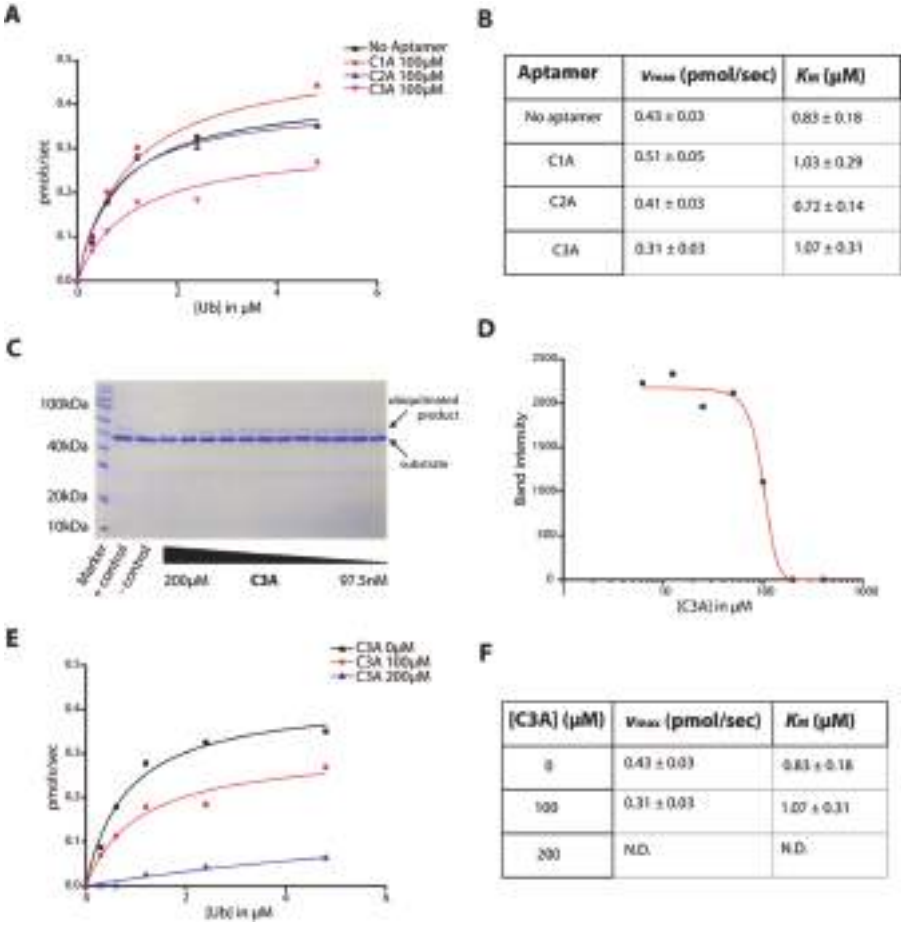


| Aptamer | $V_{max}$ (pmol/sec) | $K_M$ (μM) |
|---|---|---|
| No aptamer | 0.43 ± 0.03 | 0.83 ± 0.18 |
| C1A | 0.51 ± 0.05 | 1.03 ± 0.29 |
| C2A | 0.41 ± 0.03 | 0.72 ± 0.14 |
| C3A | 0.31 ± 0.03 | 1.07 ± 0.31 |

| [C3A] (μM) | $V_{max}$ (pmol/sec) | $K_M$ (μM) |
|---|---|---|
| 0 | 0.43 ± 0.03 | 0.83 ± 0.18 |
| 100 | 0.31 ± 0.03 | 1.07 ± 0.31 |
| 200 | N.D. | N.D. |

**Figure 4.** Aptamer mediated inhibition of HECT ubiquitination. (**A**) Rate of reaction product formation plotted against ubiquitin concentration (Michaelis-Menten) for aptamers C1A–C3A to compare inhibition rates between aptamers from representative gel data. (**B**) Resultant $V_{max}$ and $K_M$ values from the Michaelis-Menten plot. (**C**) 12% SDS-PAGE gel showing the reaction product over increasing C3A concentrations; (**D**) Logarithmic plot of C3A aptamer concentration to band intensity as measured to determine $IC_{50}$ from representative gel data (**E**) Michaelis-Menten plot of two different C3A concentrations for determination of mode of inhibition from representative gel data. (**F**) Summary of $V_{max}$ and $K_M$ values tabulated for the two C3A concentrations.

The resulting $v_{max}$ and $K_M$ are tabulated in Figure 4B and reconfirms aptamer C3A as the strongest inhibitor. This result is also consistent with our observations of aptamer binding in Figure 3. Figure 4C shows the ubiquitination assay on an example gel over a series of aptamer C3A concentrations, where substrate and reaction product are labeled (residual ubiquitin (~10 kD) and E2 (~10 kD) can also be seen). The plot of C3A concentration to band intensity of reaction product (Figure 4D) determines an $IC_{50}$ of approximately 100 μM. To determine mode of inhibition, two different C3A concentrations were tested (100 μM and 200 μM) while varying the concentration of ubiquitin substrate to determine $K_M$ and $v_{max}$ as shown in Figure 4E,F. The presence of the inhibitor caused a significant reduction in

the apparent $v_{max}$ while the apparent $K_M$ remained similar. These results imply that the aptamer acts as a non-competitive inhibitor of ubiquitination.

### *2.4. Cellular Localization, Runx2 Levels, and Bone Mineralization in Saos-2 Osteoblastic Cells*

Fixed and stained SaOS-2 cells were imaged after the transfection process to investigate differences in localization. These stained images were used to compare aptamer C3A and control, both with and without transfection reagent as shown in Figure 5A. Although the images are overexposed, we were able to gain information about the relative abundance of aptamer in the cytoplasm versus nucleus. In this representative example, aptamer C3A without transfection (CN) appears to enter the cell, but appears mostly proximal to the nucleus, whereas aptamer C3A with transfection (CT) seems to localize both in the nucleus and cytosol.

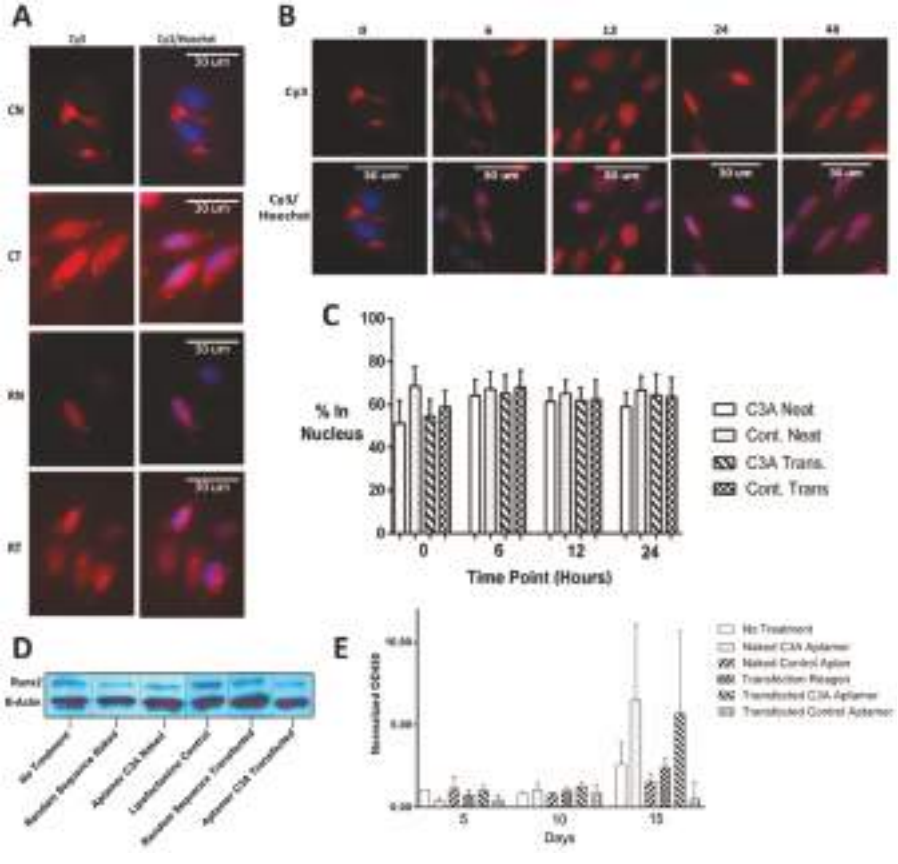


**Figure 5.** Aptamer C3A localization, and effect on Runx2 levels and bone mineralization in SaOS-2 cells. (**A**) Aptamer (Cy3) nucleus (Hoechst) overlays where: RN—random sequence control without transfection, RT—random sequence control with transfection, CN—aptamer C3A without transfection, and CT—aptamer C3A with transfection; (**B**) Aptamer and nucleus overlays over time points in hours; (**C**) Quantitative assessment of nuclear localization using MetaMorph™ software for transfected or naked (labeled as "NEAT") aptamer C3A and random sequence control; (**D**) Western Blot of Runx2 performed on SaOS-2 cell extracts; (**E**) Quantitation of extracellular matrix deposition over time using Alizarin Red assay.

After determining that aptamer enters the cells without transfection reagent, we compared localization over time by incubating aptamer C3Awith SaOS-2 cells without transfection reagent over 5 time points (Figure 5B). All aptamer samples appear to enter the cell and the images depict migration towards the nucleus over time. Percent nuclear localization over time was quantified by image intensity where hundreds of cells were batch processed using MetaMorph™ software (64-bit version, Molecular Devices Corp., Sunnyvale, CA, USA) for aptamer C3A and control, with and without transfection (Figure 5C). Whether or not transfection reagent was used, aptamers appear to enter the cell and localize partially in both the cytoplasm and nucleus to some degree. There are examples where all aptamers are exclusively in the cytoplasm for a period of time, but these results show that for most cells, a proportion (>50%) of the aptamers end up in the nucleus quickly after exposure. To see if treatment with aptamer C3A had an effect on Runx2 protein expression levels in SaOS-2 cell extracts, a western blot was performed (Figure 5D). Data were consistent with a slight reduction of Runx2 levels when cells were transfected with C3A relative to controls (Figure 5D). To determine if aptamer C3A influenced osteoblast ability to deposit extracellular matrix, SaOS-2 cells were subjected to an Alizarin Red assay to quantify calcific deposition (Figure 5E). At a timepoint 15 days after transfection it was clear that both the naked C3A aptamer and the transfected C3A aptamer were able to increase the rate of calcific deposition of the cells relative to control aptamers (Figure 5E). This data would be consistent with an observation that the C3A aptamer is able to enter the cell even in the absence of the transfection reagent and increase calcific extracellular matrix deposition. We also investigated the influence of aptamer C3A on apoptosis and observed that aptamer C3A promoted apoptosis significantly more than a random sequence control (Figure S1).

## 3. Discussion

Aptamer selections were begun with an entire HECT domain 'pre-selection'. Subsequent selections against N-lobe, C-lobe and HECT pool showed enrichment of Aptamers only against C-lobe. This indicated that the C-lobe likely had selected tight-binding aptamers early in the selection process. We observed that it was necessary to retain the flanking constant regions in the C-lobe aptamers. Two classic examples of aptamers for which the PCR constant regions were not necessary for binding are pegaptanib and the anti-thrombin aptamer, but others have been reported where constant regions were required for binding [37,38]. We surmise that the necessity of flanking regions in an aptamer varies from selection to selection.

Concerning our WWP1 truncation targets themselves (Figure 1), some structural features are relevant. First, the C-lobe portion of the related E3 ubiquitin ligase UbR5 has its crystal structure solved and was found to be active [39]. Nevertheless, we assumed our C-lobe truncation was unlikely to have activity considering previous reports had shown that the N-lobe is necessary for the ubiquitination reaction [8]. Our best C-lobe targeting aptamer C3A, which had been pre-selected against HECT domain, was shown to specifically bind HECT (Figure 3). This implies that the C-lobe truncation most likely folded into a similar structure as that in the context of the whole protein, consistent with the demonstrated activity of UbR5 [39]. Many ubiquitin ligases have been identified as disease targets. This is the first attempt to inhibit HECT ubiquitin ligase activity with an aptamer and we therefore do not have a direct comparison of binding affinity for this specific family of targets [40]. Aptamers often bind to targets with nanomolar affinities, but the $K_D$ of our C3A could be estimated in the low μM range. We were not able to obtain estimations from our other aptamers and control because they did not bind sufficiently at the tested range of concentrations, but one may conclude their binding was far weaker (Figure 3).

Ubiquitination assays to determine inhibition are well-established [41]. HECT ligases in particular are commonly studied from many angles with such assays [41]. Other groups have detected ubiquitination by anti-ubiquitin western blotting, but we found this step unnecessary given the quantitative Coomassie stain from the reaction product on the gel, which we confirmed to be ubiquitin conjugated HECT with mass spectrometry [40]. Nevertheless, $IC_{50}$ values for aptamers are rarely

reported because enzymes are typically targeted by small molecules. There are some examples, however, such as G-quadruplex aptamers against Shp2 phosphatase which inhibited Shp2 activity at 29 nM, while small molecules inhibited in the μM range [42]. Conversely, anti-sclerostin antibodies inhibit in the nM range, while aptamers for the same protein inhibit at 15 μM [19,43]. Evidence of the mode of inhibition could be seen with our Michaelis-Menten curves and apparent $v_{max}$ and $K_M$ values, which were consistent with non-competitive inhibition. Overall these pieces of evidence support the possibility that aptamer C3A binds specifically to HECT domain and inhibits its activity in a non-competitive manner (Figures 3 and 4).

There are 3 known mechanisms for DNA to enter a eukaryotic cell without transfection or a virus: pinocytosis, absorptive endocytosis, or receptor mediated endocytosis [31,44]. In our assessment of aptamer C3A localization in SaOS-2 cells, we found qualitatively that the aptamer appeared to be able to enter the cell in the presence of absence of transfection reagent (Figure 5A). Here, we can only assume that the DNA in the non-transfected samples entered by the abovementioned mechanisms. Recently, aptamers for the intracellular and membrane target nucleolin were demonstrated to enter via macropinocytosis [45]. In addition, non-specific DNA internalizing receptors exist in other cell types but are not known in osteoblasts [27,28]. Both transfected and non-transfected samples were treated with DNA for 5 h, a time frame where aptamers could conceivably diffuse passively through the nuclear pore complex (Figure 5B), which could be compared to eukaryotic cells expressing proteins from plasmids which must enter the nucleus to be transcribed [29,46]. The percentage of signal appearing in the nucleus region for the hundreds of cells we analyzed with batch processing averaged around 60% (Figure 5C). One possible reason for this could be positively charged nuclear proteins such as histones, trapping a certain proportion of the aptamers.

Regarding aptamer C3A effect on phenotype, Western blot results were not clear-cut but were consistent with a slight reduction in Runx2 levels relative to controls (Figure 5D). The extracellular matrix deposition assay was performed under the same treatment conditions as the localization experiments and increased extracellular matrix was observed in the C3A treated cells relative to controls for both transfected and non-transfected cells.

Overall these experiments show that a DNA aptamer can bind specifically to WWP1 C-lobe and inhibit its target. Observations were consistent with the DNA aptamer entering the SaOS-2 cell nucleus, inhibiting WWP1 ubiquitination of Runx2 then increasing extracellular matrix deposition. WWP1 has also recently been implicated as an oncogene indicating that further work on WWP1 inhibition is warranted [47]. Finally, a recent paper demonstrated that interference of WWP1 led to the induction of apoptosis in osteosarcoma cells [47], which is also consistent with apoptosis experiments which we performed at the characterization stage (Figure S1). Further cell-based and animal-based experiments will be required to better understand the applicability of the aptamer to promote bone mineralization.

## 4. Materials and Methods

### *4.1. HECT, C-Lobe, N-Lobe and E2 Cloning, Expression and Purification*

HECT, C-lobe and N-lobe were amplified per Platinum® Pfx Polymerase (Invitrogen, Waltham, MA, USA) guidelines from a human liver cDNA library. The following sequences were those for which the expression inserts were designed: HECT Domain (bp 1916–3047 NCBI Reference Sequence: NM_007013.3), C-lobe (bp 2687–3047 NCBI Reference Sequence: NM_007013.3), N-lobe (bp 2342–2587 in NCBI Reference Sequence: NM_007013.3). The resulting sequences, once inserted into pET28a(+) (Novagen, Madison, WI, USA) vector, gave an N-terminal hexahistidine tags. Subcloning was initiated by 1% agarose gel purification of the PCR product with Platinum® Pfx Polymerase (Invitrogen) of each insert (approx 20 cycles) using QIAquick® gel extraction kit (Qiagen, Hilden, Germany). Inserts were then digested with *Eco*RI and *Nde*I (New England Biolabs, Ipswich, MA, USA), 1% agarose gel purified and extracted, and the concentration of the insert and vector was then determined using absorbance at OD260/280 nm. Approximately 20 ng of insert and 10 ng of vector were put into

ligation reaction with 1 μL ligase in total of 10 μL per instructions of T4 DNA ligase (New England Biolabs). A frozen eppendorf of XL-1 Blue *E. coli* (Stratagene, San Diego, CA, USA) provided in house was made competent and transformed by roughly following the pET System manual (Novagen). Colonies were selected on 50 μg/mL kanamycin agar plates, grown in 1 mL cultures for exponential growth phase, DNA was purified by QIAprep (Qiagen), and sequenced by Tech Dragon Limited™, Hong Kong, China.

The pET28a(+) (Novagen) vectors containing in-frame and un-mutated insert for all three truncations of HECT and pET-15b (Novagen) containing UbE2D2 (Addgene, Cambridge, MA, USA) were transformed into *E. coli* BL21(DE3) using the vendor transformation protocol (Novagen®). Overnight starter cultures of 30 μg/mL kanamycin containing LB media seeded 2–3 L cultures of the same media. These large cultures were grown at 37 °C under shaking at 200 rpm for approximately 6 h at 37 °C and induced to express with 500 μM IPTG, and shaken at room temperature for 4–5 h (C-lobe, N-lobe, and UbE2D2) and 4 °C overnight (HECT domain). Cell pellet was harvested by centrifugation at 4000 rpm, for 25 min, at 4 °C. After careful decanting, cell pellet was stored at −20 °C until purification. Column load was prepared by resuspending cell pellets in 20 mL of sonication buffer (Tris/500 mM NaCl/20 mM imidazole/0.1% (*v*/*v*) TritonX (pH 7.4)) for every 500 mL of culture and supplemented with Complete EDTA-free EASYpack protease inhibitor cocktail (Roche, Mannheim, Germany) followed by sonication for 10 min on ice at 30% amplitude. Cell lysate was centrifuged at 13,000 rpm for 25 min at 4 °C. Supernatant was filtered and loaded onto His-trap HP $Ni^{2+}$ affinity column (GE Healthcare, Chicago, IL, USA) using a peristaltic pump. After loading, the column was transferred to Vision™ Workstation (Applied Biosystems, Waltham, MA, USA). Real time UV trace was analyzed with the accompanying Vision™ Software (SDS v. 2.3, Applied Biosystems, Foster City, CA, USA). A gradient was run from 0% mobile phase A (50 mM Tris/500 mM NaCl/20 mM Imidazole (pH 7.4)) → 100% mobile phase B (50 mM Tris/500 mM NaCl/500 mM Imidazole (pH 7.4)) over 20 min at 3.5 mL/min and ~2 mL fractions were taken by hand throughout the gradient. Fractions were stored at −20 °C. Overall, the proteins were of correct size, were derived from the correct sequence, had purities of around 95% (excluding UbE2D2), and maintained a solubility of around 50% of the starting fraction pool after one week at 4 °C. All proteins expressed in high yield (concentrations of 2–4 mg/mL) and signal during imidazole gradients generally coincided with predicted isoelectric points.

### *4.2. SELEX Procedures*

Basic methodologies and tools for aptamer selection were adapted from our labs previous methods. A random DNA library was obtained from Tech Dragon Limited, Hong Kong containing 6.9 nanomoles of single stranded DNA of the following design: Aptamers→ 3′-CTAATACGACTC ACTATAGG(N30)AAGCTTTGCAGAGAGGATCCTT-5′, Primers→ 3′-GATTATGCTGAGTGATATCC, TTCGAAACGTCTCTCCTAGGAA-5′-Biotin. DNA was reconstituted in MilliQ $H_2O$ and contained a total of $4.2 \times 10^{15}$ DNA molecules of $1.15 \times 10^{18}$ possible sequences from a variable region of $N = 30$. Determination of the amount of protein target to be used was based on the Ni-NTA Agarose Beads Handbook (Qiagen, Hilden, Germany) estimate that approximately 3 μg of protein bind to 10 μL of bead solution. The amount of target protein necessary to saturate 10 μL of bead solution was determined by exposing the beads to an increasing amount of protein, washing with selection buffer (50 mM Tris/0.05% Tween-20/0 → 1.0 M NaCl (pH 7.3)), eluting with 1.0 M imidazole in selection buffer, and visualizing on SDS-PAGE. After washing beads with protein buffer (50 mM Tris/400 mM NaCl/0.05% Tween-20 (pH 7.3)), appropriate amounts of protein were added and beads, and washed 3 times again with protein buffer. A 25 μL aliquot of library was then diluted with 200 μL of selection buffer and added to the beads, gently mixed, and set for 1 min. The beads were then washed with 1 mL of selection buffer 6–12 times depending on the round of selection. Protein bound to DNA was eluted with 50 μL elution buffer (1.0 M imidazole in TBS, pH 7.5) and 5 μL was carried on to PCR amplification with biotinylated reverse primer for ~10 cycles. The resulting double stranded amplification product from each consecutive round was separated by washing 50 μL of Dynabeads

M-280 Streptavidin magnetic beads (Invitrogen, Waltham, MA, USA) with 1 mL separation buffer (50 mM Tris/0.05% Tween-20 (pH 7.3)), binding the entire 50 µL PCR product and 900 µL separation buffer with the washed beads, washing three times with separation buffer, and eluting with 50 µL of 100 mM NaOH. DNA containing NaOH was diluted with 150 µL TBS for neutralization. Progression of the selection process was monitored by PCR and PAGE. Pools of double stranded DNA from final rounds of selections were blunt end cloned into vectors using Zero Blunt® TOPO® PCR Cloning Kit (Invitrogen) and transfection of XL-1 Blue *E. coli* (Stratagene, San Diego, CA, USA) was performed as previously mentioned. 50 colonies from 50 µg/mL kanamycin selective plates were grown in 2.5 mL cultures for approximately 10 h, and said cultures were prepared for sequencing using the QIAprep® Spin Miniprep Kit (Qiagen, Hilden, Germany). Sequencing of plasmids was performed by Tech Dragon Limited, Hong Kong, China.

### *4.3. HECT Ubiquitin Ligase Activity Assay*

A HECT ubiquitination assay was devised based on the general guidelines of the Boston Biochem® Company which specializes in ubiquitin assays. Active HECT domain and the human E2 protein (UbE2D2) were expressed in *E. coli*, purified as described previously and were kept at 100 ng/µL and 160 ng/µL, respectively, at −20 °C in ~25% glycerol. $His_6$-tagged human recombinant Ubiquitin and recombinant Human $His_6$-Ubiquitin E1 Enzyme (UBE1) (Boston Biochem®) were kept at 5 µg/µL and 250 ng/µL, respectively, at −20 °C. The reaction was optimized by starting at 250 ng E1, 300 ng, HECT, 320 ng E2, and 5 µg Ub, and then systematically altering assay parameters such as reaction volume, time, reagent amounts, and temperature. Finally, the reaction contained 2.6 µM HECT, 45.5 nM UBE1, 507.8 nM UBE2D2, and varying from 300 nM to 4.8 µM Ubiquitin depending on the experiment. The total reaction volume was 25 µL, was run for 1 h at 37 °C in assay buffer (50 mM Tris/50 mM NaCl/5 mM $MgCl_2$/5 mM KCl/25 mM DTT/5 mM ATP (pH 7.5)), and stopped by addition of 25 µL SDS-PAGE loading buffer (100 mM Tris/40% *v/v* glycerol/8% *w/v* SDS/5% *w/v* beta-mercaptoethanol/0.04% *w/v* bromophenol blue (pH 7.5)) with a final gel load of 20 µL. Identity of the reaction product band (HECT~Ub conjugate) was confirmed by MS/MS (Genome Research Center, Hong Kong, China). Gels were stained with Coomassie or Silver depending on need for quantitation and analyzed with ImageJ (NIH, Bethesda, MD, USA) and Prism® (version 7, GraphPad, San Diego, CA, USA) softwares.

### *4.4. Electrophoretic Mobility Shift Assay (EMSA)*

Briefly, 15 µL samples containing 11.3 µM → 293.9 nM HECT domain, 55.6 nM aptamer, and 4 µL of EMSA sample buffer (50 mM Tris/10% (*v/v*) Glycerol/0.02% (*w/v*) bromophenol blue (pH 6.8)) were created. The mixture was set for 60 min at 4 °C while gel was pre-run in TAE buffer at 100 V for equilibration. Samples were then loaded and run on 12% PAGE Gels which were prepared using vendor Midi Protean Cell guidelines (BioRad, Hercules, CA, USA) at 100 V for approximately 3 h until tracking dye reached bottom of the gel. Gels were stained with 3.5 µL of SYBR Gold Nucleic Acid Gel Stain (Molecular Probes, Waltham, MA, USA) per 50 mL of TAE buffer and imaged in the UV Transilluminator Imaging System (UVP, Hercules, CA, USA) and analyzed with ImageJ and Prism®. 6.5 pmol of aptamer was mixed with a series of concentrations of HECT, set for 1 h at 4 °C, run on 10% PAGE for 1.5 h at 100 V in 4 °C with minimal glycerol for gel loading, and stained with SYBR gold™.

### *4.5. Cell Culturing*

SaOS-2 Cells (ATCC® number HTB-85®), a human osteosarcoma line, were obtained in house labeled at passage 5. Cells were thawed, seeded, passaged according to the general guidelines of the Cell Culture Basics guide (Thermo Fisher Scientific, Hercules, CA, USA) in a Class II bio safety cabinet with McCoy's 5a Media (Sigma-Aldrich, St. Louis, MO, USA) supplemented with Penicillin/Streptomycin and 15% FBS, and centrifugation was performed on bench top centrifuge. Cells were stored at a controlled environment of 37 °C with 5% $CO_2$ and viewed with an Eclipse

TS100 (Nikon, Tokyo, Japan) light microscope at 4× and 10× magnifications daily. Samples to be prepared for fixed cell imaging, western blot, apoptosis, bone mineralization, and alkaline phosphatase activity were initiated by growing cells to ~80% confluency on either 6, 24, or 96 well cell culture plates (Corning Inc., Corning, NY, USA). Cells were transfected with 100 ng of aptamer and control for 4 h per Lipofectamine 2000 (Invitrogen) guidelines using McCoy's 5a Media (Sigma-Aldrich) without Penicillin/Streptomycin or FBS or treated with aptamer and control without transfection reagent for the same amount of time. Cells were then replaced with normal supplemented media after transfection, which took place once (T0) for fixed cell imaging, western blot, and apoptosis assays and three times (T0 then every 3 days) for mineralization and alkaline phosphatase assays. The cells remained alive for the course of the experiments.

### *4.6. Fixed Cell Imaging*

Cover slip containing Costar® 6 well flat bottom plates (Corning Inc., Corning, NY, USA) were prepared with sterile technique by placing cover slips into the wells with forceps in the BSC hood, rinsing with cold methanol, and rinsing 3× with ice cold sterile PBS. Cells were seeded 1:4 and grown to ~90% confluency and then treated with aptamer and controls, with and without Lipofectamine™ 2000. At each time point, wells were washed with ice cold PBS, gently fixed with ice cold methanol at −20 °C for one hour and washed with ice cold PBS. After damping dry, Acrytol® mounting media (Leica, Wetzlar, Germany) was used to mount slides, which were then dried overnight in the dark. Images were taken on an BX51 Fluorescence Microscope (Olympus, Tokyo, Japan) using brightfield and the appropriate filters for Cy3 (red) and Hoechst (blue) at 40×. MetaMorph® (Molecular Devices, San Jose, CA, USA) batch processing software was used to analyze at least 85 cells per sample.

### *4.7. Runx2 Western Blot*

Cells were first washed with ice cold PBS, then 200 µL of ice cold RIPA buffer (150 mM sodium chloride/1.0% Triton X-100/0.5% sodium deoxycholate/0.1% SDS (sodium dodecyl sulfate)/50 mM Tris (pH 8.0)) supplemented with complete EDTA-free EASYpack protease inhibitor cocktail was added and cells, scraped and recovered by pipette. Lysates were agitated at 4 °C for 30 min by light shaking and centrifuged for 20 min at 12,000 rpm on a X-15R bench top centrifuge (Beckman Coulter) at 4 °C before recovering supernatant. In this case, Rabbit derived Anti-Runx2 (Novus Biologicals, Littleton, CO, USA) and Goat derived Anti-Rabbit IgG (whole molecule) Peroxidase conjugate (Novus Biologicals®) were used at 1/500 and 1/80,000, respectively, while generally following the Western Blotting Beginners Guide (Abcam, Cambridge, UK). 1 µL of B-Actin (Cell Signaling Technology, Danvers, MA, USA) stock was included with each primary antibody incubation as a loading control. Blots were imaged with UV Transilluminator Imaging System (UVP, Hercules, CA, USA).

### *4.8. Apoptosis Assay*

Apoptosis samples were prepared as described in the cell culture section and were performed according to HT TiterTACS™ Assay kit (Trevigen, Gaithersburg, MD, USA) guidelines, read at 450 nm on a 200 SpectraMax 340PC 38 (Molecular Devices) and analyzed with Soft Max Pro (Molecular Devices) and Prism® (GraphPad) Software.

### *4.9. Bone Mineralization Assay*

Assays to detect the calcium of bone deposition generally followed the Osteoblast Differentiation and Mineralization Guide (PromoCell, Heidelberg, Germany). First, cells washed with ice cold PBS, fixed with ice cold methanol overnight, stained with 20 g/mL Alizarin Red S for 45 min at room temperature, washed 5 times with di$H_2O$, and PBS added before digital photographs were taken.

## 5. Conclusions

We successfully generated a DNA aptamer (C3A) which binds to the C-lobe of WWP1 with a binding affinity of 1.9 μM. This aptamer was demonstrated to inhibit the ubiquitination activity of WWP1 in a non-competitive manner. The aptamer could internalize into SaOS2 cells even in absence of transfection agent. The aptamer was shown to stimulate extracellular matrix deposition relative to controls. Future work can improve binding affinity by microarray maturation, employ bioinformatics methods to modify the aptamer for greater functionality [48] or generate a library that could be used alongside a microfluidic selection method [49]. By such approaches, novel therapeutic aptamers can be further developed for a variety of human disease.

**Supplementary Materials:** Supplementary materials can be found at www.mdpi.com/1422-0067/19/3/763/s1.

**Acknowledgments:** This work was supported by the Hong Kong University Grants Council under General Research Fund Grant HKU777109M.

**Author Contributions:** Wesley Tucker conceived, designed, prepared, and performed the experiments, analyzed the data, and helped prepare the manuscript. Julian Tanner conceived the study, guided the research, and helped prepare the manuscript. Andrew Kinghorn, Lewis Fraser, and Yee-Wai Cheung helped analyze data and to prepare the manuscript.

**Conflicts of Interest:** The authors declare no conflict of interest.

## References

1. Dallas, S.L.; Bonewald, L.F. Dynamics of the transition from osteoblast to osteocyte. *Ann. N. Y. Acad. Sci.* **2010**, *1192*, 437–443. [CrossRef] [PubMed]
2. Glimcher, L.H.; Jones, D.C.; Wein, M.N. Control of postnatal bone mass by the zinc finger adapter protein Schnurri-3. *Ann. N. Y. Acad. Sci.* **2007**, *1116*, 174–181. [CrossRef] [PubMed]
3. Komori, T.; Yagi, H.; Nomura, S.; Yamaguchi, A.; Sasaki, K.; Deguchi, K.; Shimizu, Y.; Bronson, R.T.; Gao, Y.H.; Inada, M.; et al. Targeted disruption of Cbfa1 results in a complete lack of bone formation owing to maturational arrest of osteoblasts. *Cell* **1997**, *89*, 755–764. [CrossRef]
4. Wein, M.N.; Jones, D.C.; Shim, J.H.; Aliprantis, A.O.; Sulyanto, R.; Lazarevic, V.; Poliachik, S.L.; Gross, T.S.; Glimcher, L.H. Control of bone resorption in mice by Schnurri-3. *Proc. Natl. Acad. Sci. USA* **2012**, *109*, 8173–8178. [CrossRef] [PubMed]
5. Jones, D.C.; Wein, M.N.; Oukka, M.; Hofstaetter, J.G.; Glimcher, M.J.; Glimcher, L.H. Regulation of adult bone mass by the zinc finger adapter protein Schnurri-3. *Science* **2006**, *312*, 1223–1227. [CrossRef] [PubMed]
6. Huang, K.; Johnson, K.D.; Petcherski, A.G.; Vandergon, T.; Mosser, E.A.; Copeland, N.G.; Jenkins, N.A.; Kimble, J.; Bresnick, E.H. A HECT domain ubiquitin ligase closely related to the mammalian protein WWP1 is essential for Caenorhabditis elegans embryogenesis. *Gene* **2000**, *252*, 137–145. [CrossRef]
7. Pirozzi, G.; McConnell, S.J.; Uveges, A.J.; Carter, J.M.; Sparks, A.B.; Kay, B.K.; Fowlkes, D.M. Identification of novel human WW domain-containing proteins by cloning of ligand targets. *J. Biol. Chem.* **1997**, *272*, 14611–14616. [CrossRef] [PubMed]
8. Verdecia, M.A.; Joazeiro, C.A.; Wells, N.J.; Ferrer, J.L.; Bowman, M.E.; Hunter, T.; Noel, J.P. Conformational flexibility underlies ubiquitin ligation mediated by the WWP1 HECT domain E3 ligase. *Mol. Cell* **2003**, *11*, 249–259. [CrossRef]
9. Roth, A.; Breaker, R.R. The structural and functional diversity of metabolite-binding riboswitches. *Annu. Rev. Biochem.* **2009**, *78*, 305–334. [CrossRef] [PubMed]
10. Tuerk, C.; Gold, L. Systematic evolution of ligands by exponential enrichment: RNA ligands to bacteriophage T4 DNA polymerase. *Science* **1990**, *249*, 505–510. [CrossRef] [PubMed]
11. Ellington, A.D.; Szostak, J.W. In vitro selection of RNA molecules that bind specific ligands. *Nature* **1990**, *346*, 818–822. [CrossRef] [PubMed]
12. Kinghorn, A.B.; Dirkzwager, R.M.; Liang, S.; Cheung, Y.W.; Fraser, L.A.; Shiu, S.C.; Tang, M.S.; Tanner, J.A. Aptamer affinity maturation by resampling and microarray selection. *Anal. Chem.* **2016**, *88*, 6981–6985. [CrossRef] [PubMed]
13. Sampson, T. Aptamers and SELEX: The technology. *World Pat. Inf.* **2003**, *25*, 123–129. [CrossRef]

14. Ulrich, H. DNA and RNA aptamers as modulators of protein function. *Med. Chem.* **2005**, *1*, 199–208. [CrossRef] [PubMed]
15. Cheung, Y.W.; Kwok, J.; Law, A.W.; Watt, R.M.; Kotaka, M.; Tanner, J.A. Structural basis for discriminatory recognition of plasmodium lactate dehydrogenase by a DNA aptamer. *Proc. Natl. Acad. Sci. USA* **2013**, *110*, 15967–15972. [CrossRef] [PubMed]
16. Zou, J.; Huang, X.; Wu, L.; Chen, G.; Dong, J.; Cui, X.; Tang, Z. Selection of intracellularly functional RNA mimics of green fluorescent protein using fluorescence-activated cell sorting. *J. Mol. Evol.* **2015**, *81*, 172–178. [CrossRef] [PubMed]
17. Daniels, D.A.; Chen, H.; Hicke, B.J.; Swiderek, K.M.; Gold, L. A tenascin-C aptamer identified by tumor cell SELEX: Systematic evolution of ligands by exponential enrichment. *Proc. Natl. Acad. Sci. USA* **2003**, *100*, 15416–15421. [CrossRef] [PubMed]
18. Stein, C.A.; Castanotto, D. FDA-approved oligonucleotide therapies in 2017. *Mol. Ther.* **2017**, *25*, 1069–1075. [CrossRef] [PubMed]
19. Shum, K.T.; Chan, C.; Leung, C.M.; Tanner, J.A. Identification of a DNA aptamer that inhibits sclerostin's antagonistic effect on Wnt signalling. *Biochem. J.* **2011**, *434*, 493–501. [CrossRef] [PubMed]
20. Dirkzwager, R.M.; Liang, S.; Tanner, J.A. Development of aptamer-based point-of-care diagnostic device for malaria using 3D printing rapid prototyping. *ACS Sens.* **2016**, *1*, 420–426. [CrossRef]
21. Cheung, Y.W.; Dirkzwager, R.M.; Wong, W.C.; Cardoso, J.; Costa, J.D.; Tanner, J.A. Aptamer-mediated plasmodium-specific diagnosis of malaria. *Biochimie* **2018**, *145*, 131–136. [CrossRef] [PubMed]
22. Fraser, L.A.; Kinghorn, A.B.; Dirkzwager, R.M.; Liang, S.; Cheung, Y.W.; Lim, B.; Shiu, S.C.; Tang, M.S.L.; Andrew, D.; Manitta, J.; et al. A portable microfluidic Aptamer-Tethered Enzyme Capture (APTEC) biosensor for malaria diagnosis. *Biosens. Bioelectron.* **2018**, *100*, 591–596. [CrossRef] [PubMed]
23. Ouellet, J. RNA fluorescence with light-up aptamers. *Front. Chem.* **2016**, *4*, 29. [CrossRef] [PubMed]
24. Praetorius, F.; Kick, B.; Behler, K.L.; Honemann, M.N.; Weuster-Botz, D.; Dietz, H. Biotechnological mass production of DNA origami. *Nature* **2017**, *552*, 84–87. [CrossRef] [PubMed]
25. Maurisse, R.; De Semir, D.; Emamekhoo, H.; Bedayat, B.; Abdolmohammadi, A.; Parsi, H.; Gruenert, D.C. Comparative transfection of DNA into primary and transformed mammalian cells from different lineages. *BMC Biotechnol.* **2010**, *10*, 9. [CrossRef] [PubMed]
26. Yu, B.; Zhao, X.; Lee, L.J.; Lee, R.J. Targeted delivery systems for oligonucleotide therapeutics. *AAPS J.* **2009**, *11*, 195–203. [CrossRef] [PubMed]
27. Zamecnik, P.C.; Stephenson, M.L. Inhibition of Rous sarcoma virus replication and cell transformation by a specific oligodeoxynucleotide. *Proc. Natl. Acad. Sci. USA* **1978**, *75*, 280–284. [CrossRef] [PubMed]
28. Akhtar, S.; Juliano, R.L. Cellular uptake and intracellular fate of antisense oligonucleotides. *Trends Cell Biol.* **1992**, *2*, 139–144. [CrossRef]
29. Bennett, R.M. As nature intended? The uptake of DNA and oligonucleotides by eukaryotic cells. *Antisense Res. Dev.* **1993**, *3*, 235–241. [CrossRef] [PubMed]
30. Loke, S.L.; Stein, C.A.; Zhang, X.H.; Mori, K.; Nakanishi, M.; Subasinghe, C.; Cohen, J.S.; Neckers, L.M. Characterization of oligonucleotide transport into living cells. *Proc. Natl. Acad. Sci. USA* **1989**, *86*, 3474–3478. [CrossRef] [PubMed]
31. Yakubov, L.A.; Deeva, E.A.; Zarytova, V.F.; Ivanova, E.M.; Ryte, A.S.; Yurchenko, L.V.; Vlassov, V.V. Mechanism of oligonucleotide uptake by cells: Involvement of specific receptors? *Proc. Natl. Acad. Sci. USA* **1989**, *86*, 6454–6458. [CrossRef] [PubMed]
32. Zhou, J.; Rossi, J.J. Therapeutic potential of aptamer-siRNA conjugates for treatment of HIV-1. *BioDrugs* **2012**, *26*, 393–400. [CrossRef] [PubMed]
33. Legendre, J.Y.; Szoka, F.C., Jr. Delivery of plasmid DNA into mammalian cell lines using pH-sensitive liposomes: Comparison with cationic liposomes. *Pharm. Res.* **1992**, *9*, 1235–1242. [CrossRef] [PubMed]
34. De Fougerolles, A.R. Delivery vehicles for small interfering RNA in vivo. *Hum. Gene Ther.* **2008**, *19*, 125–132. [CrossRef] [PubMed]
35. Mayer, G. The chemical biology of aptamers. *Angew. Chem.* **2009**, *48*, 2672–2689. [CrossRef] [PubMed]
36. Auslander, D.; Wieland, M.; Auslander, S.; Tigges, M.; Fussenegger, M. Rational design of a small molecule-responsive intramer controlling transgene expression in mammalian cells. *Nucleic Acids Res.* **2011**, *39*, e155. [CrossRef] [PubMed]

37. Ruckman, J.; Green, L.S.; Beeson, J.; Waugh, S.; Gillette, W.L.; Henninger, D.D.; Claesson-Welsh, L.; Janjic, N. 2′-Fluoropyrimidine RNA-based aptamers to the 165-amino acid form of vascular endothelial growth factor (VEGF165). Inhibition of receptor binding and VEGF-induced vascular permeability through interactions requiring the exon 7-encoded domain. *J. Biol. Chem.* **1998**, *273*, 20556–20567. [CrossRef] [PubMed]
38. Bock, L.C.; Griffin, L.C.; Latham, J.A.; Vermaas, E.H.; Toole, J.J. Selection of single-stranded DNA molecules that bind and inhibit human thrombin. *Nature* **1992**, *355*, 564–566. [CrossRef] [PubMed]
39. Matta-Camacho, E.; Kozlov, G.; Menade, M.; Gehring, K. Structure of the HECT C-lobe of the UBR5 E3 ubiquitin ligase. *Acta Crystallogr. Sect. F Struct. Biol. Cryst. Commun.* **2012**, *68*, 1158–1163. [CrossRef] [PubMed]
40. Sun, Y. Targeting E3 ubiquitin ligases for cancer therapy. *Cancer Biol. Ther.* **2003**, *2*, 623–629. [CrossRef] [PubMed]
41. Beaudenon, S.; Dastur, A.; Huibregtse, J.M. Expression and assay of HECT domain ligases. *Methods Enzymol.* **2005**, *398*, 112–125. [PubMed]
42. Hu, J.; Wu, J.; Li, C.; Zhu, L.; Zhang, W.Y.; Kong, G.; Lu, Z.; Yang, C.J. A G-quadruplex aptamer inhibits the phosphatase activity of oncogenic protein Shp2 in vitro. *Chembiochem* **2011**, *12*, 424–430. [CrossRef] [PubMed]
43. Li, X.; Ominsky, M.S.; Warmington, K.S.; Morony, S.; Gong, J.; Cao, J.; Gao, Y.; Shalhoub, V.; Tipton, B.; Haldankar, R.; et al. Sclerostin antibody treatment increases bone formation, bone mass, and bone strength in a rat model of postmenopausal osteoporosis. *J. Bone Miner. Res.* **2009**, *24*, 578–588. [CrossRef] [PubMed]
44. Patil, S.D.; Rhodes, D.G.; Burgess, D.J. DNA-based therapeutics and DNA delivery systems: A comprehensive review. *AAPS J.* **2005**, *7*, E61–E77. [CrossRef] [PubMed]
45. Reyes-Reyes, E.; Šalipur, F.R.; Shams, M.; Forsthoefel, M.K.; Bates, P.J. Mechanistic studies of anticancer aptamer AS1411 reveal a novel role for nucleolin in regulating Rac1 activation. *Mol. Oncol.* **2015**, *9*, 1392–1405. [CrossRef] [PubMed]
46. Wente, S.R.; Rout, M.P. The nuclear pore complex and nuclear transport. *Cold Spring Harb. Perspect. Biol.* **2010**, *2*, a000562. [CrossRef] [PubMed]
47. Zhang, L.; Wu, Z.; Ma, Z.; Liu, H.; Wu, Y.; Zhang, Q. WWP1 as a potential tumor oncogene regulates PTEN-Akt signaling pathway in human gastric carcinoma. *Tumour. Biol.* **2015**, *36*, 787–798. [CrossRef] [PubMed]
48. Kinghorn, A.B.; Fraser, L.A.; Lang, S.; Shiu, S.C.C.; Tanner, J.A. Aptamer bioinformatics. *Int. J. Mol. Sci.* **2017**, *18*, 2516. [CrossRef]
49. Fraser, L.A.; Kinghorn, A.B.; Tang, M.S.; Cheung, Y.-W.; Lim, B.; Liang, S.; Dirkzwager, R.M.; Tanner, J.A. Oligonucleotide functionalised microbeads: Indispensable tools for high-throughput aptamer selection. *Molecules* **2015**, *20*, 21298–21312. [CrossRef] [PubMed]


MDPI
St. Alban-Anlage 66
4052 Basel
Switzerland
Tel. +41 61 683 77 34
Fax +41 61 302 89 18
www.mdpi.com

*International Journal of Molecular Sciences* Editorial Office
E-mail: ijms@mdpi.com
www.mdpi.com/journal/ijms

MDPI
St. Alban-Anlage 66
4052 Basel
Switzerland

Tel: +41 61 683 77 34
Fax: +41 61 302 89 18

www.mdpi.com

ISBN 978-3-03897-060-6